(12)

AD A115875

AFWAL-TR-81-4019
Volume II

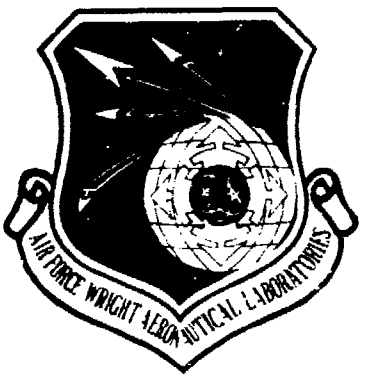

PROCEEDINGS OF THE 1980 TRI-SERVICE CONFERENCE ON CORROSION

VOLUME II

Fred H. Meyer Jr., Editor
Air Force Wright Aeronautical Laboratories
Materials Laboratory

November 1980

US Air Force Academy, Colorado

Approved for public release, distribution unlimited.

DTIC FILE COPY

DTIC ELECTE JUN 22 1982 S D E

MATERIALS LABORATORY
AIR FORCE WRIGHT AERONAUTICAL LABORATORIES
AIR FORCE SYSTEMS COMMAND
WRIGHT-PATTERSON AIR FORCE BASE, OHIO 45433

NOTICE

When Government drawings, specifications, or other data are used for any purpose other than in connection with a defin ely related Government procurement operation, the United States Government thereb ncurs no responsibility nor any obligation whatscever; and the fact that the government may have formulated, furnished, or in any way supplied the said drawings, specifications, or other data, is not to be regarded by implication or otherwise as in any manner licensing the holder or any other person or corporation, or conveying any rights or permission to manufacture use, or sell any patented invention that may in any way be related thereto.

This report has been reviewed by the Office of Public Affairs (ASD/PA) and is releasable to the National Technical Information Service (NTIS). At NTIS, it will be available to the general public, including foreign nations.

This technical report has been reviewed and is approved for publication.

Fred H. Meyer Jr.

FRED H. MEYER Jr.
Project Engineer

Paul L. Hendricks

PAUL L HENDRICKS, Technical Manager for
Corrosion Control & Failure Analysis
Materials Integrity Branch
Systems Support Division

FOR THE COMMANDER

T D Cooper

T D COOPER, Chief
Materials Integrity Branch
Systems Support Division
Materials Laboratory
Wright-Aeronautical Laboratories

"If your address has changed, if you wish to be removed from our mailing list, or if the addressee is no longer employed by your organization please notify AFWAL/MLSA, W-PAFB, OH 45433 to help us maintain a current mailing list".

Copies of this report should not be returned unless return is required by security considerations, contractual obligations, or notice on a specific document.

AIR FORCE/56780/9 June 1982 — 300

UNCLASSIFIED

SECURITY CLASSIFICATION OF THIS PAGE (When Data Entered)

REPORT DOCUMENTATION PAGE	READ INSTRUCTIONS BEFORE COMPLETING FORM
1. REPORT NUMBER: AFWAL-TR-4019 VOLUME II 2. GOVT ACCESSION NO.: AD-A115875	3. RECIPIENT'S CATALOG NUMBER:
4. TITLE (and Subtitle): Proceedings of the 1980 Tri-Service Conference on Corrosion - 5-7 November 1980 Volume II	5. TYPE OF REPORT & PERIOD COVERED: Final Technical Report 7Nov80 - 15 August 1981 6. PERFORMING ORG. REPORT NUMBER:
7. AUTHOR(s): FRED H MEYER Jr. (Editor)	8. CONTRACT OR GRANT NUMBER(s):
9. PERFORMING ORGANIZATION NAME AND ADDRESS: Materials Integrity Branch (MLSA) Materials Laboratory Air Force Wright Aeronautical Laboratories Wright-Patterson AFB, OH 45433	10. PROGRAM ELEMENT, PROJECT, TASK AREA & WORK UNIT NUMBERS: 24180704
11. CONTROLLING OFFICE NAME AND ADDRESS: Systems Support Division (MLS) Materials Laboratory Air Force Wright Aeronautical Laboratories Wright-Patterson AFB, OH 45433	12. REPORT DATE: November 1980 13. NUMBER OF PAGES: 500
14. MONITORING AGENCY NAME & ADDRESS (if different from Controlling Office)	15. SECURITY CLASS. (of this report): UNCLASSIFIED 15a. DECLASSIFICATION/DOWNGRADING SCHEDULE:
16. DISTRIBUTION STATEMENT (of this Report): Approved for Public Release, Distribution Unlimited	
17. DISTRIBUTION STATEMENT (of the abstract entered in Block 20, if different from Report)	
18. SUPPLEMENTARY NOTES	
19. KEY WORDS (Continue on reverse side if necessary and identify by block number): Corrosion	
20. ABSTRACT (Continue on reverse side if necessary and identify by block number): This report is a compilation of the papers presented at the 1980 Tri-Service Conference on Corrosion held at the Air Force Academy, Colorado on 5-7 November 1980.	

DD FORM 1 JAN 73 1473 EDITION OF 1 NOV 65 IS OBSOLETE

UNCLASSIFIED

SECURITY CLASSIFICATION OF THIS PAGE (When Data Entered)

FOREWORD

This report was compiled by the Materials Integrity Branch, Systems Support Division, Materials Laboratory, Air Force Wright Aeronautical Laboratories, Wright-Patterson AFB, Ohio. It was initiated under Task 24180704 "Corrosion Control & Failure Analysis" with Fred H Meyer Jr. as the Project Engineer. The 1980 Tri-Service Conference on Corrosion is a follow-up of six prior conferences held in 1967, 1969, 1972, 1974, 1976, and 1978.

This report (Volume II) includes all available papers from the 1980 Tri-Service Conference on Corrosion acquired after the compilation of Volume I in March 1981.

This technical report (Volume II) was submitted by the editor in August 1981.

Proceedings of Prior Conferences are available in:

1. AFML-TR-67-329 (1967)
2. MCIC 73-19 (1972)
3. AFML-TR-75-42 Vol I, Vol II (1974) (ADA 021053, ADA 029934)
4. MCIC-77-33 (1976)
5. MCIC-79-40 (1978)

The purpose of the 1980 Conference was to continue interservice Coordination in the areas of corrosion research and corrosion prevention and control. Specifically, the objectives were to make Department of Defense personnel, contractors and interested individuals aware of the important corrosion problems in military equipment, to present the status of significant corrosion research projects currently pursued by the military services and to provide a general forum for exchange of corrosion prevention and control information.

TABLE OF CONTENTS

Table of Contents (Continued)

Table of Contents (Continued)

AFWAL-TR-81-4019
Volume II

AN OVERVIEW OF THE ARMY CORROSION CONTROL PROGRAM

Milton Levy
U.S. Army Materials and Mechanics Research Center
Watertown, Massachusetts 02172

Corrosion control is of vital importance to the U.S. Army and in particular the Development and Readiness Command (DARCOM) because it continues to be a major problem that degrades Army readiness.

The Development and Readiness Command performs its mission in response to Army needs and concepts developed by the Training and Doctrine Command, the User Representative, or in response to the needs of the field commands (FORSCOM, 8th Army Korea, USAEUR). DARCOM's mission is support in the areas of: research, development, and acquisition of the Army's materiel, the readiness of that materiel once it is in the hands of troops, and the readiness of war reserves and certain stocks.

Within DARCOM, the R&D commands provide research, concept development, and initial acquisition in their appropriate commodity area. The Test and Evaluation Command oversees all development testing for the Army. The corresponding Readiness Commands provide for supply, maintenance, and follow-on procurement of end-items in their respective commodity area. The actual care, preservation, storage, and overhaul is performed at the appropriate depot(s). If a program requires intensive management, a project manager is designated and assigned to any of the Research or Readiness Commands or to HQ, DARCOM. Table 1 lists the DARCOM Major Subordinate Commands.

As the lead laboratory for Materials Technology, the Army Materials and Mechanics Research Center (AMMRC) was tasked by HQ, DARCOM to develop a DARCOM Corrosion Control Program. In cooperation with the Product Assurance Directorate, HQ, DARCOM, a Materiel Deterioration Prevention and Control (MADPAC) Program was established. DARCOM Regulation 702-24, dated 16 October 1979, prescribes policy, procedures, and responsibilities for the program which is aimed specifically at the reduction of deterioration

of Army materiel. The MADPAC Program is centrally managed by the Director of Product Assurance, HQ, DARCOM, with the assistance of AMMRC. Advice concerning the program is proffered by the Central Steering Committee which is composed of members from the subordinate commands, selected offices from HQ, DARCOM, AMMRC, and Army Materiel Systems Analysis Activity (AMSAA).

TABLE 1. DARCOM MAJOR SUBORDINATE COMMANDS

ARRADCOM	Armaments R&D Command
AVRADCOM	Aviation R&D Command
CORADCOM	Communications R&D Command
ERADCOM	Electronics R&D Command
MERADCOM	Mobility Engineering R&D Command
NARADCOM	Natick R&D Command
TARADCOM	Tank Automotive R&D Command
ARRCOM	Armaments Readiness Command
TSARCOM	Troop Support Aviation Readiness Command
CERCOM	Communications and Electronics Readiness Command
DESCOM	Depot System Command
MICOM	Missile Command
TECOM	Test and Evaluation Command
TARCOM	Tank Automotive Readiness Command

The Major Subordinate Commands are required to establish (1) a corrosion control program which covers all systems and equipment within their mission responsibility, and (2) a corrosion control action office activity for administering the program.

Program Managers are required to establish a corrosion control plan and appoint a point-of-contact for liaison with the appropriate Subordinate Command Action Office. The depots also are required to establish a corrosion control plan and appoint a point-of-contact for liaison with the appropriate Readiness Command.

The Army Materiel System Analysis Activity is required to gather corrosion data on technical equipment in the field, through field liaison visits to Army materiel users.

In addition to serving DARCOM as Lead Laboratory for corrosion and corrosion control technology, AMMRC provides management assistance to the Director of Product Assurance by reviewing, analyzing, monitoring, and coordinating the Corrosion Control Program.

Objectives of the program include: Insure maximum use of State-of-the-Art technology in the prevention of deterioration; Provide for deterioration prevention reviews encompassing the areas of design, material selection, manufacturing processes, technical documentation, product assurance, field and depot maintainability operations, feedback data, and training requirements; Insure that all applicable contracts for Army systems and associated equipment contain requirements for a deterioration prevention program. Highlights of the program include the conduct of a Triennial inspection of DARCOM facilities, the establishment of a Materiel Deterioration Information Center, the dissemination of lessons learned, the coordination of training programs, the updating of military specifications, standards, and handbooks, and the promotion of technology effort.

The theme of the 1978 Tri-Service Corrosion Conference, hosted by the Army Materials and Mechanics Research Center, was "The National Cost of Corrosion". Dr. Elio Passaglia, National Bureau of Standards, in his Keynote Address, presented data from a report to the Congress by the NBS on "Economic Effects of Metallic Corrosion in the U.S." which showed that the total costs of corrosion in the U.S. are $\sim$ \$70 billion/year with $\sim$ \$10 billion/year being avoidable, if economically best practices were used throughout the economy, but lessening the remaining costs requires advances in technology. Both basic research and applied research investigations of corrosion and corrosion control are underway.

The prime sponsor of studies of basic mechanisms of corrosion is the Army Research Office (ARO). Generally, these fundamental studies are conducted by noted researchers at academic institutions in this country. Institutions investigating corrosion fundamentals include: Arizona State University, New York University, Rensselaer Polytechnic Institute , North Carolina State University, American University, Georgia Institute of Technology, Massachusetts Institute of Technology, University of Minnesota, and Portland State University.

Direct chemical attack of structural and coating metalsby hostile substances remains a formidable problem. Basic research investigations sponsored by ARO are being made to clarify the mechanisms underlying the initiation of cracking under fretting-corrosion-fatigue in steels. Fretting, and its ramifications have had serious consequences in engine and rotating Army aircraft structural components. Investigations are underway to study fundamental mechanisms of erosion of materials in hot flowing media and to study mechanisms of protection of materials in environments encountered in gun tubes, gas turbines, and propulsion components in missiles.

The role of sulfur in the corrosion of superalloys is also being elucidated through investigations of the mechanism of migration of sulfur through single crystal and polycrystalline oxides, including NiO, CoO, Al_2O_3, Cr_2O_3, and Fe_2O_3. An improved understanding of this phenomenon will result in better materials for the hot section of aircraft engines.

An activity of practical interest concerns the chemical interaction of fiber reinforcements with aluminum alloy matrixes. This new class of lightweight, high strength materials exhibit high potential for many aircraft and bridging applications. Principles governing the corrosion behavior of aluminum-graphite and aluminum-alumina fiber composites exposed to aqueous and atmospheric service are being investigated. The ability of ion implantation to form self-healing coatings for inhibition of localized corrosion is being investigated for applications in armaments.

Another phenomena of [illegible]tical interest which requires greater understanding involves the complex behavior of stress corrosion cracking. Several studies are underway to upgrade fundamental knowledge through investigations of mechanisms of stress corrosion cracking of aluminum alloys.

Employing an electrochemical scanning potential technique, a probe has been developed which measures the likelihood of corrosion of metal surfaces, adhesion of protective coatings, and differences in materials processing which can leas to susceptible corrosion sites. This development has potential application involving detection of flaws in protective coatings on high density penetrators, propensity for corrosion of shell casings, and monitoring of protective coatings on stored missile components. Basic and applied research investigations are conducted in-house within AMMRC and the several Army laboratories at ARRADCOM, MICOM, and MERADCOM, because of expertise and experience with particular materiel.

Within the general corrosion area, in house studies are continuing, utilizing both long-time surveillance and short-time electrochemical methods, to minimize corrosion of equipment and materials of construction employed in the processing of ammunition.

Oxidation-sulfidation corrosion modes are of deep concern to designers of aircraft engines. Protective coatings for the upgraded performance of gas turbine alloys are being developed in-house.

Erosion-corrosion is a failure mechanism which can appear in Army-relevant material such as cannon tubes, gas turbine engines, rocket nozzles, and ammunition processing equipment. Solid particles entrained in a high velocity, viscous reactive media are among the conditions contributing to combined mechanical and chemical attack. Studies are underway, in-house, to identify the extent of chemical reaction between propellant gases and gun steels under gun chamber conditions of temperature and pressure. Efforts are also being made to determine the erosion constituents as well as the factors affecting the surface cracking phenomena. [illegible]ly,

the parameters governing the erosive effects of high temperature, high pressure, and high gas velocity on gun steels are being investigated.

Stress Corrosion Cracking (SCC) failure attracts attention because of its catastrophic nature. In addition to the several ARO studies described earlier, efforts are being made to upgrade the SCC resistance during the development of new Al-Zn-Mg-Li wrought and Al-Zn-Mg-Cu powder metallurgy materials through composition and thermomechanical treatments. SCC effects of humidity and up-to-150°F temperatures on commercial grades of aluminum alloys are also being determined.

High strength steels are of continuing importance to the Army. Unfortunately, these steels are highly susceptible to stress corrosion. Effects of humidity, temperature, impurities, surface treatments, and hydrogen diffusion characteristics are being investigated. Realistic missile storage parameters are being established. Also, efforts are continuing to devise an accelerated test method for evaluating SCC characteristics of armor steels.

Stress corrosion cracking characteristics are also an important consideration in the improvement of uranium alloys for armor-piercing ammunition penetrators. Effects of hydrogen, humidity, strain rate, thermal treatments, and residual stress are being studied. Protecting the surface of susceptible alloys with a compatible coating is another approach employed to elleviate the problem of corrosion-induced failure.

In-house investigations are underway to develop materials and processing techniques for protecting a variety of materials, including aluminum, cast magnesium, uranium alloys, superalloys, gun steels, magnesium-aluminum oxide, and aluminum graphite composites against the harmful effects of a wide range of environments. Metallic, intermetallic, and nonmetallic coating systems are being developed. Lead and hexavalent chromate replacement in organic and semiorganic primer paints are being studied because of toxicity and poilution effects. Army applications for these coating systems include mobility equipment, vehicle armor, aircraft structures, gas turbine turbine engines, munition processing equipment,

and high velocity armor penetrators. Evaluation of experimental and commercial coatings in natural environments is also continuing. The Clean Air Act requires the development of an entirely new range of low solvent content organic coatings (paints) to replace the presently required and used coatings.

Efforts underway have concentrated on waterborne coatings and polymers. Low solvent content coatings are being developed to replace the high volume specifications which presently include camouflage coatings, anti-corrosive primers, chemical agent resistant coatings, and pre-treatments. The water soluble alkyds appear the most promising for basic primer and camouflage use. Waterborne polyurethane, catalyzed resins, and modified polyurethane resins appear to be most suitable for applications involving severe environmental exposure, including chemical agents. The utilization of waterborne epoxy and epoxy esters, high solids alkyds, polyurethane, and epoxies are also being explored.

In summary, a new Army, centrally managed, Corrosion Control Program has been established within the Development and Readiness Command under Product Assurance Regulation. Management support by the Army Materials and Mechanics Research Center, provides close linkage between logistics and research and development. The research and development program spans the range from projects involving protective coatings, corrosion of metal matrix composites, and hot gas erosion, to those having a longer range outlook, including kinetics of materials interaction with their environments, and the identification and quantification of transient reactions and species in the degradation and reactivity of surfaces and interfaces.

Their major emphasis is the elucidation of the basic mechanisms of corrosive attack and protection, and the development of economical, new, and improved solutions for defeating the destructive effects of corrosion in Army materiel.

NAVAL AIR DEVELOPMENT CENTER
Aircraft and Crew Systems Technology Directorate
Warminster, Pennsylvania 18974

NAVAL AIR SYSTEMS COMMAND CORROSION CONTROL PROGRAM

Dr. John J. Deluccia, Naval Air Development Center
Mr. Stephen F. Saletros, Naval Air Systems Command

This is an overview of the total program of corrosion control waged by the air arm of the Navy. The NAVAIR approach to corrosion control centers on the interaction of three efforts; R and D, designs and procurement, and maintenance technology. These efforts will be discussed in reverse order.

MAINTENANCE TECHNOLOGY

There are three general levels of maintenance. They are: organizational, intermediate and depot levels. The organizational level of maintenance is concerned with inspecting, servicing, lubricating, adjusting and replacing parts, assemblies and sub-assemblies on equipment. This is performed by the squadron personnel in the fleet trying to maintain the aircraft in their deployed status. The second level of maintenance is intermediate level of maintenance is concerned with calibration, repair or replacement of damaged or unserviceable parts, components or assemblies. The third level of maintenance is performed at the depot. At depot level, the equipment receives major overhaul or complete rebuilding of parts, assemblies, subassemblies and end items including the manufacture of parts, modifications, testing, and reclamation as required. Corrosion control is practiced at each level of maintenance. The current policy requires that each command place special emphasis on the importance of the corrosion control program and lend its full support to ensure that corrosion prevention and control receives a priority for timely accomplishment. The responsibilities for corrosion control is assigned to all work centers and formal training in corrosion control is a requirement. Training of plane "captains" in corrosion prevention and detection is required and it is mandatory that they perform these duties on a daily basis.

In order to aid the sailor at the organizational or intermediate level, a number of technical manuals and publications concerned with corrosion control are provided. These are:

I - NAVAIR 01-1A-509 - Aircraft Cleaning and Corrosion Control

II - NAVAIR 16-1-540 - Avionics Cleaning Corrosion/Prevention Control

III - NAVAIR 15-01-500 - Preservation of Naval Aircraft

IV - NAVAIR 15-02-500 - Preservation of Aircraft Engines

V - NAVAIR 17-1-125 - Ground Support Equipment Cleaning and Corrosion Control

VI - NAVAIR Maintenance Publications Peculiar to Specific Aircraft Models and Related Equipment

In order to assess the damage caused by corrosion on naval aircraft and thus take corrective action, fleet personnel are trained in detecting and reporting the various forms of corrosion. With this in mind a computerized reporting system that is unique for corrosion damage has been introduced to a small sector of the fleet. This new system is called CORGRAPH.

CORGRAPH is an integration of the present Visual Information Display System/Maintenance Action Form maintenance data source document and corrosion graphics. CORGRAPH allows for specific recording of location, type and extent of aircraft corrosion. It provides a computerized data bank of corrosion data for use by cognizant field activities (CFA's) and intermediate and organizational level maintenance activities for use in developing aircraft corrosion trend analysis data.

CORGRAPH utilizes the maintenance requirement card (MRC) format which is graphically laid out in 18 inch squares. CORGRAPH has been designed to provide documentation of corrosion found during special and phase, as well as unscheduled maintenance. The card set provides step-by-step procedures and all instructions for documentation. Each card contains a card number, area title, and alpha/numeric grid used for locating and reporting corrosion. The CORGRAPH deck also lists the codes

used to identify the type and extent/treatment of corrosion found. At present, CORGRAPH is in use for the Navy's S-3 aircraft. All other models will ultimately be incorporated in this system.

COST OF CORROSION

Utilizing the existing Maintenance and Material Management System (3M) data reported by the fleet, the cost of corrosion in both dollars and manhours was computed. Some of the data is provided in Tables I and II.

TABLE I

COST OF NAVAL AIRCRAFT CORROSION*

Aircraft	Corrosion Maintenance DMMH/YR (Thousands)	Corrosion Maintenance Cost (Thousands)
A-6E	445	$ 7,414
A-7E	811	$13,511
F-4J	491	$ 8,180
F-14A	498	$ 8,292
Period JUL 79 - JUN 80		Labor Rate: $16.66

* Includes Organizational and Intermediate Levels of Maintenance Only

TABLE II

EFFECT OF CORROSION ON AIRCRAFT MAINTENANCE*

Aircraft	Total Maintenance DMMH/YR (Thousands)	Corrosion Maintenance DMMH/YR (Thousands)	% Corrosion Maintenance
A-6E	3600	445	12.4
A-7E	4349	811	18.6
F-4J	3328	491	14.8
F-14A	3086	498	16.1

* Includes Organizational and Intermediate Levels of Maintenance Only

From Table I we see that it costs $13.5 million per year for direct maintenance manhours for corrosion control of the A-7 aircraft. From Table II we find that 19 percent of all the direct, scheduled maintenance performed on the A-7 aircraft is corrosion related. It should be noted that these figures are conservative since they are based on a reporting system that does not always pinpoint the cause of malfunctions. Thus, as an example, when a piece of avionics gear malfunctions it is reported as an electrical failure although in reality corrosion of the connector pins may be at fault.

CORROSION CONTROL IN AIRCRAFT PROCUREMENT

From the direct feedback of the maintenance community, those responsible for naval aircraft materials acquisition formulate the necessary corrosion control/prevention requirments for new aircraft. These efforts are incorporated into the manual design engineering/contractual requirements for the procurement of aircraft. Specifically, the process of corrosion control in design engineering is approached as follows:

- Corrosion resistance requirements contractually imposed on manufacturer
- Design and development phase requires corrosion control engineering efforts
- Materials and process design review of all new weapons systems
- Preproduction reliability design review (PRDR) - evaluate design adequacy based on Navy technical and operational testing.

An effective method for imposing corrosion control is to establish pertinent requirements in procurement contracts. The pertintnt documents that are cited in these contracts are:

- SD-24 - General specification for design and construction of aircraft weapon systems
- MIL-F-7179 - General specification for finishes and coatings: protection of aerospace weapons systems, structures and parts

- MIL-S-5002 - Surface treatments and inorganic coatings for metal surfaces.

Additionally, corrosion control design teams consisting of appropriate service personnel as well as performing contractors are established during the design stage of new aircraft to attempt to minimize in-service corrosion problems. This has been the widely used approach on the F-18 aircraft. A capsulized example of the F-18's corrosion prevention and control plan is as follows:

F-18 CORROSION PREVENTION AND CONTROL PLAN

Chemical Treatment of Aluminum Alloys

- MIL-C-5541 ("Alodine")

  ALCLAD SHEET
  ALCLAD SHEET CHEM-MILLED, above Z90.15

- Chromic Acid Anodize

  Welded Assemblies

- Sulfuric Acid Anodize

  All structure fabricated from extrusions, bar, plate, forgings, and castings except as below, bare sheet, and chem-milled ALCLAD below Z90.15

- IVD Aluminum Coating

  All "fatigue critical" structure

FINISH SYSTEM

EXTERIOR

- One coat MMS-425 epoxy primer
- Two coats MMS-420 polyurethane enamel
- Fay surfaces, butt joints, fasteners sealed

INTERIOR

- Two coats MMS-425 epoxy primer
- Fuel tanks coated with MIL-C-27725 polyurethane

RESEARCH AND DEVELOPMENT FOR CORROSION CONTROL

The research and development effort in combatting corrosion of naval aircraft is active and aggressive. This part of the overview will address materials and processes developed by the research and development community that have provided advances in corrosion control of naval aircraft. The subjects to be covered will primarily apply to airframes, although they may also be useful for electronic equipment. First, materials currently available will be discussed, then materials still under development which look promising for the future.

Classical corrosion control involves attacking the problem from three standpoints: interfacial (coatings), internal (metal selection), and external (inhibited environment). All three aspects will be covered here.

AML-350 (MIL-C-81309) - an ultra thin water displacing corrosion preventive compound which dries to a soft film;

AMLGUARD (MIL-C-85054) - a water displacing, corrosion preventive which dries to a hard, clear finish.

The need for such materials is occasioned by the difficulty of performing corrosion control procedures in a marine environment. Areas where paint has cracked or chipped leaves bare metal exposed. The mechanism by which these compounds function is to displace water from the surface. The essential elements involved are: (1) the compound spreads over the substrate completely wetting it, (2) it is immiscible with water, therefore does not retain water, and (3) it is preferentially adsorbed, penetrating under the water droplets.

AML-350 is applied to a film thickness of 2 to 5 μm. It is composed of a petroleum sulfonate and a mineral spirits type solvent. AML-350 is intended for use on internal metallic parts and electrical connectors. It has widespread use on airborne electronic equipment.

AMLGUARD contains polymeric resins which, upon application and cure, form a dry, hard film with a thickness of 25.4 to 50.8 μm (1 to 2 mils). It is a combination of organic solvents, silicone and silicone alkyd resins, barium petroleum sulfonate, and several other additives. It also displaces water by spreading over the metal and creeping uner the water droplets. Drying occurs via solvent evaporation, leaving a solid film. Although AMLGUARD dries to the touch in 18 hours, it continues to cure for 1 to 3 months, forming a hard, flexible finish. Corrosion protection is provided by the physical barrier of the coating and also by barium petroleum sulfonate and alkyl ammonium organic phosphate performing as corrosion inhibitors. This material is intended for temporary use on external aircraft parts where if offers excellent corrosion protection.

SEALANTS

Elastomeric sealants are widely used on naval aircraft to seal out the environment. The most popular at the present time are the polysulfide sealants which contain soluble corrosion inhibitors. These are covered by military specification MIL-S-81733. Ordinary sealants can minimize corrosion of metals in high humidity environments, but cannot prevent it completly because all polymers are permeable to moisture. The inhibitive sealant is very effective when used in faying surfaces and butt joints, for wet installation of fasteners and over fasteners patterns and to insulate dissimilar metals.

It is anticipated that the use of elastomeric sealants (polyurethanes and silicones as well as polysulfides) will increase in the future due to their ability to accommodate the dynamic loads imposed on aerospace equipment without cracking.

SURFACE TREATMENTS AND COATINGS FOR ALUMINUM ALLOYS

Wit regard to surface treatments for aluminum alloys, there has been a return to anodizing for new weapons systems rather than chromate conversion coatings. Both sulfuric and chromic acid anodizing are being used. Anodized surfaces provide more corrosion protection, abrasion resistance and long-term durability than chromated surfaces.

The paint system used on naval aircraft, the MIL-P-23377 epoxy primer and the MIL-C-82386 polyurethane topcoat, has performed better than any previous system. It is durable, abrasion resistant, retains its gloss well, does not chalk or craze, and is easy to clean.

ALLOY SELECTION AND HEAT TREATMENT

The advent of the heat treatable 7000 series aluminum alloys provided a boon to aircraft designers. The high modulus, high strength, and low weight of these alloys made them ideal for the high performance of advanced aircraft. Their susceptibilities to intergranular corrosion, exfoliation, and stress corrosion cracking made them less than desirable in marine environments. It was discovered that if these alloys were systematically overaged, their susceptibilities to these forms of attack would be materially lessened if not totally eliminated. Thus the T73 temper was born. As is usually the case with most "fixes," a price had to be paid. There is an approximate 10% strength loss accompanying the T73 overaging treatment. The T73 temper replaced the standard T6 temper on many military aircraft where designs could be altered or the strength loss tolerated.

More recently newer 7000 series alloys have been developed with specific resistance to intergranular attack and environmental embrittlement. Most of these new alloys such as 7050 and 7010 owe their lessened susceptibility to the presence of zirconium and a cleaner microstructure.

The preceding paragraphs have described materials currently in use, or available, to minimize environmental deterioration of airframes. Materials and processes under development in the laboratory will now be addressed.

MATERIALS UNDER DEVELOPMENT

Water Displacing Paint

This material is a pigmented coating which will displace water, dry and subsequently afford corrosion protection. It is composed of a petroleum sulfonate, silicone-alkyd resin, organic solvents, pigments and

other organic additives. The mechanism by which this material displaces water is the same as that discussed earlier. This pigmented coating dries to a hard, flexible finish which protects the substrate from corrosion by:

1. The physical barrier of the coating
2. Corrosion inhibiting pigments; i.e., molybdates and chromates.

This water displacing paint is designed as a touch-up paint for exterior surfaces of aircraft where original paint has cracked or chipped and total repainting is not feasible. Such a situation is confronted on operational aircraft deployed on board aircraft carriers where paint touch-up is necessary but must be completed quickly and efficiently. This paint was designed to be applied during deployment and to last indefinitely until total repainting of the aircraft is necessary.

Flexible Primer

The current Navy paint scheme for high performance aircraft includes the application of MIL-P-23377 epoxy primer, MIL-S-8802 or MIL-S-81733 polysulfide sealant, and MIL-C-83268 polyurethane topcoat. This system has several limitations. The primer possessess poor low-temperature flexibility, while the sealant is difficult to apply due to its high viscosity and short pot life. The ideal solution would be a single application of an elastomeric sealant-primer with the adhesion of a primer and the flexibility of a sealant. This would also eliminate the need to handle two separate materials, resulting in a significant cost savings to the government.

A comparative evaluation of a number of inhibitive elastomeric coatings including a plysulfide, a polyurethane and an epoxy-polyurethane system is being made. Such properties as the hardness, adhesion, strength, flexibility, erosion resistance, corrosion resistance and ease of application of these materials will be determined and an optimum material selected.

Development of an Aluminum Plating Process

There is increasing pressure to eliminate the use of cadmium by DoD activities because of its toxicity. While no single coating has been found to replace cadmium in all aircraft application, aluminum has been found to be a very good alternate coating material in many applications requiring good corrosion resistance and minimal effect on fatigue properties. Only two aluminum coating processes are currently commercially feasible, vacuum deposition and ion vapor deposition. Vacuum deposition has relatively poor covering power and adhesion is often only fair. Ion vapor deposition is proprietary and facilities for its application are complex and cannot meet the demand for the coating. Other methods exist, but they have not been developed sufficiently to be of real commercial value.

The Naval Air Development Center is involved in an effort to develop a method to electroplate an aluminum coating from a molten salt bath. To date, the process has been scaled up from a small bath to a forty liter bath. It has been demonstrated that a coating of aluminum-manganese can be deposited on aluminum, titanium and steel substrates with conventional pretreatments and with excellent adhesion. The coating can be chromate conversion coated but not anodized.

Phase Transfer Inhibitors (PTI) in Crack Arrestment

A method was developed at the Naval Air Development Center by which ions could be solubilized in organic media using phase transfer catalysis (PTC). This method has been used to develop an entirely new vehicle for corrosion inhibitors. These have resulted in inorganic inhibitors incorporated in organic phases, i.e., an oxidizing anion dissolved into an organic non-polar solvent, in this case, mineral spirits.

The use of phase transfer inhibitors in pre-cracked stress corrosion cracking in aluminum alloys is presently being studied. Preliminary tests using dichromate, nitrite, borate, molybdate as well ad dichromate, phosphate, silicate inhibitor combinations show the cracking rate to be perceptibly decreased in aluminum alloy 7075-T6 and high strength steels exposed to salt laden moisture.

The field of phase transfer catalysis and organometallic chemistry appears to provide a new class of corrosion inhibitors which will probably have wide applications in materials such as coatings, corrosion preventive compounds and crack arrestment compounds.

This has been a brief discussion of the materials and processes currently being used for corrosion control on naval aircraft. Some of the more important efforts and ongoing research in the air arm of the Navy have been highlighted. Fighting corrosion is a never ending battle, but even small successes can provide a payoff in reduced maintenance manhours and improved reliability.

AFWAL-TR-81-4019
Volume II

Marine Corrosion and Fatigue

Of Graphite Aluminum Composites

by

M. G. Vassilaros[+], D. A. Davis[+], G. L. Steckel[*]

and J. P. Gudas[+]

[+]David W. Taylor Naval Ship R&D Center
Annapolis, Maryland

[*]Aerospace Corporation
El Segundo, California

ABSTRACT

The marine corrosion and fatigue performance of two types of VSB-32/Al 6061 graphite aluminum composite materials were characterized. Corrosion tests were performed in natural flowing seawater, tidal immersion and atmospheric exposure. The residual mechanical properties of the composites were evaluated after exposure. Axial fatigue tests of the standard VSB-32/Al 6061 composite were performed in air and natural seawater. Results of environmental exposures showed that the galvanic driving force dominated the corrosion of the composite materials, and the overall performance of the composites was related to both the corrosion of the surface foil and the substrate. Residual mechanical properties did not show latent effects of the environment where corrosion was not visible, but were substantially reduced in response to visible corrosion damage. The fatigue strength of the composite increased with fiber strengthening in direct response to the increase in ultimate tensile strength. The fatigue strength of the composite displayed less sensitivity to seawater than the 6061-T6 plate.

INTRODUCTION

Metal matrix composite materials are being considered for structural applications because of the range of mechanical properties attainable. The graphite/aluminum system is particularly promising because of the very high specific strength and modulus levels attainable over other alloys and composite materials. As mechanical properties of graphite/aluminum composites have been improved, it became necessary to evaluate the environmental sensitivity of the composite system and extend the characterization data into the regime of fatigue performance.

The objective of this investigation was to characterize the marine corrosion and fatigue performance of two similar types of graphite/aluminum composite materials. The approach included the production of VSB-32/Al-6061 uniaxially reinforced composite plates which were exposed in marine environments including natural flowing seawater, tidal immersion, and atmospheric exposure. Mechanical property tests of the composite material were performed prior to and after marine environment exposure. Analysis of test results were performed to correlate type and degree of corrosion attack with the residual mechanical properties of the composite.

BACKGROUND

A recent review of results of corrosion tests of graphite/aluminum has been prepared by Pfeifer[1]. This review detailed the results of corrosion exposures of T-50/Al 6061 in 3.5% NaCl and distilled water, T-50/Al 201 and T-50/Al 202 panels exposed to the marine atmosphere, Gr/Al 202 with Al 1100 interlayer foils exposed to the marine atmosphere and alternating immersion in laboratory seawater, and T-50/Al 201 with 6061 with various combinations of alloy foils including 1100, 2024, 3003, 5056, and 6061 exposed in the marine atmosphere, alternate seawater immersion, salt spray and relative humidity cabinets. The summary of the corrosion exposures as discussed by Pfeifer[1] suggested that the mode of corrosion observed with graphite/aluminum composites was predominantly pitting and severe exfoliation. Metal/matrix interfaces were found to limit corrosion resistance and both chemical and mechanical factors contributed

to corrosion. As expected, the aluminum alloy composition affected corrosion resistance, particularly when comparing the Al 6061 matrix and Al 201 matrix alloys. Finally, it was found that corrosion behavior of graphite aluminum panels were quite sensitive to fabrication process and efficiency. To date there have been no controlled experiments to evaluate the residual mechanical properties of graphite/aluminum composites.

The results of the corrosion evaluation performed to date were employed in the design of this experimental program. Specifically, Al 6061 was chosen as both a matrix and foil cladding material in order to provide some inherent corrosion resistance. Extensive NDE was performed to eliminate (as much as possible) material produced with consolidation defects. Finally, mechanical property tests were performed before and after marine exposure to determine extent of latent environmental effects, as well as quantify the degree of degradation caused by the environment.

MATERIAL

The metal matrix composite plates used in this investigation were produced from pitch-based VSB-32 fibers and a matrix of 6061 aluminum alloy. The VSB-32 fibers were supplied by Union Carbide Corporation and displayed typical properties as follows:

Tensile Strength	1720 MPa
Young's Modulus	3.8×10^5 MPa
Fiber Diameter	7-11 Mm
Numbers Fiber/Tow	2000

The fiber tows were coated with a TiB layer which was used to promote wetting during the subsequent liquid metal infiltration process. The infiltrated fiber tows appeared as aluminum wires which typically has 45 volume percent fiber as supplied by Materials Concept Inc. DWA Composites Specialties Inc. then diffusion bonded the infiltrated wires between surface foil claddings to produce the metal matrix plates.

The graphite/aluminum plates used in this investigation were produced in two configurations. The standard plates consisted of three uniaxial layers of wires between 0.15 mm thick Al 6061 surface foils which resulted in plate thicknesses ranging from 1.8 to 1.9 mm. Figure 1 is a photomicrograph of a typical corss section of the standard material. Encapsulated plates were also produced with three uniaxial layers of wire between 0.15mm thick surface foils. However, additional foils were wrapped around the wires to reduce the fiber volume and increase the transverse strength of the composite. Figure 2 is a photomicrograph of the encapsulated composite material, which was produced in thicknesses of 2.0 to 2.1 mm. A total of 8 panels of both types of composite plates were produced with planar dimensions of 216 mm x 216 mm.

EXPERIMENTAL PROCEDURES

Marine Corrosion Exposures

The marine corrosion exposures were accomplished by removing panels from the composite plates and exposing them to three types of environments for varying lengths of time. Separate specimens were exposed in each environment for corrosion characterization and residual mechanical property measurements. The planar dimensions of the two types of specimens were as follows:

Corrosion Panels	101 x 67 mm
Residual Mechanical Property Panels	101 x 101 mm

The graphite/aluminum composites were exposed with and without edge protection. Edge protection consisted of a continuous bead of RTV compound applied to the edges of selected panels.

All panels were exposed to one of three marine environments at the LaQue Center for Corrosion Technology, Wrightsville Beach, North Carolina, USA. The environments included:

(1) Complete submergence in natural, flowing seawater (0.6-0.9 m/S);
(2) Alternate immersion in tidal zone;
(3) Marine atmospheric exposure, 25 meters from the ocean.

Separate panels of both types of composite were removed for corrosion evaluation and residual mechanical property tests after 6 and 12 week exposures. Control panels of 6 mm thick 6061-T6 Aluminum plate were also exposed to the three marine environments for 6 and 12 weeks.

Residual Mechanical Properties Testing

Longitudinal and transverse tensile strength and Young's modulus were determined for the baseline and exposed plates using a standard Instron Universal testing machine. The exposed plates were nominally 100 mm square and the tensile samples were prepared from these panels according to the geometry shown in Figure 3. The longitudinal samples were 9.5 mm wide by the full length of the plates and the transverse samples were typically 38-75 mm long by 12 mm.wide. Both types of samples were the full thickness of the composite plates. In some instances, particularly when the plate edges were left unprotected, swelling at the edges required removal of a small amount of material. This is indicated by "edge corrosion" on Figure 3. Unless an excessive amount of material had to be removed from the edges, four longitudinal and five transverse samples were prepared from each plate. The samples were usually prepared by shear cutting. However, corrosion of the standard composite after the 12 week flowing seawater exposure was too severe to allow shearing and samples from these plates were prepared by hand sawing and carefully filing the edges smooth.

One mm. thick aluminum tabs were bonded to each side of the sample end in order to minimize stress concentrations at the testing machine grips. Despite the tabs, many of the longitudinal samples fractured near or within the grips. However, no correlation could be made between the fracture location and tensile strength.

Strain measurements for the Young's modulus calculations were made with a 13 mm gauge length clip-on electrical extensometer. Residual stresses which result from the composite processing were removed by loading the sample to 50% of their anticipated maximum load, unloading to 5% of maximum, and then reloading to failure. The load-extension

curve obtained during reloading was used to determine the material's modulus in the absence of residual stresses.

Fatigue Testing

The fatigue testing of the standard graphite/aluminum composite was performed on a SONNTAG SF-IU test machine, at a test frequency of 30 Hz. The fatigue specimens, shown in Figure 4, were axially loaded with a stress ratio of 0.05. Specimens were aligned using grips with a coupling of low melting temperature metal which was melted before specimen setup, then cooled after setup for the fatigue test. Specimen failure was defined as complete separation, and specimens which remained intact for more than 5×10^7 cycles were removed and designated as runouts.

The fatigue tests were performed in air and seawater. The former environment was laboratory air, approximately 24°C and 50% relative humidity. The application of seawater was accomplished by mounting a 50 ml plastic cup around the fatigue specimen test section. This reservoir was filled with natural seawater from the LaQue Center for Corrosion Technology, and the water was changed daily throughout the fatigue tests.

RESULTS AND DISCUSSION

Corrosion of Graphite/Aluminum Composites

All of the panels which were exposed to marine environments were subjected to corrosion analysis. This included the panels employed in the residual mechanical properties analysis as well as the corrosion test panels. The usual practice of describing corrosion behavior is to report weight loss, thickness reduction, and depth of pitting attack. Due to the nature of the attack observed with these composites, such descriptions were inapplicable. For example, most of the graphite/aluminum composites experienced weight gain from the oxide formed and trapped during the corrosion process. The analysis used herein will be in the form of qualitative descriptions of the corrosion and pitting behavior.

The corrosion behavior exhibited by the exposed panels is described according to five different types of attack observed in these tests. These include:

(a) Slight and incipient pitting;
(b) Pitting of surface foils;
(c) Slight blistering of surface foils;
(d) Blistering of surface foils;
(e) Edge separation of matrix, fiber and foils;
(f) Uniform edge corrosion

All types of observed corrosion attack are illustrated schematically in Figure (5), and these descriptions are included in the tabulations of corrosion test results to be presented in the following sections.

Corrosion of Graphite/Aluminum in Flowing Seawater

The results of the corrosion tests of both types VSB-32/Al 6061 composites in flowing seawater are shown in Table 1. The extent of corrosion attack experienced by the standard and encapsulated composites after six weeks exposure to flowing seawater was related to the edge protection provided each panel. When a good sealant was maintained as shown in Figure 6, no edge corrosion or blistering occurred, and the panels experienced only slight surface pitting. This pitting is typical of 6061 aluminum alloys and similar to that seen with the control exposures, Figure 7. This behavior was related to all six week exposure panels with edge protection with one exception (AC-1). In this case, a small failure of the sealant compound resulted in intrusion of seawater to the edge which caused edge attack and blistering. Panels exposed without edge protection experienced edge attack and blistering along the fiber path, Figure 6.

Both types of panels exposed for twelve weeks in flowing seawater displayed substantially different behavior than the six-week exposures. The twelve-week exposure panels displayed pitting attack as shown in Figure 8 which pierced the surface foils and allowed seawater to come in contact with the graphite/aluminum interfaces. When this situation occurred, the aluminum corrosion product blistered the composite and

exposed more matrix for corrosion attack as the corrosion process progressed from the pit. Figure 9 is a photomicrograph of a typical blister. This form of corrosion attack was not related to the edges of the panels as both the protected and unprotected panels experienced similar corrosion attack.

Corrosion of Graphite/Aluminum under Alternate Tidal Immersion

Table 2 presents results of the corrosion analysis of VSB-32/Al 6061 composites exposed to the tidal zone environment. All of the standard and encapsulated specimens experienced similar corrosion except for the effects of edge protection. The surface of the panels had incipient to light pitting as shown in Figure 10 with some pits causing small blisters as seen in the flowing seawater exposures. The edges of the corrosion panels which were protected did not experience any corrosion where the protective compound remained intact. Two panels (AB-3 and AF-3) did experience some edge attack due to bond failure of the sealant. The panels without any edge protection suffered slight to moderate edge corrosion. The encapsulated panels appeared to have slightly greater resistance to edge corrosion which is likely the result of the greater volume of aluminum in the matrix. Interestingly, the tidal environment did not show a clear exposure time dependence, and proved to be the least aggressive marine environment included in this test program.

Corrosion of Graphite/Aluminum in the Marine Atmosphere

Results of the corrosion exposures of the VSB-32/Al 6061 composites in the marine atmsophere are shown in Table 3. The surfaces of the standard and encapsulated panels experienced incipient to light pitting with some slight blistering around the pits as shown in Figure 11 (for standard material). This is typical for the 6061 aluminum alloy as shown in Figure 7. The panels with edge protection were free of edge corrosion. The panels exposed to the marine atmosphere without edge protection experienced edge corrosion which was usually severe enough to cause separation.

The twelve-week exposure panels with edge protection, Figure 11, did not appear significantly different from similar six week exposures as shown in Figure 12. The twelve week exposures without edge protection displayed advanced edge attack, Figure 11. This attack appeared to accelerate with time, indicating that the process would most probably continue until all of the aluminum matrix was oxidized.

Summary of Corrosion Exposures

The results of the corrosion exposures performed in this program show that the overall performance of the composite reflects both the performance of the graphite/aluminum substrate and the performance of the surface foils. The dominant factor in the corrosion of VSB-32/Al 6061 appears to be the galvanic cell between the graphite and aluminum with a driving force of 1.0 to 1.2 volts.[2] As long as the surface foils of the composite prevent matrix invasion, the corrosion performance was equivalent to that of the surface foils. After matrix invasion occurred, the galvanic couple was activated, and accelerated corrosion took place. The corrosion attacked both the matrix material and the matrix/foil interface, and was seen to be assisted by the production of corrosion products. There was a slight difference in the behavior of the two variations of graphite/aluminum tested due to the difference in fiber loading of the composites. However, there was no difference in inherent corrosion mechanism when comparing the standard and encapsulated materials.

Three different marine environments were included in this program. Regarding performance of the surface foils, the flowing seawater was the most aggressive, while the tidal immersion and atmospheric exposures were similar in pitting performance, but less aggressive than the flowing seawater. Where matrix invasion occurred, and free edges were exposed, the marine atmsophere and the flowing seawater were the most severe environments, and the tidal exposure resulted in a substantially decreased level of corrosion.

Residual Mechanical Properties

The purpose of the residual mechanical property tests was to evaluate possible latent effects of the marine environments on the mechanical properties of the VSB-32/Al 6061 composites. Due to the variation of fiber volume, and consolidation differences inherent in the batch processing of composite wire and plate, the mechanical properties of the unexposed plates varied not only from plate to plate, but also within each plate. Therefore, small changes in residual mechanical properties could be related to inherent material scatter, as well as effects of environmental exposures. In this context, it should be noted that a total of 24 individual panels were exposed for various durations in the three marine environments and subsequently used for post-exposure mechanical property tests. Only one panel of each type of VSB-32/Al-6061 composite was employed in evaluating mechanical properties prior to exposure.

Table 4 is a summary of the mechanical property test results from both types of graphite/aluminum composites where tests were performed in the as-received, unexposed condition. These tests show that the standard composite displays superior longitudinal strength and modulus when compared to the encapsulated composite. This clearly reflects the higher fiber volume loading of the standard material. On the other hand, the transverse tensile strength of encapsulated composite is superior as expected; again because of the difference in fiber loading (Table 4).

The residual tensile strength test results for all corrosion exposures of the standard VSB-32/Al 6061 composite are plotted in Figure 13, while similar data is presented for the encapsulated composite in Figure 14. In most cases, the data points presented in Figure 13 and 14 are the average of five tensile tests with specimens removed in such a way as to exclude material with obvious corrosion attack, except for surface foil pitting.

The results of residual mechanical property tests of the standard graphite/aluminum composite shown in Figure 13 suggests that there was no significant deleterious effect of any of the marine environments provided no evidence of corrosion attack was observed. The average tensile strength data for all exposures, (except twelve week tests in flowing seawater) fell in the range of 550-670 MPa. This range compared favorably with the data from the unexposed panel, and was consistent with the scatter inherent in the mechanical properties of these materials. In general, a tensile strength degradation on the order of 10-15% occurred in all environments for which specimens without visible corrosion attack could be tested. This is a reflection of the effects of the incipient/light pitting which occurred in all test environments.

Figure 13 also includes two other data points which were the average of tests performed on tensile specimens which had visible corrosion damage such as blistering or foil delamination. These specimens experienced twelve weeks of exposure in flowing seawater. These data show that after the matrix was invaded and corrosion occurred, there was a substantial decrease in average tensile strength. The order of this decrease reflects the severity of corrosion attack in the matrix of the standard composite material.

The residual mechanical property test results for the VSB-32/Al 6061 encapsulated composite are shown in Figure 14. All data points are average values for tensile tests performed with specimens displaying no visible corrosion damage. These data agree with the trends developed with the standard composite in that there was only slight degradation of tensile properties resulting from marine environment exposures. All data points are lower than for the standard composite because of the lower fiber loading of the encapsulated plates. The three lowest points in Figure 14, which occurred in the twelve week tidal and marine atmosphere exposures, were all developed from the same plate of material. This suggests that inherently lower mechanical properties were responsible for the results rather than effects of the environmental exposures.

The results of the residual mechanical property tests with the VSB-32/Al-6061 composites indicate that there are no latent effects with any of the marine environments which result in severe degradation of tensile properties in the case where no visible corrosion attack is evident. In the case where corrosion attack has occurred as evidenced by severe pitting, blistering and foil delamination, the composites displayed substantial reduction in tensile strength. This reduction was in response to the vigorous attack of the 6061 aluminum matrix and the matrix foil interface separation.

Fatigue of Standard VSB-32/Al 6061 Composite

The results of fatigue tests performed in air with the VSB-32/Al 6061 standard composite are plotted in Figure 15. This figure also includes similar data for 5 mm diameter Al 6061-T635 bar[3] as well as B/Al 6061 unidirectional composite[4,5]. The results indicate that the graphite/-aluminum composite shows improved fatigue properties over wrought Al-6061-T635, as observed in a previous investigation of fiber reinforced metals[4]. The graphite/aluminum fatigue strength at 5×10^7 cycles was over twice that of Al6061-T635 bar, reflecting the fact that the fibers are the load bearing members in the composite. It can also be seen that the slopes of the fatigue curves of VSB-32/Al 6061 and Al6061-T635 bar are similar, suggesting that the matrix material controls the actual fatigue failure mechanism in the composite. This is consistent with the observations of Lynch and Kershaw in evaluating the fatigue performance of B/Al 6061 composite[4]. Figure 15 also shows that the fatigue strength of VSB-32/Al 6061 is comparable with that of B/Al 6061[4,5]. This is further illustrated in Figure 16 which shows the fatigue data for VSB-32/Al 6061 and B/Al 6061 composites and Al-6061-T635 bar normalized with respect to ultimate tensile strength. This figure shows that the fatigue strength of the graphite/aluminum composite increases with ultimate strength, suggesting that this composite is not fatigue strength limited.

The results of fatigue tests performed in air and natural seawater with VSB-32/Al 6061 standard composite are shown in Figure 17. Data from air and saltwater tests performed on 13 mm diameter Al 6061-T6 bar is included in Figure 17. The Al 6061-T6 data was from rotating cantilever tests (R=-1) and fatigue equivalent stresses (R=0) shown in Figure 17 were calculated using the Goodman expression. These data indicate the deleterious effect of saltwater on fatigue properties in Al 6061-T6 was also present in the seawater fatigue performance of the VSB-32/Al 6061 composite. The degradation in fatigue properties of the composite was not as severe as in the Al 6061-T6. The respective shapes of the saltwater fatigue curves indicates that the corrosion fatigue behavior of the composite is similar to that of the wrought plate. However, the fibers attenuate the environment effects on the fatigue life of the composite.

CONCLUSIONS

The objective of this investigation was to characterize marine corrosion and fatigue performance of two similar type of graphite/aluminum composite materials. A key element in the corrosion investigation was an evaluation of the residual mechanical properties of the composite in response to environmental exposure. The following conclusions are suggested by the results of marine exposures and tests performed in this investigation:

- The overall corrosion performance of the VSB-32/Al 6061 composite reflects both the performance of the surface foils and that of the graphite/aluminum substrate;
- The dominant factor in the corrosion of the standard and encapsulated composites was the galvanic driving froce between the VSB-32 fibers and the Al 6061 matrix;
- The encapsulated composite was slightly more resistant to corrosion attack, but the corrosion mechanisms of both types of composite were similar;
- Where corrosion was not evident, there was no latent effects on residual mechanical properties due to corrosion exposure;
- Visible corrosion damage resulted in significant degradation of residual mechanical properties;
- The fatigue strength of VSB-32/Al 6061 composite increased with fiber strengthening in direct response to the increase in ultimate tensile strength;
- The reduction in fatigue strength of VSB-32/Al 6061 due to seawater environment was less than the reduction experienced with aluminum 6061-T6 plate.

REFERENCES

1. Pfeifer, Will, "Graphite/Aluminum Technology Development", Hybrid and Select Metal-Matrix Composites: State of the Art Review, American Institute of Aeronautics and Astronautics, New York, NY 1977.

2. Tuthill, A. W. and Schillwaller, C. M., "Guidelines for Selection of Marine Materials" Proceedings of Ocean Science Engineering Conference, Marine Technology Society, Washington, D. C., June 14-17, 1965.

3. Aerospace Structural Metals Handbook, Vol III, Maykuth, D. J., ed., Mechanical Properties Data Center, Battelle Columbus Laboratories, Columbus, Ohio, 1979.

4. Lynch, C. T. and Kershaw, J. P., Metals Matrix Composites,, CRC Press, 1972.

5. Toth, I. J., "Creep and Fatigue Behavior of Unidirectional and Cross-Plied Composites", Composite Materials: Testing and Design, ASTM STP 460 (1969).

6. Moore, T. D. (ed), Structural Alloys Handbook, Mechanical Properties Data Center, Battelle Columbus Laboratories, Vol. 2, Wrought Aluminum Section, pp 85 (1980).

TABLE 1

CORROSION EXPOSURE RESULTS FOR VSB-32/6061
ALUMINUM IN FLOWING SEA WATER

STANDARD

Specimen Number	Length of Exposure (weeks)	Edge Protection (yes or no)	Visual Observation surface	edge
AB-1	6	yes	SP	N
AB-2	6	no	P, B	E, corr
AC-1	6	yes	B	E
AC-2	6	no	B	E, corr
AE-3	12	yes	P, B	N
AE-4	12	no	P, B	E, corr
AF-1	12	yes	P, B	E, corr
AF-2	12	no	P, B	E, corr
		ENCAPSULATED		
BA-1	6	yes	SP	N
BA-2	6	no	P, B	E, corr
BB-1	6	yes	SP	N
BB-2	6	no	B, P	E, corr
BA-3	12	yes	B, P	N
BA-4	12	no	B, P	E, corr
BF-1	12	yes	B, P	E
BF-2	12	no	B, P	E, corr

N - No visible attack

SB - Slight Blistering; B - Blistering

SP - Slight or incipient Pitting; P - Pitting

corr - general corrosion; E - edge separation

TABLE 2

CORROSION EXPOSURE RESULTS FOR VSB-32/6061
ALUMINUM IN ATMOSPHERE

STANDARD

Specimen I.D.	Length of Exposure (weeks)	Edge Protection (yes or no)	Visual Observation surface	edge
AA-3	6	yes	SP	N
AA-4	6	no	P	E, corr
AB-5	6	yes	P	N
AB-6	6	no	P	E, corr
AE-1	12	yes	SP	N
AE-2	12	no	SP	E, corr
AF-5	12	yes	P	N
AF-6	12	no	P	E, corr
		ENCAPSULATED		
BB-5	6	yes	SP	N
BB-6	6	no	SP	corr
BC-3	6	yes	P, SB	N
BC-4	6	no	P, SB	corr
BE-3	12	yes	SP	N
BE-4	12	no	SP	E, corr
BF-5	12	yes	P, SB	N
BF-6	12	no	P, SB	E, corr

N - No visible attack

SB - Slight Blistering; B - Blistering

SP - Slight or incipient pitting; P - Pitting

corr - general corrosion; E - edge separation

TABLE 3

CORROSION EXPOSURE RESULTS FOR VSB-32/6061
ALUMINUM IN THE TIDAL ZONE

STANDARD

Specimen I.D.	Length of Exposure (weeks)	Edge Protection (yes or no)	Visual Observations surface	edge
AA-1	6	yes	SP	N
AA-2	6	no	SP	corr
AB-3	6	yes	P	corr
AB-4	6	no	P	corr
AC-3	12	yes	SP	N
AC-4	12	no	SP	E, corr
AF-3	12	yes	P, SB	corr
AF-4	12	no	SP	corr
		ENCAPSULATED		
BB-3	6	yes	SP	N
BB-4	6	no	SP	corr
BC-1	6	yes	SP	N
BC-2	6	no	SP	corr
BE-1	12	yes	SP	N
BE-2	12	no	SP	N
BF-3	12	yes	P, SB	N
BF-4	12	no	P, SB	N

N - No visible attack
SB - Slight Blistering; B - Blistering
SP - Slight or incipient pitting; P - Pitting
corr - general corrosion; E - edge separation

TABLE 4

MECHANICAL PROPERTIES OF VSB-32/6061 COMPOSITES

	STANDARD	ENCAPSULATED
Longitudinal Tensile Strength	650 MPa	510 MPa
Longitudinal Modulus	177 GPa	140 GPa
Transverse Tensile Strength	25 MPa	35 MPa
Transverse Modulus	32 GPa	32 GPa
Fiber Content of Plate	40.1%	30.6%

Reported values are the average of five tests

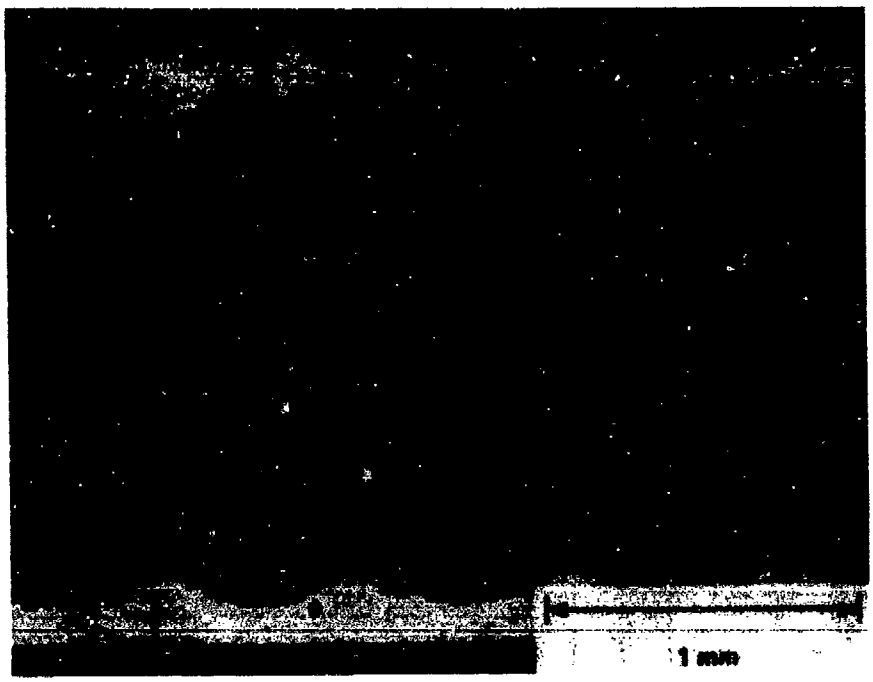

Figure 1. Photomicrograph of Cross Section of Standard VSB-32/Al 6061 Plate

Figure 2. Photomicrograph of Cross Section of Encapsulated VSB-32/Al 6061 Plate

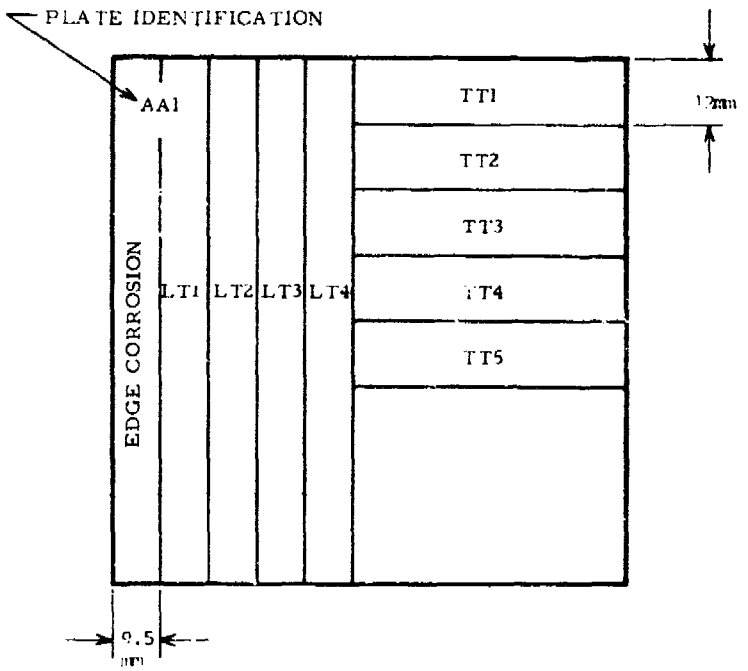

LT = Longitudinal Tensile Sample
TT = Transverse Tensile Sample

Figure 3. Typical Sample Geometry for Exposed Plates

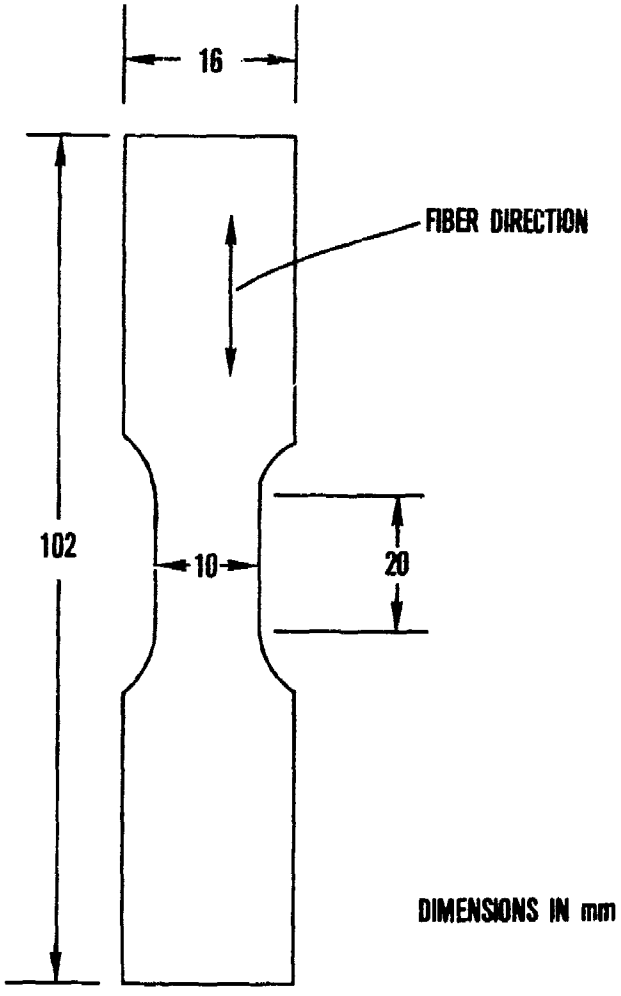

Figure 4. Drawing of Gr/Al Composite Fatigue Specimen

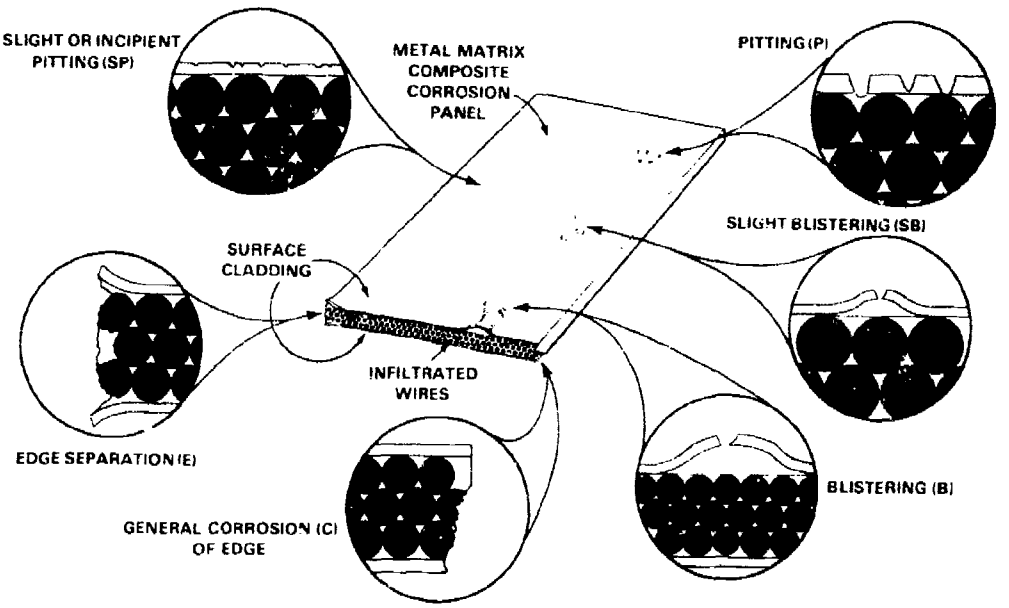

Figure 5. Schematic Illustration of Types of Corrosion Attack

Figure 6. Corrosion Panels of VSB-32/Al 6061 (Encapsulated) After 6 Weeks Exposure to Flowing Seawater

Flowing Seawater Tidal Zone Marine Atmosphere

6 WEEK EXPOSURES

Flowing Seawater Tidal Zone Marine Atmosphere

12 WEEK EXPOSURES

Figure 7. Corrosion Panels of Aluminum 6061-T6 After 6 and 12 Weeks Exposure

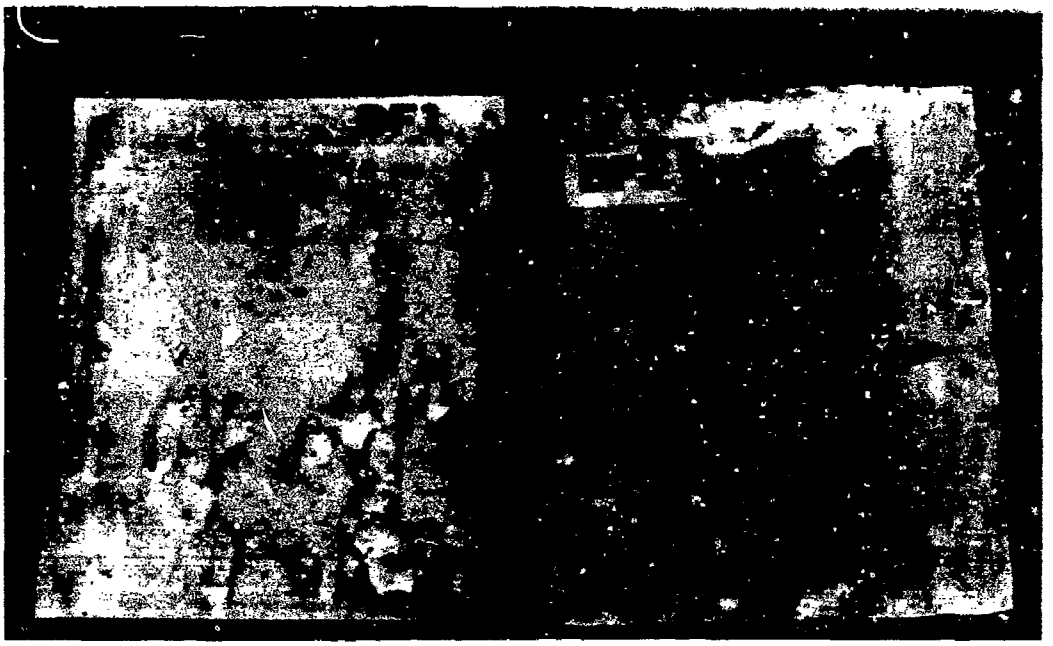

Figure 8. Corrosion Panels of VSB-32/Al 6061 (Encapsulated) After 12 Weeks Exposure to Flowing Seawater

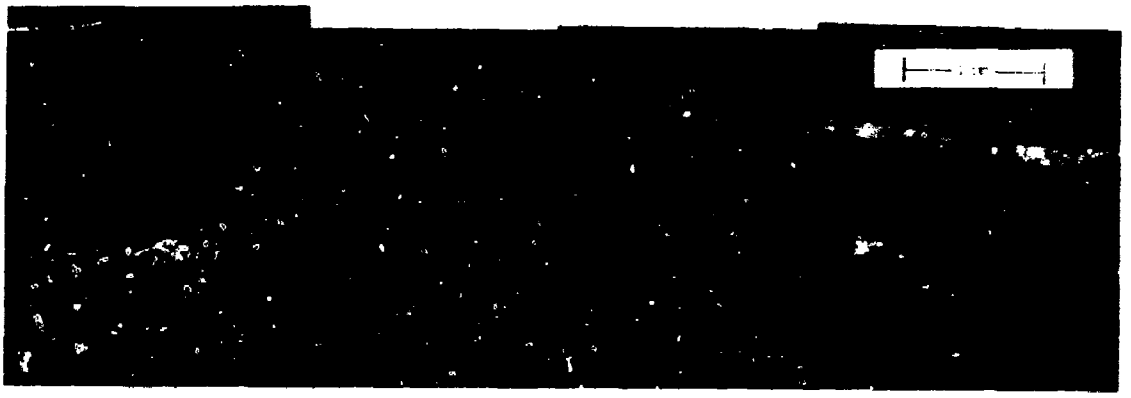

Figure 9. Photomicrograph of Blistered VSB-32/Al 6061 Composite After 12 Weeks Exposure to Flowing Seawater

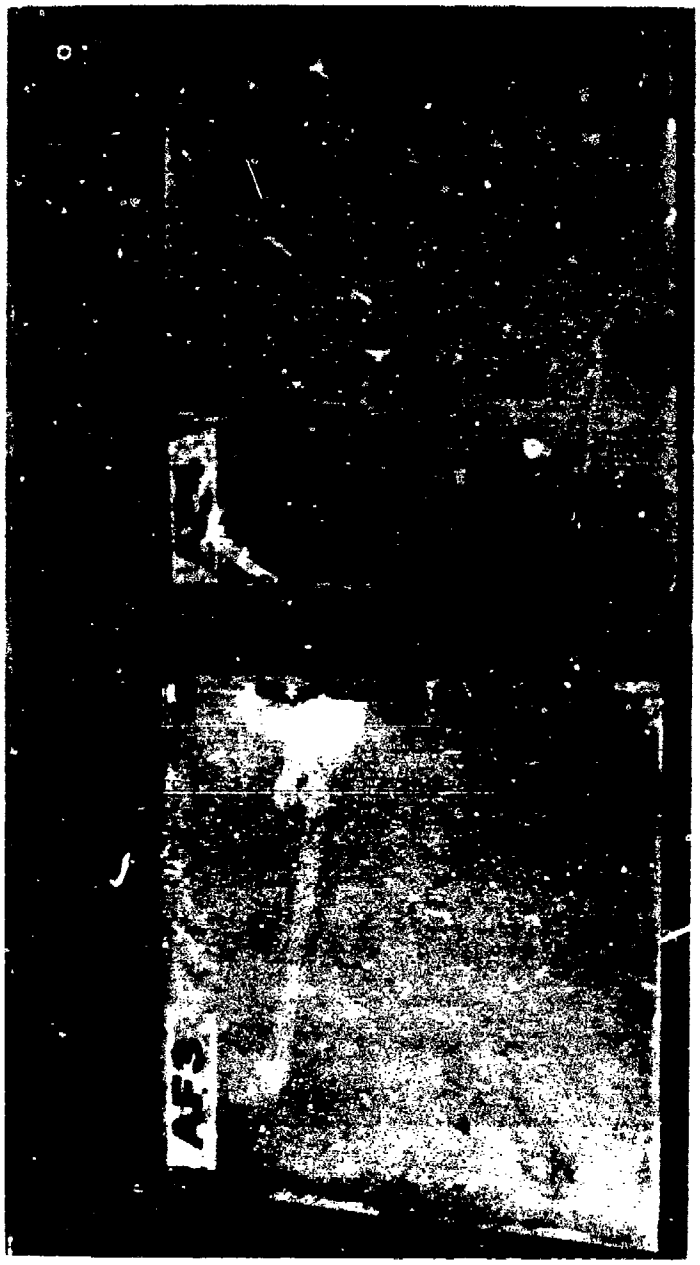

Figure 10. Corrosion Panels of VSB-32/Al 6061 After 12 Weeks Exposure to Tidal Zone Environment

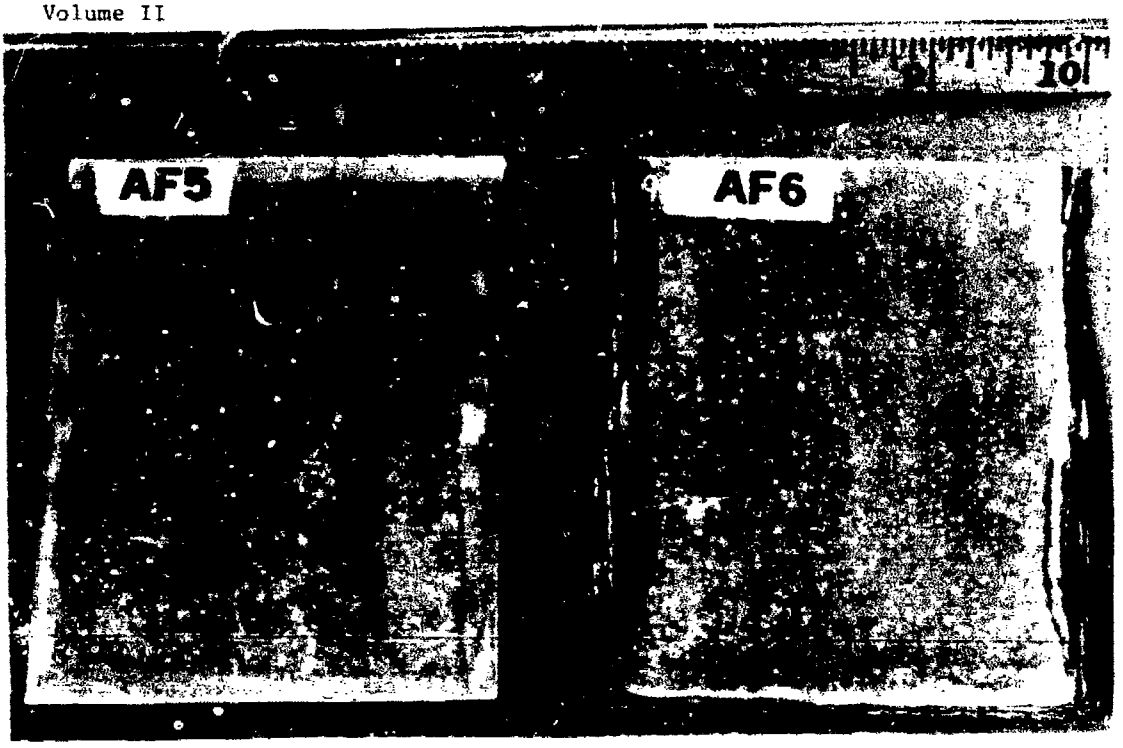

Figure 11. Corrosion Panels of VSB-32/Al 6061 After 12 Weeks Exposure to Marine Atmosphere

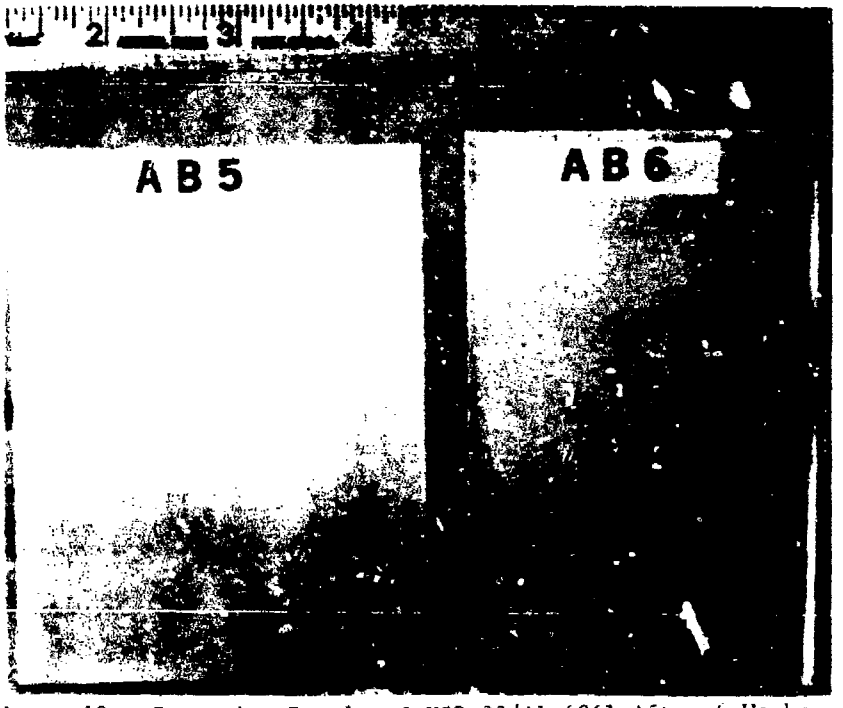

Figure 12. Corrosion Panels of VSB-32/Al 6061 After 6 Weeks Exposure to Marine Atmosphere

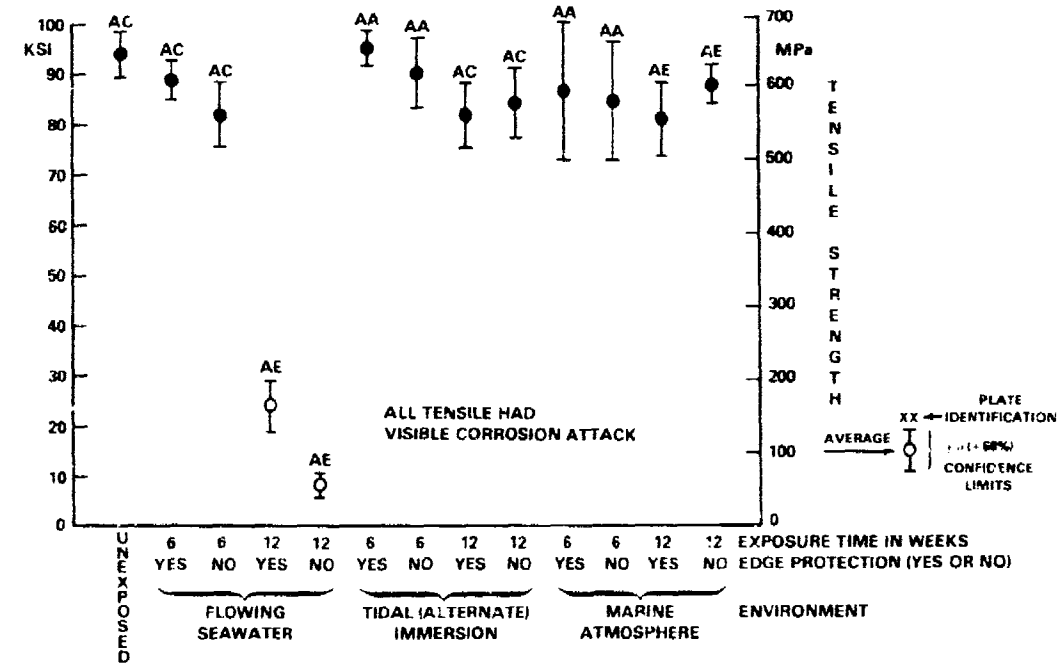

Figure 13. Residual Tensile Mechanical Properties of Standard Gr/Al Composite vs Corrosion Exposures

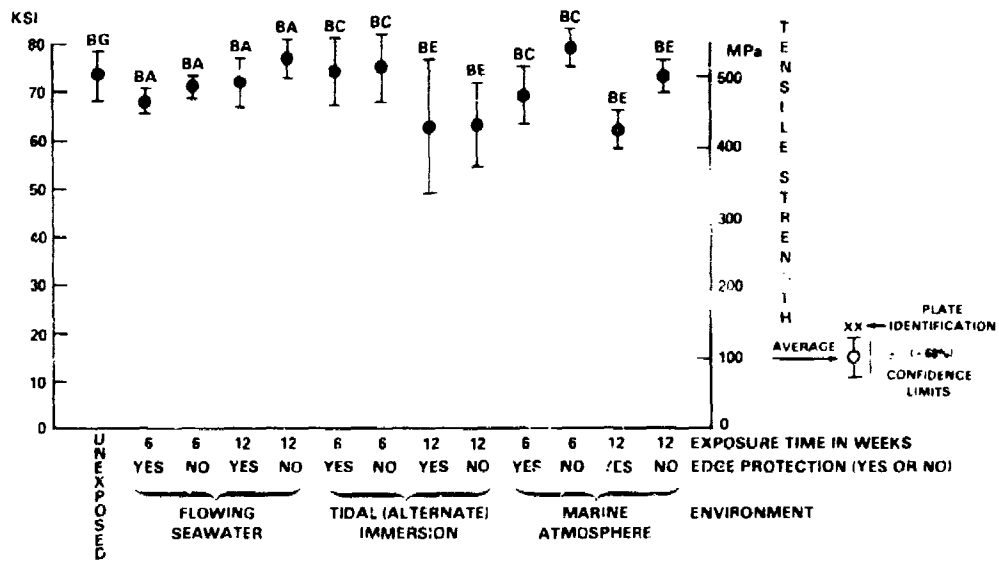

Figure 14. Residual Tensile Mechanical Properties of Encapsulated Gr/Al Composite vs Corrosion Exposures

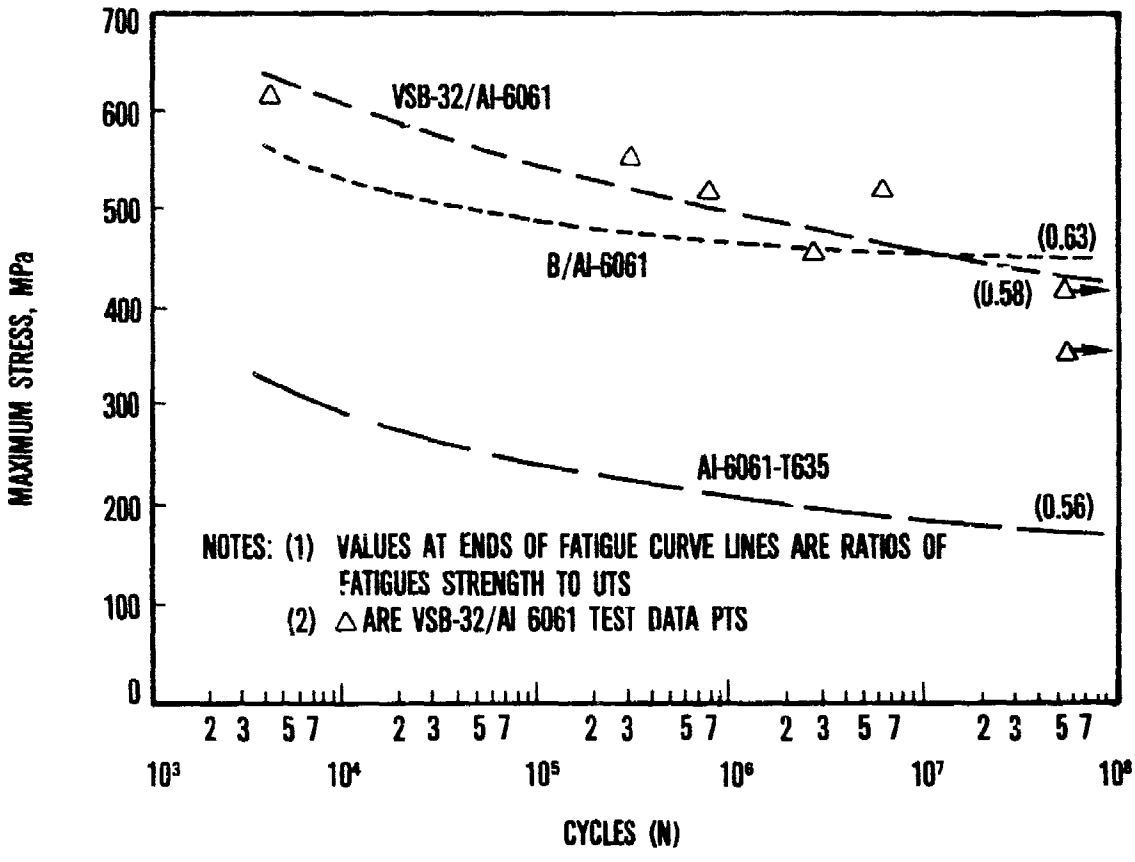

Figure 15. Axial High Cycle Fatigue Results for VSB-32/Al 6061 Composite, B/Al 6061 Composite and 5 mm Diameter Al 6061-T635 in Air

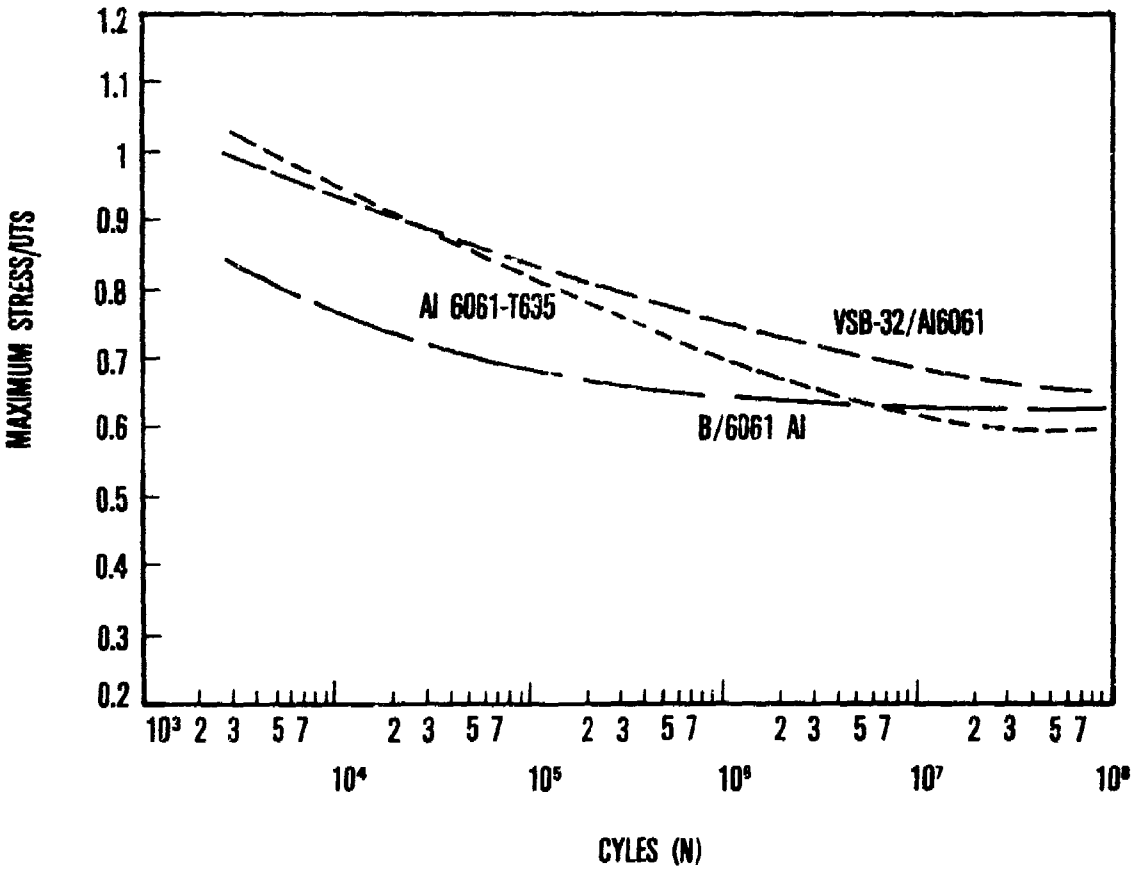

Figure 16. Normalized Axial Fatigue Data for VSB-32/Al 6061 Composite, B/Al 6061 Composite and 5 mm Diameter Al 6061-T635 in Air

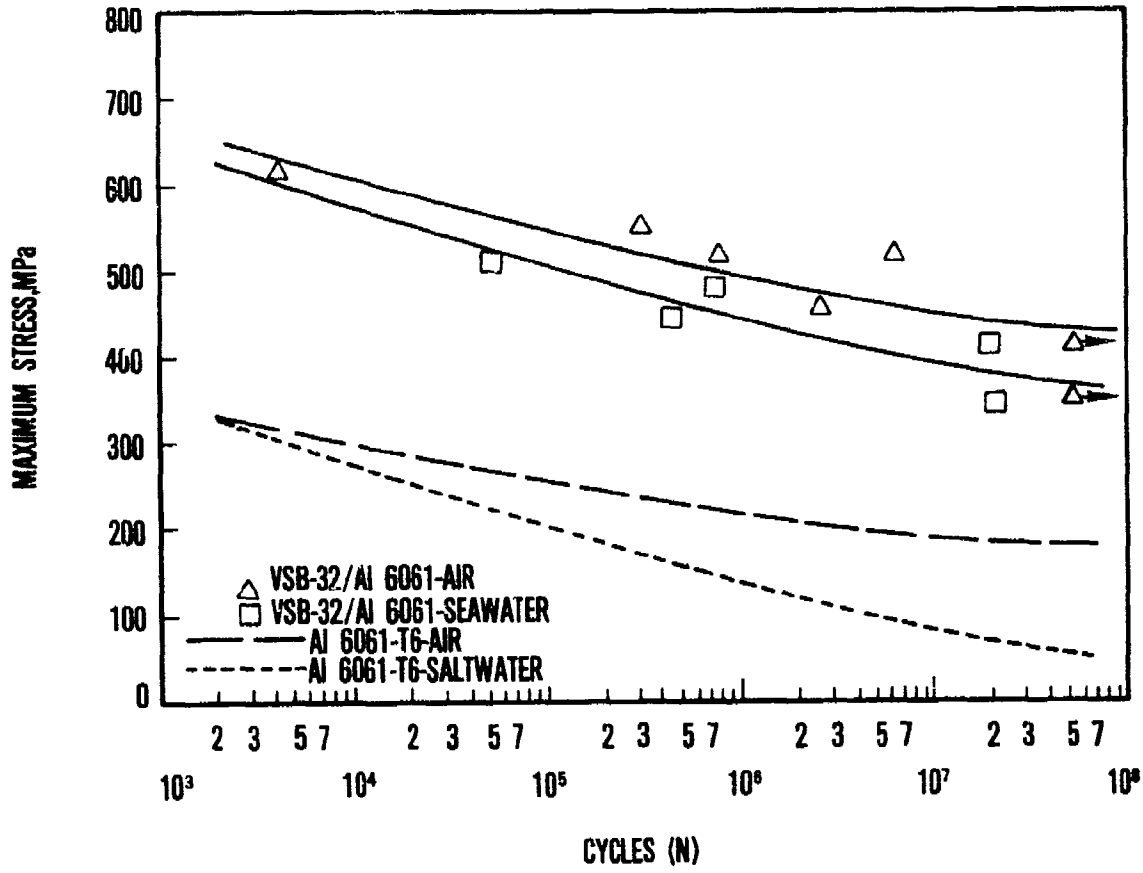

Figure 17. Axial High Cycle Fatigue Data for VSB-32/Al 6061 Composite and Al 6061-T6 Bar in Air and Salt Water

AFWAL-TR-81-4019
Volume II

THE COMBUSTION OF TITANIUM IN GAS TURBINE ENGINES

Charles W. Elrod

Aero Propulsion Laboratory
Air Force Wright Aeronautical Laboratories

The combustion of titanium in gas turbine engines has been, in recent years, a source of concern for the aircraft industry. The unpredictable nature of the titanium combustion incidents and the massive damage which can accompany an occurrence, was sufficient to initiate considerable experimental research and redesign activity in the 70s. Nearly all current aircraft gas turbine engines have suffered some metal ignition damage. This paper will summarize, in a general form, the type of incidents which have occurred, including the damage assessment and the probable causes. It is worthy to note that titanium combustion is typically a secondary event. That is, some failure preceded the metal combustion and created an environment conducive to the ignition of a titanium component. The source of failures, in most cases, was deduced from damage assessments and engine histories but does represent a relatively accurate picture of the problem. The range of potential failures will also be discussed and categorized to provide a common ground for understanding titanium combustion incidents.

The research conducted in the 70s to attempt to understand the combustion process and examine means of neutralizing or eliminating the problem will be discussed. Some of the early considerations will be described and re-interpreted based on current technology. The application of recent research and the benefits derived from that application will be explained.

INTRODUCTION

Titanium has been an integral part of the aircraft propulsion system for over 20 years. Its use is justified by a high strength-to-weight ratio, good strength retention at moderately high compressor temperatures and excellent corrosion resistance. For these reasons, titanium usage increased into the late 60s and early 70s, finding its way into nearly all the gas turbine engines developed through this period. The application of titanium, although accompanied by numerous advantages, was not without some disadvantages, including cost, machinability and combustibility. The first two are an accepted integral part of the use of titanium whereas the latter problem is an unacceptable feature, especially in an aircraft power plant.

Titanium has a wide application base in the gas turbine engine (see Figure 1). The fan/compressor is the main benefactor of titanium technology. Fan blades, vanes, cases, rotors, splitters and various support members are routinely fabricated from titanium. Similarly, the compressor blades, vanes, cases, and rotors, at least to the mid-high pressure compressor location, also benefit from titanium usage. Additional titanium can also be found in fan ducts, low pressure turbine components, nozzle members, heat shields and other miscellaneous parts.

HAZARD POTENTIAL

With this widespread use of titanium, it is obvious why a strong concern exists relative to its combustibility. But why is titanium a potential combustion hazard? Table 1 is a listing of the physical properties of some selected metals which relate to the relative combustibility of titanium. Three of the five metals listed, titanium, iron and magnesium, ignite before they melt. Thus, they do not have the benefit of the latent heat of fusion as a potential heat sink. The heat of combustion of titanium is high, albeit less than either aluminum or magnesium, however, its specific heat and probably more importantly, its thermal diffusivity, is considerably lower than aluminum or magnesium.

To put these combustibility factors in more of a relative perspective, see Figures 2, 3, and 4 which include the resistance to ignition, the relative fire severity for equal weight and the relative fire severity for equal volume, reference 1.

The relative energy to ignite the metal was found by considering surface temperature of the metal subject to a specified heat flux

$$T = 2Q\sqrt{\frac{t}{\pi K\rho c}}$$

where

T	=	surface temperature	°K
Q	=	heat flux	
t	=	time	
K	=	thermal conductivity	J/(sec)(m)(°K)
ρ	=	density	Kg/m^3
c	=	specific heat	J/(Kg)(°K)

If we now rearrange and substitute T_{ign}, ignition temperature, for T we get

$$2Q\sqrt{t} = T_{ign}\sqrt{\pi K\rho c}$$

Therefore the relative resistance to ignition for a constant heat flux over a fixed time interval is proportional to $T_{ign}\sqrt{K\rho c}$.

The relative fire severity for equal weight is determined by examining the heat of oxide formation for the metal, expressed in joules per Kilogram - mole, and dividing the heat of formation by the number of metal atoms in the oxide molecule times the atomic weight. For example, the heat of oxide formation for titanium is 94.5×10^7 J/Kg-mole, the number of titanium molecules is one and the metal atomic weight is 47.9. The energy released (E) is therefore

$$E \quad \frac{94.5 \times 10^7}{1 \times 47.9} = 1.9 \times 10^7 \text{ J/Kg}$$

The relative fire severity for equal volume is merely the energy per unit weight times the density of the metal or Eρ.

From Figures 2, 3 and 4, it can be seen that titanium has a relatively high combustibility quotient. It combines a potentially high fire severity with a relatively low resistance to ignition. Aluminum on the other hand has a potentially high fire severity but exhibits a relatively high resistance to ignition. Magnesium tends to fall in between titanium and aluminum on a comparative combustibility criteria.

Titanium, therefore, obviously warrants special consideration from a safety standpoint when its use in the gas turbine engine is intended. Studies pertaining to the ignition of titanium have been available for over 20 years, some of which were used to define the limits of acceptable titanium use, especially in the mid-60s, when interest in the potential hazards of titanium combustion in gas turbine engines began to rise. Figure 5 illustrates a typical application of the Stanford Research Institute study, reference 2, with representative stage pressure and temperature conditions plotted as an overlay. Since the pressure and temperature of a specific stage is not a constant factor, varying as a function of power setting and altitude, several different operating conditions would normally be plotted to determine the application limits. The time at each operating point could also become a determining factor for exceeding the combustibility limit. More important than these considerations, however, is the experimental basis for the curve dividing sustained combustion from non-sustained combustion. Titanium was tensile fractured in a non-flowing environment. A number of experiments, both reported, references 3, 4, 5, and 6 and unreported, have demonstrated the ill advised use of the SRI curve for setting sustained combustion limits.

More recently, the effects of velocity on sustained combustion of simulated blades have been demonstrated, references 3 and 5. As a result, the sustained combustion curve was re-developed as a function of leading edge Reynolds number and temperature, reference 7. Data from reference 5 was plotted on the N_{Rc} vs T curve and agreed quite favorably with defined combustion areas, reference 7. Figure 6 illustrates the possible use of

the N_{R_c} vs T sustained combustion curve to help define the limits for the use of titanium in a representative compressor environment. From the figure, for the compressor conditions plotted, stages 5 and 6 would represent a risk for the use of titanium 6Al-4V and similar commonly used titanium alloys. The latter distinction was made because Figure 6 does not represent the sustained combustion limits for all titanium alloys, reference 8.

Another caution should be exercised concerning the use of Figures 5 and 6 for establishing design goals and that is the lack of consideration for centrifugal effects on the combustion process, especially as it concerns melt removal. The retention and removal of molten titanium from the burning metal has been found to be an important factor in the self-sustained combustion of bulk titanium. In spite of this problem, the Reynolds number plot is currently one of the better 'quick and dirty' guides for establishing the combustion design limits for the use of common titanium alloys in the gas turbine engine.

Good design practice, however, rarely permits the 'quick and dirty' criteria to drive the design philosophy. It requires, rather, a look at the parameters involved in the problem, isolating those deemed important, and cataloging the risk associated with the potential failures. Table 2 presents a simplified summary of the factors involved in a titanium incident. Generally, the combustion process consists of an energy source creating a localized temperature rise, a fuel source (titanium) and oxygen (air). The heat source creates a condition where ignition occurs and a supply of oxygen produces a self-sustained combustion. The combustion will continue so long as titanium and air are available and the heat loss from the metal does not equal or exceed the heat generated from the oxidation process. In equation form

$$\frac{dE}{dt} = Qcond + Qrad + Qconv - Qreac - Qinput$$

During the pre-ignition phase, the equation is basically reduced to

$$\frac{\Delta E}{\Delta t} = Qcond + Qconv - Qinput$$

except for the fracture initiation sequence where Qreac becomes a dominant heat source. Once ignition has occurred, the equation can be considered

$$\frac{\Delta E}{\Delta t} = Qcond + Qconv - Qreac$$

since the heat of reaction will be a dominating heat source. The equations above are, of course, a simplified form of a much more complex problem. A detailed, generalized solution of the complex combustion process is described in references 7 and 10 and represents the best model currently available to assess the self-sustained combustion of titanium airfoils.

Before self-sustained combustion can occur, however, an ignition source must have evolved. Table 2 lists a number of potential ignition sources possible in the gas turbine engine.

The high energy rub is without question the most prevalent initial ignition source for titanium components in the gas turbine engine. High energy rubs occur as a result of blade tips rubbing against the case, or case coating, as a result of excessive radial displacement of the rotor, rubbing of blades against trapped debris; i.e., broken blades and vanes, loosened bolts, nuts or pins and numerous externally ingested objects; and rotor/stator rubs as a result of rotor axial displacement. Trapped blades and radial displacement of the rotor comprise the major sources of combustion initiation in the engine.

A very small number of incidents have resulted from aerodynamic heating, stall/surge. No distress marks resulting from rubbing were observed on either rotating or stationary components. The end result of these instances was minor trailing edge damage, an ignition but not a prolonged self-sustained combustion. In a stall event, the local temperature rises very rapidly, creating a high rate of heat flux to the blade/vane. Since convective heat dissipation is low and the conductive heat transfer, especially for thin trailing edges, is also very low the high heat input can cause localized ignition. Once the engine recovers, usually in milli-seconds, the heat removed by convection overwhelms the combustion process and effectively blows it out. Figure 7 is an example of the trailing edge burn.

A fracture initiated burn results from the exposure of unoxidized titanium to the airstream. As oxidation occurs, the exothermic reaction causes the temperature of the solid in the immediate vicinity to rise to the ignition point. Although fracture initiated combustion has occurred in the laboratory, the engine is devoid of any similar verified instances, with one questionable exception.

Molten titanium droplets are the major source of propagating a fire from its initiation site to downstream components. The titanium droplet is a high thermally reactive element. Evidence of the reactiveness of the molten titanium is seen in Figure 8 which is an exhaust plume, 8 ft. long, of molten titanium droplets from a test sample 1" x 2.3" x .060". It should be easily seen from this example the potential for massive damage from multiple blade combustion in a confined environment such as a gas turbine engine.

Once ignition has occurred, factors such as temperature, pressure, velocity, component geometry, and molten metal dispersal interact resulting in either minor or major damage. Minor damage includes both reparable and replaceable components. Major damage refers to massive destruction of the compressor, multiple blade/vane rows reduced to fractions of their original heights and sometimes, but not always, including case penetration. The difference between minor and major damage is typically a function of the rate and amount of molten titanium generated and its dissipation, i.e., separation from burning parts and impingement on downstream components.

Figure 9 is an artist's conception of a propagation scene. The blade at the left of the figure has ignited at the tip leading edge. As the burn surface regresses, molten titanium flows rearward toward the trailing edge driven by aerodynamic forces and radially outward due to aerodynamic and centrifugal forces. As the burn progresses, molten titanium builds until the aerodynamic and centrifugal forces overcome the melt surface tension thus causing dispersal of the droplets on the case and downstream components, vanes and blades. If the molten titanium separates as fine droplets widely dispersed, they will probably coat the vanes, blades and cases and extinguish. If, however, the buildup is substantial in a short

period of time, in cascade experiments the downstream blade ignites in less than two seconds, the burn will progress and ignite additional components. The effect is an extremely intense, rapidly expanding fire which continues as long as fuel (titanium) and combustion conditions permit. Events of this nature, including the most damaging, are probably over in a matter of seconds rather than minutes.

The preceding discussions and descriptions may generate fear in some concerning the potential dangers, however, the fear is probably a slight overreaction. A healthy respect is warranted and the use of titanium should be accompanied with an understanding of the problem, the type of incidents that have occurred and the potential design/material solutions which can effectively reduce the hazard.

INCIDENTS

A total of 340 recorded incidents are included in the data summarized in this section. The data gathered, from a variety of sources, is not complete. Some of the facts surrounding particular incidents are sketchy and are included and interpreted as completely as practical. In addition, a large number of minor incidents were probably overlooked in routine overhaul operations because the blades were reparable, e.g., light trailing edge burns, or beyond the tolerance limit for repair and not recognized as a significant event. The data has also been disguised to protect the proprietary rights of the sources. Also, additional plots or correlations could have been provided, however, the more parameters employed, the more likely the sources would suffer undesirable identification.

Figure 10 is an indication of rates of minor to major incidents for high bypass turbofan engines and low bypass plus turbojet engines. Also plotted are the relative number of case penetrations for each class of engine. For the high bypass engines, 58% of the incidents resulted in minor damage whereas 64% of the low bypass engines and minor damage, the ratio not being significantly different for the two classes of engine.

Case penetration, on the other hand, reveals a different picture. Fifty-seven percent to the HBTF engines had case penetrations whereas 36% of the LBTF cases were penetrated. The data indicates less resistance to case penetration by the HBTF, a conclusion which may be valid but warrants further analyses. For one thing, the majority of penetrations in the HBTF engines were at manifold locations, a fact not equally shared by the family of LBTF engines. To fully understand the implication of these comparisons would require an examination of a number of design/operational factors most of which were not available for this analysis.

Figure 11 presents the comparison of minor/major damage for gas turbine engines as a function of thrust ranges. The ratio of minor to major damage is fairly consistent with the exception of the 20-30000 lb thrust class. Once again, the implication of this deviation should come from an in-depth analysis of the engine design, operational status, and the failure mode at the time of the incident. A similar statement can be made about Figure 12 where the trend of case penetration is similar for three of the thrust classes but significantly different for the 10-20000 lb thrust class.

A comparison of incident ignition sources is contained in Figure 13. Tip rubs occur when the rotor experiences a radial displacement creating a mechanical interference between the rotor blade tips and the case. Excessive rotor movement can be caused by a number of factors including bearing failures, compressor/turbine disk failure, fan blade breakage, hard maneuvers, or hard takeoff/landings.

The FOD/IOD refers to foreign objects or internal objects (primarily but not limited to broken blades) being trapped in the flowstream such that the rotor rubs against the captured object. Most trapped debris is collected at the outer diameter of the flowpath resulting in tip rubs.

Root rubs involve the ignition of a titanium blade/vane at the inner diameter of the flowpath. Most of these occurrences are the result of either axial rotor movement or a component failure in the rotor hub region. The stall only situation was described previously.

The representation of incidents as a function of operational status is shown in Figures 14 and 15. The sea level and attitude test stand data is self-explanatory except for the lack of data on power setting. An interesting analysis could be performed on the relationship of minor/major damage and penetration/non-penetration criteria for sea level and altitude test stands as a function of power setting.

Takeoff represents a full power situation and as far as titanium combustion is concerned, a critical part of the flight envelope, since the stage pressure and temperatures are at a high level and rotor motion radially and axially are expected. Examination of Figure 15 produces a possible explanation for the high percentage of case penetrations for the HBTF, Figure 10. During takeoff, the high centrifugal forces would tend to concentrate melt on the case/manifold structure and the high pressure/high temperature environment results in a faster burn rate and an increased likelihood of self-sustained combustion, reference 5.

Once again, the data in this section was accumulated from a variety of sources with no continuity on the amount of information available. Summing the data on each of the different graphs will lead to different totals. Further, the list is not inclusive. Incidents have occurred which have not been disclosed for a variety of reasons, not the least of which is the non-recording of probable incidents at the numerous overhaul facilities.

Figure 16 is an artist's conception of typical burn patterns. The burn shown in Figure 16a, b, c, and d are progressive burn patterns. In that sequence, the initiation would probably have been at the 'b' location with 'a' being an upstream trailing edge ignition and blowout. The blades and vanes downstream from 'd' would have been replications of 'd' and could have been fabricated from metals other than titanium. Figure 17 was an example of an actual burn progression (propagation). Figure 18 is a typical example of a case penetration. Penetrations can include small holes at various locations, 360° - stage wide holes, or a massive total consumption of the entire case over the compressor section. The majority of examples are contained, fortunately, in the former category.

The preceding sections might lead to the conclusion that titanium in the gas turbine engine is a hopeless situation and its exclusion a warranted solution. In the first place, the incident rate per million flying hours is low. The number of failures compared to other material/design problems is not alarmingly excessive and there is on-going technology providing solutions to minimize the risk of ignition and self-sustained combustion. The following sections will describe some of the technology developments and design changes intended to minimize the titanium hazard.

RUB PREVENTION

Although titanium combustion is a secondary failure rather than a primary cause, it would be naive to believe all sources of primary failure could be resolved. The more likely attack is to minimize the potential for combustion once another precipitating failure occurs. The approaches are primarily concerned with the prevention of ignition.

Ignition from tip rubs can be attacked from a number of directions. One of the more obvious techniques is to open the clearances, not throughout the compressor, of course, but primarily in the critical regions. The critical regions are the latter stages using titanium, which is probably the mid high compressor region.

The early stages have two factors in their favor, first the pressures and temperatures are lower and the blades are thicker. Intuition and limited data point to an increased difficulty to ignite the thicker blade. Increasing the clearance is not a highly recommended approach because of the efficiency penalty and decrease in stall margin, a very risky approach for a stall prone compressor. Further, the clearance increases would not be on the order of 50-50 mils which may be required to prevent ignition from tip rubs following a component failure.

A more acceptable approach is the application of a rub tolerant material in which titanium rubs are suspected. The search for an acceptable rub tolerant material, especially in the tip region, has been underway for 20 years with limited success. The materials which involve the least energy

generation are also erosion prone and vice versa. The second problem with the rub tolerant material is the thickness. With weight a premium in engine design, case thicknesses are minimized, therefore leaving minimal space for the rub tolerant material. A severe rub easily penetrates compressor coating typically .015-.025. Once the coating has been penetrated, rubbing the case can be especially hazardous, particularly if it's titanium but also when the case or insert is steel.

Much has been said about the titanium on titanium rub as the prime factor in the ignition of titanium components. While rubbing titanium on titanium may generate more heat than other materials, titanium on steel, for example, can and has been an ignition source. Other materials such as plasma sprayed nickel graphite and felt metal have also resulted in titanium ignition during a hard rub. Suffice it to say, titanium will ignite in air if the energy generated during the rub is sufficient to bring the local titanium temperature to the ignition point.

One additional problem worth mentioning at this point is the potential for component failure and possible ignition when a material such as nickel graphite is sprayed directly over titanium. Heat generation at the rub surface can result in a titanium-nickel reaction at the coating/case interface. The TiN eutectic forms a low melting alloy and penetration can occur due to a melt thru or yield.

Internal rubs are similar to tip rub from the standpoint of material sensitivity to heat generation. Titanium stator seal rubbing against the titanium rotor hub is probably the worst situation for ignition. As mentioned before, the heat generation is high and two components rather than one are subject to ignition. Steel is slightly better and aluminum, if the temperature permits is preferred. An additional comment relating to titanium/steel rub should be mentioned, namely, molten steel is known to ignite titanium.

Figure 19 illustrates a concept which may prove extremely important to the tip rub ignition problem. The abrasive on the tip of the blade serves two purposes, first it isolates the titanium blade from the rub and secondly, the wear is primarily in the seal material on the case. Figure 20 shows the volume wear ratio of three blade tip treatments and a bare blade on plasma sprayed nickel graphite and a stainless steel feltmetal, reference 11. The high wear ratio of treatment T1 against the stainless steel was due to some flaking of the tip treatment, not wear. The life of the blade tip is one of the question marks left to be answered by engine tests and hours of use. The technology is basically too new to answer these questions.

MATERIAL SUBSTITUTION

The prime example of material substitution is the substitution of steel vanes for titanium vanes. The initial idea behind the move was based on the assumption the fire propagation centered around the flame holding characteristics of the stationary vanes. It is definitely true that replacing titanium vanes reduces the amount of titanium available for ignition and combustion. It does not follow that propagation will be eliminated by this substitution (see Figure 21). The vanes in this picture were steel, the blades titanium.

Figure 22 illustrates typical substitution of steel or nickel base alloys for titanium. The amount of substitution is based on the weight margin allowable for the particular engine and the degree of hazard interpreted by the manufacturer. The substitution of a steel case for a titanium case, for example, involves a serious weight penalty, but may be viewed as a necessary penalty if case penetration and subsequent burning/external damage is deemed intolerant. One point worth mentioning is that a steel case is not impenetrable but it is viewed as a less hazardous event.

A potentially superior answer is offered in references 12 and 13. The first concerns the use of a coating on the titanium component to inhibit ignition from melt impingement. The second is the substitution of a less combustible alloy, Table 3. Without going into detail on these concepts, the application would most probably be a static component where the stress effects are lower, particularly vanes and cases. In addition, the combination of a more resistant alloy with an inhibiting coating could be a highly acceptable solution.

Consistent with the use of coatings as a protection against fire propagation is the use of a coating to increase the fatigue life of the blade. Just such a coating, platinum, has been developed and applied to compressor blades, reference 14. Since blade fracture and entrapment is another of the major sources of titanium combustion, the use of a platinum coating, especially in the root area, cannot be overlooked. Figure 23 is a graph of the number of cycles to failure for a platinum coated airfoil. An increase of 25-30 percent in fatigue strength is possible with a coated airfoil, an important consideration not only for a potential fire problem but also from the standpoint of durability.

One final technology should be mentioned, although it is not a material substitution. Protective blankets or wrappings have been used to protect external fuel and oil lines as well as to increase the probability the fire will be contained in the flow path. The techniques used to date have proven fairly effective, particularly a carbon cloth type barrier used on fuel and oil lines. The blankets are a preventive feature for catastrophic failure, not a technique to minimize the fire hazard such as coating and alloy intended applications.

FIRE EXTINGUISHMENT

Very little will be said about titanium fire extinguishment in the gas turbine engine because for, practical purposes, it is an improbable action. In the first place, detection is extremely difficult since the fire occurs in the gas path with hundreds of viewing obstacles for a typical U-V detector. Secondly, the sensor would have to differentiate between a fire and sparking, which occurs in a rub that does not cause

massive combustion. Thirdly, once detection occurs, a system must be triggered to dispense an extinguishing agent to the proper location. By the time this occurs, the fire may have done its damage or at least a major portion of its potential damage. And last, the number of extinguishing agents considered acceptable is extremely limited (see Table 4).

SUMMARY

Titanium is undoubtedly a desirable material for use in the gas turbine engine. This material application is not without problem, one of the more important of which is its combustibility. This paper has discussed some of the early thinking on the subject, examined a number of documented incidents and presented a brief summary of potential solutions to the problem. Titanium combustion is an intense reaction, but its intensity can be reduced and its ignitability can be minimized. The major sources of ignition have been identified and means to reduce the ignition potential have been investigated, some of which are currently in use, while others are in the research and development phase.

Current studies are producing results which should minimize the effects of titanium combustion. Coatings, alloys, tip treatments, protective blankets and combinations of the above, consistent with good design practice, will allow the designer the luxury of considering titanium as an engine material with a much greater margin of safety and reverse the current trend of titanium removal from the gas turbine engine.

REFERENCES

1. Pelouch, J.J., "ASRDI Oxygen Technology Survey Vol VII, NASA SP-3077"

2. Littman, F.E., Church, F.M. and Kinderman, E.M., "A Study of Metal Ignitions", SRI.

3. Anderson, V.G. and Manty, B.A., "Titanium Alloy Ignition and Combustion", NADC-76083-30, 15 January 1978.

4. Fox, D.G., "Investigation of Titanium Characteristics and Suppression Techniques", AFAPL-TR-75-73, Feb 1976.

5. Elrod, C.W., and Lyon, S.R., "Self-Sustained Combustion Evaluation of Titanium 6Al-4V in an Aerodynamic Environment", AFAPL-TR-79-2047, May 1979.

6. Rihl, W.A., Key, C.F. and Gayli, J.B., "Reactivity of Titanium with Oxygen", NASA TR-R-180, 1963.

7. Glickstein, M.R., "A New Analytical Model for Prediction of Self-Sustained Combustion of Titanium Airfoils", Pratt & Whitney Aircraft Group, 1974.

8. Strobridge, T.R., Moulder, J.C. and Clark, A.F., "Titanium Combustion in Turbine Engines", FAA-RD-79-51, July 1979.

9. Anderson, V.G., and Funkhauser, M.E., "Titanium Coating Ignition Test", Pratt and Whitney Aircraft Group, Unpublished report, September 1980.

10. Glickstein, M.R., "Computer Modeling of Titanium Combustion", Tri-Service Conference on Corrosion, 5-7 November 1980, U.S. Air Force Academy, Colorado.

11. Manty, B.A., Anderson, V.G. and Hodgens, H.M., "Blade Tip Treatment - Titanium Alloy Compressor Blades", Draft Final Report, July 1980.

12. Funkhauser, M.E., "Coatings to Control Titanium Combustion", Tri-Service Conference on Corrosion, 5-7 November 1980, U.S. Air Force Academy, Colorado.

13. Lyon, S.R., and Elrod, C.W., "Alloy Effects on Titanium Combustion", Tri-Service Conference on Corrosion, 5-7 November 1980, U.S. Air Force Academy, Colorado.

14. Eckler, T.A., "Ion-Plated Coating on Titanium Alloy", AFML-TR-79-4109, August 1979.

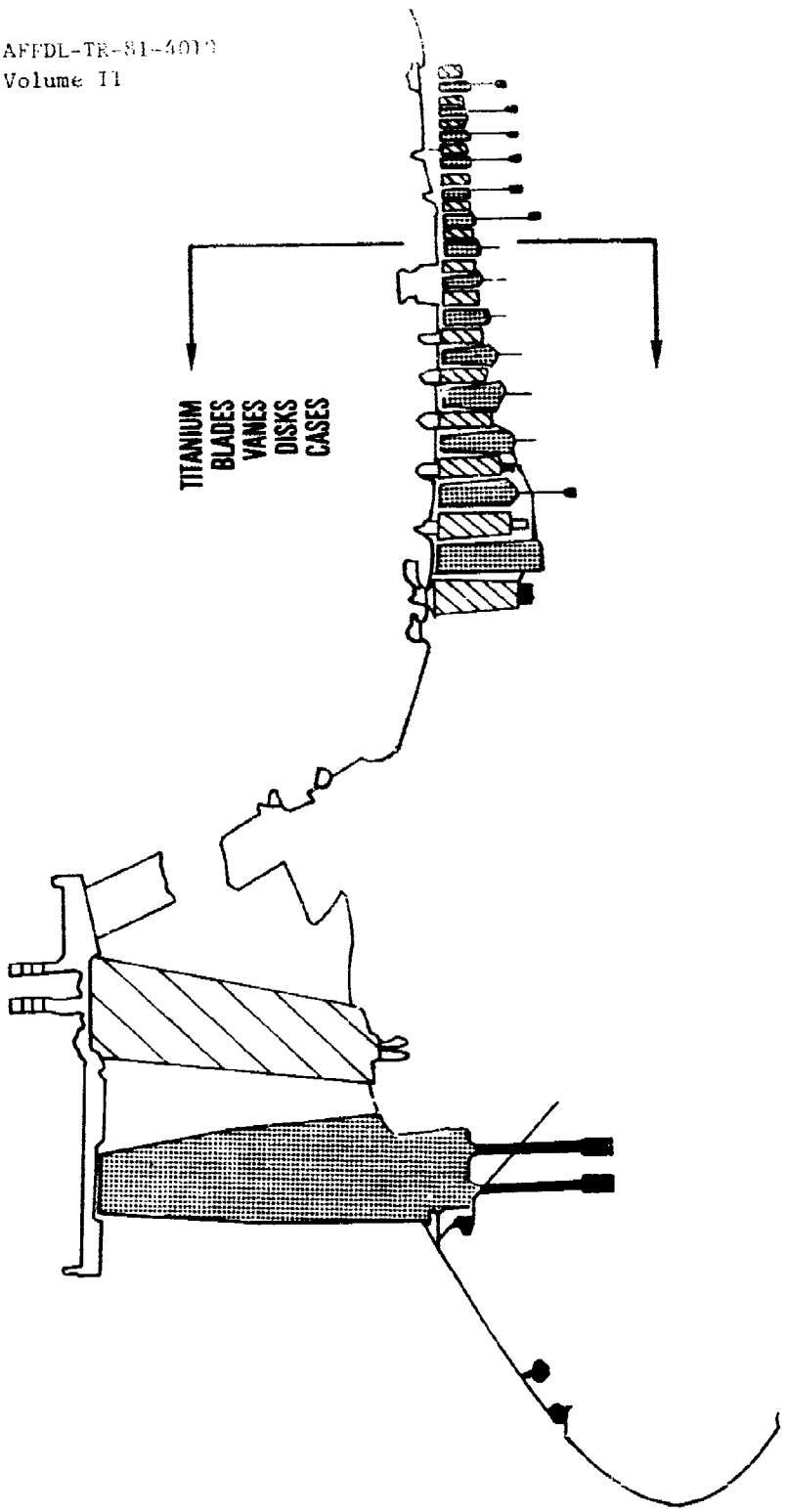

Figure 1

TABLE 1 PHYSICAL PROPERTIES OF METALS

	Titanium	Iron	Nickel	Aluminum	Magnesium
Ignition Temp	2900	1800	2550	1800	1150
Melting Temp	3250	2800	2450	1200	1200
Thermal Conductivity $W/Cm^{o}K$	.18	.8	.11	1.9	1.26
Thermal Diffusivity Cm^2/sec	.076	.23	.04	1.07	.9
Heat of Combustion J/g	19000	7000	4100	31100	25000
Specific Heat $J/Kg^{o}K$	578	503	469	938	1026

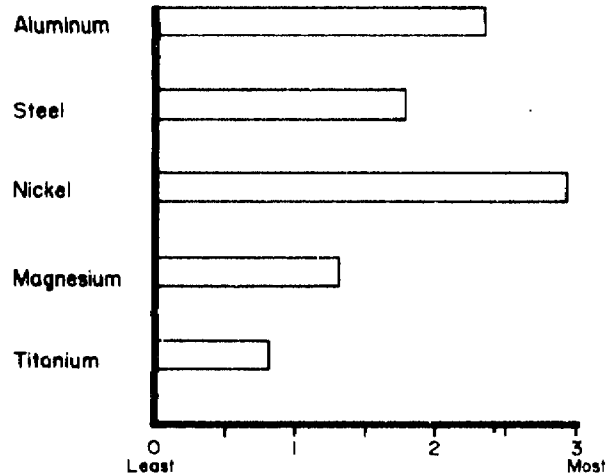

FIGURE 2 Relative Resistance

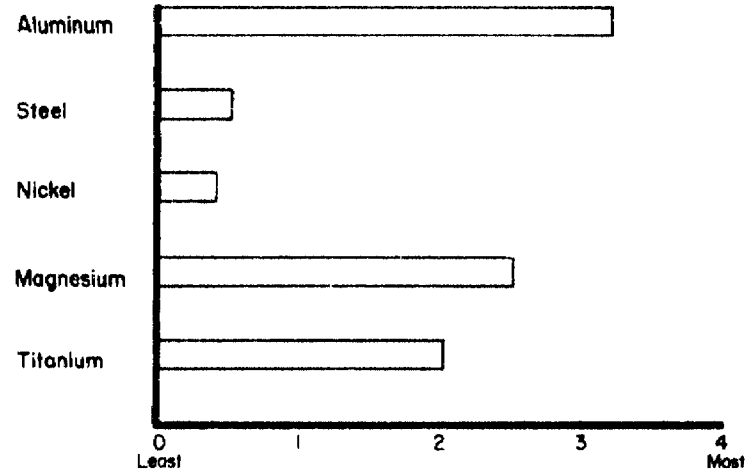

FIGURE 3 Potential Fire Severity for Equal Weight

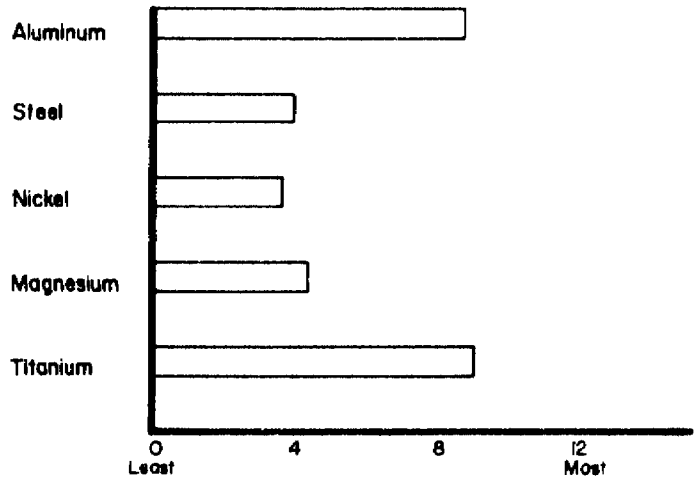

FIGURE 4 Potential Fire Severity for Equal Volume

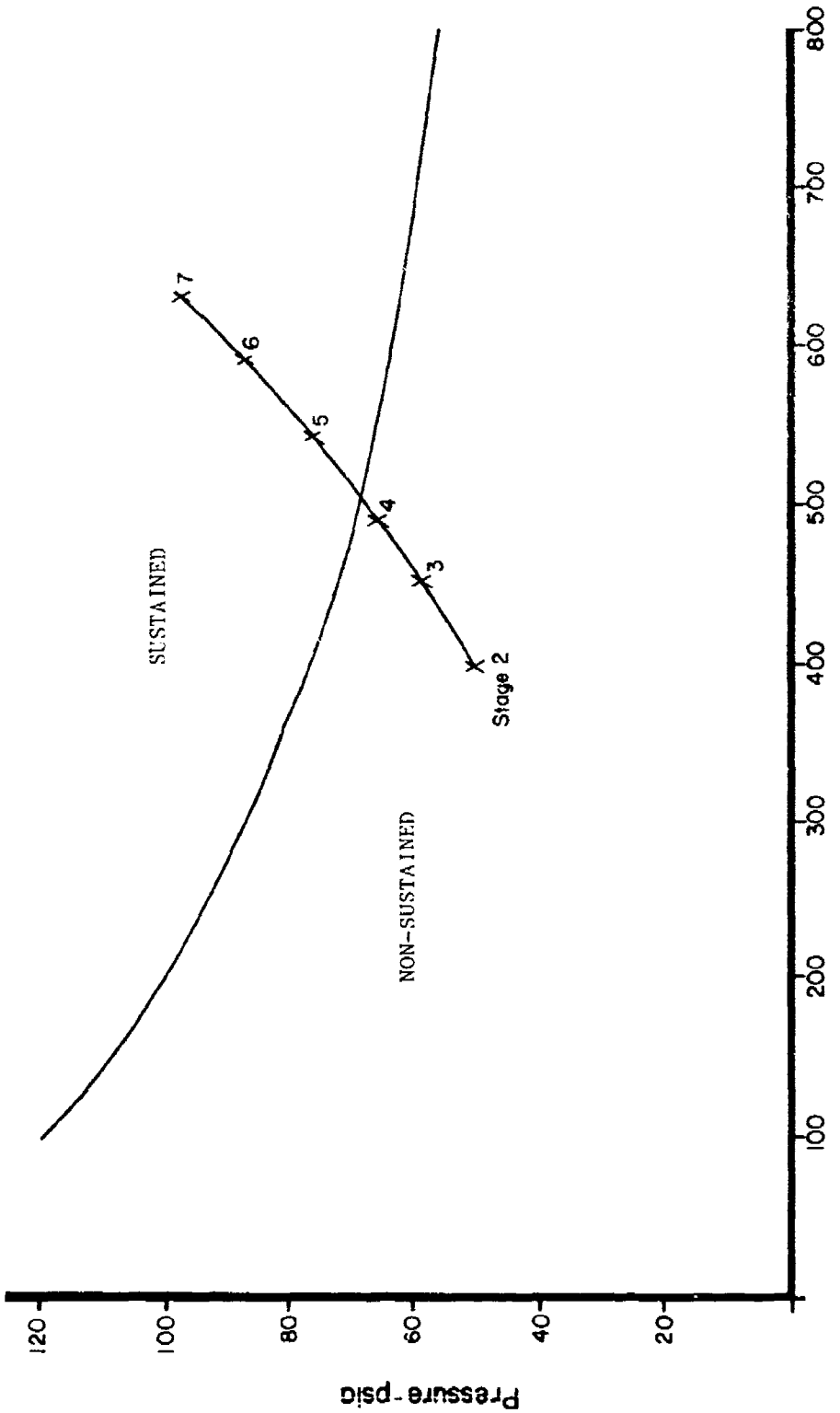

FIGURE 5 P vs T Plot of Sustained/Non-Sustained Combustion

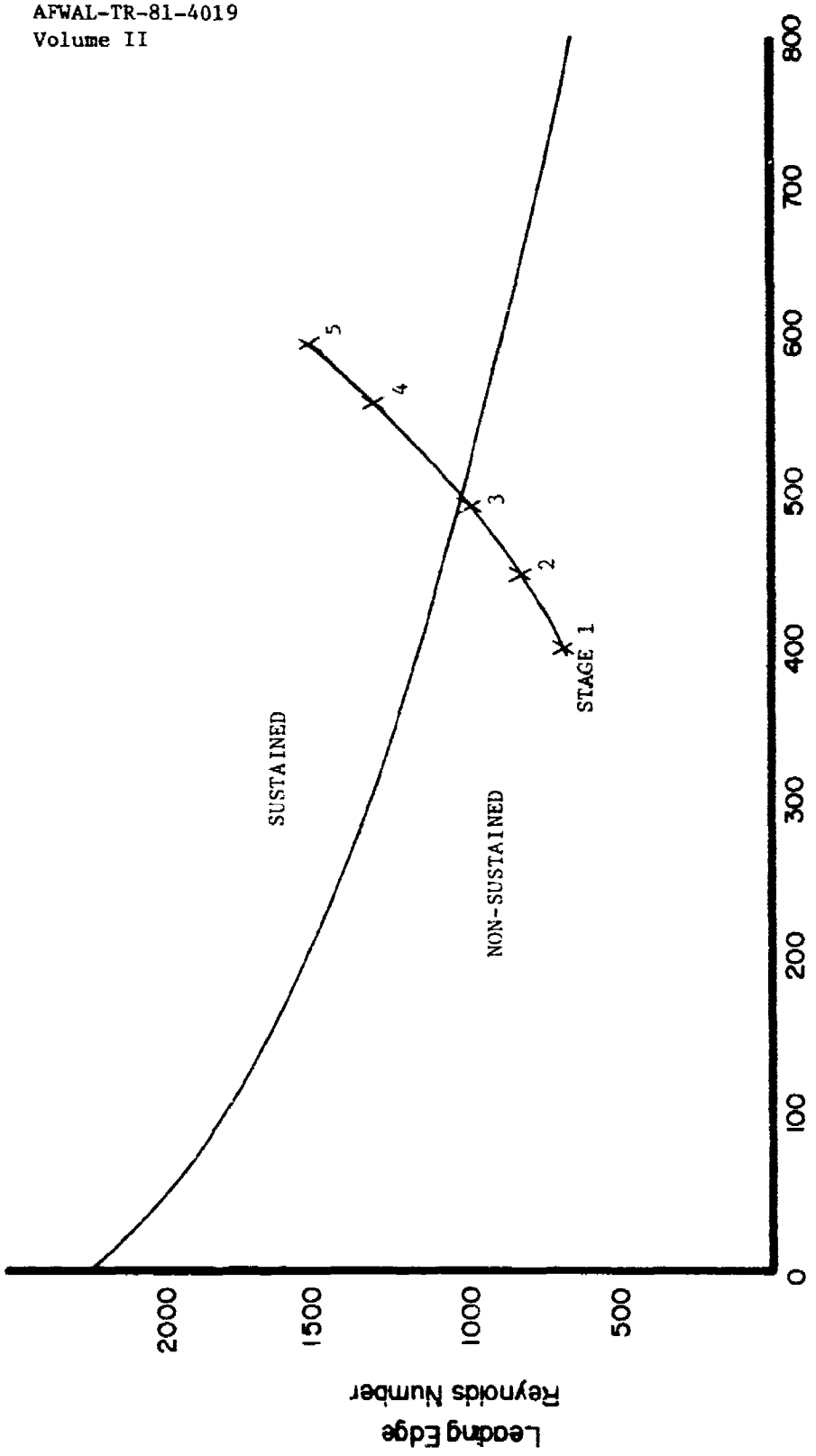

FIGURE 6 Reynolds No. Plot of Sustained/Non-Sustained Combustion

TABLE 2 FACTORS INVOLVED IN TITANIUM COMBUSTION

[ENERGY] + [TITANIUM] + [OXYGEN] ± [HEAT GAINED] - [HEAT LOSS] =

IGNITION SOURCES	COMBUSTION FACTORS	RESULTS
High Energy Rub	Temperature Pressure	Minor Damage Component Replacement Component Repair
High Heating Rates-Stall	Aerodynamics Velocity Turbulence	Major Damage Engine Replacement Loss of Aircraft
Tip Recirculation	Geometry Thickness	
Fracture	Melt Dispersal	
Melt Droplets		

FIGURE 6 Reynolds No. Plot of Sustained/Non-Sustained Combustion

FIGURE 7 Minor Trailing Edge Burn

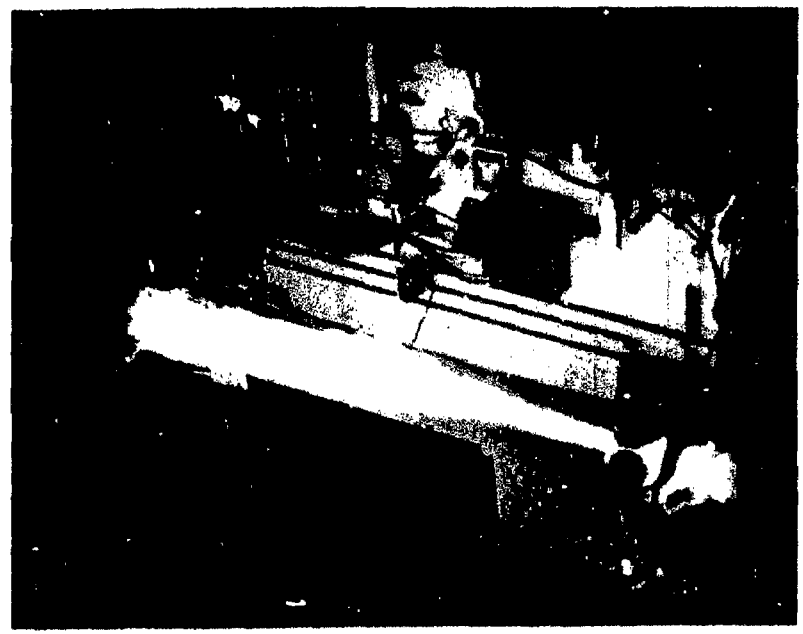

FIGURE 8 Exhaust Plume from Titanium Combustion Rig

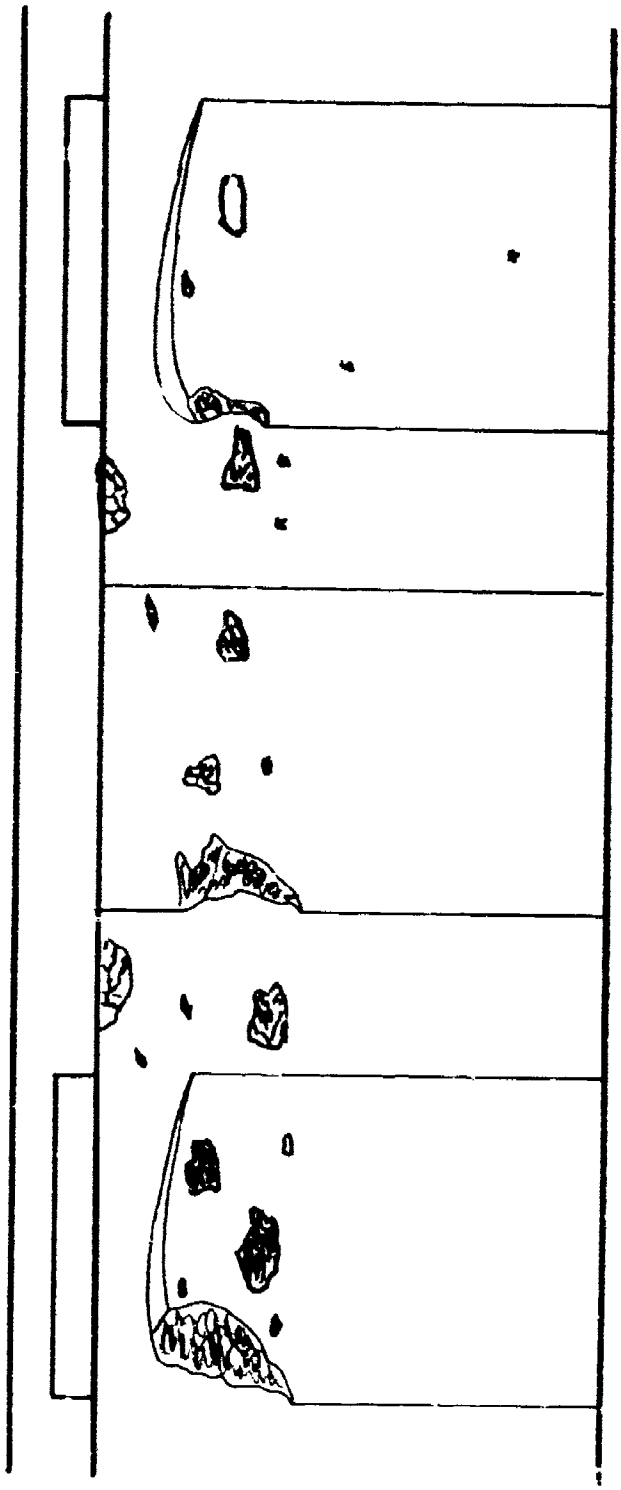

FIGURE 9 Propagation of a Titanium Fire

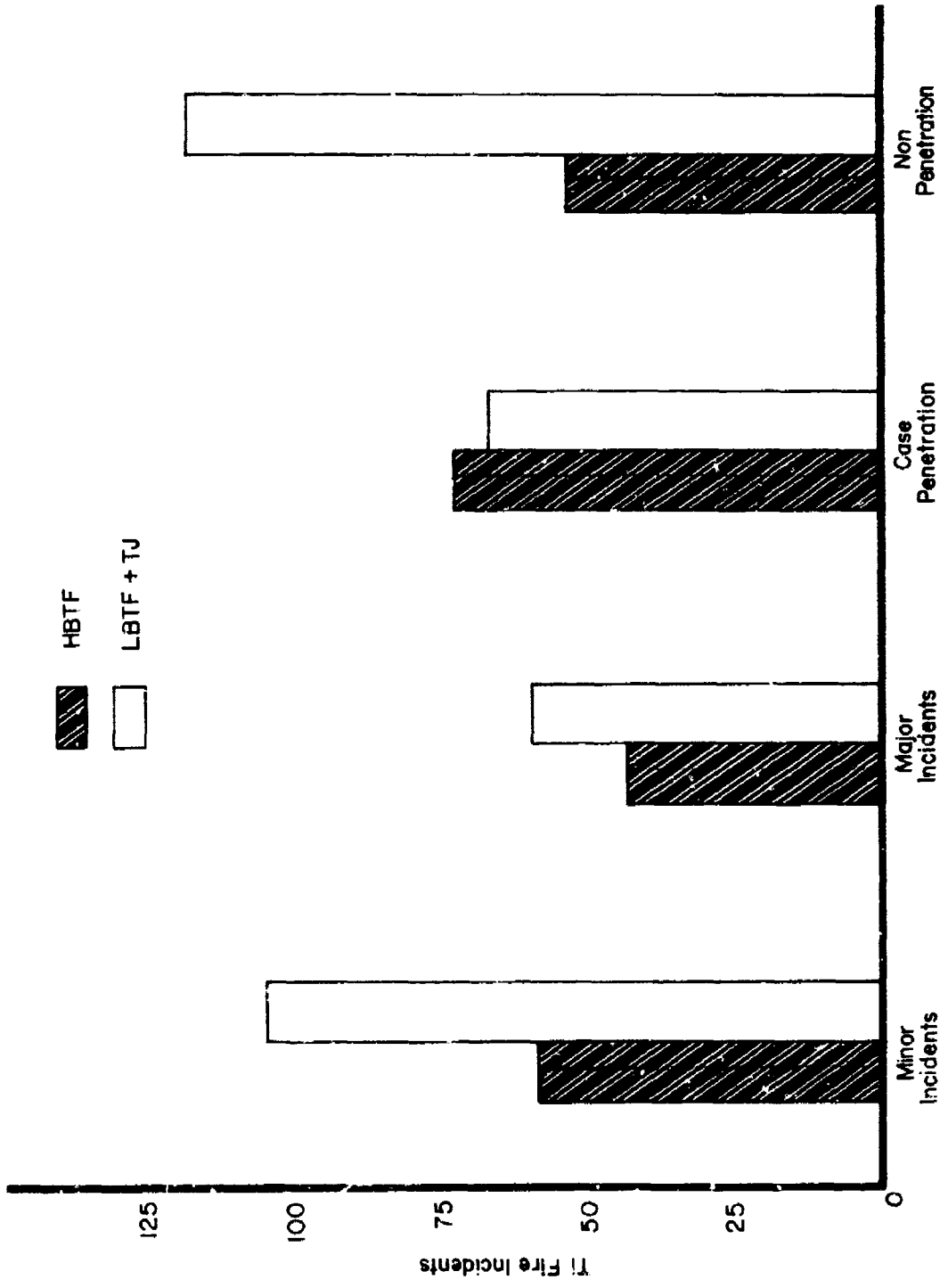

FIGURE 10 Minor/Major Incidents - Penetration/Non-Penetration for HBTF & LETF Engines

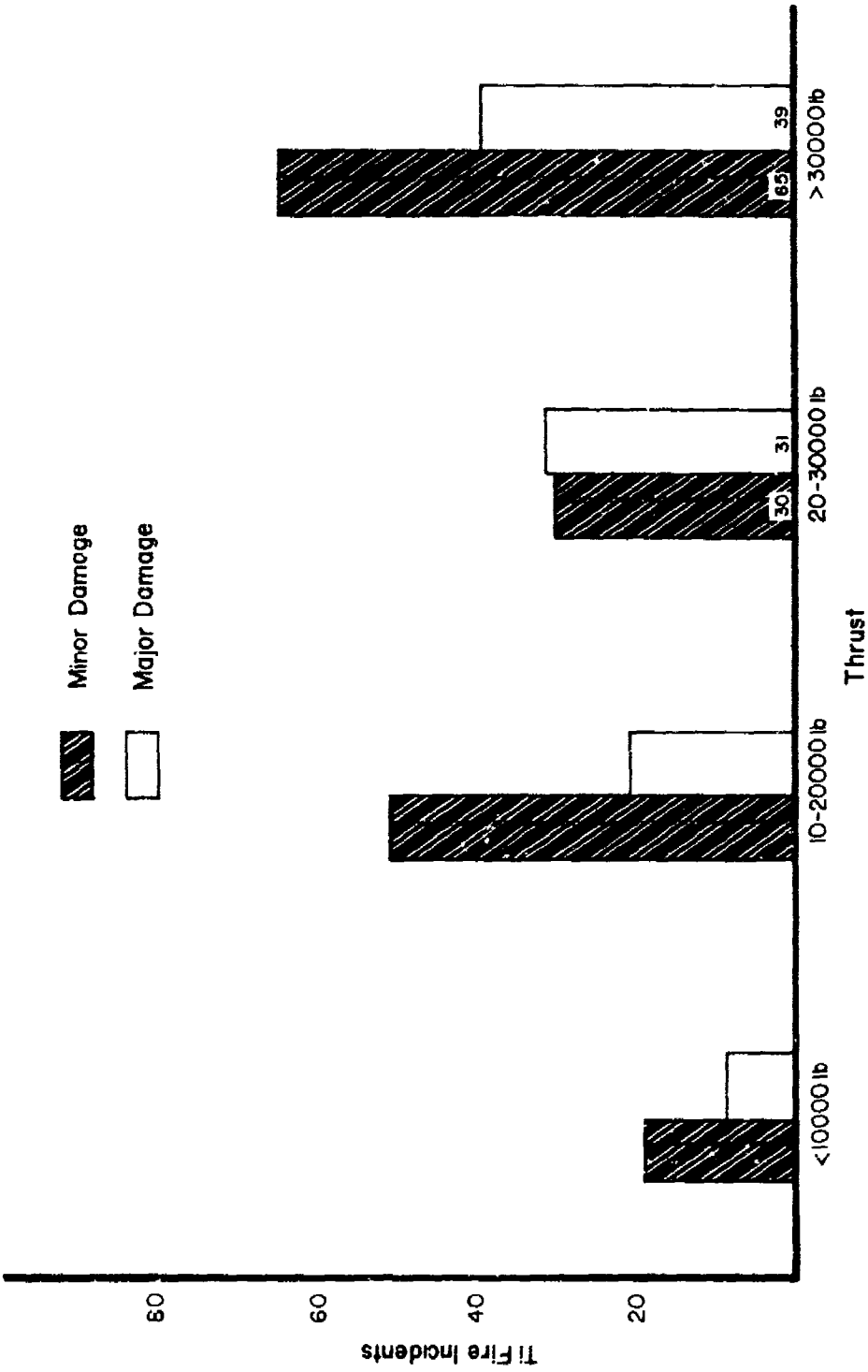

FIGURE 11 Minor/Major Incidents versus Thrust Class

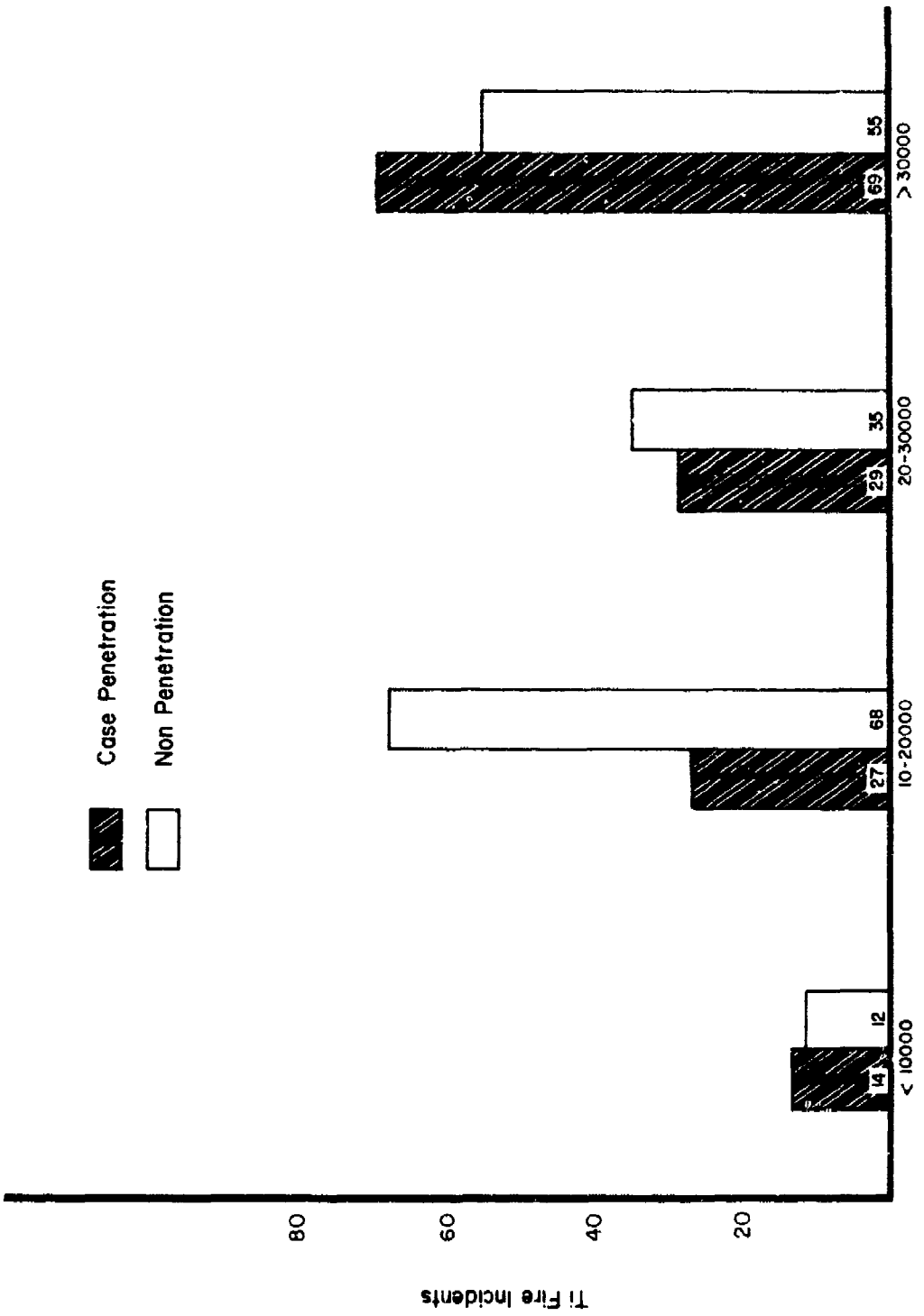

FIGURE 12 Penetration/Non-Penetration versus Thrust Class

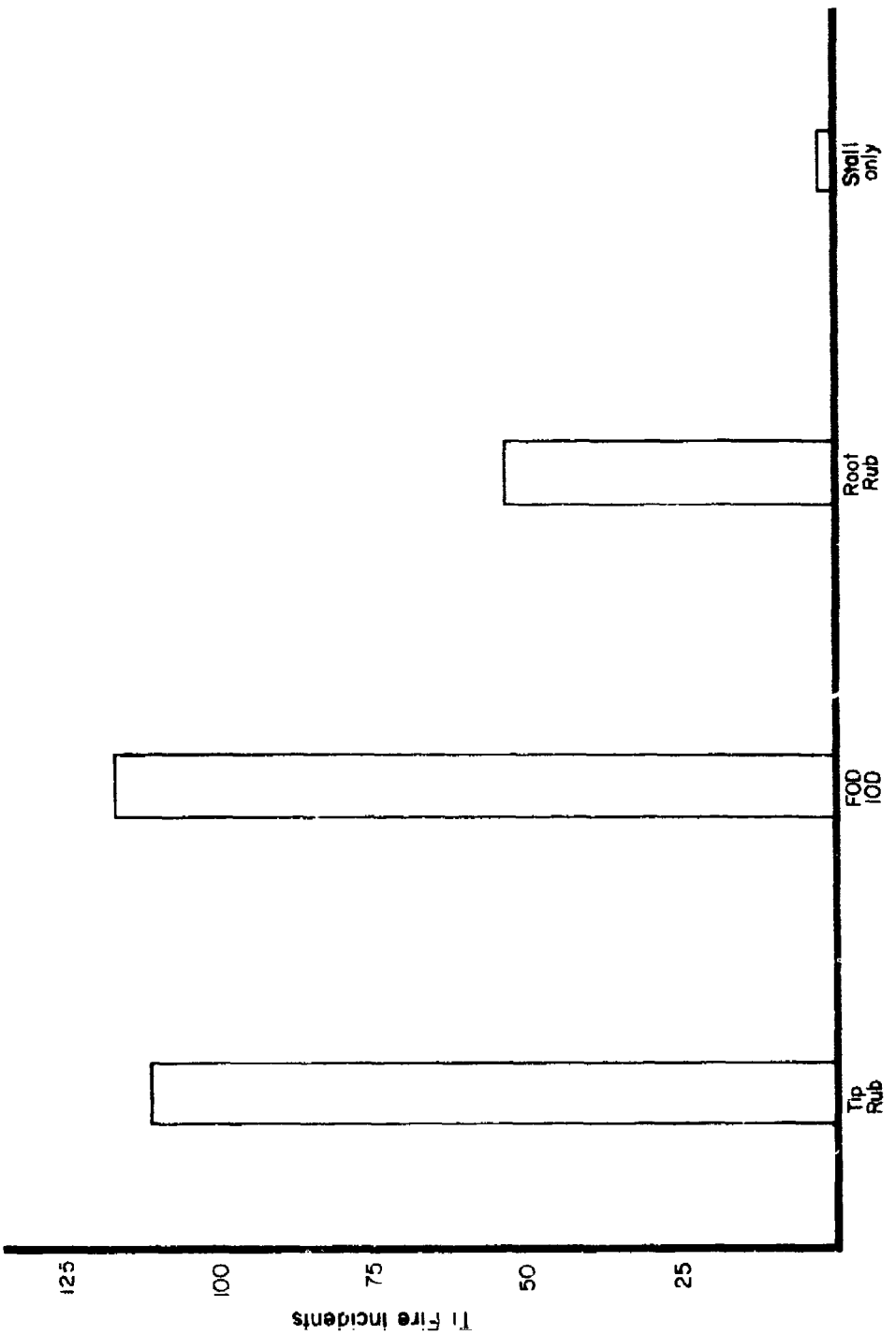

FIGURE 13 Fire Incidents as a Function of Ignition Source

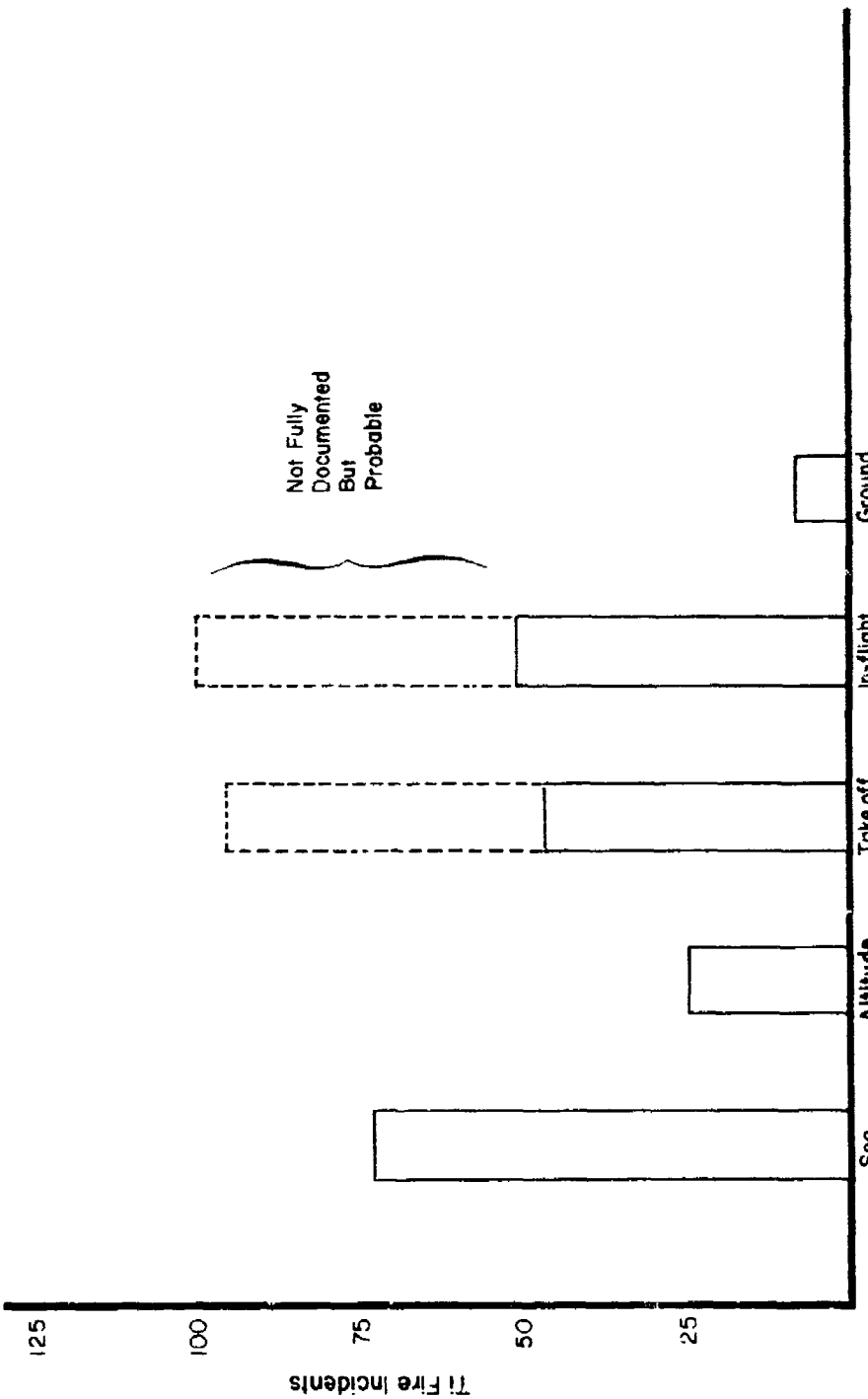

FIGURE 14 Fire Incidents as a Function of Operational Status

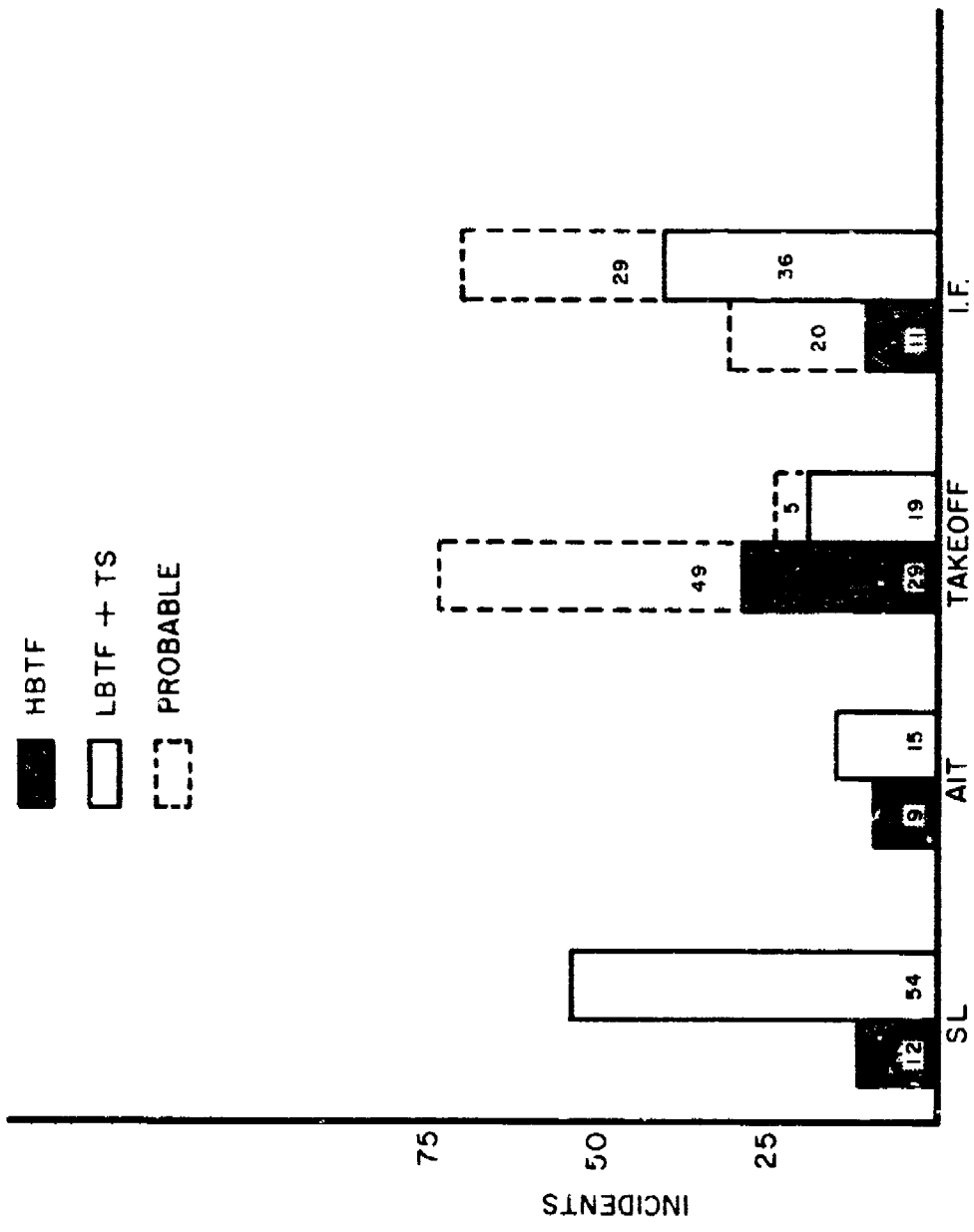

FIGURE 15: INCIDENT PER ENGINE CLASS AS A FUNCTION OF OPERATIONAL STATUS

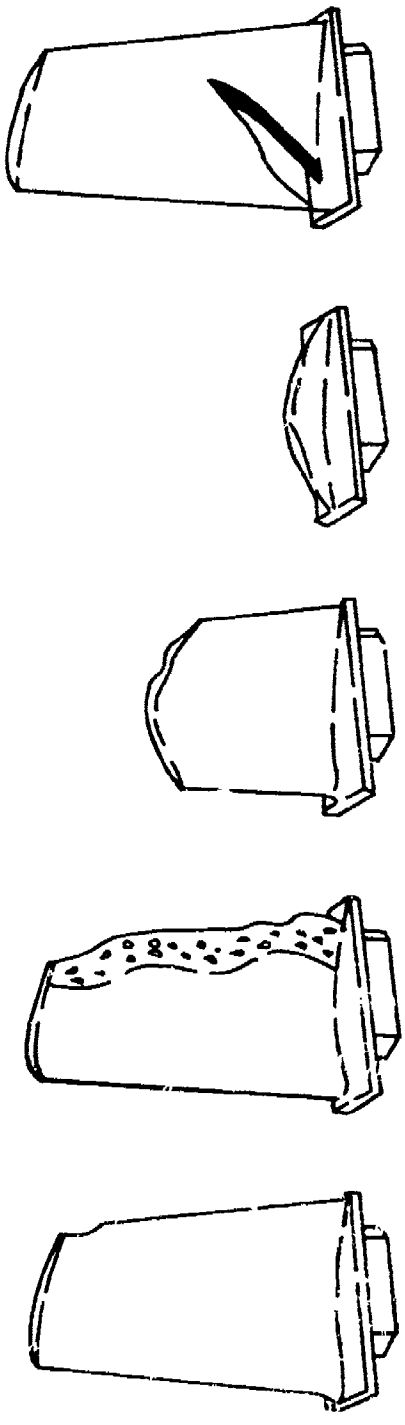

FIGURE 16 Typical Burn Patterns

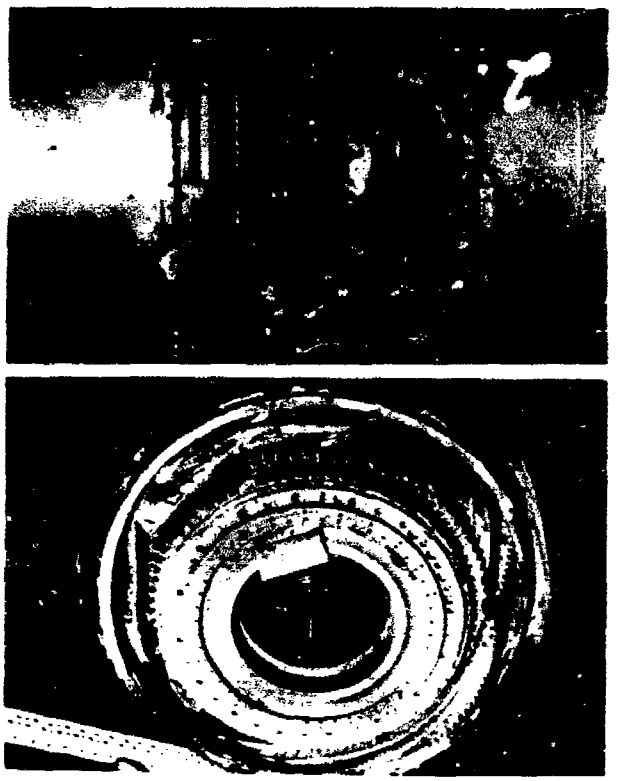

FIGURE 18 Typical Example of Case Penetration

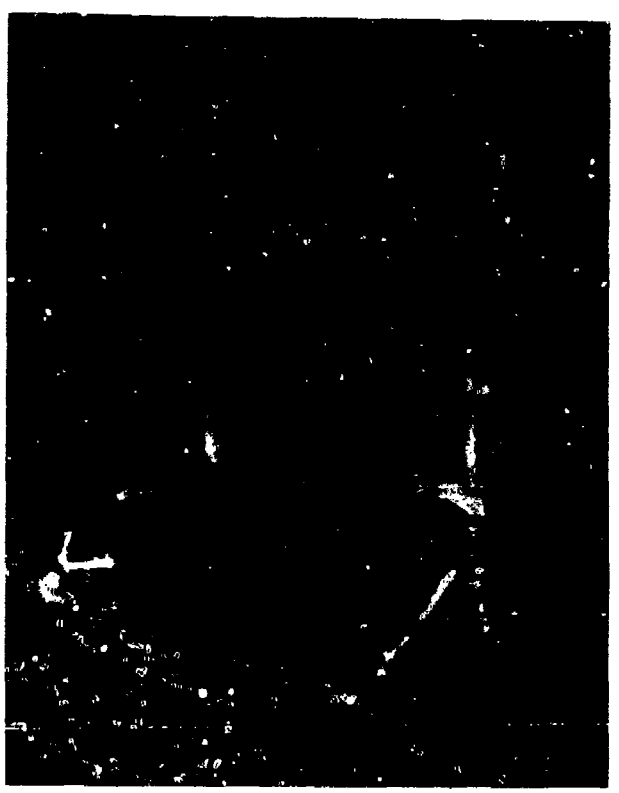

FIGURE 17 Actual Burn Progression Involving Three Mid-Engine Stages

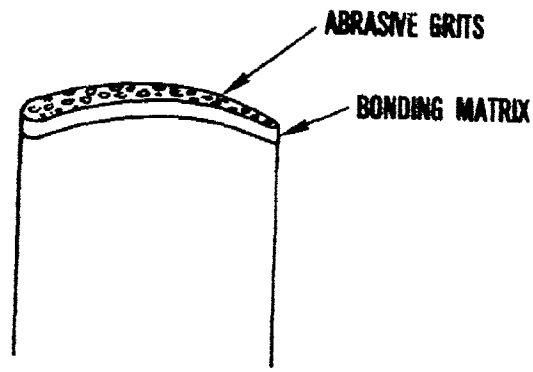

FIGURE 19 Abrasive Blade Tip

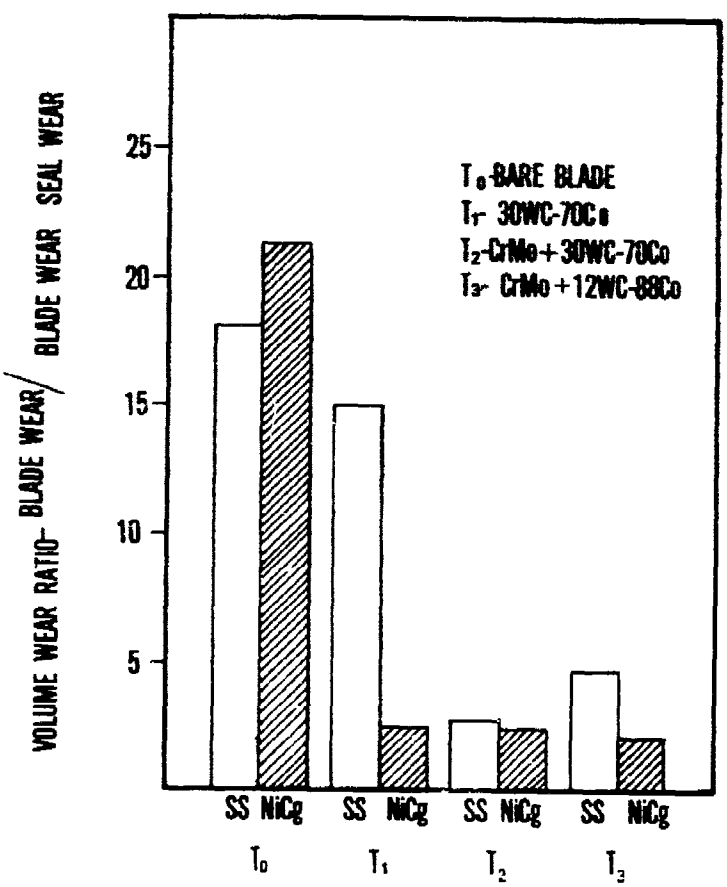

FIGURE 20 Comparative Wear of Blade Tip Treatments

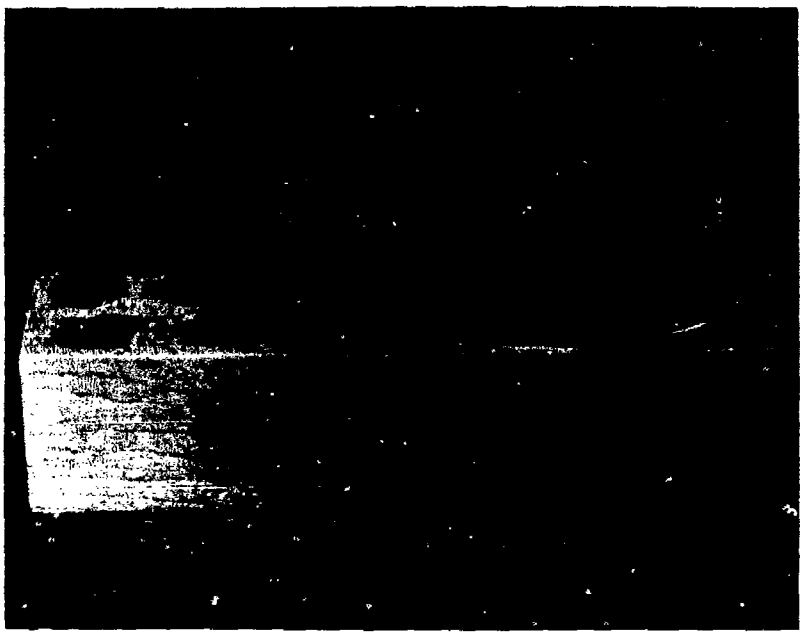

FIGURE 21 Propagation with Ti Blades and Steel Vanes

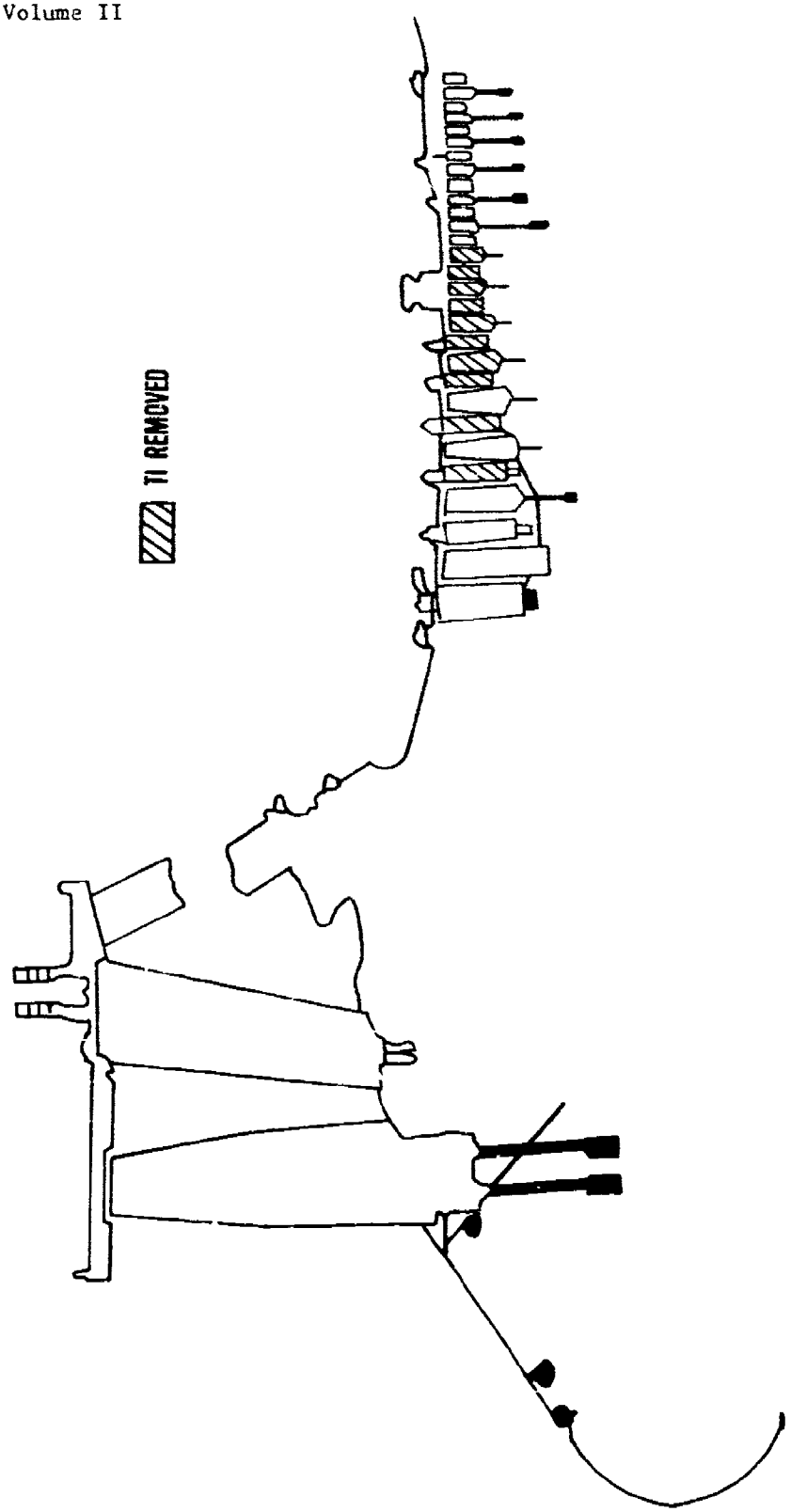

Figure 22. Typical Components Involving Titanium Removal

TABLE 3 TITANIUM ALLOYS

Common Alloys	Remarks
6Al - 4V 8Al 1V 1 Mo 6Al 2Sn 4Zr 2 Mo 6Al 2Sn 4Zr 6 Mo	• Burn relatively easily • Burn Equally well • Commonly used turbine engine alloys
Beta Alloys 3Al 8V 6Cr 4 Mo 4Zr 3Al 8V 7Cr 4 Sn 1Zr 3Al 15V 3Cr 3 Sn	• Less combustible than common alloys • Possible vane or case application
Aluminides	• Combustible up to 24 wt. % • High Al content non-combustible/poor ductility
Low Melting 13 Cu 1.5 Al 13 Cu 5 Mo 9 Fe 11 Co	• Developmental castable alloys • Less combustible than common alloys

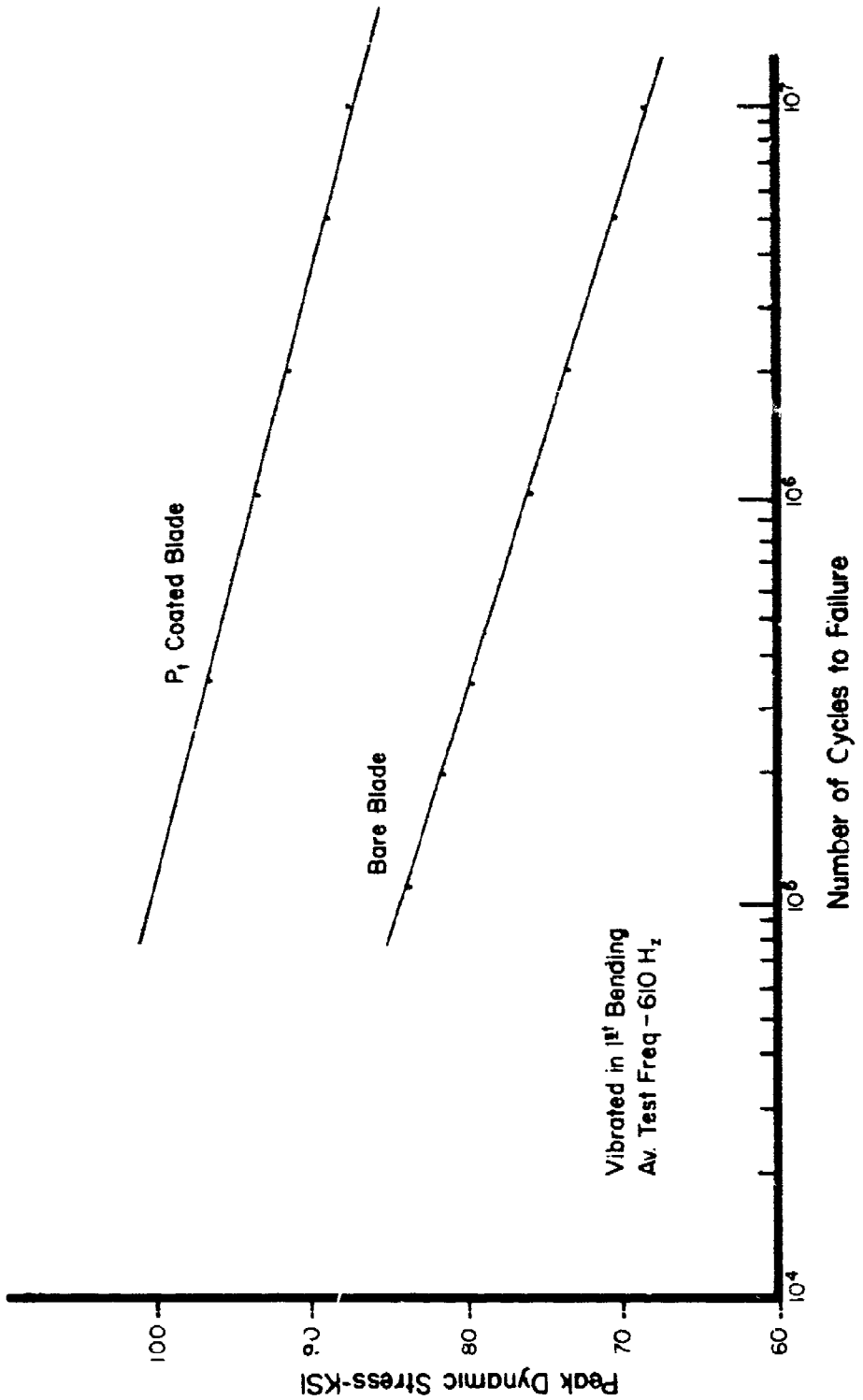

FIGURE 23 Fatigue Strength Improvement of Pt Coated Blades

TABLE 4 FIRE EXTINGUISHING AGENTS

Agent	Remarks
Carbon Dioxide	Burn rate increased 50% at 23% concentration
Nitrogen	Support titanium combustion
Foam	Ineffective for titanium fires
Carbon Tetrachloride	Ineffective for titanium fires
Water	Considered hazardous when used on titanium fires
Dibromadifluoromethane - CBr_2F_2	May support combustion when accompanied by airflow
1,2,2 trifluoropentachloropropane $C Cl_3CF_2CFCl_2$	May support combustion when accompanied by airflow
1,1,1 trifluorobromachloroethane $CF_3CHBrCl$	May support combustion when accompanied by airflow
Bromotrifluoromethane $CBrF_3$	May support combustion when accompanied by airflow
Bromochloromethane CH_2BrCl	Best of the halogens
Met-L-X Powder - NaCl+	NAPA suggests agent has been used successfully
Trimethoxyboroxine (TMB)	Found more effective than Met-L-X
Pyrene G-1	Effective if spread evenly over the fire
Dow 230 Flux	Copious quantities can control fire
Dolomite	Powder spread until fire extinguishes
Graphite	Powder spread until fire extinguishes
Sand	Has been used on titanium turnings - fine, dry

AFWAL-TR-81-4019
Volume II

COMPUTER MODELING OF TITANIUM COMBUSTION

M. R. Glickstein
Pratt & Whitney Aircraft Group
Government Products Division
West Palm Beach, Florida

ABSTRACT

Titanium and its alloys are known to undergo self-sustained combustion when ignited in aerodynamic environments. Energy in several forms, i.e., radiation, frictional heating, or aerodynamic heating can be sufficient to bring the material to the condition where self-sustained combustion can occur. This phenomenon is of interest in the aircraft industry because of the extensive use of titanium in aircraft propulsion systems.

An extensive program of analytical and experimental investigation has been in progress for the past four years to establish the parameters that govern the ignition and self-sustained combustion of titanium in propulsion system environments. An analytical model is being evolved to predict this ignition and subsequent propagation of combustion of titanium alloys. The model uses finite-element and time-marching techniques to produce simultaneous solutions of the equations governing heat and mass transfer in the aerodynamic boundary layer, transient thermal conduction in the solid metal, phase change and liquid metal flow over the solid surface. Appropriate models describe the oxidation kinetics at the metal surface, flow of liquid metal due to aerodynamic shear and centrifugal body forces, and diffusion of oxides within the molten metal. The model allows prediction of metal ignition due to a variety of sources, i.e., radiation, frictional heating, and exposure to high ambient temperatures.

The analytical model and its development over the past three years is described, and an analytical simulation of a propagating fire is compared with experimental data.

IN ODUCTION

Titanium and titanium alloys are used extensively in aerospace systems because of their high strength-to-density ratio, temperature resistance and excellent corrosion behavior. Titanium alloys have been widely applied to aircraft structural components, and to turbine engine and compressor parts. As titanium alloys have found application in different environments, especially at increasingly higher temperatures and pressures, a renewed interest has developed in their ignition and combustion behavior in air.

Within the last ten years, the incidence of titanium fires in gas turbine engines has markedly increased. Most frequently, catastrophic massive-metal fires have been observed during test cell performance evaluations. A number of factors are involved in this trend; most notably, the increase in thrust-to-weight ratio of current engines. Lower weight demands a more flexible engine and lighter components and these factors, when added to the desire for more thrust, result in increased pressure, temperature and flow, providing an environment conducive to ignition, self-sustained combustion and propagation of a titanium fire.

To date, the primary remedy has involved substitution of steels for selected titanium parts, with a resultant weight penalty, and an increase in the rotor/stator clearances with a resulting performance penalty. As these penalties may be unacceptable in certain "performance-driven" military systems, the Air Force has initiated a program to understand the phenomena and develop materials approaches to eliminate catastrophic failure.

This program includes several studies to consider various types of ignition, such as rubbing or rapid heating, and to investigate and model self-sustained combustion of titanium alloys in the gas turbine engine compressor environment.

Glickstein, et al. (Reference 1), reported the early development of an analytical model to simulate the ignition and propagation of titanium fires on massive blade-like shapes in flowing gas. Given a rectangular or airfoil shaped titanium alloy specimen in a compressor environment, and sufficient energy for ignition at a corner or edge, several factors will determine whether propagation occurs. The combination of gas-temperature, pressure and velocity control the concentration of reactants at a combusting surface, the aerodynamic shear for removal of melted materials, and the convective cooling of the surface. No prior efforts have determined the dependence of ignition or propagation on these factors. The objective of this effort was to develop an understanding of the interrelationships of the importance factors governing ignition and combustion propagation over a broad range of environmental conditions.

Since the publication of Reference 1, development of the model has continued, evolving an analytical tool for predicting the fire sensitivity of titanium in a wide variety of aerodynamic applications.

ANALYTICAL MODEL

To provide a procedure for predicting the fire susceptibility of titanium structures in aerodynamic environments, an analytical model was developed based on experimental observations (Reference 1). This model, while considering most of the observed phenomena of a propagating fire, was somewhat limited in its treatment of certain details of the process, as evidenced by comparison with test data. Furthermore, it was not capable of treating rotating airfoils, with the added complexity of centrifugal forces combining with aerodynamic shear forces in causing the removal of molten material.

In order to clarify the relationship of combustion rates, total damage and ignition, it is important to consider the entire ignition-propagation sequence with regard to the local environment. Based on observation of high speed movies and applied to a gas turbine engine environment, the following scenario can be developed to describe the titanium fire phenomena: A titanium specimen is exposed to and is in thermal equilibrium with an aerodynamic environment. Heat generated by

normal oxidation is balanced by losses to the surrounding environment. An ignition initiation event creates an imbalance in this equilibrium system. Such an event may take one of several forms, i.e., heat input due to mechanical friction, thermal radiation, aerodynamic heating or fracture which produces an atomically fresh surface. In response to one of these events, metal temperature increases in the region of heat input, resulting in increased heat generation from oxidation. Heat loss to the environment and to the sample increases accordingly to establish a new equilibrium state. If thermal equilibrium is reached with the local metal surface temperature below its melting point, ignition does not occur, and the system returns to its original state when the ignition source is removed. If melting occurs, the material ignites and, with removal of the ignition source, may cease burning if the thermal balance is insufficient to supply the necessary latent heat to continue local melting. If the rate of local heat generation is greater than the rate of losses, self-sustained combustion occurs. In the case of self-sustained combustion and subsequent propagation, test results demonstrate that a significant amount of molten material is generated at the leading edge of the specimen and adheres to and flows over the surface in response to aerodynamic forces. This flowing liquid, with considerable dissolved oxygen, continues to react as it flows, thereby maintaining its liquid state and providing additional energy to the specimen by conduction. The adherence of this molten metal in certain environments is critical to the maintenance of self-sustained combustion, and is the principal mechanism for propagation of titanium combustion at moderate-to-great airstream velocities. In general, the transport of energy along the surface in the molten flow far exceeds the capability for heat loss by conduction with the solid substrate. A more accurate description of this process must come from analytical modelling.

A. The Physical System

Figure 1 illustrates a compressor rotor blade with ignition at the airfoil leading edge and fire propagation across the blade surface. This figure shows the salient features of the process, with molten metal streaming from the leading edge of the burning zone to the downstream edge of the "melt" region, henceforth called the melt leading edge. The aerodynamic leading edge is called the stagnation region.

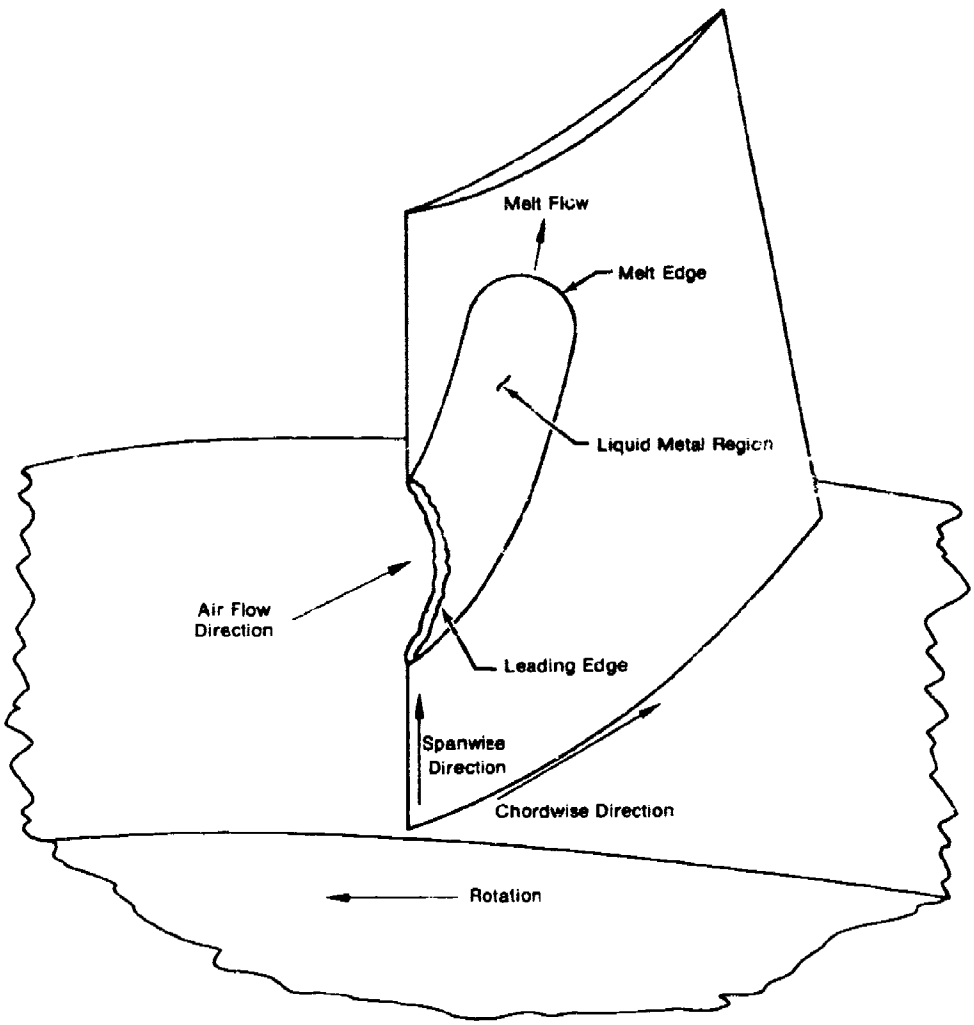

Figure 1. Features of a Burning Compressor Rotor Blade

Comparison of liquid metal velocities, evaluated from photographic data, with thermal diffusion rates in the solid airfoil substrate indicate that liquid metal flow is the primary mode of thermal propagation in a buring airfoil.

In the refined model, described herein, the detailed structure of the melt flow is examined, and a model developed for simultaneous transport of momentum, heat, and oxygen species from the liquid surface to the liquid-solid interface. The effects of oxides on the relevant physical properties are incorporated in the model, within the limitations of available data. Continuity relations are developed in integral form to allow evaluation of the melt flow processes over the surface of the airfoil. Aerodynamic melt loss considerations are included in the continuity equations, and a suggested loss model is proposed. Finally, the model geometry is expanded to incorporate the effects of centrifugal forces generated by rotation, as in the case of compressor rotors.

B. ANALYTICAL APPROACH

The gross feature of the model consists of the analysis of two regimes, the solid metal structure and the overlying liquid metal film, linked and interacting thermally. The interaction between these two regimes governs the rate of melting of the solid substrate and the rate of fire propagation over the airfoil surface. Thermal analysis of the substrate is based on a finite element technique, and evaluation of the flowing liquid metal is based on integral methods of streamline analysis. Details of the methods are described in Reference 2.

Analysis of the processes associated with each regime proceeds in a time marching fashion, with alternate evaluation of each regime at each time step.

Energy enters the system from external sources (convection, radiation, mechanical friction) or is generated by reaction at the air-metal interface. The principle reactions in the titanium-oxygen system are assumed to occur at the metal-gas interface. Energy is lost from the burning surface by

convection and radiation to the surroundings, and by conduction into the substrate. The net balance of these energy flows governs the rate of melting of the solid substrate.

The reaction rate at the metal surface, either as slow oxidation or as rapid combustion, is governed by the rate at which oxygen can flow from the air to the surface and bond with free metal in the substrate. The overall process is governed by the most restrictive step in the foregoing chain of events. The most restrictive step is dependent on the surface temperature, amount of surface oxides, and the nature of the boundary layer mass diffusion process.

The governing process is assumed to be the most restrictive of the following: (1) oxygen diffusion through the surface oxides at low temperature (parabolic kinetics), dependent on surface temperature and amount of accumulated oxides, (2) linear kinetics at high temperatures, dependent on surface temperature only, or (3) oxygen diffusion rate through the aerodynamic boundary layer.

Parabolic or linear kinetics are assumed to occur on the solid surfaces, but based on experimental observations, the rate controlling process during combustion appears to be oxygen diffusion through the aerodynamic boundary layer. The details of the assumed kinetics are described in References 1 and 2.

The corresponding reaction rate at the surface is:

$$g_r = H_\infty \frac{dM}{dt} \qquad (1)$$

where H_∞ is the heat of reaction per mass of oxygen, based on the reaction assumed to occur at a particular condition. Post-test analysis of burned airfoil specimens indicated the primary reaction product resulting from slow oxidation is TiO_2 while rapid combustion results in approximately equal weights of TiO and Ti_3O_5. The corresponding heats of reaction have been incorporated in the model, i.e., TiO_2 is assumed to result from solid surface oxidation, while 50% TiO-Ti_3O_5 is assumed to result when combustion occurs on a molten surface.

C. Thermophysical Properties

The physical properties of titanium relevant to the overall combustion model include the thermodynamic properties, defining the state and internal energy, and the transport properties, defining the rate of the various transport processes. These properties in general are dependent on the metal temperature, alloying elements and amount of oxygen present, and the crystalline structure. Because of insufficient data, the present analysis has not included alloying effects, but has as far as possible included the effect of temperature, phase, and oxygen content. The effect of temperature and oxygen content are considered in evaluating the melt viscosity and thermodynamic state, and the effect of temperature is considered on the thermal conductivity and oxygen diffusivity.

Figure 2 shows a phase diagram for the titanium-oxygen system, developed by Schofield and Bacon (Reference 3). Oxygen in titanium is seen to act as a phase stabilizer resulting in the occurrence of α-Ti at temperatures above the normal α-β transition, and increasing the liquidus temperature significantly. It is further noted that the presence of dissolved oxygen causes the occurrence of a solidus-liquidus temperature range, or two-phase region, at low concentrations.

A corresponding thermodynamic phase diagram was constructed, based on thermodynamic data for pure titanium (Reference 3).

The presence of oxygen is assumed to act only as a phase-stabilizer causing the effect of the energy of α-β transition to be shifted to the melting temperature range. While the resulting enthalpy diagram, shown in Figure 3, may not be entirely correct, it provides a workable basis for modeling the heat transfer through the melt flow.

The net effect of oxygen diffusion into the liquid film is to produce a thickened suspension of solid particles in the outer region of the film. The suspending liquid retains the properties of pure liquid at the equilibrium temperature, and the overall effect of the suspended solids is an increase in the viscosity. Basing the viscosity of the liquid on the data

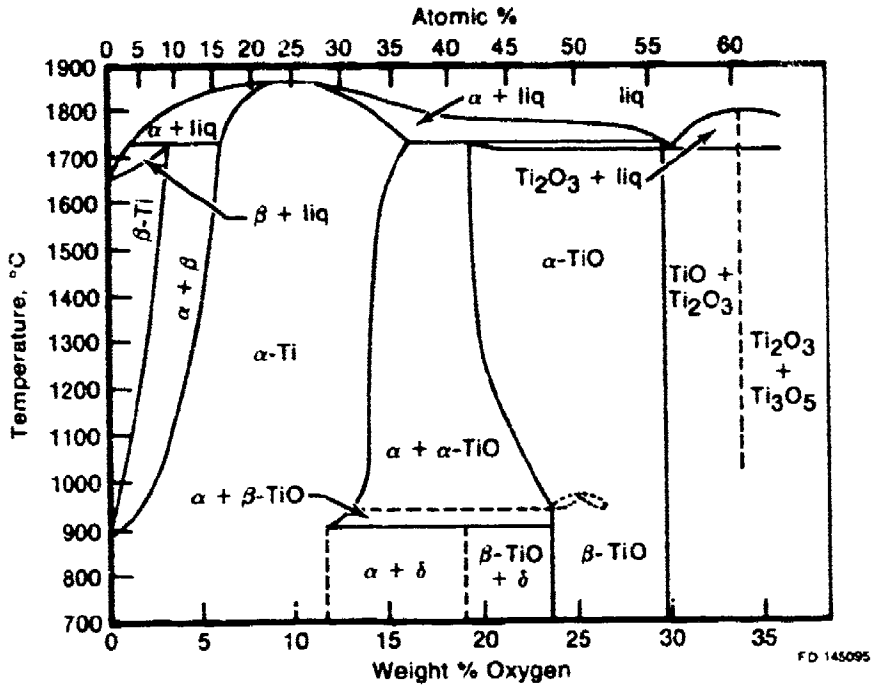

Figure 2. The Ti-O Phase Diagram Up to 35 Wt % Oxygen After Schofield and Bacon

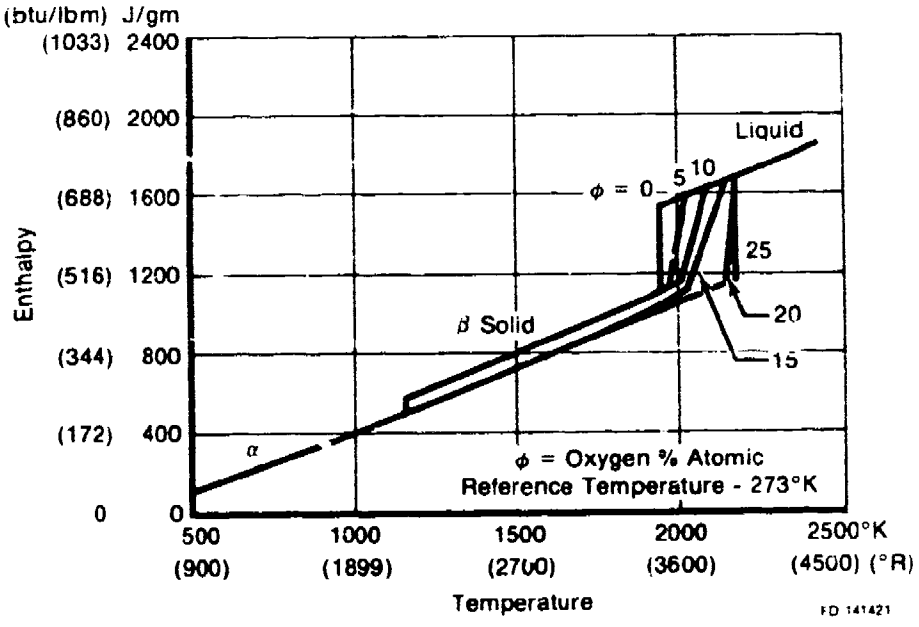

Figure 3. Enthalpy of Titanium-Oxygen System as Function of Temperature

of Orr (Reference 5), a model for the viscosity of molten two-phase titanium takes the form:

$$\frac{\mu}{\mu_o} = \frac{\left[1 - 2.86\left(\frac{H_{l_1} - H_l}{H_{l_1} - H_{s_1}}\right)\right]^{1.8}}{\left[1 + 7.54 \times 10^{-3}(T - T_o)\right]} \qquad (1)$$

where μ_o is the dynamic viscosity of liquid titanium in the oxygen-free condition at the melting temperature T_o, μ_1 is the voscosity at temperature T_1 and oxygen concentration ϕ_1 (H_1, H_{ℓ_1}, H_{s_1}) are the enthalpies at concentration ϕ_1 and respective temperature T_{ℓ_1} and T_{s_1}, liquidus temperature and solidus temperature.

Data is not available on the effect of oxygen on the other transport properties in the liquid state, nor for that matter for pure titanium in the liquid state. The data of Roe, Palmer, and Opie (Reference 6) for oxygen diffusivity in titanium is extrapolated to the melting temperature, and treated as temperature dependent only. The data of Touloukian (Reference 7) for thermal conductivity is treated in the same manner.

D. Structure of the Melt Flow

In the flowing melt region a liquid layer of thickness δ is assumed to flow on the surface, driven by aerodynamic forces in the direction of air flow, and by centrifugal forces in the radial outward direction. Oxygen flows in the aerodynamic boundary layer to the liquid surface, reacts with the melt, and the resulting heat and oxides diffuse into the melt layer. Shear stress across the melt is assumed constant, and momentum transport is considered small by comparison. Figure 4 illustrates the features of the flowing liquid layer. The coordinates (x, y, z) are in the chordwise, normal, and spanwise directions, respectively. The velocity components (u, v) represent the local liquid velocity in the two surface directions and are seen to vary with distance from the surface. The temperature and oxygen concentration at the outer surface are T_1 and ϕ_1, and at the inner surface are T_o and ϕ_o. Oxygen flows into the melt layer at a rate $\dot{m}_o$, and the liquid-solid interface recedes or advances (melting or solidification) at a velocity U.

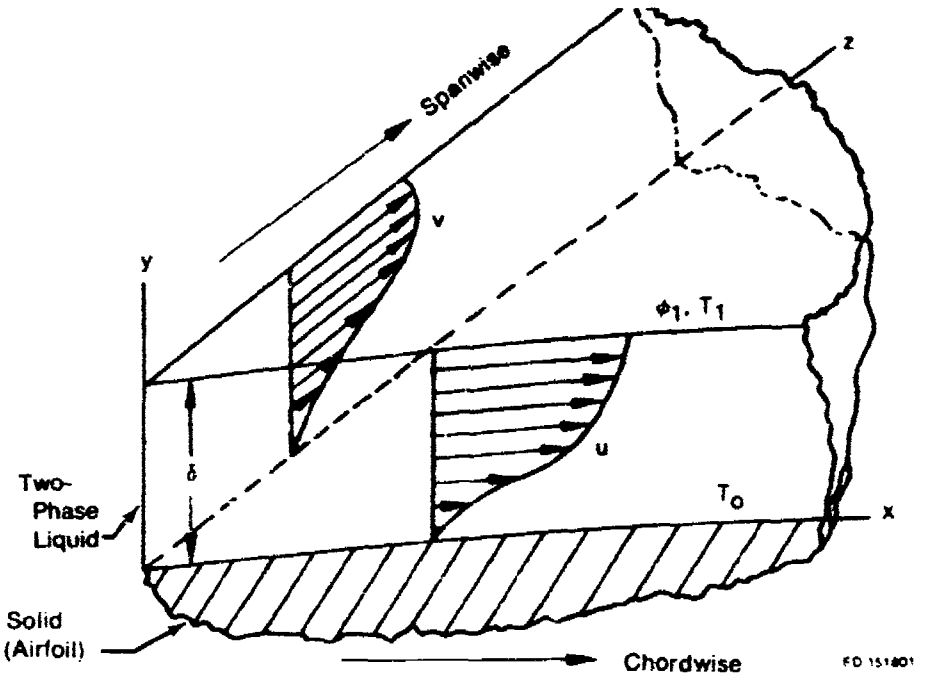

Figure 4. Features of Liquid Flow Model

Melting is assumed to occur at the solid-liquid interface in the oxygen-free state. Diffusion of oxygen into the liquid from the reaction surface results in the precipitation (re-solidification) of oxygen-rich titanium from the melt, as shown in Figure 5. Thermodynamic and phase-equilibria are assumed during this process.

The solidified material is assumed to occur in distributed particulate form, in thermal equilibrium with the oxygen-free liquid. Figures 6 and 7 show the thermodynamic and phase relations of the state points defined in Figure 5. States (a) and (b) correspond to oxygen-free titanium, and (c) is the condition at the air-melt interface. In Figure 6, state C corresponds to the condition in the melt at the air-melt interface if there were no oxygen diffusion. The temperature at C' is T'_1, determined by one-dimensional conduction without heat sinks. Solidification is assumed to be a net constant energy process, i.e., the local enthalpy of the liquid-solid system remains constant as solids precipitate. Solids and liquid are in local thermal equilibrium and the solidification process

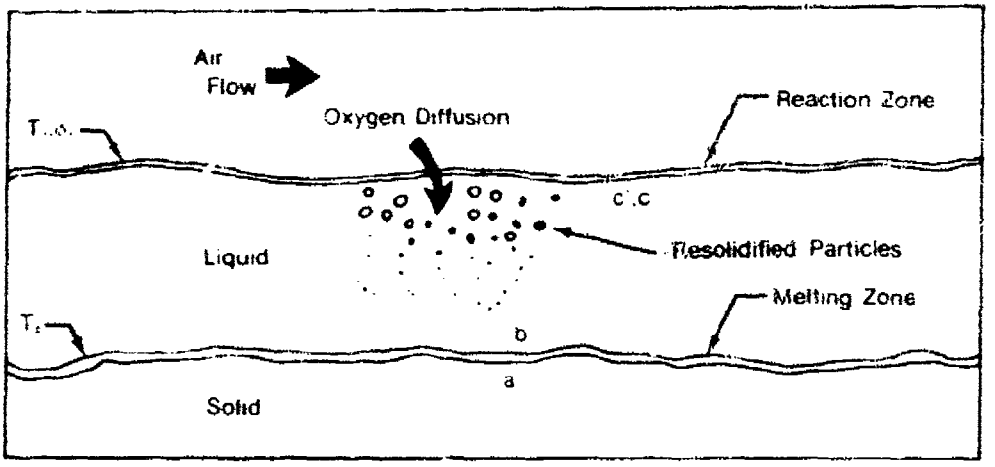

Figure 5. Features of Melting-Diffusion Model

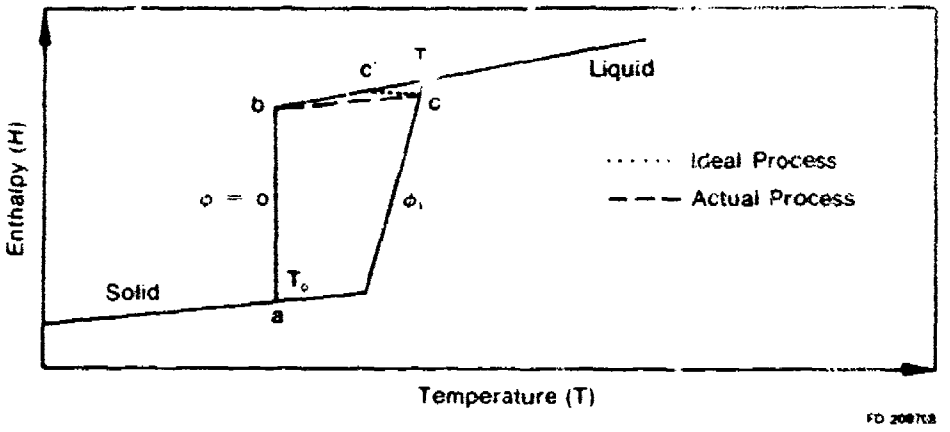

Figure 6. Thermodynamic Model of Melting-Diffusion Process

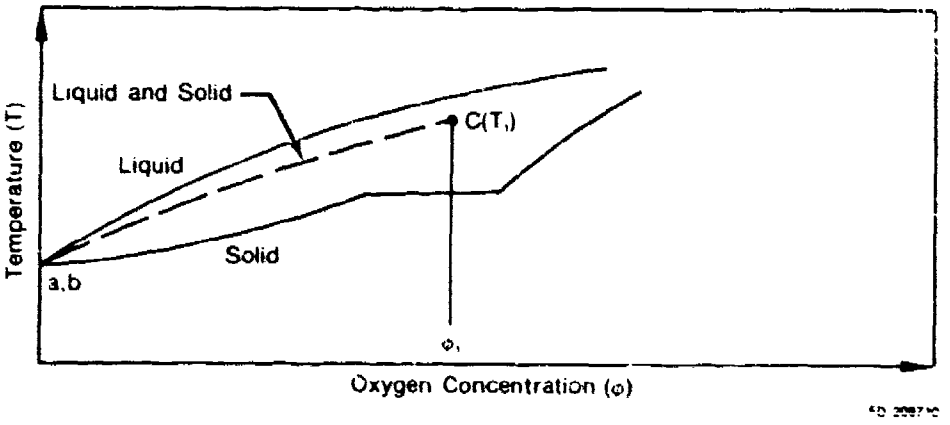

Figure 7. Phase Model of Melting-Diffusion Process

is accompanied by an increase in temperature due to release of the heat of fusion. The idealized process path is C'-C, in Figure 6. The final equilibrium temperature at state C is T_1.

E. INTEGRAL TRANSPORT EQUATIONS

In Figure 1 the melt region is illustrated with a single streamline. The melt flow field can be considered as composed of a set of streamlines originating in the stagnation region and ending at the downstream edge of the melt region, as shown in Figure 8. If a coordinate system is described by (S,J), where S is the distance along the streamline and J is the streamline number, analysis of the melt flow can be performed along each streamline. Let the liquid flow rate in a streamline at a point (S,J) be $\rho\bar{F}$, then $\bar{F}$ is a vector quantity aligned in the direction of the streamline. The flow vector $\bar{F}$ can be described as composed of components (f) in the chordwise and (h) in the spanwise directions. Thus,

$$\bar{F} = if + jh \tag{2}$$

where i and j are unit vectors in the component directions. The direction of the streamline can be described by the angle (ψ) with the chord, where

$$\tan \psi = f/h \tag{3}$$

The melting airfoil adds to the streamline flow in the amount ρU per unit length of streamline. If the fraction of flow rate lost to the airstream is ξ per unit length, then the rate of change of flow in the streamline is

$$\frac{d\bar{F}}{ds} = \bar{s}U - \xi\bar{F} \tag{4}$$

where $\bar{s}$ is a unit vector in the direction of the streamline, and the derivative is taken in the direction of flow. This expression can also be written in terms of the flow components as:

$$\frac{df}{ds} = U \cos \psi - \xi f \tag{5a}$$

$$\frac{dh}{ds} = U \sin \psi - \xi h \tag{5b}$$

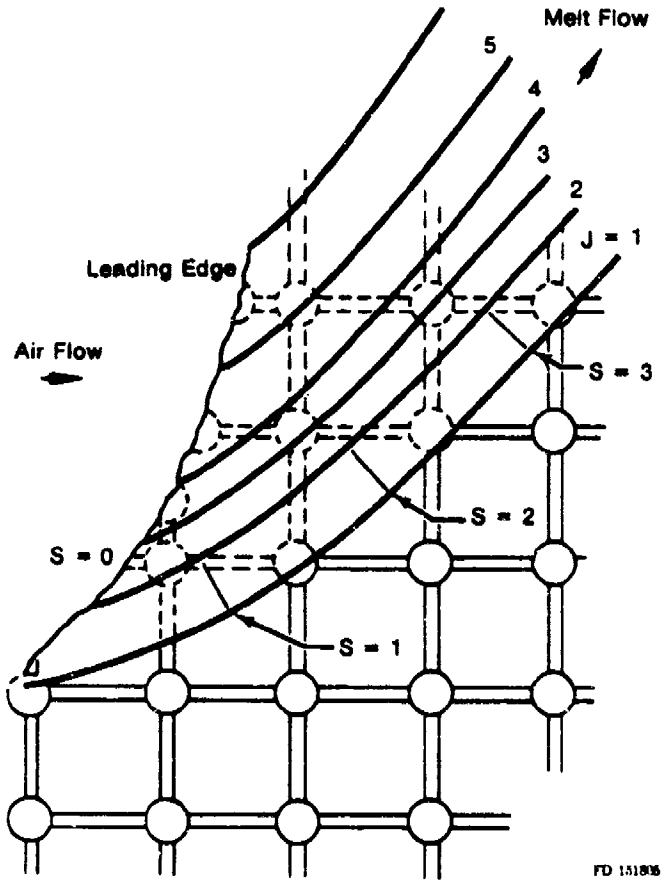

Figure 8. Streamline Coordinate System

In a similar fashion, the flow rate of oxygen carried along the surface by the melt is (g), and is related to the melt flow by

$$g = \rho F \bar{\phi} \tag{6}$$

where

$$F = \sqrt{f^2 + h^2}, \tag{6}$$

and $\bar{\phi}$ is the local bulk concentration of oxygen in the melt.

The rate of change of g along the surface is given by:

$$\frac{dg}{ds} = \dot{m}_o - \xi \phi_1 \rho F \tag{7}$$

The concentration at the liquid surface (ϕ_1) is presumed to describe the average concentration of the melt loss at the surface.

The set of equations (5a, b) and (7), describe the change in liquid mass flow and oxygen content of the streamlines as they flow over the surface.

F. Local Transport Processes

Integration of the integral transport equations requires evaluation of the initial conditions, i.e., values of (f, h, g) at the stagnation point. In addition, these transport functions must be related to the local transport processes to allow evaluation of the physical variables, such as local velocity, temperature, and concentration.

1. Axial (Chordwise) Velocity Profile

The melt flow is assumed to be laminar, with constant shear stress, and with no slip at the liquid-solid interface. Assuming the velocity profile to be represented by a second degree equation:

$$u = a + b\eta + c\eta^2 \tag{8}$$

where

$$\eta = y/\delta$$

The shear stress τ, must be equal to the aerodynamic shear, determined from boundary layer analysis, and is related to the velocity profile by:

$$\tau = \frac{\mu_0}{\delta}\frac{du}{d\eta}\Big|_{y=0} = \frac{\mu_1}{\delta}\frac{du}{d\eta}\Big|_{y=\delta} \tag{9}$$

where subscripts '1' and '0' refer to evaluation at conditions at the liquid and solid surfaces. With the no-slip conditions ($u = 0$, $y = 0$) and Equation (9), the constants in Equation 8 can be determined, yielding the velocity equation:

$$u(\eta) = \frac{\tau\delta}{\mu_0}\eta + \frac{\tau\delta}{2\mu_0}\left(\frac{\mu_0}{\mu_1} - 1\right)\eta^2 \tag{10}$$

The axial component of flow in the streamline (per unit width is:

$$\rho f = \int_0^\delta \rho u dy = \frac{\rho\delta^2\tau}{\mu_0}\int_0^1 \left[\eta + \frac{1}{2}\left(\frac{\mu_0}{\mu_1} - 1\right)\eta^2\right] d\eta \tag{11}$$

Hence

$$f = \frac{\tau\delta^2}{6\mu_0}\left[\frac{\mu_0}{\mu_1} + 2\right] \tag{12}$$

2. Radial Velocity Component

Fluid motion in the radial direction is driven by centrifugal body force (β), and resisted by aerodynamic shear stress (τ_0) due to the motion of the liquid relative to the air stream. A simple analysis, balancing radial forces, shows that the shear stress generated by body forces varies linearly from the liquid surface to a maximum at the solid surface. The aerodynamic shear stress is found to be constant across the melt. The total stress is:

$$\tau = \beta\delta(1-\eta) - \tau_0 \tag{13}$$

where

$$\beta = \rho \bar{R} \omega^2 \quad \text{and} \quad \tau_0 = C_f \frac{\rho_a v_i^2}{2} \tag{14}$$

The centrifugal force depends on the radius to the blade midspan ($\bar{R}$) and the rotational speed (ω) of the compressor stage. The aerodynamic shear stress, is a function of the local friction coefficient (C_f) and the relative liquid velocity at the air-liquid interface (v_l). Approximating the velocity profile by a second degree polynomial,

$$v(\eta) = a + b\eta + c\eta^2 \tag{15}$$

the laminar relation between shear stress and velocity gradient is combined with Equation 13 and integrated to yield the velocity profile:

$$v(\eta) = \frac{\beta\delta^2}{\mu_0} \left[\eta - \frac{\eta^2}{2} \right] - \frac{\tau_0 \delta}{\mu_0} \left[\eta - \frac{1}{2} \left(\frac{\mu_0}{\mu_1} - 1 \right) \eta^2 \right] \tag{16}$$

the surface velocity (v_l) is determined by combining Equations 14 and 16, for $\eta = 1$, yielding:

$$v_l = \frac{-1 + \sqrt{1 + \rho_a C_f \beta \delta^3 \left(\frac{\mu_0}{\mu_1} + 1 \right)}}{\frac{\rho_a \delta C_f \left(\frac{\mu_0}{\mu_1} + 1 \right)}{2 \mu_0}} \tag{17}$$

The radial flow component is now calculated in the same manner as the axial component, resulting in the relation:

$$h = \frac{\beta\delta^3}{3\mu_0} - \frac{\tau_0 \delta^2}{6\mu_0} \left(\frac{\mu_0}{\mu_1} + 2 \right) \tag{18}$$

3. Oxygen Concentration Profile

The distribution of oxygen mass function (ϕ) is assumed to be a third order power function of the distance from the solid surface:

$$\phi(\eta) = a + b\eta + c\eta^2 + d\eta^3 \tag{19}$$

The coefficients are evaluated by satisfying the following conditions at the solid and liquid surfaces:

a. Flow rate of oxygen into the liquid surface is equal to the diffusion rate into the melt.

b. Diffusion rate in the liquid goes to zero at the solid-liquid interface.

c. The oxygen concentrations in the liquid and solid are zero at the interface.

The resulting concentration profile must be related to a reference value. Relating to the liquid surface:

$$\phi(\eta) = (3\phi_1 - \Gamma)\,\eta^2 + (\Gamma - 2\,\phi_1)\,\eta^3 \tag{20}$$

where $\Gamma = \delta\,\dot{m}_0/\rho\,D_1$, and D_1 is the oxygen diffusivity at the surface temperature T_1.

The bulk concentration, $(\bar{\phi})$, is obtained by integration of the product of the velocity and concentration profiles:

$$\bar{\phi} = \frac{\int_{\eta}^{1} \phi \bar{V} d\eta}{\int_{\eta}^{1} \bar{V} d\eta} \tag{21}$$

where $\bar{V}$ is the liquid velocity vector. Combining Equations 10, 16, and 20, and performing the integration indication indicated in 21 yields a relationship between the bulk and liquid surface concentrations $(\bar{\phi}, \phi_1)$. The surface concentration is the positive root of the following quadratic equation:

$$F_1\,\phi_1^2 - 2F_2\,\Gamma\,\phi_1 + 2\,\Gamma^2 - 100\,\bar{\phi}^2 = 0 \tag{22}$$

where

$$F_1 = \left[\frac{13 + 8\psi}{2 + \psi} \right]^2 + \left[\frac{13B - 13\pi - 8\pi\psi}{2B - 2\pi - \pi\psi} \right]^2$$

$$F_2 = \left[\frac{13 + 8\psi}{2 + \psi} \right] + \left[\frac{13B - 13\pi - 8\pi\psi}{2B - 2\pi - \pi\psi} \right]$$

$$B = -\frac{\beta\delta}{\tau} \; ; \pi = \frac{\tau_o}{\tau} \; ; \psi = \frac{\mu_o}{\mu_1}$$

G. SURFACE MELTING RATE

Heat transfer into the flowing melt consists of the sum of several components, heat generation due to chemical reaction at the surface, discrete surface heat input (i.e., laser radiation), and convective and radiant exchange with the surrounding environment.

The net difference between these heat flows, and the heat flow into the solid substrate by conduction, determines the rate of melting of the substrate. Writing an energy equation for the solid-liquid interface in generalized vector form:

$$\rho H_{sl} \bar{U} = \bar{q}_s - \bar{q}_k \qquad (23)$$

where

$\bar{U}$ = velocity of melting surface

$\bar{q}_s$ = net surface heat flux normal to surface

$\bar{q}_k$ = conduction heat flux into solid substrate

H. STAGNATION REGION ANALYSIS

Integration of Equations 5 and 7, with evaluations of the corresponding local processes, defines the development of melt flow over the airfoil surface. However, this evaluation requires that conditions at the stagnation point be known to provide initial conditions for the integration. Specifically, these quantities are required to start the calculation, the melt thickness (δ), the bulk concentration ($\bar{\phi}$), and the melting velocity at the leading edge (U). Figure 9 shows a cross-sectional view of the leading edge with the relevant features.

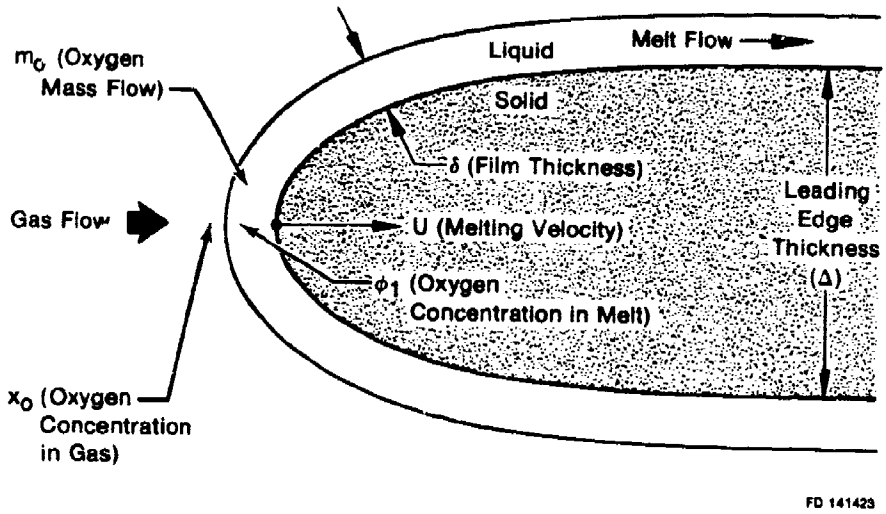

Figure 9. Stagnation Point Region of Burning Airfoil

Based on post-test examination of burned specimens, the cross-sectional shape of a melting leading edge will be considered an elliptic cylinder with an aspect ratio R (width/length).

The initial concentration is determined by expanding Equation 7, taking the limit as S→0, and noting that the aerodynamic shear stress vanishes at the stagnation point. This results in an expression for the bulk stagnation concentration:

$$\bar{\phi} = \frac{\dot{m}}{\rho U} \tag{24}$$

Consider the starting point for streamline (J=1) in Figure 8, noting that the leading edge is yawed to the direction of airflow. Figure 10 shows a large planform view of the leading edge and the relative directions of the various heat fluxes and the melting velocity.

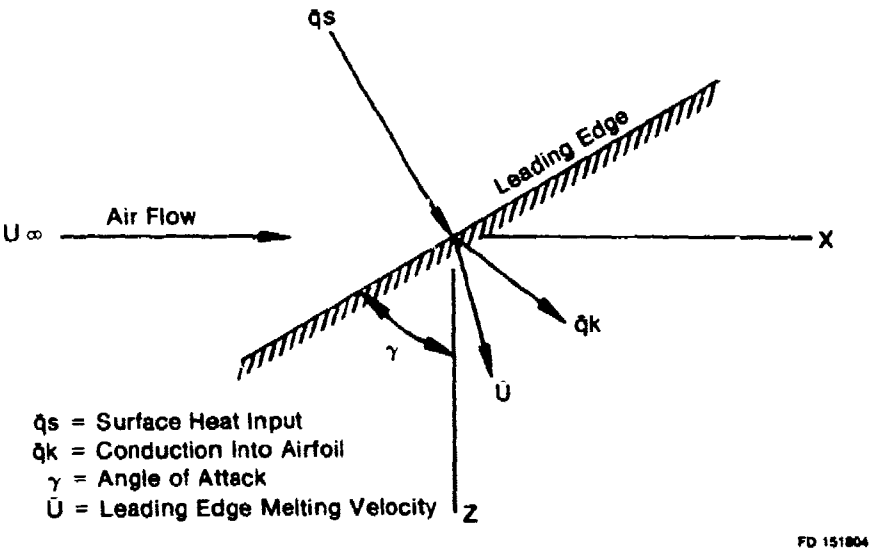

Figure 10. Heat Flow and Velocity Relationship at Burning Leading Edge

The leading edge is at a yaw angle (γ) to the airstream. The surface heat flux ($\bar{q}_s$) is normal to the leading edge, and the internal conduction flux ($\bar{q}_k$) points in the direction of maximum temperature gradient in the solid. The magnitude and direction of the melting velocity is determined by the vector addition defined in Equation 23. It is worthy of note that the melting velocity at the leading edge lies in the plane of the airfoil leading edge at an angle defined by the heat transfer. Over the remainder of the airfoil surface the melting velocity vector is oriented normal to the airfoil surface, since the surface and internal fluxes are aligned everywhere except at the leading edge. It is the effect of the internal conduction term in Equation 23 that controls the relative burning rates in the chordwise and spanwise directions, observed in the combustion tests.

The initial melt thickness is found by taking Equations 5a, b to the limit at the stagnation point. Writing these equations in terms of components normal to the leading edge, and considering the variation of aerodynamic shear stress and centrifugal force as the stagnation point is

approached, an expression is derived relating initial melt thickness to the other parameters at the leading edge. The resulting equation in (δ) is:

$$\frac{\delta^3 \beta \sin\gamma}{R\Delta} + \delta^2 \rho_\infty U_\infty^2 \frac{d C_{f_0}}{dn} \cos^2\gamma = 12 \mu_\infty U \tag{25}$$

where β is defined by Equation 14, R and Δ are the leading edge aspect ratio and thickness. The derivative of the friction coefficient is evaluated at the stagnation point and is found to be a function of R, Δ, and the leading edge Reynolds number.

I. STREAMLINE CONTINUITY

Independent analysis of flow in adjacent streamlines does not implicitly avoid continuity conflicts, such as intersection of streamlines. To ensure that continuity is satisfied, a condition of streamwise continuity is imposed on the solutions for streamline thickness. If the width of a streamline is (W), then continuity requires that (FW) be constant along the streamline, where F is the magnitude of the flow vector. This statement is expressed by:

$$\frac{d}{ds} W^2 (f^2 + h^2) = 0 \tag{26}$$

If local rates of changes of shear stress and body force are considered secondary, Equation 26 can be expanded into:

$$\frac{d\delta}{ds} = - \frac{\delta(f^2 + h^2) \frac{dW}{ds}}{W(2f^2 + 3h^2 + hf \frac{\tau_0}{\tau})} \tag{27}$$

This relation expresses the required correction in the calculated growth of the melt thickness necessary to satisfy streamline continuity.

J. MELT LEADING EDGE FLOW

Analysis of the motion of the liquid front (melt leading edge) over the solid structure requires considerations of the two-dimensional nature of the flow, including effects of both aerodynamic and body forces. Figure 11 shows the melt leading edge region isolated as a free body.

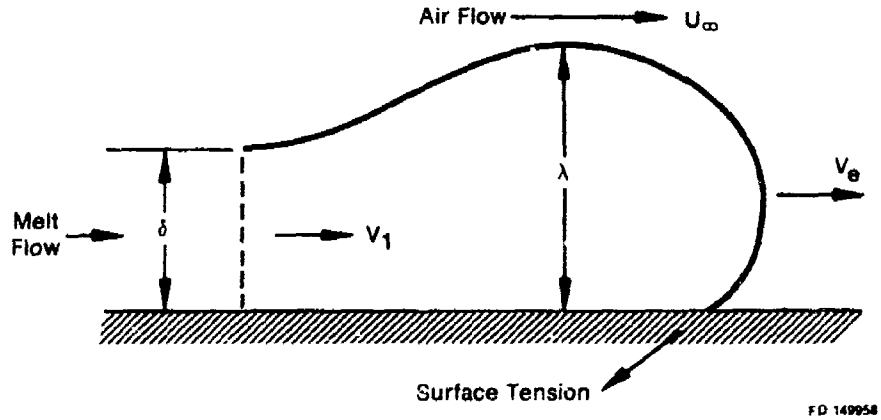

Figure 11. Leading Edge of Melt

The sum of forces acting on the fluid must be zero for steady motion. These forces include the aerodynamic drag force (F_D), the component of surface tension parallel to the solid surface (ζ), and the internal forces due to momentum change in the liquid as its velocity is reduced within the leading edge region (F_{int}). If the liquid velocity is V_1 as it approaches the leading edge zone, and the edge moves at an average velocity V_e, the internal force is equal to the liquid momentum change, or:

$$F_{int} = \dot{m}\,(V_1 - V_e) = \rho\delta V_1\,(V_1 - V_e). \tag{28}$$

Considering continuity of flow

$$\rho\delta V_1 = \rho\lambda V_e = \rho F \tag{29}$$

where F is the magnitude of the flow vector defined in Equation 2. Combining these expressions.

$$F_{int} = \frac{\rho F^2}{\lambda}\left(\frac{\lambda}{\delta} - 1\right) \tag{30}$$

The aerodynamic drag is

$$F_D = C_D \frac{\rho_a U_\infty^2}{2}\lambda\cos^2\psi \tag{31}$$

Summation of forces yields the relation

$$\frac{C_w \rho_s U_e^2}{2} \lambda \cos^2 \psi + \frac{\rho F^2}{\lambda} \left(\frac{\lambda}{\delta} - 1 \right) - \zeta = 0 \qquad (32)$$

This is solved for the leading edge thickness, λ which is then combined with Equation 29 to yield V_e, the velocity at which melted titanium spreads over the airfoil in the direction of the streamlines.

K. COMPUTING PROCEDURES

In general, the program proceeds through several main functional areas for each time increment in the simulation.

These function areas are as follows:

1. Evaluation of temperature field in solid airfoil,
2. Test for occurence of ignition,
3. Analysis of flowing melt processes,
4. Evaluation of spread of melt-covered region,
5. Evaluation of change in airfoil geometry due to melting, and
6. Return to (1).

Figure 12 shows the operational flow and required conditional transfers. Logic diagrams for the various operational blocks are expanded in Reference 8.

L. COMPARISON WITH TEST DATA

Figure 13 shows the comparison of simulation results with photographic data from the combustion test of an uncambered airfoil of Ti 8-1-1. The specimen has a leading edge thickness of 0.012 inch, a midchord thickness of 0.050 inch, and a chord of 1.00 inch. The combustion test was performed with at an air temperature of 800°F and pressure of 90 psia, with a velocity of 400 ft/sec.

While not identical in appearance, the model simulation displays the basic characteristics of the experimental data.

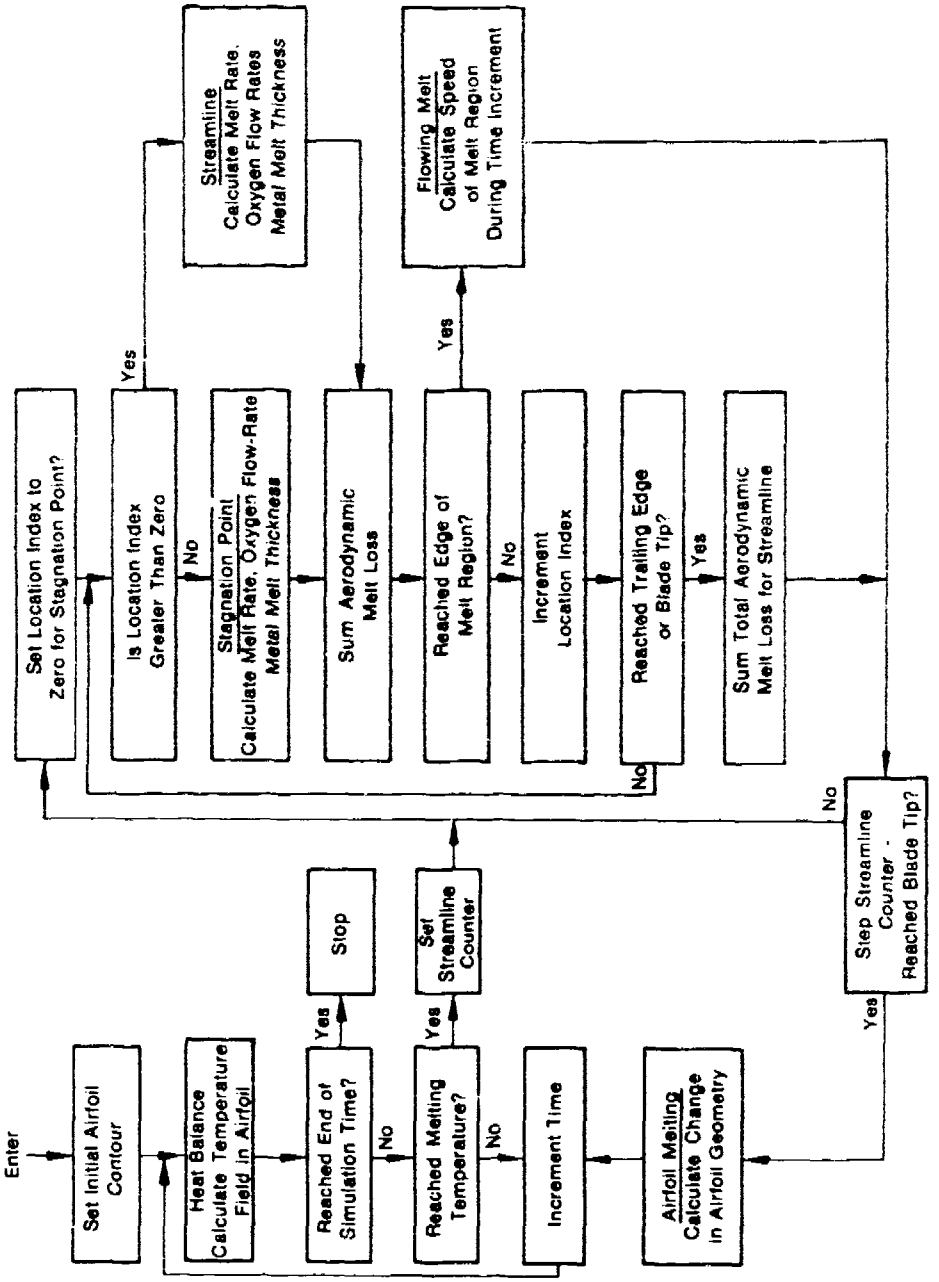

Figure 12. Generalized Combustion Program Logic

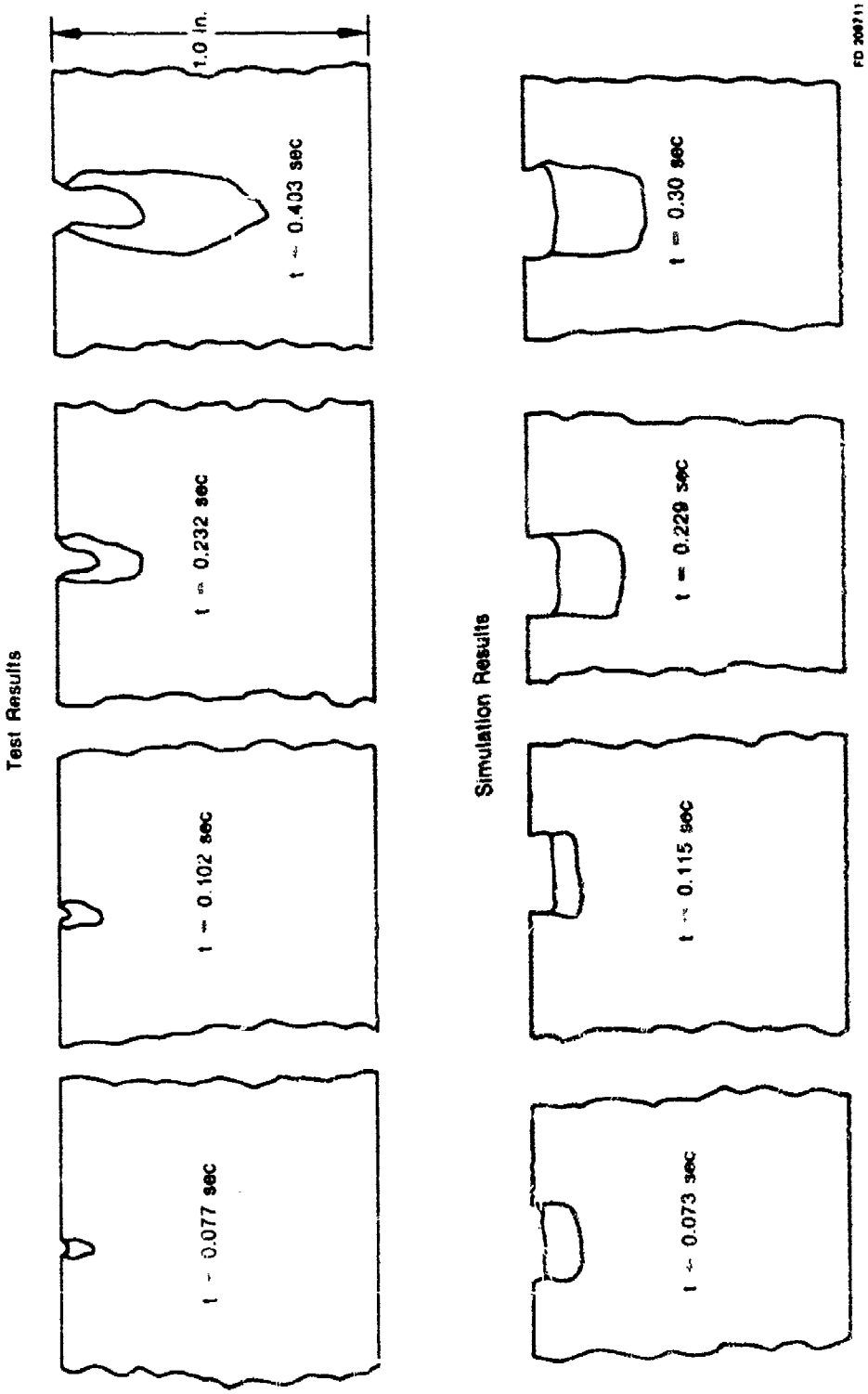

Figure 13. Comparison of Combustion Test and Model Simulation

SUMMARY OF RESULTS

The self-sustained combustion of a selected titanium alloy (Ti-8Al-1Mo-1V), has been investigated over a range of temperatures, pressures and flow-velocities encompassing the typical gas turbine engine compressor environment.

A basic analytical model has been developed to simulate the ignition and self-sustained combustion of stationary titanium alloy airfoils in gas turbine environments, and the model has been programmed for computer evaluation. Preliminary results with the model indicate that it is generally in good agreement with the test data in predicting the lower limits of self-sustained combustion and in simulating liquid metal flow; however, some details of the model required further development to provide a predictive technique generally applicable to a wide range of gas turbine engine environments.

The analytical model was further generalized and programmed for computer solution to include the effects of centrifugal body forces on liquid metal flow and propagation, thus extending its application to analysis of compressor stators and rotors. Also, to provide better agreement with observed experimental behavior, liquid flow models were expanded to include aerodynamic coupling mechanisms controlling loss of melt from the surface, and physical property models were developed to include the effect of absorbed oxygen on thermodynamic and transport properties.

ACKNOWLEDGMENT

Development of the analytical models described in this paper was performed under two subsequent Air Force programs, Contract F33615-76-C-5041 (AFML) and Contract F33615-79-C-2003 (AFAPL).

LIST OF SYMBOLS

Notation

C_D	=	aerodynamic drag coefficient
C_F	=	coefficient of friction
C_p	=	specific heat
D	=	oxygen diffusivity in metal
$\overline{F}$	=	melt flow vector
F	=	melt flow scalar
f	=	chordwise component of melt flow
g	=	oxygen convective flow in melt
h	=	radial component of melt flow
H	=	enthalpy of metal
H_{ox}	=	heat of reaction per unit mass of oxygen
H_f	=	latent heat of fusion
i,j	=	unit vectors in chordwise and radial directions
M	=	mass of oxygen bonded on surface
$\dot{m}_o$	=	oxygen mass flux
n	=	direction normal to surface
$\overline{q}_s$, q_s	=	surface heat flux vector, scalar
$\overline{q}_k$, q_k	=	internal conduction vector, scalar
R	=	leading edge aspect ratio
$\overline{R}$	=	radius to mid-span of blade
S,J	=	streamline position and location indices
s	=	distance along streamline
t	=	time
T	=	temperature in melted metal
T_g	=	gas temperature
T_m	=	melting temperature
T_n	=	node temperature
U	=	melting velocity of surface
U_∞	=	free-stream air velocity
u, v	=	chordwise and radial velocity components (melt)
$\overline{V}$, V	=	liquid metal velocity vector, scalar
W	=	width of streamline
X,Y,Z	=	chordwise, normal, radial coordinate system
β	=	centrifugal body force per volume
γ	=	leading edge yaw angle
Γ	=	mass transport ratio (Eq. 20)
δ	=	liquid metal film thickness
Δ	=	local thickness of airfoil
ζ	=	component of surface tension parallel to surface
η	=	dimensionless distance from solid surface
λ	=	thickness of liquid metal leading edge
μ	=	dynamic viscosity of liquid metal
ξ	=	fraction of melt flow loss from surface
ρ	=	metal density
ρ_∞	=	air density
τ	=	aerodynamic shear stress in chordwise direction
τ_r	=	aerodynamic shear stress in radial direction
ϕ	=	local oxygen mass-fraction in liquid metal
ϕ	=	bulk (mean) oxygen mass-fraction in liquid metal
ψ	=	streamline angle relative to chord
ω	=	rotational speed of blade

LIST OF SYMBOLS

Notation

Subscripts

`	=	solid
'	=	liquid
"	=	liquid-solid interface
'	=	liquid metal-air interface

REFERENCES

1. "Ignition and Self-Sustained Combustion of Titanium Alloys," Third DoD Laser Effects Vulnerability and Countermeasures Meeting, 19 July 1977, San Diego, CA (with B. A. Manty, S. R. Lyon, and C. W. Elrod).

2. "Final Report of Titanium Combustion Research Program," AFML-TR-79-4001, Air Force Materials Laboratory, WPAFB, Ohio, March 1979.

3. Schofield, T. H. and A. E. Bacon, *Journal of the Institute* of Metals, Vol. 84 (1955-56), p. 47.

4. "Casting Properties of Titanium Alloys," O. N. Magnitskiy, 1968, Translation by Foreign Technology Division, WPAFB, 1970.

5. Orr, Clyde, Jr., and Dalla Valle, J. M., "Heat Transfer Properties of Liquid-Solid Suspensions, *"Chem. Eng. Prog. Symposium No. 9*, 1954.

6. Roe, W. P., H. R. Palmer, and W. R. Opie, "Diffusion of Oxygen in Alpha and Beta Titanium," Transactions of the ASM, Vol. 52 (1960) pp. 191-200.

7. Touloukian, Y. S., *Metallic Elements and Their Alloys*, TPRC Databook, Vol. 1, Purdue Research Foundation, Lafayette, Indiana, 1964.

8. "Titanium Airfoil Combustion Program User's Manual for Deck CCD 1152-O.O," AFML-TR-79-4001, Air Force Materials Laboratory, WPAFB, Ohio, March 1979.

AFWAL-TR-81-4019
Volume II

STRESS CORROSION CRACKING IN DEPLETED URANIUM -2 W/O MOLYBDENUM ALLOY PENETRATORS

By C. R. Crowe*

D. F. Hasson**

H. A. Newborn*

J. A. Joyce**

* Naval Surface Weapons Center, Silver Spring, Maryland 20910

** U. S. Naval Academy, Annapolis, Maryland 21402

Abstract

High kinetic energy rounds are required for a variety of defense systems and dense uranium alloys are well suited for this application. A problem area involves storag of the rounds for extended periods in marine environments. Uranium is highly susceptible to general atmospheric corrosion and, more critically, to stress corrosion cracking (SCC). To date, coating schemes have achieved limited success in alleviating these problems. In general, alloying of uranium with elements such as molybdenum, tends to improve resistance to uniform corrosion but results in a multi-phased structure and high SCC susceptibility.

Stress corrosion cracking in alloys in salt laden, moist air environments has been studied by cantilever beam testing. Crack growth kinetics were continuously monitored during the test. Threshold stress intensity values for SCC, K_{1scc}, range from 24.4 MPa.$m^{1/2}$ to 15.6 MPa.$m^{1/2}$ for DU-3/4 Ti and DU-Quint, respectively. Values for U-2Mo in two heat treated conditions were slightly less than the DU-3/4 Ti threshold. Data are presented in a "safe zone" plot of flaw size vs. stress. Fractographic investigations by SEM revealed mixed fracture modes with both transgranular and intergranular fracture occurring.

The SCC failure mechanism is caused by the conjoint action of localized stress and a corrosive medium. Earlier work has shown that crack propagation is rapid in U-2Mo. Presently, rounds are produced by hot rolling and grinding of U-2Mo bar or rod stock. Stress corrosion cracking in penetrators fabricated in this way has been reported during long-term exposures to humid air. Cracking was linked to the presence of residual stresses and oxycarbonnitride inclusions in the material. These inclusions provide regions of stress concentration and localized corrosive attack which serve as sites for crack

initiation. Tensile stresses are necessary for crack propagation and these may result from corrosion product wedging and/or residual tensile stress produced during fabrication of the round. Since α-uranium is very anisotropic mechanically, some internal stress always remains locked into any polycrystalline part even after "stress relief" heat treatments.

Acknowledgments

The authors would like to extend their appreciation to Messrs. F. Rider, R. Jones, D. Eller, and Dr. M. Norr for technical assistance. Funding for this work was provided by Naval Sea Systems Command, and the Naval Surface Weapons Center under Independent Research Projects.

INTRODUCTION

A depleted uranium -2 weight percent molybdenum alloy (U-2Mo) has been selected as penetrator material for various defense systems. One problem with the use of U-2Mo, as well as other uranium based alloys, is that the alloy is susceptible to stress corrosion cracking (SCC) during storage in moist air environments, especially if sodium chloride is also present. Indeed, catastrophic SCC failure of penetrators during long-term exposure to humid air has been observed (Figure 1).

During the last five years, detailed studies of the stress corrosion cracking problem have been conducted at the Naval Surface Weapons Center (NSWC). These studies have linked the SCC phenomena with the presence of both residual stresses and oxycarbonitride inclusions in the material.[1,2] The inclusions provide regions of stress concentration and localized corrosive attack and serve as sites for crack initiation. Tensile stresses are necessary for SCC crack propagation. Tensile stresses in rounds result from corrosion product wedging and/or residual tensile stress produced during fabrication of the round. Internal stresses in parts produced from depleted uranium alloys result from the concomitant factors of plastic deformation, thermal strains, and phase transformations during fabrication. In other uranium alloy munitions the $\lambda \rightarrow \alpha'$ transformation is of such magnitude as to sometimes cause centerline void formation.[3]

Initial penetrators were fabricated at NL Industries, Albany, NY, by grinding hot rolled U-2Mo rod. Since this technique is time consuming, expensive, and wasteful of material, other production techniques have been examined. The feasibility of forging the rounds has been demonstrated by NETCO, Long Beach, CA., and casting techniques have been developed at Nuclear Metals, Inc., Concord, MA. Each of the manufacturing methods produce different internal stress states which must be assessed as to their effect on the stress corrosion cracking phenomena.

A correlation of the stress distributions with SCC crack propagation characteristics is presented.

Diagnostic tests were also performed on the rounds including hardness and yield strength measurements, moist nitrogen environmental tests, and microstructural determinations. In addition, detailed chemical analysis was performed on the rounds for comparison with inclusion content in the microstructure. Scanning electron microscopy was performed on SCC fracture surfaces.

The results of measurement of residual internal stress distributions occurring in rounds manufactured by these methods is described.

Although rounds using other DU alloys were not produced, SCC kinetics in U-3/4 Ti, and U-3/4 Quint alloys are also reported with those of U-2Mo in moist salt laden air using precracked cantilever beam specimens for comparison. The fracture mechanics approach for stress corrosion tests as suggested by Brown and Beachem[4] is used. This data is then utilized to construct the so called "safe-zone" plot for the use of the alloys in moist salt laden air.[5,6]

EXPERIMENTAL PROCEDURES

I. MATERIALS

Table 1 lists the representative samples from forged and cast batches tested, along with a description of post-working heat treatments. Chemical analysis of the rounds was performed by Ledoux and Co. with the results listed in Table 2.

Hardness measurements were made using both the Rockwell "C" and Knoop microhardness scales. The mean values are tabulated in Table 3 along with yield strength data for the various lots. Compressive stress-strain curves were measured using the cylindrical portion of the rounds for the tests.

A 0.2% offset yield stress determination was made, though inherent inaccuracy is recognized due to the low length to diameter ratio of 1.6:1 of the specimens and the anelastic behavior of uranium alloys.

A round from each batch was cut lengthwise, mounted, polished, and etched for metallographic examination. The etchant which produced the best results was one part each of nitric acid, acetic acid, and water, adding a few drops of hydrofluoric acid. Illustrative microstructures are shown in Figure 2.

All materials used in SCC testing were processed and fabricated into specimens by Rockwell International Corporation, Rocky Flats Division except for tensile and Charpy V-notch specimens which were machined by the Army Mechanics and Materials Research Center, Watertown, Massachusetts from Rockwell International material.

The chemical analyses of the alloys used in SCC tests are provided in Table 4. Oxygen, hydrogen and nitrogen analyses were not obtained. These elements are, however, present in the microstructure in the form of blocky carboxynitride inclusions and hydrogen, after exposure to the environment, in the form of very small lenticular uranium hydride inclusions near the surfaces.

The materials were fabricated into rectangular plate according to the thermomechanical processing schedules given in Table 5. Designations for the various treatments are also indicated in Table 5.

Some specimens of the U-2Mo QOA were reheat treated to form a two phase structure by quenching from the $\alpha + \gamma$ phase field. The resulting microstructure is shown in Figure 3(a). The morphology consists of a dispersion of retained γ, rich in molybdenum, imbedded in a low molybdenum α matrix. There is no optical evidence in the micrographs that the banded martensitic variant of the α phase, α_b', was formed during the quench. The prior γ ASTM grain size is 2 to 3. Large rectangular precipitates, which presumably are carboxynitrides, are also found in the fracture topology.

The quenched and overaged U-2Mo QOA microstructure is seen in Figure 3(b). It consists of small precipitates of δ along prior γ grain boundaries and psuedo-lamellar (α + δ) in the grain interior. The prior γ grain size is ASTM 2 to 3. Again, there are some small blocky carboxynitride inclusions dispersed throughout the microstructure.

In Figure 3(c), the microstructure for the uranium -3/4 Quint (U-3/4 Quint) is given. The structure is similar to the quenched and overaged U-2Mo. In this case, however, the ASTM grain size number is 3 to 4.

The microstructure of the as extruded uranium -3/4 w/o titanium (U-3/4 Ti) material is presented in Figure 3(d). The structure is the acicular form of martensitic α_a', and is very similar to what one would expect for a γ quenched and overaged material. The morphology shows some decomposition at the prior γ grain boundaries and inside the martensitic needles. Some inclusions are also observed. The prior γ average grain diameter is 300 μm.

The mechanical properties of these alloys are given in Table 6 at several humidity levels. Tensile and Charpy V-notch bars were machined from cantilever beam bars after SCC testing. The Poisson's ratio was assumed to be 0.22. Charpy data is shown in Figure 4.

II. RESIDUAL STRESS MEASUREMENTS

The most widely used mechanical method giving a three-dimensional evaluation of internal stresses in metals is the boring-out method proposed by Mesnager[7], developed by Sachs[8], and discussed widely in the literature[9]. Boring-out experiments were performed on rounds fabricated by grinding hot rolled rod, by forging, and by casting.

The experimental method consisted of boring out the center of a projectile in a succession of small layers and measuring the resultant

mechanical relaxations in the length and diameter of the remaining portion of the round after each bore. In the present experiments 120 Ω Magnaflux PA-09-062 AH-120 gages were used to measure relaxation strains. The gages were mounted to the cylindrical section of the rounds with either Eastman 910 cement or M-Bond 610 adhesive. Some difficulty was experienced in maintaining adherence of the gage because of oxidation of the alloy at the adhesion site. Short times between gage mounting and boring minimized this problem. Eastman 910 proved to be the better adhesive choice. The gages were coated with a silicon-phenolic resin to protect them from oil, water, and impact damage during handling.

Borings were performed with extreme care under a 40:1 mixture of water and water soluble oil. This was to prevent overheating with resultant annealing and to prevent introducing erroneous stresses during cutting of the metal. A photograph of the set-up without the coolant is shown in Figure 5.

Strain measurements were made after each bore when the relaxation was complete. A BLH model 120C strain gage power supply and bridge was used.

III. SCC TESTING

Stress corrosion testing was performed on the depleted uranium alloys to obtain crack growth kinetics. The test apparatus was a cantilever beam fixture similar to that proposed by Brown and Beachem[4]. Cantilever beam specimens were instrumented with a crack-opening-displacement gage to continuously monitor crack growth rate. A schematic of the test arrangement is shown in Figure 6. The system is capable of distinguishing crack opening displacement changes of 1×10^{-3} mm which gives a system resolution of 0.5 mm for a period of one month. Crack growth rates of 3.5×10^{-4} mm/hr can be detected in less than seven days.

Prior to testing, the specimens were fatigue precracked to insure a sharp notch. Crack orientation was TS. Fatigue precracking was performed in a cantilever configuration for the 12.7 mm x 12.7 mm x 152.4 mm samples on a constant deflection Krauss-Tatnal machine and in three point bending for the 25.4 mm x 25.4 mm x 152.4 mm samples on a closed-loop machine. The fatigue schedule was well within the criteria established in ASTM E399-74 with the ratio of the maximum stress intensity of the fatigue cycle, K_f (max) to the Young's modulus E, equal to $8.01 \times 10^{-5} m^{1/2}$ for the final 1.5% overall length of notch plus crack. The ratio of K_f(max) to K_{IC} was at most 0.3; and the plastic zone radius, using Irwin's approximation, at the beginning of the SCC test was 1.38×10^{-5} to 1.76×10^{-5} m.

The specimens were dipped in a 3.5 percent salt distilled water solution. The specimens were allowed to dry in laboratory air. The specimens were then installed in the cantilever beam test apparatus with zero applied load for one hour in a closed container designed to maintain 98 percent relative humidity. The solution in the container was a super-saturated solution of $CaSO_4.5H_2O$ in distilled water as specified by ASTM E104-51 (Reapproved 1971), located about 35 mm below the specimen. After the one hour necessary for the atmosphere to equilibrate around the specimen, the test load was applied. Room temperature and room relative humidity were continuously monitored. Additional details of this test procedure are given in reference 10.

RESULTS AND DISCUSSION

Illustrated examples of residual stress distributions for various rounds tested are shown in Figures 7 and 8. A generalized comparison of stress distribution versus fabrication technique shows the ground, hot rolled, material to have large tangential tensile stresses on the surface (of the order of 380 MPa) whereas forged and cast penetrators are either in a compressive surface stress state or exhibit considerably lower tensile surface stress (max 100 MPa).

The surface stress state is critical in determining susceptibility to stress corrosion cracking. A large tensile surface stress component coupled with flaws or inclusions results in SCC failures. The ground, hot rolled material #16 and #18 exhibit this type of stress distribution. "As forged" rounds 3808, 3811, and 3798, however, showed compressive stress states on the surface. This minimizes the likelihood of stress corrosion failures; and, indeed, no SCC failures have been observed in forged penetrators.

The cast rounds of lots 1 and 2 and the forged rounds of lots A and C show minimal stress. In comparison, the cast lot 4 sample which has been cast and remelted three times retained a higher stress level. Also, the "as forged" lot F and lot D rounds showed this trend. It was believed that heat treatment of the forged rounds might achieve some stress relief. The data indicates that this assumption is not correct for all heat treatments.

Another interesting result is that in many instances large hydrostatic tensile stresses were present along the centerline of the rounds. Although no centerline porosity was observed metallographically, the possibility of this occurring remains. Centerline porosity has been a problem in parts fabricated from U-3/4 Ti. Sachs boring out data for a 34.9 mm dia (1-3/8 in)

by 101.6 mm long (4 in) U-3/4 Ti bar water quenched from 800°C showed high centerline tensile stresses with σ_ℓ= 758 MPa (110 Ksi) and σ_t= 586 MPa (85 Ksi)[3]. The stresses decreased monotonically toward the outer surface and became compressive with σ_ℓ= -345 (-50 Ksi) and σ_t= -552 (-80 Ksi). Results on a 25.4 mm dia (1 in) rod are reported to be similar. Northcutt reports fabrication procedures which prevent centerline void formation in DU-3/4 Ti long rod penetrators.[11]

Stress corrosion cracking (SCC) is a fracture process caused by the conjoint action of stress and corrosive environment. Surface tensile stresses are necessary for SCC. To quantify safe operating stresses it is common practice to use the concepts of linear elastic fracture mechanics. This approach assumes that the propagation of cracks is predictable in terms of the magnitude of the tensile stresses at the crack tip and that the opening of the crack is controlled by the stress intensity factor, K. The K level which causes fast fracture solely because of overload is designated K_{IC}. The threshold (if it truly exists) above which SCC occurs is designated K_{ISCC}. Figure 9 schematically shows expected da/dt vs. K_I data with three stages, I, II, and III of kinetic behavior.

Typical normalized crack length-time curves are shown in Figure 10. Although at first glance the curves appear relatively smooth, they contain fine details which suggests that "crack propagation is irregular." First, many samples exhibited a rapid increase in crack length during the early part of the test as illustrated by curve A. This produces an initially decreasing crack growth rate, da/dt, with increasing K_I as shown in Figure 11 for a DU-3/4 Ti alloy. This behavior is possibly caused by crack tip blunting due to corrosion and/or residual stressee. Secondly, cracks frequently increased their crack lengths with rapid jumps in length over relatively short periods of time as indicated by curve B of Figure 10. This behavior

causes fluctuating da/dt with increasing K_I and occurs in both large and small steps as shown in Figure 12 for a DU-2Mo QOA material. The DU-2Mo ($\alpha + \gamma$) and DU-3/4 Quint materials behaved similarly. This behavior could also be due to residual stresses or corrosion product wedging.

All alloys showed stage II and III crack growth behavior. Stage I crack growth kinetics were not observed even though growth rates as low as 10^{-9} m/sec were measured. This contrasts with the work of Magnani[12] on a DU-4.5 w/o Nb alloy which showed a distinct stage I in low humidity air at a comparable sensitivity.

Initial stress intensity, K_I, as a function of time-to-failure (TTF) is shown in Figure 13. For SCC resistance in salt laden moist air, the alloys rank in the order DU-3/4 Ti, DU-2Mo QOA, DU-2Mo ($\alpha + \gamma$), and DU-3/4 Quint. Threshold values, K_{ISCC}, are listed in Table 7 and ranged from 24.2 MPa·$m^{1/2}$ to 15.6 MPa·$m^{1/2}$. K_{ISCC} values for the DU-2Mo alloys were not significantly lower than the value for DU-3/4 Ti. Fracture toughness decrease because of exposure to the environment, however, was much more significant for the DU-3/4 Ti and DU-3/4 Quint alloys than it was for DU-2Mo.

Interpretation of SCC fracture surfaces examined by SEM was difficult because corrosion obscured many fracture features. Some general fracture trends were, however, evident. Typical fracture surfaces for U-2Mo are shown in Figure 14(a)-(c). Figure 14(a) shows the fracture surface of U-2Mo QOA near the boundary of the transition of slow crack growth to fast crack growth. The fracture morphology is predominantly mixed intergranular and quasicleavage with separation at $\alpha + \delta$ lamella a frequent observation. This fracture morphology at higher K values, Figure 14(b), does not contain intergranular fracture but appears to show mixed quasicleavage and ductile dimple tearing. Figure 14(c) shows the morphology of the U-2Mo ($\alpha + \gamma$) at high K. It, too, consists of quasicleavage and dimples; however, there is

a much larger fraction of ductile fracture and the involvement of the large blocky precipitates in the fracture is evident. These observations are in agreement with those of Fishman and DeJarnette[13], but differ somewhat from the observations by Koger and Bennett[14] on higher Mo content alloys. The latter authors observe a preponderance of intergranular fracture in aqueous chloride environments.

Fracture surfaces for U-3/4 Ti were more uniform in appearance as K increased. Typical fractures are shown in Figure 15(a) and (b). In Figure 15(a), separation at α' platelets is apparent and the fracture appears ductile between platelets, although definite dimple morphology was not observed. A higher magnification view, shown in Figure 15(b), shows some quasicleavage with secondary cracking apparent. A cross-sectional micrograph is shown in Figure 15(c) which shows only a slight, but definite, tendency to cleave α' platelets.

Stress corrosion cracking fracture morphology of U-3/4 Quint is shown in Figure 16(a) through (c). The region of slow crack growth was flat and transgranular with some ductile appearance as shown in Figure 16(a). At higher K values a transition in fracture mode to intergranular separation along prior γ grain boundaries occurs. The intergranular separation is not smooth as would be expected with grain boundary decohesion, but consisted of mixed quasicleavage in ill-defined river patterns connected by distorted regions as shown in Figure 16(c).

CONCLUSIONS

The principal results of this investigation and the conclusions drawn from them are as follows:

1. Depending on manufacturing method, residual surface stresses may be either tensile or compressive. Tensile stresses should be avoided since

they aggravate SCC. Hot rolled and ground rounds showed the highest level of residual surface tensile stresses which were often above the SCC threshold, σ_{SCC}, in magnitude. Forged and heat treated rounds and cast rounds also showed tensile residual stresses on the surface. These stresses, however, were lower in magnitude and below σ_{SCC}.

2. Direct correlation of SCC behavior between residual stress level, measured K_{ISCC} values, and the moist nitrogen test was obtained.

3. Large hydrostatic tensile stresses were observed along the centerline of some rounds, thus, introducing the possibility of centerline void formation. Centerline void formation was not, however, observed.

4. There is little difference in SCC resistance between U-3/4 Ti, U-2Mo, and U-3/4 Quint alloys in salt laden moist air environments. U-3/4 Ti and U-2Mo show a slightly higher resistance than does U-3/4 Quint.

5. U-3/4 Ti and U-3/4 Quint show a much larger decrease of toughness when exposed to the environment than does U-2Mo.

6. Stage I crack growth kinetics were not observed in these alloys at crack velocities as low as 10^{-9} m/sec.

7. Continuous monitoring of crack growth rate revealed that crack propagation is not continuous.

REFERENCES

1. S. G. Fishman and C. R. Crowe, Pract. Metallog., 13, 184 (1976).

2. S. G. Fishman and C. R. Crowe, in Case Studies in Fracture Mechanics (AMMRC; Watertown, MA:1977) MS 77-5.

3. A. M. Ammons, in Physical Metallurgy of Uranium Alloys, J. J. Burke, et. al., ed. (Brook Hill: Chestnut Hill, MA: 1976) p525.

4. B. F. Brown and C. D. Beachem, Corr. Sci., 5, 745 (1965).

5. B. F. Brown, Stress Corrosion Cracking in High Strength Steels, and in Titanium and Aluminum Alloys, (Naval Research Laboratory, Wash.,D.C.,1972)1.

6. J. G. Kaufman, Marshall Space Flight Center Rept., No. NAS-8-21484, May 31, 1973.

7. M. Mesnager, Comptes Rendus, 169, 1391 (1919).

8. G. Sachs, Z. Metallkunde, 19, 29 (1929).

9. J. J. Lynch, in Residual Stress Measurements, R. G. Trenting, et.al., eds. (ASM: Metals Park, Ohio: 1952)51.

10. J. A. Joyce, D. F. Hasson, and C. R. Crowe, J. T. E. V. A., 8, 293 (1980).

11. W. G. Northcutt, Union Carbide Corp., Oak Ridge Y-12 Report Y-2128,1978.

12. N. J. Magnani, in Advances in Corrosion Science and Technology, 6, M. G. Fontana and R. W. Staehle, eds., (Plenum: New York: 1976) 89.

13. S. G. Fishman and H. DeJarnette, Corr., 33, 351 (1977).

14. J. W. Koger and R. K. Bennett, Union Carbide Oak Ridge Y-12 Plant Report No. Y-2063, 1976.

LIST OF FIGURES

Table 1

Manufacturing Detail for Rounds
Tested for Internal Stress Distribution

Round Identification	Manufacturer	Method Used to Produce Rounds
16', 18'	NL Industries	Hot rolled then machine ground
3798'	NETCO	Solution treated @ 850°C, 40 min. OQ → aged 582°C, 8 hrs, then forged 2 blows @ 500°C
3808'	NETCO	As Forged @ 620°C, 1 blow
3811'	NETCO	As Forged @ 500°C
Lot A #4	NETCO	Forged @ 500°C heat treated 575°C, 1 hr R_c 28/32
Lot B #2	NETCO	Same as Lot A
Lot C #5	NETCO	Forged @ 500°C heat treated 525°C, 1 hr R_c 33/34
Lot D #3	NETCO	Forged @500°C, heat treated 450°C, 1 hr R_c 34/35
Lot F #1 #2	NETCO	Forged @ 500°C
Cast Lot I #6	NMI	Cast → solution heat treated @ 850°C, 40 min, OQ → aged @ 582°C, 8 hrs 340/460 ppmC
Cast Lot II #8	NMI	230/470 ppmC recycled
Cast Lot IV #7	NMI	930-960 ppmC recycled

Table 2

Chemical Analysis of the Depleted Uranium Rounds

	FORGED					CAST		
	A (ppm)	B (ppm)	C (ppm)	D (ppm)	F (ppm)	I (ppm)	II (ppm)	IV (ppm)
Aluminum	50	70	60	50	100	30	70	70
Copper	10	10	10	10	200	70	70	30
Iron	15	15	15	15	40	20	20	20
Magnesium	7	5	7	7	30	5	10	10
Manganese	15	7	5	5	10	20	30	20
Nickel	40	40	20	20	70	150	150	70
Lead	15	15	10	10	30	5	5	2
Silicon	300	250	10	10	30	400	700	700
Cobalt	20	20	20	15	20	20	20	20
Zirconium	10	10	10	10	10	10	10	10
Oxygen	520	800	550	190	130	250	200	140
Hydrogen	4	2	2	2	3	2	1	1
Nitrogen	30	30	30	40	40	30	20	40
Carbon	235	280	220	160	215	300	530	1000
Molybdenum (wt pct)	1.89	1.88	2.11	2.20	1.98	1.98	2.10	1.89
U remains	97.98	97.96	97.79	97.75	97.93	97.89	97.72	97.90

Data taken by Ledoux and Co., Teaneck, NJ

Table 3

Hardness and Strength Data

Lot	Hardness (Rock. C) ± 2	Yield Strength MPa(Ksi)
A	29	658.4(95.5)
B	28	No Data
C	33	742.5(107.7)
D	34	823.2(119.4)
F	31	637.7(92.5)
I	32	715.0(103.7)
II	32	657.7(95.4)
IV	31	740.5(107.4)

Table 4 - Chemical Analyses in Weight Percent for Depleted Uranium Alloys used in SCC Tests

	Alloy		
	U-2Mo	U-3/4 Ti	U-QUINT
Mo	2.00	96×10^{-4}	0.84
Nb	—	$<10 \times 10^{-4}$	0.70
Zr	—	—	0.86
Ti	$<1 \times 10^{-4}$	0.71	0.44
V	$<1 \times 10^{-4}$	$<1 \times 10^{-4}$	0.16
Al	25×10^{-4}	35×10^{-4}	75×10^{-4}
Si	5.5×10^{-4}	127×10^{-4}	97×10^{-4}
Fe	60×10^{-4}	45×10^{-4}	140×10^{-4}
Cu	10×10^{-4}	10×10^{-4}	15×10^{-4}
C	100×10^{-4}	10×10^{-4}	40×10^{-4}
U	Balance	Balance	Balance

Table 5 - Thermomechanical Processing of Depleted Uranium Alloys used in SCC Testing

Alloy	Processing
U-2Mo QOA	γ extruded into rectangular plate at 100°C, solution treated for 2 hours and helium quenched; and aged at 500°C for 5 hours and air cooled.
U-2Mo (α+ γ)	As per U-2Mo QOA above plus: solution treat at 800°C for two hours, and water quenched: heated to 615° for five hours and water quenched: aged at 400°C for five hours, and slow cooled.
U-3/4 Quint	As extruded at 1000°C
U-3/4 Ti	As α extruded at 630°C

Table 6 - Mechanical Properties of Depleted Uranium Alloys In Dry Air and Salt Laden Moist Air

Material	%RH	0.2% Y.S. (MPa)	UTS (MPa)	%e (4D)	*** Rc	E(GPa)
U-2Mo QOA	0	796	1243	6.7	37.0	159
	98	735	1043*	-**		
U-2Mo ($\alpha+\gamma$)	0	642	952	3.0	37.0	164
	98	735	1126*	-**		
U-3/4 QUINT	0	721	1305	11.9	37.0	160
	66	728	1016*	1.5		
	98	742	1058*	1.6		
U-3/4 Ti	0	824	1339	7.1	37.0	172
	66	823	1036*	1.4		
	98	762	920*	1.5		

* Max Stress at fracture
** Specimen failed at artificial notch
*** Avg. of 5 readings

Table 7 - Comparison of Fracture Toughness and Threshold Stress Intensity for Depleted Uranium Alloys in 98% Relative Humidity Salt Laden Moist Air

Alloy	K_{IC} (MPa·$m^{1/2}$)	K_{ISCC} (MPa·$m^{1/2}$)
U-2Mo QOA	48.6	20.8
U-2Mo (α+ γ)	27.9	21.5
U-3/4 Quint	43.3	15.6

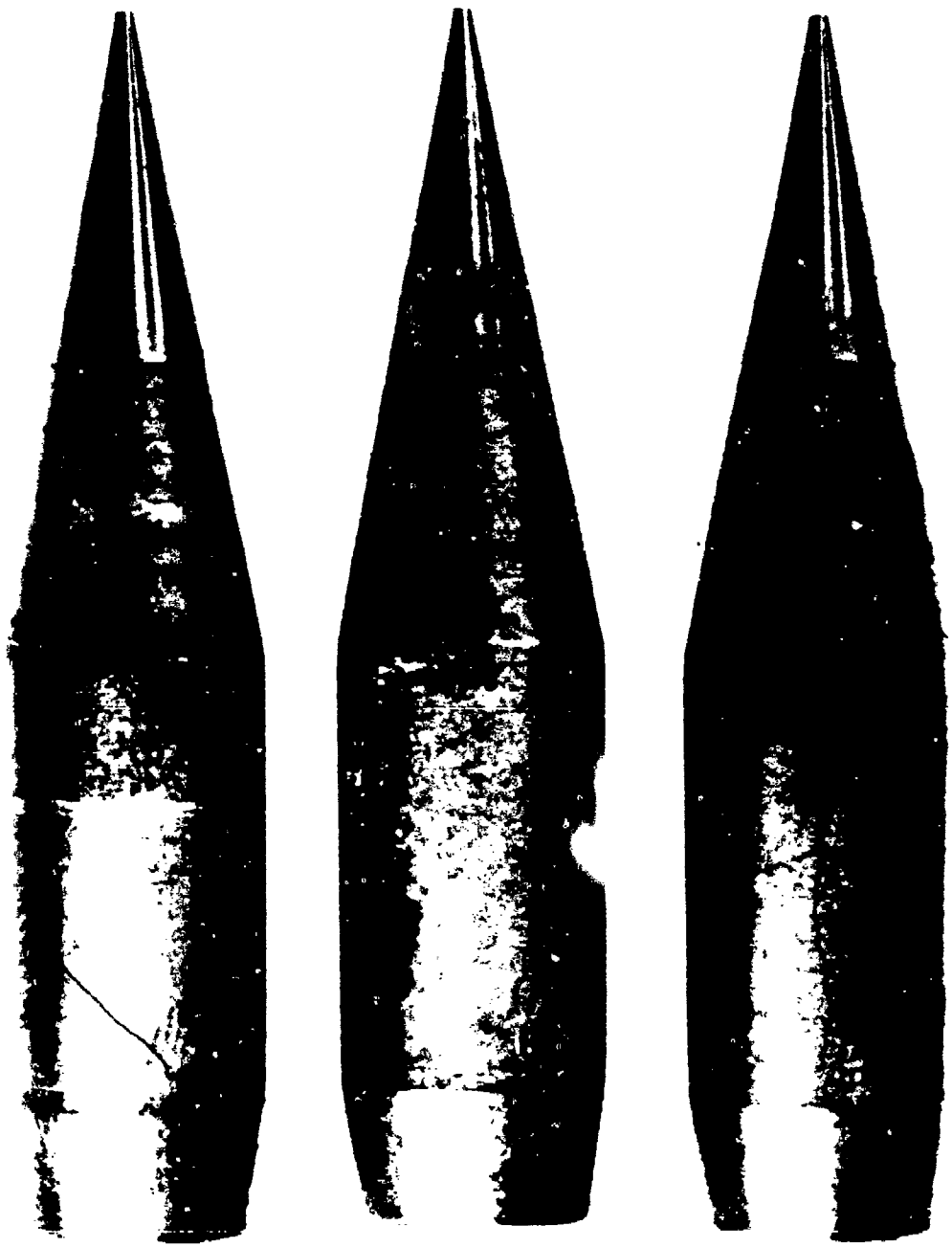

(A) HOT ROLLED AND GROUND

(B) FORGED

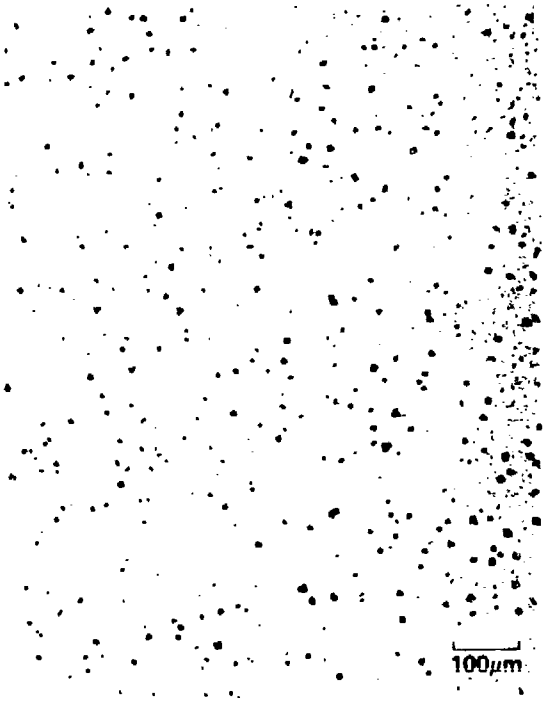

(C) CAST

FIGURE 2 INCLUSIONS OBSERVED IN PENETRATORS

(a)

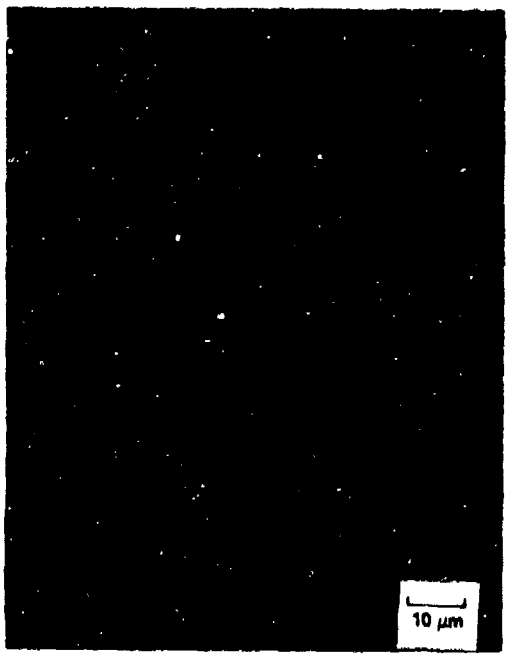

(b)

(c)

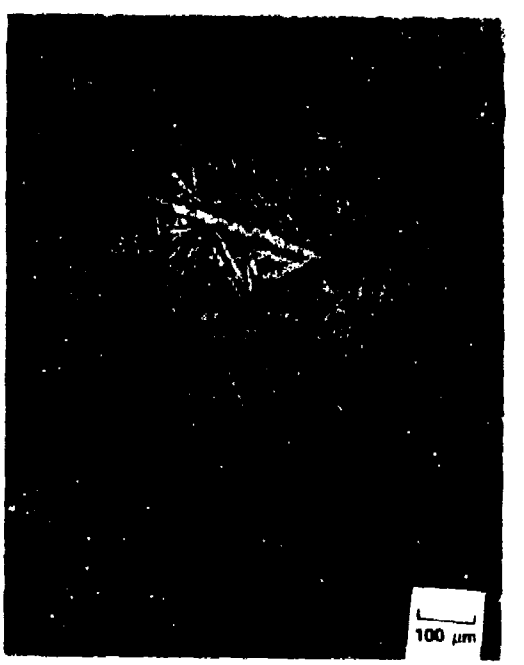

(d)

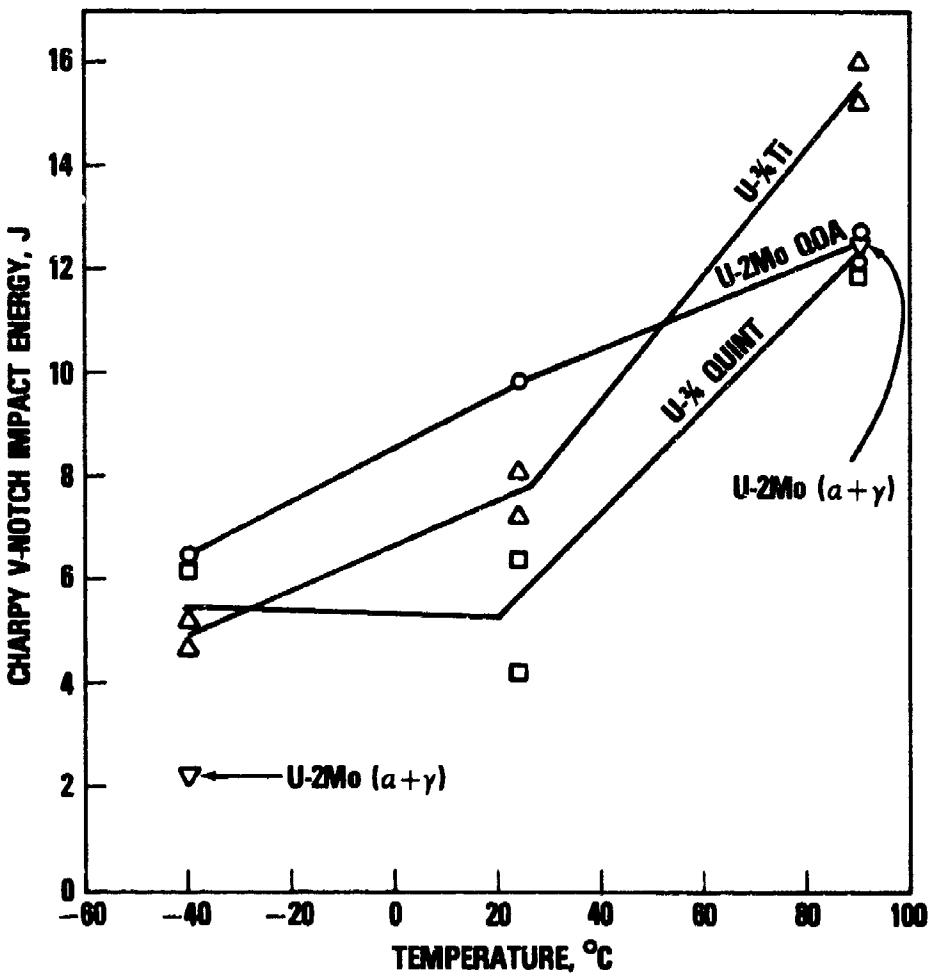
CHARPY V-NOTCH IMPACT ENERGY, J
TEMPERATURE, °C
U-¾Ti
U-2Mo QQA
U-¾ QUINT
U-2Mo (α+γ)
U-2Mo (α+γ)
0
2
4
6
8
10
12
14
16
-60
-40
-20
0
20
40
60
80
100

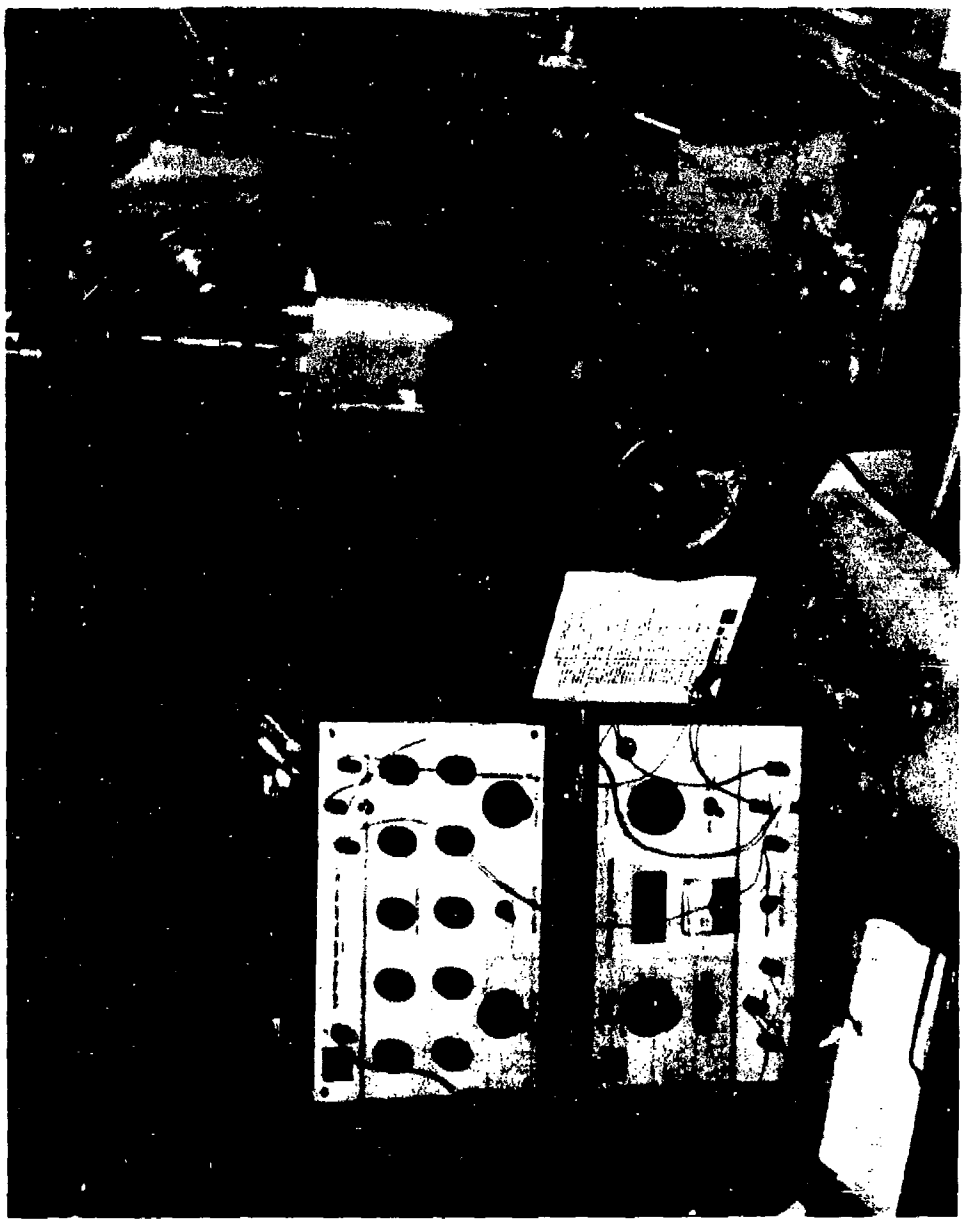

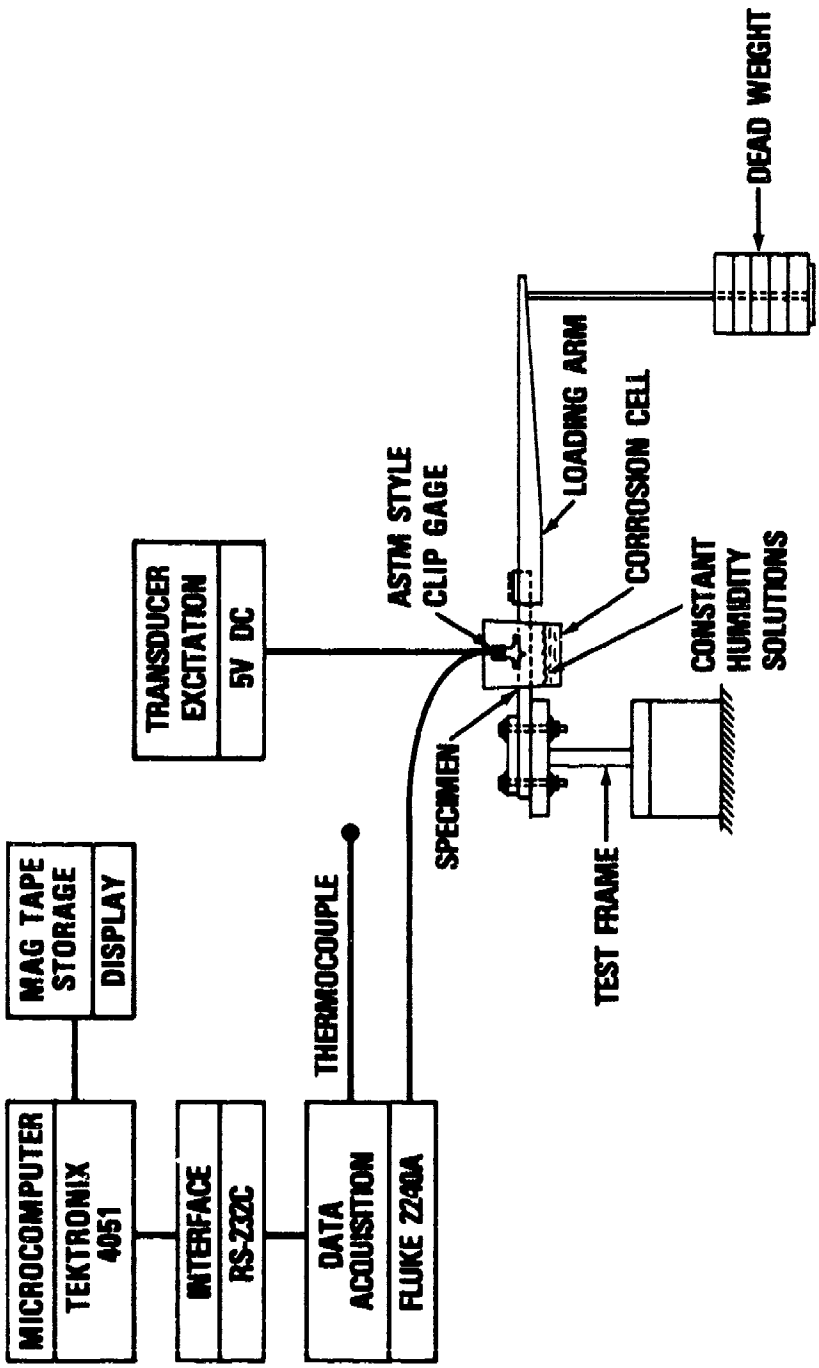
DEAD WEIGHT
LOADING ARM
CORROSION CELL
CONSTANT HUMIDITY SOLUTIONS
ASTM STYLE CLIP GAGE
TRANSDUCER EXCITATION
5V DC
SPECIMEN
TEST FRAME
THERMOCOUPLE
MAG TAPE STORAGE
DISPLAY
MICROCOMPUTER
TEKTRONIX 4051
INTERFACE
RS-232C
DATA ACQUISITION
FLUKE 2240A

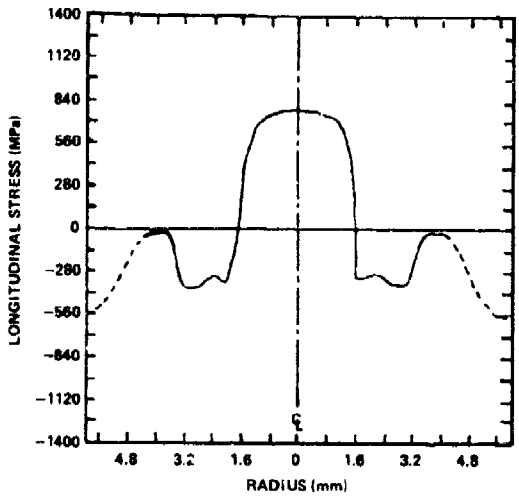
LONGITUDINAL STRESS (MPa)
1400
1120
840
560
280
0
-280
-560
-840
-1120
-1400
4.8
3.2
1.6
0
1.6
3.2
4.8
RADIUS (mm)

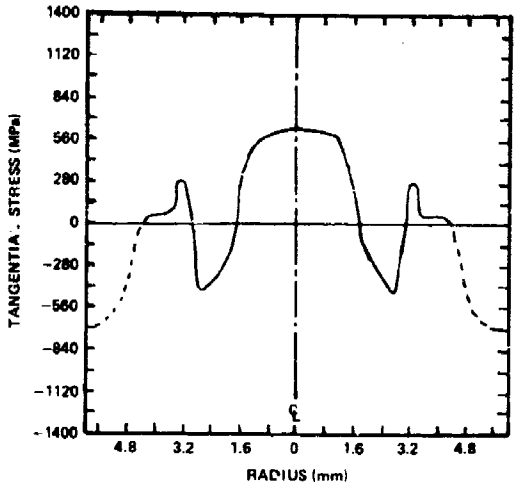
TANGENTIAL STRESS (MPa)
1400
1120
840
560
280
0
-280
-560
-840
-1120
-1400
4.8
3.2
1.6
0
1.6
3.2
4.8
RADIUS (mm)

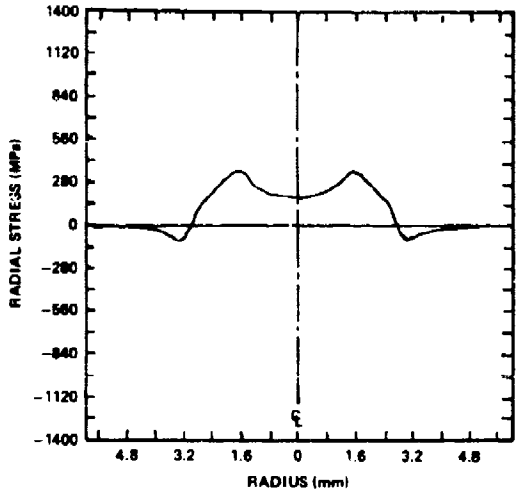
RADIAL STRESS (MPa)
1400
1120
840
560
280
0
-280
-560
-840
-1120
-1400
4.8
3.2
1.6
0
1.6
3.2
4.8
RADIUS (mm)

(A) HOT ROLLED AND GROUND # 16

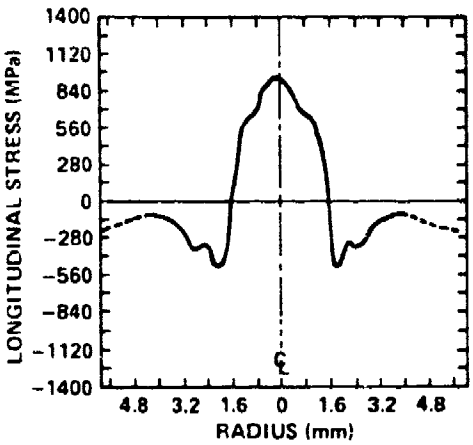

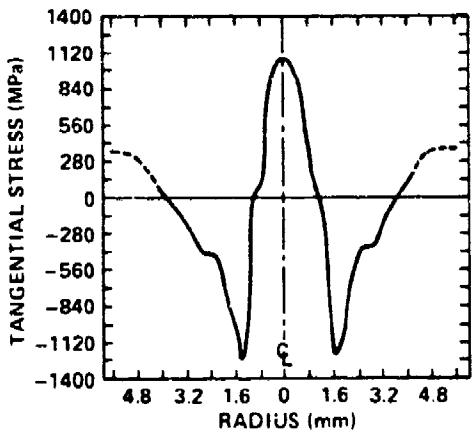

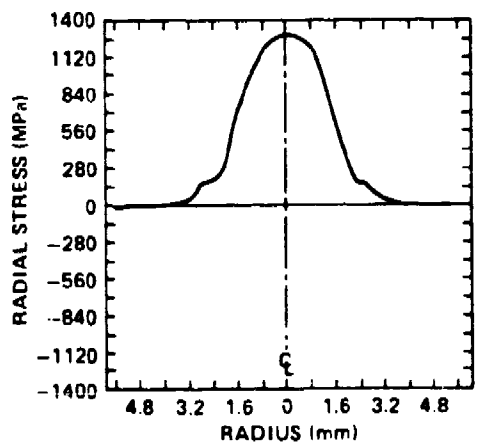

(B) CAST LOT # I

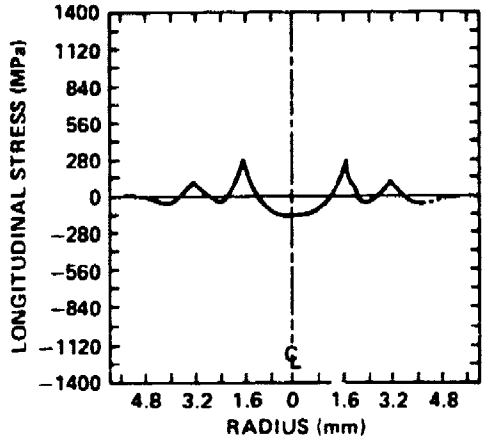

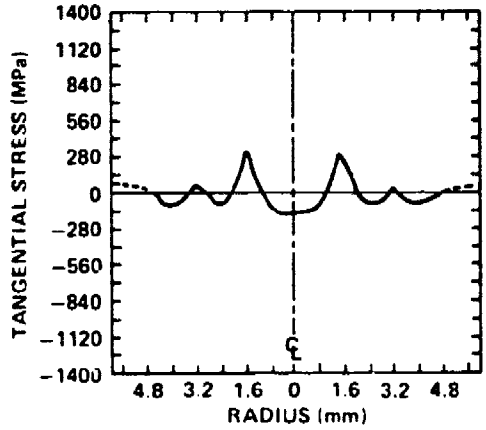

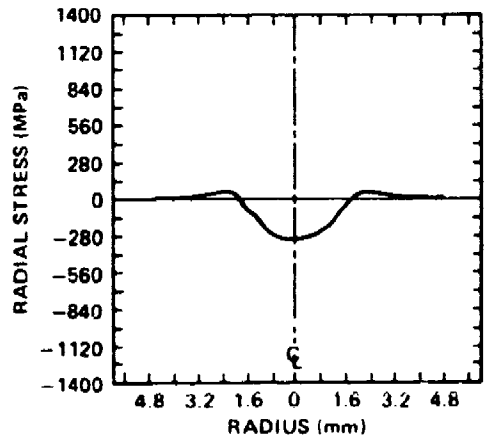

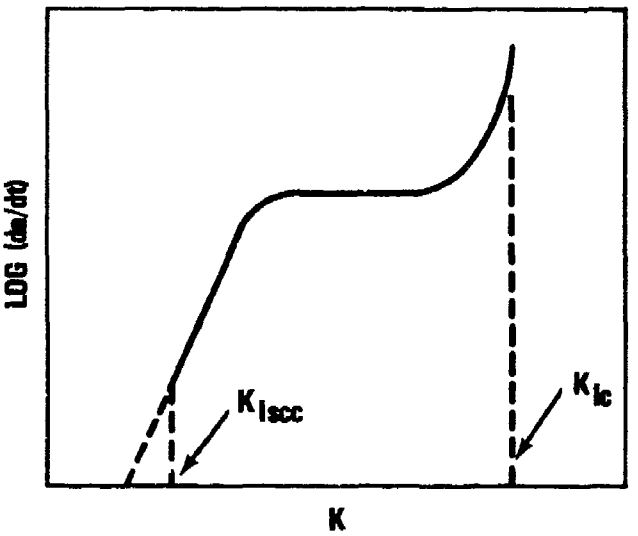
LOG (da/dt)
K_{Iscc}
K_{Ic}
K

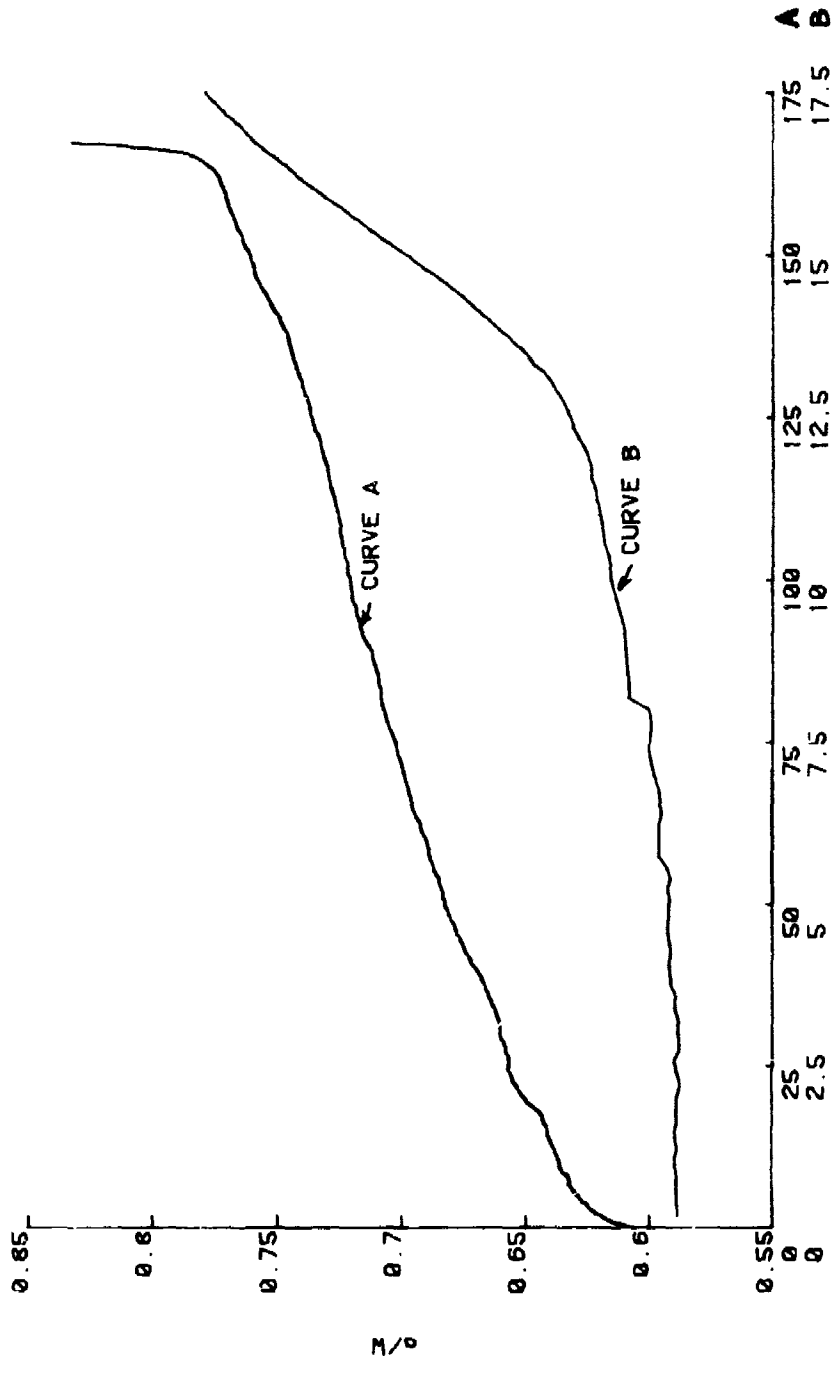
A
B
0.85
0.8
0.75
0.7
0.65
0.6
0.55
M/o
0
25
50
75
100
125
150
175
0
2.5
5
7.5
10
12.5
15
17.5
TIME hours
CURVE A
CURVE B

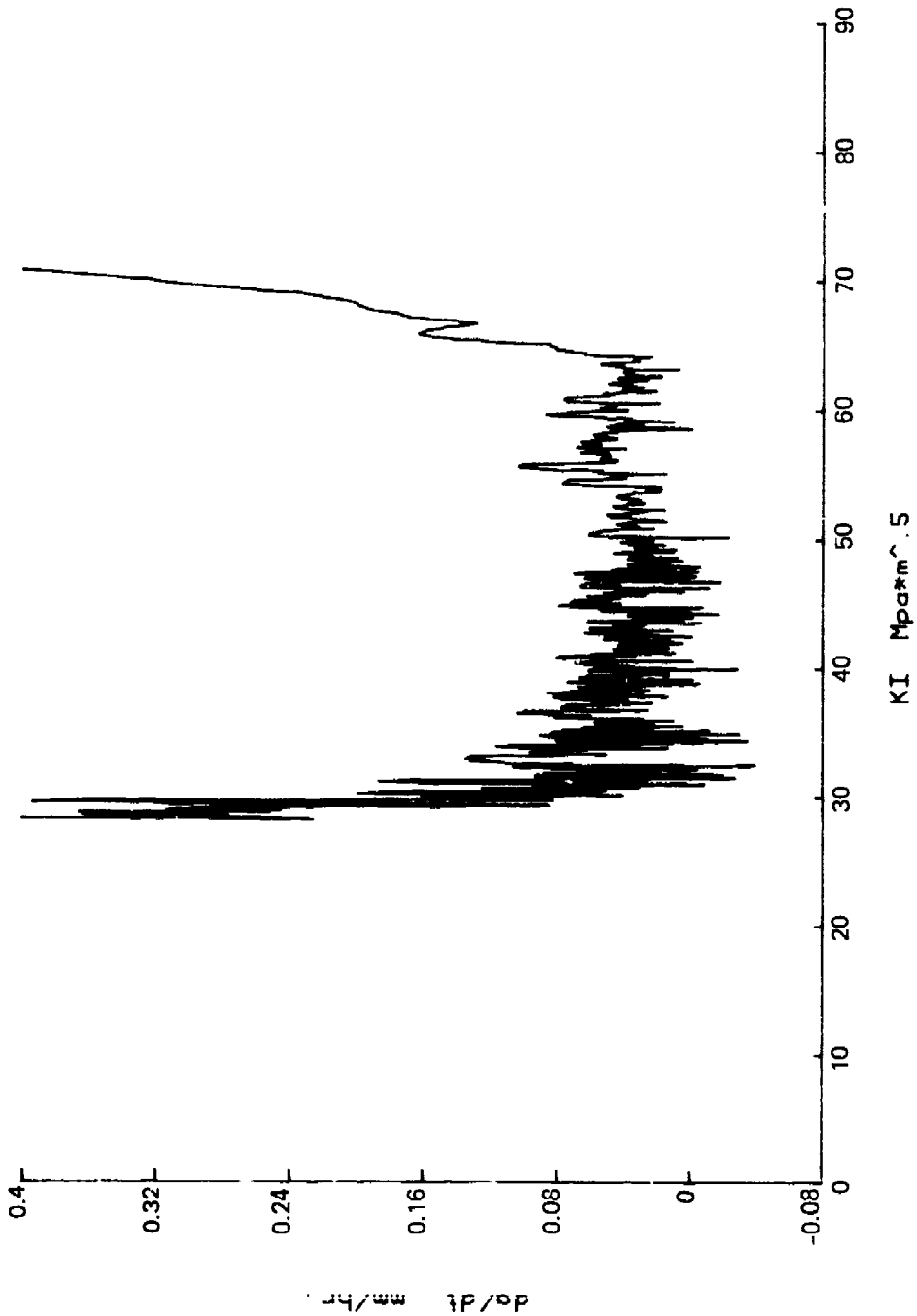
0.4
0.32
0.24
0.16
0.08
0
-0.08
0
10
20
30
40
50
60
70
80
90
KI Mpa*m^.5

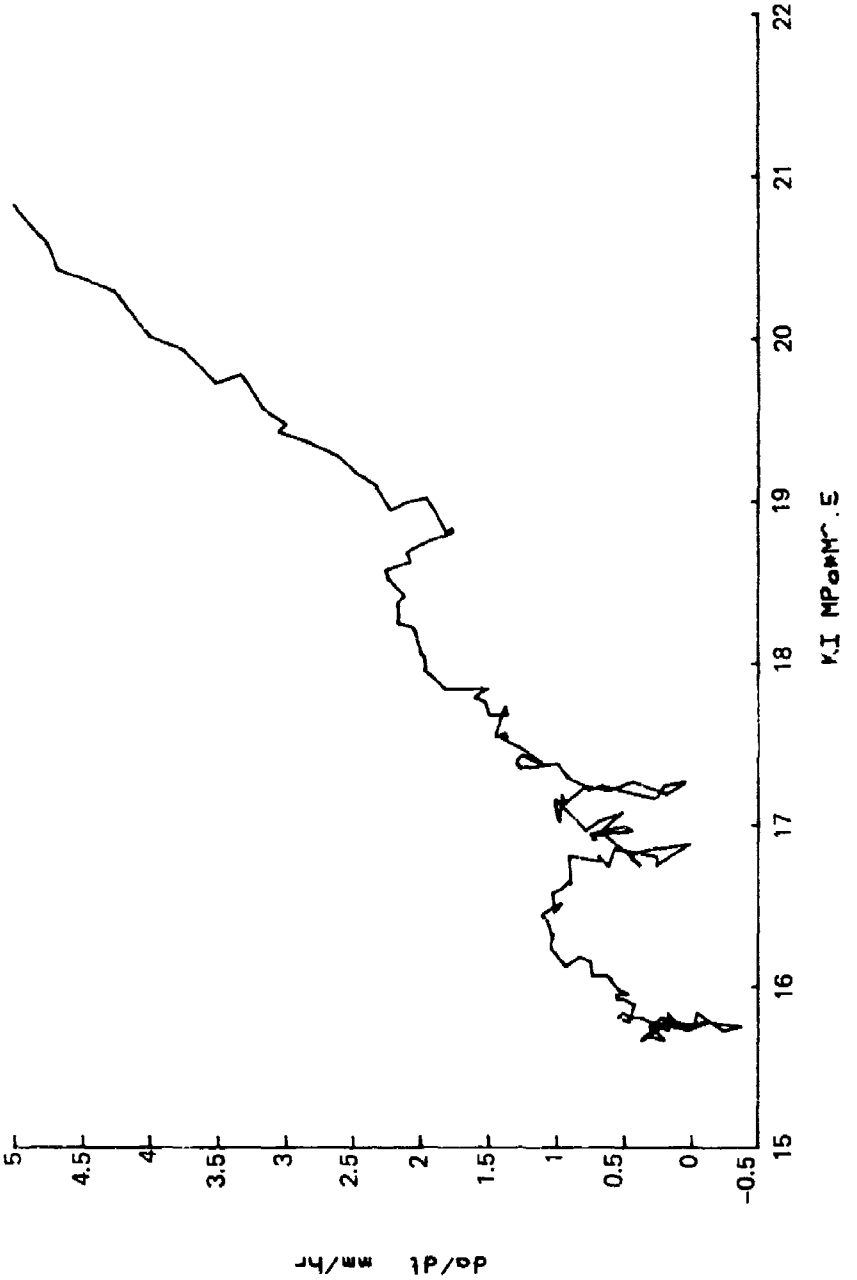
5
4.5
4
3.5
3
2.5
2
1.5
1
0.5
0
-0.5
15
16
17
18
19
20
21
22
K.I MPa√m
da/dt mm/hr

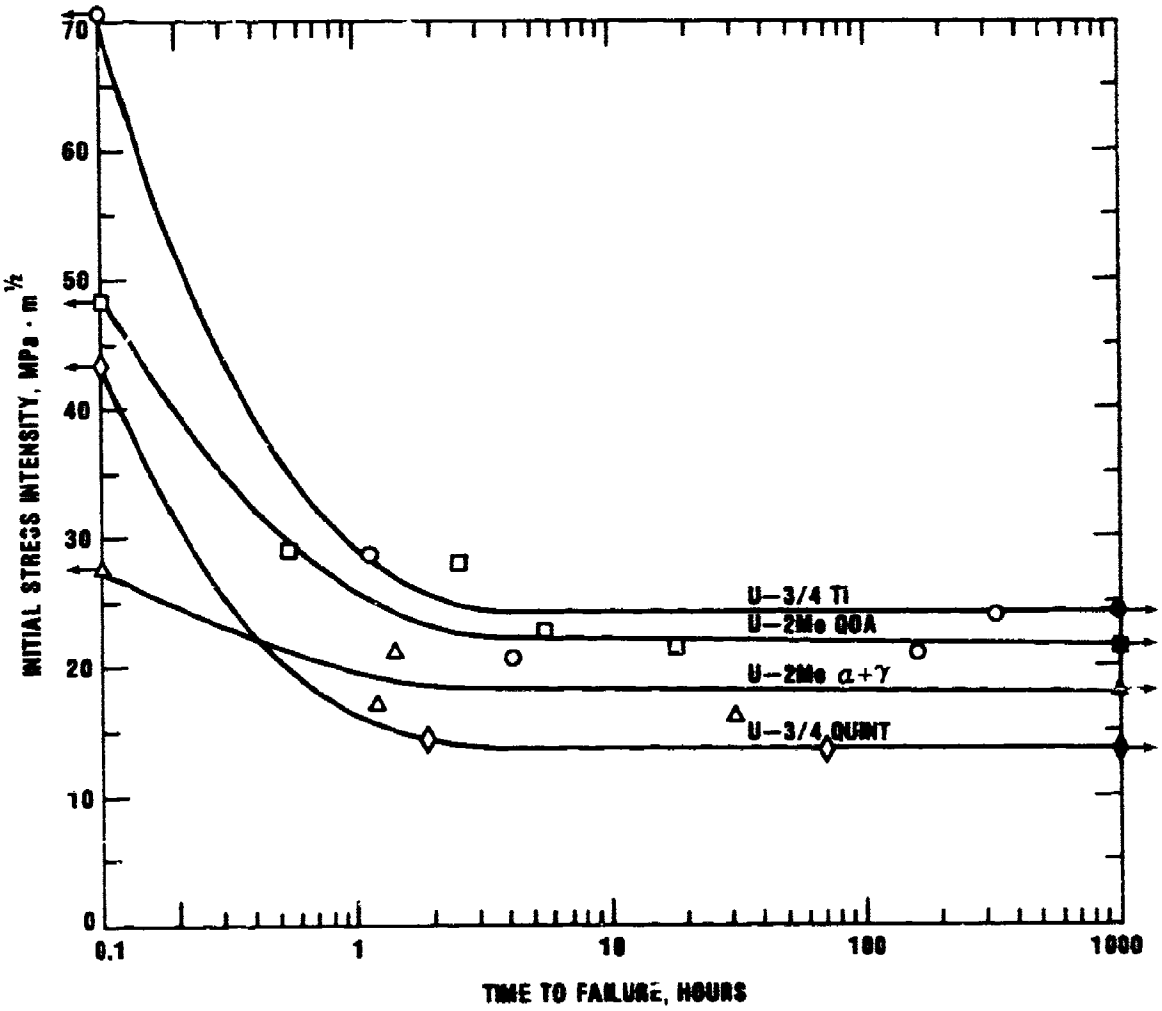
70
60
50
40
30
20
10
0
0.1
1
10
100
1000
INITIAL STRESS INTENSITY, MPa · m^½
TIME TO FAILURE, HOURS
U–3/4 Ti
U–2Mo QQA
U–2Mo α+γ
U–3/4 QUINT

(a)

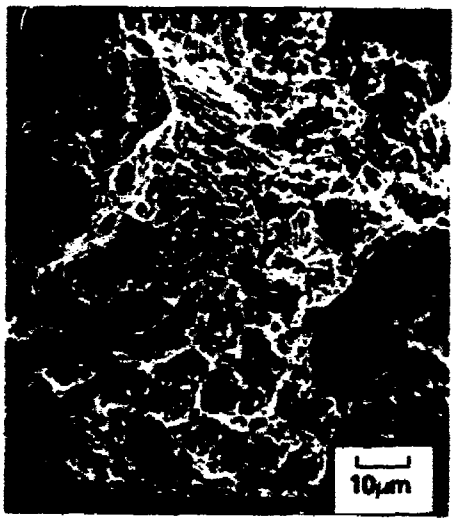

(b)

(c)

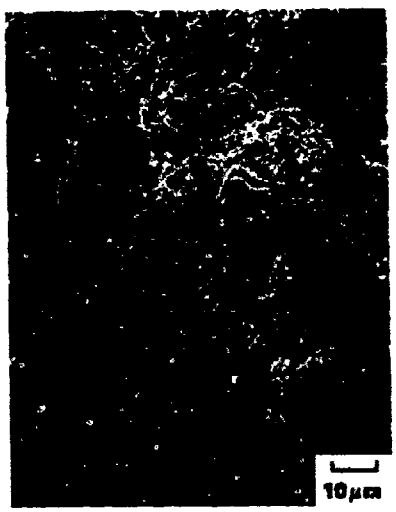

(a)

(b)

(c)

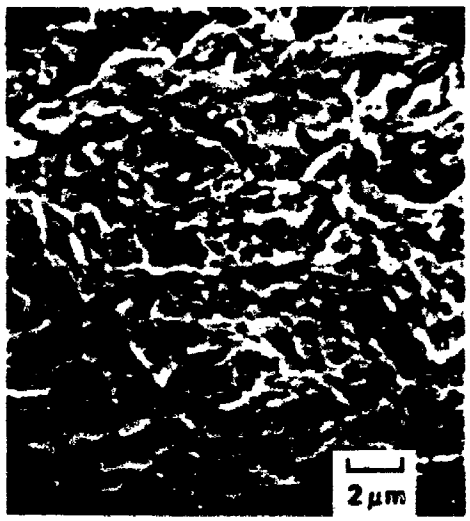

(a)

(b)

(c)

AFWAL-TR-81-4019
Volume II

RESEARCH ON MULTIPURPOSE CORROSION INHIBITORS FOR AEROSPACE MATERIALS IN NAVAL ENVIRONMENTS

V. S. AGARWALA

Naval Air Development Center
Warminster, Pennsylvania 18974

A study to formulate corrosion inhibitor systems for the control of common aircraft corrosion and corrosion assisted failures has been conducted. The mechanisms of principal driving corrosion processes and control are considered to devise new multipurpose inhibitor systems which can protect high-strength structural alloys from catastrophic failures such as stress corrosion cracking, corrosion fatigue, hydrogen embrittlement, exfoliation and wear.

BACKGROUND

Corrosion damages in Naval aircraft range from simple general corrosion to complete failure of structural parts much below their design strength level. According to new estimates (NBS and 3M data) the Navy spends nearly $450 million dollars annually in corrosion costs on aircraft alone. Based on failure reports from the fleet, the major corrosion damages appear in the form of structural breakdown such as exfoliation, stress corrosion cracking, corrosion fatigue or hydrogen embrittlement. They mostly originate from pitting and/or crevice corrosion type of attack. These are generally caused by imperfections in the structure or porosity and breakdown in the protective films and coatings. Since paints and finishes used for this purpose are only temporary barriers to the environment, they are likely to break down easily and provide active centers for more accelerated attack of the underlying metal. Thus, the presence of a corrosion inhibitor in the system is essential to provide corrosion protection to the underlying metal.

In an earlier study[1] it was determined that the mechanisms involved in various corrosion failures have some basic common factors as the governing rules of the process. Principally they are classfied as follows:

1. Anodic dissolution of metal

$$M \longrightarrow M^{+n} + ne^- \qquad \text{REACTION (1)}$$

2. Cathodic reduction of hydrogen

$$H^+ + e \longrightarrow H \text{ atomic} \longrightarrow 1/2\ H_2$$

$$H \text{ atomic} \longrightarrow H \text{ absorbed} \longrightarrow H \underset{\text{(Metal)}}{\text{ absorbed}} \qquad \text{REACTION (2)}$$

3. Breakdown of passivity (auto catalytic)

$$M^+ + H_2O \longrightarrow M.OH + H^+$$

$$M.O + 2H^+ \xrightarrow{Cl^-} M^+ + H_2O$$

4. Plastic deformation (mechanical and metallurgical)

$$\text{Emergence of Slip Steps} \longrightarrow \text{New Active Surfaces}$$

Thus, reactions 1 and 2 proceed. Here the symbols have their usual meaning and M stands for any metal such as iron.

Among these reactions, reaction 2 is probably the most critical in causing structural damages. Since all of the above reactions are of an electrochemical nature, they can be mechanistically controlled by chemicals; i.e., by utilizing the selective reduction-oxidation (redox) properties of certain inorganic compounds. Currently a number of inorganic compounds are known which can be classified as corrosion inhibitors. They mostly

1. Agarwala, V.S., "Accelerated Environmental Testing of Aerospace Materials for the Study of Stress Corrosion Cracking and Hydrogen Embrittlement," Oct 1977, NRC Senior Associateship Report, Nat. Acad. Sci., Washington, DC.

control either anodic or cathodic reactions. However, as corrosion failures result from a combination of several of the above reactions, a single inorganic compound will be unable to perform a multifunctional task. Thus, a combination of several different redox systems is most essential for the effective control of corrosion and corrosion assisted failures.

OBJECTIVES

To analyze the mechanisms of corrosion and corrosion assisted failures with a view to devising new multipurpose versatile inhibitors or inhibitor systems which can protect high-strength structural alloys from catastrophic failures such as stress corrosion cracking, corrosion fatigue, hydrogen or environmental embrittlement, exfoliation and wear. It is also anticipated that this research will provide meaningful data, test results and methods which may be used to produce a product or procedure that can be of immediate use to naval aircraft.

PROGRESS

Selection and determinations of inorganic compounds as functional corrosion inhibitors and their formulation into one versatile inhibitor system are the key elements of this program. A rapid electrochemical technique was, therefore, required to perform the screening and selection process. Earlier[2] a technique was developed by which inorganic compounds could be linked with a quaternary ammonium salt by an anion exchange reaction, which makes them soluble in many organic solvents. Use of this method, thus, reduces the difficulty of retaining the redox functional properties of the additives compounded in the formulation (mixture) without encountering interference. In another program[3], it was also established that inorganic compounds dissolved in organic solvents were much more efficient and long lasting as inhibitors than their counterpart in aqueous phase.

The electrochemical method developed for inhibitor selection was a galvanic corrosion monitor probe as shown in figure 1. The probe works on the principles of a galvanic cell and is comprised of a series of plates of two different metals (steel and copper) sandwiched together alternately separated by an electrical insulator and encapsulated in epoxy. An electronic zero-resistance ammeter circuit connects them externally while the edges of the plates are ground, polished, and exposed to the environment. The environmental condensation on these plates forms a thin film of electrolyte which completes the galvanic circuit. The galvanic output of this cell becomes a measure of the corrosivity of the condensed film

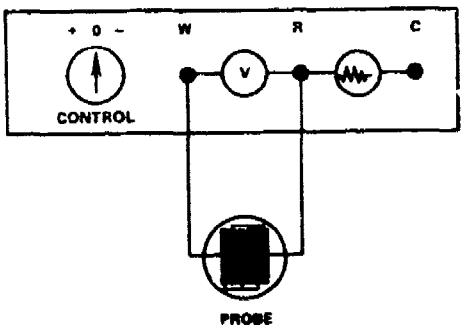

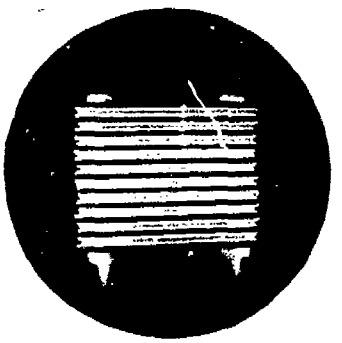

FIGURE 1 - INSTRUMENTATION FOR CORROSION MONITOR PROBE

2. Ohr, J., and Clark, K.G., "The Chemistry and Application for the Solubilization of Chromate Salts in Non-Polar Organic Solvents," NAVAIRDEVCEN Report No. NADC-78017-60.

3. DeLuccia, J.J., and Agarwala, V.S., "Research on Catastrophic Damage Phenomena and Damage Control in Naval Aircraft Alloys," IR Work Unit No. GC153, 1978 IR/IED Annual Report.

(or environment). The outdoor (e.g., aircraft carrier) and indoor (in simulated environmental chamber) testing of this probe has been successful in measuring the severity of the naval environment. This technique was used to evaluate potential corrosion inhibitors. However, in these evaluations the probe was half submerged into the test solutions containing the inhibitor and the salt etc. A plot of corrosion monitor probe output versus time under some test conditions is shown in figure 2. The results illustrate a direct correlation between the monitor output and the corrosion and/or inhibitive properties of the test media. Using this technique a large number of compounds are evaluated as potential anodic (or passivating type) inhibitors. Chemicals like dichromates, nitrites, osmiates, permanganates, etc. fall in this category.

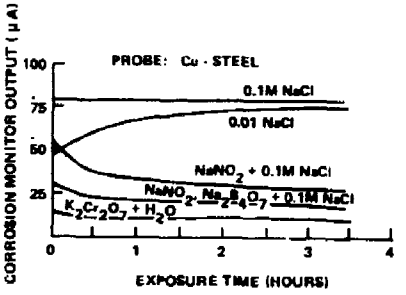

FIGURE 2 - EVALUATION OF CONDIDATE INHIBITORS USING A CORROSION MONITOR PROBE (STEEL/COPPER)

In order to evaluate cathodic type inhibitors; i.e., those which control the hydrogen evolution reaction, an electrochemical hydrogen permeation technique was used. The details of the method are described elsewhere[4]. However, in these investigations the electrolyte in the input chamber (i.e., where H is evolved cathodically) was added with the test inhibitors to determine their effects on the hydrogen evolution reaction and/or hydrogen entry into the metal (Armco iron). The results of such a measurement are illustrated in figure 3. Among the compounds tested the dichromate, palladate and lanthanum nitrate have produced a very significant decrease in H permeation rate from that of the control without an inhibitor. The dichromate has shown the maximum cathodic inhibition as the rate of H diffused through the metal was lowered by almost 50%. Several other potential candidate inhibitors are also being evaluated currently. Based on the above knowledge and the experience gained from the earlier work[3] a few formulations have been made and evaluated. Adogen 464, known chemically as methyl trialkyl (C_8-C_{10}) ammonium chloride, was used as a phase transfer catalyst to dissolve the inorganic compounds in mineral spirites. The tests were performed to investigate the effects of some of the combination inhibitors on low-cycle fatigue life of AISI 4340 steel (260-280 ksi) when exposed to high humidity and chloride containing environments. The details of

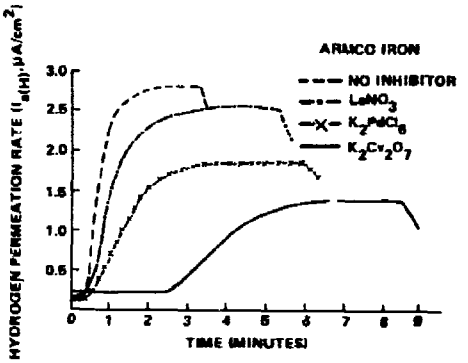

FIGURE 3 - EFFECTS OF INHIBITORS ON HYDROGEN PERMEATION IN IRON

4. *Agarwala, V.S., and DeLuccia, J.J., "Effects of a Magnetic Field on Hydrogen Evolution Reaction and Its Diffusion in Armco Iron," Proceedings of 7th International Congress on Metallic Corrosion, 1978, Rio de Janiero, Brazil.*

these tests are described elsewhere[5]. A summary of the data obtained is given in table I. As shown in table I, the results clearly demonstrate that the concept of combining several functional inhibitors into one system was very effective in retarding crack growth rate. In particular, a combination inhibitor system containing dichromate, nitrite and borate compounds (c.f. table I) showed an excellent fatigue life for 4340 steel compared to the results shown by their individual components. However, when chloride was also added to the environment, the effect of inhibition disappeared until molybdate was added. This is because molybdate has been known to counteract the effect of chloride by influencing the kinetics of repassivation.

The effect of these inhibitors was also studied on a high strength 7075-T6 aluminum alloy for their stress corrosion cracking (SCC) inhibition properties. For this evaluation, double cantilever beam (DCB) specimens were used and pop-in cracked under a constant load applied by two bolts. The technique used was developed by Hyatt[6] for determining SCC resistance of aluminum alloys. Because of the simplicity of this method a number of test specimens can be tested at the same time. The test chamber in these tests was kept at room temperature and a high relative humidity (>95%) was maintained at all times. Addition of inhibitors and salt solution (3.5% NaCl) into the notch area of the specimen was done by putting a drop of these liquids through a very thin wick of cotton inserted in the notch.

	INHIBITORS APPLIED TO NOTCH AREA	MECHANISMS INVOLVED	CRACK GROWTH RATE MICRO-IN./CYCLE	STRESS INTENSITY FACTOR ΔK, KSI $\sqrt{IN.}$	FATIGUE LIFE, CYCLES
	DRY AIR ONLY	NO CORROSION	12	70	17,000
MOIST AIR ONLY	NO INHIBITOR USED	SEVERE CORROSION AND H. E.	110	33	1,800
	DICHROMATE	PASSIVE FILM FORMATION	42	52	8,800
	NITRITE + BORATE	MOSTLY pH ADJUSTMENT	65	36	3,300
	HEXAPALLADATE	ACCELERATE H RECOMBINATION	45	>40	4,000
	LANTHANUM NITRATE	H GETTERING ACTION	50	>40	4,800
	DICHROMATE + NITRITE + BORATE	PASSIVATION AND pH ADJUSTMENT	27	55	9,000
	CERATE + NITRITE + BORATE	PASSIVATION AND pH ADJUSTMENT	38	45	8,400
MOIST AIR + CHLORIDE	NO INHIBITOR USED	SEVERE CORROSION AND SEVERE H.E.	150	32	1,200
	DICHROMATE + NITRITE + BORATE	NO PASSIVATION, SEVERE H. E.	200	34	1,200
	MOLYBDATE	SOME PASSIVATION AGAINST CHLORIDE	61	46	4,500
	DICHROMATE + NITRITE + BORATE + MOLYBDATE	PASSIVATION, pH ADJUSTMENT AND CHLORIDE RESISTANCE	28	48	8,500

TABLE I - EFFECT OF FUNCTIONAL PROPERTIES OF VARIOUS CRACK ARRESTMENT INHIBITORS ON LOW-CYCLE FATIGUE OF HIGH STRENGTH 4340 STEEL

5. *Agarwala, V.S., and DeLuccia, J.J., "New Inhibitors of Crack Arrestment in Corrosion Fatigue of High-Strength Steels," Corrosion, 36(4), pp. 208-212, 1980.*

6. *Hyatt, M.V., "Use of Pre-cracked Specimens in Selecting Heat Treatments for Stress Corrosion Resistance in High Strength Al Alloys," Corrosion, Vol. 26 No. 11, pp. 487-503, 1970.*

FIGURE 4 - ENVIRONMENTAL TEST CHAMBER CONTAINING DCB SPECIMENS FOR DETERMINING SCC OF 7075-T6 Al ALLOYS

Only a drop of the test solutions were added once a week. The crack growth of the specimen was monitored periodically. The results obtained from this test are shown in figure 5 as crack growth rate versus stress intensity factor (da/dt versus K_I) curves for an inhibitor combination of dichromate + nitrite + borate + molybdate (DNBM), in two environmental conditions. A marked crack growth retardation effect was observed for DNBM as demonstrated by the shift in the da/dt versus K_I curves to a much higher stress intensity value. In other words, the K_{ISCC} Value For 7075-T6 aluminum alloy was increased by a factor of two when these inhibitors were used. Efforts are continuing to evaluate several other inhibitors.

FUTURE PLANNING

Electrochemical investigation of selected candidate corrosion inhibitors will be continued to study their anodic and cathodic (hydrogen permeation) effects. Several other formulations will be made in other possible alternate non aqueous media to seek greater stability of the compounds present. Evaluation of the inhibitors will be continued and extended to other forms of corrosion such as exfoliation and wear.

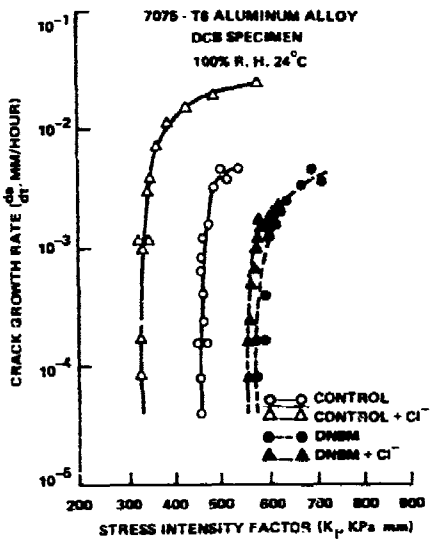

FIGURE 5 - EFFECT OF INHIBITORS ON STRESS CORROSION CRACKING PROPERTIES OF 7075-T6 ALUMINUM ALLOY

The research as planned is expected to translate into useful products, procedures and techniques for fleet application. Progress has already been made in the development of the corrosion monitor probe and a forumulation for inhibiting corrosion fatigue in high-strength steels.

Biography

Name: Koelling, James H.

Present Affiliation: 3M St Paul, Minnesota

Title: Technical Manager Industrial Tape Division

Field of Interest/Responsibilities: Pressure Sensitive Tapes: Product Development, Product Engineering, and Technical Service worldwide.

Previous Affiliations/Titles: Colonel United States Army (Retired) 30 years service in the RA and USAR

Professional Musician - self employed

Academic Background: B.S. Chemical Engineering, Iowa State University
Graduate study: University of Iowa, University of Minnesota, Drake University and Macalester College work toward PhD in Education.

U.S. Army Command and General Staff College, graduate of The Army War College

Society Activities/Offices: Technical Association of the Pulp and Paper Industry: Chairman, Winding Committee, Finishing and Converting Division

Reserve Officer's Association
Cheerhaven Inc. Dalton GA: Member, Board of Directors

Publications/Papers: 1980 papers only:
Pressure Sensitive Tapes for the Electronics Industry ASME
Splicing Materials and Methods: TAPPI
Repulpability of Splicing Materials and Test Methods: TAPPI
Energy Curable Adhesive Systems: AMP Inc.
beam curable Imaging Systems for Hybrid Micro Circuits: Sanyo, Japan, ITT and TI, USA
Tapes for preferential masking during Metal Plating: Airline Plating Conference
Splicing Materials for $CaCO_3$ Low Binder Coatings on Gravure Papers: Haindl Paper GMBH Germany, and Timavo, Trieste

The title of my presentation is "Pressure Sensitive Tapes to Prevent Corrosion on Metal Surfaces".

To tell the truth about it, tapes really don't do much to prevent corrosion; but they do assist in many ways as an industrial tool allowing you people to apply corrosion preventing coatings to metallic surfaces. So we thought we might have a little fun with sticky tapes and, at the risk of insulting your intelligence, talk a little bit about what tapes are in general.

(Backing Slide)
You can see here in front of you that we, the industry, make pressure sensitive tapes out of a number of materials. The backing is the part that is not sticky and, as you can see, we make tapes out of paper, we make tapes out of cloth, we make tapes out of foil; and foil, as the industry tells us, is any kind of metal that is 6 mils or thinner. We make tapes out of green pool table felt and whatever else you might like to try. So you have seen in your business and in your day-to-day activities, I am sure, tapes made out of all of these different materials and maybe some others.

Let's take a look at the next slide and see what adhesives are made of. Generally, the pressure sensitive tape industry makes adhesives out of three different kinds of chemistry. When we say rubber resin, we mean, of course, natural rubber which is chemically pretty much isoprene; but we also think of all the synthetic rubbers available today: butadiene styrene, butadiene acrylonitrile, and some of the new block copolymers. Shell Co. has something called "Kraton". Many different kinds of synthetic rubbers provide some very interesting characteristics.

First of all, rubber resin adhesives can be very sticky. They stick to your fingers. They stick to most surfaces tenaciously - right away; but they are not very long aging. They do tend to oxidize and dry-out and in a matter of a relatively short period of time lose holding power.

The acrylate adhesives, on the other hand, tend to be permanent -- whatever that word may mean. People ask us what is the difference between the word acrylic and the word acrylate; and one of our smart marketing guys said "the difference is that one is a noun and the other is an adjective". And that is really what they are, so when we banty the words acrylate and acrylic around, this is typical of what we mean.

Acrylates are esters of acrylic acid that has reacted with an alcohol. Although they do tend to be a little bit sensitive to water, they are not soluble in water; but when we have high concentrations of moisture, the acrylate adhesives do not do too well. Again, to quote our marketing man, "When any of us get involved with mixtures of alcohol and water, we tend to get a little bit unglued also". This is what happens to acrylate adhesives.

Silicone adhesives, on the other hand, are very much like rubber adhesives except you substitute silicon atoms for the carbon atoms that you have in rubber molecules; whether they are natural or synthetic rubbers. Silicones are characterized by high strength at elevated temperatures - but not very tacky to begin with. So the industry (and their are many of us in the industry) has these same three kinds of adhesives for a variety of applications.

Let us just take a look at some of the chemistry that is involved in the acrylate adhesives. They are reaction products of acrylic acid and one of the alcohols. The first (Slide) one you see is something you might call 2-ethyl hexylacrylate. Depending on where you went to school, you might call it something else.

The second one as you can see has two methyl groups attached. We call that 2-5 dimethyl hexyl acrylate; so these would be products that are made from acrylic acid and 2 ethyl hexyl alcohol or 2-5 dimethyl hexyl alcohol. These are products that are tacky or sticky by them-

selves. They do not require any wood rosins or other additives to make them sticky, but they do have very interesting chemical resistance.

Let's take a look at one more. Typically, acrylate adhesives are copolymerized. They are copolymerized with acrylic acid; so if you look at the bottom line, you will see that in the middle, we have (Slide) the acid carboxyl functionality of the typical organic acid as well as the acrylate ester formulation.

They are copolymerized with acrylic acid so are not totally, in many cases, esters, but are copolymerized with the acrylic acid.

Here is the one exception where pressure sensitive tapes really do (Slide A) act to minimize metallic corrosion. This is a picture which shows the use of a polyester film with a pressure sensitive adhesive on one side to separate two dissimilar metals to minimize galvanic corrosion.

This is a piece of tape that is being put down on part of the (Slide A) air frame which is subsequently covered with a skin surface. The significant thing here is that the chemical resistance, in this case, of an acrylate adhesive makes it permanent, non-aging, and not subject to drying-out. This is a piece of tape that will last pretty much for the life of the aircraft & separate those two metals, effectively preventing galvanic corrosion.

We think it is important to have an adhesive system which is permanent. This is why we use the acrylate adhesive systems. We also think it is necessary to have a backing material which is dimensionally stable over a wide temperature range. This is why we use polyester film backings. And when I say we, I mean the pressure sensitive tape industry, not just necessarily our particular company.

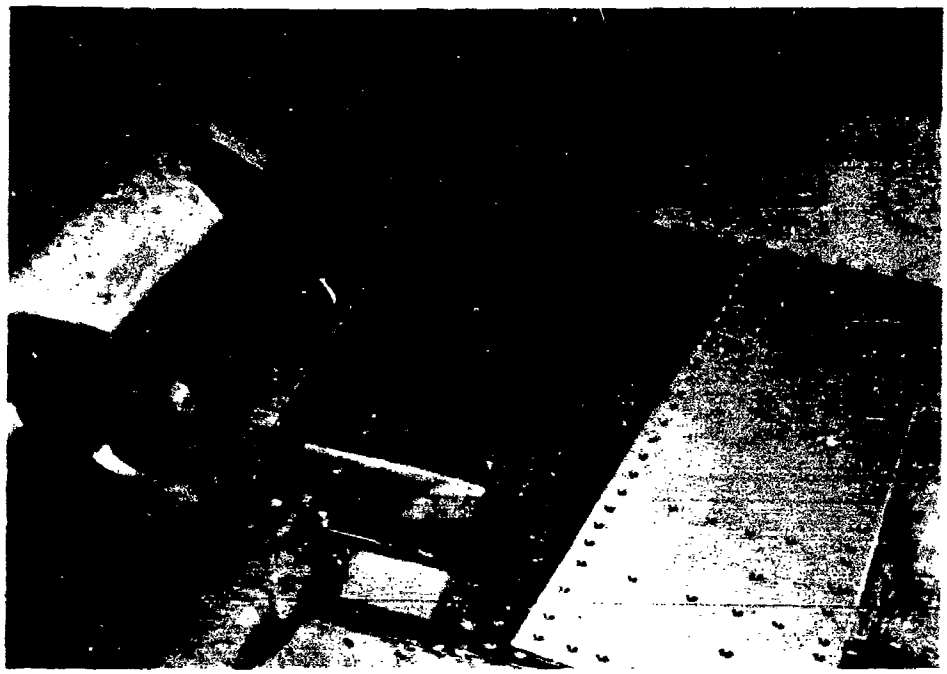

Slide A

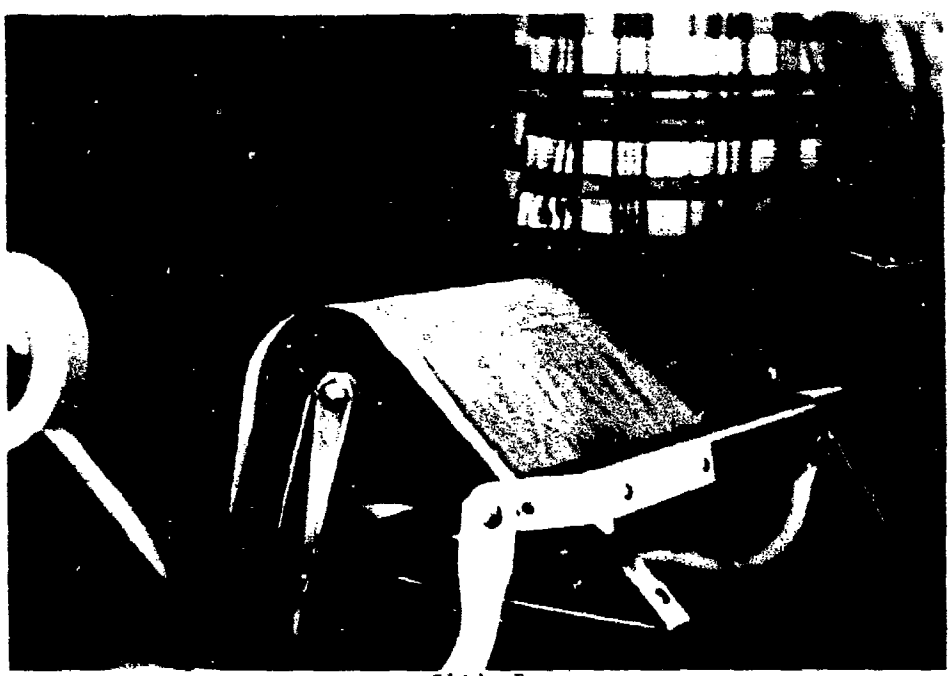

Slide B

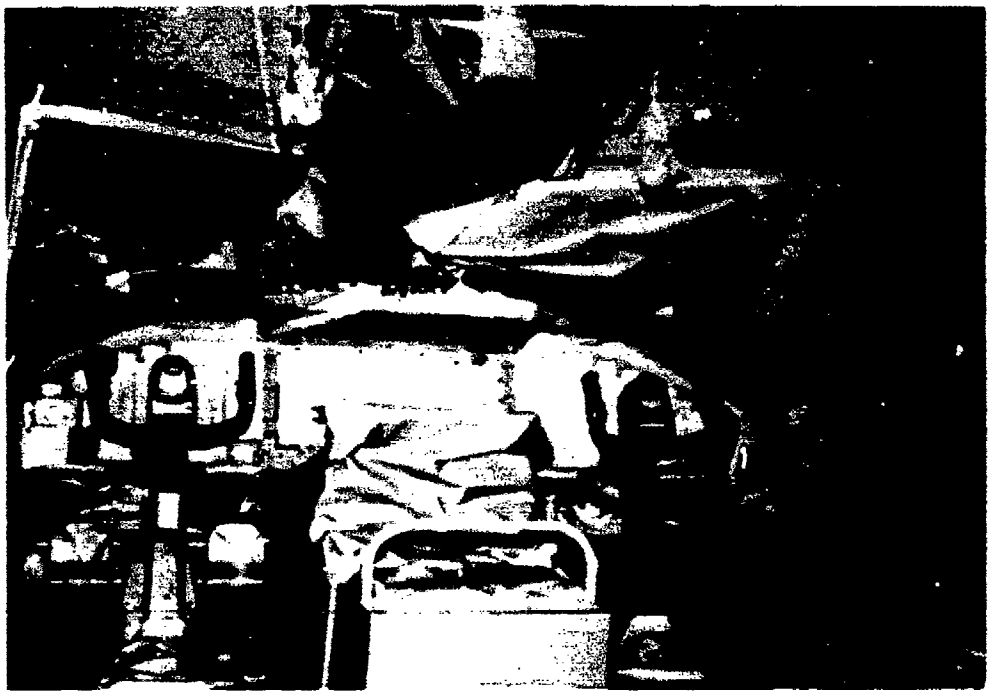

Slide C

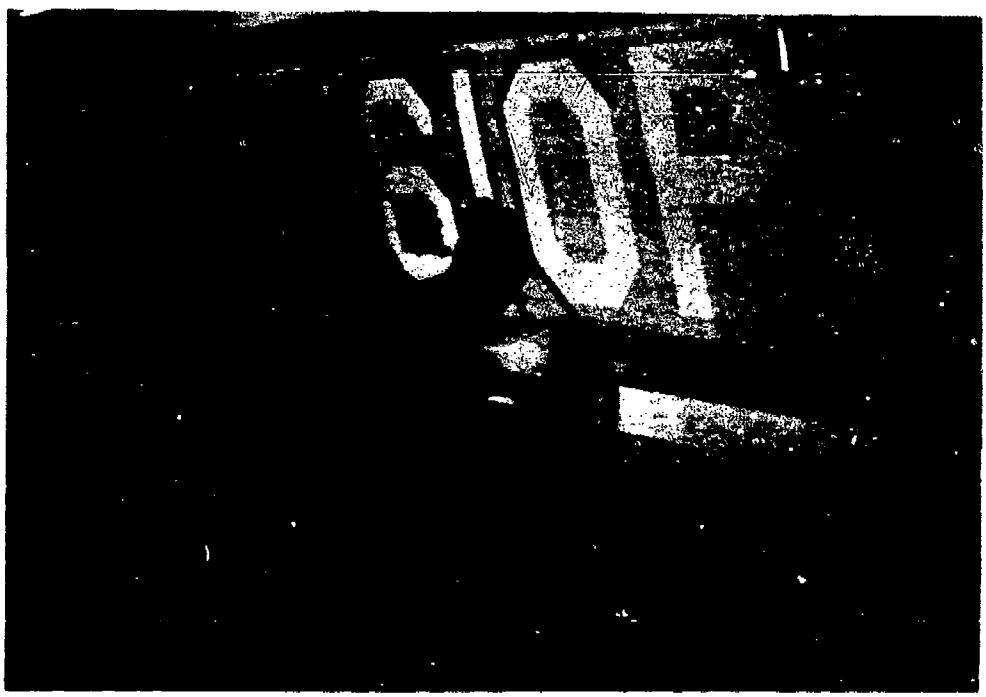

Slide D

Pressure sensitive tapes really contribute a great deal toward the prevention of corrosion as they assist you in applying corrosion resistant coatings.

This is what is called an apron taper. This combines a masking tape (Slide B) and a piece of paper used in the taping of an aircraft.

This is not really a slide on corrosion, but it is the interior of a C-5A. (Slide C)

There are 13 different colors in the cockpit of this airplane. You see it masked, so that paint can soon be applied. Tape and masking paper are very effective industrial tools in allowing you to do this kind of job.

This is a very interesting picture. It is strictly paint masking, but of course, the chemistry of paints changes every day. Paint (Slide D) is applied to the aircraft in order to prevent metallic corrosion. The tape is simply an industrial tool which allows you to apply paint where you want paint to go and to keep paint away from where you do not want it.

Rubber resin adhesives, typically used in masking tapes, allow you to mask-off an aircraft, or ship, or military vehicle and pull that tape off after the job of applying corrosion prevention coatings is completed. Without pressure sensitive tapes, you really can't do these jobs totally.

This is a helicopter and the picture (Slide E) simply shows a stenciling operation - once again, the utility of a pressure sensitive tape is an important industrial tool - allowing you to apply a corrosion prevention material.

This is another picture that shows that the pressure sensitive (Slide F) tapes can be die cut in odd formations and shapes. This is a triangular section being applied on the canopy of the airplane as a masking material prior to painting.

Here is something relatively new in the pressure sensitive tape (Slide H) industry. It is a shot of a plasma spray; and what we are showing here is that pressure sensitive tapes (and not the typical roll of masking tapes that would never withstand a situation like this) can be designed to do the unusual. There are pressure sensitive tapes made out of aluminum foil backing, glass cloths, and laminates and combinations of the two that will withstand a plasma spray operation and allow you to spray the plasma coating on one surface and keep it off areas you do not want coated. This particular shot was taken at Tinker AFB.

This is a bit mundane, also, but when you are applying corrosion prevention coating, for example, hard chrome, there are certain (H) areas of the parts which do not require chrome to be applied. If you look carefully, you will see small areas of yellow tape. This is a polyvinyl chloride tape which is put around the parts in those areas where you do not want chrome plating to be applied. The solution is to get an industrial tape with chemical resistance to do the job.

Slide E

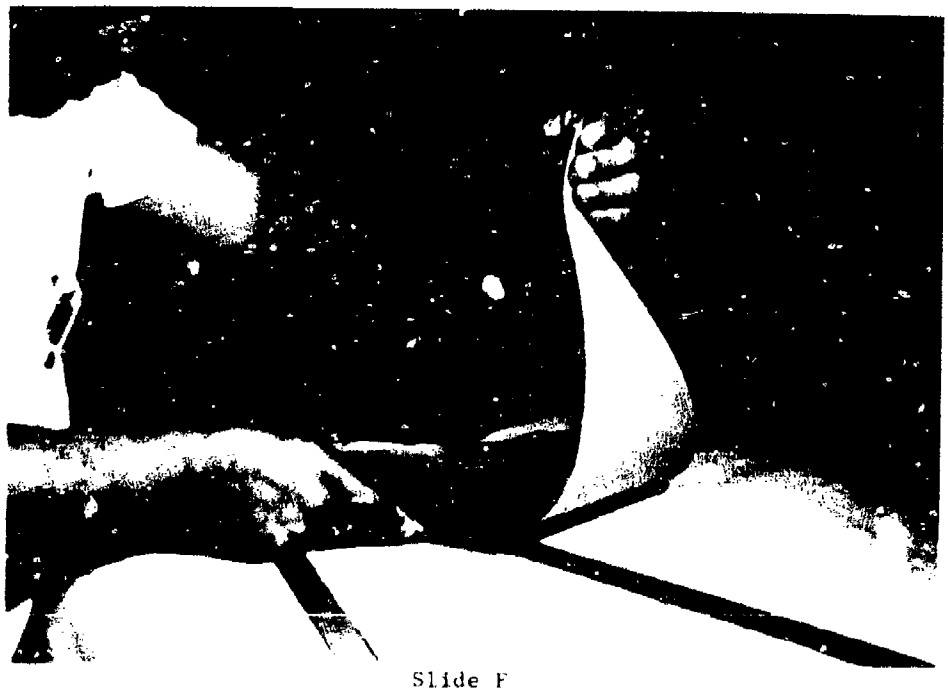

Slide F

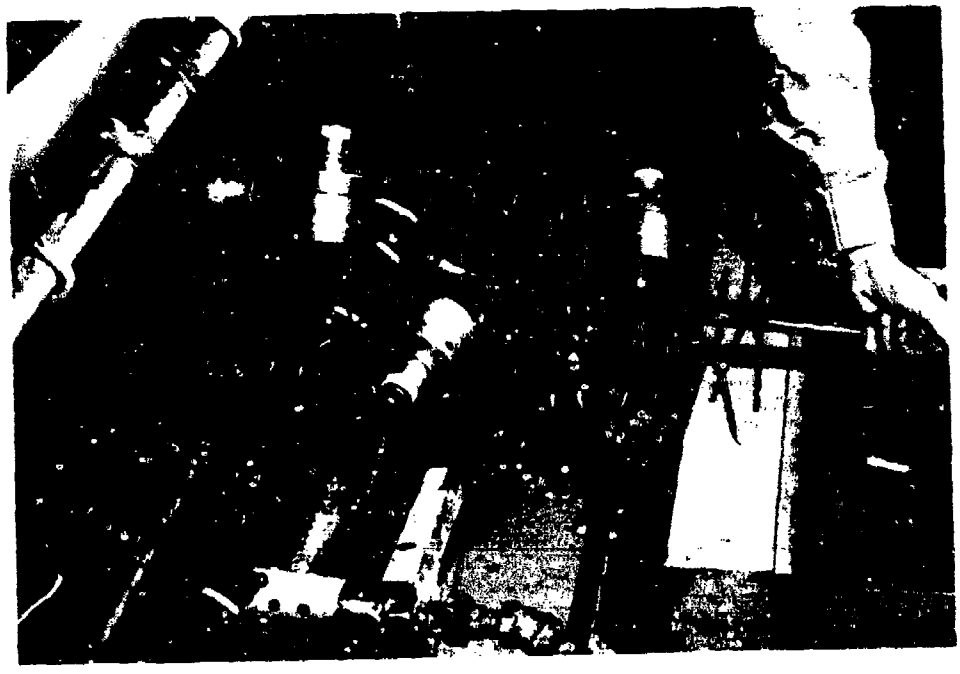

Slide H

Slide I

The formulation of vinyl tapes is something that our industry has worked on for many years. We use special plasticizers in the formulation of the backing. There are both monomeric and polymeric plasticizers, but they all have the chemical resistance for use in plating baths - and provide masking to prevent chrome from being applied to certain areas of the metal part. So when we think of a piece of vinyl chloride film, we are thinking about something much less sophisticated than the specially formulated backing on vinyl tapes. The chemistry of plating tapes is complex - the chemistry of the adhesive, and the chemistry of the backing. They do allow you to do a plating job and apply a corrosion inhibitor.

This is a series of pictures where again we are stretching the point a little while talking about corrosion inhibition. From time to time we have to take the old paint off and reapply a new coat of paint to improve corrosion inhibition.

This is a picture of a 707 (Slide I). This gentlemen is putting masking tape on the windows of this aircraft. This particular masking tape happens to be a metal foil. He is actually attaching the tape only to the frame around the edge of the window, because the acrylic adhesive that we use on this tape does stick quite well to the acrylic windows. Therefore, the adhesive surface is not in contact with the window, but is actually blocked-off and covered by paper. This gentlemen is putting on these pre-cut window masks and attaching the adhesive only to the framework of the window.

Now let's look at paint stripping. This is a rather dim picture of an aircraft. (Slide J) This shows the use of metal foil tape prior to the paint stripping operation. The chemistry of the acrylate adhesive resists the alkaline paint strippers. The aluminum foil has enough resistance to the alkaline paint strippers to last during the process. The adhesive is such that after the paint stripping operation, the tape will come off cleanly without adhesive residue on the aluminum metal.

Slide 3

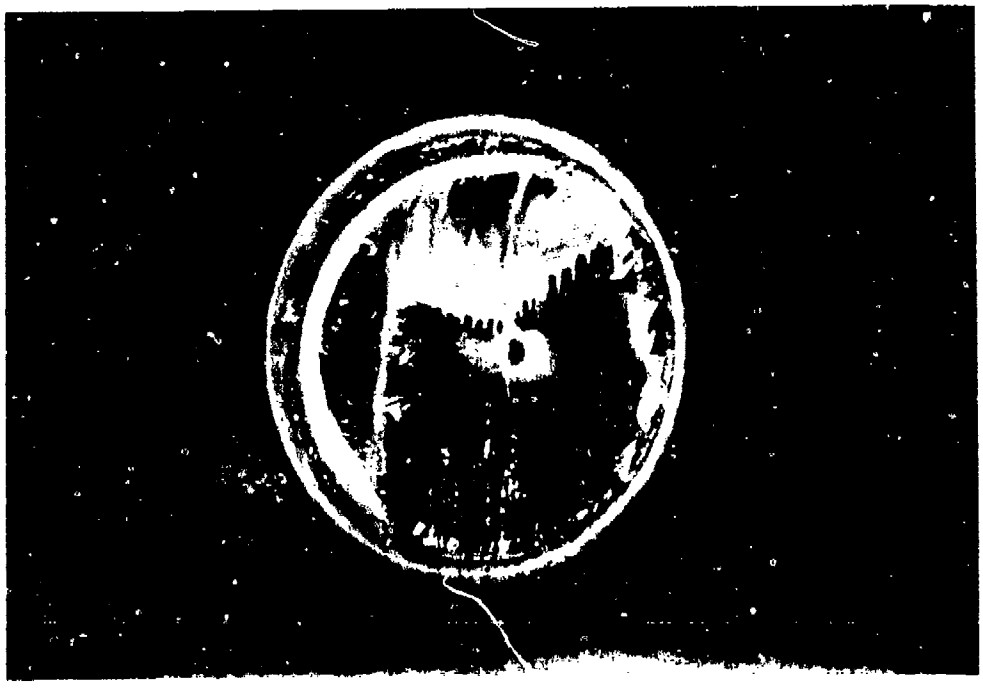

Slide L

Slide M

This picture (Slide K) shows a different aircraft, but obviously, this is an engine intake that has a polyethylene film which has been adhered with tape. Then again, we are counting on the chemical resistance of the combination of the metal foil tape and the adhesive to resist the paint strippers.

Here is a typical shot that you ladies and gentlemen have seen many times (Slide L) where the paint stripper is being sprayed on the airplane. The plastic film is held on with a pressure sensitive industrial tape which has sufficient chemical resistance to allow the old corrosion inhibiting material to be selectively removed before applying the new.

This is a roll of pressure sensitive tape that is being applied to an (Slide M) acrylic canopy that is being formed. Now it doesn't have much to do with corrosion, but nevertheless, it does show another example of pressure sensitive tapes having good chemical resistance.

Tapes have been used for many years as erosion inhibitors, particularly on helicopters where polyurethane tapes have been applied to the leading edge of rotor blades - main rotor blades as well as tail rotor blades. I have had a couple of tours in Viet Nam with an Aviation Battalion, and we literally kept aircraft flying simply because we had tapes that could be used on aircraft in order to prevent both rain and sand erosion.

There was a time a few years ago when we had the Berlin Corridor which was controlled by the Russians and the maximum flying altitude allowed in flying from West Germany into Berlin was 10,000 ft. As you know, there were very difficult weather conditions many times. I think that Pan American kept their aircraft flying simply by being able to cover the leading edges of the wings with erosion inhibitor materials which were really pressure sensitive tapes - sticky on one side with a resilient polyurethane material as the backing.

There is a rather strange use of pressure sensitive tapes that we in the industry don't really support. That is the use of a pressure sensitive tape to measure the effectiveness of coatings you put on a piece of metal. There are two specifications, one Federal and one Military, that prescribe the use of pressure sensitive tapes to measure the anchorage of a coating which has been applied to metal. We in the industry do not think that these are very effective because there are so many variables involved in how the tape is applied, how long it is on, how quickly and rapidly you can pull it off and at what angle the tape is removed, that we think we may not be measuring anchorage with validity. So this use of pressure sensitive tapes, from the tape industry viewpoint, is not typically recommended although very very widely used.

Tapes have been used as sacrifical corroders. For example, we have made tapes out of zinc foil with a permanent pressure sensitive adhesive, and applied them on certain military vehicles. We have also put such tape on aircraft and on trucks and allowed the "tape" to sacrificially corrode away, thereby protecting the surface to which it is applied. This again is quite a remote and unusual use for pressure sensitive tapes.

We have all heard about mothballing airplanes and mothballing military equipment. The Marine Corps for many many years had a facility in Barstow, California, where vehicles were stored. Pressure sensitive tapes have been used as a preservation material for many many years in this type of application. The Navy and Air Force utilize this preservation technique on aircraft near Tucson, Arizona, also as both corrosion preventors and corrosion inhibitors. On some aircraft that have been stored in the mothball fleet for 10-15 years, the tapes can be pulled off, and with a minimum amount of cleanup and maintenance, the aircraft is virtually on its way. So, we believe that pressure sensitive tapes have really done quite a good job in helping to preserve military equipment for a number of years and eliminate, or certainly minimize corrosion that would have taken place because the item had been in storage.

I would now like to talk to you about some of the technologies evolving in the pressure sensitive tape field. For many many years people have said we certainly would like to have a tape that sticks well to aircraft, vehicles, or to a cardboard box for that matter, and then, at the snap of a finger, the tape should pull off easily and cleanly. The industry has said for many years that this is impossible. But no longer, because of some very interesting new chemistry.

Due to this interesting, new technology, we now have energy-responsive adhesives that will allow you to have a tape that is very sticky, and then, but subjecting it to ultra violet or to electron beam radiation, you can kill the tack to whatever level you want. So when you are using tape as a corrosion inhibitor, or if you are using a tape as a packaging material, or if you are using tape as a masking material, or for whatever purpose, we now have in our industry the technology to give you a very sticky tape and then have it literally fall-off when you want it to. All of this can occur without adhesive residue, and without excessive expense.

This is actually a silicon wafer (Slide N) which has been etched with circuitry that will go into a hybrid microcircuit. To process this wafer, a pressure sensitive tape is used to hold it as it is being sliced, sawed or diced. After the wafer has been cut into many small pieces, the individual die can be picked off easily because one can detackify the tape down to where it has no tack. It was strong enough to hold the wafer during processing and then detackifiable so the individual die can be picked off with a vacuum probe or by a needle cluster coming up from underneath.

(Slide O) This is a blown-up picture of a 3" diameter silicone wafer which has circuitry and has been diced and sawed through. You can see two of the little die which had been individually removed. This is the
(Slide P) machine that does the sawing and cutting and you can see here again the pressure sensitive tape down near the bottom, sticky side up, holding the wafer as it is being sawed. The adhesive is then de-

tackified so the individual pieces can be pulled off.

(Slide Q)This is a similar application which involves the back side of the silicon wafers being polished. Again, a very sticky tape holds them down but we have the ability to detackify the adhesive so wafers will literally fall off.

Another thing our industry is doing which we thought you might be interested in is in the area of measuring hydrogen embrittlement. There is some new interesting technology in the pressure sensitive tape area that allows one to measure quantitatively the amount of hydrogen entrapped in a structural member, and therefore, estimate the amount of hydrogen embrittlement that has occurred because of that entrapment.

The patent for this process is held by McDonnell-Douglas and tape is used as a tool. In the determination, a patch, similar to a "Band-Aid" is made. The "bandage" portion of the patch is a coating of Neodymium metal on a smooth substrate. The "tape" portion of the "Band-Aid" is a neutral, high temperature tape of low permeability. (usually including aluminum foil).

The patch is placed over the area selected for the test, and secured in place with the tape. The test piece is then heated to drive hydrogen out. The hydrogen reacts with the neodymium metal forming a visible color change at the reaction site. The patent states that by measuring the reaction site and applying the proper calculations, a close approximation of the hydrogen content can be calculated. This helps to predict whether, or how much embrittlement has occurred and what can be expected in terms of the strength of the member.

The old days of the twenty five cent roll of paper masking tape to help paint an aircraft and put a coating on it that will resist corrosion have left.

We are not the only company that makes pressure sensitive tapes, and we think we have a very strong, vibrant industry. We hope that pressure sensitive tapes do provide a useful tool for your people in whatever phase of corrosion prevention and control you work.

AFWAL-TR-81-4019
Volume II

Scanning Electrode Techniques in Corrosion*

H. S. Isaacs and B. Vyas

Brookhaven National Laboratory

Upton, New York 11973

July 1981

*Research carried out under the auspices of the United States Department of Energy under Contract No. EY-76-C-02-0016

TABLE OF CONTENTS

LIST OF FIGURES

LIST OF FIGURES (Cont'd)

AFWAL-TR-81-4019
Volume II

Scanning Electrode Techniques in Corrosion*

H. S. Isaacs and B. Vyas

Brookhaven National Laboratory

Upton, New York 11973

ABSTRACT

The principles, advantages, and implementations of scanning reference electrode techniques are reviewed. Data related to pitting, intergranular corrosion, welds and stress corrosion cracking are presented. The technique locates the position of localized corrosion and can be used to monitor the development of corrosion and changes in the corrosion rate under a wide range of conditions.

*Research carried out under the auspices of the United States Department of Energy.

INTRODUCTION

The definition of localized corrosion usually is restricted to specific types of attack often related to the presence of chlorides. This definition may be broadened to incorporate all other cases where corrosion takes place at specific areas of the metal surface. General corrosion rates in most systems have been measured and design allowance can be made for the metal losses during the expected life of the system. Problems arise when the corrosion becomes localized and the penetration rate of the metal is orders of magnitude greater than the predicted general corrosion. Localized forms of corrosion, therefore, take a far greater toll than the incorrect choice of materials having unacceptable general corrosion rates.

During localized corrosion,[1,2] the electrochemical dissolution is well separated from the cathodic reactions. This makes an *in situ* study of the anodic and cathodic reactions amenable to direct measurement and to clearly separate the anodic and cathodic reactions in contrast to general corrosion where the reactions can take place in close proximity. *In situ* measurements such as mapping of potentials in solution or the physical separation of anodic and cathodic areas and measuring the currents flowing between them have been used successfully to identify the processes during corrosion.[3,16]

Figure 1 shows a schematic of the flow of current in the electrolyte from a localized anodic to the surrounding cathodic areas and equipotentials set up around the localized electrode. By scanning a "passive" reference probe with a fine capillary tip parallel and in close proximity to the metal surface the potential distribution in the liquid can be measured. The potential changes are most rapid over the localized electrode and a potential maximum or minimum is observed over its center. In the SRET work presented here, the sign convention

adopted is opposite to that generally used in order to show anodic areas as potential peaks and cathodic areas as minima. Thus, the SRET is an in situ technique to locate the anodic and cathodic sites and study the electrochemical processes during localized corrosion, without altering the processes taking place, changing the local environment over the corrosion site or influencing the rate of corrosion. The scanning technique has been recently reviewed.[11]

Areas around a weld have been studied separately using a liquid drop drawn across the sample. The potential variations and the polarization characteristics as a function of the drop position were measured.[3] In another study,[4] an insulating coating over a weld area was perforated with a micro-hardness indentor, and a liquid drop was placed over the perforation and the potential and the polarization characteristics of the underlying deformed metal was determined.

The flow of current from the anodic to the cathodic areas can also be determined without sectioning samples. In an early work on water line corrosion, Evans and Agar[5] calculated the current from the measured equipotential lines during the corrosion of zinc. A scanning reference electrode technique (SRET) was used to measure the potential variation in the solution. An agreement of within 10% was obtained between the measured corrosion rates from weight loss and the calculations from the equipotential surfaces.

Jaenicke and Bonhoeffer,[6,7] Copson[8] and Rozenfeld[9] measured the potential distribution around galvanic couples and calculated the corrosion rates and the surface current density distributions. Measurements of potential distribution during corrosion of bismuth-cadmium and zinc-aluminum alloys were also studied.[7] More recent measurements of couples of iron and copper have been conducted by Heldebrand and Schwenk.[10]

EXPERIMENTAL TECHNIQUE

The potential fields generated in the electrolyte due to local corrosion sites can be measured by scanning a microtip reference electrode over a horizontal exposed surface facing up. The equipment built at Brookhaven National Laboratory is shown schematically in Fig. 2.[12,13] The microtip reference electrode is held by a mechanical stage attached to low friction, linear bearings for smooth motion in the X and Y direction, and driven by two stepping motors. The mechanical stage can be automatically programmed to scan both in the X and Y directions parallel to the specimen surface. The length of the X direction can be varied up to 26 mm, and, at each end of the X scan, the Y direction can be shifted to a set value (from 30 m to 200 m). Thus, an area of the surface is scanned by a rectangular wave. The linear speed of the scan in the X direction can be varied from 0.1 mm/sec to 300 mm/sec.

Alternatively, potential fields on cylindrical samples can be obtained by keeping the probe stationary while rotating the sample.[14,15] The microtip reference electrode measures the potential variations along the circumference of the sample as the potential field around the sample rotates with the sample. A schematic of such an instrument is shown in Fig. 3.[15] A motor is used to rotate a cylindrical metal specimen in the electrolyte such that the rotational motion of the sample is synchronized to produce a signal which is proportional to the angular position of the sample with respect to the probe. The microtip reference electrode is made to scan in the vertical direction (parallel to the cylindrical axis). If the signal of the sample rotation is fed to the X direction and signal of scan of the probe to the Y direction, the surface scan of the cylindrical specimen is obtained. The size of the area examined on the specimen surface can be controlled by regulating the length over which the microtip refer-

ence electrode moves along the axis of the sample and controlling the time per revolution of the specimen.

The potential field in the electrolyte during localized corrosion is the difference in the potential measured by the microtip reference electrode and a reference electrode placed more than 10 mm away from the sample surface. The two signals are fed into a differential electrometer and the resultant potential amplified to the desired amount. The potential fields can be plotted on a X-Y recorder by feeding the signal from the X position of the motor to the X amplifier of the recorder the sum of the Y position of the motor and the amplified potential difference to the Y amplifier of the recorder. Thus, one obtains a two dimensional plot of the potential field variations at a plane parallel to the sample surface. The signals can also be recorded on a storage oscilloscope and photographed. Alternately, the amplified potential difference can modulate the intensity of the cathode ray tube of an oscilloscope,[11] or plot the equipotential lines from an analyzer.[15]

APPLICATIONS

Pitting Corrosion

Pitting corrosion is a highly localized form of corrosion attack of passive metal surfaces and is generally directly related to the presence of chlorides or bromides. The development of pitting is sensitive to almost all variables associated with the interface between the metal and the electrolyte. These variables include the chloride concentration, the presence of other anions which may act as pitting inhibitors, the composition of the metal, its surface preparation and history and the electrochemical potential.[16-22]

The pitting behavior of stainless steels was investigated by Rosenfeld and Danilov using the adjacent reference electrode technique.[16] Their measure-

ments were carried out in a solution containing about 0.05M $FeNH_4(SO_4)_2$ and 0.1 or 0.56M NH_4Cl. They could detect pits after 30-60 secs after contact with the solution. Initially the rates of dissolution of all the pits were similar, however, with time, some of the pits stopped corroding or showed decreased rates. Observations of the pits under the microscope showed that they were covered by a film or shielding layer resulting from the attack of the metal by chloride ions penetrating the oxide film. Destroying the shielding layer led to passivation. The authors considered the rupture of the shield assisted the diffusion of the "passivator" into the pit. The process of passivation took a relatively long time, of the order of tens of minutes, after disruption of the shield. Also, the time for deactivation of the pits increased with the size of the pits.

The currents from the pit were related to the square root of time. The current densities, therefore, decreased and assuming a hemispherical pit, the surface area varied linearily with time. This result is in agreement with work by other investigators.[17,18]

The SRET has been used to study the pitting of type 304 stainless steels in a ferric chloride solution[12,21] composed of 0.4M $FeCl_3$ and adjusted to pH 0.9.[20] The change in the number of active pits were studied as a function of time and surface preparation. On exposing the steel to the solution, the potential of the specimen increased rapidly above the pitting potential with the generation of active pits. With time, the potential of the specimen decreased as the active pits grew and the number decreased. However, small potential increase were observed when pits passivated. The active and repassivated pits were separated using the SRET. The active pits were always covered by a film and contained a dark green solution. Fig. 4 shows a sequence of scans

represented by potential surfaces for an electropolished surface at the times shown. Each peak is associated with the currents from active pits. On the first scan, initialed one minute after exposure, fourteen pits could be identified. The number of active pits decreased and only one pits was active after 26 minutes. When the final pit was subjected to a jet of solution, it repassivated. The anodic currents polarizing the cathodic reaction then ceased and the potential rose rapidly above the pitting potential and the sequence of events observed on first contacting the specimen with the chloride solution was repeated.

It was suggested that the film over the active pits was the passive oxide film originally on the metal surface that was undermined by the pitting process.[12] This possible explanation was investigated by varying the surface preparation of the stainless steel prior to pitting.

The results were found to be consistent with the changes in the properties of the original oxide layer over the pit before it was undermined by the pitting process. The thicker the oxide, the greater was the protection afforded to the growing pit and the longer the pits remained active. When the metal was abraded, stresses in the oxide film lead to short half-lives (< 1 sec). The half-lives of pits on abraded surfaces was low ($\sim$ 5 min.) even after oxidation at 250°C in comparison to similarly oxidized electropolished surfaces which gave a half-life of 480 minutes.

Intergranular Corrosion

Intergranular corrosion (IC) is defined as the localized attack, at the grain boundaries of steels. This form of corrosion is particularly severe in stainless steels which are sensitized. Sensitization is caused by (1) heat treating the alloy in the temperature range of 500-850°C for a few hours and

quenching; (2) cooling slowly through the above mentioned temperature range and; (3) welding.[23,24] It is generally believed that sensitization leads to the precipitation of chromium rich carbides at the grain boundaries and the depletion of chromium adjacent to the boundary.[25] This depletion has been observed by scanning transmission electron microscopy.[26] The depletion of chromium at the grain boundary leads to IC of stainless steels in certain environments.

The SRET has been used to determine the accelerated corrosion of grain boundary region in sensitized type 304 stainless steel. Fig. 5(A) is a potential scan during the IC of a large grain size (diameter ~ 3 mm), sensitized (600°C for 24 h) type 304 stainless steel in 2.5N H_2SO_4 at room temperature at a potential of -200 mV vs. SCE. Fig. 5(B) is a line drawing of the etched boundaries on metallographic observation after the test showing a clear relation between the etched boundaries (dark lines) and the peak maximum in Fig. 5(B) (dotted lines). The potential peaks were observed only in the case of sensitized type 304 stainless steel, while solution annealed (1100°C for 3 hrs) samples exhibited no peaks and no grain boundary etching in this solution.

The dependence of intergranular corrosion on the electrochemical potential of type 304SS in 2.5N H_2SO_4 can be determined by slowly increasing the potential (0.3 V/h) of the sample in the anodic direction and scanning the surface simultaneously. In the potential region where sensitized type 304SS is susceptible to IC, peaks are observed on scanning, while in the potential region, where the material does not undergo IC no peaks are observed. The material is susceptible to IC between -280 mV to +80 mV vs. SCE and then again in the transpassive region (> 820 mV vs. SCE), as shown in Fig. 6. This result is consistent with the observation of IC of this steel in the Strauss test and the nitric acid test.[27]

Welds

In welding, it is assumed that corrosion behavior of the weld metal and the parent metal is similar. However, this is not always the case, particularly when austenitic stainless steels are considered. The weldment, i.e. the weld metal and the adjacent parent metal affected by the heat of the welding, may be susceptible to varying degrees of preferential attack. The weld metal may corrode more or less than the parent metal due to differences in composition or metallurgical condition.[24] In addition, the base metal heated during the welding may corrode as a result of metallurgical changes caused by heating cycles.[23] The factors that can influence the type and degree of preferential attack depend on 1) composition and structure of base and weld metal, 2) metallurgical changes in the parent metal due to welding, 3) welding process and procedure, 4) size of material welded, and 5) the type of the environment.[28]

The SRET has been successfully used to identify the preferential attack of type 304 stainless steel weldments. The type of preferential attack observed are 1) attack of the ferrite in the weld matrix, 2) fusion boundary corrosion, 3) intergranular corrosion of the sensitized material in the heat-affected zone of the base metal.[13] A type 304 stainless steel weldment was tested in 2.5N H_2SO_4 at room temperature at various potentials. The potential regions exhibiting the different types of preferential attacks are shown in Fig. 7.

Sensitization in the heat affected zone adjacent to the weld is probably the most common cause of intergranular corrosion and intergranular stress corrosion cracking in stainless steels in service. In order to determine the susceptibility of a given weldment to these forms of localized attack, it is necessary to develop a test which will give 1) the location of the sensitized zone, and 2) a quantitative measure of the degree of sensitization. The SRET meets the above

mentioned requirements and has been successfully used to give the location and the degree of sensitization of the weldments for various welding process variables. The details of the test are given in detail elsewhere.[13]

Stress Corrosion Cracking

Stress corrosion cracking in metal systems is concerned with the nucleation and propagation of cracks in stressed metals induced by the environment. In order to understand the mechanism of cracking in any particular metal-environment system, it is necessary to determine the electrochemical reaction(s) that take place at the crack tip. The SRET provides an ideal system to study this reaction and in this section, an example is given of SCC of type 304 stainless steel in a chloride solution. The electrolyte used was 20 molal LiCl controlled at 90°C.

Fig. 8 shows the potential peaks observed after the cracking had progressed into the metal. The propagation of the potential peaks was studied. Fig. 9 gives the magnitude of potential peaks along the length of the crack at various times taken from figures similar to Fig. 8. The shape of these plots which are non-symmetrical, indicates that although the dissolution rate was greatest at the crack tip, the entire crack remained active. These observations are consistent with most theories of stress corrosion cracking, i.e. rapid dissolution takes place at the high stress intensity at the crack tip where fresh metal is continuously exposed to the corrosive environment.[29] However, the persistent anodic dissolution of the crack surfaces shown using SRET, during cracking and after the specimens fail, is in conflict with models which suggest that the crack surface must passivate to account for crack propagation. The SRET suggests that the exposed metal remains active but with decreased dissolution rates.

SUMMARY

The SRET has been shown to offer a technique for studying localized forms of corrosion including pitting, intergranular corrosion and stress corrosion cracking. These processes are associated with relatively rapid dissolution rates and observable potential variation in solution. The technique is also useful in separating preferential dissolution or cathodic reactions under controlled potentials where external currents flow.

Other electrochemical measurements e.g. polarization techniques, can give detailed information about processes under study, but, difficulties arise in the complete separation of the anodic and cathodic areas and duplicating the conditions operative during corrosion. The SRET overcomes these difficulties, and offers an approach for in situ determination of the corrosion processes and allows for clarification of the factors involved, without extraneous effects influencing the corrosion.

TABLE 1. Variations of Pit Half-Life with Surface Preparation

Surface treatment	Pit half-life,* min
Electropolished and cathodically polarized	<1
As electropolished	22
Electropolished and oxidized at 110°C for 24 hr	90
Electropolished and oxidized at 165°C for 24 hr	150
Electropolished and oxidized at 240°C for 24 hr	430
Electropolished and oxidized at 250°C for 2 hr	480
Electropolished and oxidized at 300°C for 22 hr	340
Electropolished and oxidized at 375°C for 2 hr	270
Abraded with 600 grade SiC	<1
Abraded and oxidized at 250°C for 8 hr	5

*Maximum variation of 20%

REFERENCES

1. Localized Corrosion - Cause of Metal Failure ASTM, STP 516, American Society of Testing & Materials, 1972.

2. Brown, B.F., Kruger, J. and Staehle, R.W., Eds., Localized Corrosion, National Association of Corrosion Engineers, 1974.

3. Lajain, H. Z.F. Werkstofftechnik, Vol. 2 (1971), p. 19.

4. Lajain, H. Werkstoffe und Korrosian, Vol. 23 (1972), p. 537.

5. Evans, U.R. and Agar, J.N., see Evans, U.R., The Corrosion and Oxidation of Metals, Edward Arnold Ltd., 1960, p. 862; Evans, U.R., Journal of the Iron and Steel Institute, I, Vol. 141, 1940, p. 219.

6. Jaenicke, W., Z. Physik Chem., Vol. A191, 1943, p. 350.

7. Jaenike, W. and Bonhoeffer, K.F., Z. Physik Chem., Vol. 193, 1944, p. 301.

8. Copson, H.R., Journal of the Electrochemical Society, Vol. 84, 1943, p. 71.

9. Rozenfeld, I.L. Atmospheric Corrosion of Metals, National Association of Corrosion Engineers, 1972, p. 83.

10. Hildebrand, H. and Schwenk, W., Werkstaffe und Korrosion, Vol. 23, 1972, p. 364.

11. Isaacs, H.S. and B. Vyas, Electrochemical Corrosion Testing ASTM, STP 727, F. Manfield and V. Bertocci, Eds., American Society for Testing and Materials, 1981, p. 3.

12. Isaacs, H.S., in Ref. 1, p. 158.

13. Vyas, B. and Isaacs, H.S., Intergranular Corrosion of Stainless Alloys, ASTM, STP 656, R.F. Steigerwald, Ed., American Society for Testing and Materials, 1978, p. 133.

14. Bhansali, J.J. and Hepworth, M.T., Journal of Physics E. Scientific Instruments, Vol. 7, 1974, p. 681.

15. Gainer, L.J. and Wallwork, G.R., Corrosion, Vol. 35, 1979, p. 61.

16. Rosenfeld, I.L. and Danilov, I.S., Corrosion Science, Vol. 7, 1967, p. 129.

17. Engell, H.J. and Stolica, N.D., Z. Phys. Chem., Vol. 20, 1959, p. 113.

18. Sato, N., Nakagawa, T., Kudo, K. and Sakashita, M.S. in Ref. 1, p. 447.

19. Isaacs, H.S. and Kissel, G., Journal of the Electrochemical Society, Vol. 119, 1972, p. 1628.

20. Wilde, B.E. and Williams, E., Journal of the Electrochemical Society, Vol. 117, 1970, p. 775.

21. Galvele, J.R., in Passivity of Metals, R.P. Frankenthal and J. Kruger, Eds., The Electrochemical Society Inc., 1978, p. 285.

22. Wilde, B.E. and Williams, E., Electrochimica Acta, Vol. 16, 1971, p. 1971.

23. Cowan, R.L. and Tedmon, Jr., C.S., Advances in Corrosion Science and Technology, Vol. 3, 1973, p. 293.

24. Henthorne, M., Localized Corrosion - Cause of Metal Failure, ASTM, STP 516, 1972, p. 66.

25. Tedmon, Jr., C.S., Vermilyea, D.A. and Rosolowski, J.H., J. Electrochem. Soc., Vol. 118, 1971, p. 192.

26. Pande, C.S., Suenaga, M., Vyas, B., Isaacs, H.S., and Harring, D.F., Scripta Met., Vol. 11, 1977, p. 601.

27. ASTM Designation, Recommended Practice for Detecting Susceptibility to Intergranular Attack in Stainless Steel, 1970.

28. Clarke, W.L., Cowan, R.L. and Walker, W.L., Intergranular Corrosion of Stainless Alloys, ASTM, STP 656, R.F. Steigerwald, Ed., American Society for Testing and Materials, 1978, p. 99.

29. Latanision, R.M. and Staehle, R.W., in Fundamental Aspects of Stress Corrosion Cracking, R.W. Staehle, A.J. Forty and D. van Rooyen, Eds., National Association of Corrosion Engineers, 1969, p. 278.

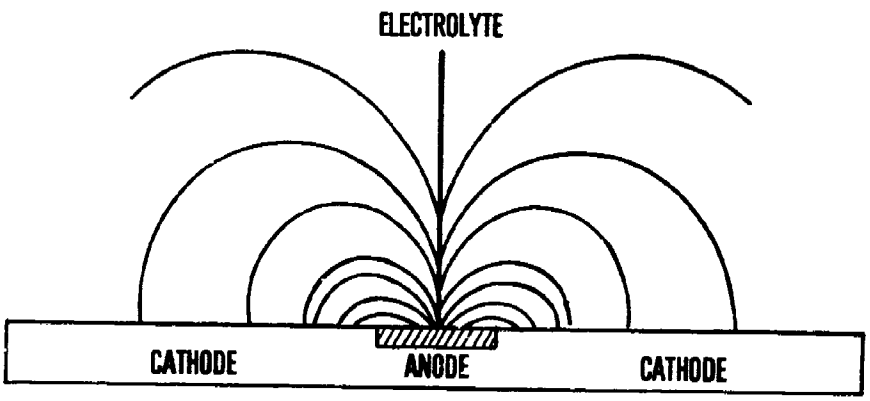
ELECTROLYTE
CATHODE
ANODE
CATHODE

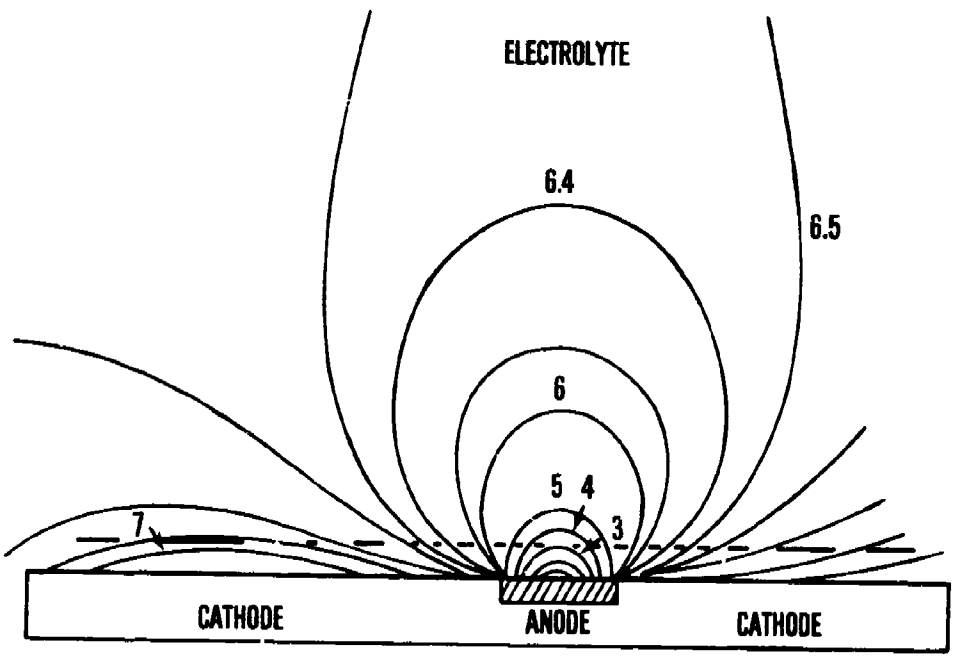
ELECTROLYTE
6.4
6.5
6
5
4
3
7
CATHODE
ANODE
CATHODE

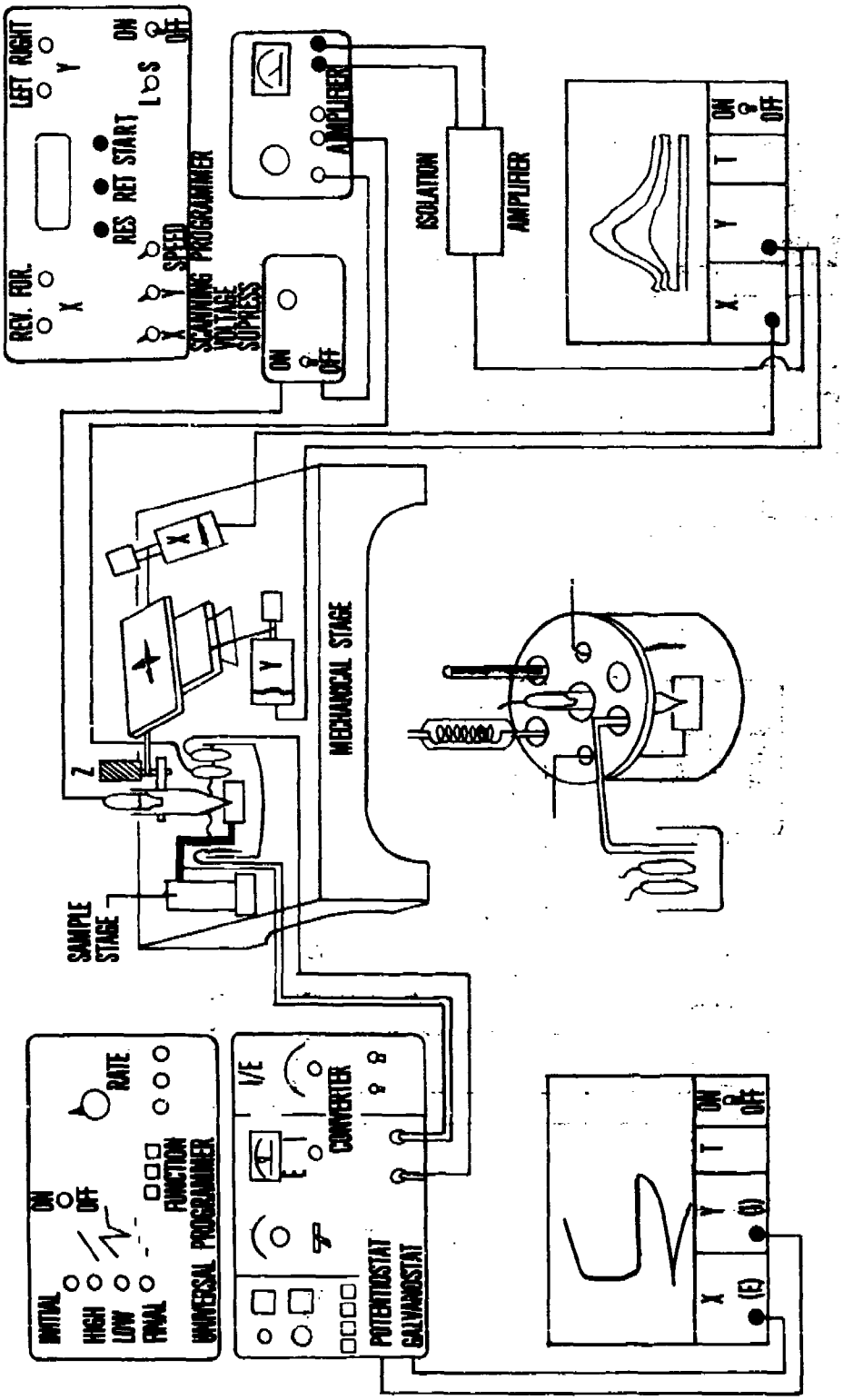
LEFT RIGHT
Y
ON
OFF
RES RET START
SPEED
REV. FOR
X
SCANNING PROGRAMMER
VOLTAGE SUPPRESS
ON
OFF
AMPLIFIER
ISOLATION
AMPLIFIER
ON
OFF
T
Y
X
MECHANICAL STAGE
Z
SAMPLE STAGE
RATE
ON
OFF
FUNCTION
INITIAL
HIGH
LOW
FINAL
UNIVERSAL PROGRAMMER
I/E
CONVERTER
POTENTIOSTAT
GALVANOSTAT
ON
OFF
T
Y
(I)
X
(E)

Figure 2

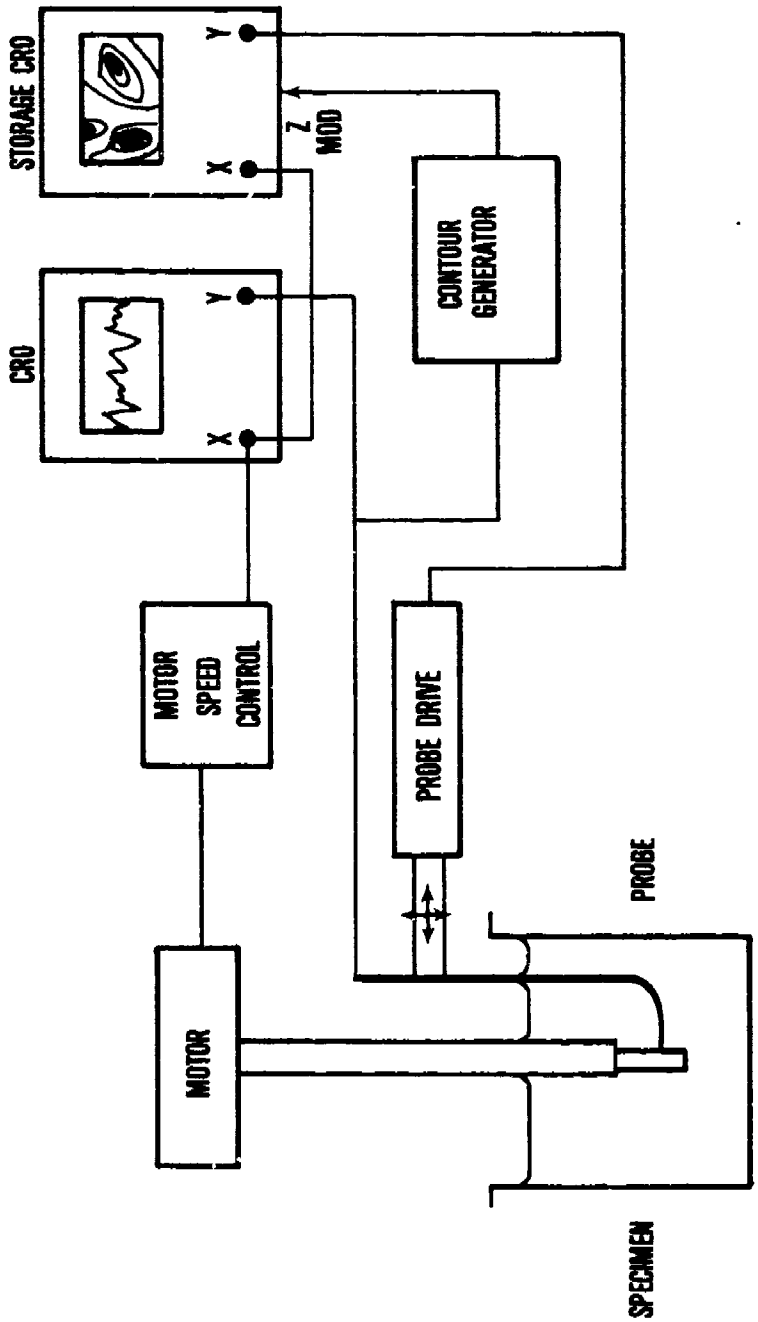
STORAGE CRO
Y
X
Z MOD
CRO
Y
X
CONTOUR GENERATOR
MOTOR SPEED CONTROL
PROBE DRIVE
PROBE
MOTOR
SPECIMEN

Figure 3

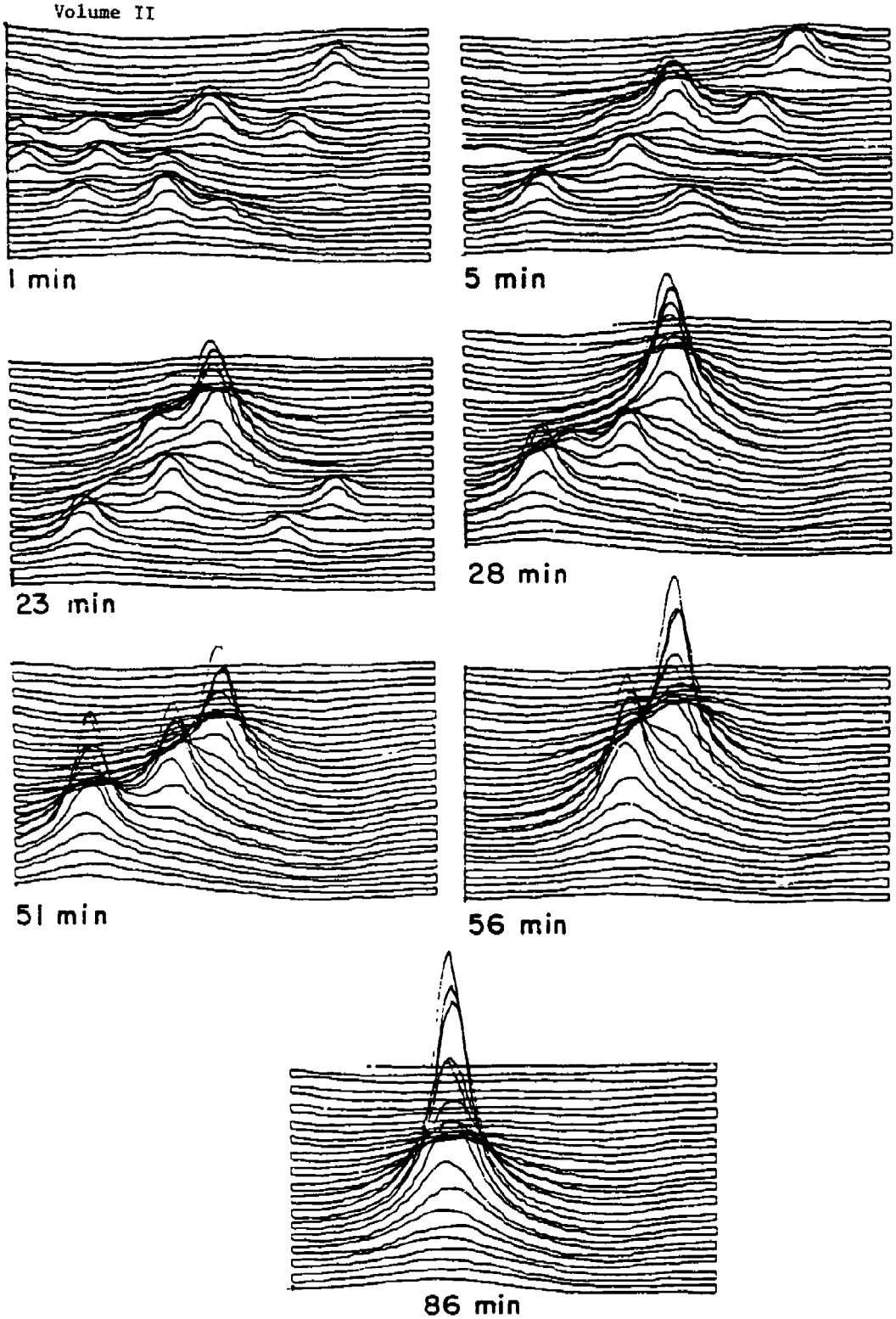

Figure 4

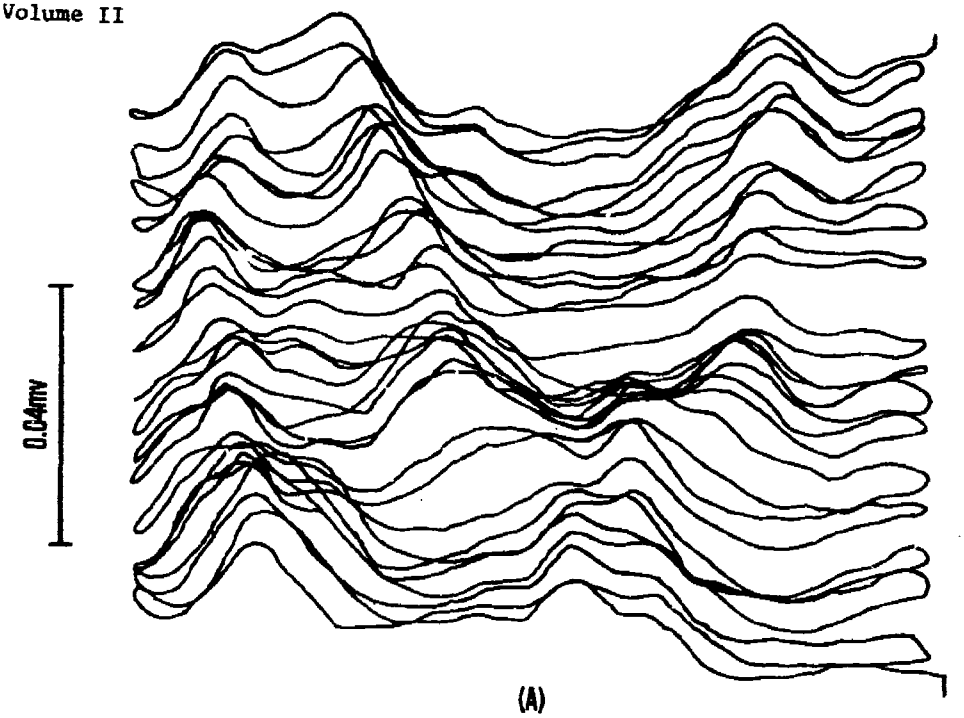

(A)

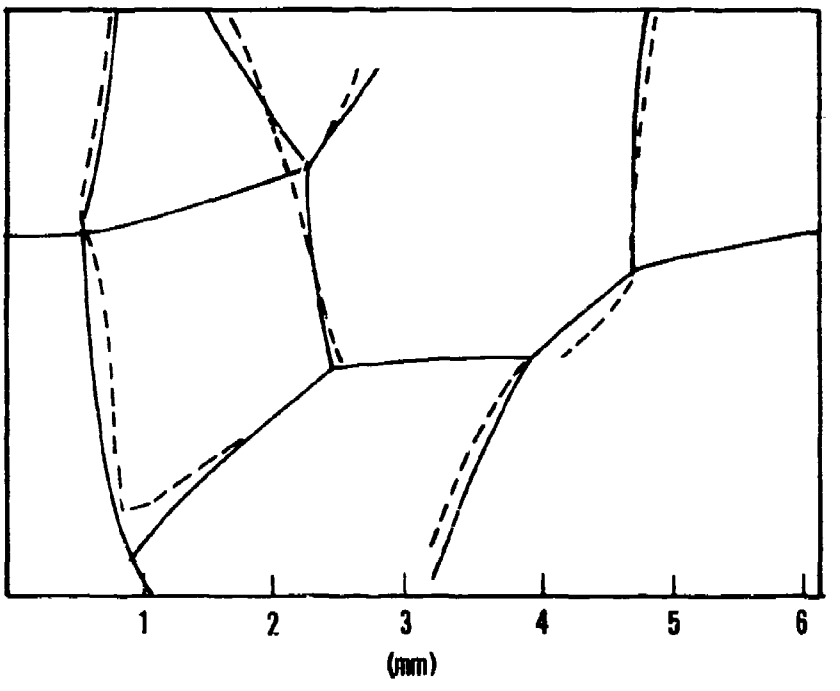

(B)

Figure 5

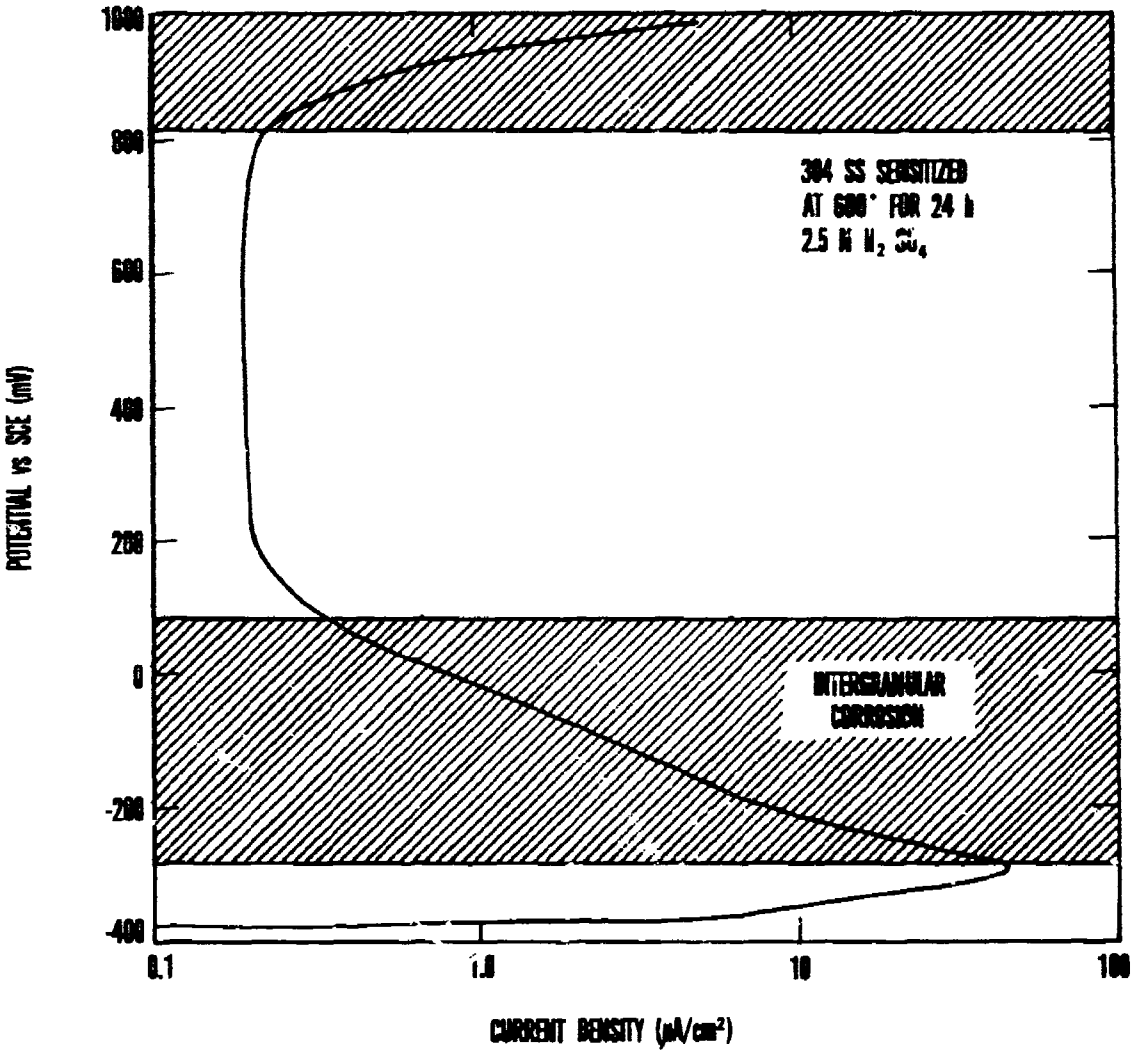
304 SS SENSITIZED
AT 600° FOR 24 h
2.5 M H_2SO_4
INTERGRANULAR
CORROSION
POTENTIAL vs SCE (mV)
CURRENT DENSITY (μA/cm²)
0.1
1.0
10
100

Figure 6

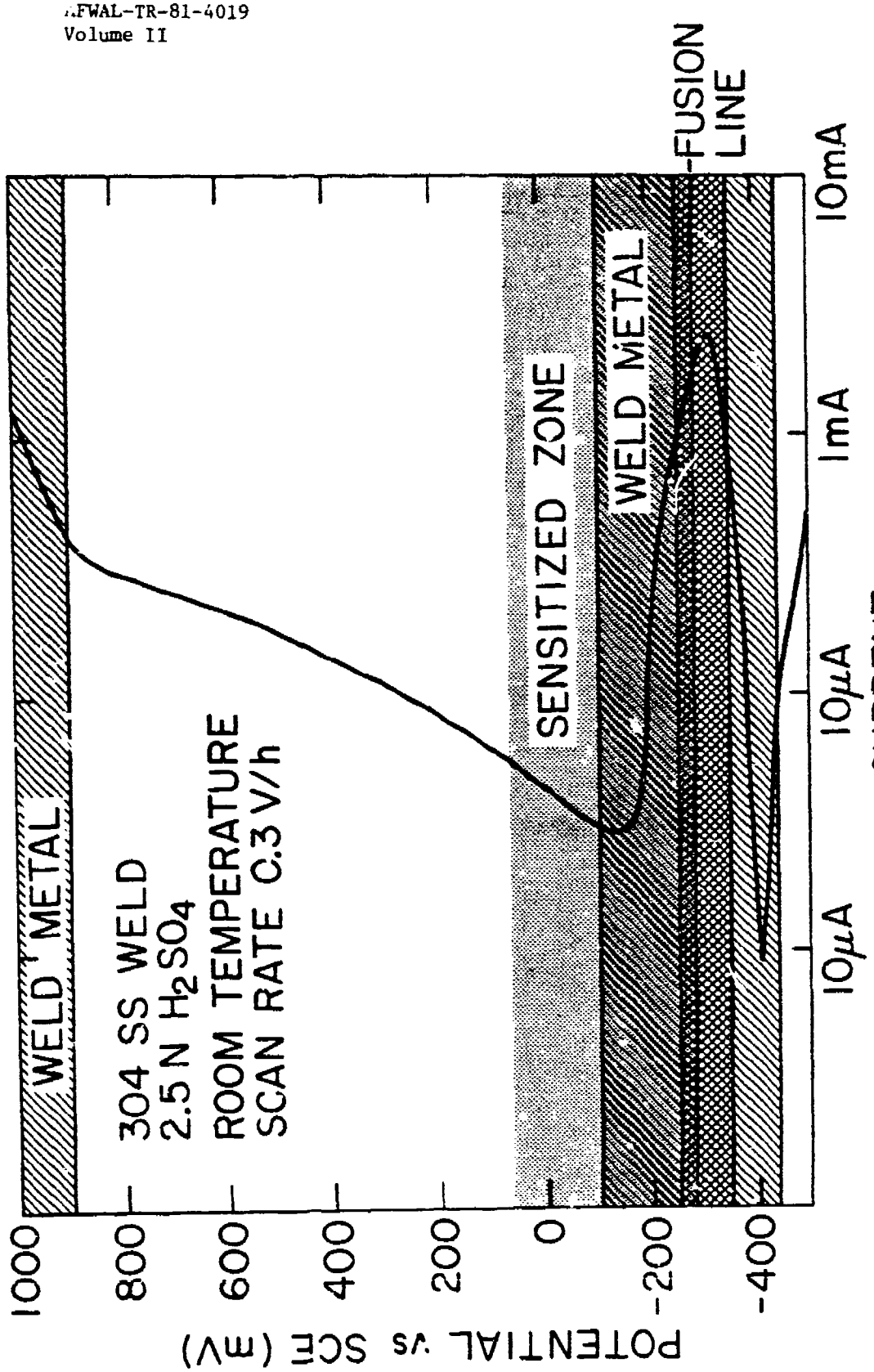
POTENTIAL vs SCE (mV)
1000
800
600
400
200
0
-200
-400
10μA
1mA
10mA
CURRENT
FUSION LINE
WELD METAL
SENSITIZED ZONE
WELD METAL
304 SS WELD
2.5 N H_2SO_4
ROOM TEMPERATURE
SCAN RATE C.3 V/h

Figure 7

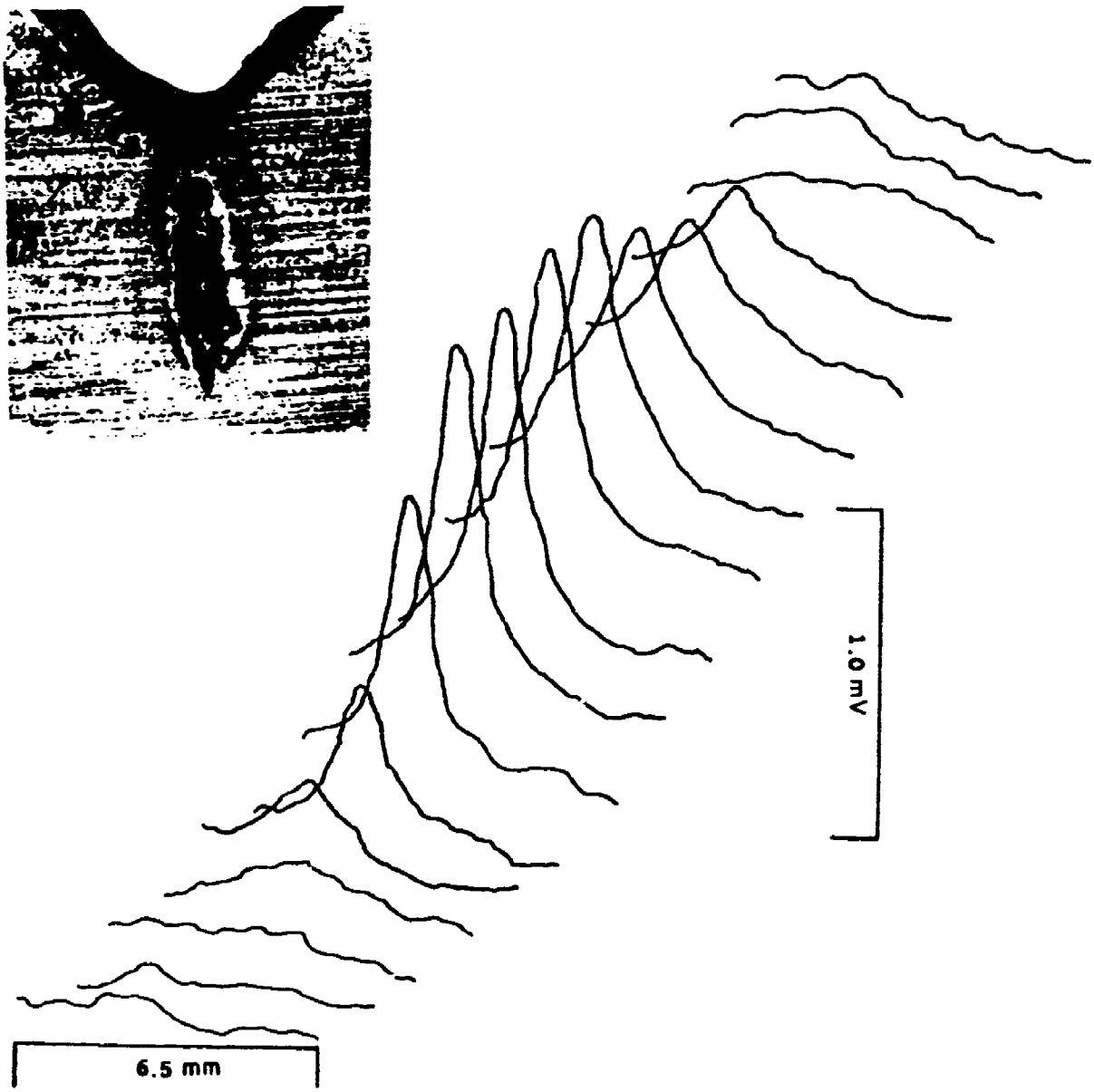

Figure 8

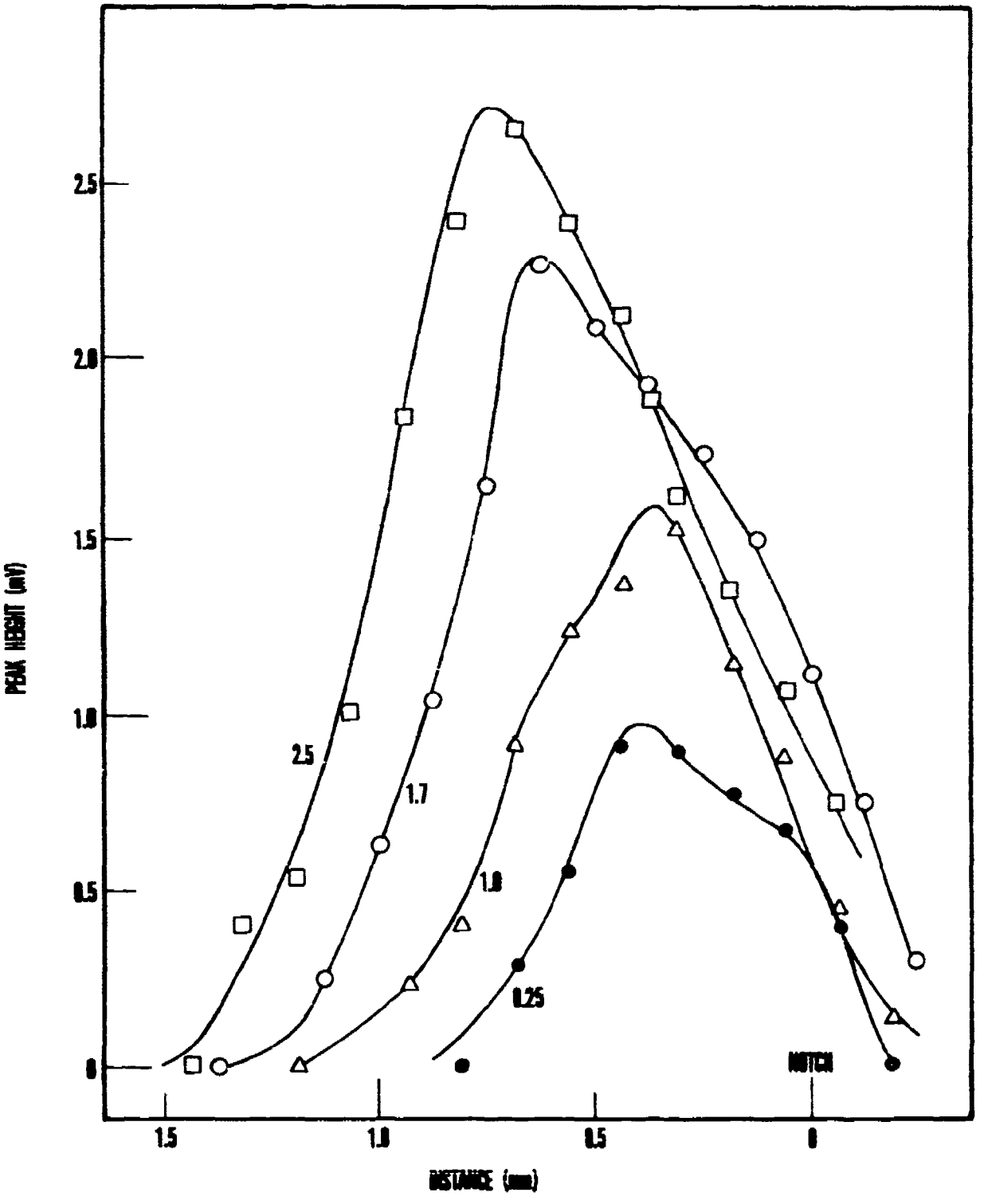
PEAK HEIGHT (mV)
2.5
2.0
1.5
1.0
0.5
0
2.5
1.7
1.0
0.25
NOTCH
1.5
1.0
0.5
0
DISTANCE (mm)

Figure 9

AFWAL-TR-81-4019
Volume II

ACCELERATED TESTING IN CONTROLLED ATMOSPHERES

M. Khobaib and Frank C. Chang*
Systems Research Laboratories, Inc.
2800 Indian Ripple Road
Dayton, OH 45440

C. T. Lynch
Air Force Wright Aeronautical Laboratories
AFWAL/MLLN
Wright-Patterson Air Force Base
OH 45433

*Present address: Army Materials and Mechanics Research Center, Watertown, MA 02172

ABSTRACT

Available methods for accelerated testing of corrosion behavior do not yield accurate or reliable results for predicting the service life of aircraft components and materials which degrade or fail due to environmental attack. Research has been conducted in controlled atmospheres on the localized environmental enhancement of crack-growth rates of aerospace alloys in order to provide the basis for development of realistic accelerated corrosion tests. Initial emphasis has been placed on investigations of environmental conditions for accelerating reactions which lead to catastrophic failure of high-strength alloys. Corrosion-fatigue and rising-load experiments have been conducted on 4340 steel and 7075-T6 aluminum using accelerating pollutants such as sulfur dioxide and ambient air to 100% relative humidity (RH) air in a specially designed atmospheric chamber. Initial results indicate that a realistic environmental enhancement of crack-growth rates can be employed to develop accelerated tests which can be related to actual in-service degradation. For materials with high stress-corrosion susceptibility, the threshold for crack growth (K_{ISCC}) was estimated to be 45 - 46 MPa $\sqrt{m}$ for 4340 steel at a 1440-MPa yield-strength level, as compared to 49 - 52 MPa $\sqrt{m}$ as determined by means of rising-load tests and 44 - 46 MPa $\sqrt{m}$ by fracture analysis in 1000 ppm SO_2 at 80% RH. Thus, a rapid and reproducible method for K_{ISCC} determination appears feasible.

INTRODUCTION

The enormous cost of corrosion prevention and control for aircraft has been brought to light in a recent report published by NBS [1]. Several similar studies have been conducted within the Air Force regarding the total cost of corrosion prevention and control for aircraft. The inescapable conclusion is that total corrosion costs in terms of life-cycle management and maintenance of aircraft represent an intolerable burden to the Air Force in maintaining force effectiveness at a reasonable cost to the taxpayer. The 1978 NBS report [1] estimated the total corrosion cost to be 70 billion dollars nationally. For the Air Force the direct cost of corrosion maintenance in the field and at the depot level was estimated at that time to be 750 million dollars, and the total corrosion cost including facilities was estimated to be in excess of one billion dollars. During the 1975 and 1977 AFOSR-AFML Corrosion Workshops, improved accelerated tests were cited as being a major area of need requiring further research [2,3]. One of the major problems in effectively reducing aircraft-corrosion maintenance costs has been the inability of the research community to develop realistic corrosion tests which give meaningful results in a reasonable length of time. Despite the need for this development, there are no accurate methods for accelerated testing for corrosion which yield reliable results for predicting the service life of aircraft components and materials which degrade or fail due to environmental attack. Current alternatives involve the use of 1) gross tests such as salt-water immersion which yield relative corrosivity values that have no quantitative relation to service life or 2) outdoor atmospheric exposure tests which require experiments of three to five years duration or longer and are specific to one local environment. Furthermore, the immersion tests make use of high salt concentrations which do not represent realistic conditions, except for marine environments. Thus, the results have no real-time basis for extrapolation to real conditions. Fundamentally, the corrosion reactions from immersion tests are completely different from those in typical high-humidity air environments containing small concentrations (ppm to ppb range) of contaminants (e.g., SO_2, NO_X, Cl^-) which accelerate the corrosion reactions.

Therefore, we have initiated a program to provide the basis for the development of realistic accelerated tests which can be used to predict the long-range corrosion behavior of materials under actual service conditions. Test environments are based upon reasonable variations in the concentration of corrosion-accelerating pollutants, humidity, and temperature, using primary and secondary air-quality standards to establish concentration base levels for accelerating pollutants such as sulfur dioxide. Controlled atmospheric experiments are being conducted for general corrosion and for localized environmental enhancement of crack-growth rates. Crack-growth studies include low-cycle corrosion-fatigue, rising-load, and constant-slow-strain-rate tests. Some of the results are reported in this paper for 4340 steel and 7075-T6 aluminum alloys under rising load and low-cycle fatigue.

The state-of-the-art in accelerated-corrosion testing methods as described in the ASTM Book of Standards and approved by NACE requires the aforementioned use of gross tests such as salt fog and alternate salt-immersion tests with their lack of quantitative values for corrosivity or relative corrosivity and no direct relationship to service experience. Atmospheric outdoor tests where panels are exposed to various environments require a time scale which precludes rapid materials-selection decisions or paint-protection measure evaluations. These tests are limited to specific environments and seldom take into account stress factors which may accelerate the localized corrosion and enhance crack growth leading to premature failure. Cyclic loading is, of course, also precluded. Establishing realistic test environments requires, at a minimum, a reasonable selection of atmospheric environmental variables coupled with stress factors which aerospace components are expected to experience. The selection of appropriate air-quality standards is difficult and should be based upon knowledge of ambient-air pollutant levels and experimental work to determine the relative importance of these pollutants. The effects of SO_2 for high-strength steels and NO_2 for high-strength aluminum alloys must be related to the interaction of these gases with water vapor and airborne particulates and to causal factors. In this paper, the design and layout of the experimental apparatus for simulating the environment and the initial results obtained in environmentally accelerated crack-growth studies conducted on high-strength steels and aluminum alloys are given. Experiments have been conducted in dry and humid air and then in more aggressive environments containing a mixture of SO_2 and humid air. Rising-load tests have been used to determine the apparent K_{ISCC} for 4340 steels and high-strength aluminum alloys in these environments. Fractographic analysis has been employed to correlate the results and the types of failure that have occurred.

EXPERIMENTAL

Materials

A 50.8-mm-thick plate of 4340 steel of aircraft quality obtained from Jorgensen Steel was used. The steel was heat treated to yield strengths of 1240, 1345, and 1440 MPa. The high-strength Al 7075-T6 alloy with a yield strength of 440 MPa was obtained from Rockwell International in the form a 76.2-mm-thick plate. Research-grade SO_2 and N_2 were employed. Distilled water was used throughout the experiments.

The critical stress-intensity factor, K_{IC}, the threshold stress intensity for stress-corrosion cracking, K_{ISCC}, and crack-growth data were obtained using compact-tension plane-strain fracture-toughness specimens as shown in Fig. 1. Both steel and aluminum specimens were machined in the short-transverse (ST) orientation.

All fractured surfaces were examined visually and then by light microscopy. The specimens were then ultrasonically cleaned in acetone, deionized water, and methyl alcohol. The light-microscopic observation was followed by scanning electron microscopy (SEM) for detailed examination of the fractured surfaces.

Test Methods

For fracture-toughness determinations the compact-tension specimens were precracked to 2.54 mm by fatigue cracking according to ASTM specifications. Two specimens from each heat treatment were loaded monotonically to failure to determine the stress intensity at fracture, K_{IC}.

The apparent threshold for sustained-load stress-corrosion cracking, K_{ISCC}, in humid air and in different mixtures of humid air and SO_2 was estimated using the accelerated rising-load procedure [4]. The testing technique utilized was identical to the procedure used for K_{IC} fracture-toughness testing (ASTM Test for Plane-Strain Fracture Toughness of Metallic Materials E 399-72) [5], except that a slower rate of loading was employed and the specimen was exposed to the environment while being loaded. These tests were conducted with standard 19.05-mm-thick compact-tension specimens. The specimens were precracked to crack lengths of 2.54 mm at stress intensities below 15 MPa $\sqrt{m}$ for steel and 7 MPa $\sqrt{m}$ for Al 7075-T6 (R - 0.1 and f - 0.1 Hz). A special environmental chamber (to be described in detail later) was used to maintain and control the constituents of the specific environments required for the tests. The specimens were loaded in air, in 80% relative humidity, in 1000 ppm SO_2 + 80% RH, and in 1000 ppm SO_2 + 100% RH, at fixed loading rates corresponding to 5, 22, and 88 N/min. K_{ISCC} values were estimated from the load-displacement record, using the five-percent secant offset procedure similar to that used for the K_{IC} testing [5]. The results are given in Tables I and II.

All corrosion-fatigue tests were conducted at room temperature using a 100 KN Materials Testing System (MTS) machine. The crack length was monitored through crack-opening-displacement (COD) measurements during fatigue testing. To determine the crack length from COD data, compliance measurements were carried out for both high-strength steels and aluminum alloys. Tests were conducted in air, and crack lengths were determined using optical and COD measurements simultaneously on the MTS machine. The COD was measured by a double-cantilever displacement gauge prepared in accordance with the ASTM designation [5]. The displacement gauge was calibrated to measure COD from 0 to 1.25 mm ± 0.0125 mm using a Daytronic strain-gauge amplifier. The COD was recorded as a function of cycles.

A sinusoidal tension-tension waveform was employed for all fatigue-crack-growth-rate tests. Most of the tests were conducted at an R ratio (K_{min}/K_{max}) of 0.6 and a frequency of 0.1 Hz. The slow frequency and high R ratio were utilized

to facilitate the observation of environmental effects. Limited tests were conducted at frequencies of 0.25 and 0.5 Hz also. All specimens were initially precracked according to ASTM specification E 399-72 [5] on the same MTS machine on which the corrosion-fatigue tests were conducted.

No significant differences were found in the COD/load and crack length/load curves. The crack length, a, was calculated from the analytical compliance relationship [6]

$$a/W = 1.001 - 4.6695\ U + 18.460\ U^2 - 236.82\ U^3 + 1214.94\ U^4 - 2143.6\ U^5$$

where

$$U = \frac{1}{\sqrt{\frac{EB\ (COD_{Max} - COD_{min})}{P_{Max} - P_{Min}} + 1}}$$

E is the Young's modulus and P the stress. W and B are the dimensions indicated in Fig. 1. The stress-intensity values were calculated from [6]

$$K = \frac{P}{BW^{1/2}} \frac{(2+a/w)[(0.886+4.64(a/w)] - 13.32(a/w)^2 + 14.72(a/w)^3 - 5.6(a/w)^4}{(1-a/w)^{3/2}}$$

where B and W are the dimensions indicated in Fig. 1 such that B and a > 2.5 $(K_{IC}/YS)^2$, with K_{IC} being the fracture toughness and YS is the tensile yield strength. The crack-length-versus-number-of-cycles data were converted to fatigue-crack-growth rates (da/dN) using a computer program [6]. Seven to eleven data points were fitted to a second-order polynomial, and the derivative (da/dN) was then obtained for the middle data point. This process was then repeated over the entire range of data.

Controlled-Atmosphere Environmental Chamber

The environmental chamber and the gas-train assembly are shown in Fig. 2. The chamber is made of 316 stainless steel while the grips, pull rods, and pins are made of 17-4 PH steel which exhibits good resistance to wet SO_2 and wet NO_2 environments. It is a leak-proof system with bellows and other attachments to attain high vacuum. The temperature inside can be controlled from 0 to 1000°F. The unit is installed in a closed-loop MTS machine for conducting mechanical tests in simulated realistic environments.

The test atmospheres were supplied through the gas train which consists of a gas mixing and delivery system. High-purity bottled gases (SO_2 and dry air in this case) were metered by Matheson flowmeters 601 and 603 and then mixed in the mixing tube. The concentration of SO_2 in the chamber is routinely measured by calibrated Gastec analyzer tubes. Special gas-sampling outlets are provided in the chamber. The relative humidity (RH) inside the chamber is controlled by means of a BMA dry and wet bulb hygrometer. The water vapor is added in the form of steam by boiling distilled water in a flask maintained at a constant temperature. The steam flow is controlled by the output voltage of the BMA controller which monitors the opening and closing of the solenoid valve on the steam line. The steam is injected into the gas mixture prior to its entry into the chamber in order to obtain the required mixture of SO_2 and RH air.

Gas pressures used in all the tests have been slightly above atmospheric to provide positive flow through the environmental chamber. The gas inlet and outlet are positioned specifically to minimize the channeling effect. The gas is circulated inside the chamber by means of a circulating fan (placed inside the chamber) to maintain a uniform environment throughout the chamber. Negligible condensation occurred during these tests except in the case of 100% RH. The fatigue-crack-propagation data previously discussed were obtained using compact-tension plane-strain fracture-toughness specimens (Fig. 1). Tests were conducted in the controlled atmosphere inside the environmental chamber as described. The inert dry nitrogen was used as a control, while the 80% RH air, 1000 ppm SO_2 + 80% RH, and 1000 ppm SO_2 + 100% RH were used as representative aggressive environments for stress corrosion and environmentally accelerated corrosion fatigue.

RESULTS AND DISCUSSION

Crack Propagation

The fatigue-crack-propagation behavior of many ferrous and nonferrous alloys can be schematically represented as in Fig. 3 [8]. The rate of crack growth depends strongly upon K at K levels approaching K_C or K_{IC} at the high end and at levels approaching an apparent threshold at the low end, with an intermediate region that depends upon some power of K or ΔK. The upper end corresponds to the onset of unstable fracture, while the lower end corresponds to the fatigue "threshold" ΔK_{th} [9,10] which appears to be related to the metallurgical structure [11].

The environment-enhanced fatigue-crack-growth response of high-strength metals may be broadly characterized in terms of three general patterns of behavior [12], as illustrated schematically in Fig. 4. The first type of behavior represents those material-environment systems where fatigue-crack-growth rates are enhanced by the presence of an aggressive environment through a synergistic action of corrosion and cyclic loading. This is "below K_{ISCC}" behavior [13-15] and applies to materials which are not susceptible to stress corrosion where $K_{ISCC} > K_{IC}$. This behavior is classified as true corrosion fatigue. The second type of behavior is representative of those systems where there is a substantial environment-enhanced sustained-load crack-growth component [16,17] which occurs whenever the stress intensity in the cycle is above K_{ISCC}. This behavior is classified as stress-corrosion fatigue. The most common type of behavior pertains to material/environment systems which exhibit stress-corrosion fatigue above K_{ISCC} and also true corrosion fatigue at all stress-intensity levels. Such behavior lies between the two extremes and is shown in Fig. 4(c).

Crack Growth Behavior of Al 7075-T6 and 4340 Steel

The accelerated atmospheric effects resulting from the variation of the relative humidity upon observed crack-growth rates were investigated. The low-cycle corrosion-fatigue data are expressed in terms of crack-growth rate da/dN as a function of the stress-intensity-factor range ΔK. The dependence of crack-growth rate upon the humidity level in air for Al 7075-T6 is shown in Fig. 5. At high levels of humidity such as 80% RH, the crack-growth rates were substantially increased as compared to those in dry air ($\leq$ 5% RH). The immersion results for crack growth in aqueous solutions are shown for the sake of comparison. While increasing relative humidity also increases the crack-growth rates,

the change in crack-growth rate from gaseous environment to total-immersion aqueous environment is much more significant. This rate is also less realistic for estimating corrosion reactions except where standing water is present. Similar results on several aluminum alloys have been obtained by other workers [18-25]. The commonly accepted explanation of crack-growth acceleration due to a high level of humidity is the pressure mechanism of hydrogen embrittlement suggested by Broom and Nicholson [19] which requires a water-metal surface reaction and proposes that the increase in the rate of fatigue-crack growth results from the synergistic action of a mechanical process--fatigue, which creates a sufficient amount of fresh surface--and the chemical reaction of water vapor with the resulting fresh surface.

Figure 6 represents the crack-growth-rate data on 4340 steel with a yield strength of 1345 MPa obtained at three levels of humidity. In all these tests a frequency of 0.1 Hz and a load ratio R of 0.1 were used. While the shapes of the three curves are similar, noticeable differences exist in the crack-growth rates at high K levels. Note that although the differences in crack-growth rates (at different humidity levels) are small, very definite differences are present. The differences found are reproducible within an experimental error of da/dN less than the Δda/dN values. Similar differences in crack-growth rates were observed for Al 7075-T6. These differences become more pronounced when one considers data on cycles to failure. These data are shown in Table III for both Al 7075-T6 and 4340 steel. Similar increases in crack-growth rates of high-strength 4340 steel due to water vapor were observed under both sustained and cyclic loading by Lynch and other workers [26-32]. Dahlberg [33] has demonstrated more distinct differences in the crack-growth rates of 4340 steel tested at different humidity levels when an R ratio of 0.8 was used. However, the differences in crack-growth rates with increasing humidity levels were similar to those obtained in the present investigation where smaller R ratios were used.

Although several mechanisms have been suggested for hydrogen embrittlement [34-37] (such as the decohesion model [36] and the pressure model [37]), no single theory gives a complete description of the problem. For high-strength steels, however, in "hydrogen-producing" atmospheres (e.g., H_2, H_2O, H_2S), decohesion theories are widely accepted [38-41, 37] (for monotonic and cyclic loading). Also the general concensus is that the presence of water vapor in the atmosphere enhances crack-growth rates for both high-strength aluminum alloys and steels.

Crack Propagation of Al 7075-T6 and 4340 steel in humid SO_2

The corrosion-fatigue tests with high-strength aluminum alloys were extended to more aggressive environments of a mixture of 80% RH and 1000 ppm SO_2. Two sets of tests using stress ratios of 0.6 (R = 0.6) and 0.8 (R = 0.8) were conducted with frequencies ranging from 0.1 to 1 Hz. The crack-growth results for R = 0.6 are shown in Fig. 7, while Fig. 8 shows the da/dN-vs-ΔK plot for a stress ratio of 0.8. Frequency has very little effect from 0.1 to 0.5 Hz at both stress ratios, but there is a surprising difference in the behavior at 1 Hz. At a stress ratio of 0.6, and a frequency of 1 Hz, crack-growth rates decrease at higher K-values compared to the rates obtained at frequencies of 0.1 and 0.5, while the crack-growth rates are almost the same at these higher

K-levels for all three frequencies at a stress ratio of 0.1. However, the rates are comparatively higher at lower K-levels, at a frequency of 1 Hz. There is no easy explanation for such behavior, and more tests must be conducted to clearly define such differences in behavior. However, the effect of stress ratio is more distinct than that of frequency. At a stress ratio R = 0.6, the da/dN-vs-ΔK curve has a more pronounced intermediate or second region, while there is little evidence of a normal intermediate region (as shown in Fig. 8) at a stress ratio R = 0.8, except at a frequency of 1 Hz. This difference in the intermediate region of the da/dN-vs-ΔK curve has been reported to be stress-ratio and frequency dependent [24,42].

It appears that there is a near plateau region followed by a maximum in the da/dN-vs-ΔK curves obtained at a stress ratio of 0.6, but it is not very well defined, in contrast to the case of 1440 MPa steel. Hence, no attempt was made to determine K_{ISCC} from a similar extrapolation as has been done in the case of 1440 MPa steel. The K_{ISCC} values in humid SO_2 were determined by the rising-load method; the results are shown in Table I. The difference in the K_{IC} value and the apparent K_{ISCC} value was not very great. This leads to the conclusion that either the rising-load test for determination of K_{ISCC} does not hold sufficiently for this material-environment system or the humid SO_2 atmosphere has a small and insignificant embrittling effect upon Al 7075-T6 at a strength level of 440 MPa. This contrasts markedly with the results for 4340 steel.

High-strength 4340 steel at yield strengths of 1240 MPa and 1440 MPa was tested at a load ratio of 0.6 and a frequency of 0.1 Hz. The atmospheres were ambient air, dry nitrogen, 80% RH air, and 1000 ppm SO_2 in 80% RH air. The crack-growth results for 1240 MPa steel are shown in Fig. 9, while Fig. 10 shows the da/dN-vs-ΔK plot for 1440 MPa steel. A comparison of these two figures shows that there is a greater enhancement in the crack-growth rates for 1440 MPa steel as compared to 1240 MPa steel due to the SO_2 environment. These data show a plateau intermediate region followed by a maximum of the da/dN-vs-ΔK plot obtained for 1440 MPa steel tested in the 1000 ppm SO_2 + 80% RH environment. A similar, but less-pronounced maximum is obtained for 1240 MPa in this same environment. The ambient air and 80% RH plots, however, follow the normal trend [8]. This difference in the nature of the plot (or appearance of a plateau followed by a maximum) is expected when the K level exceeds the K_{ISCC} value for the metal-environment system. In general, this follows the trend of Fig. 4(c) which is most significant because the extrapolation from this slope change to the abscissa of the plot produces the K_{ISCC} value as shown in Fig. 4(c). Accordingly, the K_{ISCC} values have been obtained from Figs. 9 and 10 and are 55 and 46 MPa $\sqrt{m}$ for 1240 MPa and for 1440 MPa steels. The accuracy of this estimate has been further verified by the rising-load method and fractographic observations. The K_{ISCC} value obtained from 1440 MPa steel by such extrapolation is in very close agreement with the K_{ISCC} values obtained from the other observations. The high value of K_{ISCC} obtained for 1240 MPa steel could not be supported by either rising-load or fractographic observations. Such high values of K_{ISCC} obtained by extrapolation of da/dN-vs-ΔK curves have been reported previously [43]. However, the K_{ISCC} value obtained by such extrapolation for 1440 MPa steel is quite consistent and accurate. The validity of this extrapolation is supported by the results of Austen, et al. [44], on high-strength 835M30 steel in a 3.5% NaCl environment. However, the high value of K_{ISCC} obtained for 1240 MPa steel requires further studies in several environments. A more detailed investigation of the nature of the da/dN-vs-ΔK plot is required when there is a very small

difference in K_{ISCC} and K_C values for the metal-environment system. In this case 1240 MPa steel is not so susceptible as 1440 MPa steel to hydrogen-assisted stress-corrosion cracking in the environmental conditions of the test, and the results apparently are intermediate between the first two cases of the schematic presentation of Fig. 4. In such a case, further detailed study of frequency/load/R ratio effects may be necessary to improve the determination of K_{ISCC} by extrapolation.

Modified Rising-Load K_{ISCC} Tests

The approximate values of K_{ISCC} obtained for 1240 MPa and 1440 MPa steels in various environments are shown in Table I. Only two loading rates of 22 and 88 N/min were used. The values quoted in Table I must be taken as the higher-limit estimates because of the rapid K rates utilized and the limited nature of the test procedure. More experiments at slower rates should improve the approximation of K_{ISCC} values. The K_{ISCC} values for Al 7075-T6 were estimated by a modified step-by-step loading practice. The schematics of the procedure are shown in Fig. 11. The results are given in Table II.

Fractographic Analyses

Fractographic analyses of the fracture surfaces of the specimens were conducted to provide further information concerning the crack-tip mechanism in corrosion fatigue of 4340 steels at different K levels in humid SO_2 environments. The fracture features of Al 7075-T6 fatigued in humid SO_2 will be reported in a later paper.

Figure 12 shows fractographs taken from the surface of a 1240 MPa steel specimen tested in 1000 ppm SO_2 + 80% RH. These fractographs indicate that at low values of K, 40.5 MPa $\sqrt{m}$, the surface features are very ductile [Fig. 12(a)]. At higher values of K, there is little evidence of intergranular fracture. The fracture is mainly transgranular and ductile in nature. No substantial component of intergranular fracture could be found, even in the fracture zone corresponding to high values of K, ≈ 57.5 MPa $\sqrt{m}$ (near the fast fracture) [Fig. 12(b)]. Different fracture-surface characteristics were obtained for 1440 MPa steel corrosion fatigued in 1000 ppm SO_2 + 80% RH.

Figure 13(a) shows the ductile nature of failure at low K values of 35 - 36 MPa $\sqrt{m}$, while Fig. 13(b) shows the mixed mode of failure, corresponding to a K value of ≈ 40 MPa $\sqrt{m}$. Figure 13(c) is a typical fractograph obtained in the fracture zone corresponding to a K value of ≈ 46 MPa $\sqrt{m}$. The entire fractured surface was scanned several times, and a definite intergranular failure mechanism was observed over the entire cross section when the K value exceeded 45 - 46 MPa $\sqrt{m}$. The value of K_{ISCC} was approximated by careful measurement of the crack length and found to be ≈ 46 MPa $\sqrt{m}$, which is in agreement with the K_{ISCC} value obtained from the da/dN-vs-ΔK plot; this value falls within good approximation of the value obtained by the rising-load method.

Figure 14 shows the fractographs obtained from the fractured surface of 1240 MPa steel tested in dry N_2, which are shown for comparison. The fractured surfaces [Fig. 14(a)] are characteristic of ductile failure, containing dimpled rupture. In Fig. 14(b) the dimples can be more clearly seen at higher magnification.

CONCLUSIONS

The presence of water vapor in the atmosphere accelerates the crack-growth rates of high-strength steels and aluminum alloys. Crack-growth rates increase with increasing relative humidity, with the effect being more pronounced in steel at a yield strength of 1440 MPa as compared to 1240 MPa.

There is a significant increase in crack-growth rates (and corresponding decrease in cycles to failure) for high-strength alloys in full immersion to aqueous solutions as compared to 100% RH air atmosphere.

Corrosion-fatigue crack-growth rates increase from ambient air to 80% RH air to 80% RH air + 1000 ppm SO_2. This is true for all alloys, with the effects being more pronounced in the 1440 MPa steel than in the 1240 MPa steel.

The value of K_{ISCC} can be extrapolated from the corrosion-fatigue curve, providing the conditions of load, frequency, and R ratio are optimized. The results of rising-load corrosion-fatigue extrapolation and fractography experiments are in excellent agreement for the 1440 MPa steel. Thus, a rapid determination of K_{ISCC} is provided for susceptible alloys. For aluminum the embrittling effect in high humidity and SO_2 atmosphere is insufficient to obtain an accurate K_{ISCC} value from the corrosion-fatigue curve.

ACKNOWLEDGMENTS

The authors express their thanks to F. M. Thornton for reducing the experimental data and to M. B. Strope for assisting in the fractographic analysis.

REFERENCES

1. L. H. Bennett, J. Kruger, R. L. Parker, E. Passaglia, C. Reimann, A. W. Ruff, and H Yakowitz, Economic Effects of Metallic Corrosion in the United States, Parts 1 and II, NBS Special Publication 511-1,2 (U. S. Department of Commerce, National Bureau of Standards, Washington, D.C., May 1978).

2. M. Hoch and J. Gwinn (eds.), Proceedings of the AFOSR/AFML Corrosion Workshop, AFML-TR-77-175 (Air Force Materials Laboratory, Wright-Patterson Air Force Base, OH, 1975).

3. E. D. Verink, Jr. (ed.), AFOSR/AFML Workshop on Corrosion of Aircraft (St. Augustine, FL, September 13-15, 1977) (The University of Florida, Gainsville, FL, 1977).

4. W. G. Clark and J. D. Landes, Stress Corrosion - New Approaches, ASTM STP 610 (American Society for Testing and Materials, Philadelphia, PA, 1976), p. 108.

5. ASTM E399-72, Standard Test for Plane-Strain Fracture Toughness of Metallic Materials, 1972 Annual Book of ASTM Standards (American Society for Testing and Materials, Philadelphia, PA, 1972).

6. N. E. Ashbaugh, Technical Report AFML-TR-79-4127 (Air Force Materials Laboratory, Wright-Patterson Air Force Base, OH, September 1979).

7. ASTM E647-78T, Tentative Test Method for Constant-Load-Amplitude Fatigue Crack Growth Rates Above 10^{-8} m/cycle, 1978 Annual Book of ASTM Standards (American Society for Testing and Materials, Philadelphia, PA, 1978).

8. B. F. Brown (ed.), Stress Corrosion Cracking in High Strength Steels and in Titanium and Aluminum Alloys (U. S. Government Printing Office, Washington, D.C., 1972).

9. P. C. Paris, "Testing for Very Slow Growth of Fatigue Cracks," MTS Closed Loop Magazine 2(5) (1970).

10. R. J. Bucci, W. G. Clark, Jr., and P. C. Paris, in Stress Analysis and Growth of Cracks, ASTM STP 513 (American Society for Testing and Materials, Philadelphia, PA, 1972), p. 177.

11. J. A. McMillan and R. P. Wei, Met. Trans. 1, 1741 (1970).

12. A. J. McEvily and R. P. Wei, "Fracture Mechanics and Corrosion Fatigue," in Proc. Int. Conf. on Corrosion Fatigue - Chemistry, Mechanics and Microstructures (Storrs, CT, 1972) (National Association of Corrosion Engineers, Houston, TX, 1972), p. 381.

13. J. M. Barsom, "Corrosion Fatigue Crack Propagation Below K_{ISCC}," Eng. Fract. Mech. 3, 15 (1971).

14. J. P. Gallagher, "Corrosion Fatigue Crack Growth Rate Behavior Above and Below K_{ISCC}," J. Materials 6, 941 (1971).

15. J. P. Gallagher and R. P. Wei, "Corrosion Fatigue Crack Propagation in Steels," in Proc. Int. Conf. on Corrosion Fatigue - Chemistry, Mechanics and Microstructure (Storrs, CT, 1972) (National Association of Corrosion Engineers, Houston, TX, 1972), p. 409.

16. R. P. Wei. J. Eng. Fract. Mech. 1, 633 (1970).

17. R. P. Wei and J. D. Landes, Mat. Res. and Std. ASTM 9, 25 (July 1969).

18. N. J. Wadsworth, A. Nicholson, and J. Hutchins, "The Effect of Atmospheric Corrosion on Metal Fatigue," Phil. Mag. 3, 1154 (1958).

19. T. Broom and A. Nicholson, "Atmospheric Corrosion Fatigue of Age Hardened Aluminum Alloys," J. Inst. Met. 39, 183 (1960-1).

20. F. J. Bradshaw and C. Wheeler, Appl. Mat. Res. 5, 112 (1966).

21. A. Hartman, Int. J. Fract. Mech. 4, 167 (1965).

22. R. P. Wei, Int. J. Fract. Mech. 4, 159 (1968).

23. R. P. Wei and J. D. Landes, Int. J. Fract. Mech. 5, 69 (1969).

24. A. Hartman and J. Schijve, Eng. Fract. Mech. 1, 615 (1970).

25. W. P. Wei, et al., "Fracture Mechanics and Surface Studies of Fatigue Crack Growth in Al Alloys," Report 9 (IFSM-79-93) (Lehigh University, Bethlehem, PA, April 1979) (Contract N00014-75-C-0543).

26. C. T. Lynch, F. W. Vahldiek, and F. W. Thornton, in Proceedings of the 1978 Tri-Service Conference on Corrosion (October 4-6, 1978, New Orleans, LA).

27. P. M. Che-Yu Li, P. M. Talda, and R. P. Wei, Int. J. Fract. Mech. 3, 29 (1967).

28. H. H. Johnson and A. M. Willner, Appl. Mat. Res. 4, 34 (1965).

29. G. G. Hancock and H. H. Johnson, Trans. Met. Soc. AIME (April 1966).

30. G. L. Hanna, A. R. Troiano, and E. A. Steigerwald, Trans. ASM 57, 658 (1968).

31. W. A. van der Sluys, Trans. ASME 89D, 28 (1967).

32. J. P. Gallagher, "Environmentally Assisted Fatigue Crack Growth Rates in SAE 4340 Steel, "Ph.D. Dissertation (Dept. of Theoretical and Applied Mechanics, Univ. of Illinois, Urbana, IL, 1968).

33. E. P. Dahlberg, Trans. ASM 58, 46 (1965).

34. H. H. Johnson and P. C. Paris, Eng. Fract. Mech. 1, 3 (1968).

35. H. H. Johnson, "On Hydrogen Brittleness in High Strength Steels," in Proc. Conf. Fundamental Aspects of Stress Corrosion Cracking (Ohio State University, Columbus, OH, 1967).

36. R. A. Oriani and P. H. Josephic, Acta. Met. 22, 1065 (1974).

37. C. Zappfe and C. Sims, Trans. AIME 145, 225 (1941).

38. A. W. Thompson and I. M. Bernstein, in Advances in Corrosion Science and Technology (R. W. Staehle and M. G. Fontana, eds.), Vol. 7 (Plenum Press, NY, 1973).

39. R. P. Wei and J. D. Landes, Mat. Res. Stds. 9, 25 (1969).

40. I. M. Austen and P. McIntyre, Met. Sci. 13, 420 (1979).

41. R. O. Ritchie, M. H. Castrocedeno, V. F. Zackay, and E. R. Parker, Met. Trans. A. 9A, 35 (1978).

42. K. Walker, in ASTM STP 462 (American Society for Testing and Materials, Philadelphia, PA, 1970), pp. 1-14.

43. R. O. Ritchie, S. Suresh, and J. Toplosky, M.I.T. Fatigue and Plasticity Lab Report No. FPL/R/80/1030 (Massachusetts Institute of Technology, Cambridge, MA, January 1980) (Contract DE-AC02-79ER10389,A000).

44. I. M. Austen and E. F. Walter, "Quantitative Understanding of the Effects of Mechanical and Environmental Variables on Corrosion Fatigue Crack Growth Behavior," in Proceedings Int. Conf. Effect of Environment on Fatigue (Institute of Mechanical Engineers, London, 1977), pp. 1-10.

TABLE I

APPARENT K_{ISCC} VALUES OBTAINED BY RISING LOAD TESTS

SPECIMEN #	ENVIRONMENT	LOADING RATE N/min	*APPARENT K_{ISCC} MPa $\sqrt{m}$	YIELD STRENGTH MPa
2B	1000ppm SO_2 + 80%RH	22	55	1440
3B	1000ppm SO_2 + 80%RH	88	49	1440
10A	1000ppm SO_2 + 80%RH	22	72	1240
23A	1000ppm SO_2 + 100%RH	22	70	1240
29A	80% RH	22	78	1240
15A	50% RH	22	78	1240

* THESE VALUES ARE APPROXIMATE.

TABLE II

APPARENT K_{ISCC} VALUES OBTAINED FROM RISING LOAD TEST

SPECIMEN	ENVIRONMENTAL	LOADING RATE (N/MIN.)	HOLD TIME	APPARENT K_{ISCC} OR K_{IC} (MPa)
STA-36	80% RH	88	TO FAILURE	165.3
STA-33	80% RH	88	80 MPa FOR 24 HR.	
		22	90 MPa FOR 24 HR.	
		22	105 MPa FOR 24 HR.	
		22	110 MPa FOR 100 HR.	
		22	TO FAILURE	177.8
STA-1	1000 PPM SO_2 + 80% RH	88	TO FAILURE	175.2
STA-24	1000 PPM SO_2 + 80% RH	88	125 MPa FOR 24 HR.	
		22	134 MPa FOR 50 HR.	
		22	142 MPa FOR 50 HR.	
		22	TO FAILURE	150.0

TABLE III

SPECIMEN LIFE IN CYCLES

4340 STEEL 1335 MPa		
SPECIMEN #	RH	N_f (cycle)
1	DRY AIR ≤5 %	60,174
2	65%	40,593
3	100%	33,864
Al 7075-T651		
SPECIMEN #	RH	N_f (cycle)
1	DRY AIR ≤ 5%	40,347
2	80%	26,950
3	100%	41,005

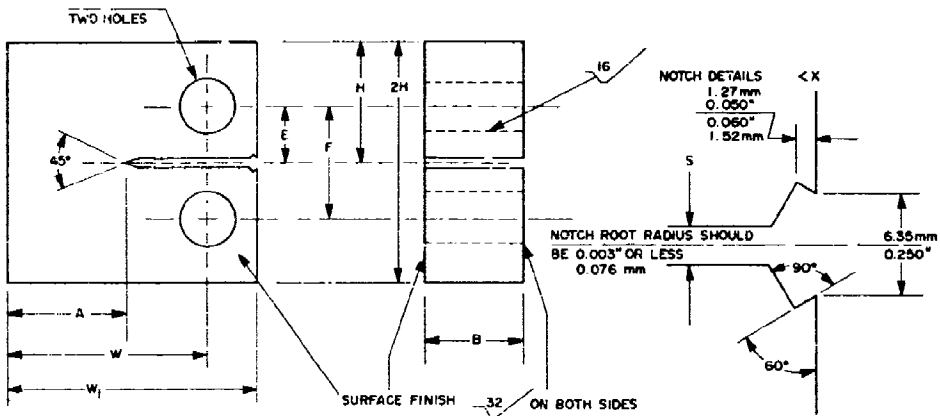

MATERIAL	B	A	W	W_1	S	E	F	H	D
ALUMINUM	25.4mm	29.2mm	50.8mm	63.5mm	2.36mm	13.97mm	27.94mm	30.48mm	12.7mm
STEEL	19.05mm	22.22mm	38.10mm	47.62mm	1.90mm	10.46mm	20.95mm	22.86mm	9.52mm

Figure 1. Compact-Tension Specimen.

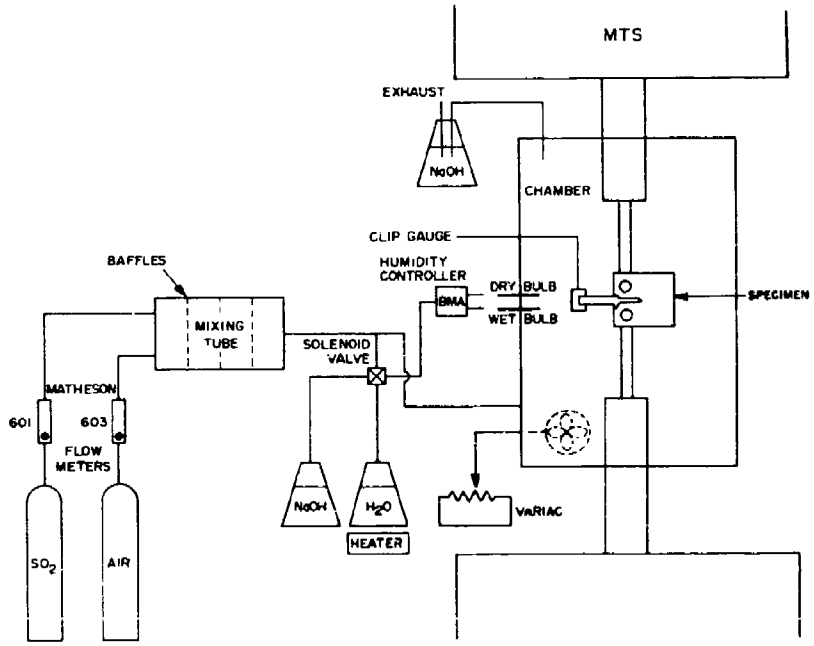

Figure 2. Gas Train and Environmental Chamber.

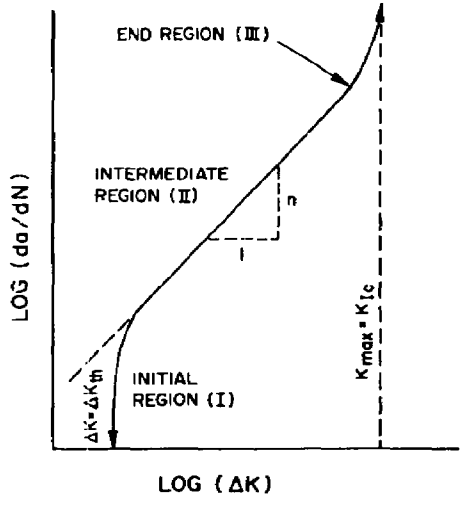

Figure 3. Schematic Diagram of Fatigue-Crack-Growth-Rate Behavior.

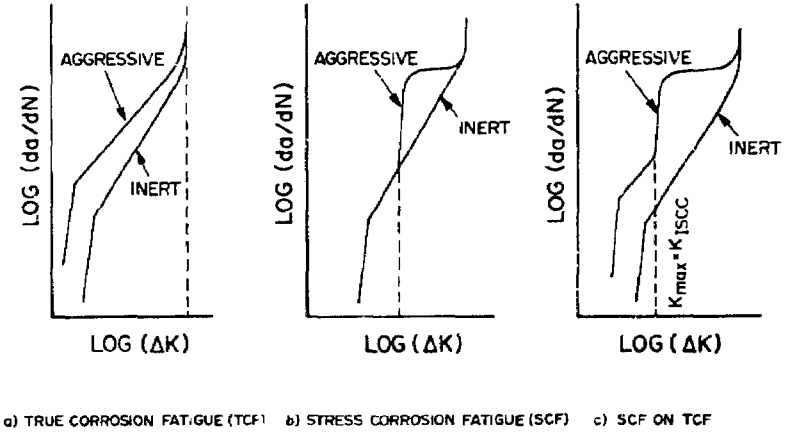

Figure 4. Types of Fatigue-Crack-Growth Behavior.

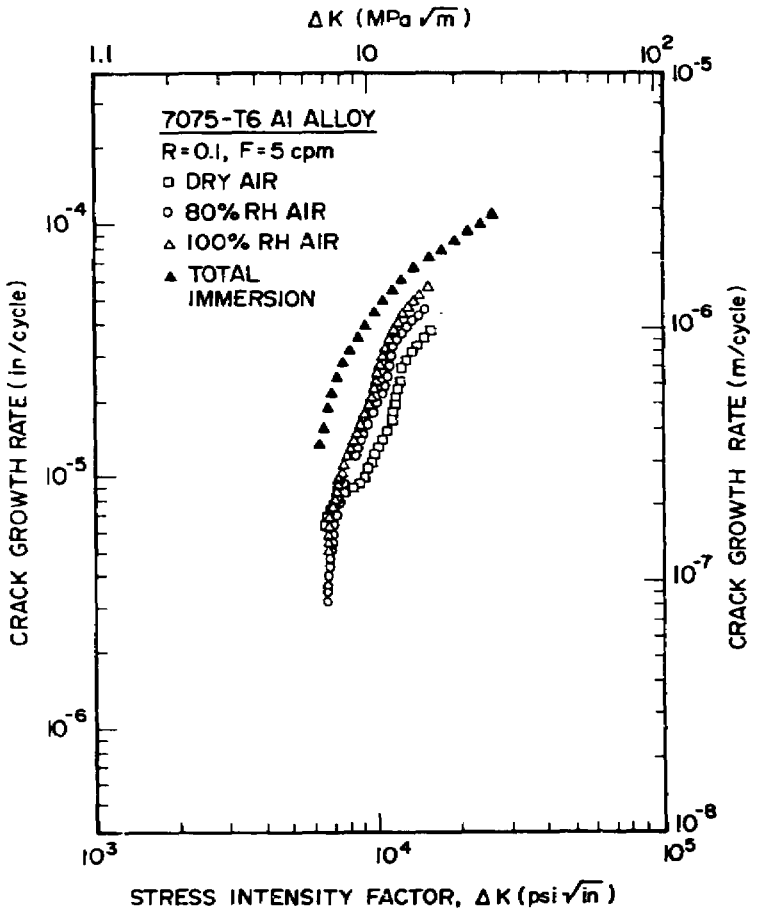

Figure 5. Crack-Growth Rate Data Obtained for Al 7075-T6 Tested at Various RH Levels.

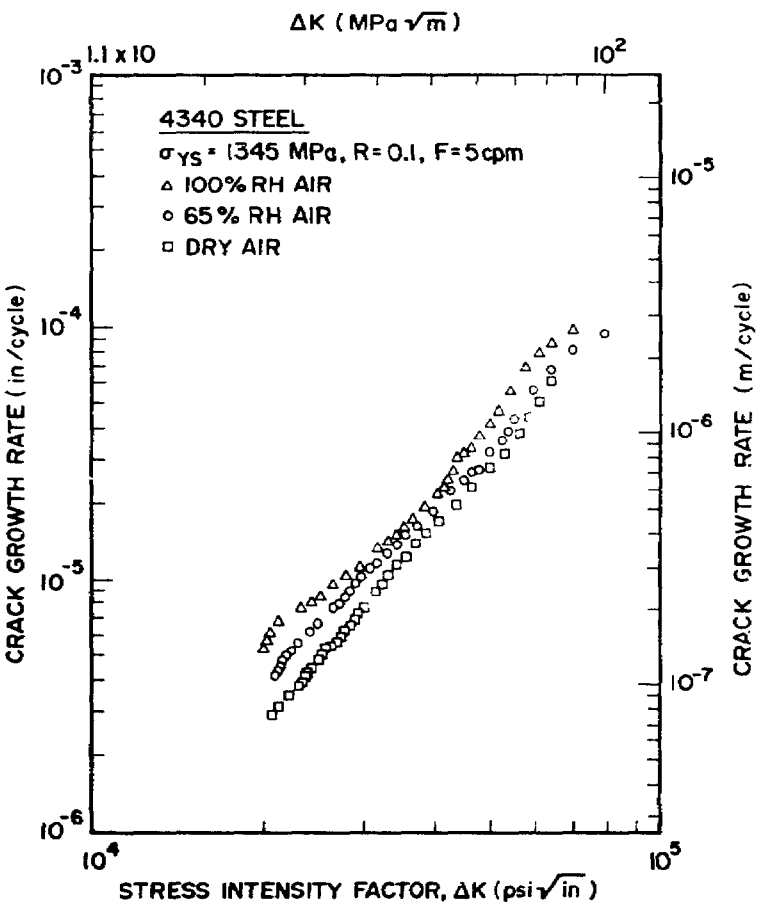

Figure 6. Crack-Growth-Rate Data Obtained for 4340 Steel (1345 MPa) Tested at Various RH Levels.

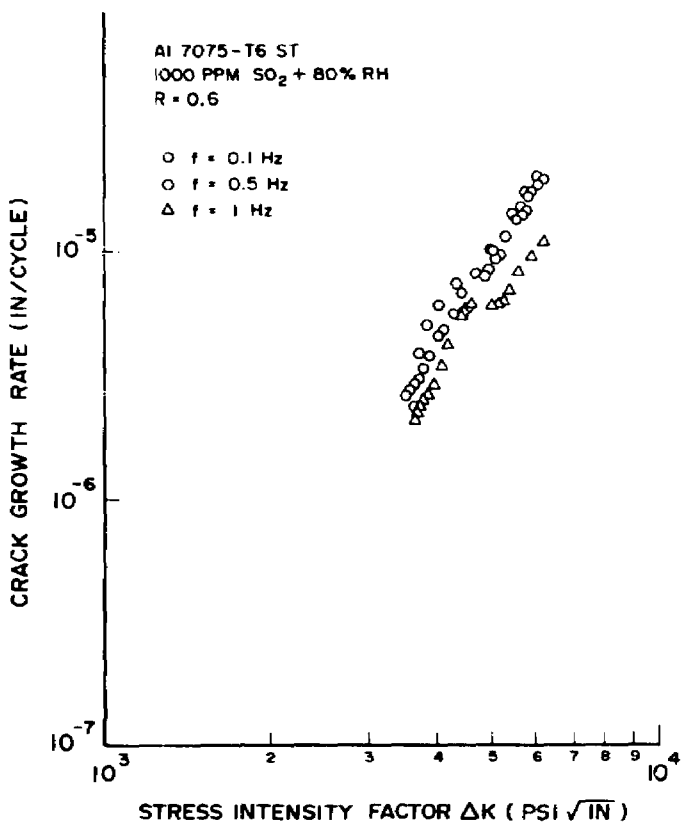

Figure 7. Crack-Growth-Rate Data Obtained for Al 7075-T6 Tested in 1000 ppm SO_2 + 80% RH Environment at a Stress Ratio of 0.6.

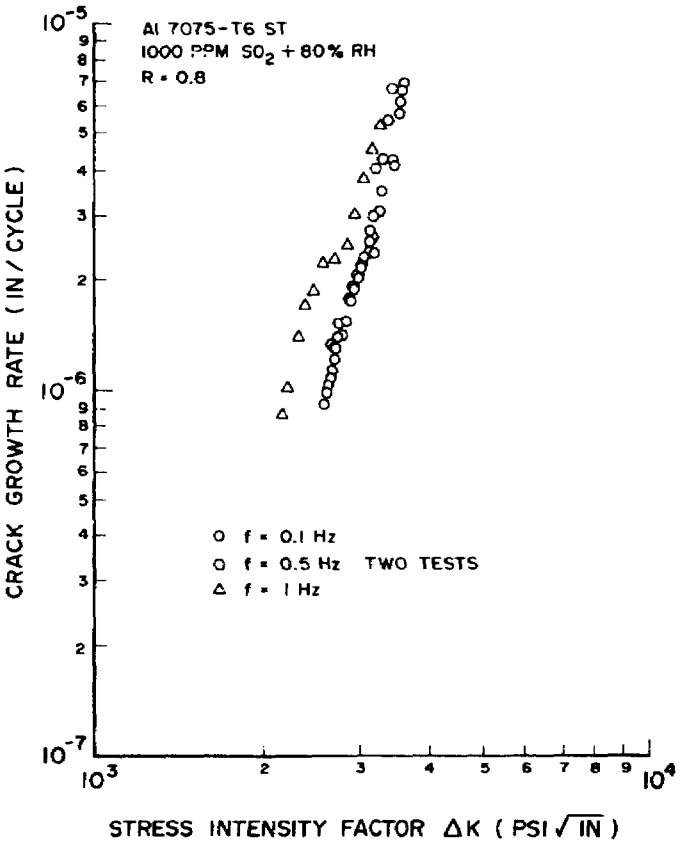

Figure 8. Crack-Growth-Rate Data Obtained for Al 7075-T6 Tested in 1000 ppm SO_2 + 80% RH Environment at a Stress Ratio of 0.8.

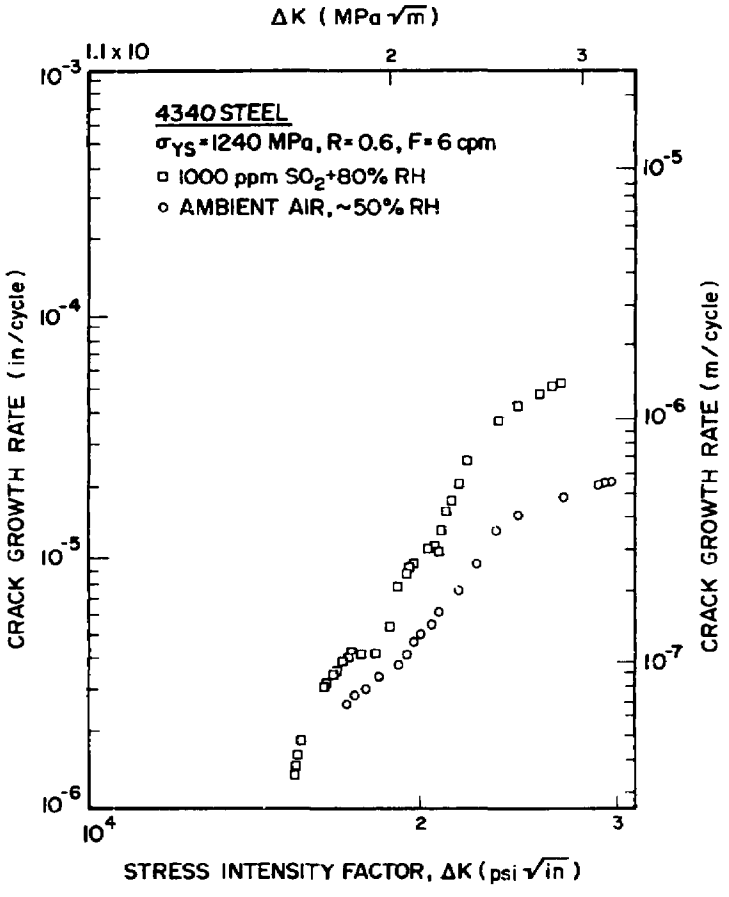

Figure 9. Crack-Growth-Rate Data Obtained for 4340 Steel (1240 MPa) Tested in 1000 ppm SO_2 + 80% RH Environment.

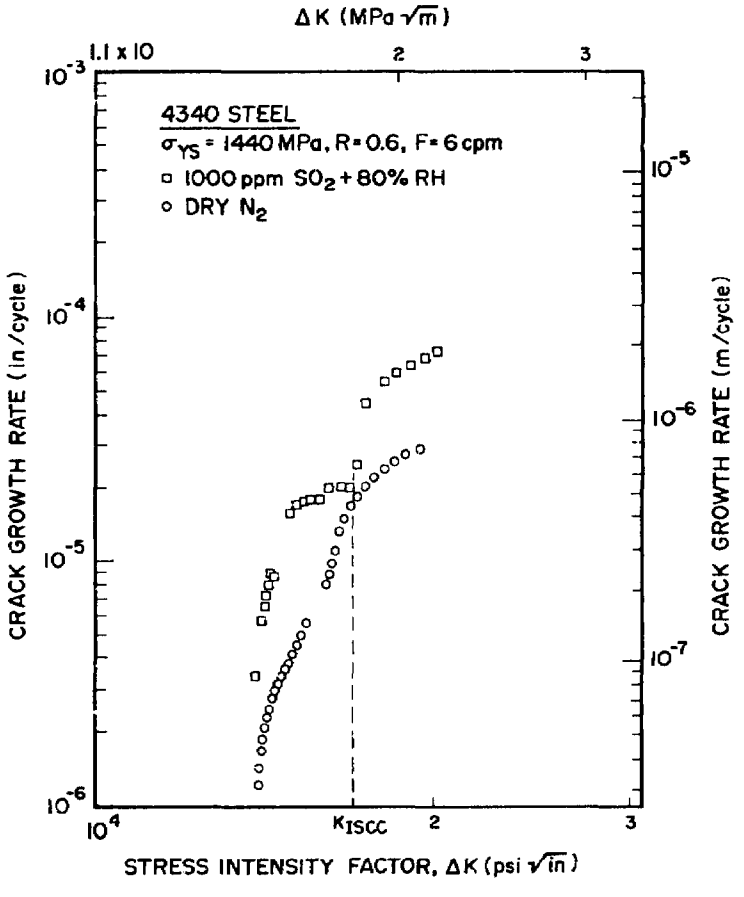

Figure 10. Crack-Growth-Rate Data Obtained for 4340 Steel (1440 MPa) Tested in 1000 ppm SO_2 + 80% RH Environment.

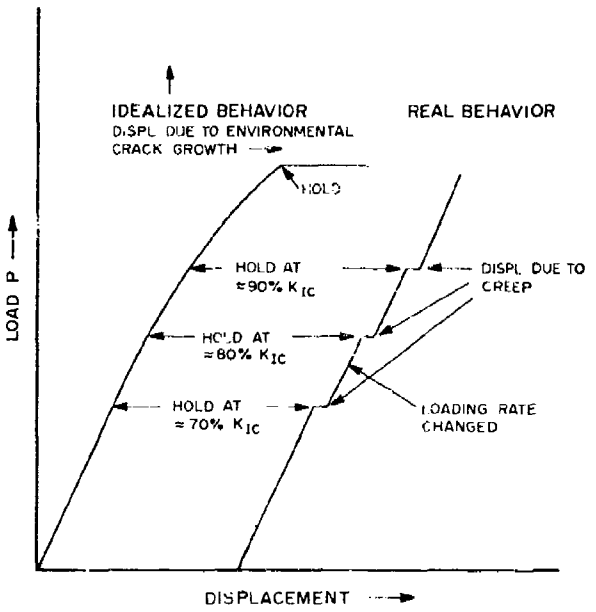

Figure 11. Schematic Diagram of Step Loading in Rising-Load Test for Al 7075-T6.

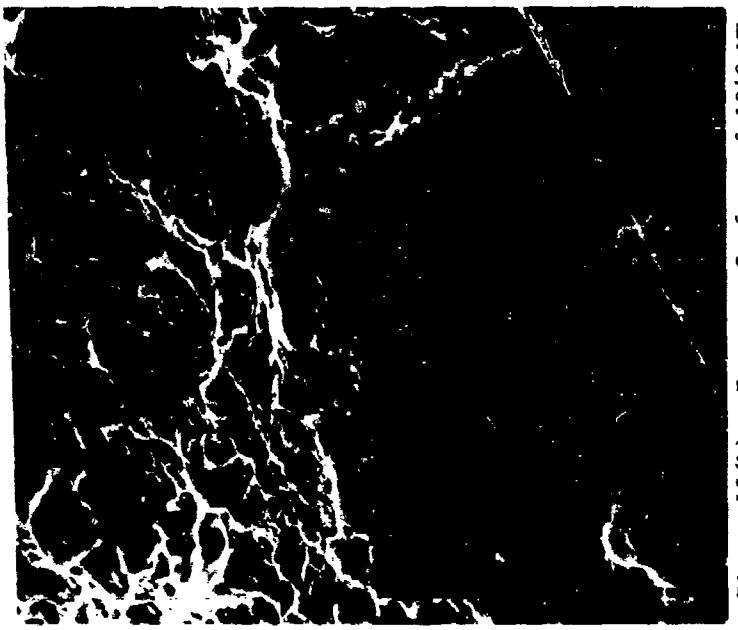

Figure 12(b). Fracture Surface of 1240 MPa Steel Tested in 1000 ppm SO_2 + 80% RH Environment at 57.5 MPa $\sqrt{m}$ (×3500).

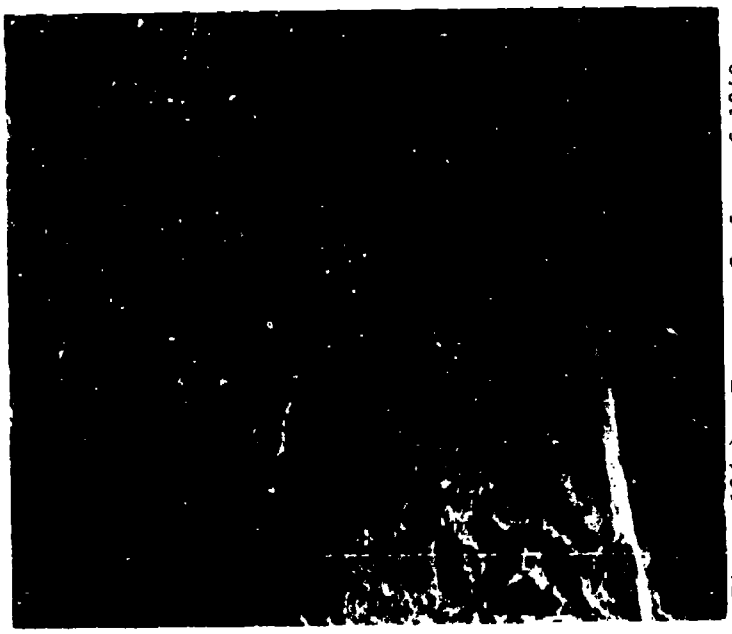

Figure 12(a). Fracture Surface of 1240 MPa Steel Tested in 1000 ppm SO_2 + 80% RH Environment at 57.5 MPa $\sqrt{m}$ (×600).

Figure 13(a). Ductile Morphology Obtained for 1440 MPa Steel, Resulting from Test in 1000 ppm SO_2 + 80% RH Environment in the Range 35-36 MPa $\sqrt{m}$ (×600).

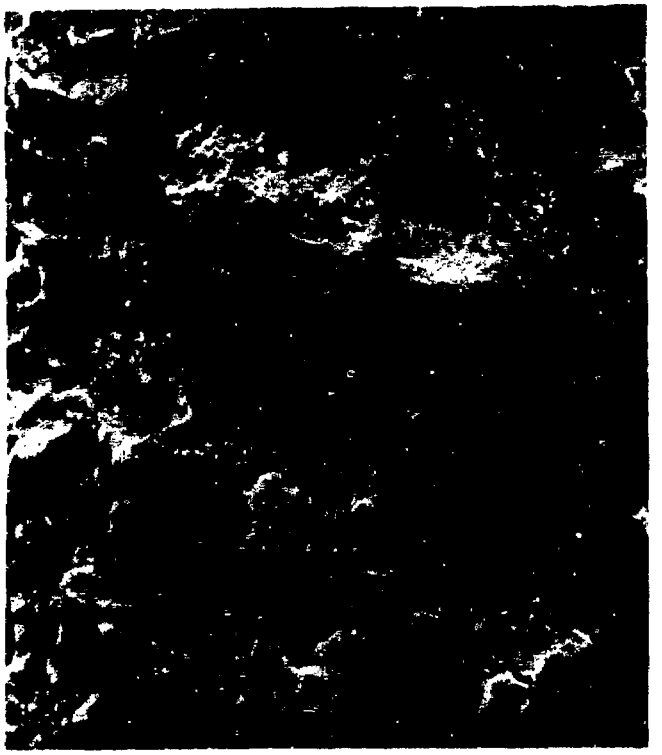

Figure 13(b). Mixed-Mode Fracture Obtained for 1440 MPa Steel, Resulting from Testing in 1000 ppm SO_2 + 80% RH Environment at 40 MPa $\sqrt{m}$ (×1100).

Figure 13(c). Intergranular and Brittle Failure Obtained for 1440 MPa Steel Resulting from Test in 1000 ppm SO_2 + 80% RH Environment in the Range 45-46 MPa $\sqrt{m}$ (×1100).

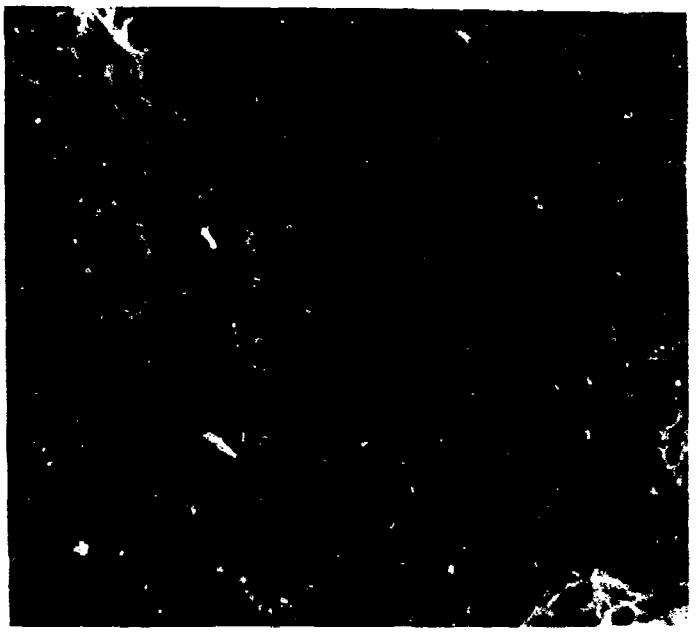

Figure 14(b). Higher Magnification of 14(a) Showing Dimple Rupture (×5000).

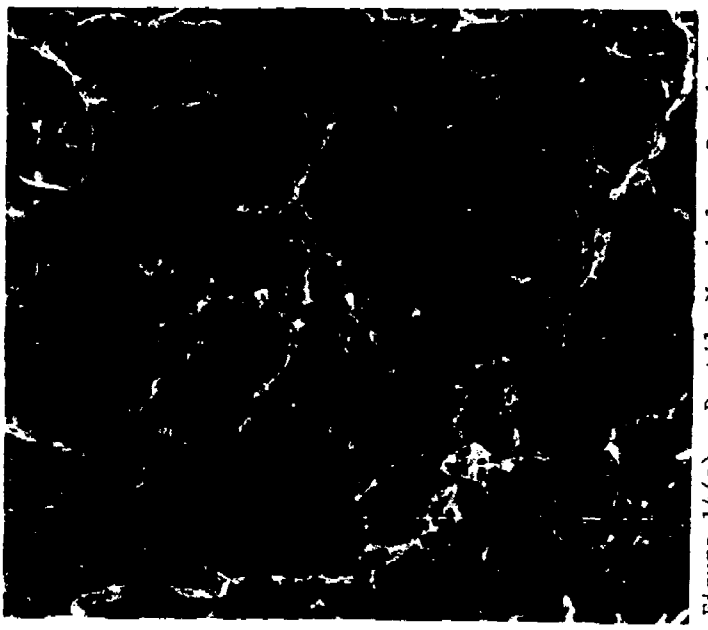

Figure 14(a). Ductile Morphology Resulting from Test Conducted in Dry Nitrogen (×2200).

AFWAL-TR-81-4019
Volume II

CORROSION PROBLEMS IN AIRCRAFT COMPONENTS--

CASE STUDIES OF FAILURES

W. R. Coleman, R. J. Block and R. D. Daniels
University of Oklahoma
Norman, Oklahoma 73019

Abstract

Case histories describing the analysis of failures of aircraft engine and accessory components are presented. In each case corrosion is identified as a causative or contributive factor to the failures.

Failures of cartridge pneumatic starter breech chambers have been observed in a number of jet engines. The failures are usually attended by significant damage to the aircraft. Failure analysis is often made difficult by excessive flame erosion of the fracture surfaces. Stress corrosion cracking, induced by residual or thermal stresses and the presence of corrosive combustion products, was observed in a breech chamber made of 4340 steel. Failure appears to have been the consequence of the geometry of the component coupled with use of a medium alloy steel in an extremely hostile environment.

An in-flight failure of the engine tail cone from an A-7D aircraft involved the loss of about one-third of the length of the assembly. The potential danger associated with an in-flight separation of several feet of metal tube is immediately obvious. The cone was fabricated from A-286 alloy. Failure originated at the junction between a longitudinal seam and a circumferential weld which joined a stiffener to the outside of the cone. Evidence of thermal and ordinary fatigue was noted and stress corrosion cracking in the weld nugget and base metals was documented.

Bursting of a 2024 aluminum bydraulic cylinder barrel on the inner landing gear door actuator of an F-101 aircraft was the result of fatigue and overload. However, the failure was found to have been induced by surface pitting. The failure initiated beneath an identification band which encircled the component. Similar failures have been observed in the main landing gear actuating cylinders of C-141 aircraft (2014 aluminum). Placing tightly fitting bands on such components appears to invite corrosion due to differential aeration. The pitting induced by crevice type corrosion sufficiently elevates the stresses locally that failure by mechanical means can occur.

Introduction

The work described here is part of a project dealing with failure analysis of aircraft engine and accessory components carried out in the School of Chemical Engineering and Materials Science at the University of Oklahoma. The work is sponsored by the Oklahoma City Air Logistics Center,

AFLC, U.S. Air Force. Where documentation is available on the failure history of a class of components or information is available on the service conditions of a particular component, it is often possible to deduce the circumstances leading to a specific failure. Otherwise, the analyses are limited to characterizing the failure according to the basic mechanisms that are indicated.

Corrosion as a causative or contributive agent to the process is indicated in a large number of failures we have analysed. This paper presents case studies of failures in three very different types of components which appear to share the common thread of being corrosion-related failures.

Breech Chamber Failures

One of the most frequently failed components for which analyses have been required is the breech chamber used in cartridge/pneumatic starters on a variety of aircraft engines. The chambers are part of the pressure containing system and hold a burning charge. The combustion products which are produced are directed toward the turbine to effect a quick start of the engine. Operating conditions typically involve a 20 second burn time, pressures in the neighborhood of 700 psi and metal temperatures of about 1100°F. Failure usually will produce damage to the neighboring engine and airframe structures as the burning gases escape through a rupture in the system.

Two types of breech chambers have been examined in some detail. One type is produced as an investment casting using the cobalt base alloy Stellite 21. These chambers show only mechanical failures by overload at the bayonet closure. There appears to be some question about the adequacy of the pressure relief system in this group of components. However, no corrosion induced failures have been observed. The second group of chambers is fabricated from 4340 steel heat treated to hardnesses in the range, Rockwell C 40 to 45. Examination of failed components indicates that after some service the material degrades to hardnesses in the neighborhood of Rockwell C 35. Stress analysis indicates that the corresponding reduction in strength renders the design marginal from a purely structural-mechanical standpoint.

Figures 1 and 2 show examples of typical failures in the steel breech chambers. The dome blows out at a location opposite the hot gas discharge nozzle. The failures occur in the region of highest stresses (according to stress analysis) at the change in section where the dome meets the body of the chamber. The photographs show the internal heat shields exposed by the failure. The shields are not sealed to the discharge duct and are not pressure containing components. Circulation of the cartridge combustion products can occur around the shields making cleaning of the residues difficult and uncertain.

Analysis of the failures is often made difficult by flame erosion and deterioration of the fracture surfaces. The changes produced obliterate necessary details of the fracture origin. The internal surfaces of the failed components are generally covered by a heavy layer of combustion products and are generally degraded by corrosion. Figure 3 is a photomicrograph of a cross-section through the failed chamber wall adjacent to the fracture origin. The photograph shows pitting of the internal wall. The pitting was noted to be quite deep in some places. Figure 4 shows a higher magnification view of the cross-section at the failure origin. One may note jagged, branching cracks which appear to follow the prior austenitic

grain boundaries in the heat treated structure. Some of the cracks contained a heavy deposit of oxide scale indicating their existence over prolonged periods prior to the failure. The cracks shown in the photograph are reasonably clear of oxide indicating they are of relatively recent origin.

The internal surfaces of the chambers which are exposed to the combustion products are not coated for corrosion protection. The external surfaces, specifically the dome, are covered with a coating of electroless nickel. The logic of this design is not immediately obvious in view of the potential sources for the most serious corrosion attack. Further, it should be recognized that the coating is inherently quite brittle. As the chamber is used it is subjected to internal pressure and thermal stresses in each service cycle. These stresses induce brittle cracking of the coating as shown in Figure 5. Corrosion attack of the base metal was often noted to be associated with these cracks. Figure 6 shows a typical example. The corrosion observed is most probably the result of galvanic coupling of the more noble nickel coating with the active steel chamber. The galvanic corrosion process appears to be a slowly progressing failure mechanism which should be capable of inducing fracture in the absence of other more rapid processes. The other processes do operate and an externally induced failure has not been observed thus far.

A particularly striking example of galvanic corrosion produced by the nickel coating was exhibited by a chamber which failed due to a complete separation encircling the bayonet locking connector. This chamber also contained the fracture at the hot gas nozzle, shown in Figure 7. The failure appears as a brittle, jagged crack extending about halfway around the nozzle. The fracture is of the same character as the fractures shown in Figures 3 and 4. This crack morphology is usually taken as evidence of failure by stress corrosion cracking (SCC). On the external surface of the chamber there is a craze pattern of trenches that extends beyond the failure crack at the base of the nozzle, Figure 8. Figure 9 shows a cross-section through the trenches associated with the craze pattern.

In evaluating SCC problems it is traditional to try to identify the source of stress and the specific corrosive agent responsible for the failure. Here it may be recognized that the cartridge contains a variety of materials that are capable of inducing pitting and SCC. The charge is an ammonium nitrate-based material in an (acid) organic binder. The potential for damaging species exists in both the combustion residues and any unburned cartridge material which is deposited on the chamber walls. The combustion products are likely to be hygroscopic and their deposition on inaccessible areas of the chamber further compounds the problem.

The most probable source of persistent stress (leading to SCC) is derived from the thermal cycles the chamber experiences. The rapid changes in body cross-section are conducive to uneven heating and cooling of the metal and localized regions of high stress due to notch effects. These are further intensified by pitting attack and general corrosion which acts to raise the local stresses. Finally, degradation of the strength properties of the metal also would contribute to catastrophic failure of the assembly.

Exhaust Tailcone Assembly

An unusual problem for which failure analysis was required involved the separation of a portion of the exhaust tailcone from an A-7D aircraft. About one-third of the assembly fell away from the airplane during a flight over Pittsburgh, Pennsylvania and the part was never recovered. Figure 10 shows an overall view of the portion of the cone that remained. The original cone tapered from about three to two feet in diameter, was about six feet long and was formed from sheet approximately 0.020 inches in thickness. The structure was stabilized with circumferential stiffeners on the outside. The piece that fell off in-flight was large enough to do considerable damage.

Figure 11 shows one of the stiffeners. Failure occurred in the body of the tailcone adjacent to the stiffener. Figure 12 details the stiffener which is resistance welded to the body in a skip or stitch weld pattern. The continuous longitudinal weld used to join the body is shown in Figure 13. The body material is A-286, a precipitation-hardened iron-base superalloy.

The contour of the fracture surface which encircled the body of the tailcone indicated that the origin of the failure occurred at the junction between the longitudinal and circumferential welds. Figure 14 and 15 are scanning electron micrographs of the fracture surface near the failure origin. As demonstrated by the photographs the majority of the failure exhibited dimple rupture evidencing failure due to simple overload. More detailed examination, in this same area revealed a pattern of metal degradation on the inside surface of the tailcone. Figures 16 and 17 show a network of coarse and fine cracks extending into the metal.

A cross-section was made through the junction of the longitudinal weld in the body and the circumferential stiffener weld at the stiffener adjacent to the large end of the cone (shown in Figure 10) where no failure had occurred. Figure 18 shows a photomicrograph of the weld nugget and the parent metal from both the stiffener and the body. In the more detailed view of Figure 19 one may note severe intergranular degradation of the weld which has isolated many of the metal grains. Figures 20 and 21 show intergranular attack of the parent metals.

The jagged, branched character of the cracks shown in the photomicrographs are indicative of stress corrosion cracking. The geometry of the tailcone configuration at the failure origin appears to be capable of producing the persistant stresses required for SCC. The crossing of a longitudinal and a circumferential weld would normally result in residual stresses when the metal cooled from the final weld. These stresses may not anneal out at the temperatures produced during normal use of the assembly.

The photomicrographs also demonstrate that the structure as revealed by electrolytic oxalic acid etching shows clearly defined grain boundaries or the "trench" type structure defined by ASTM A-262. The metal is thus shown to be disposed toward intergranular corrosion because of precipitate formation in the grain boundaries. The specific agent responsible for crack formation was not determined, but may be assumed to be a component of the engine exhaust gas stream.

Hydraulic Cylinders

The last class of component failures to be discussed involves various types of hydraulic cylinder bodies. Figure 22 shows an overall view of the inner landing gear door actuator cylinder from an F-101 aircraft. The material was reported to be 2024-T4 aluminum; this was verified by chemical analysis and hardness measurement. Figure 23 shows a close up view of a through wall crack in the cylinder. The metal surface is pitted and there is evidence of an identification band having been located in this area. The bands are typically attached with a rubber-like adhesive material.

Figure 24 shows the fracture surface associated with the crack. The area shown is believed to be the origin of the failure. Here the metal exhibited a "woody" appearance. A more detailed view of this area, revealed by SEM is presented in Figure 25. The metal shows the results of corrosion attack and typical exfoliation damage. It appears likely that this damage initiated the failure process. Areas of the fracture surface adjacent to the origin showed clear evidence of fatigue striations (Figures 26 and 27) obviously introduced as the cylinder was pressure cycled in use.

Transverse cross-sections through the cylinder beneath the banded area showed incipient cracks extending from the outside surface inward. It is a crack of this type that is presumed to have caused the failure. There are some well recognized dangers associated with the partial isolation of metal surfaces exposed to oxygenated corrosion media. Metals are susceptible to corrosion damage due to differences in oxygen concentration across the exposed surfaces. Moisture permeable films act to partially isolate the metal from oxygen in the environment and become preferred sites for corrosion attack. The process is often called differential aeration attack. The effect is much more pronounced with metals like aluminum that depend upon oxygen for production and repair of a normally protective surface film. Under conditions of oxygen deprivation the passive film may become damaged and the metal will be susceptible to rapid pitting attack.

A number of failures were studied all of which appeared to be associated with identification bands attached to hydraulic cylinders. Figure 28 shows the main landing gear actuating cylinder from a C-141 aircraft. The material is 2014-T6 aluminum. The closer view of the surface shown in Figure 29 shows a crack which has opened in the wall beneath the band. Figure 30 shows an area of the surface where a small piece of metal was lost either because of a forging defect or because it was isolated by corrosion. The appearance of a normal, overload fracture in the cylinder wall (Figure 31) may be compared with the fracture surface near the failure origin (Figures 32 and 33). The latter exhibits the same woody appearance which characterizes exfoliation attack. Here again attack was induced by differential aeration and was the result of a band attached to the cylinder surface. Once initiated, failure proceeded by fatigue as evidenced by the striations shown in Figure 34.

A similar type of failure was found in another C-141 hydraulic cylinder. The woody, darkened area on the fracture surface at its origin was examined with the electron probe microanalyser. This area was found to contain a number of contaminents, including chlorine, potassium and calcium. These are considered significant indications of water residues and particularly damaging species to which aluminum is susceptible.

Conclusions

The case histories discussed above present examples of corrosion due to relatively simple and well known mechanisms. Corrosion as a potential source of failure obviously must be acknowledged along with mechanical considerations in the design and maintenance of aircraft accessory components.

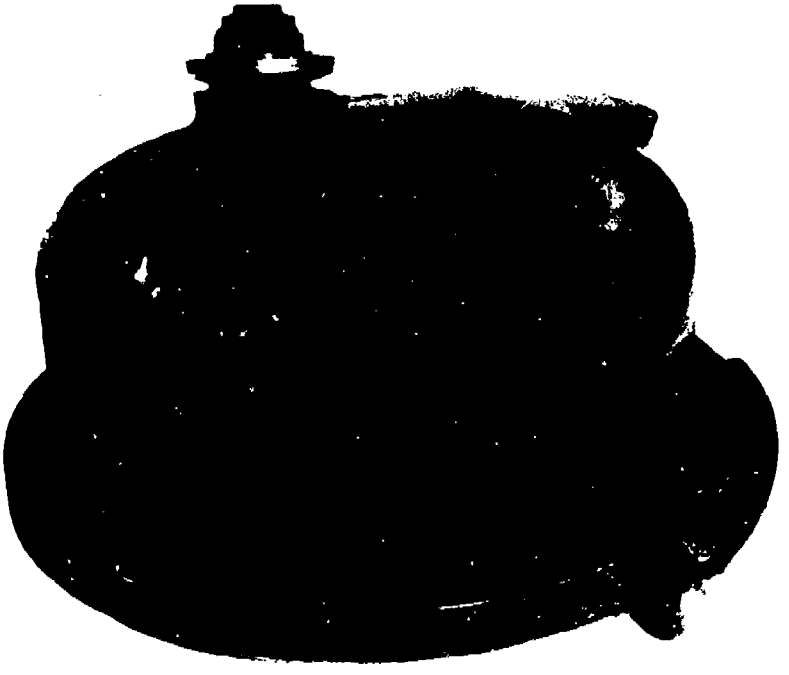

Figures 1 (above) and 2. Breech chambers which have suffered dome blowout failures.

Figure 3 150 X Nital-Picral Etch

Photomicrograph of a cross section through the breech chamber wall. Internal wall (left vertical edge) exhibits a pitted surface. Prior austenitic grain boundaries are outlined by a jagged crack.

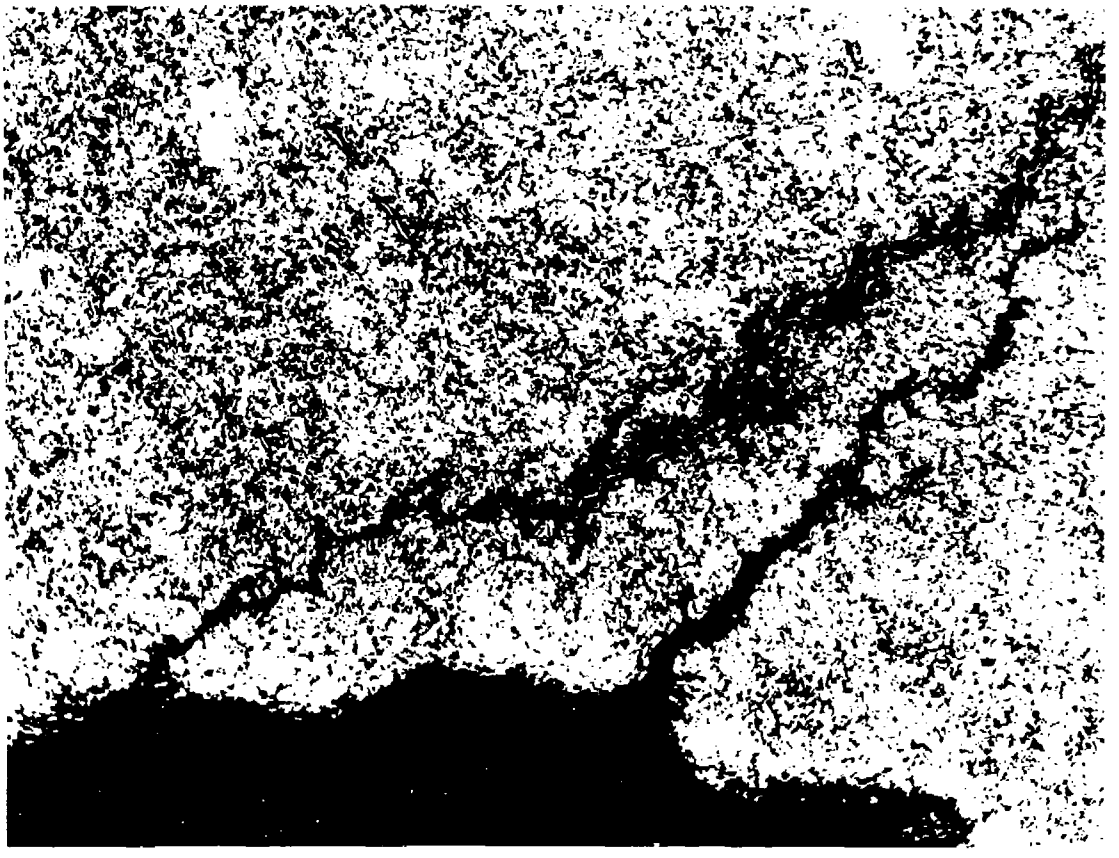

Figure 4 300 X Nital-Picral Etch

High magnification view of the jagged crack shown in Figure 3. The stress corrosion crack winds through a microstructure of tempered martensite; hardness Rockwell C 35.

Figure 5 300 X Nital-Picral Etch

Figure 6 300 X Nital-Picral Etch

Photomicrographs revealing nature of brittle nickel coatings.

Figure 7. Fracture encircling the hot gas nozzle of a chamber which has also failed in the bayonet lock.

Figure 8. Craze pattern of trenches extending beyond the main failure and at the base of the nozzle.

Figure 9 300 X Nital-Picral Etch
Cross section through the trenches associated with the craze pattern identified in Figure 8.

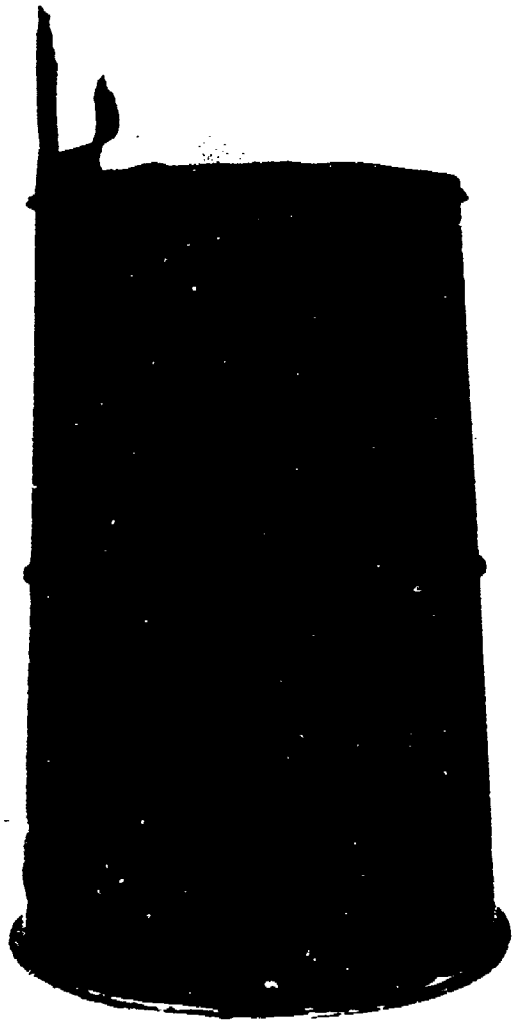

Figure 10. Overall view of the separated tailcone assembly. A-7D aircraft.

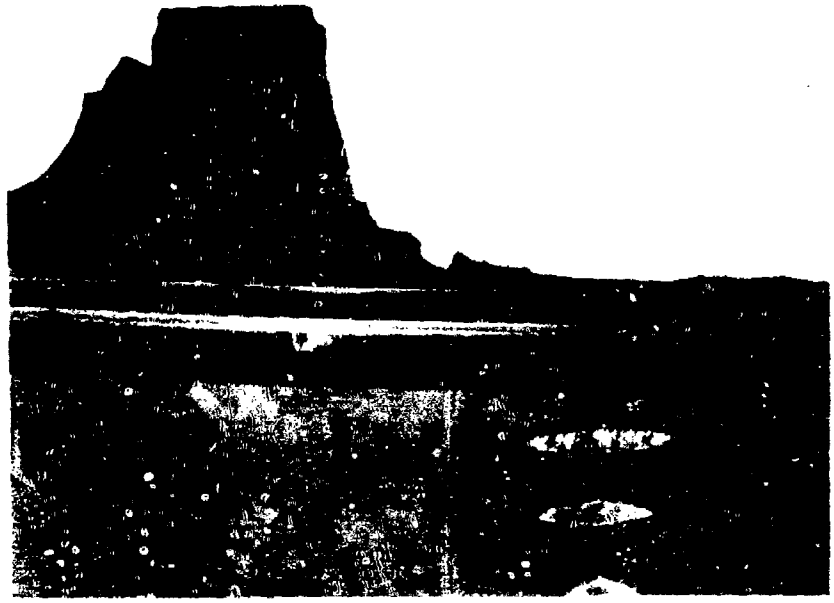

Figure 11. Close up view of the tailcone stiffener.

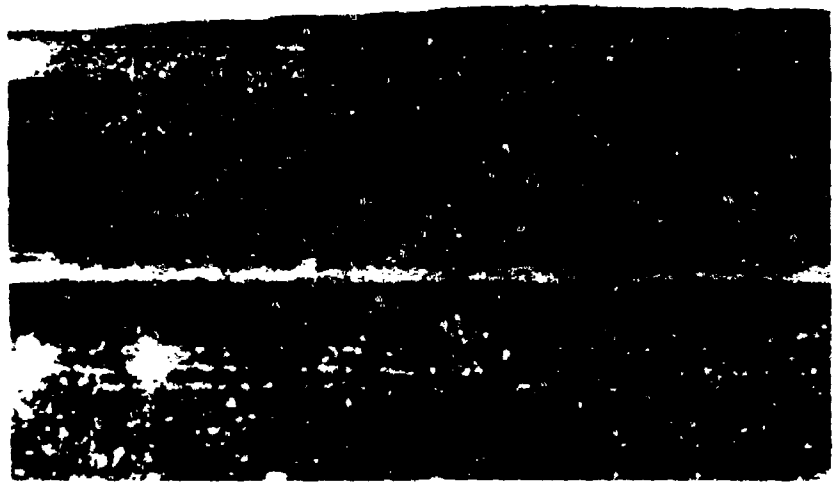

Figure 12. Detail of stiffener showing resistance stitch weld.

Figure 13. Continuous longitudinal weld used to join the body.

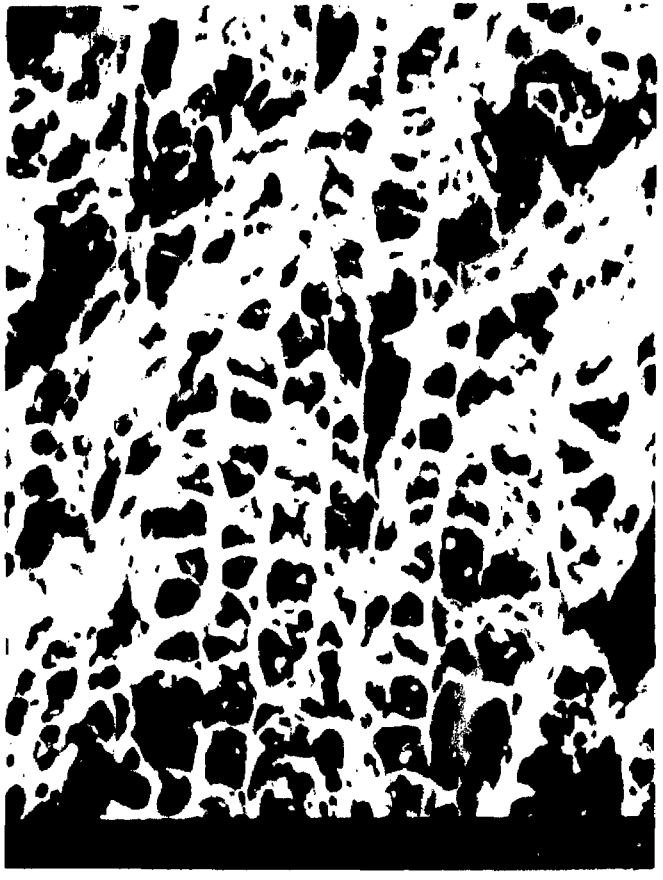

Figures 14 (left) and 15. Scanning electron micrographs of the tailcone fracture near the failure origin. Low and high magnification views indicating dimple rupture due to simple overload.

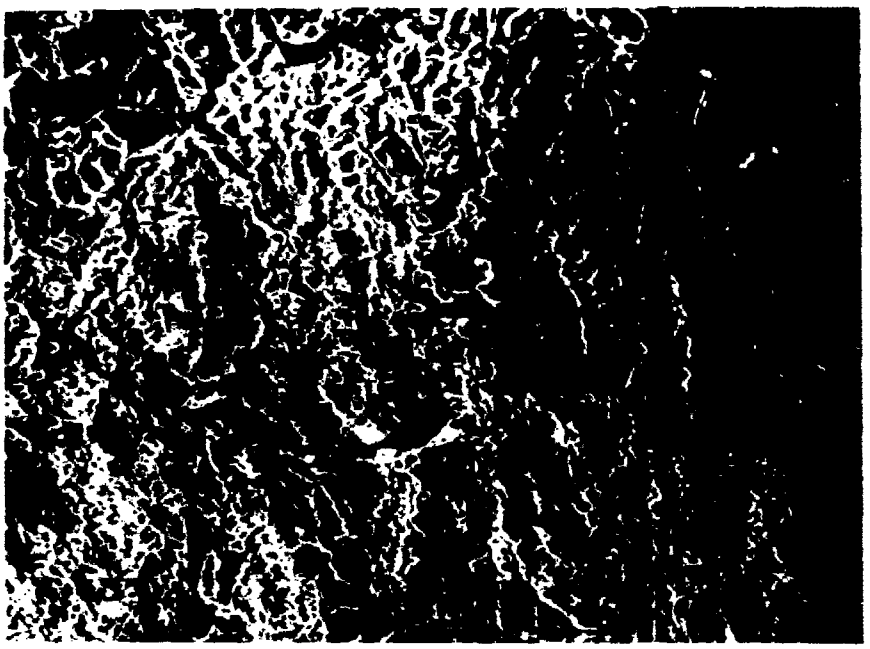

Figures 16 (left) and 17. Low and high magnification scanning electron micrographs showing crack network adjacent to the failure extending into the metal wall.

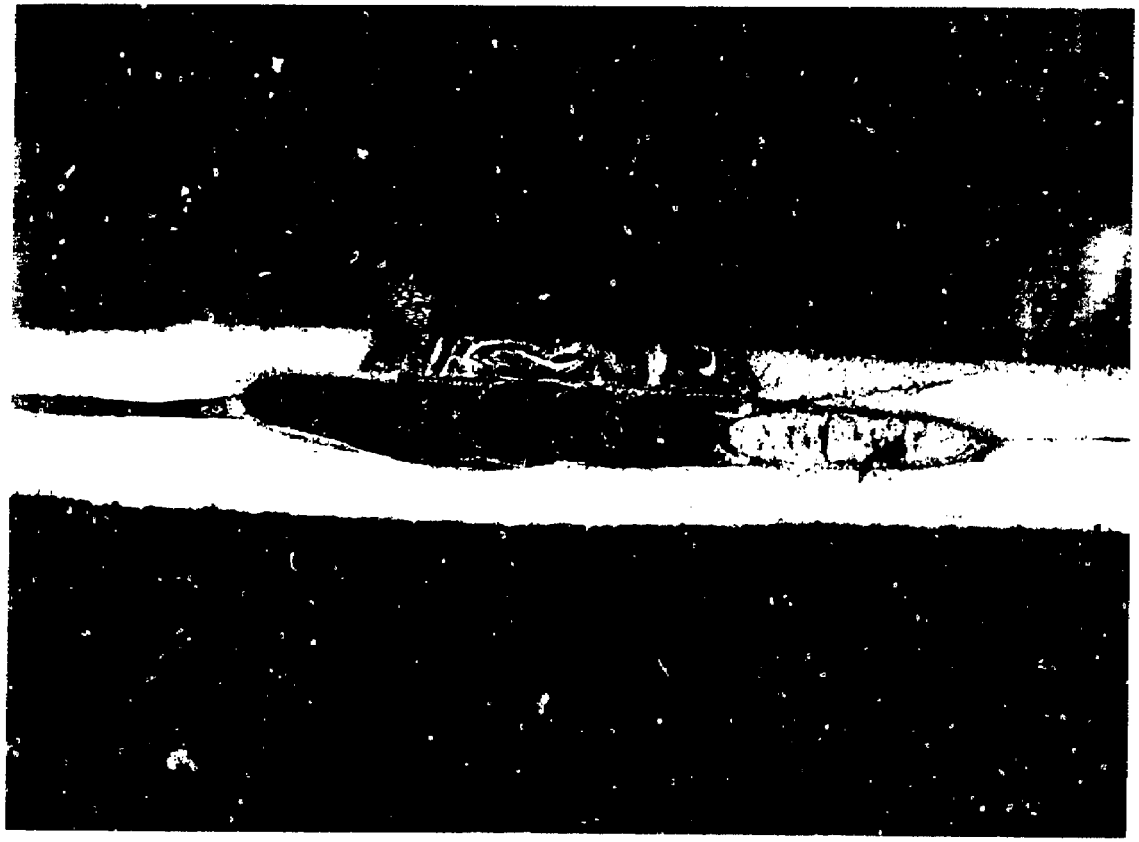

Figure 18 230 X Electrolytic: 10% Oxalic Acid

Weld nugget and parent metal from the stiffener and the body. Figures 19 and 20 show high magnification views taken near the left extreme of the weld nugget.

Figure 19 100 X Electrolytic: 10% Oxalic Acid

Figure 20 130 X Electrolytic: 10% Oxalic Acid

Severe intergranular degradation of the weld and parent metal.

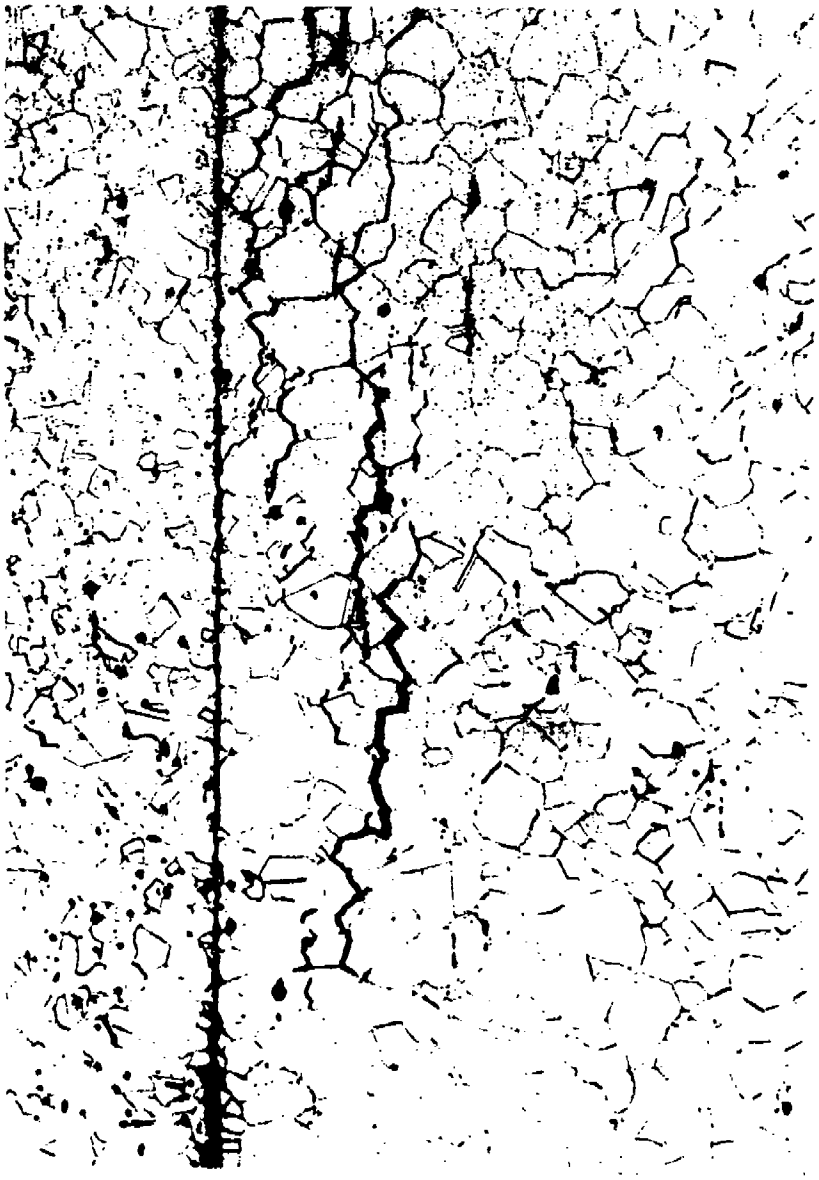

Figure 21 200 X Electrolytic: 10% Oxalic Acid
Intergranular attack extending outward in directions opposite of the weld nugget.

Figures 22 (above) and 23. Selected views of the inner landing gear actuator cylinder exhibiting a failure oriented longitudinally in the cylinder wall.

Figure 24. Fracture surface associated with the longitud-
failure in the cylinder wall.

Figures 25 (left) and 26. SEM views of the fracture surface shown in Figure 24. "Woody" features dominate the image in Figure 25 which appeared to have initiated the evidence of fatigue failure in Figure 26.

Figure 27. Another view of fatigue striations in the cylinder wall.

Figure 28. Overall view of the failed main landing gear cylinder. Note the anomaly in the wall.

Figures 29 (above) and 30. Close up views of the fracture in the longitudinal wall. Note the light stripes around the outside diameter in Figure 29.

Figures 31 (above) and 32. Areas in the failed wall exhibiting different fracture modes. Normal ductile failure remote from the origin (Figure 31) contrasted with a laminated or exfoliated character in the vicinity of the origin (Figure 32).

Figure 33. Example of exfoliation attack near the failure origin. Again characterized by the laminations in the wall.

Figure 34. Fatigue within the laminated areas of the cylinder wall.

VITAE

WILLIAM R. COLEMAN, Ph.D. candidate in Metallurgical Engineering School of Chemical Engineering and Materials Science, University of Oklahoma. Mr. Coleman earned the B.S. and M.S. in Metallurgical Engineering from the University of Oklahoma in 1978 and 1979. His research currently involves surface effects in crystal plasticity, heat treatment processes, and failure analysis.

ROBERT J. BLOCK, Professor of Chemical Engineering and Materials Science, University of Oklahoma. Dr. Block earned the B.S. in Metallurgy from the Massachusetts Institute of Technology in 1956, and the Ph.D. from the University of Illinois in 1963. Dr. Block has been on the faculty of the University of Oklahoma since 1963. His research interests include crystal plasticity and surface effects on plastic deformation. He is a frequent consultant on problems involving failure analysis and product liability.

RAYMOND D. DANIELS, Professor of Chemical Engineering and Materials Science, University of Oklahoma. Dr. Daniels earned the B.S. (1950) and M.S. (1953) in physics, and the Ph.D. in Metallurgy (1958), all from Case Western Reserve University. He has been employed by the National Bureau of Standards and the Union Carbide Corporation. He has been on the faculty of the University of Oklahoma since 1958. His research interests include hydrogen embrittlement of metals and corrosion. He is presently serving on the Board of Directors of the National Association of Corrosion Engineers.

COLEMAN BLOCK DANIELS

AFWAL [illegible]
Volume II

AIRCRAFT ANTENNA CORROSION CONTROL

J. S. Shaffer
Naval Air Development Center
Warminster, Pennsylvania

INTRODUCTION

Antennas have been determined to be the most corrosion prone components in the Navy's airborne electronic systems. Corrosion of antenna installations affects structural integrity and causes degradation of transmitted and recieved signals and undesirable random and static electrical discharges in sensitive electrical and electronic communication and armament systems. A considerable amount of maintenance time spent on antenna systems are to correct damage caused by corrosion. In an attempt to alleviate this problem an AERMIP (Aircraft Equipment Reliability Improvement Program) was funded to provide aircraft antenna corrosion prevention/control improvements. In the first phase of this program the major causes of corrosion and related antenna failures were identified. These results[1] were reported at the last Tri-Service Conference in 1978.

In the next phase of this program improved corrosion preventive materials and processes for aircraft antennas were proposed. Representative antenna installations were selected for a fleet evaluation of these maintenance procedures. A test plan was developed that provided the guidelines for conducting the fleet evaluations to assess the effectiveness of these materials and processes. Under Commander, Air Force Pacific (COMNAVAIRPAC) and Commander, Air Force Atlantic (COMNAVAIRLANT) sponsorship and in coordination with the appropriate Fleet Wings, the test plan maintenance procedures and material applications were applied to various types of aircraft antennas. The test period covered 180 days.

Aircraft antennas can be classified into four types: whip, long wire, rigid and flush/dome. Figures 1 through 6 provide illustrations of the different antenna types. The installation depicted in Figure 4 shows the use of a gasket between the antenna and airframe skin. It should be noted that not all rigid (or blade) type antennas use this gasket.

The antenna installations selected for evaluations along with the fleet maintenance activities which performed the maintenance procedures are listed in Table I. The main basis of selection was that the antennas should represent the different types each with its own distinctive corrosion problems. For example, the P-3 HF long Wire antenna is subject to corrosion and arcing due to water intrusion into the tensioner assembly and the insulator; the H-46 HF radio antenna has a whip antenna mounted on the lower skin that has a particular problem due to water entrapment around the electrical attachment inside of the fuselage; and the A-7 Lower TACAN/IFF antenna has a major problem due to the presence of water and other fluids in a bathtub-like area where the coaxial lead penetrates the fuselage skin to the antenna. Similarly, the H-3 No. 1 UHF/Comm Normal (lower) and Alternate (upper) antennas are skin mounted and require a conductive gasket between the antenna base and the skin. These antennas are subject to the same moisture intrusion as the A-7 aircraft, yet the A-7 installation requires no conductive gasket. The H-3 Doppler has a particularly bad problem because that portion of the antenna interior to the aircraft is located in the fuselage low point area and, therefore, subject to a variety of standing fluids.

Table II lists the corrosion maintenance data for the selected antenna. Data was obtained from the Naval Maintenance Support Office (NAMSO), Aviation

Type Equipment History Inquiry Report, NAMSO 4790-A2098-01, for a one year period, 1 January through 31 December 1978. The list contains aircraft, antenna nomenclature, total maintenance actions reported with the no defect actions eliminated, total related corrosion maintenance actions and corrosion percentage. The numbers are based on the corrective maintenance actions performed at the first two levels of maintenance; the organizational or squadron level and the intermediate level. Data for the third or depot level conducted by the Naval Air Rework Facilities cannot be obtained in the NAMSO data system. The numbers reflect the magnitude of the corrosion problem in these antennas. The corrosion maintenance actions attributable to corrosion damage range from 11 to 18%.

AIRCRAFT CORROSION CONTROL MAINTENANCE PROCEDURES EVALUATION

The fleet evaluation was designed to get inputs from the using technicians relative to the use (application/removal) as well as the durability and effectiveness of the corrosion preventive materials and procedures.

Selections of materials for this fleet level corrosion control were based on the following considerations:

1. There should be no detrimental effects on the operation of systems or components.

2. They should possess demonstrated effective corrosion preventive properties.

3. They should be easily utilized in the fleet environment.

4. Insofar as possible, they should be materials that presently are available in the Naval Aviation supply system.

GENERAL ANTENNA MOUNTING PROCEDURE

During the implementation of the test program these procedures were applicable to any of the rigid type antenna bases (blade, whip, or long wire mast base). The step-by-step actions for cleaning, application of corrosion preventives and sealing of these antenna bases were:

a. Removed dirt, oil, and grease from contact surfaces of the antenna and aircraft skin using cleaning cloth dampened with dry cleaning solvent.

b. Removed minor surface corrosion with an abrasive mat

c. On areas where the corrosion products were abrasively removed, applied Chemical Conversion Coating, MIL-C-81706, Class 3, to the bared surface. The class 3 material was used because it provides a thinner coating with lower electrical resistivity.

A-7 TACAN/IFF ANTENNA MOUNTING PROCEDURES

This procedure is applicable to the A-7 aircraft lower TACAN/IFF antenna, and was evaluated on two A-7E aircraft at the Naval Air Station, Lemoore, California.

Since the A-7 lower TACAN/IFF antenna installation did not require a conductive gasket, the following mounting procedures were used:

a. Removed anodize on screw countersink areas of antenna base in order to provide good electrical conductivity from the base to the screws.

b. Applied Chemical Conversion Coating, MIL-C-81706, Class 3, on bared countersink areas.

c. Applied an even coating of Corrosion Preventive Compound, MIL-C-16173, Grade 4, on both the aircraft skin surface and the flat side of the antenna base which mates against the aircraft skin. The Grade 4 material is a soft, tacky to the touch, coating when it dries and has been used for many years as a general preservative on naval aircraft.

d. Conducted electrical resistance test to check for a good grounding connection. The grounding specification requires the resistance not to exceed 0.1 ohms. (The milliohmmeter reading for these antenna installations were both 0.02 ohms.)

e. Applied a fillet of corrosion inhibited polysulfide sealant, MIL-S-81733, Type II, around the outside of the antenna base on one aircraft and a fillet of MIL-S-8802 polysulfide sealant without inhibitors on the antenna on the other aircraft to form a watertight seal.

f. Covered the fastener heads with Corrosion Preventive Compound, MIL-C-16173, Grade 4.

H-3 AIRCRAFT #1 UHF NORMAL AND ALTERNATE ANETNNA

The H-3 aircraft #1 UHF antennas require a conductive gasket; therefore, the base-to-skin mounting procedure was as follows:

a. Placed a heavy coating of Corrosion Preventive Compound, MIL-C-16173, Grade 4, around the lower coax cable and on the outside of the coax connector so that this corrosion preventive compound would be inside of the gasket circle when the antenna base was mated to the fuselage skin.

b. Installed the antenna base as described in paragraphs a and b of the A-7 TACAN/IFF ANTENNA MOUNTING PROCEDURE.

c. Conducted electrical resistance test to check for a good ground connection. (The milliohmmeter reading on these antenna installations were all 0.01 ohms.)

d. Continued the installation procedures as described in paragraphs e and f of the A-7 TACAN/IFF ANTENNA MOUNTING PROCEDURE.

AIRCRAFT ANTENNA COAXIAL CONNECTORS

Corrosion inside of an antenna coaxial connector is a principal cause of antenna performance degradation (Figure 7). Therefore, the cleaning and preserving of the antenna connectors is important to reduce effects of

moisture intrusion. Throughout the test program the cleaning and preserving of these connectors were accomplished during the various installations by the following procedures:

a. With the connector sections mated, corrosion was removed with an abrasive mat.

b. Connectors were opened and internal sections were cleaned.

c. The internal areas were sprayed with a water displaying corrosion preventive compound MIL-C-81309, Type III. The MIL-C-81309 material forms an ultra thin tacky (soft) film that is designed so that it is displaced by the wiping action of a sliding electrical contact, yet the film is self healing (reforms) in non-contact areas after displacement. The resultant lack of disruption to DC continuity through the male/female type of connections due to a MIL-C-81309, Type III, film has been well established.[3,4]

d. The connectors were then mated and a coating of another water displacing corrosion preventive compound, MIL-C-85054[5], was applied to the exterior surface of the connector. This material dries to a relatively thick (1 to 2 mils) hard, clear finish and has been used successfully on naval aircraft to protect exterior skin surfaces in areas where paint has chipped or cracked leaving exposed bare metal.

P-3 AIRCRAFT LONG WIRE/DIRECTION FINDER (DF) SENSING ANTENNA CORROSION PREVENTION PROCEDURE

At the Naval Air Station, Moffett Field, two P-3C aircraft were selected for the Long Wire Antenna Test procedure. This test was performed to develop a means of minimizing a moisture intrusion problem in the antenna insulator. The following installation procedures were used for corrosion prevention on the P-3C aircraft long wire/DF antenna:

a. Removed dirt, oil and grease from the long wire/DF attachment components with Dry Cleaning Solvent, P-D-680.

b. Removed surface corrosion on the antenna mast cable shackle, clevis bolts, etc., with an abrasive mat.

c. Cleaned by wiping with Cleaning Cloth, dampened with Cleaning Compound Solvent, MIL-C-81302. This step removes any petroleum residue and other materials left by the use of the abrasive mat.

d. With the long wire/DF antenna installed, applied a coating of Corrosion Preventive Compound, MIL-C-85054, Type I, over the attaching hardware.

e. Applied Adhesive Sealant, RTV 3140, clear, MIL-A-46146, where the wire feeds into the insulator.

f. Applied Adhesive Sealant, RTV 3140, clear, MIL-A-46146, where the wire feeds into the take-up tension assembly, and over the tension take-up assembly alignment slot.

H-46 AIRCRAFT LONG WIRE/DIRECTION FINDER (DF) SENSE ANTENNA CORROSION PREVENTION INSTALLATION PROCEDURE

The H-46 aircraft Long Wire/Direction Finder (DF) Sense Antenna is a whip antenna mounted on the lower skin and has a corrosion problem due to water entrapment around the antenna electrical attachment inside of the fuselage. This antenna is subject to two types of corrosion damage:

a. Corrosion and arcing due to water intrusion into the insulator assembly.

b. Corrosion around the base of the mast due to steel screws through aluminum parts and water seepage between the base and the skin.

The following corrosion prevention test plan procedures were used on an H-46 aircraft to evaluate techniques to minimize the foregoing problems.

a. Preparation of the individual antenna parts involved removal of surface corrosion on the mast cable shackle, clevis bolts, etc., with an abrasive mat.

b. Removed dirt, oil and grease from long wire/DF attachment components with Dry Cleaning Solvent, PD-680.

c. Cleaned by wiping with Cleaning Cloth, dampened with Cleaning Compound Solvent, MIL-C-81302.

d. The corrosion preventive procedures for mounting the antenna mast are described in the GENERAL ANTENNA BASE MOUNTING PROCEDURE.

e. With the long wire/DF antenna installed, applied a coating of Corrosion Preventive Compound, MIL-C-85054, over the attaching hardware.

f. Applied Adhesive Sealant, RTV 3140, clear, MIL-A-46146, where the wire feeds into the insulator.

H-3 UHF-VHF/ADF (ARA-25) ANTENNA

The principal cause of maintenance requirements on this antenna is traditionally due to a water intrusion problem. Therefore, a special sealing procedure for the ADF antenna was evaluated along with the normal antenna installation anti-corrosion procedures. The following procedures were performed:

a. With antenna removed, removed grease, oil and dirt from the aircraft mounting areas with Cleaning Cloth, dampened with Dry Cleaning Solvent, PD-680.

b. Removed surface corrosion from the ADF antenna with an abrasive mat.

c. Cleaned the corrosion controlled antenna and aircraft mounting areas and areas to be sealed with MIL-C-81302.

d. Assembled the antenna, but omitted installation of the extruded rubber dust cover channel. Sealed the circumference of the mated dust cover and antenna cavity to the casting with Sealing Compound, MIL-S-81733, Type II. Also sealed around the circumference of the mated plastic plate to the antenna cavity, as well as sealing on top of the external fasteners of the dust cover.

e. Before installing the antenna, coated the inside lip, where the antenna is mounted, as well as the surrounding area with Corrosion Preventive Compound, MIL-C-85054.

f. After the sealant was cured, installed the antenna and applied Corrosion Preventive Compound, MIL-C-85054, over the antenna mounts.

g. Cleaned and preserved electrical connectors in accordance with the procedure in the AIRCRAFT ANTENNA COAXIAL CONNECTORS paragraph.

h. Sealed the exterior circumference of the antenna and aircraft mating surface with Sealing Compound, MIL-S-81733.

FLEET EVALUATION RESULTS

Throughout the evaluation the designated fleet squadrons submitted reports describing the results pertaining to the specific antenna procedures applied to their particular aircraft. The following general summary of the submitted reports is provided:

a. Throughout the 180-day evaluation, all the test items were reported from excellent to satisfactory, and none showed evidence of corrosion or problems with the materials used.

b. All reports indicated that the solvents, cleaning materials, etc., had no effect on the sealants or corrosion preventive materials applied to the test items.

c. Throughout the evaluation period, there was only one reported failure. This was on the ADF (ARA-25) antenna on the SH-3H aircraft. The report indicated this failure was discovered during troubleshooting of a discrepancy of the UHF/DF system. During the ADF antenna removal approximately three ounces of water was noted to run out from the antenna area. No corrosion, however, could be detected on the antenna exterior. The technician noted that there was no indication that the presence of this water was the cause of the functional failure of the ADF antenna.

Specific test results included the following:

a. In the evaluation of sealants as applied around the bases of antennas, the two assigned A-7E lower TACAN/IFF antennas were removed (Figure 8) with no difficulty in the removal due to the sealant applied around the circumference of the bases. The inspection of the sealants indicated that MIL-S-8802 and MIL-S-81733 both are effective in resisting deterioration due to solvents, detergents, cleaning materials, etc. Upon removal of the antenna, a combination of fluids (hydraulic oil and water) were present; however, the Corrosion Preventive Compound, MIL-C-16173, Grade 4 prevented these fluids from affecting the antenna and the aircraft skin mounting area. There were no visible

signs of corrosion. When the antenna connectors were disconnected they were in the same material condition as when they were connected at the beginning of the evaluation period. There was no evidence of external connector corrosion. As the photos (Figure 9) show, the antenna coaxial connector appears to be clean after the six months tests even though the photo clearly shows that fluids, foreign matter, etc. from the inside of the aircraft are all around the base of the connector.

b. The P-3C evaluation results indicate that the procedures of applying Adhesive Sealant, RTV 3140, clear, MIL-A-46146, to the HF Long Wire antenna insulator wire connection ends were beneficial for preventing moisture from entering the insulator in this area. The use of Corrosion Preventive Compound, MIL-C-85054, Type I, over the attaching hardware was also effective in preventing corrosion in these areas. However, the procedure for applying the Adhesive Sealant, RTV 3140, clear, MIL-A-46146, over the tensioner (Figure 10), alignment slot was not adequate. The sealant appeared to be lifted from the alignment slot area.

c. The H-3 test plan procedures applied to the Doppler AN-APN-182, No. 1 UHF/COMM (normal and alternate) and the ARA-25 antennas were very satisfactory in preventing corrosion attack in these areas. The corrosion preventive compounds, sealants and method of applying these materials appear to be a very effective way of protecting these normally corrosion-prone areas. The Doppler antenna mounting area had no evidence of corrosion, even though upon removal there was water, hydraulic fluids, etc., present due to the lack of proper drainage.

Evaluation of results on the No. UHF/COMM normal (lower fuselage) and alternate (upper fuselage) antenna anti-corrosion procedures utilized on the antenna base and aircraft structure mating area indicated that the preventive methods employed did preclude moisture from entering the critical base and coaxial connector areas - even though the No. 1 UHF lower fuselage antenna was generally saturated with fluids. The same situation also applied to the ARA-25 antenna.

SPECIAL ANTENNA COAXIAL (COAX) CONNECTOR TESTING

Coax lines are used for the transmission of RF energy in the frequency range from 30 MHz to 3GHz, although there is some overlap with waveguide RF transmission which is used for frequencies above 300 MHz. This means, however, that most of the NAV/COM equipment utilizes coax lines and, therefore, coax connectors where a transmission line mates to an antenna. By far, the principal cause for rejection of NAV/COM antennas is corrosion degradation within the coax antenna connector.

Traditionally no preservatives have been used inside of a coax connector because of fears that any foreign material would alter the characteristic capacitance created by the spacing and insulation between the inner and outer conductors. This characteristic is particularly critical in those lines for which changes in capacitance is used as a sensor in the system - such as in a capacitive type of fuel quantity indicating system. Any change in the dielectric between the inner and outer conductor also can affect the impedance of an antenna line (connector).

Special tests with relatively sensitive measuring equipment were made to determine the electrical (RF transmission) effects incurred by the introduction

of MIL-C-81309, Type III, Water Displacing Corrosion Preventive Compound into coax connectors between sections of coax line. The tests were conducted using TDR (Time Domain Reflectometry) and FDR (Frequency Domain Reflectometry) equipment to sweep a coax assembly over a frequency range of 2 to 11 GHz. Two runs were made on the line/connector assembly with no corrosion preventive applied to display the repeatability of the test when no change is introduced to the test item. Following that, runs were made with MIL-C-81309, Type III, Class 2, applied to both sections (male and female) of the connector.

No attenuation of signal or change in characteristic impedance resulted from the presence of MIL-C-81309 material in the coaxial connectors over the frequency range measured.

Concurrent with the foregoing electrical testing, the effectiveness of MIL-C-81309, Type III, in this application was tested by fleet activities. Reports received from fleet activities throughout the evaluation period revealed no problems with antenna performance or maintenance associated with coax connectors. The disassembly of the connectors at the end of the test period revealed no evidence of corrosion inside of the coax connectors. In the case of the connectors on the A-7, corrosion inside of connectors has been such a problem that there is a requirement at every 28 days for the connectors to be opened and cleaned due to this internal corrosion problem. For the connectors involved in this evaluation, however, none were opened and cleaned or otherwise maintained during the six-month evaluation period - yet, all were clean and free of corrosion when inspected at the end of the evaluation.

CONCLUSIONS

1. The 180 day fleet evaluation was an overwhelming success. The maintenance personnel who were implementing the new procedures on the designated aircraft found them to be effective in cleaning and removing corrosion products and experienced no difficulty in applying the prescribed sealants and water displacing corrosion preventive compounds. When the antennas were removed at the completion of the evaluation all sites were free of corrosion.

2. The introduction of MIL-C-81309, Type III, Class 2, Corrosion Preventive Compound material into antenna coaxial connectors during the fleet evaluation, as well as the test conducted with the TDR (Time Domain Reflectometry) and FDR (Frequency Domain Reflectometry) equipment, demonstrated no detrimental effects to the antenna systems. Also, the use of Corrosion Preventive Compound, MIL-C-85054, as a moisture barrier on the exterior of coaxial connectors provided the fleet with a very effective corrosion preventive procedure.

3. Standardized corrosion control materials and procedures can be effectively used by fleet level activities for better corrosion protection of antennas.

REFERENCES

(1) Shaffer, I. S., Carrato, A. F., and Hoffner, J. A., "Aircraft Antenna Corrosion Proceeding of the 1978 Tri-Service Conference on Corrosion," pp 325-332.

(2) Wieczorek, R. M. and Ketcham, S. J., "Qualification Testing of Corrosion Inhibitive Sealants under MIL-S-81733B," Report no. NADC-78264-60, Naval Air Development Center, Warminster, PA Jan 1979

(3) Knight, W., "Use of Water Displacing Corrosion Preventive Compound (MIL-C-81309A) on Aircraft Electrical Connectors," Report No. MA-7109, Naval Air Development Center, Warminster, PA Feb 1971

(4) Soroka, J., "Failure Analysis Techniques for Electronic Devices and Components," Report No. NADC-78091-60, Naval Air Development Center, Warminster, PA 1980

(5) Pilla, G. J., and De Luccia, J. J., "A Corrosion Preventive Compound for Aerospace," Metal Progress, May 1980, pp 57-59.

TABLE I. ANTENNAS USED IN FLEET EVALUATION

Aircraft	Nomenclature	Performing Maintenance Activity
A-7	Lower TACAN/IFF	NAS Lemoore, CA
H-3	No. 1 UHF/COMM (Normal)	NAS North Island, CA
H-3	No. 1 UHF/COMM (Alternate)	NAS North Island, CA
P-3	Long Wire DF Sensing	NAS Moffett Field, CA
H-46	Long Wire DF Sensing	NAS North Island, CA
H-3	Receiving Transmitter (Doppler)	NAS North Island, CA

TABLE II. ANTENNA CORROSION CORRECTIVE MAINTENANCE

Aircraft	Nomenclature	Total Maintenance Actions	Total Corrosion Maintenance Actions	Percent Corrosion
A-7	Lower TACAN/IFF	281	240	85%
H-3	No. 1 UHF/Comm (normal)	155	103	66%
H-3	No. 1 UHF/Comm (alternate)	58	33	57%
P-3	Long Wire DF Sensing	186	21	11%
H-46	Long Wire DF Sensing	133	28	21%
H-3	Receiver Transmitter (Doppler)	653	139	21%

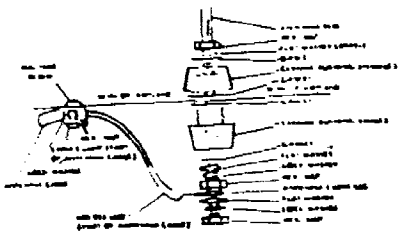

Figure 1.
Typical Whip Antenna

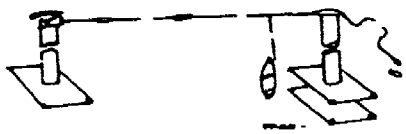

Figure 2.
Typical Long Wire Antenna

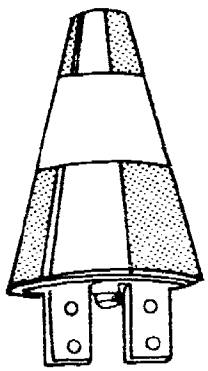

Figure 3.
Typical Rigid Antenna

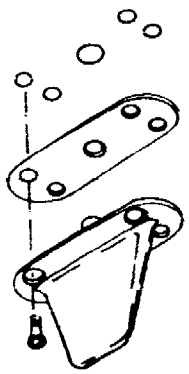

Figure 4.
Typical Rigid Antenna
(with Gasket)

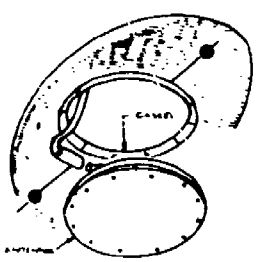

Figure 5.
Typical Flush
Mounted Antenna

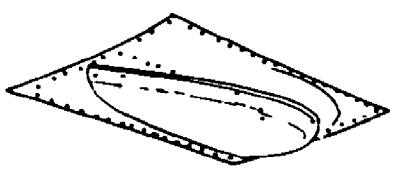

Figure 6.
Typical Dome Mounted
Antenna

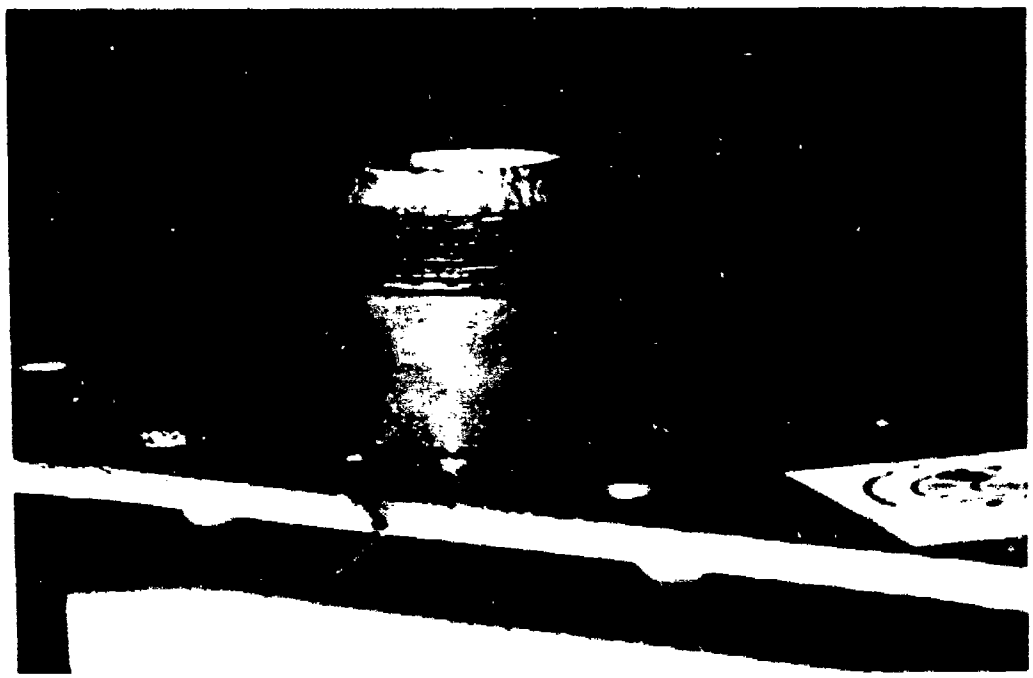

Figure 7. Corrosion on Lower TACAN/IFF Antenna Coaxial Connector

Figure 8. Sealed A-7 Lower TACAN/IFF Antenna

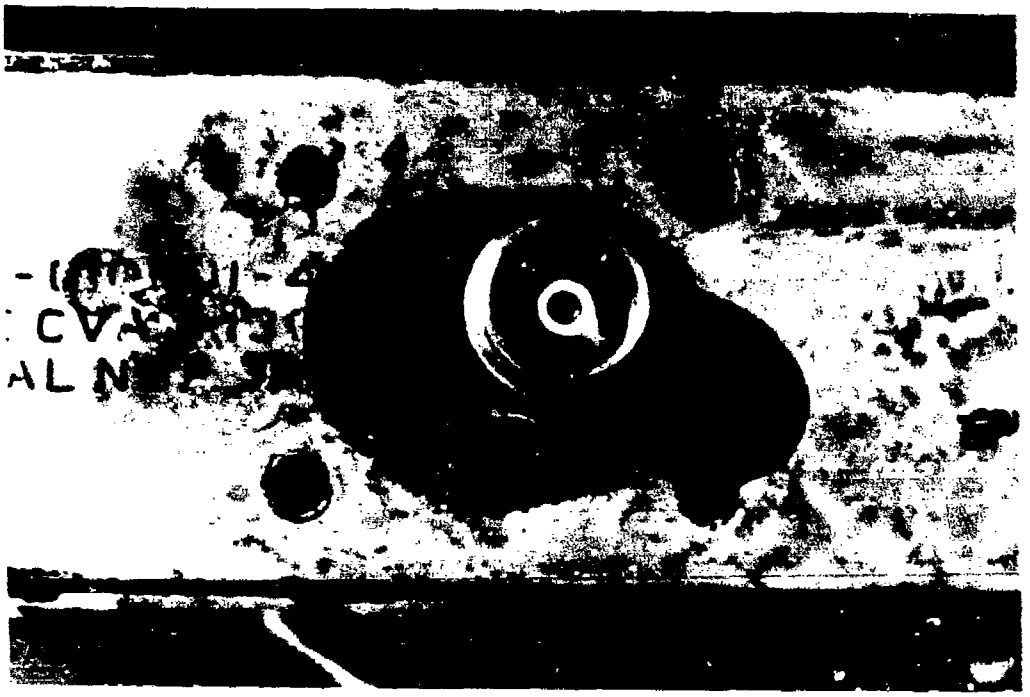

Figure 9. A-7 Lower TACAN/IFF Antenna Coaxial Connector

Figure 10. P-3 HF Long Wire Tensioner

AFWAL-TR-81-4019
Volume II

THE USAF CORROSION TESTING PROGRAM AND A CORROSION SEVERITY INDEX ALGORITHM

Dr. Fred T. Fink and Dr. Robert Summitt
Department of Metallurgy, Mechanics and Materials Science
Michigan State University
East Lansing, Michigan 48824

INTRODUCTION

Several studies have centered on the total costs of corrosion prevention and control within the past few years (1-5). Direct costs of corrosion maintenance for major aircraft systems have been estimated to be in excess of $750 million per year, and total corrosion costs, including those for facilities, are estimated to be in excess of $1 billion per year (4). A key factor in controlling costs is the ability to optimize corrosion repairs based upon need. The current program of fixed time interval depot maintenance of aircraft does not correspond to the actual corrosion damage level of individual units (6). The scheduling of depot maintenance could be based on the cumulative exposure to corrosion risk if the risk factors were quantified and relations between exposure and damage were known.

One approach to quantifying risk is to classify the environmental severity according to the nature and intensity of ambient corrosive factors. It has been acknowledged that some environments are more corrosive than others, and environments are commonly classified as industrial, urban, or marine, thus indicating their approximate severity (7,8). It is also established that certain environmental constituents, e.g., sea salt and sulfur dioxide, increase the relative aggressiveness of the environment (9, 10). An environmental classification, based on the atmospheric constituents present, might be used as a guide in establishing maintenance schedules for aircraft.

1. THE CORROSION SEVERITY CLASSIFICATION SYSTEM

1.1 Environmental Variability

The variability of environmental corrosion severity has been well established by atmospheric testing programs (8, 11-14). Relative severity is commonly indicated by designating an environment as rural, urban,

industrial, marine, or an appropriate combination of these terms. Moreover, many studies (7, 9) have shown that certain environmental factors, e.g., moisture, salt, and pollutants, are responsible for rapid corrosion observed in environments containing them. Consequently an environmental rating scale which takes into account those factors could provide a useful indication of relative severity.

It would be difficult to devise a rating system which would predict corrosion damage to every metal. Different metals display widely diverse behavior in a given environment. Some alloys are more resistant in marine locations than industrial, and the reverse is true of others. Several factors which influence corrosion are present in a unique combination for a given site, and precise information relating the corrodibility of a specific alloy to every environmental factor is not available. In the case of aircraft, the concern is with a limited number of alloys, a few each of aluminum, steel, titanium, and magnesium.* A precise rating scale is not needed for logistic decisions, but merely a relative rating. It is commonly known that aircraft corrode more severely in some environments than others. Finally, since military aircraft spend most of their lifetime on the ground at the home airbase (6), a system for classifying the severity of airbase environments is reasonable.

1.2 Atmospheric Corrosion in Aircraft

Tomashov (7) distinguishes the following types of atmospheric corrosion:

(1) "Wet atmospheric corrosion" caused by visible droplets of condensed moisture on the surface. Such moisture may result from dew, frost, rain, snow, or spray;

(2) "Moist atmospheric corrosion," which occurs at relative humidity less than 100%, and proceeds under a very thin, invisible layer of electrolyte formed on the surface by capillary action, physical, or chemical adsorption;

* The scope of this study is restricted to corrosion of structural alloys, excluding engines and avionics. Materials of these latter systems, however, probably will respond to environmental corrosive factors in a similar way (6).

Both wet and moist atmospheric corrosion occur in aircraft. Water accumulates on metal surfaces as condensation (dew, fog, from humid air on cold post-flight surfaces), rainfall on exterior surfaces and through open hatches, and various inadvertent spills.

Thus the range of corrosion problems in aircraft may be categorized as:

(1) Wet and moist corrosion of bare unprotected metal surfaces;

(2) Wet and moist corrosion of protected metal surfaces subsequent to failure of protective coatings. Protective coatings fail because of solar radiation, atmospheric contaminants (mainly ozone and other oxidants, particulates, fuel, and exhaust gases), high speed air ablation, and mechanical abrasion and flexure;

(3) Corrosion caused by contaminants of human origin including spilled beverages, human waste, hydraulic fluids, and battery acids.

The first and second categories of corrosion may be related to environmental factors which accelerate corrosion of metals or degradation of protective coatings, hence an environmental rating system would be relevant to them. The third category is a housekeeping problem. Although it should be relatively easy to control and prevent such damage, it is in fact a serious problem in USAF aircraft.

1.3 Factors Affecting the Rate of Corrosion

The rate of metallic corrosion in the atmosphere is determined by three sets of variables:

(1) Weather conditions, especially those relating to moisture;

(2) Atmosphere pollutants, both natural and anthropogenic;

(3) The nature of the metal.

The relationship of weather and pollutants to the corrosion of aircraft alloys of interest in PACER LIME will be discussed in some detail.

1.3.1 Weather

Weather parameters include temperature, precipitation, solar radiation, wind direction, wind speed, relative humidity, dew point, cloud cover, and

fog (10). All can affect the rate of corrosion, but water (and therefore those parameters related to water) will produce the largest influence. Vernon (17, 18) has shown that a given metal corrodes rapidly when the relative humidity exceeds a critical value, but corrodes slowly or not at lower humidity. The value of the critical humidity varies from one metal to another, and the presence of various pollutants can change the value as well as the corrosion rate. The critical humidity for ferrous alloys is about 70% in the absence of other factors; in the presence of sulfur dioxide, however, it is reduced to about 60%. Similarly in the presence of SO_2, the critical RH is about 70% for aluminum. Unfortunately very few data are available for other metals.

A film of moisture will deposit from humid air on metal surfaces of aircraft (19) under several conditions: if the metal is colder than the air (immediately following high altitude flights), if hygroscopic salts (corrosion products, pollutant deposits) are present, or through simple chemisorption. The film thickness, from 2 or 3 to several hundred molecular layers, will be determined by the humidity value as well as the nature of the adsorption process (7). Consequently, relative humidity alone is not sufficient to determine relative corrosivity, but it can provide a good first approximation.

Dew, fog, and rain, on the other hand, we exposed surfaces immediately. Dew condensation occurs when air cools to its dew point temperature, corresponding to 100% RH. The air itself need not cool to this point before moisture accumulates. The requirement is that the metal surface be sufficiently cooler than the surrounding air. At 80% RH, for example, the surface must be only 6°F cooler than the air (19).

There has been much discussion (10) on the effects of rainfall. Rain is thought to promote corrosion by providing moisture and washing away soluble corrosion products. It is also believed to retard corrosion by washing away pollutant deposits. Thus light rain would be harmful, but heavy rain would be beneficial.

The beneficial effects appear to be unimportant to aircraft corrosion, because, generally, paint protects aircraft surfaces exposed to the washing effects of rain, whereas corrosion occurs underneath the paint at cracks, etc., where the washing is ineffective. Interior surfaces carelessly exposed to rain, however, are wetted and not washed, and water is harmful to the less well protected surfaces. Accordingly, rain should be considered a harmful source of moisture.

Air temperature, humidity, solar radiation, cloud cover, and wind speed affect the rate of water evaporation. Temperature strongly influences the rate of corrosion reactions, thus corrosion rates would be expected to increase as the temperature rises. But oxygen, dissolved in the water electrolyte, is required for most corrosion reactions and the solubility of gases decreases with increasing temperature.

Rozedfeld (9) considers in some detail the interaction of temperature and moisture, and points out that the time of wetness will vary with temperature. Thus corrosion rates are greater in northern regions, where temperatures are low, than in warmer southern regions because moisture remains on metal surfaces longer at the cooler northern temperatures. A combination of high temperature with prolonged moisture contact, however, will result in severe corrosion. For example, corrosion of marine pilings in summer is rapid near the water surface where they are wetted by rain. It remains difficult to predict the effect of temperature on corrosion processes in the atmosphere.

1.3.2 Pollutants

Atmospheric pollutants are natural and anthropogenic airborne substances present at harmful concentrations. These substances usually are described as follows (20), including only those known to contribute to corrosion (21):

(1) "Particulates" includes both solid and liquid material in particle size from 0.1 to 100 μm. Dust, grit, fly ash, and visible smoke particulates larger than 20 μm settle to the ground somewhat quickly. Smaller particles remain suspended much longer and may be dispersed over

extremely wide areas. Thus large particulates potentially might cause corrosion problems close to the source (sea salt-spray is a special case), whereas small particulates can be important factors at great distances from their source.

Particulates vary in chemical composition. They generally are classified according to the source (22): (1) salts from sea spray and salt flats; (2) dust from agricultural lands; (3) soots from the incineration of agricultural wastes the burning of fuels; (4) agricultural and industrial dusts. Ninety per cent of airborne particulates originate from natural sources. Very few monitoring stations report the chemical compositions of particulates, but provide only total concentrations. Thus, although the corrosiveness of various particulates may vary widely, there is no way to take account of the differences, because data are not available. Geographical proximity to salt, however, is a notable exception. The corrosivity of salt is well established, but for other particulates, there exist only a few studies (22) which show corrosion to be more severe in industrialized areas with high particulate concentrations. These studies are ambiguous, however, because other corrosive factors are present.

The presence of salt greatly increases corrosion rates for nearly all metals (7, 9), hence the proximity of salt sources will be of much concern. Environments where airborne salt concentrations are high will be high risk environments. When soluble salts, e.g., sodium chloride or ammonium sulfate, are present, corrosion products usually are water soluble and readily removable. Corrosion products which form in the presence of water only, however, usually are weakly soluble, thus not readily removed, and serve a protective function to the underlying metal. In addition, many anions remove primary oxide films or displace oxygen layers which are passivating (9).

There is a synergistic effect between salt deposits and the atmospheric water content. The deliquescent salts undergo a phase transformation from dry crystal to a solution droplet when the ambient water vapor pressure exceeds that of a saturated solution of the highest hydrate (7). The relative humidities at which this transformation occurs for ammonium sulfate,

sodium chloride, and ammonium nitrate are 80, 86, 75, and 62 percent, respectively. Thus salt deposits both attract moisture to metal surfaces and provide the electrolyte solution required for corrosion.

(2) Sulfur enters the atmosphere in a variety of forms, including sulfur dioxide, SO_2, hydrogen sulfide, H_2S, and sulfate salt particulates (23). About two thirds of all atmospheric sulfur comes from natural sources, mainly as H_2S from bacterial action which later is converted to sulfur dioxide.

Sulfur dioxide initially is oxidized photochemically to sulfur trioxide, which then combines with water to form sulfuric acid. The primary oxidation process may follow several different paths and can proceed rapidly in polluted atmospheres. In air containing nitrogen dioxide and certain hydrocarbons, sulfur dioxide is oxidized in a photochemical reaction process that produces aerosols containing sulfuric acid. Also, sulfur dioxide can be oxidized in water droplets that contain ammonia, the end product being ammonium sulfate aerosol. Both sulfuric acid and sulfate salts thus formed are removed by precipitation and, to a lesser extent, by gravitational settling.

Hydrogen sulfide is emitted by some industrial operations and by catalytic converter-equipped automobiles. Hydrogen sulfide, like sulfur dioxide, is oxidized in the air and eventually converted to sulfur dioxide, sulfuric acid, and sulfate salts.

On a local or regional basis, the mechanisms by which sulfur compounds are removed from the air may produce significant effects. In the 1960's as the concentration of sulfur compounds in the air over Europe began to rise, so did the acidity of precipitation (24). Both phenomena are attributed to increased use of sulfur-containing fuels.

Many materials, in addition to metals, deteriorate in the presence of atmospheric sulfur in one form or another (23). Ferrous alloys, in particular, corrode more rapidly in the presence of SO_2, the effect apparently being synergistic with moisture.

In the U.S., ambient SO_2 levels have decreased in recent years because of reduced usage of coal and enforcement of "environmental protection" legislation (25). It appears likely, however, that energy consideration will force the U.S. to use more coal, and SO_2 concentration probably will reach levels no lower than they are today and may even increase.

(3) Hydrocarbons (26) mostly come from natural decomposition of organic matter. Anthropogenic sources are important, however, because they may be highly concentrated geographically where they are not rapidly dispersed. The most notable example is the Los Angeles basin, where the sources are automobile engines. The fate of the hydrocarbon pollutants involves the reaction with oxides of nitrogen to form photochemical smog, which include a variety of secondary pollutants such as ozone, nitrogen dioxide, and peroxyacetyl nitrates. Hydrocarbons themselves are not damaging either to metals or protective coatings, but photochemical oxidants are harmful to both (27).

(4) Nitrogen oxides (28), NO_x, arise from both natural and anthropogenic sources. The former mainly are organic decomposition, the latter the internal combustion engine. Internal combustion initially yields nitric oxide, NO, which by itself is relatively harmless. In the atmosphere, however, NO oxidizes to nitrogen dioxide, NO_2 which is harmful both directly as an irritant and indirectly in the formation of photochemical smog. The chemical reactions occuring in the presence of NO_2, hydrocarbons, and sunlight are complex but yield an atmsophere which is aggressive in the destruction of organic materials such as paint films and protective coatings.

The corrosive effects of NO_x and photochemical oxidants (27, 28) probably are indirect. These pollutants may decompose protective finishes on aircraft resulting in premature failure of the coating and exposure of underlying metal. It should be remembered that the nature of local pollutants is relevant to the type of aircraft corrosion problems to be expected. In the industrial eastern U.S., smog containing SO_2 will produce direct metal corrosion to the interior and exposed metal parts of an aircraft, whereas a Los Angeles photochemical-type smog will damage finishes and seals, followed by corrosion of underlying metal.

1.4 Establishing Environmental Quality Standards for Corrosion

Corrosion accelerates when the following environmental factors are present:

(1) Humidity, rainfall, and solar radiation;

(2) Proximity to the sea or other salt sources; and

(3) Pollutants, mainly sulfur oxides, particulates, photochemical oxidants, and nitrogen dioxide.

The prevalance of these environmental factors varies widely from one geographical location to another even within relatively small areas (29). Moreover, there is much evidence to show that environmental corrosivity becomes increasingly severe as these factors increase. Thus, it is reasonable to assume the existence of a critical value for each factor, either alone or in combinations, which could be used to establish environmental severity. The critical value may sharply divide slow and rapid corrosion, such as for iron and aluminum in the presence of SO_2 versus humidity (cf. Rozenfeld (9), pp. 106 and 109). Alternately, the variation of damage with the environmental parameter may be gradual, such as the repainting of houses vs. particulate concentration (cf. Stoker and Seager (30), p. 98). Where such critical values are known, they can be utilized directly as environmental quality standards.

Unfortunately, data are nearly nonexistent for all environmental factors except humidity. Most laboratory studies of pollutant effects on corrosion have used concentrations much higher than any found in even the most polluted environments. Much effort (22, 23, 26-28) has been devoted to establishing critical concentration levels with respect to human health, plant, and animal welfare which form the basis of ambient air quality standards. A critical concentration for materials damage, however, may be higher or lower than these.

A set of working environmental corrosion standards (WECS) might be developed by consideration of the following:

(1) The range of values for the several ambient parameters, which will establish limits of environmental exposure, if not the damage to be expected. Such data include maxima, minima, medians, and percentiles for the measured parameter. Since the acutal environments are known to vary

in corrosion severity, it follows that critical concentrations for practical use must be within the range of ambient levels, perhaps near the median values or higher.

(2) Ambient air quality standards established by the Environmental Protection Agency are concerned primarily with human health, as noted above. Nevertheless, they do summarize careful consideration of all available evidence by a host of scholars and bureaucrats. The values represent the highest levels believed safe for human health and comfort.

(3) Experimental studies which relate corrosion damage with pollutant concentrations and weather variables may provide information for establishing WECS.

1.4.1 Ranges of Ambient Parameters

Within the United States, a number of air quality parameters are measured by several agencies. Weather data are collected by the National Weather Service, the USAF Environmental Technical Applications Center (ETAC), and others. Weather data most commonly are measured at aerodromes because weather is a critical factor in aircraft operational safety. Air quality data - measurements of a limited number of pollutants - are collected by federal, state, municipal, and private air monitoring stations, the results are compiled by state agencies and, nationally, by the U.S. Environmental Protection Agency. Many monitoring stations - especially private ones - were established to track specific pollution sources, e.g., certain manufacturing operations, thus their data may reflect highly localized conditions. Despite these limitations, the national data as compiled by EPA are the only data available to assess the range of exposure.

Graedel and Schwartz (31) analyzed ambient atmospheric conditions and quality based on National Weather Service and EPA data. Weather data spanned 30 years from more than 200 measuring sites, and air quality data, mostly from CY 1973, represented as few as 82 to as many as 3760 measuring sites for several pollutants. Graedel and Schwartz's objective was to determine the range of environmental parameters to which materials are exposed in the U.S. and thus establish "bench marks" for laboratory or field testing. Weather data analyzed by the authors were mean annual temperature and mean

annual absolute humidity. Pollutant data were the annual median of hourly averaged continuous data for each measuring site.

We note three results of Graedel and Schwartz for each atmospheric parameter: The median of the 50th percentiles, the median of the 99th percentiles, and the maximum value reported (Table 1). The 50th percentile median represents "average of averages" values reported, whereas the 99th percentile median is the level exceeded at only 1% of all air quality sites. Graedel and Schwartz define the 99th percentile median as Atmospheric Upper Limit Values, AULV, or "mean high water marks" which may be used for design purposes with the expectation that 99% of the applications will encounter levels below the AULV. The maximum value was the highest mean reported.

The distribution of means as shown by Graedel and Schwartz is more-or-less Poisson-like for all factors except ozone and SO_2. For ozone, a large number of sites reported values below 20 $\mu g/m^3$ and a substantial number were grouped between 30 and 60 $\mu g/m^3$. Nevertheless, the median, 36 $\mu g/m^3$, probably is a valid demarcation between high and low concentrations. Sulfur dioxide data from 447 monitoring sites were highly skewed toward low values. Indeed, the maximum number of sites reported values at the median and mean value of 43 $\mu g/m^3$, and only 17% of monitoring stations reported means greater than 53 $\mu g/m^3$. Because of this, the significance of the median value of SO_2 is placed in a different light than for the other parameters. This is especially unfortunate because of the peculiar role of SO_2 in corrosion.

Critical levels of atmospheric factors probably lie between the median values and the worst-case maxima or even the AULV's. Clearly the AULV's represent the most hostile environments for individual atmospheric factors in the CONUS, and this worst 10% level would be inappropriate to use in a practical environmental rating scale. It may be noted that the list of monitoring stations (their Table 2) which exceed the AULV's includes San Bernadino, CA only once (for nitrate ion particulates), whereas Travis, CA and Charleston, SC are not mentioned. All three of these have been shown

to be severe environments, the first for paint degradation and the latter two for metallic corrosion (6, 32).*

1.4.2 Proximity to the Sea and Other Sources of Salt

Several studies (8, 11, 13, 33, 34) have shown that accelerated atmospheric corrosion near the seashore is correlated with airborne sea salt. Establishing a critical distance from the shore, however, is difficult because there is little quantitative information relating corrosion to atmospheric salt concentrations, or even relating salt concentrations to distance from the shore.

The study of atmospheric aerosols (36) has centered mostly on the distribution of particle sizes, rather than the mass of aerosol per unit volume, i.e., micrograms per cubic meter of particulate, as measured at air monitoring stations. The upper limit of aerosol particle size is determined by sedimentation processes. Particles larger than 20 μm radius remain airborne for a short time and are found only in the vicinity of their source. Hence, an atmospheric aerosol by definition consists of particles between 0.1 μm and 20 μm radius. Aerosol particles commonly are classified as "Aitken" particles, $\leq$ 0.1 μm radius, "large" particles, 0.1 - 1.0 μm radius, and "giant" particles 1 μm radius in size. Larger particles settle from the air rapidly whereas smaller particles persist in the atmosphere for long times and travel large distances, and serve as condensation points for rainwater precipitation. Thus measurements of sodium chloride particulates vs. distance from the sea may suggest values for the critical distance.

1.4.2.1 Salt in Rainwater

The concentration of sodium chloride in rainwater is high near and over the ocean, but diminishes inland (35). Concentrations over the sea are 8.0 μg/l, and over land in the central U.S. are 0.1 μg/l (35). The concentration decreases logarithmically with distance from the sea up to 500 km in the U.S., and is constant at greater distances.

*The corrosive severity of Travis and Charleston has been attributed primarily to their proximity to salt water, which in turn should indicate high concentration of seal salt. Graedel and Schwartz's list does include several sites near the ocean which exceed their particulate AULV.

It is unlikely, however, that chloride in rainwater is relevant to aircraft corrosion. The exterior surfaces of aircraft exposed to rain are protected by paint, whereas, most interior surfaces are not exposed to rain. Moreover, the decrease of chloride in rainwater occurs over large distances, whereas the decrease in corrosion damage is quite abrupt (9, 11). Corrosion rates 10 km from the shore are approximately the same as corrosion rates far inland. Consequently, the critical proximity should not be determined from rainwater chloride concentrations.

1.4.2.2 Particulate Sodium Chloride

Duce et al. (32) have measured the concentration of sodium chloride and other ions in the air at various elevations and distances from the sea-shore on Hawaii Island, HI. All measuring sites were downwind of off-shore trade winds. Their results show chloride concentrations at all sites varying widely with ambient weather conditions. Their primary interest was the variation of chloride and other ionic components vs. elevation above sea level, rather than distance from shore. Nevertheless, the results show a consistent, monotonic decrease in chloride concentration with increasing distance from the shore.

Also included are two additional reported values for giant particle chloride concentrations, one over the ocean and one near the shore in Massachusetts. The over-ocean values should be compared with Junge's summary (36) (p. 162) of salt concentration vs. wind velocity measurements, which illustrate the wide variability of such data.

Hudson and Stanner (34) found in Nigeria that sodium chloride concentration in the air varies within wide limits and depends strongly on the distance from the shore. The sodium chloride content in the air is about .22 milligrams per cubic meter. The amount of salt that settles out on the surface under these conditions reaches values from 10 to 1000 milligrams per square meter per year. Corrosion tests were conducted at various distances from the shore with simultaneous determination of airborne salt concentration. The relationship between salt deposits and distance from the sea as well as corrosion rates vs. distance from the sea are calculated.

Available evidence shows that giant particle chloride concentrations in the atmosphere are reduced by about 1 order of magnitude at a distance of 3/4 km from breaking surf. At distances of about 15 km the concentration reaches a value which remains nearly constant further inland.

Junge (39) (p. 176) has drawn together the available data on giant salt particulates vs. distance from sea. Values of 5 $\mu g/m^3$ at distant point inland.

The available data on atmospheric corrosion near marine environments suggests that the decrease in corrosion rate parallels this decrease in giant salt particulates, and "marine atmospheres are aggressive in direct proportion to concentration of (airborne) NaCl particles" (Rozenfeld (9)).

Most studies suggest a critical distance of less than 1.5 km for sites where strong off-shore winds are not prevalent. Allowing for the variability of weather, however, it seem prudent to extend this to 4.5 km.

1.4.3 U.S. National Ambient Air Quality Standards (NAAQS)

The Federal Clean Act (Public Law 91-640) directed the Environmental Protection Agency (EPA)

" to publish proposed national primary and secondary ambient air quality standards based upon air quality criteria, (also issued by EPA). Primary ambient air quality standards define levels of air quality which (the EPA judges) necessary, based on air quality criteria and allowing an adequate margin of safety, to protect the public health. Secondary ambient air quality standards define levels of air quality which (EPA) judges necessary, based on the air quality criteria to protect the public welfare from any known or anticipated adverse effects of an air pollutant." (40)

Air quality criteria published by EPA summarize the scientific knowledge relating pollutant concentrations and their adverse effects. They were issued to assist the development of air quality standards. In developing criteria many factors were considered, including the chemical and physical characteristics of the pollutants, the techniques available for measuring them, exposure time, relative humidity, and other conditions of the environment. The criteria attempted to consider the contribution of all

variables to the effect of air pollution on human health, agriculture, materials, visibility, and climate. Air Quality Standards on the other hand legislate pollutant concentrations that the government determines should not be exceeded in a specific geographic area. Primary standards were intended to protect public health, whereas secondary standards were intended to protect public welfare. In the case of some pollutants, the primary and secondary standards are the same, whereas for others, notable sulfur oxides and particulates, the secondary standards are lower. These standards are listed in Table 2.

It is difficult to determine how EPA based the NAAQS on the respective Air Quality Criteria (22, 23, 26-28). Comments submitted to EPA, subsequent to the first publication of standards, "reflected divergences of opinion among interested and informed persons as to the proper interpretation of available data on the public health and welfare effects of the six pollutamts . . ." (41), suggesting that others could not follow the logic used in developing standards.

"Current scientific knowledge of the health and welfare hazards of these air pollutants is imperfect." (41) Indeed! The Clean Air Act, however, required the promulgation of standards by a specific data. Using the available scientific evidence, any standard value could be established within a wide range.

In responding to comments on the initial standards, EPA did state the basis for setting several of the standards. The standard for carbon monoxide

"was based on evidence that low levels of carboxyhemoglobin in human blood may be associated with impairment of ability to discriminate time intervals . . . In the comments, serious questions were raised about the soundness of this evidence (and) extensive consideration was given to this matter. The conclusions reached were that the evidence regarding impaired time-interval discrimination have not been refuted and that a less restrictive national standard for carbon monoxide would therefore not provide the margin of safety which may be needed to protect the health of persons especially sensitive to the effects of elevated carboxyhemoglobin levels.

The only change made in the national standards for carbon monoxide was a modification of the 1-hour value. The revised standard affords protection from the same low levels of blood carboxyhemoglobin as a result of short-term exposure. The national standards for carbon monoxide, as set forth below, are intended to protect against the occurrence of carboxyhemoglobin levels above 2%.

"National standards for photochemical oxidants have also been revised. The revised national primary standard of 160 micrograms per cubic meter is based on evidence of increased frequency of asthma attacks in some asthmatic subjects on days when estimated hourly average concentration of photochemical oxidant reached 200 micrograms per cubic meter. A number of comments raised serious questions about the validity of data used to suggest impairment of athletic performance at lower oxidant concentrations. The revised primary standard includes a margin of safety which is substantially below the most likely threshold level suggested by this data.

"National standards for hydrocarbons have been revised to make these standards consistent with the above modifications of the national standard for photochemical oxidants. Hydrocarbons are a precursor of photochemical oxidants. The sole purpose of providing a hydrocarbon standard is to control photochemical oxidants. Accordingly the above described revision of the national standards for photochemical oxidants necessitated a corresponding revision of the hydrocarbon standards.

"National standards for nitrogen dioxide have been revised to eliminate the proposed 24-hour average value. No adverse effects of public welfare have been associated with short term exposure to nitrogen dioxide at levels which have been observed to occur in the ambient air. Attainment of the annual average will, in the judgement of the EPA, provide an adequate safety margin for the protection of public health and will protect against known and anticipated adverse effects on public welfare."

We conclude that the NAAQS are of little relevance to corrosion in aircraft.

1.4.4 Experimental Studies Relating Corrosion to Environment

Several studies have attempted to develop quantitative relations between corrosion and environmental parameters. These will be discussed as possible indications of critical values.

Upham (42) conducted atmospheric exposure studies at established air monitoring sites in St. Louis and Chicago. His results showed approximately linear relationships between corrosion rates and SO_2, TSP, and surface sulfation rates for low-carbon, low-copper mild steel panels. Mansfield (43, 44) has extended this work to a wider variety of materials at St. Louis sites, but analysis of the results is not complete.

Guttman (21) conducted a long term exposure program using zinc at a single site and compared the results with environmental conditions. He showed that the most important factors are time of wetness and atmospheric concentration of SO_2, and, further, that the time of wetness is a consequence of ambient relative humidity. He found temperature not to be important. Using a curve-fitting technique, Guttman obtained an empirical equation

$$y = 0.00546A^{0.815} \quad (B + 0.0289),$$

where

y = corrosion loss, mg/3x5-in panel,
A = time of wetness, hr., and
B = SO_2 concentration during the time panels were wet, ppm.

This equation suggests a linear dependence of corrosion damage on SO_2 concentration, which would imply that there is no critical concentration. Guttman did not relate time of wetness to weather parameters, thus it doesn't help this study.

Haynie and Upham (45), in an extension of Guttman's work with zinc, assumed a linear dependence of corrosion on mean relative humidity and mean SO_2 concentration. Zinc specimens were exposed at a number of U.S. Public Health Service Continuous Air Monitoring Program (CAMP) sites. Corrosion damage to the samples was compared with CAMP pollutant data

and weather data from the nearest weather station. Statistical analysis yielded

$$y = 0.00104\ (RH - 49.2)\ SO_2 - 0.00664\ (RH - 76.5)$$

where

y = zinc corrosion rate, μm/yr.,
RH = mean relative humidity, %, and
SO_2 = mean SO_2 concentration, $\mu g/m^3$.

This equation suggests that zinc will not be wet below RH of 76.5% in the absence of SO_2 and, furthermore, increasing humidity above that point inhibits corrosion. Haynie and Upham view this as consistent with the formation of a protective carbonate film. In the presence of SO_2, however, their equation indicates a linear dependence on the product of RH with SO_2 and a linear dependence on SO_2. Again, critical values of each parameter are not indicated.

Equations such as these can be used to predict the useful life of galvanized iron products which are scrapped when the zinc coating is perforated. Haynie and Upham have made such predictions for various environments and their results compare well with experience.

Haynie and Upham (46) conducted a more extensive study of the corrosion of enameling steel and atmospheric factors. Specimens were exposed at 56 sites on the National Air Specimens Network (NASN) coordinated by the EPA. Weight loss data were obtained at one year and two years and were correlated with mean weather data (RH and temperature) and pollutant concentrations (SO_2, TSP, sulfate ion $SO_4^=$, and nitrate ion NO_3^-). Correlation analysis identified the variable set which was used in multiple regression analysis. Haynie and Upham found that corrosion of steel is a function primarily of $SO_4^=$, NO_3^-, RH, and time. Temperature, TSP, and SO_2 appeared to be insignificant. Because of an observed covariance between $SO_4^=$, and SO_2^-, together with many other studies which had shown a relation between corrosion and SO_2, Haynie and Upham suggested that $SO_4^=$ may be merely a "proxy" variable for SO_2. When $SO_4^=$ data were excluded from their analysis, the empirical fit was nearly as good with SO_2 as with $SO_4^=$.

The relation between corrosion for this steel and the environmental factors considered was best expressed as

$$\text{corr.} = 183.5 \sqrt{t} \exp (0.0642\ \text{Sul} - 163.2/\text{RH}),$$

where

t = time, yr.,

Sul = mean concentration $SO_4^=$ or SO_2, $\mu g/m^3$, and

RH = relative humidity, percent.

By transposing the time factor to the left hand side, Haynie and Upham show the dependence of "pseudocorrosion rate," corr./$\sqrt{t}$, on SO_2 concentration and relative humidity.

Environments where RH and SO_2 are high should be more corrosive and maintenance to equipment will be required more frequently. The frequency of a given maintenance operation would be inversely proportional to the time required for corrosion to reach a specified depth. Thus a crude estimate of the ratio of maintenance frequency in a SO_2 polluted environment to that in a cleaner environment is given by Haynie and Upham as

$$\text{MFR} = \exp (.006\ SO_2),$$

or

$$\text{MFR} = \exp. [.006\ (SO_{2a} - SO_{2b})],$$

where MFR - maintenance frequency ratio, and a, b refer to two different environments.

Haynie, Spence, and Upham (47) have studied the corrosion of weathering steel and galvanized steel in a laboratory chamber with various combinations of humidity, radiation, and pollutants. Experiments were conducted in atmospheres containing SO_2, NO_2, O_3, and water vapor, each at two different concentrations as listed in Table 3, and the results were compared with corrosion rates in clean humid air. This two-level factorial arrangement was selected to identify environmental factors statistically. It may be noted from Table 3 that the three "low" pollutant concentrations are essentially equal to the primary NAAQS values, and considerably higher than the 50th percentiles of Graedel and Schwartz (31). Absolute humidities are

very high compared with the ambient 50th percentiles. The "high" values of the several factors are many times greater than the extreme values of the U.S.

Analyzing the results, Haynie et. al. conclude that only SO_2, humidity, and their interaction are significant factors in the corrosion of weathering steel. For galvanized steel, only the direct effects of the two were of importance. Thus, they view NO_2 and O_3 as having little or no effect on the corrosion of these alloys.

Their corrosion rate results, reproduced in part in Table 4 however, suggest otherwise. (We must admit we do not have access to their complete analysis). Corrosion rates, the largest increase being for SO_2. From these data, it appears that NO_2 and O_3 do accelerate corrosion rates, although not as much as SO_2.

1.4.4 Working Environmental Corrosion Standards (WECS)

After considering the existing literature on materials degradation and environmental factors, we conclude that there are no firm guidelines for setting WECS, with the exception of humidity. Metallic corrosion is definitely accelerated in the presence of SO_2 and high humidity, and probably accelerated by NO_2, oxidants, and many particulates. Organic protective finishes are deteriorated by solar radiation, oxidants, some particulates, and possibly by NO_x and SO_2. Published research does not tell us, however, at what level these factors become significantly damaging.

Accordingly, we adopt the view that critical values lie within the range of ambient values, because accelerated corrosion has been observed in existing environments. We adopt two sets of WECS based on the analysis of Graedel and Schwartz (31). The first set are their 50th percentile values plus 20 percent of the difference between the 99th and 50th percentiles. These are listed in Table 5. The values for proximity to salt or sea are based on the analysis presented earlier. The solar radiation values are based on the mean (July) values for the continental U.S.

These WECS have been used in the Corrosion Severity Index Algorithms (described in a subsequent section) and the results compared with experimental environmental ratings. The agreement is sufficiently good that the values of Table 5 together with the Algorithms may be used to compute accurate relative environmental severity for corrosion in aircraft.

1.5 Environmental Severity Algorithms for Aircraft Corrosion

We propose a set of algorithms, based on locally-measured environmental factors which rely in part on maintenance experience as contained in AFM 66-1 records. A feature of this approach is that the authority to set maintenance intervals is left in the hands of local management. These decisions would be based on locally measured meteorlogical and pollutant conditions and would be subject to change dictated by local experience.

1.5.1 Corrosion Maintenance in Aircraft

Excluding housekeeping, corrosion maintenance involves

(1) washing of exterior surfaces,

(2) repair of replacement of protective coatings and sealants, and

(3) treatment and repair of corroded components.

Environment elements which corrode metal are not necessarily the same as those which deteriorate paint and sealants.

Consequently, no single algorithm can classify an environment with respect to all three corrosion problems. Instead three decision algorithms are required to determine intervals for:

- aircraft washing
- complete repainting, and
- corrosion inspection/maintenance.

Each algorithm would assess the level of local contaminants and, via a decision-map process, lead to recommended intervals for each maintenance cycle.

1.5.1.1 Aircraft Washing

Aircraft are washed both to maintain appearance and to remove soil deposits which may damage the paint. There are several sources of soil: engine exhausts, fuels, and lubricants; airborne particulates; and the workers' shoesoles during maintenance and servicing operations. Soil deposits will attract and retain moisture from humid air and gaseous pollutants, particularly SO_2. Thus, the damaging effects of soil are compounded by high humidity and pollutant concentrations. It is not likely that surface soils accelerate paint degredation by sunlight or gaseous oxidants, but there is no evidence to support this view. Thus, aircraft washing intervals selected to protect the paint and exposed metal should be related to particulates (and proximity to the sea), SO_2, (possibly) NO_2, and humidity. USAF recommended washing intervals, for several years, have been 45, 60, and 90 days, depending on local conditions. Practical washing intervals, which are consistent both with environmental risk factors and rigorous climates, are 30, 60, and 120 days. We designate these as A, B, and C, respectively.

The Washing Algorithm (Figure 3) first determines if the distance to the sea is less than the WECS distance. If it is, washing interval A is recommended; if not, particulate concentrations are compared with WECS. If the ambient level exceeds the standard, then the ambient SO_2 concentration is checked. If SO_2 is higher than WECS, interval A is recommended; if lower, interval B.

If particulates are below the standard, SO_2 concentration again is queried: If high, interval B is recommended; if low, moisture factors are considered. High moisture values -- either RH or rainfall greater than WECS -- lead to interval B recommendation; low values yield interval C.

1.5.1.2 Painting

Aircraft are painted primarily to protect metal surfaces. Protective finish maintenance is effected at three levels: (a) minor touchup; (b) major touchup; and (c) complete strip-repaint. Minor and major touchup are effected at field or intermediate level maintenance, whereas complete repaint is authorized only at depot-level for large aircraft (52). The

need for touchup painting must be determined at field-level inspection: an environment-based algorithm should not be used. The following paint-interval algorithm refers to complete strip/repaint maintenance.

As before, three intervals, A, B, and C, are recommended. Paint systems currently in use -- epoxy or polysulfide primers and polyurethane finish coat -- should provide a service life of 10+ years in the mildest environments (53). Consequently, the A, B, and C intervals may be equated to 36, 72, and 120 months, respectively. These intervals may not correspond to the PDM intervals for a particular aircraft system. For example, C-141A aircraft currently are on a 42 month cycle, and B-52's are on 48 months. If 120 months is the maximum expected service life for the paint finish, and the PDM interval is y months, then y should be compared with the intervals recommended by the Repaint Algorithm, i.e., 36, 72, or 120 months. The interval closest to the PDM interval should be selected.

Environmental factors which deteriorate paint are, in order of severity, solar radiation, oxidants, and sulfur dioxide absorbed on soil deposits. Soil deposits themselves might be included, but there is insufficient information to relate repaint schedules to the nature of the soils. Thus, only sunlight, oxidants, and SO_2 are considered. The repaint algorithms (Figure 2) compares the solar radiation level, ozone and sulfur dioxide concentrations with the WECS values. High values for all three result in the A interval recommendation, whereas low values for all three lead to the C interval. Various combinations of high values lead to the B interval.

1.5.1.4 Corrosion Damage

The Corrosion Damage algorithm (CDA) is of a different nature than those for washing and repainting, which recommend maintenance intervals appropriate to the environment. Corrosion repairs routinely are effected simultaneously with phased and isochronal maintenance efforts, and it would be both undesirable and difficult to impact their scheduling.

Accordingly, the CDA is intended as a guide for anticipating the extent of corrosion damage and for planning the personnel complement and time required to effect their repairs.

The Algorithm (Figure 1) considers first distance to salt water (or salt flats), leading either to the very severe (AA) rating or a consideration of moisture factors. After moisture factors, pollutant concentrations are compared with WECS either for SO_2, TSP, or O_3. High values for any one of the three pollutants together with a high moisture factor leads to the (AA) rating, but if all are low, together with a high moisture factor, the severe (A) rating results. Low moisture factors with a high pollutant value result in the moderate (B) rating, whereas if all are low, rating (C) results.

1.5.1.5 Use of Environment Algorithms

The above algorithms are readily compared with the appropriate local environmental parameters to yield corrosion maintenance ratings; the use of a computer obviously is not necessary. The algorithms could be used in a modified for within the base-level computer system and , with appropriate automatic data input, can provide monthly revisions for maintenance needs recommendations.

1.5.1.6 Environmental Applications

Environmental Severity Algorithms have been used to establish preliminary ratings for most airbases of interest to USAF. These ratings are listed in Appendix 3*. These ratings are based essentially on comparisons of the Working Environmental Corrosion Standards with local geographical and environmental data. Modifications to the algorithms were necessary in order to use the available data format, but the results are not significantly affected. No responsibility is assumed for the accuracy of the data, particularly with respect to its relevance to a specific airbase, since the monitoring site may have been located at some distance from the airbase in question. If more accurate and reliable data should become available, they may be used to compute more appropriate ratings.

*Available from the authors.

1.5.1.7 Environmental Data

The following environmental data were collected for USAF, AFRES, and ANG airbases, from the sources indicated.

(1) Mean annual relative humidity, mean annual temperature, mean annual rainfall. Source: USAF Environmental Technical Applications Center, "Worldwide Airfield Climatic Data," Vols. I-VIII, 1970. (54)

(2) Mean solar radiation for July. Source: Baldwin, J. L., "Climates of the United States," U.S. Department of Commerce, Washington D. C., 1973. (55)

(3) Ambient concentrations of SO_2 particulates, NO_2, and O_3. Source: U.S. Environmental Protection Agency, "Air Quality Data -- 1976 Annual Statistics," March 1978, EPA-450/2-78-009. (56)

(4) Distance to salt water or other salt source and prevalent wind direction with respect to the nearest urban/industrial area. Source: U.S. Department of Commerce, "Sectional Aeronautical Charts," Washington, D. C., 1979. (57)

Additional discussion of some of these points is required. Data were collected only for continental US airbases because pollutant data were available only for them. The algorithms could be used in abbreviated form with only weather and geographical data. In some case this would lead to useful results. For example, Anderson AFB, Guam would receive A, (probably) B, and AA ratings for washing, repaint, and corrosion severity, respectively, based only on these parameters. Ratings for less unique environments, however, would be ambiguous, and we chose not to compute them.

Weather data reported by ETAC are variable-year averages of hourly measurements and were obtained by weather stations located at the specific airbase in question. These stations did not report solar radiation measurements, hence the source listed in item (3) was used. These latter data are mean values for wide geographical regions and were computed from US Weather Bureau measurements. Values for July are used because these are near the maximum for the northern hemisphere. July values would be inappropriate elsewhere. Mean annual RH and temperature were used to compute mean annual absolute humidity.

Sulfur dioxide and particulate concentrations were available in the cited EPA documents as mean annual values and thus are directly compared with WECS. In the case of the NO_2 and O_3, however, available data frequently provided only first and second hourly maxima, which cannot be compared with the WECS annual mean values. Accordingly, we have substituted for these pollutants a secondary WECS equal to the 50th percentile of Graedel and Schwartz (29) plus 0.8 of the difference between their 99th and 50th percentiles. The modified algorithm compares this secondary WECS with the reported hourly maximum.

Unlike the ETAC data, EPA's pollutant data were not measured at the airbase in question. We have selected data from the nearest EPA monitoring station and upwind of the airbase wherever possible. In the data listings (Appendix 3#), latitude and longitude of both the relevant monitoring station and the airbase are included, together with the wind direction from the airbase.

2. PACER LIME -- Atmospheric Corrosion Testing

2.1 OBJECTIVE

The experimental phase of PACER LIME was intended to provide a calibration for the corrosion severity index (CSI) algorithm. Corrosion of selected alloys would be used to compare environmental corrosivity at several airbases selected to span the range of actual environments. Comparative evaluation of the alloys tested was not a consideration.

2.2 THE TESTING PROGRAM

2.2.1 TESTING SITES

Warner-Robins AMA, in 1971, selected eleven test sites, seven CONUS, two USAFE and two PACAF airbases. Close consideration, however, reduced the number of overseas test sites to two. Test sites were selected on the basis of the Interim CSI algorithm, represented a wide range of environmental severities, but most "moderate," two were "severe" and one "very mild." Unfortunately, no useful data were obtained from the "severe" locations. Mild sites included Davis-Monthan AZ, and F. E. Warren WY. Moderate locations chosen were Andrews DC, Barksdale LA, Hickman HI,

Available from the authors.

Norton CA, Robins GA, Tinker OK, and Wright-Patterson OH. Severe sites were MacDill FL. and RAF Lakenheath England.

Exposure sites were a few hundred yards distance from operational areas unusual environmental factors were rare, e.g., a wash rack at 200 yards (Barksdale), fuel depot at 100 yards (Norton), and fuel depot and sewage treatment plant at 300 yards (Robins). Stand location details are not available for Andrews, Hickman, MacDill, and F. E. Warren.

2.2.2 TEST METHODS AND MATERIALS

Test stands (ASTM G 50-76. (1)) Fastened test panels by means of poreclain insulators at 30° to the horizontal and facing prevailing winds. Stand installation was accomplished at eight sites in March 1972, two more in September 1973, and the last one in late summer 1975.

Six alloys* were tested in three different configurations. Three aluminum alloys 2024 T3 (clad) 7075 T6 and 7079 T6 (clad), steel 4340, magnesium AZ31B and titanium Ti 6AL 4V. An assembly made from one panel of each aluminum alloy was also exposed. The assemblies were riveted with four cadmium plated rivets. Panel sizes were 12.7 x 14.3 cm for all materials. In addition 12.7 x 29.8 cm panels were provided for 2024 T3, 7075 T6 and magnesium. Thus, corrosion should represent the behavior of aircraft.

Initial setup and specimen handling followed ASTM G 1-72 and G 50-76 (1).

At six month intervals, panels were removed, scrubbed with a rubber stopper under flowing water, acetone-rinsed, dried and weighed.

2.3 PROBLEMS

The setup procedure was too flexible, but since test stands were set up by personnel from Warner-Robins, this does not seem to have been a difficulty. There is evidence (e.g., weights recorded to the nearest 0.0001) that care was taken at every step of the program.

*From hindsight, it is unfortunate that a low carbon steep and perhaps zinc were not included, since these metals are so common in published corrosion tests.

The decision to remove, clean, and weigh every panel at six month intervals was unfortunate. The task of multiple weighings results in a greater chance of error on the part of the laboratory personnel.

The cleaning procedure was selected to avoid the hazards of chemical cleaning methods. Chemical methods remove corrosion products more effectively than the stopper-rubbing technique, hence yield more accurate weight loss measurements. Since many actual weight changes were quite small, the resultant errors are probably significant.

In addition to these problems, the program was plagued with numerous difficulties from the onset. At most locations the required equipment (balance) or personnel were lacking, hence panel weighings could not be done locally. Only Robins, Tinker, Wright-Patterson, and Lakenheath possessed the needed capability. Specimens from other sites were removed, packaged, and shipped to Robins or to Tinker for measurements.

In 1974 all data from MacDill were lost* because of personnel changes. A new set of panels was installed, but the test stand soon was destroyed by weather* and testing was discontinued. The late-installed stand at Lakenheath was destroyed by weather and testing was discontinued after only six months. This was especially unfortunate because both Lakenheath and MacDill were believed to be severe environments.

Steel panels were found to corrode so rapidly that the surface-marked identifications were obliterated; a new marking method was developed. Finally, when an attempt was made in 1975 to analyze the data it was discovered that no initial weights had been recorded for most panel sets.

3. RESULTS

3.1 DATA REDUCTION

Data were tabulated, keypunched and entered into a CDC 6500 Computer. Mass change per unit area vs. time was computed. Anomalous values were noted and checks were made to determine whether they resulted from tabulation or keypunch errors, and corrections made. In addition a subroutine calculated

*Not uncommon occurrences even in programs operated by the most experienced workers, cf. References 3, 4. 5.

mean mass change and rejected data more than three standard deviations from the mean.

A curve-fitting algorithm plotted mass change for all panels for each alloy and each base, and corrosion rates were computed.

4. DISCUSSION

Compared with the amount of data this study might have yielded, useful information actually obtained is meager. Panels tested number 1089. As noted, experimental values for each panel type were averaged for each test site, thus reducing potential corrosion rate values to 110. Only 33 apparently valid corrosion rates, in fact, could be computed. We also have pointed out the difficulty of taking such data seriously when they are surrounded by obviously-invalid data measured simultaneously by the same personnel. But for evaluative purposes, the results must be accepted at face value and compared with measurements by other workers and with the environmental ratings of the corrosion severity algorithms.

4.1 OTHER RESULTS

Carter (6) reported weight loss measurements on aluminum alloys exposed to industrial, rural, and marine environments. The alloys studies were identical to none in this study, but one contained copper and had a nominal composition similar to that of 2024. His corrosion rates were 70×10^{-6} and 5×10^{-6} kg/m^2-dat for severe industrial and rural environments, respectively. Marine and rural environments produce quite similar results and were relatively non-corrosive. Environmental pollutants -- mainly SO_2 -- increased pitting attack, rather than general corrosion.

Pearlstein and Teitell (7) reported four year weight loss data for 2024 T3 and AZ31B exposed at three different sites in the Panama Canal Zone. Highest corrosion rates for both alloys were observed at the marine site and lowest in a rain forest. Weight losses in 2024 T3 were negligible in the latter environment. Pearlstein and Teitell comment, however, that weight loss measurement may not be meaningful because 2024 exhibited extensive blistering and exfoliation corrosion without substantial weight loss. Their results for both alloys are about an order of magnitude larger than our highest corrosion rates.

McGeary et al. (3) report seven year weight loss data for several aluminum alloys exposed at four sites (Kure Beach NC, Point Reyes CA and State College PA). Lowest corrosion rates were observed at the rural site for all alloys, and except for 7075 T6, highest rates were found at the moderately severe industrial environment. For 7075 T6, the highest rate occurred at the 80-foot Kure Beach NC site. Corrosion rates at marine and industrial sites are quite similar, however, and reported difference may not be significant, in contrast with Carteris (6) findings for a copper-containing aluminum alloy.

Additional data for aluminum alloys are shown in Tables 7-9. Industrial environments were the most severe, whereas marine environments were somewhat milder. Ailor's seven year values (8) are in good agreement with those of McGeary et al. (3). Ailor notes that intergranular and exfoliation corrosion were more dominant in marine environments, whereas weight loss and pitting corrosion were prevalent at industrial sites.

4.2 CORROSION RATES COMPARED WITH ENVIRONMENT

Sufficient PACER LIME data are available for environmental comparisons for AZ31B, 2024 and 7075 alloys only. In the case of 4043 and the aluminum assembly, there are but four data values each. For 7079 there also are only four values, but there are literature corrosion rates which warrant environmental comparison.

For each site, the CDA yields a two-letter scale, viz., BB, AB, etc. The first rating is derived from less-tolerant threshold values for environmental parameters, and the second from a more-tolerant set. Thus a second-letter "A" indicates a more severe environment than does a first letter "A." Ratings range from mildest "C" through "B" and "A" to the most severe "AA." For data plotting, these letters are assigned a numerical scale 1 to 4 for C to AA, and the two-letter values are summed. Thus, an "AB" environment yields the sum of 5, and "AA, AA" yields 8.

Data for the magnesium alloy, Figure 1, shows a remarkable good correlation with the CDA rating, with one or two discrepancies. ASTM data for State College PA and Newark NJ are high for their environmental ratings. The PACER LIME data, however, are consistent.

In the case of 2024 T3 Alcald, Table 8 nearly all the results are consistent, with the exception of the ASTM McCook IL and Richmond VA values. The data for 7075 T6, Table 7 are similar to those of 2024 T3. The four PACER LIME 7079 T6 data points are plotted with ASTM results, and are consistent with the CDA ratings.

5. CONCLUSION

The experimental phase of PACER LIME was designed to calibrate the Corrosion Factor Equation by measuring weight losses of panels exposed at several airbases. The results are less useful than expected:

(1) Although alloys tested were typical aircraft alloys, they were not especially suitable for measuring environmental corrosivity by weight-loss methods. The aluminum alloys are relatively resistant to general corrosion, weight losses were small, and potential experimental errors large. The titanium alloy did not corrode and yielded no data.

(2) Test sites which yielded data were quite similar and more-or-less, whereas the mild and severe test sites were unproductive.

(3) Experimental methods were flawed:

(a) Rubber-stopper rubbing to remove corrosion products is not reproducible and not effective.

(b) Removing cleaning, and weighing all panels at six-month intervals was unfortunate because information was lost and technicians were overburdened.

(4) This was a complex program, with significant potential for expanding knowledge or corrosion. Resources committed to it, however, were inadequate.

(5) Although misfortune can be expected, PACER LIME received more than its share.

With these facts, together with scant data from the experiment, it is difficult to give serious weight to the apparent relative corrosivity of each test site. Despite flaws in the experiment, however, the results are consistent with those of other workers, the results agree with USAF

maintenance experience, and the results confirm environmental ratings from the Corrosion Damage Algorithm.

We conclude that the experimental phase of PACER LIME was successful in supporting a priori environmental corrosion severity ratings. Its success did not extend far enough, however, to provide a basis for a more accurate rating system.

TABLES AND FIGURES

Table 1. Ranges of Environmental Ambient Parameters, Continental U.S.[19]

	50th Percentile	99th Percentile	Maximum Reported
Total Sustended Particulates, $\mu g/m^3$	61	185	500
Sulfur Dioxide, $\mu g/m^3$	43	186	410
Photochemical Oxidants, as ozone, $\mu g/m^3$	36	90	110
Nitrogen Oxides			
as NO, $\mu g/m^3$	25	88	98
as NO_2, $\mu g/m^3$	72	135	150
Temperature, °C	11.8	23.3	25.7
Humidity, absolute, g/m^3	7.1	16.5	18.3

Table 2. National Ambient Air Quality Standards [8,9]

	Primary	Secondary[a]	
Sulfur dioxide	80	60	$\mu g/m^3$, annual arithmetic mean
	365	260[b]	$\mu g/m^3$, 24-hour maximum
		1300[c]	$\mu g/m^3$, 3-hour maximum
Particulate matter	75	60	$\mu g/m^3$, annual geometric mean
	260	150	$\mu g/m^3$, 24-hour maximum
Carbon monoxide	10	10	mg/m^3, 8-hour maximum
	40	40	mg/m^3, 1-hour maximum
Photochemical oxidants	160	160	$\mu g/m^3$, 1-hour maximum
Hydrocarbons	160	160	$\mu g/m^3$, 6 to 9 AM maximum
Nitrogen dioxide	100	100	$\mu g/m^3$, annual arithmatic mean

[a] Maximum values are not to be exceeded more than once per year.

[b] ". . . as a guide to be used in assessing implementation plans to achieve the annual standard."

[c] ". . . as a guide to be used in assessing implementation plans to achieve the 24-hour standard."

Table 3. Working Environmental Corrosion Standards (WECS)

	Annual Mean	
	I	II
Suspended Particulates, $\mu g/m^3$	61	86
Sulfur dioxide, $\mu g/m^3$	43	72
Ozone, $\mu g/m^3$	36	47
Nitrogen dioxide, $\mu g/m^3$	64	78
Absolute humidity,* g/m^3	7.1	9.0
Proximity to sea or salt source, km	4.5	2
Solar radiation, July (Langleys)	600	650
Rainfall, cm total	125	150

*Absolute humidity is the product of relative humidity and the mass of water in one cubic meter of water-saturated air at a given temperature.

Table 4. Environmental Ratings for Selected Test Sites

Site	Test Type	Corrosion Damage Algorithm Rating
Altus AFB OK	C-141A base	A,B
Andrews AFB MD	PACER LIME	A,B
Barksdale AFB LA	PACER LIME	A,B
Charleston AFB SC	C-141A base	AA,B
Corpus Christi TX	Other	AA,AA
Davis Monthan AFB AZ	PACER LIME	B,C
F.E. Warren AFB WY	PACER LIME	C,C
Kure Beach NC:	Other	
80 ft		AA,AA
800 ft		AA,A
McCook IL	Other	A,B
McChord AFB WA	C-141A base	A,C
McGuire AFB NJ	C-141A base	B,C
Newark NJ	Other	A,B
Norton AFB CA	C-141A base	A,A
Panama Canal Zone:	Other	
Marine*		AA,AA
Open Field*		AA,AA
Rain Forest*		AA,AA
Point Reyes CA	Other	AA,A
Richmond VA	Other	A,B
Robins AFB GA	PACER LIME	A,B
State College PA	Other	B,B
Tinker AFB OK	PACER LIME	B,C
Travis AFB CA	C-141A base	AA,A
Wright-Patterson AFB OH	PACER LIME	A,B

*Reported corrosion rates [35] suggest a higher rating than AA,AA.

Table 5. Materials Tested in PACER LIME Program

Code	Number of Panels	Size	Materials
01	12 ea	12.7 x 14.3 cm	2024 T3 (clad)
03	12 ea	12.7 x 14.3 cm	7075 T6
05	12 ea	12.7 x 14.3 cm	7079 T6 (clad)
07	12 ea	12.7 x 14.3 cm	4340
09	12 assemblies	12.7 x 14.3 cm	*
11	12 ea	12.7 x 14.3 cm	Mg AZ31B-O
13	12 ea	12.7 x 14.3 cm	Ti 6Al 4V
15	5 ea	12.7 x 29.8 cm	2024 T3 (clad)
17	5 ea	12.7 x 29.8 cm	7075 T6
21	5 ea	12.7 x 29.8 cm	Mg AZ31B-O

99 Total panels for each test stand.

*The assemblies were made from one panel each of

(clad) 2024 T3
7075 T6
(clad) 7079 T6

each panel was 12.7 x 6.4 cm. The assemblies were riveted with 4 cadmium plated rivets and assembled as shown in Figure 2.

Table 6. Corrosion Rates For Four Year Exposure in the Panama Canal Zone (afer Pearlstein and Teitell [35]).

	Marine	Openfield	Rain Forest
2024 T3	9.75×10^{-5}	8.9×10^{-6}	negligible
AZ31B-O	4.3×10^{-4}	2.2×10^{-4}	$1.3. \times 10^{-4}$
			kg/m^2-day

Table 7. Corrosion Rates for Seven-year Exposure at Several Test Sites (after McGeary et al [36]).

	Kure Beach 80-foot (E. Coast Marine)	Newark NJ (moderately severe industrial)	Point Reyes CA (W. Coast marine-1900 ft)	State College PA (rural)
2024 T3 Alclad	1.62×10^{-6}	2.04×10^{-6}	0.76×10^{-6}	0.34×10^{-6}
2024 T3 bare	3.77×10^{-6}	4.28×10^{-6}	2.97×10^{-6}	0.52×10^{-6}
7075 T6	5.67×10^{-6}	4.90×10^{-6}	4.61×10^{-6}	0.66×10^{-6}
7079 T6 Alclad	1.98×10^{-6}	2.96×10^{-6}	(lost)	0.43×10^{-6}
				Kg/m^2-day

Table 8. Corrosion Rates for Seven-year Exposure of 2024 T3 Aluminum at Several Test Sites (after Ailor [37]).

	Kure Beach NC 800-ft (E. Coast Marine)	Corpus Chisti TX 150-ft (Gulfcoast Marine)	Richmond VA (moderate industrial)	McCook IL (industrial)
1 year	7.62×10^{-6}	14.5×10^{-6}	23.6×10^{-6}	52.9×10^{-6}
2 years	1.89	5.92	18.0	33.2
7 years	2.17	2.57	4.40	7.14
				kg/m^2-day

Table 9. Corrosion Rates for One-year, Two-year, and Seven-year Exposure of Aluminum and Magnesium Alloys (after Copson [39], Pettibone [40,41], and Coburn [42].

	Kure Beach NC 80 ft lot	Newark NJ	Point Reyes CA	State College PA
	Corrosion rate x 10^6	kg/m^2-day		
2024 T3 Alclad				
1 year	2.40	2.77	1.73	0.60
2 years	1.74	2.25	1.43	0.52
7 years	1.62	2.04	0.76	0.34
7075 T6				
1 year	9.87	5.77	7.75	1.18
2 years	6.85	4.34	6.33	0.90
7 years	2.46	3.29	1.15	0.42
7079 T6 Alclad				
1 year	1.28	2.63	0.99	0.60
2 years	2.26	2.68	2.28	0.60
7 years	*	4.85	*	0.49
AZ31B-H24				
2 years	86.7	134	71.1	90.3
7 years	71.6	129	55.5	68.1

* data considered unreliable

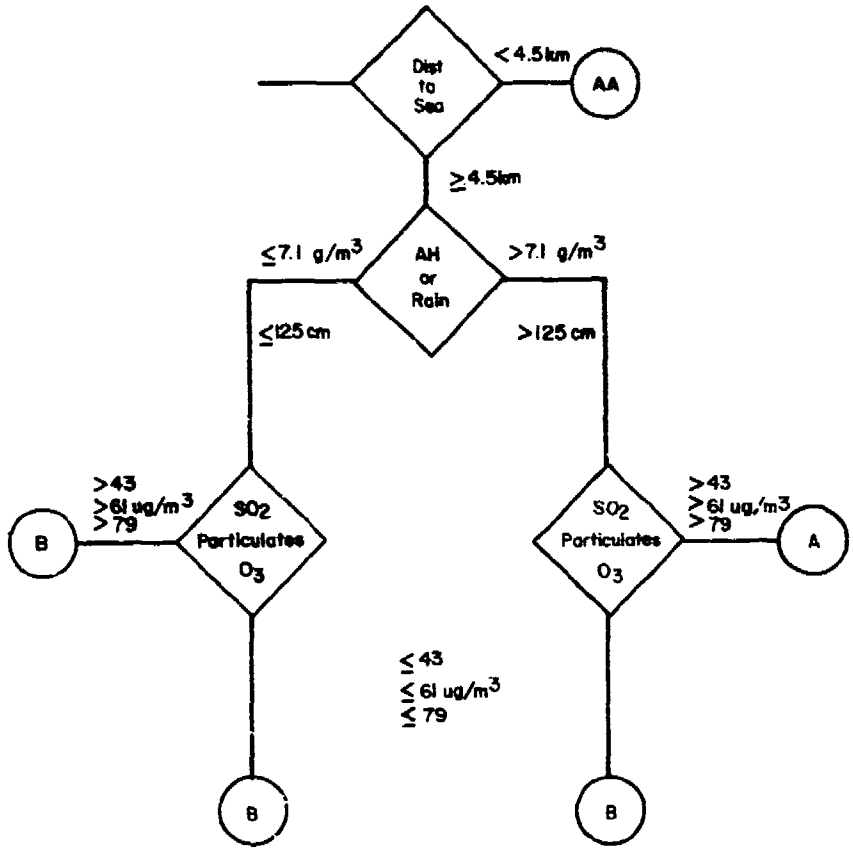

Figure 1. Corrosion Damage Algorithm for aircraft using set I of Working Environmental Corrosion Standards (Table 3).

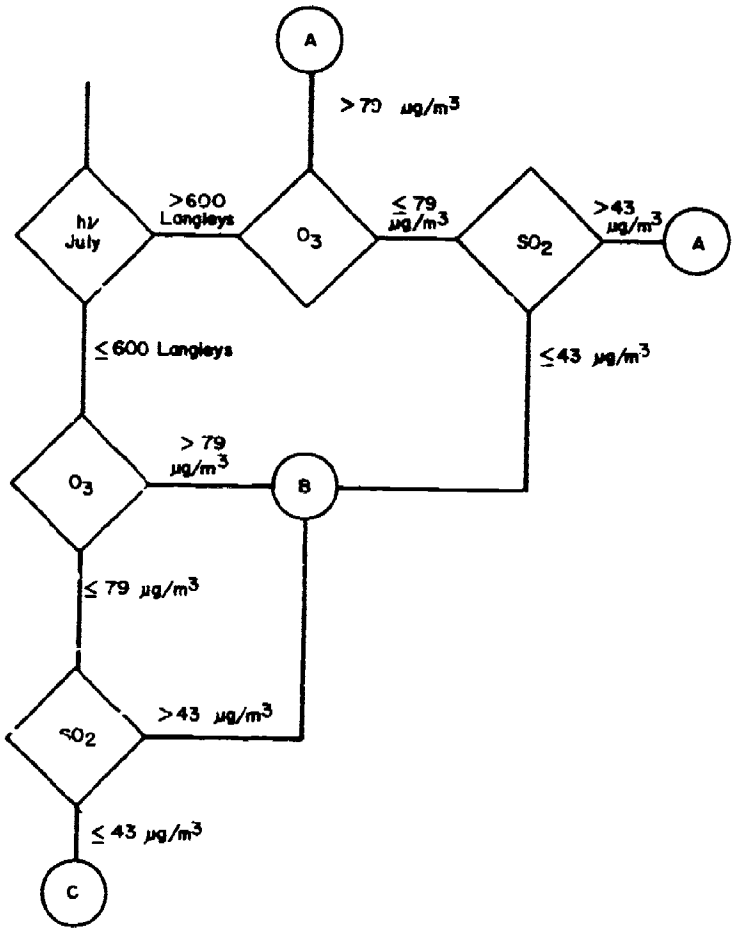

Figure 2. Aircraft Complete Repaint Algorithm.

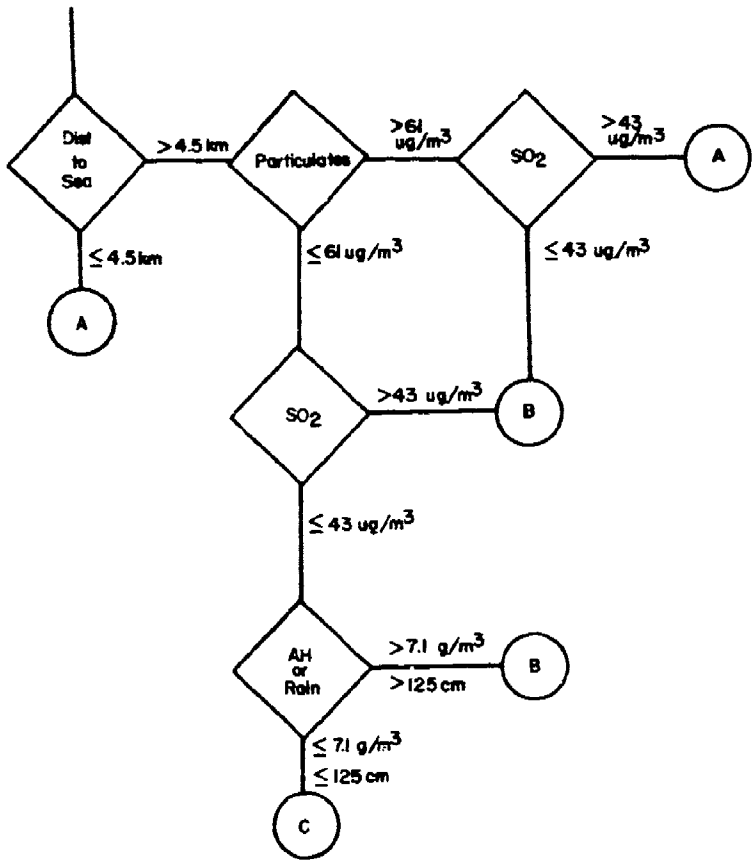

Figure 3. Aircraft Washing Interval Algorithm.

REFERENCES

1. N. D. Tomashov, "Theory of Corrosion and Protection of Metals," Translated and edited by E. H. Tytell, I., Geld and H. S. Preiser, McMillan, New York 1966.

2. W. H. Ailor, "ASTM Atmospheric Corrosion Testing: 1906 to 1976," "Atmospheric Factors Affecting the Corrosion of Engineering Metals, ASTM STP 646," S. K. Coburn, Ed., American Society for Testing and Materials, 129-151, 1978.

3. I. L. Rozenfeld, "Atmospheric Corrosion of Metals," B. H. Tytell, Trans., National Association for Corrosion Engineers, Houston, TX, 1972.

4. P. J. Sereda, "Weather Factors Affecting Corrosion of Metals," Corrosion in Natural Environments, ASTM STP 558," American Society for Testing and Materials, 7-22, 1974.

5. H. Guttman, and P. J. Sereda, "Measurement of Atmospheric Factors Affecting the Corrosion of Metals," "Metal Corrosion in the Atmosphere ASTM STP 435," American Society for Testing and Materials, 326-359, 1968.

6. P. R. Grossman, "Investigation of Atmospheric Exposure Factors that Determine Time-of-Wetness of Out-Door Structures," "Atmospheric Factors Affecting the Corrosion of Engineering Metals, ASTM 646," S. K. Coburn, Ed., American Society for Testing and Materials, 5-16, 1978.

7. H. S. Stoker, and S. L. Seager, "Environmental Chemistry: Air and Water Pollution," 2nd edn., Scott, Foresman and Co., Glenview, IL, 1976.

8. Federal Register 36, 1502 (1971).

9. Federal Register 36, 8186 (1971).

10. J. B. Upham, "Atmospheric Corrosion Studies in Two Metropolitan Areas," J. Air Pollution Control Association 17, 398-403 (1967).

11. F. Mansfield, "Results of Thirty-Six Months Exposure Study in St. Louis, MO," CORROSION/78, Houston, TX, 1978.

12. F. Mansfield, "Regional Air Pollution Study Effects of Airborne Sulfur Pollutants on Materials," EPA 600/4-80-007, January 1980.

13. F. H. Haynie, and J. B. Upham, "Effects of Atmospheric Sulfur Dioxide on the Corrosion of Zinc," Materials Performance 9, 35-40 (1970).

14. F. H. Haynie, and J. B. Upham, "Correlation Between Corrosion Behavior of Steel and Atmospheric Data," "Corrosion in Natural Environments ASTM STP 558," American Society for Testing and Materials, 33-51, 1974.

15. F. H. Haynie, J. W. Spence, and J. B. Upham, "Effects of Air Pollutants on Weathering Steel and Galvanized Steel: A Chamber Study," "Atmospheric Factors Affecting the Corrosion of Engineering Materials, ASTM STP 646," S. K. Coburn, Ed., American Society for Testing and Materials, 30-47, 1978.

16. United States Air Force Environmental Technical Applications Center, "Worldwide Airfield Climatic Data," Vols. I-VIII, Washington, D. C., 1970.

17. U. S. Environmental Protection Agency, "National Air Quality and Emissions Trend Report, 1976," EPA-450/1-77-002.

18. U. S. Environmental Protection Agency, "Air Quality Data - 1976 Annual Statistics," March 1978, EPA-45-/2-78-009.

19. T. E. Graedel, and N. Schwartz, "Air Quality Reference Data for Corrosion Assessment," Materials Performance 16, 17-25, August, 1977.

20. C. E. Junge, "Air Chemistry and Radioactivity," Academic Press, New York, 1963.

21. C. E. Junge, and R. Gustafson, "On the Distribution of Sea Salt Over the United States and Removal by Precipitation," Tellus 9, 164 (1957).

22. J. C. Hudson and J. F. Stanner, J. Iron and Steel Inst., 180, 271 (1955).

23. ASTM, "Corrosiveness of Various Atmospheric Test Sites as Measured by Specimens of Steel and Zinc," "Metals Corrosion in the Atmosphere, ASTM STP 435," American Society for Testing and Materials, 360-391, 1968.

24. R. A. Duce, J. W. Winchester, and T. W. Van Nahl, "Iodine, Bromine, and Chlorine in the Hawaiian Marine Atmosphere," J. Geophysical Res. 70, 1775 (1965).

25. R. S. Pueschel, R. J. Charleson, and N. C. Ahlquist, "On the Anomalous Deliquescence of Sea-Spray Aerosols," J. Appl. Meteorol. 8, 995-998, (1969).

26. C. E. Junge, "The Chemical Composition of Atmospheric Aerosols I: Measurements at Round Hill Field Station, June-July 1953," J. Meteorol. 11, 323-333 (1954).

27. U. S. Department of Health, Education and Welfare, "Air Quality Criteria for Particulate Matter," January 1969, National Air Pollution Control Administration Publication AP-49.

28. U.S. Department of Health, Education and Welfare, "Air Quality Criteria for Sulfur Oxides," January 1969, National Air Pollution Control Administration Publication AP-50.

29. U.S. Department of Health, Education and Welfare, "Air Quality Criteria for Hydrocarbons," March 1970, National Air Pollution Control Administration Publication AP-64.

30. U.S. Department of Health, Education and Welfare, "Air Quality Criteria for Photochemical Oxidants," March 1970, National Air Pollution Control Administration Publication AP-63.

31. U.S. Environmental Protection Agency, "Air Quality Criteria for Nitrogen Oxides," January 1971, National Air Pollution Control Administration Publication AP-84.

32. J. L. Baldwin, "Climates of the United States," U.S. Department of Commerce, Washington, D. C., 1973.

33. R. Summitt and F. T. Fink, "PACER LIME: An Environmental Corrosion Severity Classification System," Air Force Materials Laboratory, Wright-Patterson AFB, OH (in press).

34. V. E. Carter, "Atmospheric Corrosion of Aluminum and Its Alloys," Metal Corrosion in the Atmosphere, ASTM STP 435," American Society for Testing and Materials, pp. 257-270, 1968.

35. F. Pearlstein and L. Teitell, "Corrosion and Corrosion Prevention of Light Metal Alloys," CORROSION/73, Anaheim, CA, Paper no. 114, 1973.

36. F. L. McGeary, T. J. Summerson and W. H. Ailor, Jr., "Atmospheric Exposure of Nonferrous Metals and Alloys -- Aluminum: Seven-Year Data," "Metal Corrosion in the Atmosphere, ASTM STP 435," American Society for Testing and Materials, pp. 141-174, 1968.

37. W. H. Ailor, Jr., "Performance of Aluminum Alloys at Other Test Sites," "Metal Corrosion in the Atmosphere, ASTM STP 435," American Society for Testing and Materials, pp. 258-307, 1968.

38. W. H. Ailor, "Seven-Year Exposure at Point Reyes, California," Corrosion in Natural Environments, ASTM STP 558," American Society for Testing and Materials, pp. 75-81, 1974.

39. H. R. Copson, "Report of Subcommittee VI on Atmospheric Corrosion," Proc. ASTM 59, 176 (1959).

40. J. S. Pettibone, "Report of Subcommittee VI on Atmospheric Corrosion," Proc. ASTM 61, 205 (1961).

41. J. S. Pettibone, "Report of Subcommittee VI on Atmospheric Corrosion," Proc. ASTM 62, (1962).

42. S. K. Coburn, "Report of Subcommitee VI on Atmospheric Corrosion," Proc. ASTM 66, (1966).

43. R. Summitt, "Corrosion Tracking and Prediction for C-141A Aircraft Maintenance Scheduling," AFML-TR-78-29, Air Force Materials Laboratory, Wright-Patterson AFB, OH, 1978.

44. R. Summitt, "Forecasting Corrosion Damage and Maintenance Costs for Systems of Large Aircraft: Environmental Corrosiveness," CORROSION/80, Chicago, March 6-10, 1980.

AFWAL-TR-81-4019
Volume II

FAILURES OF THE M72A2 LAW ROCKET SYSTEM

G. A. Bruggeman
Army Materials and Mechanics Research Center
Watertown, Massachusetts 02172

ABSTRACT

Over a period of several years, the M72A2 LAW Rocket has experienced a number of malfunctions traceable to failures of either the rocket motor closure or the rocket motor itself. Both of these components are made of 7001 aluminum alloy heat treated to the T6 temper, an alloy known to possess low fracture toughness properties and also to be highly susceptible to stress corrosion cracking. The role of stress corrosion in a number of these malfunctions is discussed, and the remedies chosen to alleviate each problem as it occurred are described. Comparisons are made between the mechanical and physical properties of material from production lots manufactured during different time periods, and comments are made regarding factors that would appear to be contributing to the on-going stress corrosion problem.

INTRODUCTION

The M72 LAW system was developed in the early 1960's as an individual antitank weapon used extensively in Army and Marine Corps units. The system consists of a self-contained lightweight shoulder-fired launcher and a high explosive antitank (HEAT) rocket (Figure 1). The rocket is made up of the warhead, joined through a closure assembly (which houses the fuze) to an aluminum rocket motor. When fired at 70°F, the burning propellant develops a chamber pressure on the order of 600 psi which propels the rocket from the launcher with a muzzle velocity of about 450 feet per second.

From very early in its history and continuing to the present time, the LAW has experienced a series of problems, some as the result of deficient engineering practice on the part of the manufacturer, but most stemming from inadequacies in the mechanical and physical properties of the aluminum alloy used in the rocket motor and closure. The aluminum alloy used in both of these components is 7001-T6, an age hardenable alloy developed by Harvey Aluminum in the mid 1950's to provide an alloy with higher mechanical properties than any other commercially available alloy of aluminum. Typical properties of 7001 are compared in Table 1 with the properties of other aluminum-zinc-magnesium alloys, all heat treated to the T6 temper (i.e., the maximum strength condition). At the time it was developed, the claim was made that corrosion characteristics of 7001, including resistance to stress corrosion, were comparable to the other high strength 7xxx series alloys.

The strength requirements imposed by the rocket motor design adopted for the LAW mandated the selection of 7001-T6 as the motor material. Figure 2 presents the results of a finite element stress analysis of the LAW rocket motor during launch, showing a maximum effective stress of 83,000 psi occurring in the throat

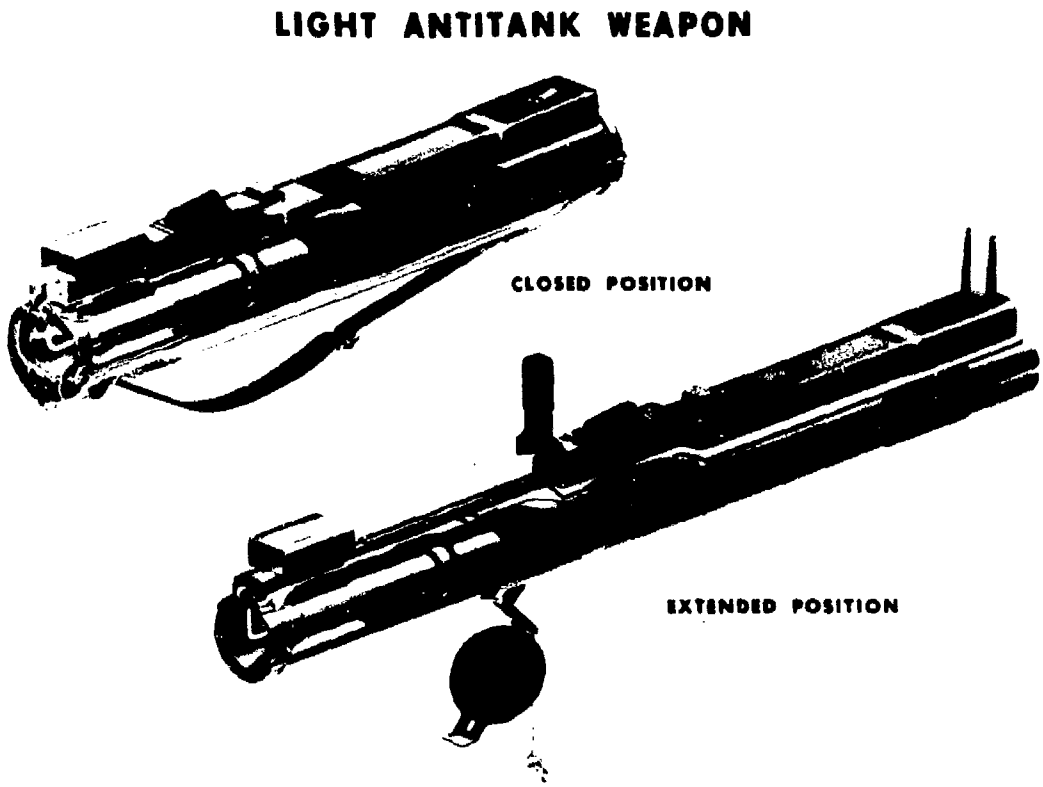

Figure 1. The M72A2 LAW system.

Table 1. TYPICAL TENSILE PROPERTIES OF 7XXX ALUMINUM ALLOY EXTRUSIONS

	YS ksi	UTS ksi	Elong %
7001-T6	84	92	5
7178-T6	78	86	5
7075-T6	72	80	7
7079-T6	70	79	7

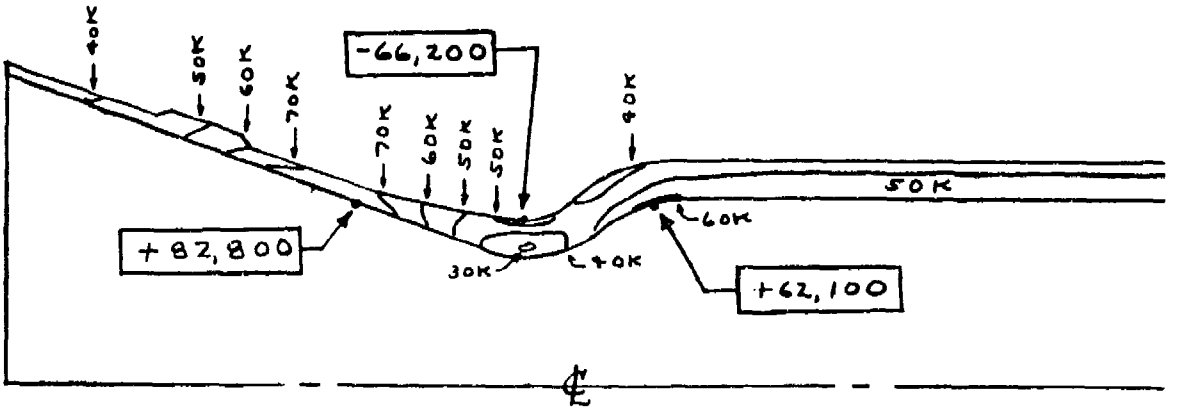

66MM LAW ROCKET MOTOR BODY - AFT SECTION

EFFECTIVE STRESSES

Material - 7001 - T6 Aluminum
Yield Strength - 84,500 psi
Internal Pressure - 9,100 psi
Exit Pressure - 1,050 psi
Acceleration - 4,000 G's

Figure 2. Finite element stress analysis of the LAW rocket motor during launch-effective stresses.

area of the rocket nozzle. Of the commercially available aluminum alloys, only 7001-T6 has a yield strength high enough to withstand this level of stress. Unfortunately, at the time when this alloy selection was made, the concepts of fracture mechanics were not widely used, and the potential for catastrophic failure inherent in the use of a material with low fracture toughness and high stress corrosion susceptibility was not adequately appreciated.

What follows is a brief case history of the LAW problems from AMMRC's first involvement through one of the most recent failure investigations. Various data obtained in the course of these investigations and elsewhere will be summarized in an attempt to give insight into the nature of the corrosion phenomena involved.

CLOSURE PROBLEMS

The first series of malfunctions with which AMMRC became involved occurred in the time period around 1970[1], and was traced to a structural weakness in the rocket closure and the warhead/closure joint. There were two types of failures encountered: (1) the closure split longitudinally due to setback forces upon launch and metal parts were expelled from the rear of the launcher, or (2) separation occurred at the warhead/closure joint, sometimes causing premature warhead

1. Carr, Frank L., Larson, Frank R., and McElaney, Francis X., *Metallurgical Analysis of the M72 LAW Closure Failure Part II*, Army Materials and Mechanics Research Center, AMMRC TN 72-2, February 1972.

detonation. Corrosion was not implicated in any of these malfunctions, but extensive mechanical property data were collected during the course of the malfunction investigation which demonstrated the low fracture toughness of 7001-T6 aluminum. The results of many tests of specimens taken from the LAW closure and the statistical analysis of that data showed the average yield strength to be 83.1 ksi with the lower 99 percent confidence limit at 76.8 ksi, well below the specified minimum yield strength of 84.5 ksi. Also, the average plane strain fracture toughness value was found to be 14.0 ksi$\sqrt{in}$ with the lower 99 percent confidence limit at 11.6 ksi$\sqrt{in}$.

With the extremely poor flaw tolerance of 7001-T6 aluminum now in evidence, coupled with its known stress corrosion susceptibility, recommendations were made to replace 7001 in all components of the LAW with a higher toughness alloy. However, because of other factors at play at the moment, the decision was made to retain 7001 in the system but to reduce the stress in the closure and strengthen the warhead/closure joint through the application of a fiberglass overwrap. While this corrective action was effective in providing a solution to the immediate problem of closure failures, it failed to take into account the basic deficiencies of the material and its use elsewhere in the system, with the result that a new series of failures developed less than five years later.

ROCKET MOTOR FAILURES - PART 1

This new round of malfunctions was confined to rocket motors produced by a single manufacturer (hereafter referred to as Manufacturer A). The typical failure signature is illustrated schematically in Figure 3. Upon firing, failure of the

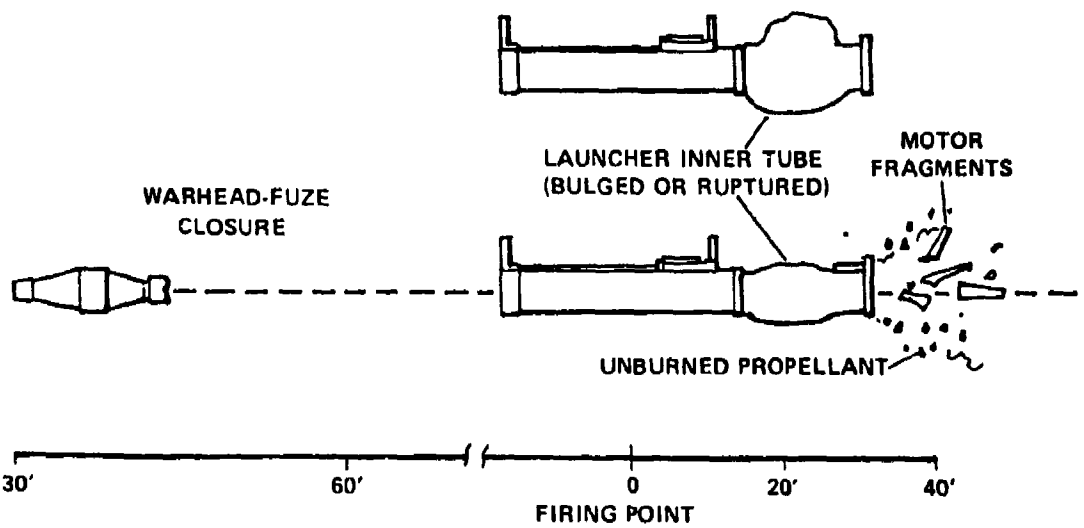

Figure 3. Schematic representation of typical LAW rocket motor malfunction.

rocket motor occurred with little or no rocket travel in the launcher, expelling unburned propellent and motor fragments to the rear and propelling the warhead and closure a short distance forward of the launch point. The launch tube was bulged or ruptured, but miraculously no serious operator injury took place.

Typically, the rocket motor broke into two or three major fragments, as shown in Figure 4, with the primary fracture path running longitudinally the full length of the motor. Following the chevron markings on the fracture surface allowed the fracture path to be traced back to the point of primary origin, which almost invariably was located on the nozzle rim. Secondary fracture origins in the throat of the nozzle were often activated by the bending forces which developed following the initial fracture. Close examination of the fractures showed the primary origins to be stress corrosion cracks on the order of one millimeter (0.040 inch) in depth (Figure 5), which exhibited the intergranular appearance typical of stress corrosion in the scanning electron microscope, as shown in Figure 6. Verification of stress corrosion cracks in the nozzle rim as the operative failure mechanism was obtained by test firings of rockets with machined notches cut into the rim of the nozzle; the failure signature that resulted was identical to the actual malfunctions. It was later demonstrated that the condition leading to the formation of these stress corrosion cracks was most likely introduced by one of the proof tests used as a quality assurance measure during motor production.

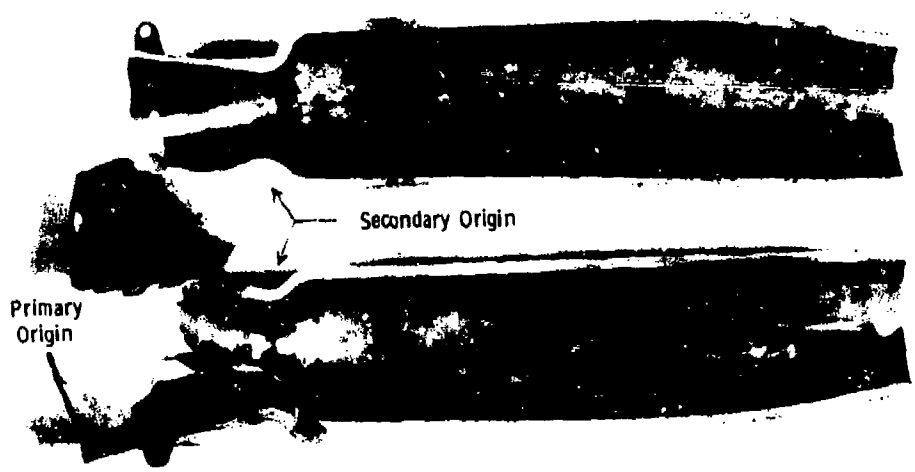

Figure 4. Typical LAW motor failure.

Figure 5. Primary fracture surface in LAW motor failure showing the primary initiation site (Reference 2). Mag. 3.5X

Figure 6. Fracture surface at primary initiation site showing intergranular fracture (Reference 2). Mag. 1500X

Fracture toughness measurements performed on specimens taken from motors of the affected manufacturer produced K_{IC} values as low as 7 ksi$\sqrt{in}$ with the average being 10-11 ksi$\sqrt{in}$. Taking K_{IC} = 10 ksi$\sqrt{in}$ and assuming a stress of 45 ksi (35 ksi launch plus 10 ksi residual stress) a critical flaw depth of 0.3 mm (0.012 inch) was calculated, supporting the contention that the observed stress corrosion cracks were indeed supercritical[2].

2. *Malfunction Investigation Program, Rocket, He, 66-MM:AT, M72 Series (LAW) - Metallurgical Program*, U. S. Army Armament Research and Development Command Report, Pittman-Dunn Laboratory, April 1976.

Again, the situation should have been clear that the basic problem stemmed from the use of 7001-T6 aluminum, a material with very low flaw tolerance and with high stress corrosion cracking susceptibility. Nevertheless, the decision was made to salvage the remaining stockpile by again overwrapping the affected component (this time the rocket motor) with fiberglass. In detail, the fix involved machining a small quantity of material from the nozzle rim to remove any stress corrosion cracks already present, followed by a fiberglass overwrap of both the rim and the throat areas of the rocket nozzle, as shown in Figure 7. The throat wrap was for the purpose of reinforcing the most highly stressed area of the motor and to arrest any cracks which might initiate and propagate from the nozzle rim. The rim wrap was to prevent ejection of metal fragments from the rear of the launcher in the unlikely event of a motor failure. Firing tests of pre-flawed motors showed the wrap to be effective in both these points. The basic deficiencies of 7001-T6 aluminum were still ignored, however, and history was soon to be repeated.

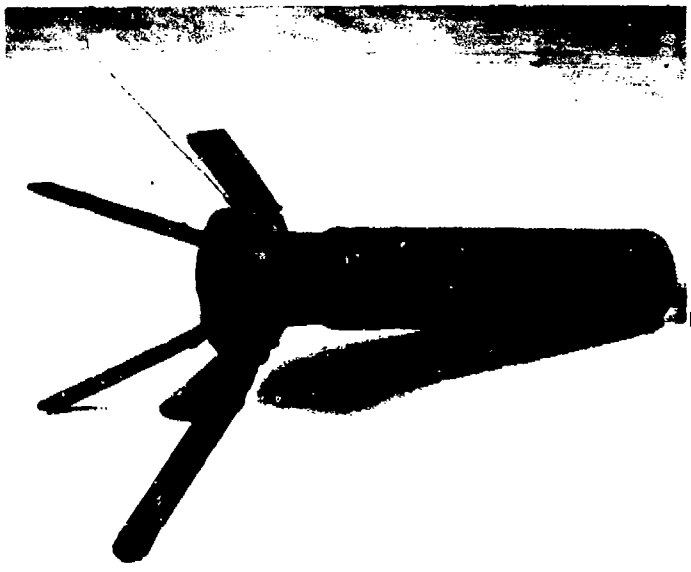

Figure 7. Fiberglass wrapped LAW rocket motor.

ROCKET MOTOR FAILURES - PART 2

In the span of a few weeks in mid 1978 two malfunctions occurred in fiberglass wrapped rocket motors. The failure signature resembled, in most aspects, the signature of the previous motor failures: a few large fragments with a primary longitudinal fracture. Figure 8 shows the motor fragments recovered from one of these malfunctions along with a diagram of the fracture path[3]. The primary fracture initiation site is at point A, the base of the fin slot on the lug rim, rather than at the rim of the nozzle as in the earlier malfunctions. A finite element stress analysis of the wrapped motor had shown that the region of maximum stress would be moved away from the throat of the nozzle to the lug rim by the

3. Bruggeman, Gordon A., *An Investigation of the Failure of a Fiberglass-Wrapped M72A2 LAW Rocket Motor*, Army Materials and Mechanics Research Center, AMMRC TN 79-2, January 1979.

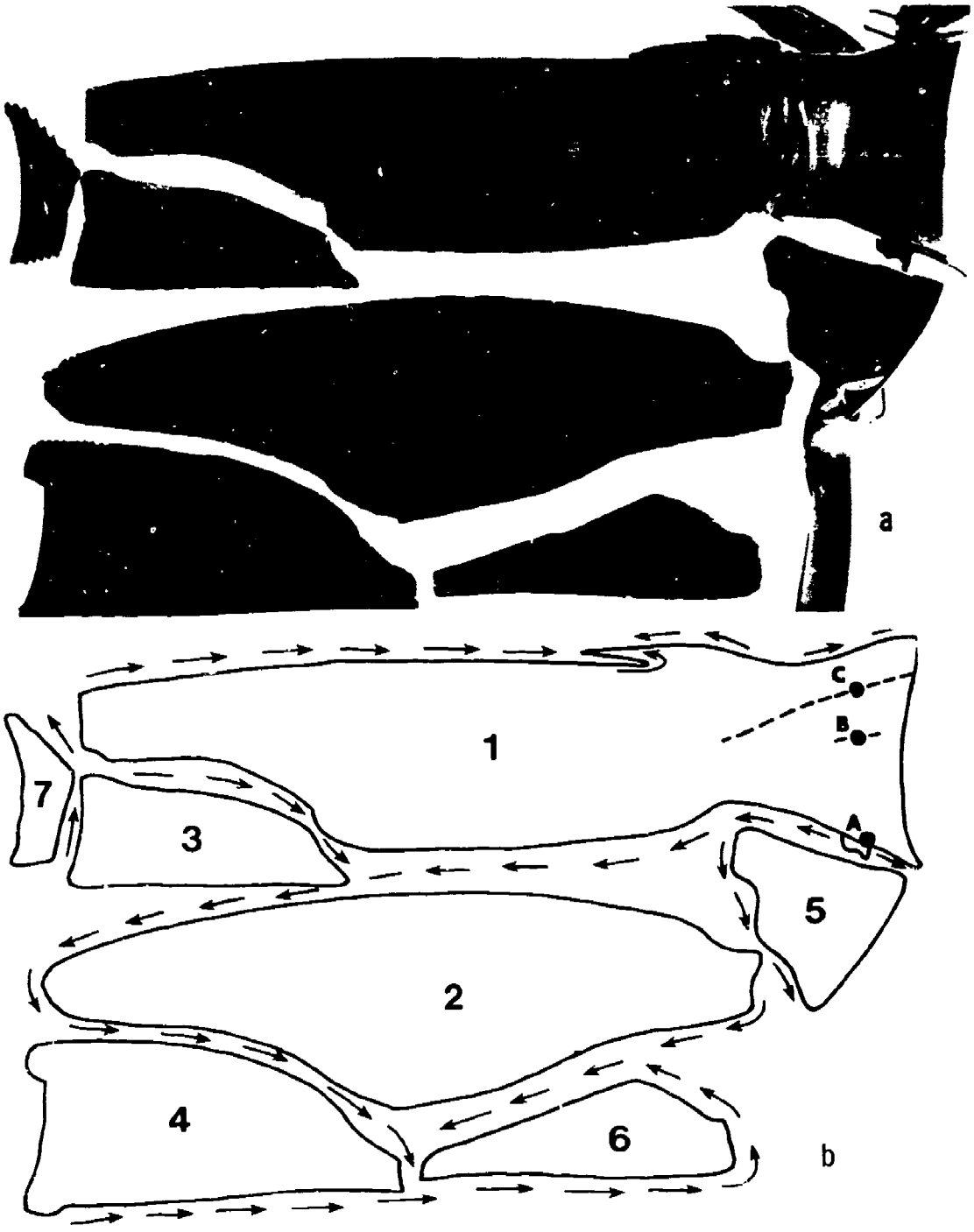

Figure 8. Fragments from fiberglass wrapped LAW motor failure (Reference 3).

application of the fiberglass. Thus the failure of the wrapped motor appears to have initiated at a location near the point of maximum stress. Secondary crack initiation sites were also located in equivalent locations B and C at the base of other fin slots on the lug rim. These secondary cracks were unrelated to the primary fracture and apparently developed independently.

Examination of the fracture surface near the primary initiation point again gave evidence of intergranular fracture and crack branching (Figure 9), suggestive of a stress corrosion failure mechanism. Similar features were observed at the

a. Mag. 500X

b. Mag. 1000X

Figure 9. Primary fracture initiation site in fiberglass wrapped motor failure showing (a) "mudcracking" and intergranular fracture, and (b) crack branching (Reference 3).

secondary crack initiation sites at B and C, as well. However, no pre-existing flaws could be identified. It was speculated that the anodized coating at the base of the fin slots may have been damaged when the fins were moved for the fiberglass wrapping operation, and that this contributed to a later corrosion problem.

One other point of interest was the failure of the throatwrap to arrest the crack propagating from the lug rim, in contrast with what had been demonstrated earlier. Apparently, relaxation of the wrap during long-term storage reduced its crack arresting effectiveness.

DISCUSSION

From the picture of LAW performance thus far presented, it would appear that all LAW systems, regardless of their manufacturer, have been subject to problems of stress corrosion and poor flaw tolerance because of their common usage of 7001-T6 aluminum. Interestingly, this has not been the case. Of three manufacturers involved in LAW production over the years, one has had a far worse malfunction record than the others. Table 2 compares the motor failure rates compiled from several years of firing experience by the three manufacturers. Manufacturer A has clearly had the more difficult time whereas the experience of Manufacturer C has been extraordinarily good. It may be useful to compare various material and process parameters from the three producers to gain insight into the cause of this difference in performance.

Table 3 compares some typical chemical compositions obtained from sample rocket motors of the three producers along with the specified chemistry for 7001. Note that Manufacturer B had used a high zinc version of 7001 aluminum (alloy designation ZG93), but beyond that, there appears to be little in the way of significant differences between the alloys. In recent years, Manufacturer C has chosen to restrict the zinc, magnesium, and copper levels to the lower end of the 7001 chemistry range, to significantly reduce the maximum amounts of iron and silicon, and to place tight controls on the maximum sodium and hydrogen levels. Even without these restrictions, however, Manufacturer C reportedly has had uniformly trouble-free experience. The iron concentrations, often related to poor ductility and a loss in toughness, are no worse for Manufacturer A than for Manufacturer B.

Table 4 summarizes mechanical property data obtained from motors produced by the three manufacturers. With the exception of one data set (i.e., Manufacturer C, circa 1975), all data entries represent the results of from four to eight tests. From a ductility and fracture toughness standpoint, the data from Manufacturer B motors seem the least desirable, with the Manufacturer C (circa 1979) motors showing up the best. More or less as expected, the leaner chemistry of the more recent Manufacturer C motors has had the effect of modestly lowering the strength and raising the ductility and toughness. The mechanical properties of Manufacturer A's motors appear to be quite good and certainly do not reflect the poor firing record experienced by that producer. However, recall that earlier data obtained during the first rocket motor malfunction investigation[2] by the U.S. Army Armament Research and Development Command (ARRADCOM) had produced some K_{IC} values as low as 7 ksi$\sqrt{in}$, so there may be greater variability in Manufacturer A's product than was detected by current tests.

Table 2. COMPARISON OF LAW FIRING EXPERIENCE (MOTOR FAILURE RATE)

Manufacturer	Number Fired	Failure Rate
A	150,000	1/30,000
B	2,000,000	1/400,000
C	800,000	0/800,000

Table 3. CHEMICAL COMPOSITION - LAW ROCKET MOTORS (WEIGHT PERCENT)*

	Zn	Mg	Cu	Cr	Si	Mn	Fe	Ti
7001	6.8/8.0	2.6/3.4	1.6/2.6	0.18/0.35	0.35	0.20	0.40	0.20
A	(5.0)/7.9	2.9/3.1	1.8/2.0	0.16/0.24	0.15/0.31	0.01/0.14	0.11/0.40	0.01/0.08
B (ZG93)	7.3/8.8	2.4/2.7	1.8/1.9	0.17/0.18	0.24/0.39	0.19	0.38/0.40	0.04/0.07
C	7.0/7.5	2.8/3.3	1.9/2.6	0.11/0.18	0.08/0.13	0.01/0.02	0.10/0.14	0.01/0.03
7278	6.8/7.2	2.7/3.0	1.7/2.1	0.18/0.22	0.2	0.02	0.2	0.03

*Double numbers represent range; single numbers represent maximum.

Table 4. MECHANICAL PROPERTIES OF LAW ROCKET MOTORS*

Manufacturer	Y.S. ksi	U.T.S. ksi	Elong %	RA %	K_Q ksi$\sqrt{in.}$
A	81.7 ± 3.1	95.1 ± 2.4	10.0 ± 0.6	21.5 ± 4.9	15.6 ± 2.0
B	84.7 ± 2.8	91.9 ± 1.2	8.0 ± 0.9	11.3 ± 4.3	13.4 ± 1.4
C (circa 1975)	83.1 ± 4.0	98.3 ± 0.3	10.0 ± 0.7	22.3 ± 1.9	15.6 ± 2.4
C (circa 1979)	79.0 ± 2.9	95.8 ± 0.2	11.7 ± 1.6	17.0 ± 5.1	17.5 ± 1.7

*Indicated variability is one standard deviation.

Figure 10 compares the longitudinal microstructures taken from the nozzle area of the three manufacturers' motors. Manufacturers A and C both exhibit recrystallized microstructures whereas Manufacturer B's motors contain a cold worked, unrecrystallized microstructure in this area (partial recrystallization is achieved away from the nozzle). The dark second phase particles in all the microstructures are chromium and iron bearing intermetallics. The maximum size and volume fraction of these intermetallics appears greater for Manufacturers A and C. Quantitative metallography performed on these microstructures tended to confirm this observation with typical data appearing in Table 5. On this basis one might expect that Manufacturer C would have as many problems as Manufacturer A, but this has not occurred.

Since stress corrosion cracks in the nozzle rim would grow only under the influence of a residual tensile stress, the residual stresses in the nozzle were measured by means of the standard X-ray method using a Rigaku MSF Strainflex X-ray unit. The measured hoop stress in the nozzle rim exhibited considerable variability, both between motors and between locations on a single motor, as evidenced in Table 6. The condition of Manufacturer C's motors is by far the most desirable from a stress corrosion standpoint, but one might expect Manufacturer B to have the same SCC problems as Manufacturer A, which has not been the case.

Table 7 summarizes significant aspects of the manufacturing processes used by the three producers, highlighting some of the differences that exist. In so far as is known (not all details are available in their entirety) the major differences lie in the initial preparation of the extrusion slug and in the final aging treatment. Discussing the latter point first, Manufacturer A used a single step aging treatment whereas Manufacturer B employed a two step process. Manufacturer C's aging treatment is not known, but judging from the electrical conductivity values measured on the motor bodies (which can often reflect the state of heat treatment in aluminum alloys) it would seem to resemble that of Manufacturer A. The higher conductivity measured on Manufacturer B motors would indicate a more advanced or complete state of aging (all other things being equal) and might explain the lack of stress corrosion failures, in spite of other factors being unfavorable. The susceptibility of Manufacturer C motors might be expected to approach that of Manufacturer A motors on the basis of this measure of the state of aging, however, which is contrary to the evidence.

The extrusion slugs were prepared differently by all three manufacturers. Manufacturer A purchased air melted direct chill (DC) cast and extruded bar stock which was annealed prior to extrusion of the rocket motors. Manufacturer B vacuum melted an aluminum billet which was then forged into the final extrusion slug. Manufacturer C vacuum melted, DC cast, and homogenized the aluminum billets which were hot extruded to the diameter of the final extrusion slug. What is perhaps the most significant of the process differences (and the one factor which is consistent with the difference in performance) is the fact that Manufacturers B and C melted under vacuum, which will have the effect of lowering the level of residual gases, principally hydrogen, in the melt. In view of increasing evidence concerning the role of hydrogen in the embrittlement and stress corrosion of aluminum[4], reduced hydrogen levels can be expected to have a beneficial effect.

4. Christodoulou, L., and Flower, H. M., *Hydrogen Embrittlement and Trapping in Al-6%Zn-3%Mg*, Acta Met., v28, 1980, p. 481-487.

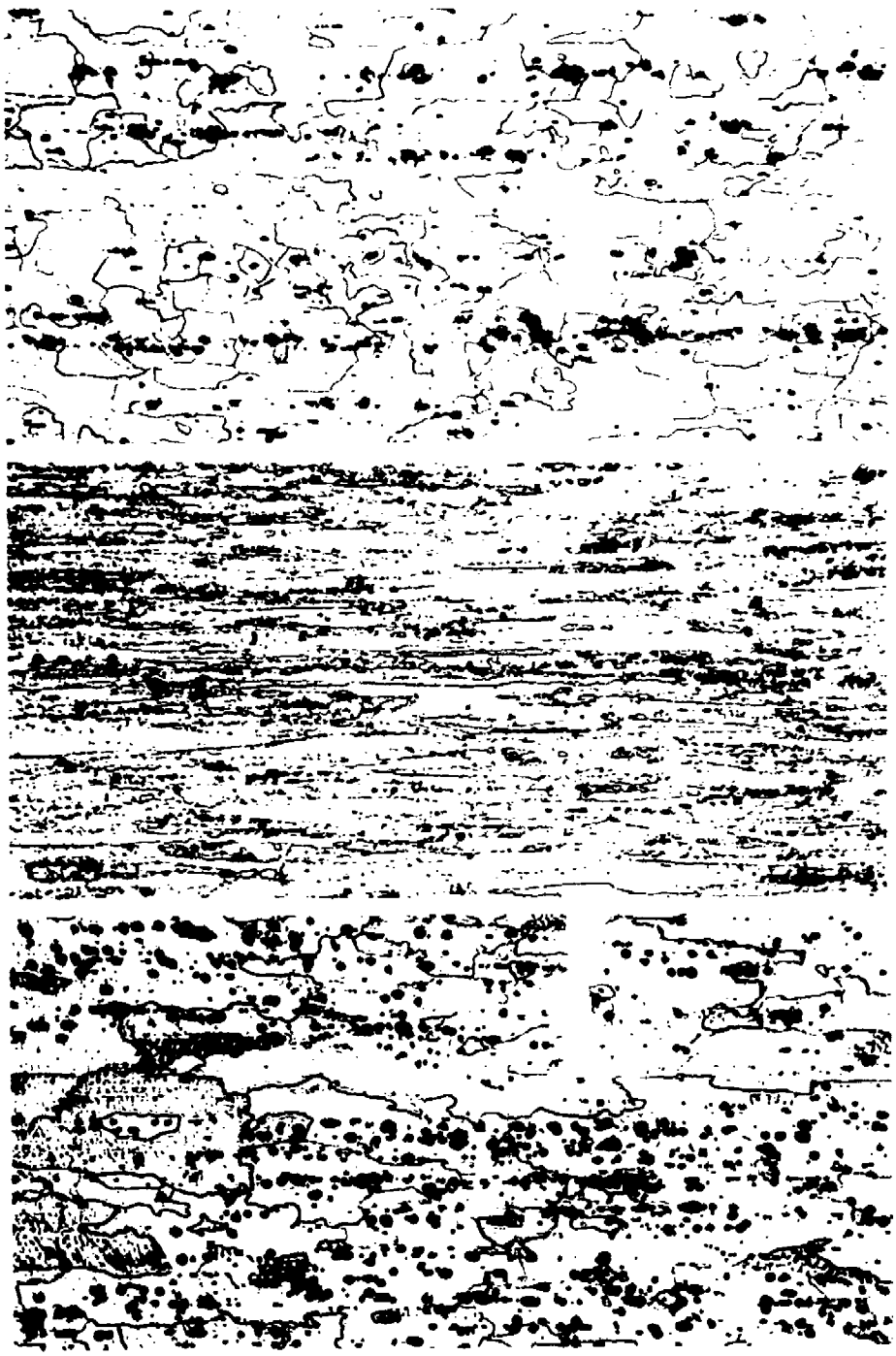

Figure 10. Typical longitudinal microstructures in the nozzle area of motors produced by the three manufacturers. Mag. 200X

Table 5. MICROSTRUCTURAL ANALYSIS OF DISPERSOID PHASE

Manufacturer	Volume Fraction	Maximum Diameter (Micrometers)
A	0.05-0.09	9.1
B	0.08-0.10	6.4
C	0.07-0.16	8.5

Table 6. RESIDUAL STRESSES AT THE NOZZLE RIM IN LAW ROCKET MOTORS

Manufacturer	Residual Hoop Stress
A	9 ksi Compressive to 20 ksi Tensile
B	6 ksi Compressive to 33 ksi Tensile
C	0 to 5 ksi Compressive

Table 7. DIFFERENCES IN MANUFACTURING PROCESS

	A	B	C
Melting	Air	Vacuum	Vacuum*
Condition of Extrusion Slug	DC Cast, Extruded, Annealed	Forged	DC Cast, Homogenized, Extruded
Solution Treat 30 min. at 870°F	X	X	X
Water Quench Temperature	RT	RT	RT
Age	24 hrs. at 240°F	3 hrs. at 250°F & 3 hrs. at 325°F	?
Conductivity % IACS	29.3	32.9	29.5

*Na and H controlled to low levels.

It is not possible, nor is it the intent here, to draw conclusions concerning the relative importance of various metallurgical and process parameters in stress corrosion of aluminum alloys generally or in malfunctioning of the LAW rocket system specifically. It does appear evident that subtle differences in processing result in subtle differences in the character of the metal in the final product, which may, in turn, have profound effects on such things as the stress corrosion characteristics. It is beyond the ability of existing material and product specifications to adequately control these subtleties. Lacking this, therefore, it is necessary that materials selected for critical applications be tolerant of the inevitable processing variability and production defects which present-day quality control measures are unable to screen out. In the case of the selection of 7001 aluminum for use in the LAW, this obviously was not done.

ACKNOWLEDGEMENTS

ARRADCOM fractographic and fracture toughness data from the early rocket motor malfunction investigation were provided by Mr. J. Rinnovatore and Mr. J. Mulherin, respectively. Dr. J. Kohatsu and Mr. C. Gazzara, both of AMMRC, performed the metallographic and X-ray residual stress analyses, respectively.

AFWAL-TR-81-4019
Volume II

THE DEVELOPMENT OF MULTIFUNCTIONAL CORROSION INHIBITORS FOR AEROSPACE APPLICATIONS

M. Khobaib
Systems Research Laboratories, Inc.
2800 Indian Ripple Road
Dayton, OH 45440

F. W. Vahldiek
and
C. T. Lynch
Air Force Wright Aeronautical Laboratories
Materials Laboratory (AFWAL/MLLN)
Wright-Patterson Air Force Base, OH 45433

ABSTRACT

The development of inhibitors for aerospace applications such as automated rinsing of aircraft requires systems of high solubility, low toxicity, and reasonable cost which are effective on a wide variety of high-strength corrosion-susceptible alloys. Chromate-based products, in combination with polyphosphates, have been reasonably effective against corrosion of ferrous and nonferrous metals and alloys and are presently the most widely used inhibitors. The use of chromates, however, has been the subject of ecological concern, and the present investigation involves the development of non-toxic, multifunctional water-soluble inhibitors. The performance of a large number of nonchromate inhibitors has been studied and a borax-nitrite-based formulation developed which inhibits the corrosion of both ferrous and nonferrous alloys. This formulation consists of a combination of low-toxicity components and is effective in preventing localized corrosion and accelerated crack growth as well as general corrosion. Effectiveness in aggressive environments including synthetic urine has been demonstrated. Applications include lower-bay, galley, and related areas of large aircraft and automated aircraft rinse facilities. Field evaluations are underway.

INTRODUCTION

During the past four years, a considerable number of studies have been conducted in the United States regarding the total cost of corrosion prevention and control for aircraft. The inescapable conclusion is that total corrosion costs in terms of life-cycle management and maintenance of aircraft represent an intolerable burden to the U. S. Air Force in maintaining force effectiveness at a reasonable cost to the taxpayer. A recent study conducted by NBS [1] has indicated that the total corrosion cost for one year (1976) was more than 70 billion dollars nationally, with costs to the USAF estimated to exceed one billion dollars. In order to minimize these costs, the USAF has been searching for ways to combat corrosion in all its forms. Several years ago a study [2] conducted by the U.S. Navy on corrosion prevention in carrier-based aircraft revealed that by merely rinsing the aircraft with water to remove detrimental particles such as salt and ash, a considerable savings could be realized in terms of corrosion maintenance. By late 1975, the USAF had made a decision to build a rinse facility for the F-4 aircraft and to install it under AFLC/WRALC and TAC at MacDill Air Force Base, FL. At the corrosion managers conference at WRALC in the fall of 1975, questions concerning hard-water rinsing as opposed to inhibited or demineralized-water rinsing were discussed [3]. In the rinsing of aircraft, the possibility exists that water will be trapped in crevices or so-called dry-bay areas and that trapped hard water will cause serious corrosion problems and hence completely jeopardize any advantage of hard-water rinsing as a corrosion-control method. Therefore, the incorporation of a low concentration of a non-toxic water-soluble inhibitor into the rinse facility was suggested.

The use of inhibitors to reduce costs also received impetus as a result of the conclusions reached at the 1975 AFML-AFOSR Corrosion Workshop [4]. The expanded use of inhibitors to reduce the costs and problems associated with corrosion in aerospace systems was recommended as a cost-effective, flexible, and widely applicable approach. In this regard one of the major cost items for depot repair has been due to corrosion in the lower surfaces of particularly larger aircraft, such as the C-130 and C-141A. Generally inaccessible and hard to inspect, these areas (referred to as "bilge" areas) act as traps for dirt and moisture which accelerate corrosion and result in major corrosion damage that requires large-scale structural repair. In addition to lower cargo bay areas, hot spots for corrosion are found in the galley and latrine areas. Warner Robins Air Logistics Center Corrosion Management Office, GA, has often cited the need to investigate the development of corrosion inhibitors for this type of application that would be simple to apply or use. Bilge inhibitors in package form have already been reported in use by the Royal Air Force in Great Britain [3], but they are reported to contain chromates which would not be satisfactory from a toxicity standpoint for the Air Force. Some commercial use has been made of water-displacement compounds, but these have limited life, are difficult to apply, and are toxic in application. The magnitude of the cost of bilge-area rework is indicated from recent figures for depot work on the C-141A, on which 1182 hours were required per aircraft for a cost in excess of two million dollars per year for the entire C-141A force.

Although chromate-based [5,6] corrosion inhibitors have been widely used to combat corrosion of ferrous and nonferrous metals and alloys, the use of chromates has recently been the subject of ecological concern. The present investigation was carried out to search for alternatives to chromates, one such

alternative being a borax-nitrite-based inhibitor. The value of borax nitrite as a corrosion inhibitor has long been recognized [7,8]. Earlier work [9] has shown a borax-nitrite combination to be very effective in controlling general corrosion as well as crevice corrosion of high-strength steels. However, this combination was not found to be effective against the corrosion of other ferrous and nonferrous metals and alloys. The present study was conducted first to develop a nontoxic multifunctional corrosion inhibitor (which would be effective against corrosion of ferrous and nonferrous metals and alloys--mainly aluminum and copper alloys) to be incorporated into the USAF Automated Rinse Facility at MacDill Air Force Base in Tampa, FL. The second objective was to use this system as the basis for the further development of a nontoxic, multifunctional corrosion inhibitor system which would be applicable to incorporation into hot-spot corrosion-prone areas such as the lower bay areas of large aircraft.

Several hundred inhibitor compounds and formulations were surveyed with regard to their effect upon electrochemical behavior, general corrosion, galvanic corrosion, crevice corrosion, and corrosion fatigue. As a result a borax-nitrite-based inhibitor was developed and is currently being evaluated in the Automated Rinse Facility at MacDill Air Force Base. This solution contains no chromate, is biodegradable, and offers other important advantages over chromate-based combinations which will be discussed. The Rinse Facility was placed in operation in 1978; and in tests begun in late 1979, inhibitors were added. Efforts have been initiated to track corrosion maintenance costs of F-4 aircraft undergoing the inhibited rinse operation.

In the follow-on effort new formulations have been developed for use in the lower cargo bay, galley, and latrine areas of large aircraft. These inhibitors

have proven effective in laboratory tests in extremely aggressive environments over long periods of time.

GENERAL CONSIDERATIONS FOR INHIBITORS

Several commercial inhibitors are available for various service applications such as cooling-tower circuits, central-heating systems, and automotive radiators. These formulations are normally combinations of several classes of inhibitor compounds, some functioning as anodic inhibitors and others as cathodic inhibitors. Commercial experience has shown that such combinations are often more effective due to some synergistic [10] effect. Unfortunately, most of them are optimized for a specific application. The results of work conducted at the Air Force Wright Aeronautical Laboratories/Materials Laboratory have demonstrated an encouraging inhibition effect of borax-nitrite upon high-strength steels [11]; chromates have not been found to be so effective in the presence of chloride ions [12]. The promising results of the borax-nitrite combination were observed in crack-growth experiments--both in static test and cyclic corrosion-fatigue tests--but this combination per se was not effective in inhibiting the corrosion of high-strength aluminum alloys, copper, and other alloys used in aircraft structures and in the Rinse Facility. However, the encouraging results obtained on high-strength steels served as the impetus for further exploration.

A substantial number of corrosion-preventive compounds (called CPC's) are also available commercially. These are based upon the use of water displacing compounds, protective organic films, and surfactant agents in a solvent vehicle. Their chief disadvantages appear to be limited effective life, the requirement of clean and uncorroded surfaces, cost, and toxicity of the carrier solvents.

In order to systematize the development of new inhibitor formulations and current commercial products, it is desirable to establish some guidelines for selection of inhibitors for further experimental screening. In Table 1 some of the more important considerations and possible compound types are listed. Most of these are obvious considerations, with a few being particularly important for aerospace or other applications where high-strength alloys are utilized. These considerations require effectiveness to retard or eliminate hydrogen embrittlement, stress-corrosion cracking, and corrosion fatigue which can lead to catastrophic cracking failure in high-strength alloys [11].

The first and foremost task in the screening of the inhibitors was the question of toxicity. All the inhibitor formulations which were obviously toxic (based upon information in the literature [13]) were eliminated first--chromates, aniline, and arsenic additions being obvious examples. It is also important that the materials used be cost effective and readily available. They should be economical and have long-term effectiveness. For bilge areas of aircraft, effectiveness should last between major field maintenance operations and ideally between programmed depot maintenance intervals.

The use of the other guidelines delineated in Table 1 is discussed in more detail in a previous report on the development of the rinse inhibitors [14]. These guidelines led to a selected list of inhibitor compounds and formulations for subsequent experimental screening. Special solutions were employed, as discussed in the experimental section, to reproduce the rinse water used at the Automated Rinse Facility and to reproduce more aggressive media based upon possible high-chloride contamination of the rinse water upon recycling after use

on the aircraft. For bilge environments it was necessary to develop special solutions for synthetically reproducing the most aggressive media expected to be present in the lower-bay areas of large aircraft. This included the use of a synthetic-urine solution which simulated natural urine in corrosive action as subsequently described.

EXPERIMENTAL

Since the inhibitor was being developed for aircraft rinsing and for aircraft galley and dry-bay areas, the materials chosen to be tested were those commonly used in aircraft structures and in the Rinse Facility. Three high-strength aluminum alloys--2024-T3, 7075-T6, and 7050--along with high-strength steel, 4130, 4340, cast iron, and 70-30 brass were obtained from a local supplier (Jorgenson Steel, Dayton, OH).

Standard 60 × 30 × 3.125 mm test coupons were used for immersion tests on aluminum alloys. Smaller rectangular sheets with dimensions 75 × 25 × 3.125 mm were used for high-strength steel, brass, and cast iron. These were mechanically polished with emery paper up to 400, cleaned thoroughly in acetone and alcohol, and in several instances finally degreased with petroleum ether. A hole, nearly 5 mm in diam., was made close to one end; and the specimens were suspended by means of a fish line (nylon thread). The maximum duration of these tests has been up to 30 months, but most of the test specimens were immersed in the respective electrolytes for 90 days.

The working electrodes for the electrochemical tests were 25-mm-square pieces which were carefully mounted in resin and were tapped with 3-48 thread for attaching to the electrode holder. All electrochemical tests were carried out in accordance with ASTM Standard G5-72, "Standard Recommended Practice for Standard Reference Method for Making Potentiostatic and Potentiodynamic Standardization Measurements." The measurements were conducted using an automated PAR unit consisting of a corrosion cell, potentiostat/galvanostat, log converter, programmer, and X-Y recorder.

A series of systematic tests were conducted which involved the screening of 1) anodic inhibitors (single component, multicomponent), 2) cathodic inhibitors (single component, multicomponent), 3) a combination of anodic and cathodic inhibitors, and 4) multifunctional systems containing the anodic-cathodic inhibitors. The screening of a large number of combinations was conducted by the potentiodynamic polarization technique and weight-loss methods.

In the immersion tests, the weight loss per unit of surface area of the specimens in different electrolytes was converted to mpy (mils per year). The percentage inhibitive efficiencies were not calculated because the final selection of the inhibitor was based upon the visual observation (where there was no change in surface appearance) and polarization results. In some cases, pieces of aluminum, high-strength steels, brass, and cast iron were suspended together in one electrolyte to check the effectiveness of inhibitors against interfering ions. Finally, the effectiveness of the inhibitor for metallic

parts prone to galvanically coupled conditions was also examined. Galvanic couples were prepared as shown in Fig. 1. Pieces of aluminum, steel, brass, and cast iron were connected through a stainless-steel rod and individually bolted with stainless-steel nuts.

Low-cycle corrosion-fatigue tests [15] were conducted to determine the effectiveness of the inhibitor formulations in retarding crack growth. The rinse inhibitor containing 0.35% (w/o) borate + 0.05% nitrite + 0.1% nitrate + 0.01% silicate + 50 ppm phosphate + 30 ppm MBT and a modified formulation for bilge solution inhibition containing 0.35% (w/o) borate + 0.2% nitrite + 0.2 % nitrate + 0.01% silicate + 50 ppm phosphate + 50 ppm MBT + 125 ppm Richonate 1850 were used for this purpose. Compact-tension plane-strain fracture-toughness specimens, (Al 7075-T6) as shown in Fig. 2, were used to determine the crack-growth rate in the presence of uninhibited and inhibited tap water and saline solution and in uninhibited and inhibited natural and synthetic urine. A detailed description of the corrosion-fatigue tests on high-strength aluminum alloys is given in Ref. [15]. Sinusoidal tension-tension cycling was used at a frequency of 0.1 Hz. All tests were performed at a maximum load of 5328N (1200 lbs.) and a stress ratio, $R(\sigma_{min}/\sigma_{max})$, of 0.1. The specimens were initially precracked to a fatigue-crack length of ~ 2.54 mm (0.10 in.). The crack length was monitored using a double-cantilever-beam gauge and an amplifier-recorder system. The crack-opening displacement (COD) was recorded as a function of fatigue cycles.

In order to determine the crack lengths from COD data, compliance measurements were carried out for all aluminum alloys. Tests were conducted in air, and crack lengths were determined using optical and COD measurements simultaneously

on the MTS machine. No significant differences were found in the COD/load and crack-length/load curves. The crack length, a, was calculated from the analytical compliance relationship [16].

$$a/w = 1.001 - 4.6695\ U + 18.460\ U^2 - 236.82\ U^3 + 1214.94\ U^4 - 2143.6\ U^5$$

where

$$U = \frac{1}{\sqrt{\frac{EB(COD_{Max} - COD_{Min})}{P_{Max} - P_{Min}}} + 1}$$

E is the Young's modulus, and P the stress. W and B are the dimensions in dicated in Fig. 2. The stress-intensity values were calculated from

$$K = \frac{P}{BW^{1/2}} \quad \frac{(2 + a/w)[0.886 + 4.64(a/w)] - 13.32(a/w)^2 + 14.72(a/w)^3 - 5.6(a/w)^4}{(1 - a/w)^{3/2}}$$

where B and W are the dimensions indicated in Fig. 2 such that B and a > 2.5 $(K_{IC}/YS)^2$, with K_{IC} being the fracture toughness and YS is the tensile yield strength. The crack-length-vs.-number-of-cycles data were converted to fatigue-crack-growth rates (da/dN) using a computer program [16]. Seven to eleven data points were fitted to a second-order polynomial, and the derivative (da/dN) was then obtained for the middle data point. This process was then repeated over the range of data. The da/dN-vs.-ΔK curves were then constructed based upon test data of uninhibited and inhibited solutions.

Commercial inhibitor solutions and aerosols were obtained from the manufacturers or commercial vendors. Reagent-grade chemicals and distilled water were used to make solutions, with the exception of the use of tap water for typical hard-water simulation. The most aggressive solutions used were an aqueous solution containing 0.1M sodium chloride to represent a highly contaminated rinse solution after multiple recycling in the Rinse Facility and the synthetic urine used to simulate the corrosive behavior of natural urine. Most of the tests were conducted in tap water (Wright-Patterson Air Force Base, Dayton, OH). Several tests were performed in the water obtained from the Automated Rinse Facility at MacDill Air Force Base in Tampa, FL. The analysis of the rinse water at MacDill is shown in Table 2. The composition of the synthetic solution, consisting of the most aggressive components of natural urine, is given in Table 3. The corrosive behavior of the synthetic urine was found to closely approximate that of natural urine and was used in most subsequent testing. The polarization behavior of synthetic urine is found to be almost identical to that of natural urine on Al 7075-T6, as shown in Fig. 3.

RESULTS AND DISCUSSION

From the hundreds of polarization and immersion tests that have been conducted in this investigation, a number of representative results have been selected for discussion in this paper. It is important to understand that optimizing inhibitor formulations for aggressive environments such as 0.1M sodium chloride in water and synthetic urine requires many more experiments than will be described here. Initially any new formulation was tested with Al 7075-T6; if the anodic-polarization curve looked encouraging (in terms of current density and the amount of passive region), the performance of the formulation was

checked with high-strength steel and brass. It was found that formulations for aggressive environmental effects that were inhibitive toward the corrosion of high-strength aluminum alloys were generally protective toward other aerospace alloys such as high-strength steels. The converse of this, however, was generally not true.

Figure 4 shows the anodic and cathodic polarization of Al 7075-T6 and Al 2024-T3 in one of the inhibitor formulations. As expected, there is a small difference in the anodic current at the nose level. The difference is more apparent in the cathodic curve; although not clearly shown, the anodic part of the curve has a larger passive region for Al 2024-T3. These two results simply indicate that Al 2024-T3 is more effectively inhibited than Al 7075-T6, possibly due to the fact that Al 2024-T3 is more corrosion resistant than Al 7075-T6 under these conditions. The results of anodic polarization tests of Al 7075-T6 in Wright-Patterson Air Force Base tap water, distilled water, 0.1M NaCl, and one of the inhibitor formulations (0.35% sodium borate, 0.05% sodium nitrite, 0.1% sodium nitrate, 0.01% sodium metasilicate pentahydrate, 50 ppm sodium metaphosphate, and 30 ppm sodium salt of MBT) are shown in Fig. 5.

It is interesting to note that nearly the same level of current density is providing the passivity for aluminum in both distilled water and the inhibited solution. However, the results of the long-time immersion tests show the difference in the corrosion rates of aluminum in these solutions (see Table 3).

Figure 6 shows the performance of the borax-nitrite-base inhibitor as compared to that of sodium nitrate, 1% sodium dichromate, and one of the most promising

commercial inhibitors screened in this investigation. The corrosion current extrapolated against the passive region is least for the borax-nitrite-base inhibitor; at the same time, better passivity is achieved by this formulation. This formulation was found to be effective in inhibiting the corrosion of high-strength steels, aluminum alloys, and copper-bearing materials such as brass.

Borates alone are not particularly effective as inhibitors except for perhaps a limited number of ferrous alloys in mild environments. Nitrites provide a degree of protection to iron and carbon steel in tap water similar to that provided by the chromates; however, higher inhibitor concentrations are required with increasing chloride content to protect against local corrosion [17]. A mixture of borate and nitrite, however, was found to be very effective in the corrosion inhibition of high-strength steels. The borax-nitrite system does not provide satisfactory inhibition to aluminum. Silicates, phosphates, and nitrites are the most commonly known passivators of aluminum. In addition silicates and phosphates [18] provide corrosion inhibition to iron and high-strength steels. The nitrates [19] are known to provide protection to aluminum and its alloys against attack by chloride ions. Hence, a mixture of borate, nitrite, silicate, nitrate and phosphate in the proper concentrations should provide inhibition to iron, steel, and aluminum. Sodium mercaptobenzothiazole was added to the formulation due to the problems expected from the presence of copper ions in the Rinse Facility. The sodium salt of MBT is known [20] to provide inhibition to copper and its alloys. This explains the excellent inhibition provided to aluminum, brass, and steel by the rinse formulation developed in this study as shown by the anodic-polarization results in Fig. 6 and the immersion results in Table 3.

Generally the exact concentration of inhibitor needed depends upon the quality of the water, especially upon the chloride content. The breakdown of the passivity with increasing concentration of chloride ions is demonstrated in Fig. 7. The results show that up to 1000 ppm NaCl, the passive region still occupies nearly 400-mV portion of the anodic curve and that the corrosion current remains the same. This establishes a conservative limit for effective use of this inhibitor in tap water, even in the presence of 500 - 600 ppm NaCl.

Extensive weight-loss tests were conducted to supplement the polarization experiments. Although these tests are time consuming, they have certain advantages over polarization tests, where small mistakes could result in erroneous conclusions. The results of several weight-loss tests are shown in Table 4, and the corrosion rates calculated represent the average values obtained from five to ten tests. The best results were obtained with the formulation of sodium borate, sodium nitrate, sodium nitrite, sodium metasilicate, sodium phosphate, and sodium salts of MBT which was found to be effective in inhibiting the corrosion of aluminum, copper, and steel in Tampa, FL, water (see Table 2). It is interesting to note the difference in corrosion rates of Al 2024-T3 and Al 7075-T6 when immersed in distilled water and inhibited tap water. According to the anodic-polarization curve, the passivity of aluminum is achieved both in distilled water and inhibited water at the same current-density level as that shown in Fig. 5. However, the long-time immersion test results show a corrosion rate of 0.34 - 0.57 mpy for Al 2024-T3 and 0.051 to 0.95 for Al 7075-T6 in distilled water from weight-loss measurements; no corrosion was detected in the borax-nitrite-base inhibitor solution. This illustrates the need for conducting weight-loss tests in parallel with fast screening polarization tests for adequate evaluation of inhibitor-formulation effectiveness. To

expand the experimental variables of importance, some immersion tests were conducted where a) the solution was stirred, b) only the lower-half portion of the specimen was immersed, c) the specimen was intermittently immersed and dried, and d) the specimen was sprayed with the inhibitor solution. The performance of the borax-nitrite-based inhibitor was excellent in all of these situations.

When the more aggressive synthetic urine environments were employed, it was necessary to improve the effectiveness of the inhibitor system. Figure 8 is the anodic polarization plot of Al 7075-T6 in the synthetic-urine solution with the rinse inhibitor [14] added. The values of Tafel slopes and corrosion current calculated from linear polarization tests are given in Table 5. Concurrent with the polarization tests, immersion experiments were conducted. These results are given in Table 6. These results show that only limited protection is provided by the rinse inhibitor in this aggressive environment. The anodic-polarization curve (Fig. 8) indicates a very small passive region. However, the current density corresponding to the break-down potential (pitting potential) has been lowered as compared to that in synthetic urine. Since the synthetic (and natural) urine contains nearly 1% sodium chloride and since sodium nitrate is known to provide inhibition against chloride ions, several formulations with higher concentrations of nitrites and nitrates were used in the development process. The immersion results in Table 6 suggest that better protection is provided by formulation Nos. 2 and 3. This is mainly the effect of higher nitrite and nitrate concentrations, as indicated earlier. Long-term immersion resulted, however, in the pitting of aluminum and steel. This is

thought to be due to the local breakdown of the passive layer by ions present in the complex chemistry of the synthetic urine. At the same time the corrosion rates as shown in Table 5 decreased only by a small amount and there was only slight improvement in the breakdown (of passivity) potential.

Several modifications of rinse-inhibitor formulations [14] by additions of small concentrations of film formers, chloride absorbers, and a number of chelating agents were tested. Figure 9 shows the effect of the addition of low concentrations of isopropylamine, Triton X-114, and Estersulf. The anodic polarization curves exhibit a large passive region, and the linear polarization results shown in Table 5 represent marked lowering of the corrosion current. The immersion test results on Al 7075-T6 were found to be excellent for some of these formulations. There was no visible corrosion, upon close inspection after six to ten months of immersion. No weight loss could be detected and was reported as negligible. This is consistent with the observation that amines, along with silicates and nitrites, [21,22] provide passivation for aluminum. Vermilyea, et al., [23] have also reported that satisfactory passivation is provided to aluminum by salts of organic acids (sulphonic acid, stearic acid, etc.).

Problems were encountered when pieces of aluminum, steel, and brass were immersed together in the synthetic urine. Some of the formulations which exhibited excellent inhibition to aluminum alloys failed to protect the metals under these conditions. Table 7 gives immersion results for selected formulations. There was evidence that copper ions were dissolving out from the brass and interfering with the inhibiting effect of these formulations. When different metallic materials are present simultaneously in one aggressive electrolyte, it becomes necessary to use a combination of different inhibitors in order to provide protection from the effect of interfering ions on all the materials

present. For the combination of steel and copper or copper and aluminum, in which the corrosion of steel--and particularly of aluminum--is frequently increased by copper ions, corrosion of the copper itself may not be significant. In view of this, the concentration of mercaptabenzothiazole or benzothiazole was increased in some formulations. $ZnSO_4$ was also included in several formulations to provide additional protection to steel. The immersion results of some of these combinations are shown in Table 7. Figure 10 contains the anodic polarization curves for aluminum, brass, and steel. The weight-loss measurements combined with the polarization results show that very effective inhibition is provided by 0.35 w/o borate + 0.2 w/o nitrite + 0.2 w/o nitrate + 0.01 w/o silicate + 50 ppm phosphate + 50 ppm MBT + 125 ppm Richonate 1850. Weight-loss results clearly demonstrate the much improved protection provided by this formulation.

Certain formulations which are effective for general corrosion inhibition actually accelerate corrosion in crevice situations and are crack accelerators. In order to evaluate the effectiveness of the inhibitors in all practical applications, low-cycle corrosion-fatigue tests were conducted. Figure 11 illustrates the corrosion-fatigue behavior of Al 7075-T6 in synthetic urine and synthetic urine inhibited by the formulation developed as a result of the present study. The air result is shown for comparison. The reduction in the fatigue-crack-growth rate due to the addition of the inhibitor can be clearly observed. It is interesting to note that the crack-growth rate is two to three times lower in Region II, as compared to the air value, and five to six times lower than that obtained in uninhibited synthetic urine. The difference in the crack-growth rates in air and inhibited synthetic urine may be due to the fact that the air value is not a vacuum value and, in general, is higher. This

Some problems have arisen with the maintenance of a discrete population of aircraft within the test group and the control group, since some aircraft have been transferred to other stations. It now appears, however, that at least one-half of both groups will be maintained at MacDill Air Force Base for a sufficient time to complete a two to three year test program. As far as the authors know, this is the first attempt to actually track maintenance costs in the use of aircraft rinsing facilities. The general observation has been that this practice is "beneficial," but no cost-effectiveness studies have been conducted.

A view of the Rinse Facility at MacDill Air Force Base is given in Fig. 13. The holding tanks for rinse water, major piping and pumping systems, return tanks, etc., are located underground. Only the control facilities are above ground. The inhibitors are added to a tank holding ~ 11,000 liters of water (~ 3,000 gallons). A forced-air system mixes the inhibitors to effect full dissolution within about 1 min. after addition, and a conductivity bridge is used to monitor inhibitor concentration in the rinse water. When an aircraft passes over an induction coil on the runway, it triggers the rinse system to deliver ~ 560 liters of rinse water in a 15 - 20 sec. time period, pumping at ~ 2,250 liters/min. at the maximum point after startup. Water jets below the runway/taxiway surface direct water to various parts of the aircraft. An F-4 aircraft as it taxis through the facility is shown in Fig. 14.

The method of monitoring the rinse-inhibitor concentration by following the change in conductivity is shown in Fig. 15. Laboratory experiments have shown this to be a reliable and accurate method. The Rinse Facility provides for discharge of the effluent water periodically as contaminants build up

suggests that the introduction of the inhibitor nearly eliminates the environmental influence upon the crack growth. For applications involving high-strength aerospace alloys, it is important to establish this inhibition or elimination of the environmental acceleration of crack-growth rates in the corrosion-inhibiting medium.

In a similar manner the rinse inhibitor has been found to eliminate the environmental effects on crack-growth rates. In Fig. 12 da/dN-vs.-ΔK is shown for Al 7075-T6 in the rinse inhibitor formulation.

RINSE-FACILITY APPLICATION

The borax-nitrite-based inhibitor with additions of nitrate, polyphosphate, metasilicate, and mercaptobenzothiazole was recommended for use in the Rinse Facility as a result of the research efforts in 1978. Experimental use commenced in the summer of 1978 with inhibitors added to the rinse water. In August of 1979 a full-scale test program to evaluate the use of an inhibited rinse was begun on F-4 aircraft stationed at MacDill Air Force Base, FL. The missions of these aircraft emphasize over-sea water exercises at low altitudes; MacDill Air Force Base itself is surrounded on three sides by salt water. In addition the Tampa industrial area contributes substantial suspended particulates and sulfur dioxide to the atmosphere. Thus, it is considered to be a prime area for conducting such tests for the use of automated rinsing to reduce contamination of surfaces and subsequent increased corrosion on operational aircraft. Twenty-five F-4 fighter aircraft were selected to use the Rinse Facility, and a second group of twenty-five F-4's not using the facility was designated as a control group. This test program is still underway, and it is planned that tracking of maintenance costs and corrosion damage will be completed within the next year.

and for the removal of oily water to appropriate disposal facilities. In actual practice, 100 - 200 liters of water are lost on the runway and not returned to the holding tanks after each aircraft rinse. Fresh water is added to the holding tank at this point, and tracking of the inhibitor concentration is essential in determining when additional inhibitors should be added. While this could be accomplished automatically, in the current test it is done manually. Recent experiments have indicated that the action of the rinse-inhibitor formulation may be improved by small additions of a surfactant material (in the parts-per-million level). This change in the rinse-inhibitor composition is planned for late spring of 1981.

CONCLUSIONS

Multifunctional nonchromate inhibitors have been developed for the USAF Automated Rinse Facility to reduce corrosion maintenance costs by removing corrosive contaminants from aircraft which operate in aggressive environments such as those encountered near the sea coast. These inhibitor systems are low cost, water soluble, nontoxic formulations which are effective against general corrosion, localized corrosion, and environmentally assisted crack growth under conditions of stress corrosion and corrosion fatigue.

A synthetic-urine solution has been formulated and found to experimentally reproduce the corrosion behavior of natural urine which is considered to be the most aggressive corrosive environment in the lower-cargo bay, galley, and comfort-station areas of large aircraft.

Extensive polarization and immersion experiments have been conducted to determine and optimize the effectiveness of various inhibitor systems in aggressive media.

A borax-nitrite-based inhibitor containing small additions of nitrate, silicate, phosphate, and mercaptobenzothiazole has been found to provide excellent corrosion protection for the high-strength aluminum and steel alloys used in aerospace applications and for the copper-bearing alloys used in electronic components and in parts of the Rinse Facility. For the bilge environments this inhibitor formulation was improved to provide long-term effectiveness in very aggressive environments. The new formulation is also a borax-nitrite-based inhibitor with 0.35% (w/o) borate, 0.2% nitrite, 0.2% nitrate, 0.01% silicate, 50 ppm phosphate, 50 ppm MBT, and 125 ppm Richonate 1850.

Environmental effects upon crack-growth rates of aluminum and high-strength steel alloys were eliminated--reducing the rates in corrosion fatigue as compared to those obtained in air.

A test program using these inhibitors is currently underway in the USAF Automated Rinse Facility at MacDill Air Force Base, FL. Tracking of maintenance costs and corrosion damage is being conducted to determine the effectiveness of the inhibited rinse in reducing corrosion costs.

REFERENCES

1. L. H. Bennett, J. Kruger, R. L. Parker, E. Passaglia, C. Reimann, A. W. Ruff, and H. Yakowitz, Economic Effects of Metallic Corrosion in the United States, Part I and II, NBS Special Publication 511-1,2 (U. S. Department of Commerce, National Bureau of Standards, Washington, D.C., May 1978).

2. J. DeLuccia, Naval Air Development Center, Warminster, PA, Private Communication, 1-2 December 1975.

3. Data presented at AFLC Corrosion Managers Conference, WRALC, Robins AFB, GA, October 1975.

4. "1975 AFML-AFOSR Corrosion Workshop." AFML-TR-77-175 (Air Force Materials Laboratory, Wright-Patterson AFB, OH, 1977).

5. Corrosion Inhibitors (C. C. Nathan, ed.) (National Association of Corrosion Engineers, Houston, TX, December 1974).

6. The Corrosion and Oxidation of Metals (Second Supplementary Volume) (U. R. Evans, ed.) (Edward Arnold Publishers, Ltd., Great Britain, 1976).

7. J. Green and D. B. Boies, "Corrosion-Inhibiting Compositions," U. S. Patent No. 2,815,328, 3 December 1957.

8. J. T. Bregman and D. B. Boies, Corrosion 14, 275 (1958).

9. K. Bhansali, C. T. Lynch, F. Vahldiek, and R. Summitt, "Effect of Multifunctional Inhibitors on Crack Propagation Rates of High Strength Steels in Corrosive Environments," Prepared discussion presented at the Conference on the Effect of Hydrogen on Mechanical Behavior of Materials, Moran, WY, 7-11 September 1975.

10. F. N. Speller, Discussion, Proc. ASTM 36 (Part 2), 695 (1936).

11. C. T. Lynch, F. Vahldiek, K. J. Bhansali, and R. Summitt, "Inhibition of Environmentally Enhanced Crack Growth Rates in High Strength Steels," Symposium on Environment Sensitive Fracture of Engineering Materials, AIME Meeting, Chicago, IL, 26 October 1977. Proceedings Volume, AIME, 1979, pp. 639-658.

12. C. T. Lynch, K. J. Bhansali, and P. A. Parrish, "Inhibition of Crack Propagation of High-Strength Steels through Single- and Multi-Functional Inhibitors," AFML-TR-76-120 (Air Force Materials Laboratory, Wright-Patterson AFB, OH, 1976).

13. N. I. Saz, Dangerous Properties of Industrial Materials (Second Edition) (Reinhold Publishing Corporation, NY, 1963).

14. M. Khobaib, "Development of Corrosion Inhibitors," AFML-TR-79-4127, Part II (Air Force Materials Laboratory, Wright-Patterson AFB, OH, September 1979).

15. M. Khobaib, C. T. Lynch, and F. W. Vahldiek, "Inhibition of Corrosion Fatigue in High-Strength Aluminum Alloys," To be published in Corrosion.

16. N. E. Ashbaugh, "Mechanical Property Testing and Materials Evaluation and Modeling," AFML-TR-79-4127, Part I (Air Force Materials Laboratory, Wright-Patterson AFB, OH, September 1979).

17. J. Weber, Br. Corr. J. 14(2), 69 (1979).

18. S. O. Lahandy and L. Kastelan, Proc. 4th European Symposium on Corrosion Inhibitors, Ferrara, Italy, 1975, p. 223.

19. H. Bohni and H. H. Uhlig, J. Electrochem Soc. 116, 906 (1969).

20. J. B. Cotton and I. R. Scholes, Br. Corr. J. 2. 1 (1967).

21. G. Schick, Mater. Perf. 23 (February 1975).

22. A. H. Roebuck and T. R. Pritchett, Mater. Perf. 16 (June 1966).

23. D. A. Vermilyea, J. F. Brown, and D. R. Ochae, J. Electrochem. Soc. 783 (June 1970).

TABLE 1

INHIBITORS

A. GENERAL Considerations

1. Multifunctional
   - Cathodic
   - Anodic
   - Chloride Absorbers
   - Buffers
2. Solubility Range
3. Influence on Hydrogen Entry Rates
4. Toxicity
5. Cost

B. COMPOUNDS

1. Cathodic: Polyphosphate, Zinc, Silicate
2. Anodic: Orthophosphate, Chromate, Ferrocyanide, Nitrite
3. Combinations:
   - Polyphosphate-Chromate
   - Polyphosphate-Ferrocyanide
   - Borax-Nitrite
   - Benzoate-Nitrite
   - Silicate-Chromate
4. Film Formers:
   - Emulsified or Soluble Oils
   - Octadecylamine
   - Long-Chain Amines
   - Alcohols and Carboxylic Acids

C. GENERAL CONSIDERATIONS

1. Stress Corrosion and Corrosion Fatigue
2. Special Bilge Environments
3. Long Term Effectiveness
4. Method of Application

TABLE 2

CITY OF TAMPA - WATER DEPARTMENT

AVERAGE DAILY ANALYSIS OF FINISHED WATER

	Color Units	Total Hardness $CaCO_3$	Total Alkalinity $CaCO_3$	Calcium Hardness $CaCO_3$	pH Units	Resid. Chlorine	Temp °F
Max.	4	[illegible]	118	164	7.6	3.5	81
Min.	3	171	103	142	7.4	2.7	77
Average	3	181	110	154	7.5	3.2	79

JUNE MONTHLY COMPOSITE
COMPLETE ANALYSIS
(Results expressed in milligrams per liter)

Calcium	Ca	61.6
Magnesium	Mg	7.00
Sulfates	SO_4	55.
Chlorides	Cl	57.
Fluorides	F	0.32
Sodium	Na	36.0
Potassium	K	3.2
Nitrates	NO_3	0.08
Silica	SiO_2	4.4
Manganese	Mn	0.0
Iron	Fe	0.08
Bicarbonates	HCO_3	136
Phosphates	PO_4	0.26
Aluminum	Al	0.30
Total Solids		350
Total Hardness	$CaCO_3$	180
Total Alkalinity	$CaCO_3$	112
Non-Carb. Hardness	$CaCO_3$	68
Amonia-Nitrogen	NH_3	ND
L.A.S.	MBAS	0.03
Copper	Cu	0.03
Color	Units	3
Turbidity	Units	0.7
pH	Units	7.6
Temperature	°F	76
Sp. Conductivity	MMhos	425
B.O.D. (5 days at 20°C)		0.2

TABLE 3

INGREDIENTS OF SYNTHETIC URINE

(wt in gm/liter)

Urea	20.60
5-Hydroxyindoleacetic Acid	0.0045
Uric Acid	0.052
Glucuronic Acid	0.431
Oxalic Acid	0.031
Citric Acid	0.462
Glycolic Acid	0.042
Creatine	0.0721
Guanidinoacetic Acid	0.027
Formic Acid	0.013
Glucose	0.072
Ammonium Sulfate	4.00
Potassium Phosphate	0.175
Potassium Chloride	0.0100
Potassium Bromide	0.008
Sodium Chloride	10.00
P-Cresol	0.087
Creatinine	1.500
Acetone	0.0001
Hydroxyquinoline-2 Carboxylic Acid	0.0028
Potassium Sulfate	0.134

TABLE 4

IMMERSION TEST RESULTS

No. of Tests	Electrolyte	pH Initial	pH Final	Surface Appearance 2024-T3	Surface Appearance 7075-T6	Corrosion Rate (mpy) 2024-T3	Corrosion Rate (mpy) 7075-T6	Remarks
5	Tap Water (WPAFB)	7.62	8.48	Stained; several pits.	Couple of oxide patches; several pits.	0.034 to 0.65	0.38 to 0.78	Should be inhibited.
5	0.1M NaCl in Distilled Water	6.95	7.50	Entire surface corroded; several pits.	Entire surface corroded; several pits.	1.38 to 1.98	1.54 to 2.4	Should be inhibited.
5	NALCO 39L (18cc/liter) in Tap Water	9.24	9.00	Looks as original.	Looks as original.	$<10^{-4}$	$<10^{-4}$	Very good.
3	Betz 545 (500 ppm) in Tap Water	8.83	8.42	Corners and edges badly pitted; surface fairly clean.	Entire surface dark; several pits.	0.017 to 0.063	0.028 to 0.054	Poor.
5	Calgon Inhibitor CS (4000 ppm) in Tap Water	8.90	8.80	Light tinted scale all over; no visible pits.	Light tinted scale all over; no visible pits.	0.067 to 0.088	0.083 to 0.092	Poor.
3	1% Sodium Dichromate in Tap Water	5.80	5.80	Surface looks as original.	Surface looks as original.	$<10^{-4}$	$<10^{-4}$	Very good.
3	0.1% (Sodium Metasilicate + Sodium Polyphosphate) in Tap Water	8.64	8.45	Surface looks as original.	Surface looks as original	$<10^{-4}$	$<10^{-4}$	Very good.
8	0.35% Sodium Borate + 0.05 Sodium Nitrite + 0.1 Sodium Nitrate + 0.01 Sodium Silicate + 50 ppm Polyphosphate + 30 ppm MBT in Tap Water	8.78	8.64	Surface looks as original.	Surface looks as original.	$<10^{-4}$	$<10^{-4}$	Excellent.

TABLE 5

TAFEL SLOPES AND CORROSION CURRENTS
IN DIFFERENT ELECTROLYTES
OF Al 7075-T6

ELECTROLYTE (wt%)	TAFEL SLOPES (mV/decade) ba	bc	i_{corr} ($\mu A/cm^2$)
Synthetic Urine	100	135	6.24
Synthetic Urine + Rinse Inhibitor	120	160	3.42
Synthetic Urine + Rinse Inhibitor + 0.15 Nitrite + 0.1 Nitrate (INH)	160	130	2.44
Synthetic Urine + INH + 75 ppm Triton X-114	100	150	0.78
Synthetic Urine + INH + 100 ppm Estersulf	120	90	1.08
Synthetic Urine + INH + 100 ppm Isopropylamine	120	80	1.41
Synthetic Urine + INH + 125 ppm Richonate 1850	100	125	0.544
Synthetic Urine + INH + 125 ppm Richonate + 500 ppm $ZnSO_4$ + 50 ppm MBT	120	135	0.63

TABLE 6

IMMERSION TEST RESULTS ON Al 7075-T6

TYPE NO.	ELECTROLYTE (wt%)	mpy	pH INITIAL	pH FINAL	TIME OF EXPOSURE	SURFACE APPEARANCE
1	Synthetic Urine	0.23	5.6	5.8	3 Mo.	Nearly 20% surface area pitted.
2	Natural Urine	0.18	5.8	6.0	3 Mo.	Nearly 25% surface area pitted.
3	Synthetic Urine + Rinse Inhibitor	0.12	8.30	8.25	3 Mo.	Several pits on the surface.
4	Synthetic Urine + Rinse Inhibitor + 0.15 Nitrite + 0.1 Nitrate	0.078	8.35	8.35	3 Mo.	Surface clean, very light corrosion.
5	Synthetic Urine + Rinse Inhibitor + 0.25 Nitrite + 0.2 Nitrate	Negl.	8.40	8.35	3 Mo.	Clean as original. No sign of corrosion.
6	No. 4 + 25 ppm Triton X-114	Negl.	8.30	8.30	3 Mo.	Clean as original. No sign of corrosion.
7	No. 4 + 75 ppm Estersulf	Negl.	8.35	8.30	3 Mo.	Clean as original. No sign of corrosion.

TABLE 7

TEST RESULTS OF Al, BRASS, AND STEEL SPECIMENS IMMERSED TOGETHER

SPECIMEN	ELECTROLYTE (wt%)	pH INITIAL	pH FINAL	TIME OF EXPOSURE	SURFACE APPEARANCE
Al 7075-T6	0.35 Borate + 0.2 Nitrite + 0.2 Nitrate + 0.01 Silicate + 50 ppm	8.45	8.30	3 Mo.	50% area pitted.
Brass	Phosphate + 25 ppm MBT (INH) + 250 ppm Isopropylamine in			3 Mo.	Slowly dissolving into solution.
Steel	Synthetic Urine,			3 Mo.	Several pits.
Al 7075-T6	INH + 25 ppm Triton X-114 in	7.75	7.60	3 Mo.	Several large pits.
Brass	Synthetic Urine.			3 Mo.	Clean but dull.
Steel				3 Mo.	Pitted - dull.
Al 7075-T6	INH + 25 ppm Triton X-114	7.65	7.60	3 Mo.	Clean and shiny.
Brass	+ 100 ppm $ZnSO_4$ in			3 Mo.	Clean.
Steel	Synthetic Urine.			3 Mo.	One corner pitted.
Al 7075-T6	INH + 75 ppm MBT + 125 ppm Richonate	8.25	8.20	3 Mo.	Clean and shiny as original.
Brass	1850 in Synthetic Urine.			3 Mo.	Clean, as original.
Steel				3 Mo.	Clean, as original.
Al 7075-T6	INH + 50 ppm Estersulf	8.30	8.20	3 Mo.	Clean, few pits.
Brass	in Synthetic			3 Mo.	Clean.
Steel	Urine.			3 Mo.	Clean, but several fine pits.
Al 7075-T6	ANL Guard in Synthetic Urine.	6.90	6.95	3 Mo.	Nearly 20% area badly pitted.
Brass				3 Mo.	Nearly 20% area badly pitted.
Steel				3 Mo.	More than 50% area badly pitted.
Al 7075-T6	1% Boeshield T-9 in Synthetic Urine.	5.10	5.15	3 Mo.	Several large pits and number of small pits.
Brass				3 Mo.	Dull, one pit.
Steel				3 Mo.	Several large pits and number of small dark pits.

Figure 1. Galvanic Couple.

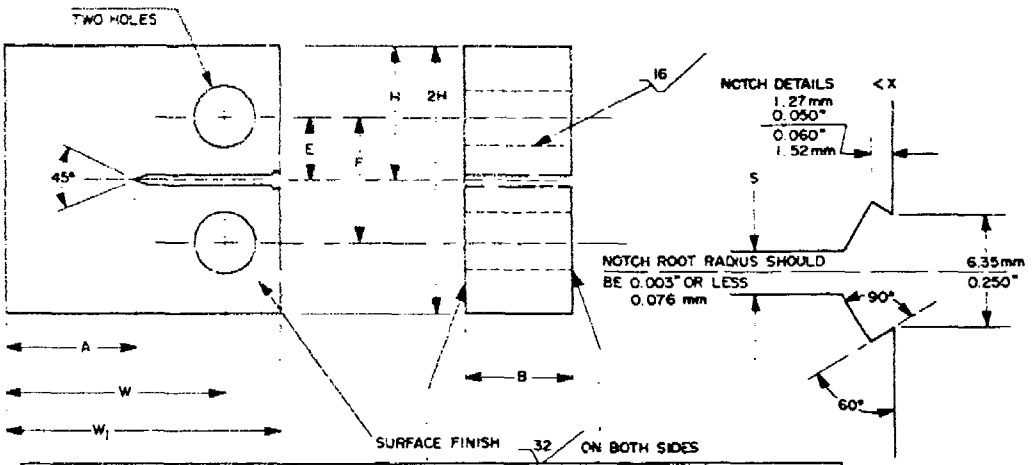

MATERIAL	E	A	W	W_1	S	E	F	H	D
ALUMINUM	25.4mm	29.2mm	50.8mm	53.5mm	2.35mm	13.97mm	27.94mm	30.48mm	12.7mm
STEEL	19.05mm	22.22mm	38.10mm	47.62mm	1.90mm	10.46mm	20.95mm	22.86mm	9.52mm

Figure 2. Compact-Tension Specimen.

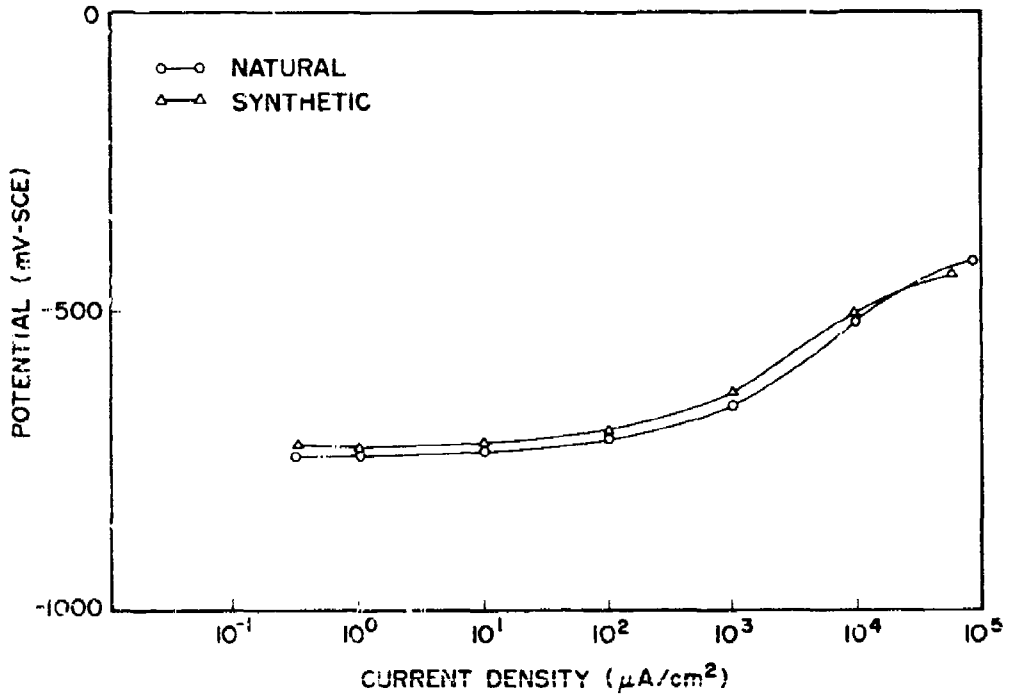

Figure 3. Comparison of Anodic Polarization Behavior of Al 7075-T6 in Synthetic and Natural Urine.

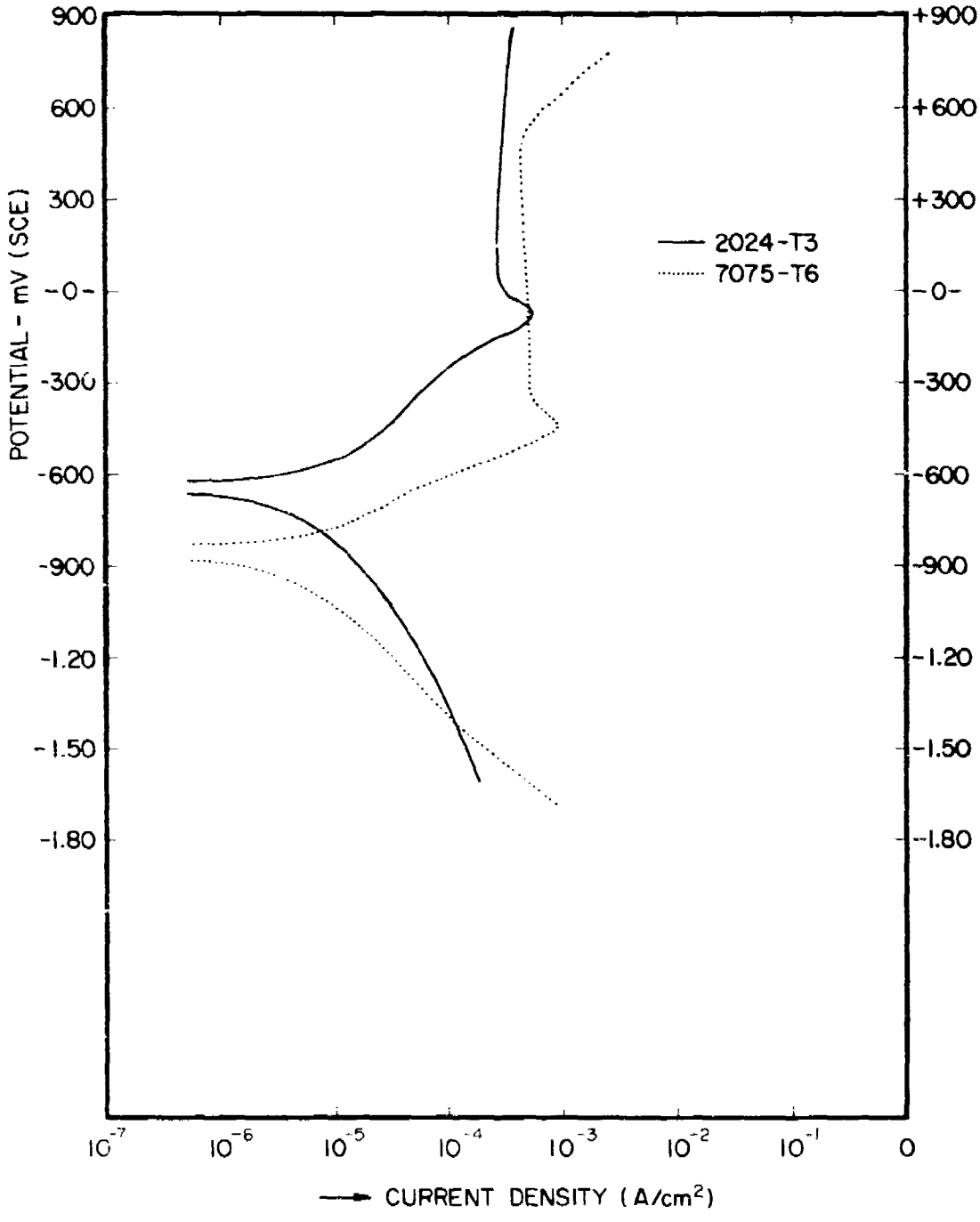

Figure 4. Anodic and Cathodic Polarization Curves for Al 2024-T3 and Al 7075-T6 in an Inhibited Solution.

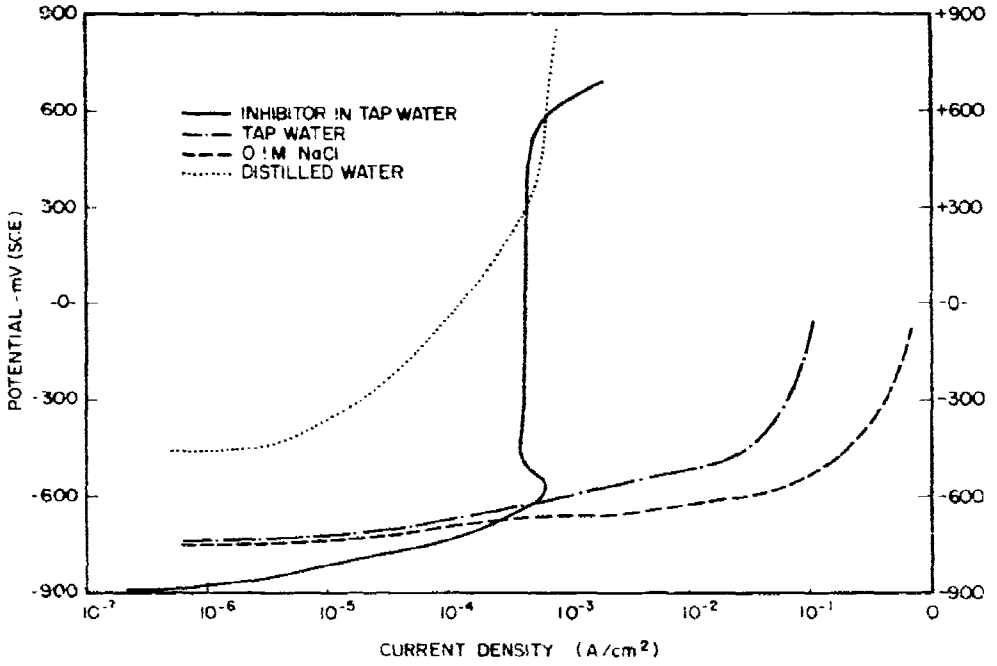

Figure 5. Anodic Polarization Curves for Al 7075-T6 in Tap Water, Distilled Water, 0.1M NaCl and Inhibitor.

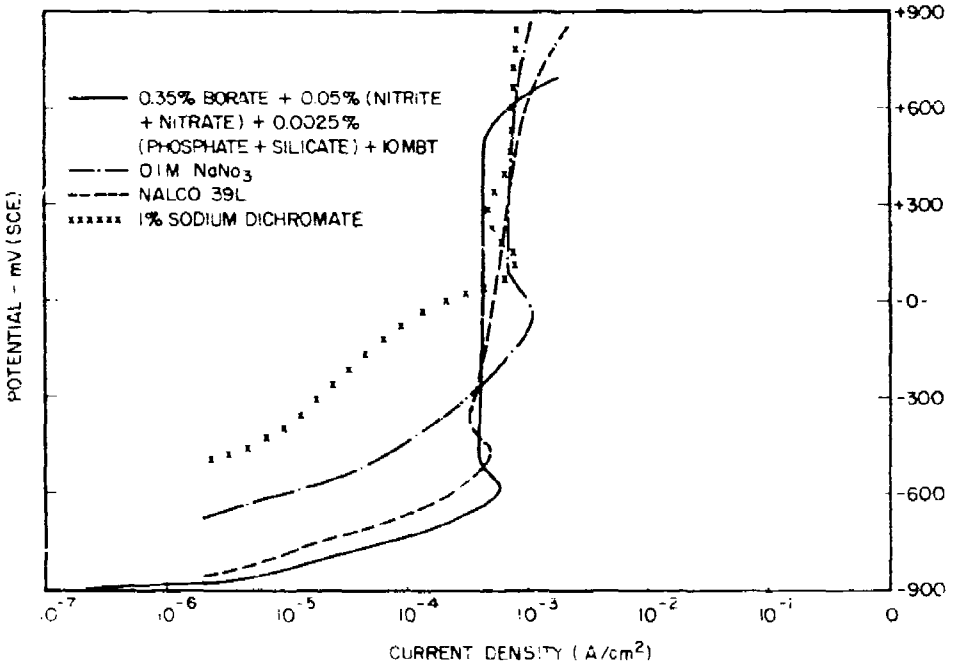

Figure 6. Anodic Polarization Behavior of Al 7075-T6 in Different Inhibitors.

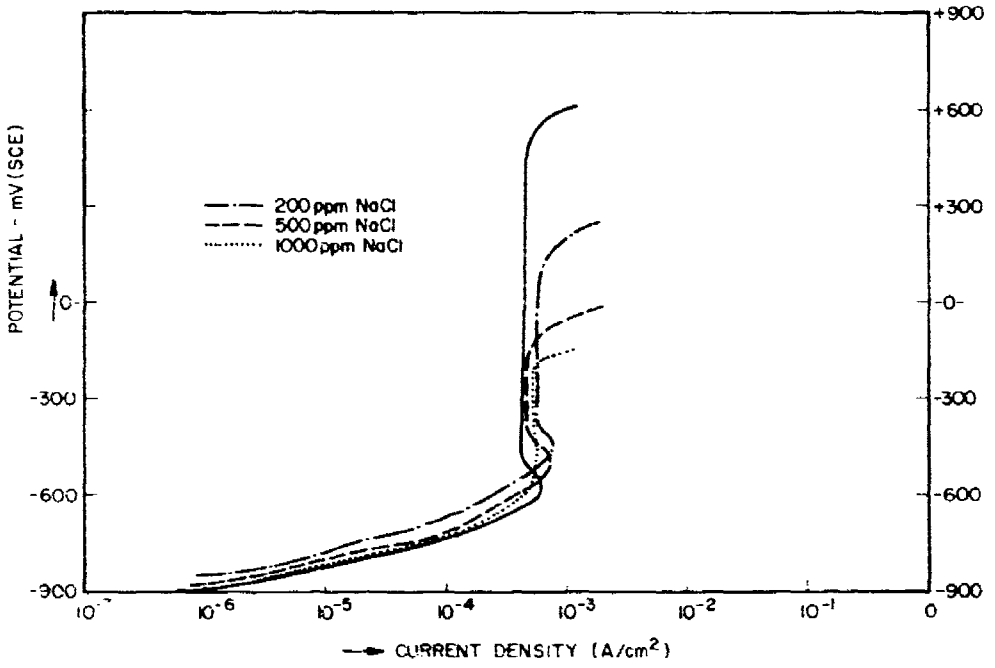

Figure 7. Effect of Increasing Chloride Concentration Upon the Pitting Behavior of Al 7075-T6 in an Inhibited Solution.

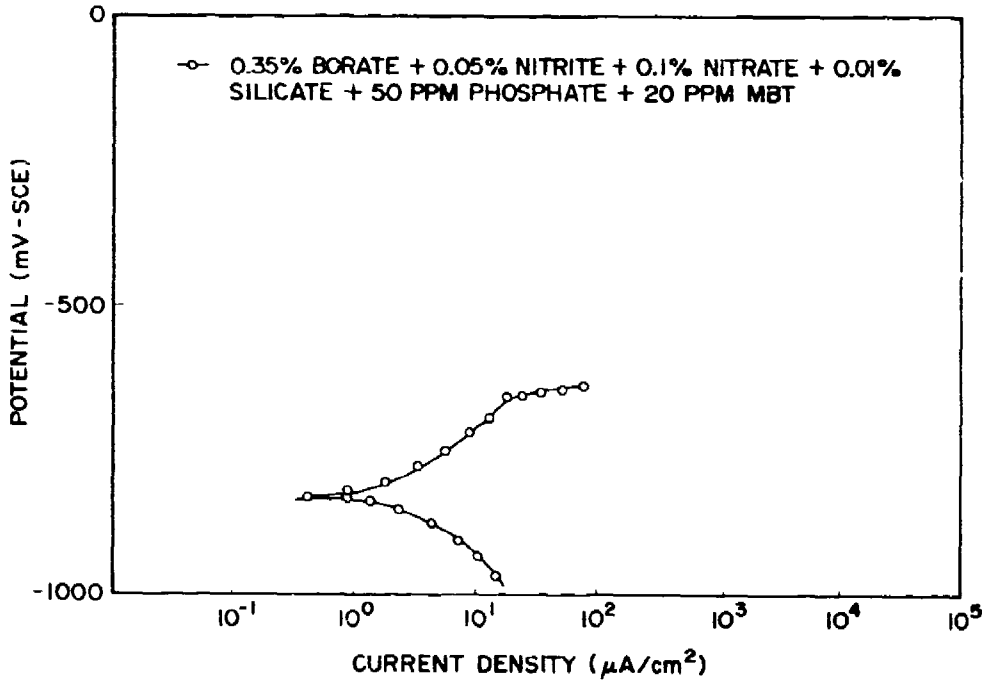

Figure 8. Anodic and Cathodic Polarization Behavior of Al 7075-T6 in Synthetic Urine Inhibited by Rinse Formulation.

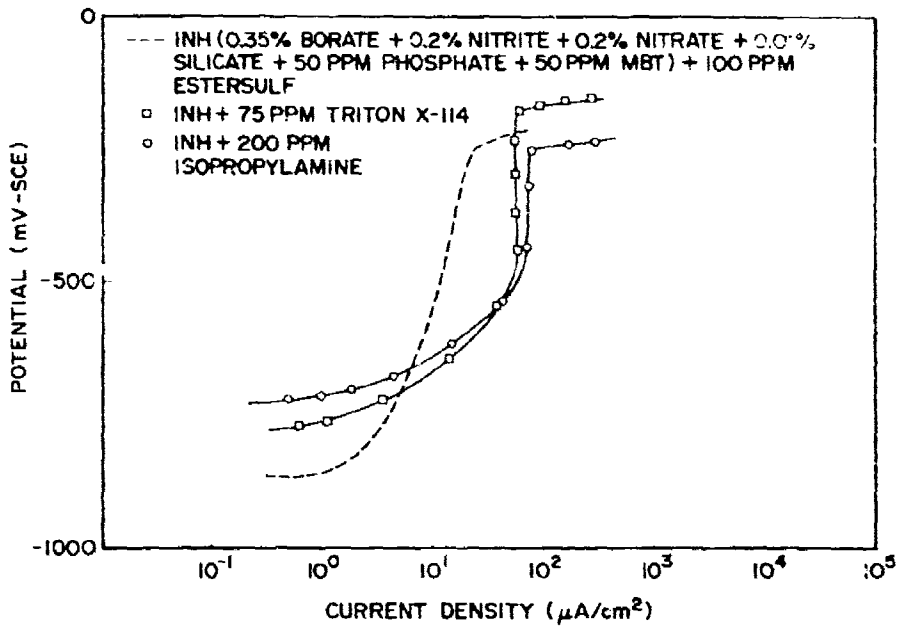

Figure 9. Effect of Addition of Estersulf, Triton X-114, and Isopropylamine Upon the Anodic Polarization of Al 7075-T6.

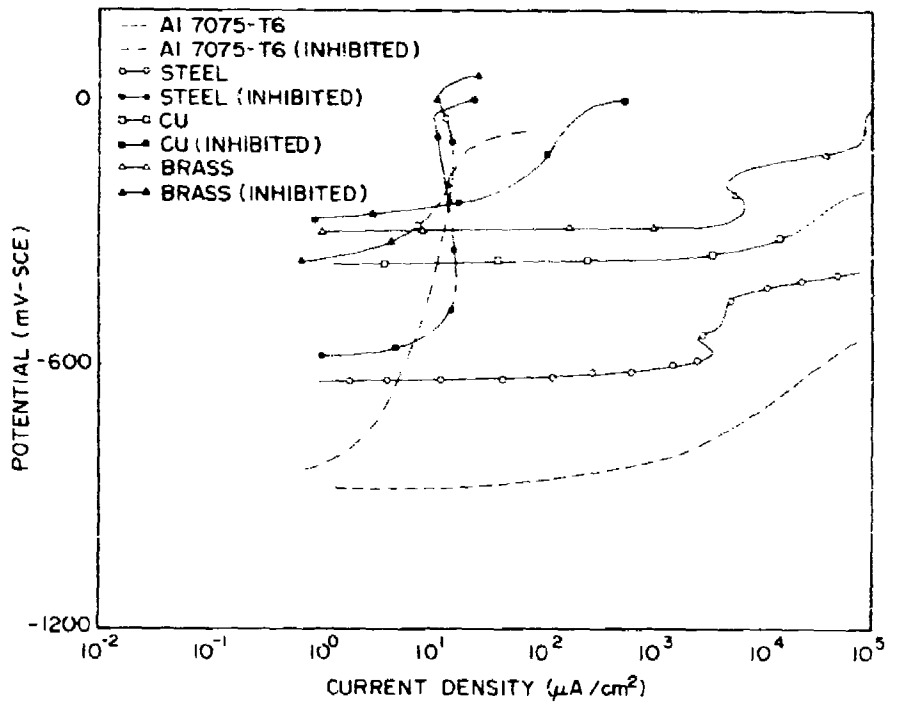

Figure 10. Anodic Polarization Behavior of Al 7075-T6, Steel, Copper, and Brass in Inhibited Synthetic Urine.

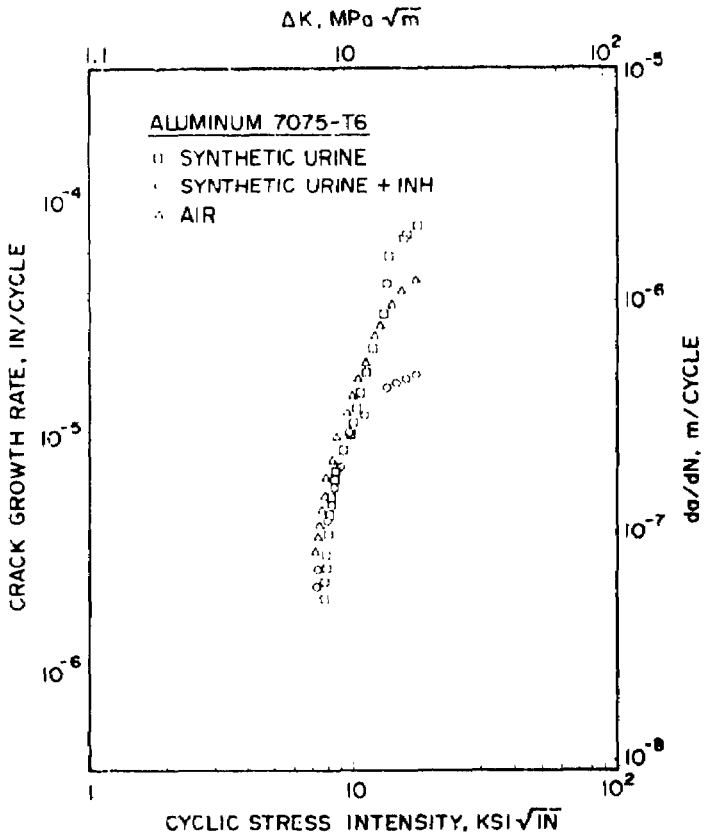

Figure 11. Comparison of Crack-Growth Rates of Al 7075-T6 in Air and Inhibited and Uninhibited Synthetic Urine.

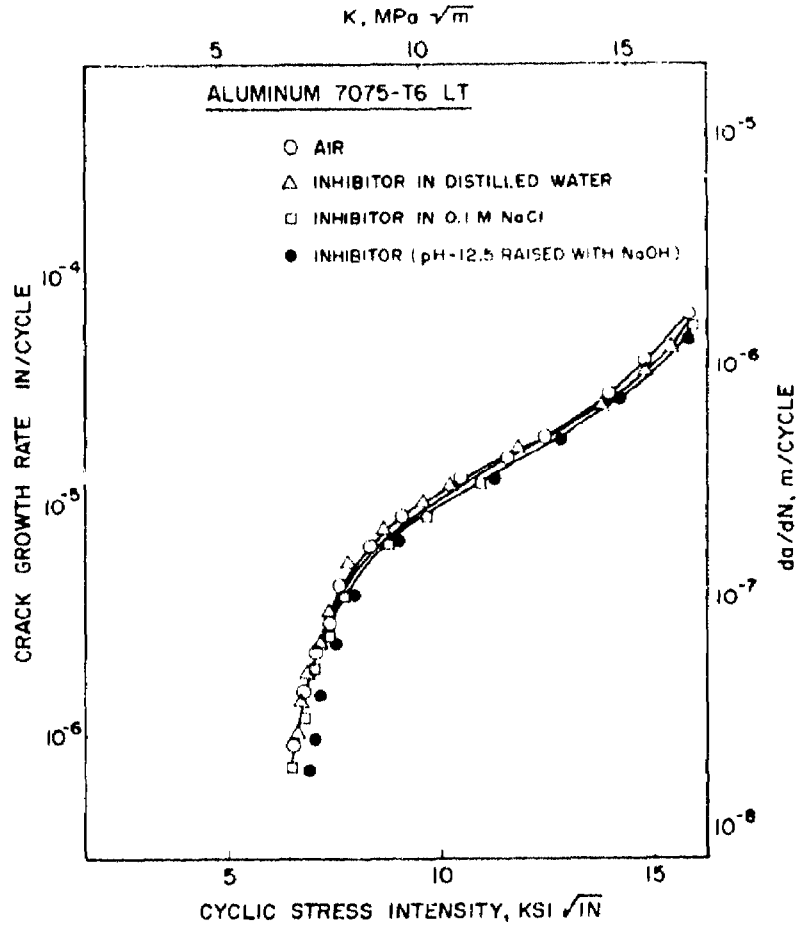

Figure 12. Effect of Rinse Inhibitor Upon Crack-Growth Rates of Al 7075-T6 LT.

Figure 13. View of the USAF Automated Rinse Facility.

Figure 14. F-4 Aircraft Taxiing Through the Rinse Facility.

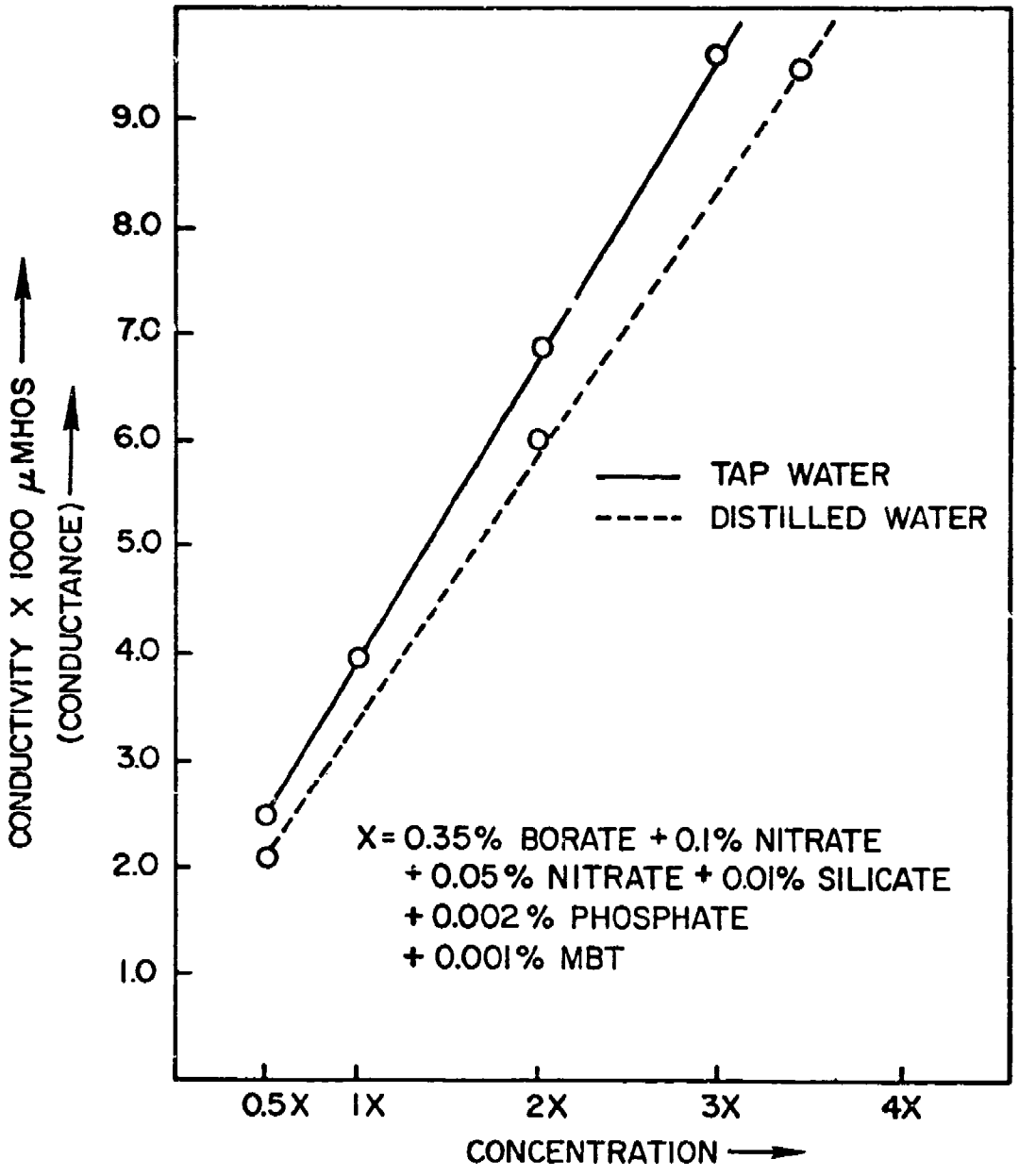

Figure 15. Calibration Chart of Conductivity as a Function of Inhibitor Concentration.

Corrosion Control in Commercial Airplanes

J.C. McMillan
Chief, Materials Technology-Airplane Programs

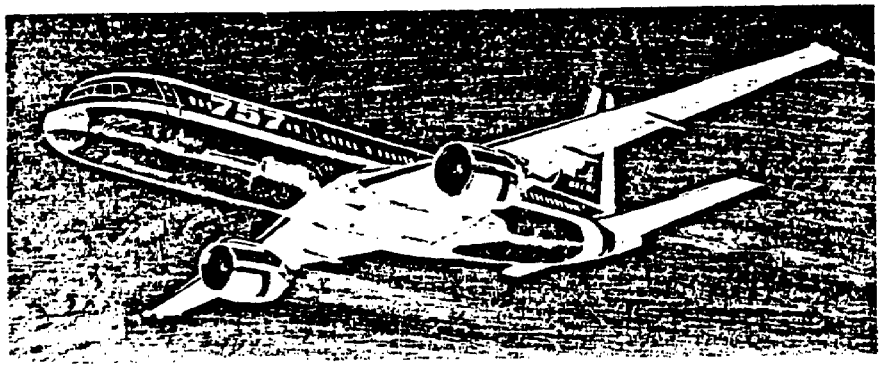

Boeing Commercial Airplane Company

November 5-7, 1980

Tri-service Conference on Corrosion ■ United States Air Force Academy, Colorado

BMT80-188

Corrosion Control in Commercial Airplanes

In production airplane

- Monitor fleet experience
- Identify corrosion problems
- Initiate correction action
  - Production change
  - In service action
  - Establish new design guidelines

New airplane designs

- Establish design objectives
- Design for avoidance
- Design for protection

Evolution of Major Corrosion Improvements

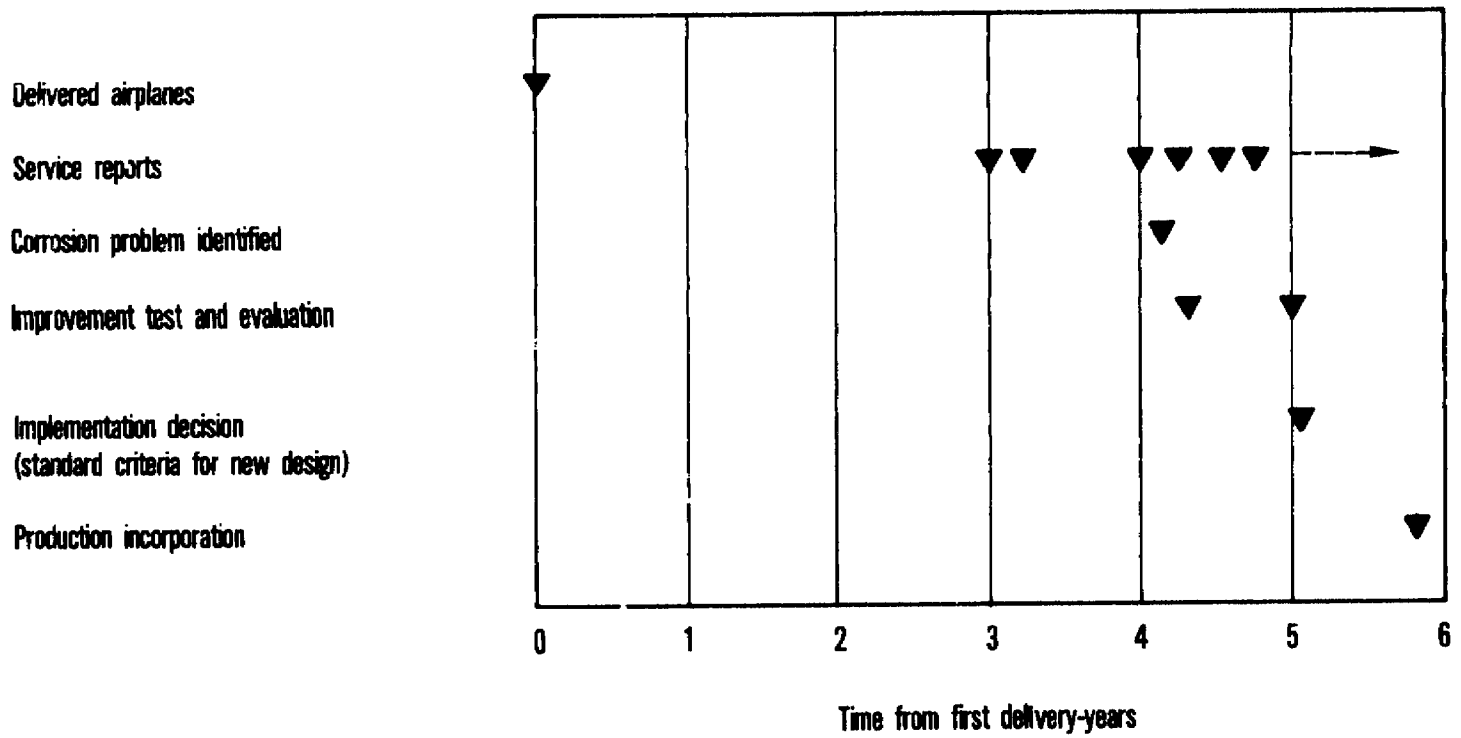

Corrosion Control Improvements
New Airplane Starting Point

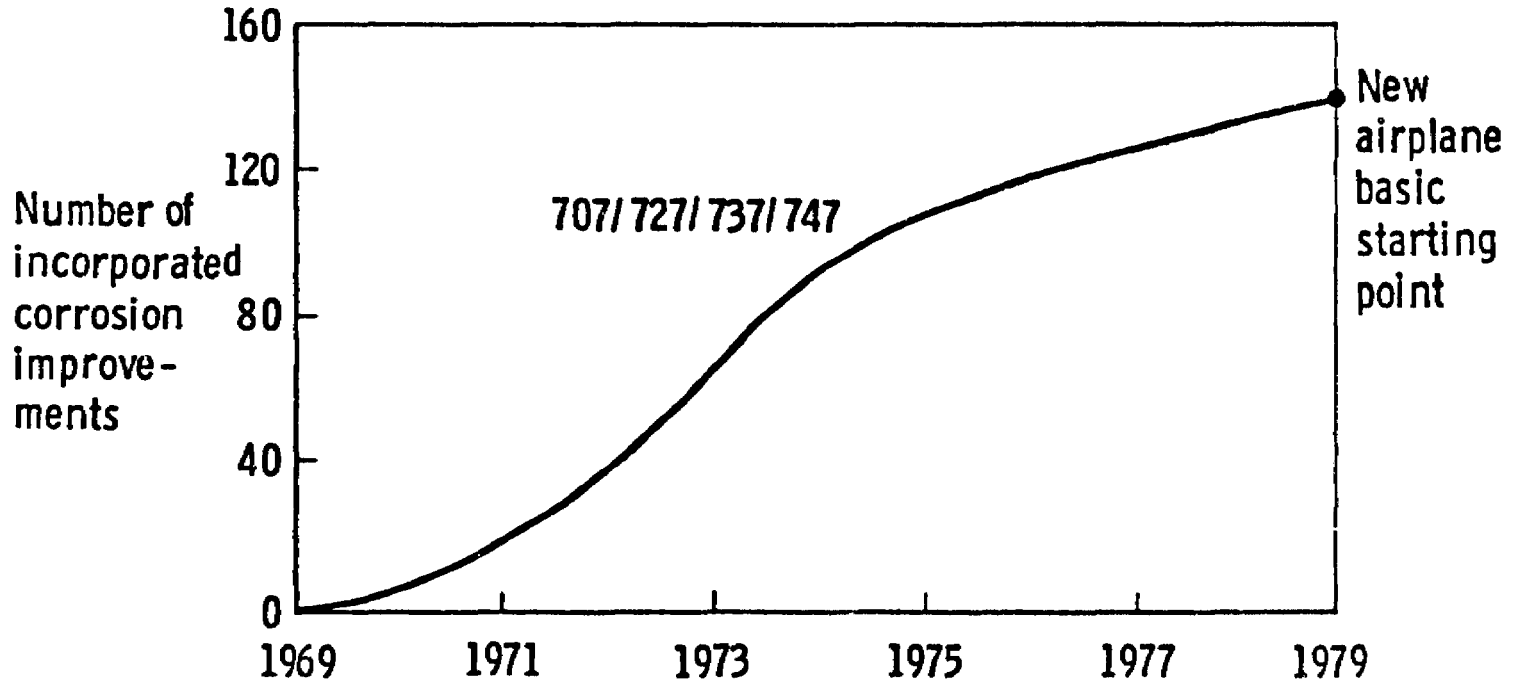

BMT80-52-A

New Airplane Corrosion Control
Objectives

- Control corrosion to assure structural integrity of the airplane with normal airline maintenance over a 20 year period

New Airplane Corrosion Control
Corrosion Control Design Handbook

BMT80-208

New Airplane Corrosion Control Organization

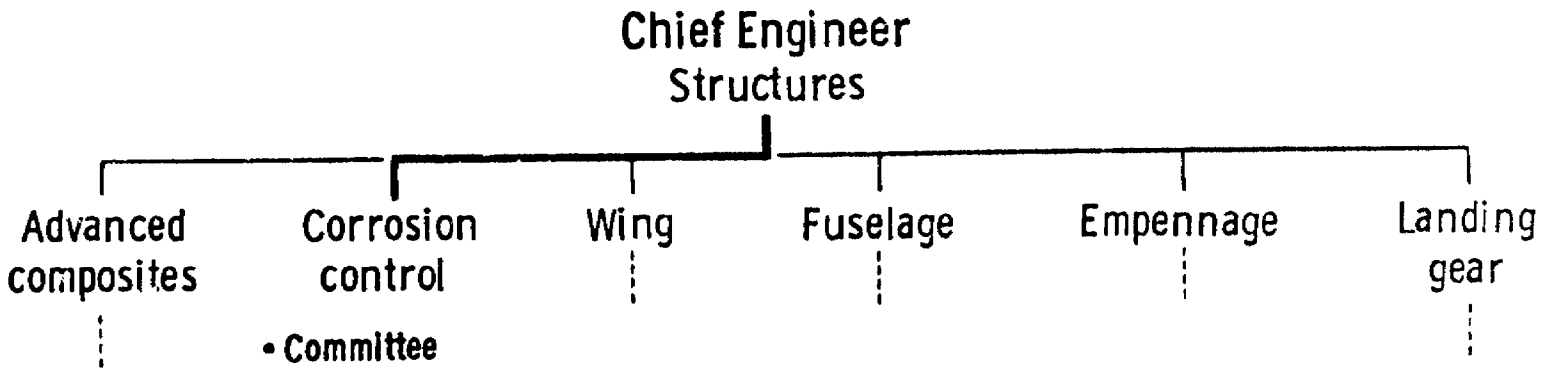

- Committee
  - -Design
  - -Stress
  - -Materials
  - -Systems
  - -Interiors
  - -Manufacturing
  - -Quality control
- Policy
  - -Design
  - -Sealing
  - -Drainage
  - -Finishes

BMT80-32-A

New Airplane Corrosion Control
Design for Corrosion Avoidance

- Materials and processes selection
- Entries, galleys and lavatories
- Drainage

New Airplane Corrosion Control
Materials Selection

- Aluminum alloys
  - Extensive use of stress corrosion and corrosion resistant tempers
  - No 7079 alloy
- Magnesium
  - No structural applications

New Airplane Corrosion Control
Metal Bonding Guidelines

- Phosphoric acid anodize surface preparation
- Corrosion inhibiting adhesive primer
- Corrosion resistant-nonperforated core
- No bonding in bilge
- No cold bonding
- No bonded 7075 clad
- High toughness, high durability 250° F cure adhesives

New Airplane Corrosion Control
Metal Bonding Applications

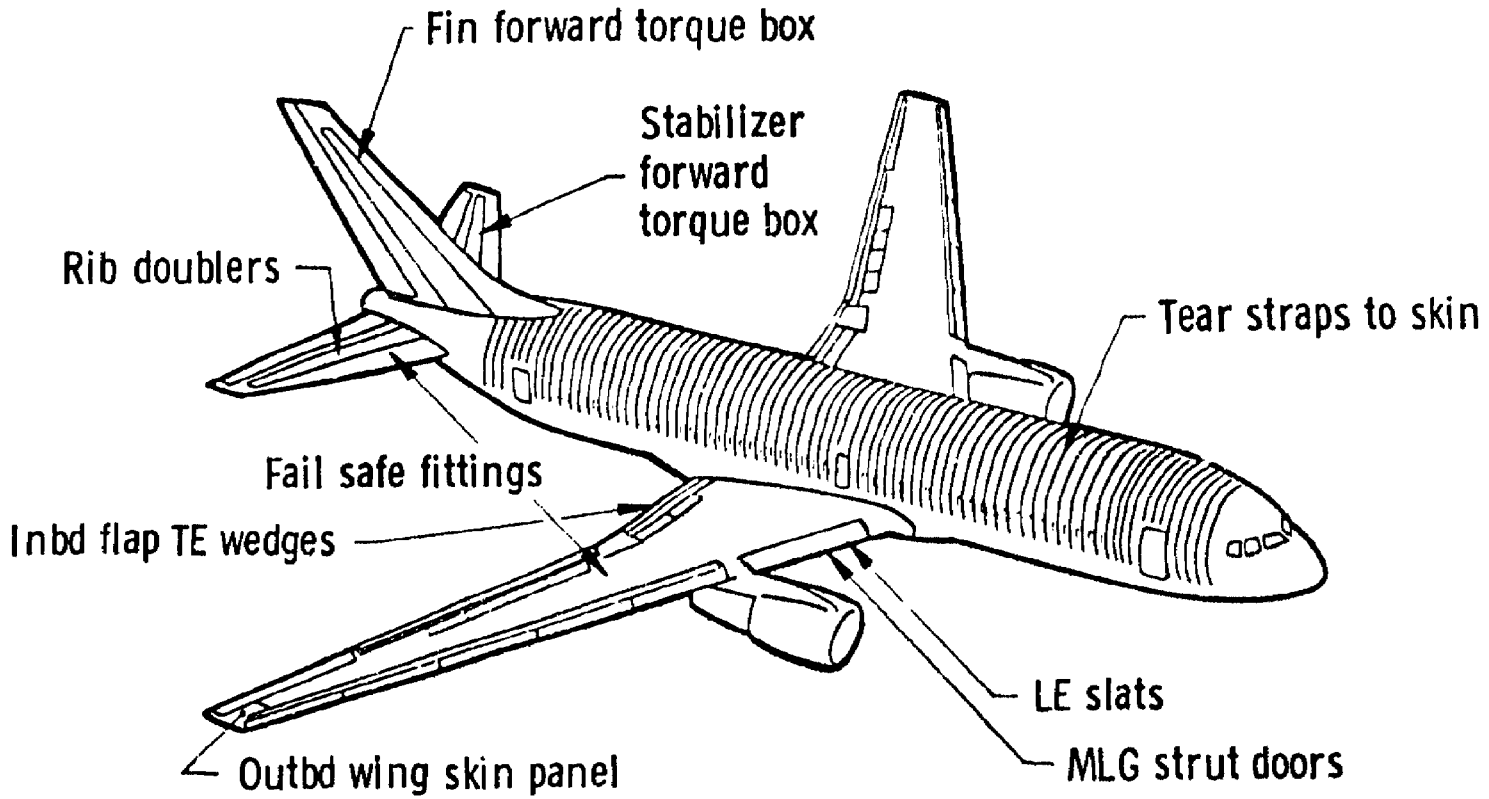

New Airplane Corrosion Control
Galleys and Entries

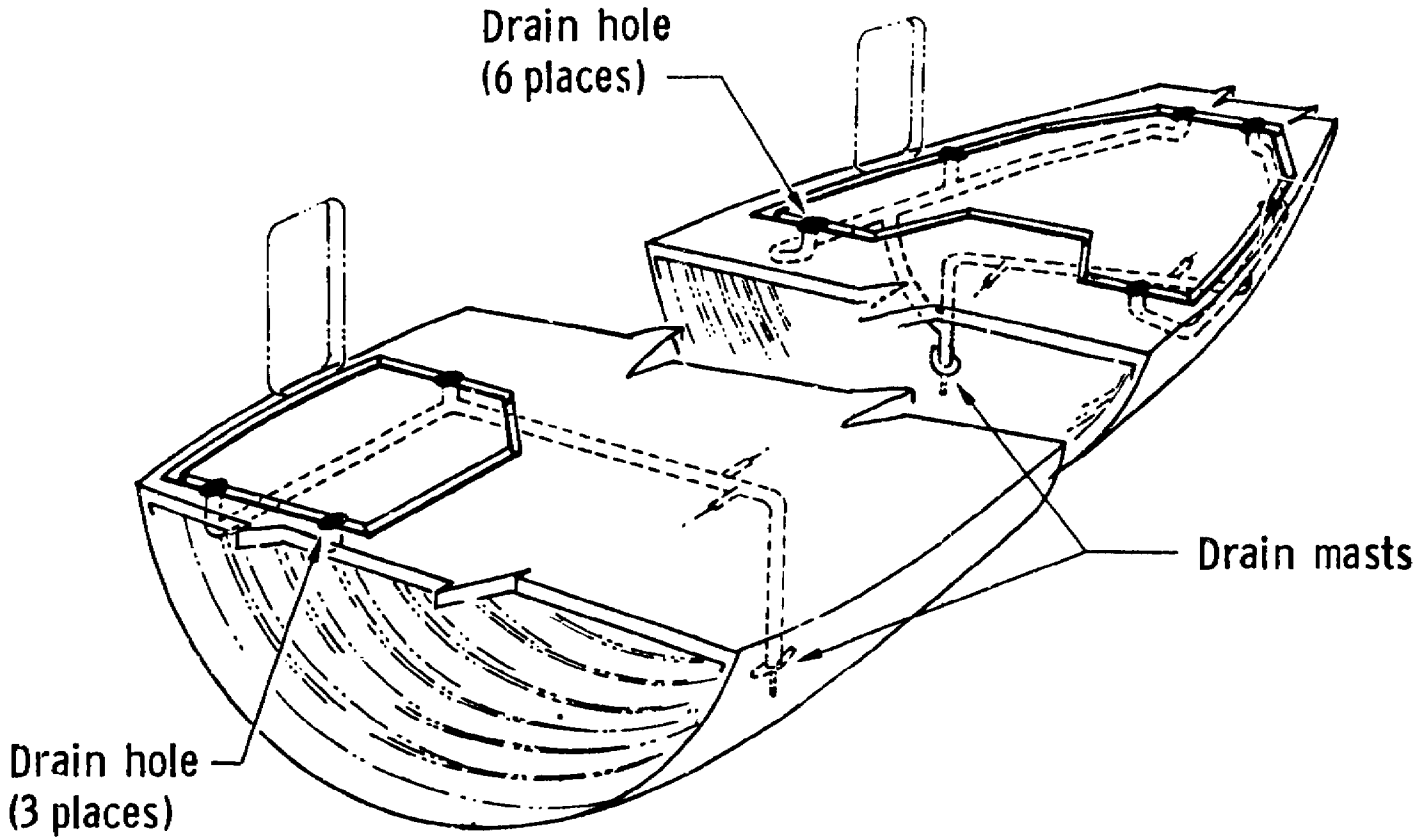

BMT80-199

New Airplane Corrosion Control
Drainage - Lower Lobe/Bilge

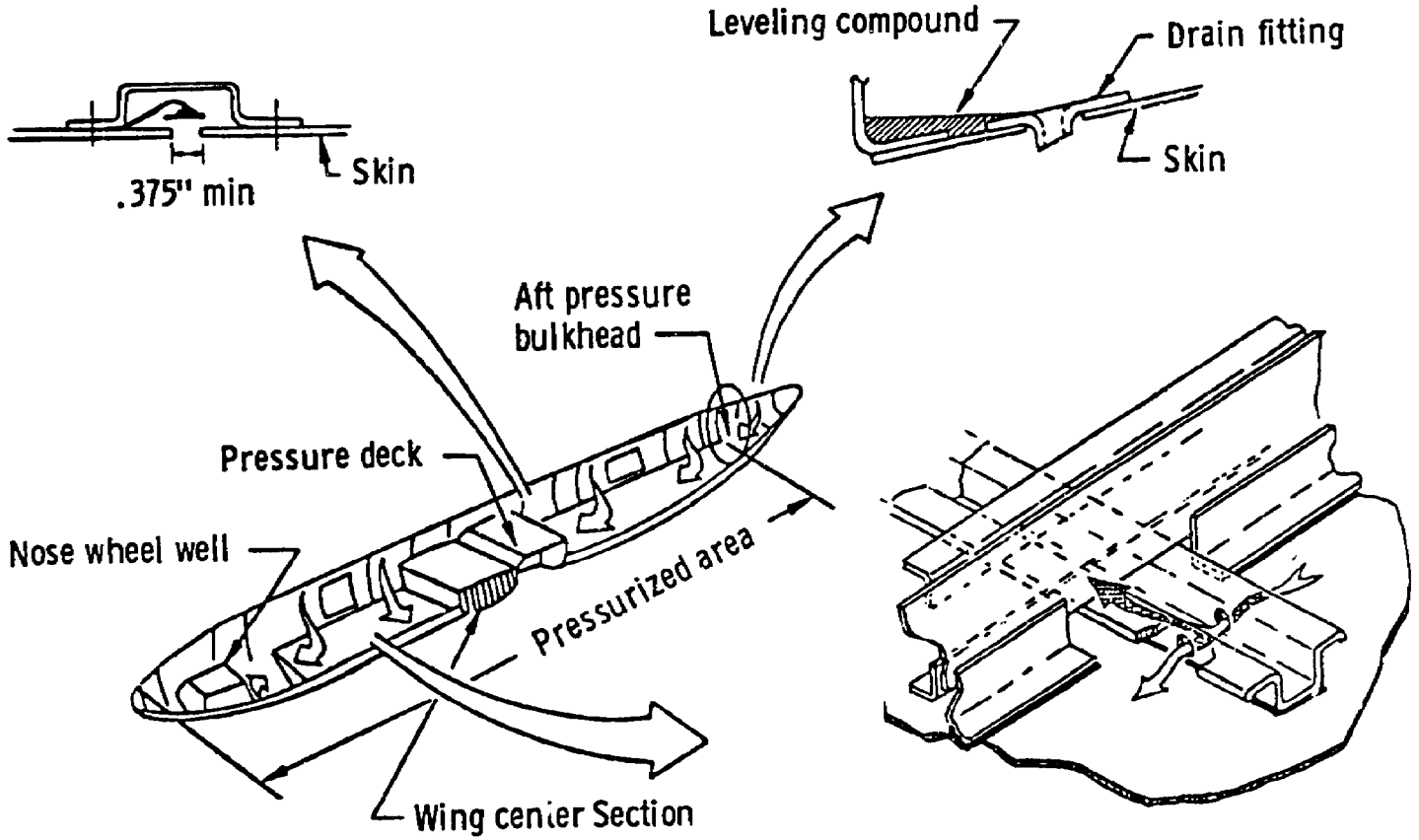

BMT80-48 - A

New Airplane Corrosion Control
Design for Corrosion Protection

- Basic finish systems
- Priming and enameling
- Sealing
- Fastener installation
- Advanced Composites
- Organic corrosion inhibiting compounds

New Airplane Corrosion Control
Basic Finish-Details

Aluminum

Interior – Anodize and primer-bare
Alodine and primer- clad

Exterior – Alodine all clad
Anodize and primer-bare

Steel

Interior – Cad plate and primer- < 220 ksi
Ti/cad plate and primer- > 220 ksi

Exterior – Plus enamel

Titanium

Aluminum interface-primer
Hydraulic fluid areas-protective coating

New Airplane Corrosion Control
Sealing-Wing

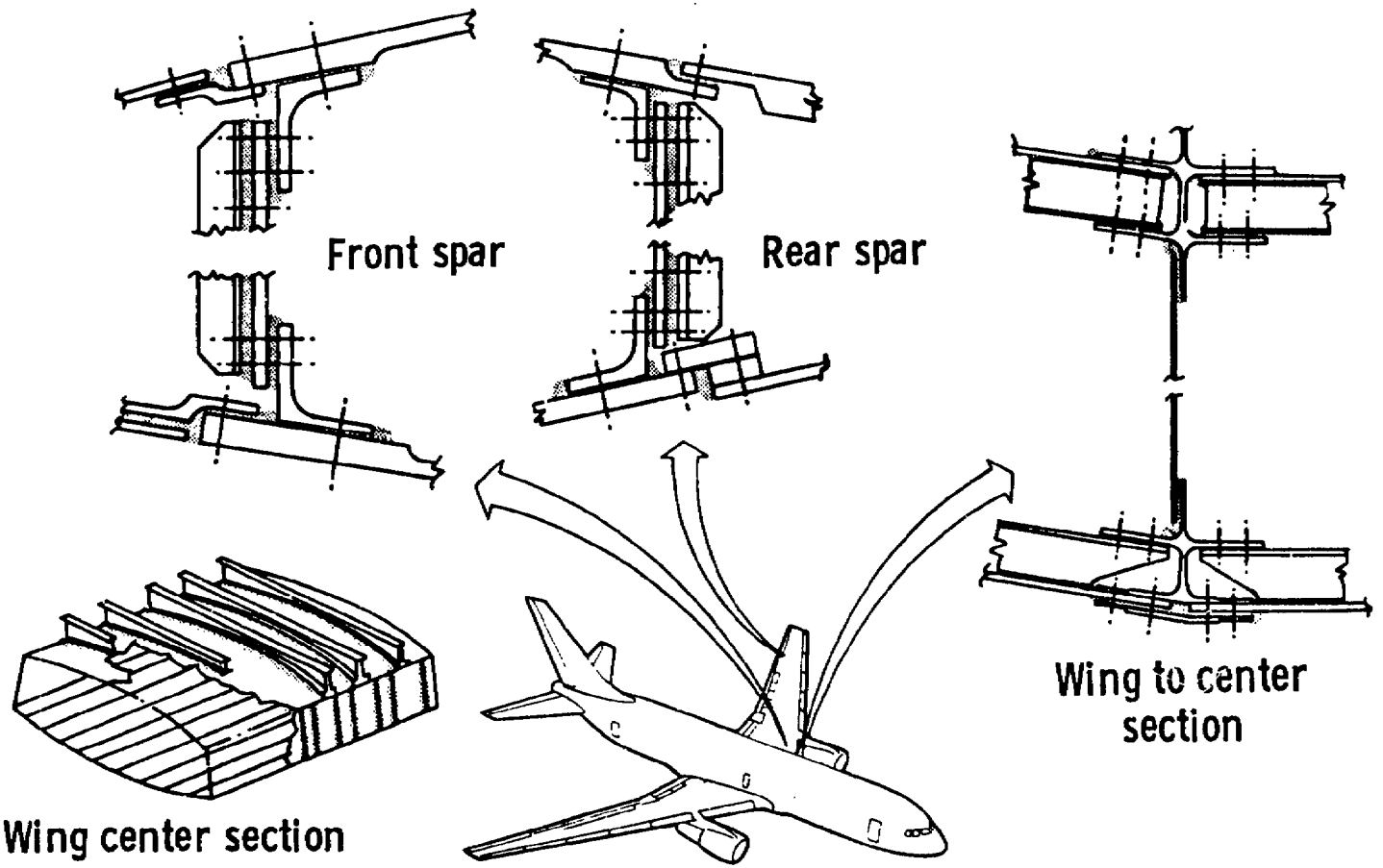

BMT80-200

New Airplane Corrosion Control
Fastener Installation

- Wet installation- All permanent nonaluminum fasteners penetrating exterior skin

- Wet installation and/or cap sealing- Many fasteners in known corrosion prone areas

- Titanium fasteners- Aluminum coated

New Airplane Corrosion Control
Advanced Composites

- Extraordinary corrosion protection measures required when graphite reinforced parts are directly coupled with aluminum

New Airplane Corrosion Control
Graphite/aluminum Protection Measures

Aluminum detail

-Anodize, prime, enamel

Graphite detail

-1 ply fiberglass or kevlar cocured on graphite faying with aluminum and extending 4 inches beyond

- Remainder of graphite surface
  - Tedlar film, fiberglass or kevlar ply, or pinhole filler plus 2 coats of primer
  - Graphite cut edges, sealant or primer plus enamel

Assembly

- Fay surface seal
- Fasten with aluminum coated titanium fasteners, wet sealant installed
- Use aluminum or cadmium plated CRES washers, nuts or collars on aluminum side and cap seal

New Airplane Corrosion Control
Graphite/aluminum Protection Details

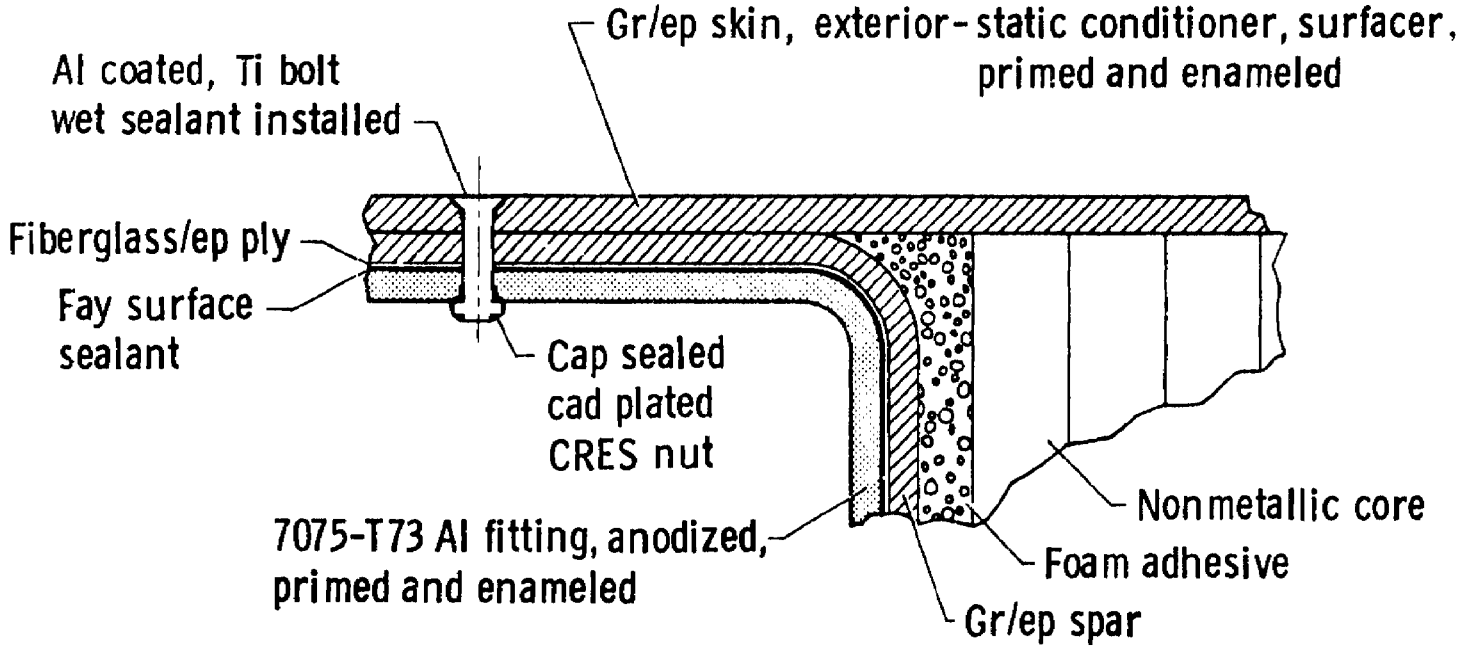

BMT80-206

New Airplane Corrosion Control
Organic Corrosion Inhibiting Compound

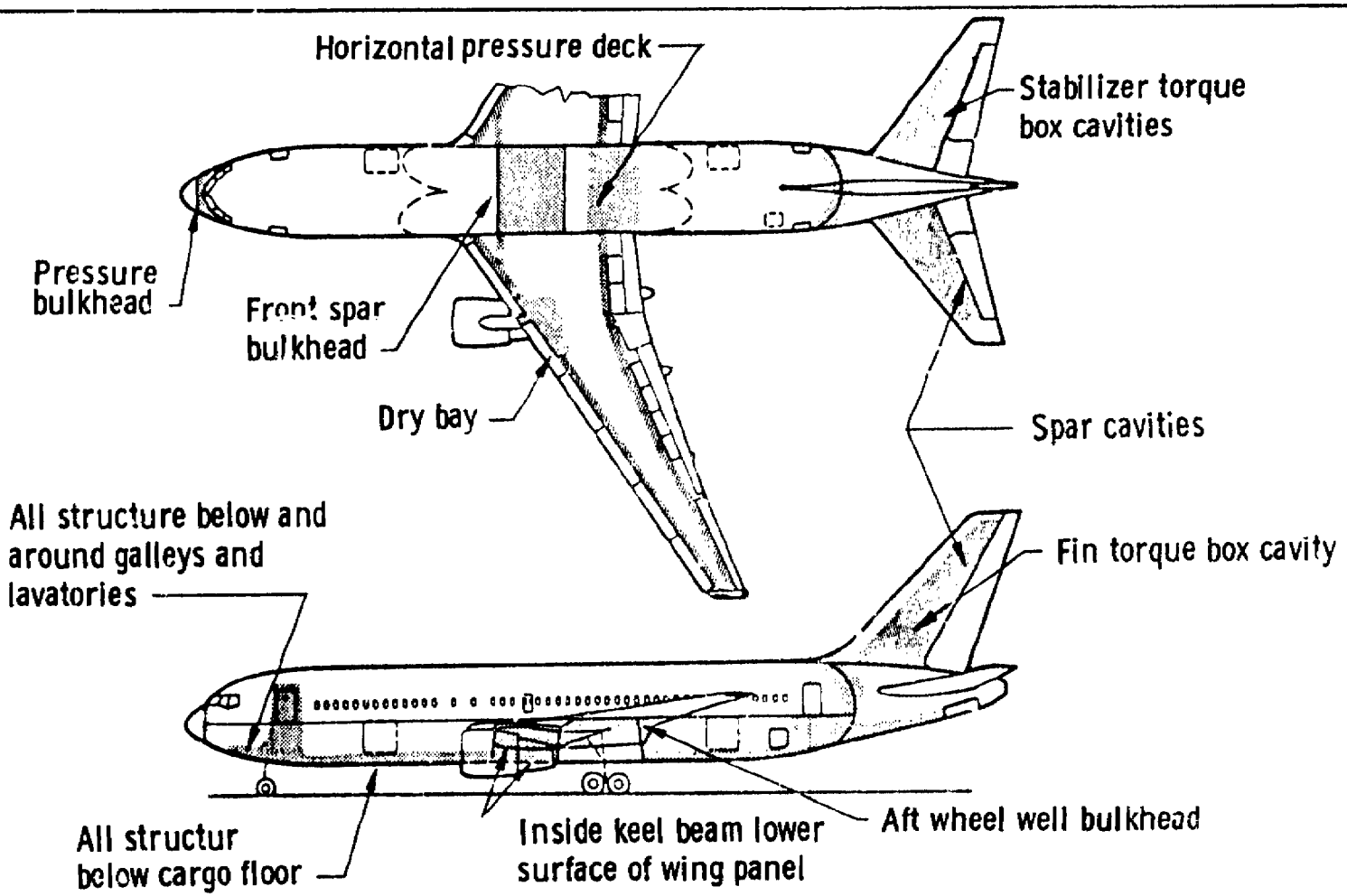

BMT80-207

Corrosion Control in Commercial Airplanes
Summary

- Evolutionary process
  - Production improvements
  - New design standards
- New design objectives
  - Assure 20 year structural integrity with normal maintenance
- Design for avoidance
  - Materials and processes
  - Entries, galleys and lavatories
  - Drainage
- Design for protection
  - Finish systems
  - Sealing
  - Corrosion inhibitors

Biography

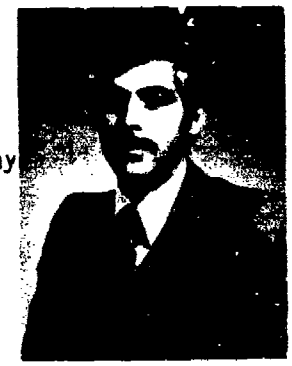

Name: J. Corey McMillan

Present Affiliation: Boeing Commercial Airplane Company

Title: Manager, Materials Technology

Field of Interest/Responsibilities:

Responsible for all materials and processes engineering activities within Boeing Commerical Airplane Company

Previous Affiliations/Titles:

Academic Background:

B.S. Metallurgical Engineering, University of Washington

M.S. Metallurgical Engineering, University of Washington

Society Activities/Offices:

Publications/Papers:

Numerous papers and publications in the general areas of fractography, fracture, fatigue, adhesive bonding and corrosion control.

Biography

Name: Daniel B. Arnold

Present Affiliation: Boeing Commercial Airplane Company

Title: Technology Supervisor

Field of Interest/Responsibilities:

Composites, Adhesive Bonding, Finishes, and Sealants

Previous Affiliations/Titles:

Academic Background:

B.S. Chemical Engineering- University of Washington
B.A. Business Adminstration- University of Washington

Society Activities/Offices:

Publications/Papers:

AFWAL-TR-81-4019
Volume II

Improvements in Corrosion Resistance of Adhesive Bonded Structure

Daniel B. Arnold

Boeing Commercial Airplane Company

November 5-7, 1980

Tri-service Conference on Corrosion ■ United States Air Force Academy, Colorado

BMTBO-203

IMPROVEMENTS IN CORROSION RESISTANCE OF ADHESIVE-BONDED STRUCTURE

SLIDE 1

This paper will report the improvements in corrosion resistance of adhesive-bonded structure and be a compendium of the technical changes that have taken place to advance adhesive-bonding technology. It is appropriate that this particular paper will be presented at a corrosion conference, because adhesive bonding has been one of the most serious corrosion problems for Air Force as well as commercial vehicles.

SLIDE 2

This slide portrays the historical flow chart of the paper, as well as the progress that has been made with adhesive bonding over the past 15 years. The paper will trace each of the eight steps as we go through the presentation.

SLIDE 3

Adhesive bonding has long been used as a low-cost fabrication procedure for aerospace structure; however, it has not been without problems, as we will see in the future slides here. The process was originally used by Hawker DeHavilland and Fokker to bond metal to wood structure in the late 1940s. This was done to increase the thicknesses and strengths of wooden structure and aircraft wings. Fokker initially used the process to laminate thin sheets of aluminum together during periods of shortage when thicker sectioned extrusions or plate were not available to make the wing skins on Fokker aircraft.

SLIDE 4

The extent of usage of adhesive bonding has not grown precipitously, but has been a gradual increase starting with the Boeing fleet of aircraft in the mid-1950s. Initially, metal-to-metal and honeycomb bonding were used relatively sparingly on the B-52 and KC-135 types of aircraft. However, as the demand for lower cost fabrication techniques and lighter weight aircraft evolved, with the 727, 737, and 747 adhesive bonding became a more popular means of fabrication of structure. Most recently, the amount of adhesive-bonded structure has actually declined in the 757 and 767. That structure has been replaced with composite and hybrid types of components.

SLIDE 5

This slide shows the extent of usage of adhesive bonding on the Model 747. As you can see, there is quite extensive use on the fuselage, empennage, and wings. In the fuselage area, adhesive bonding is used to bond metal-to-metal doublers, tear straps, and reinforcements around windows and door areas. In the wing structure, adhesive bonding is used for control surfaces, particularly the spoilers, flaps, and ailerons. In each of these cases, multiple suppliers were used to supply the various components of the aircraft. Thus, it became necessary to have uniform bonding specifications for each of the Model 747 suppliers.

SLIDE 6

Extensive usage of adhesive-bonded structure on the 747, as well as on other aircraft that were emerging in the late 1960s, was not without problems. Specifically, there were delamination and corrosion on a large variety of components, including both metal-to-metal and honeycomb types of structure. The experience in the commercial industry was similar to the experience with military aircraft. The following four photographs detail the types of problems that were typical of service failures.

SLIDE 7

This photograph shows the delamination of an inner skin of a honeycomb panel. Notice that there is lifting of this skin along the edges of the honeycomb. In addition, there is both doubler and skin separation on the external surface.

SLIDE 8

Slide 8 shows the delamination area along the edge of a honeycomb panel in which the face sheet has been peeled off, revealing the areas of corrosion and delamination. Notice that the delamination starts from the edge of the panel as well as from the fastener holes and radiates away from those exposed edges into the center of the bonded area.

SLIDE 9

This slide shows a delaminated body skin doubler leaving behind the external skin on the surface of the airplane. Notice again that the delamination initiates at the fastener holes and propagates radially from these holes. This is due to the ingression of moisture through the fastener holes.

SLIDE 10

This slide shows a severe case of corrosion in which the waffle pattern doubler has completely peeled away from the external skin, leaving behind serious corrosion. Notice also that the delamination occurs from both the doubler and the external skin, indicating that the problem exists with both of these pieces of the bonded assembly. Also, this type of delamination was accelerated by the environment. In this case, the panel was exposed in the bilge of an aircraft, and the fluids that existed in the area accelerated the corrosion.

SLIDE 11

This quotation is typical of the industry mood toward the usage of bonded structure. What is most critical here is that the quote says that the current technology is not satisfying the requirements of the Air Force. The error with this particular quotation is that the technology used was not the up-to-date, proven technology that could be used to solve the corrosion problems. In other words, the problems that exist today are a result of implementation of the incorrect materials and processes in prior designs and in the fabrication of parts in the late 1950s and early 1960s.

SLIDE 12

Thus far, we have shown the problems with adhesive-bonded structure; we are now going to talk about how we should define those particular problems. It must be understood that it is not possible to solve any technology problem unless you really understand the mechanisms of the failure itself. Thus, an in-depth study of the failure mechanisms occurring in adhesive-bonded structure was necessary.

SLIDE 13

Crevice-cell corrosion is one of the most prevalent mechanisms that occur with adhesive-bonding delamination failures. What happens is that a galvanic cell is set up between the clad material and the base metal. This electromotive difference is supposed to exist because the cladding is placed on the external surface of the base metal as a sacrificial barrier that will corrode away, leaving behind the structural base material. However, when cladding is placed in a bondline, this particular mechanism is not desirable. In other words, it is not desirable to have this sacrificial layer in the interface between the two adherents. What occurs chemically during a crevice corrosion attack is that once a crack is initiated through dissolution of the cladding at the edge of a panel, the crack actually propagates and is accelerated by the crevice itself. In the lower sketch, there is a pH gradient from one end of the crack to the other. The tip of the crack is very acidic, and the tail of the crack is basic because of its oxygen enrichment. The crack tip with the increased acidity has a higher etch rate and actually accelerates crack growth as it grows into the structure. The acidic solution dissolves not only the cladding, but also the aluminum oxide as it progresses through the part. This is the most classic and prevalent type of adhesive-bonding failure.

SLIDE 14

The characteristics of delamination are typified in the photograph and sketch shown in this slide. With the crevice corrosion delamination, the initial failure is an interfacial separation of the adhesive from the substrate. The second step is progressive delamination continuing across the panel, accelerated by the pH gradient in the crevice. It is also accelerated by low stresses acting on the adhesive bond, peeling the adherends apart. As noted previously, the cracks start at a free surface and propagate inward toward the panel center.

SLIDE 15

Crevice corrosion that exists in metal-to-metal bonding also exists in honeycomb bonding. In this photograph, delamination has occurred in the edgeband area of a honeycomb panel, exposing the honeycomb itself to further corrosion.

SLIDE 16

A second classical type of failure is shown here. Once water has progressed into the honeycomb area, the honeycomb foil itself is corroded and separation of the adhesive occurs from the foil itself. Thus, we have a lifting of the face sheet from the core, leaving behind a corroded surface of the cells. For this mechanism to occur, there must be water and relatively low stresses present. The water ingresses either through fasteners or through the hydroscopic adhesive that bonds the face sheet to the honeycomb core. The stresses exist due to air loads or fitup stresses.

SLIDE 17

With the establishment of these failure mechanisms, it became necessary to develop new adhesive test methods that would define the materials and processes necessary to improve the technology. It had become obvious that the traditional static test had not provided the discriminating evaluations necessary to select the proper processes and adhesives.

SLIDE 18

This slide shows a 737 body skin doubler that was returned from service, severely delaminated in certain sections of the adhesive-bonded area, but undamaged and still bonded in other areas. The traditional lap-shear and peel tests on the bonded area of the panel showed that the residual strength was on the order of 5100 psi lap shear and some 72 in.-lb of peel. However, if instead of testing the panel or the coupons using a static type of test, we use dynamic tests coupled with an environmental exposure, we can detect the type of failure that occurred in the delaminated section. As shown in the upper photograph, we fabricated a wedge test specimen and exposed it to a low cleavage type of stress and to an environment of humidity or salt spray. With this combined stress and environmental exposure, the specimen delaminated rapidly; as a matter of fact, it took only a matter of hours for the crack to propagate several inches down the length of the specimen. The crack grew interfacially, which is the same type of failure as occurred in the delaminated area of the panel. In the lower photograph, the peel test specimen had a room-temperature peel strength of 72 in.-lb; however, when we added moisture to the crevice of the peel specimen, the peel strength essentially went to zero and failure mode shifted from being cohesive within the adhesive layer to adhesive between the primer and the adherend, again typifying the type of failure that was seen in the delaminated zone of the panel.

SLIDE 19

If we now compare a good panel with a poor panel (i.e., a panel that has gone through service and not delaminated versus a panel that has gone through service and delaminated), we can see in the upper two comparisons of lap-shear portashear that there is no difference in the shear strength of the good and the bad panel. However, in the third comparison, the wedge test shows that the good panel had essentially no crack growth, whereas the delaminated panel had a precipitous crack growth that occurred in a matter of hours. In the fourth comparison, the toughness of the adhesives was measured; the good adhesive maintained its toughness until it was plasticized by the moisture, and then the toughness dropped off. With the poor adhesive that delaminated in service, the toughness dropped off quite rapidly and, in fact, we were not even measuring the toughness of the adhesive, but instead were seeing an interfacial failure, again typical of the type of failure seen in the panel.

SLIDE 20

Because of the large amount of honeycomb bonding, it became necessary to develop a honeycomb specimen that could be a self-contained static or dynamic test specimen and that could be exposed to an environment at the same time it was being loaded. In this photograph, such a specimen was fabricated by bonding a honeycomb specimen and then clamping this specimen in a fulcrum fixture to impart a bending load to the specimen. This specimen is self contained and can be exposed in the environmental chamber.

SLIDE 21

This slide shows the same type of specimen, only instead of a static load, it has been fitted with a bellows and the same fulcrum arrangement and cyclic stress can be applied. A 1-hour cure cycle was chosen because it represents the Webber chamber simulation of a ground-air-ground airplane flight cycle.

SLIDE 22

This slide shows the ground-air-ground environmental cycle. In the upper left, the humidity is varied from 100% to 0% and back to 100%, while at the same time the temperature is cycled from 140°F to -60°F and back to 140°F. The pressure in the chamber is also changed from sea level to a simulated altitude of 40,000 feet. In the right center, you can see a photograph of the inside of the chamber with a number of these different types of coupons sitting on the racks. The lower part of the slide shows a comparison of old and new-technology adhesive-bonded structure. Reading across, we can see that with no stress there were approximately 100 cells filled with water after 4000 cycles with the old-technology alkaline system, and no water was absorbed even up to 8000 cycles with the newer technology. If a static stress was applied, 50 or more cells filled with water after 700 cycles, whereas there was no water absorbed up to 8000 cycles with the new technology. If a cyclic load and environmental cycle were applied, it is seen that the old technology failed relatively quickly in 250 to 300 cycles, whereas the new technology endured over 8000 cycles without an ingestion of moisture or any propagation of failure.

SLIDE 23

As a result of adhesive resin technology changes and test procedures, a whole new family of test methods has been developed. Instead of using static testing, fatigue testing is used; instead of ambient conditions, a range of temperatures is tested. Instead of a dry exposure, combined moisture along with the fatigue and temperature environment is used. Instead of using a single load, we use a synergestic loading, wherein multiple loads are applied to a panel in much the same way as they are applied to the airplane itself. Instead of using small specimens, we use larger ones that can simulate the types of loading that exist in aircraft structure.

SLIDE 24

Armed with the new test techniques, we are now going to highlight some of the material and process changes that have occurred in the past 10 years. These changes have improved the corrosion resistance of bonded structure from relatively poor performance to a much improved capability.

SLIDE 25

This slide shows the elements that make up an adhesive bond. It is not just a simple interface between two pieces of metal, but actually a complex combination of oxide, primer, adhesive and, in the case of sandwich structure, honeycomb core. Each of these elements has seen a significant improvement in corrosion resistance over the past few years.

SLIDE 26

This slide shows the wedge test coupon discussed earlier and also shows how this particular speicmen was used to develop a new surface preparation; in this case, phosphoric acid anodizing. The curve at the lower right typifies the type of crack growth rate that was experienced with poor interfacial resistance of older surface preparations as compared with the phosphoric acid anodized surface preparation. This simple wedge test specimen has led to one of the most dramatic improvements in adhesive-bonding processes that has occurred in the past few years.

SLIDE 27

The chart shows the phosphoric acid anodize process in boxed format. On the left is shown the six steps necessary for FPL etch (for those of you who are not familiar with FPL etch, it is the sulfuric acid/sodium dichromate etch process). On the right is shown the eight steps that are necessary for the phosphoric acid anodize process. The main difference is in step six, where instead of rinsing and drying the parts, they are immersed in a phosphoric acid anodize bath and anodized for 20 minutes. This particular process creates a measured thickness of porous anodic coating on the adherend.

SLIDE 28

Perhaps one of the most dramatic changes that has taken place in adhesive-bonded structure has been the incorporation of corrosion-resistant honeycomb core. On the left is shown the older, uncoated honeycomb; on the right, the metal, organic-coated, corrosion-resistant honeycomb core. These particular specimens have been exposed to a salt spray environment for 25 days. On the left, the honeycomb core specimens, as well as the foil itself, are severely pitted; whereas on the right, there is no corrosion attack on the edges of the honeycomb foil or on the foil. In addition to the two changes that we have discussed here (phosphoric acid anodize and corrosion-resistant core), there have been a number of other changes to improve the corrosion resistance of bonded honeycomb structure. Specifically, the clad adherends have been changed to bare adherends to eliminate the problem of clad dissolution. Corrosion-resistant primers have been implemented. In the past, either no primers, or primers that were susceptible to moisture degradation, were used. Lastly, toughened epoxy adhesives have been used; not only do they have better toughness and resistance to peeling, but they also have higher resistance to moisture ingression. Thus, the amount of moisture that reaches the interface of the bond has been decreased.

SLIDE 29

Shown next are some of the recent test results and experimental work in the area of phosphoric acid anodizing and comparison of phosphoric acid anodzing with other surface preparations.

SLIDE 30

This slide shows cross sections or edges of three different types of oxide in electron microscope photographs. On the left is shown the traditional sulfuric acid/sodium dichromate (FPL) etch and the relatively thin oxide layer that is developed with that process. In the center is shown the phosphoric acid anodize process on 7075 bare alloy. On the surface of the anodize is seen a flake type of oxide structure. On the right photograph is shown a phosphoric acid anodize on 2024-T3 clad material; the traditional needle and very deep pore type of oxide structure can be seen. Contrasting these photographs, it can be seen that the anodize on clad material has a thickness of 5000 angstroms. The anodize on the bare material has an oxide thickness of 2500 to 3000 angstroms, and the oxide developed by the FPL etch has a thickness of 400 to 500 angstroms. Also contrasting these different types of oxide, it can be seen that the one on the far right with the needle-like structure would have a much greater surface area for bonding to a liquid adhesive primer.

SLIDE 31

This slide shows a family of micrographs with three different types of adhesive primers applied over the surface of the oxide itself. On the left photograph, there is partial primer penetration into the oxide pores; in the center photograph, there is complete penetration; and in the right photograph, there is an excessive amount of primer built up on the oxide surface. A thicker rubber coating can be seen on the surface of this particular specimen.

SLIDE 32

This photograph was taken from a cross section of an anodized surface that had been sliced into a thin wafer on a microtome device. The microtoming procedure is being developed for biological inspection and, in this case, is applied to the sectioning of an anodized surface impregnated with a primer resin. On the left photograph is shown the structure of a bare phosphoric acid anodized surface and on the right, a clad anodized surface. Both of these are shown at the same magnification and show the same type of cellular honeycomb structure for each. In both cases, the oxide wall thicknesses are on the order of 50 to 100 angstroms and the diameters or cross sections of the pores themselves are on the order of 300 to 500 angstroms. It can also be seen that the pores are all completely filled with resin such that the oxide is stabilized and there is no open structure to collapse during loading of the specimen.

SLIDE 33

This slide shows a cross section of the base metal/oxide/primer interface and the interaction between the multiphased primer and the oxide itself. Note that there are at least two phases in the adhesive primer and there is an enrichment at the interface of the second phase. Note also that there is penetration of the adhesive primer down into the cellular structure of the oxide. Ignore for the moment the artifact that exists in the center of the oxide itself. These are sectioning artifacts that occur during specimen preparation that were not present during the original bonding.

SLIDE 34

This slide is an enlargement of slide 33 showing the oxide interface with both base metal and the primer itself. Note again that in the center there is a sectioning artifact and that across the artifact there are necking pieces of material, indicating that the primer has penetrated to the bottom of the oxide pore. Note also that there is a base oxide layer at the bottom of each of the pores between the base metal and the oxide structure.

SLIDE 35

With the advancements that have been made in adhesive bonding, it is now possible to commit this technology to every greater applications in the aerospace industry.

SLIDE 36

This slide shows the YC-14 advanced medium STOL transport that was built by Boeing for the Air Force. In this particular aircraft, adhesive-bonding technology was applied to the primary structure of the aircraft. Specifically, the vertical fin and the horizontal stabilizer torque boxes were bonded aluminum honeycomb structure.

SLIDE 37

This sketch shows the details used in the fabrication of the YC-14 empennage and the type of honeycomb structure used for this application of bonded technology.

SLIDE 38

This slide shows the application of adhesive bonding to the 767 aircraft that is emerging today at The Boeing Company. On the 767, there are the traditional applications of metal bonding for tear straps and doublers, as well as for fail-safe structure and rib structure in the empennage area. However, there is an absence of some of the control surfaces that had traditionally been bonded aluminum honeycomb structure; these have been replaced with graphite structure.

SLIDE 39

Bonded aluminum structure is in competition with graphite structure as an alternative means of fabrication of aerospace components. The future of adhesive bonding is going to depend upon the advancements that can be in terms of reducing the weight of aluminum structure compared to graphite structure, such that the advantages that now exist for graphite are reduced through the use of lighter weight and stronger aluminum face sheet structure such as aluminum-lithium alloys or metal-matrix composites. In this way, bonded aluminum structure will become more attractive from a weight standpoint when compared with graphite structure.

SLIDE 40

This slide summarizes the trends occurring in adhesive-bonding technology. Specifically, the use of bonding has emerged from secondary to primary structure and, in the future, will be used for more and more high-temperature applications. At the same time, it has become necessary to establish meaningful test techniques that duplicate the loads and environments seen by the components in service. It has been necessary to simulate the types of surface failure and to identify the failure mechanisms that cause bond separation, corrosion, and delamination. What has evolved is a technology that is stable in the environments of moisture, temperature, and fatigue exposure seen on aircraft today.

HISTORICAL FLOW CHART

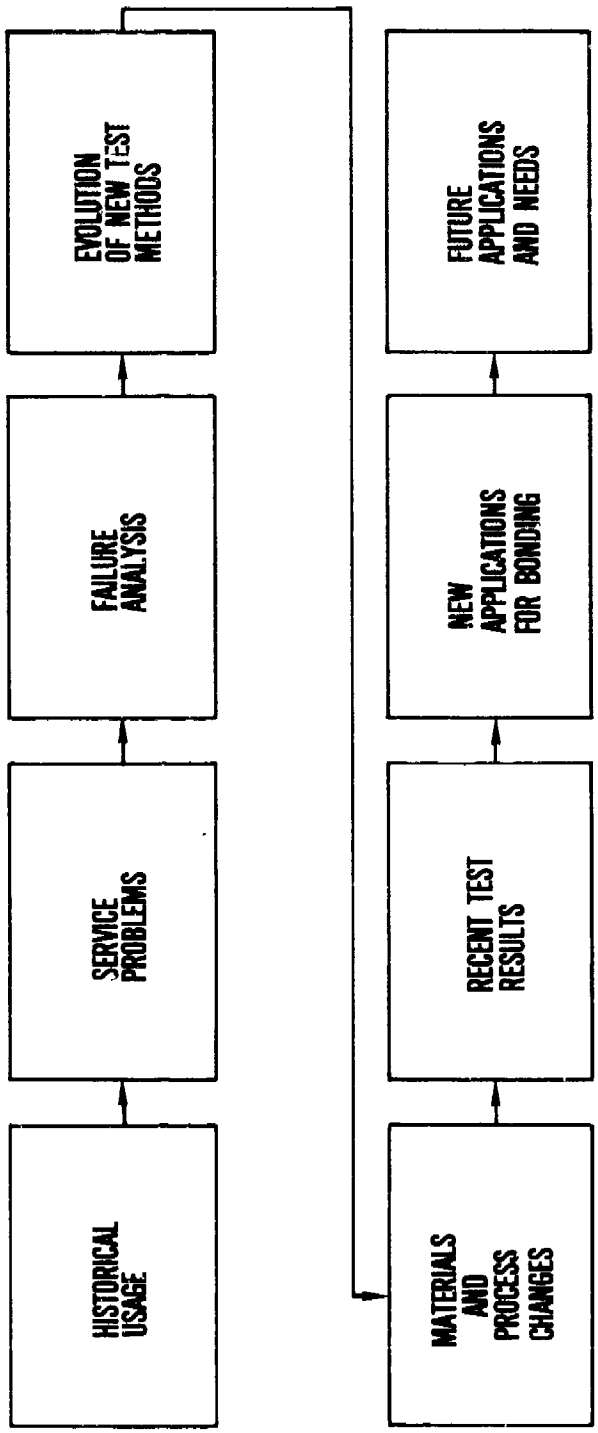

HISTORICAL FLOW CHART

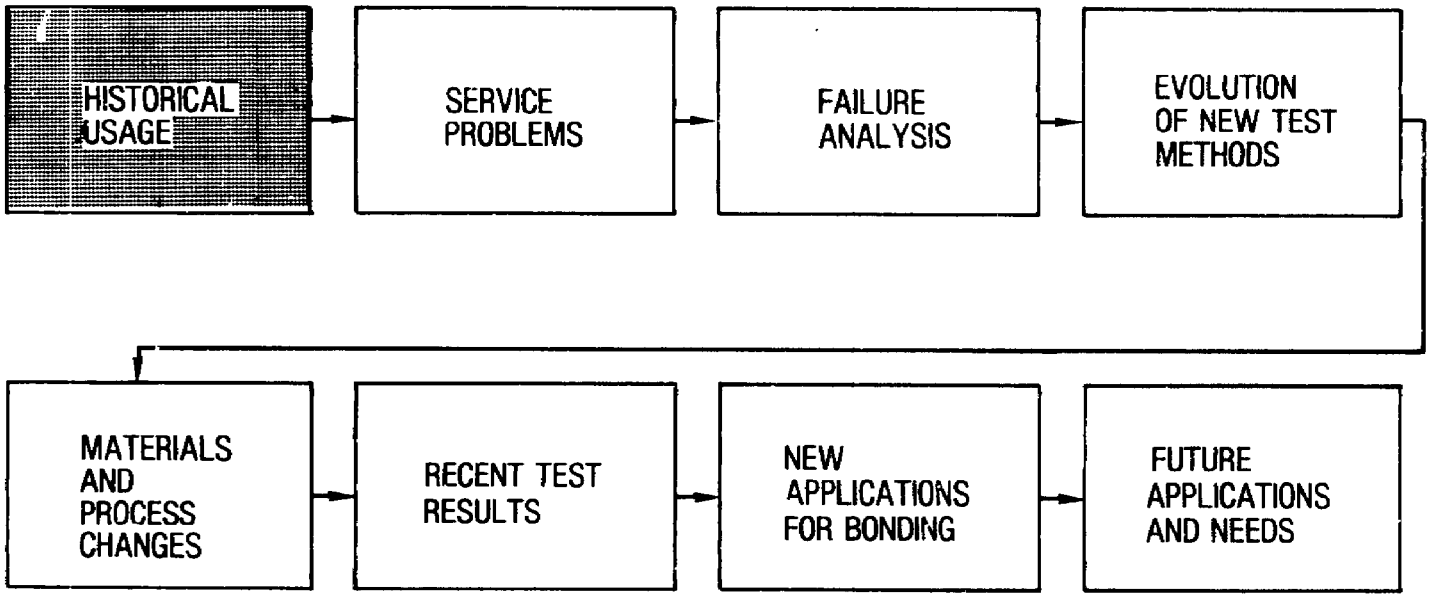

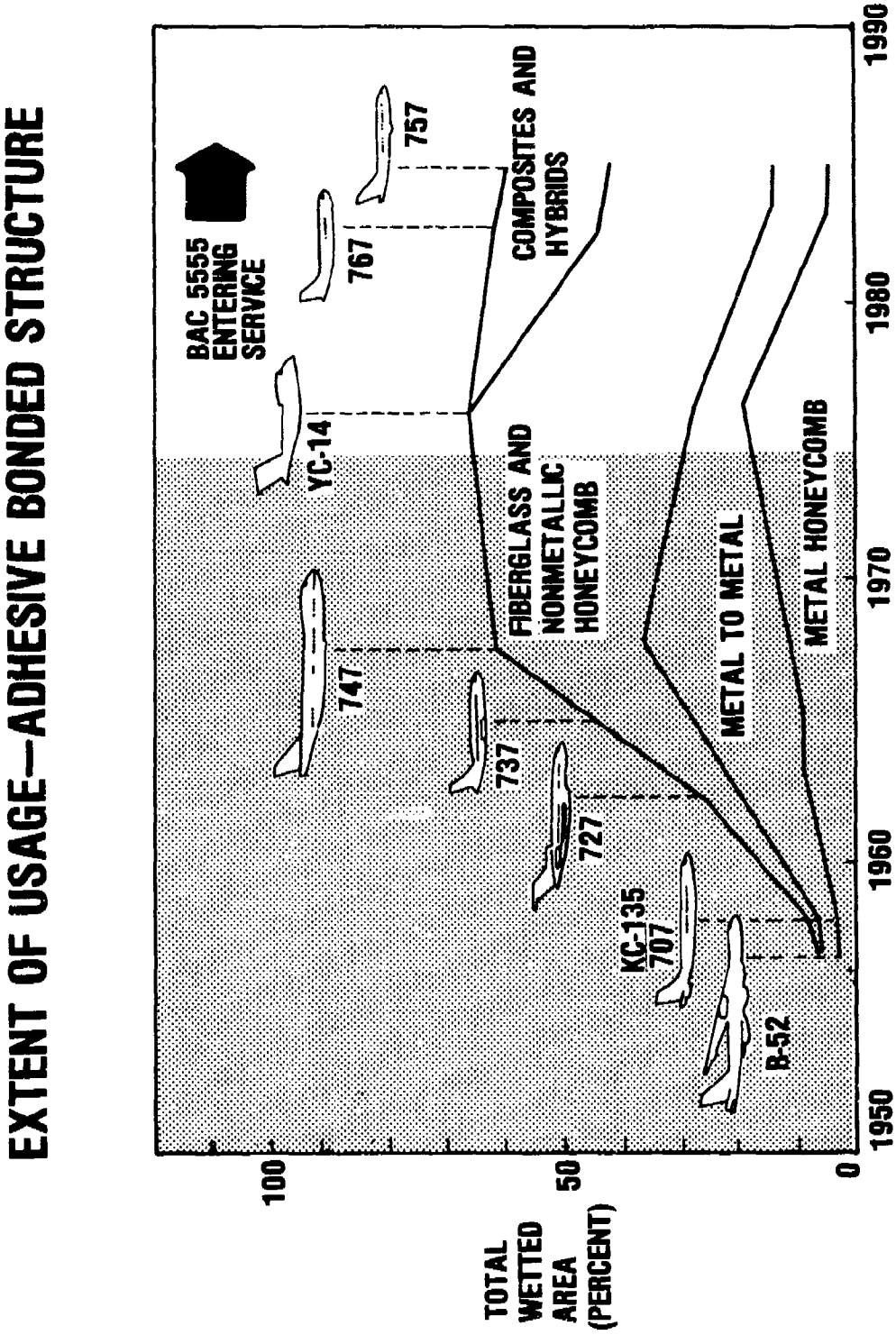
EXTENT OF USAGE—ADHESIVE BONDED STRUCTURE
TOTAL WETTED AREA (PERCENT)
100
50
0
1950
1960
1970
1980
1990
BAC 5555 ENTERING SERVICE
YC-14
747
737
727
KC-135
707
B-52
767
757
COMPOSITES AND HYBRIDS
FIBERGLASS AND NONMETALLIC HONEYCOMB
METAL TO METAL
METAL HONEYCOMB

747 ALUMINUM HONEYCOMB USAGE

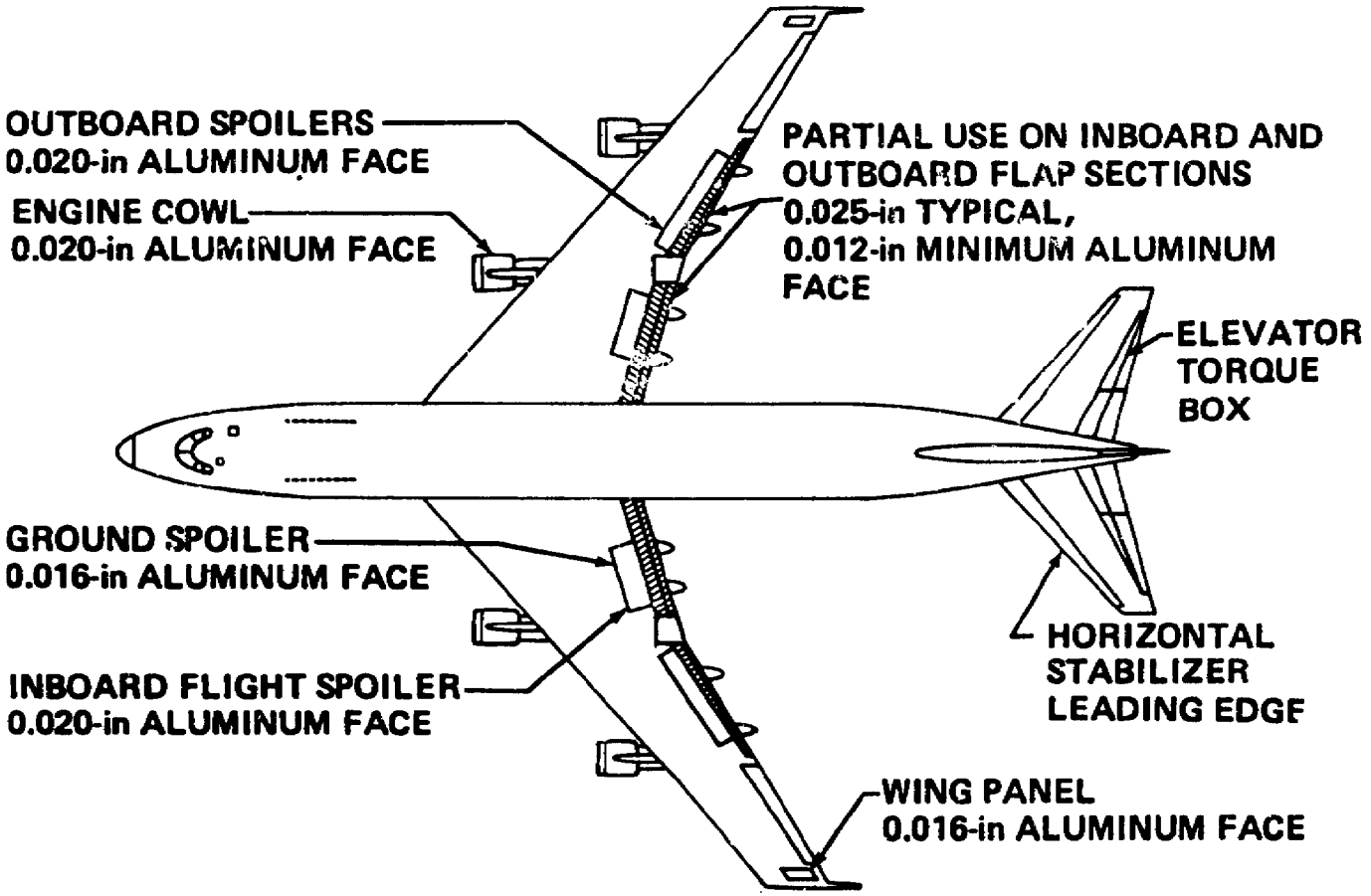

HISTORICAL FLOW CHART

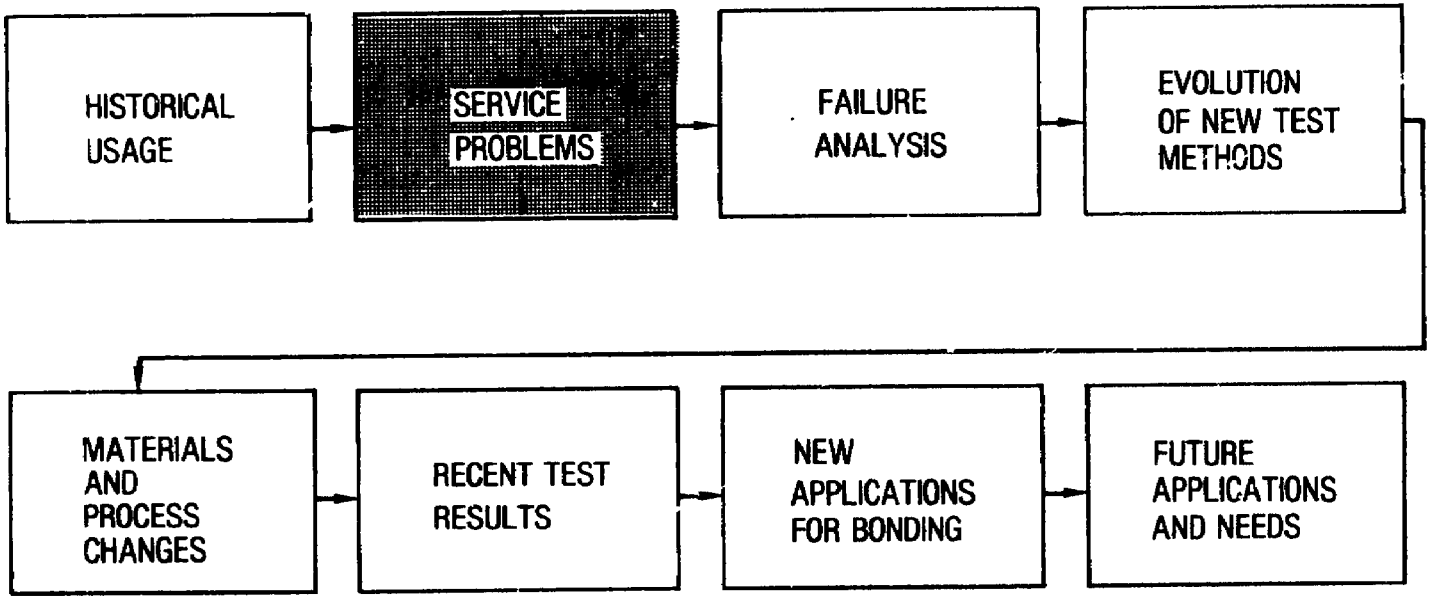

EXAMPLES OF HONEYCOMB SERVICE FAILURES

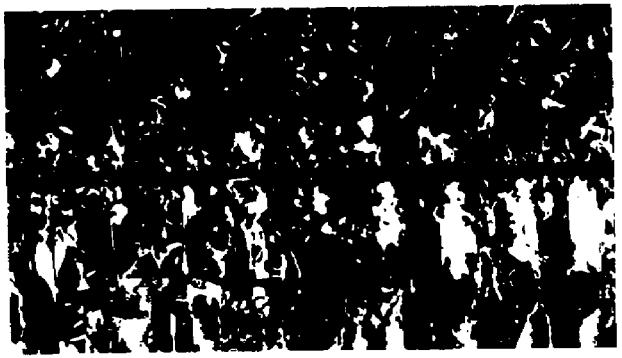

WATER INGESTION

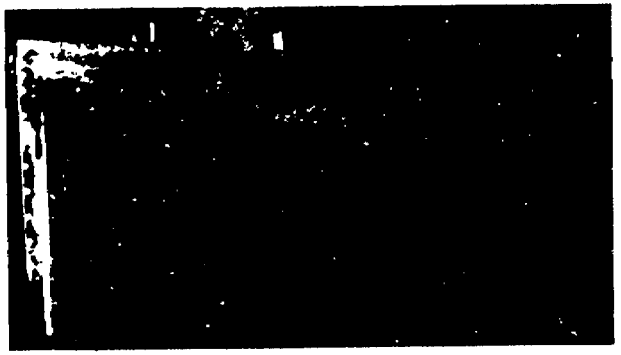

DELAMINATION

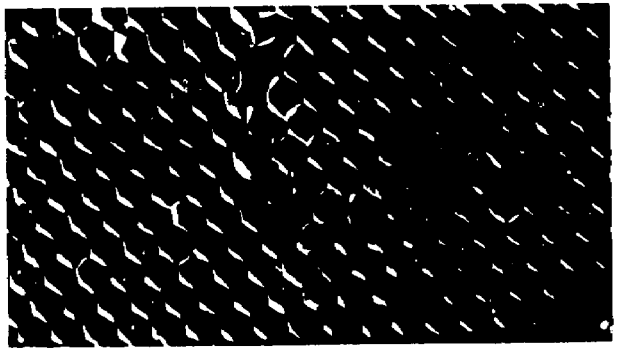

CORE DISBOND

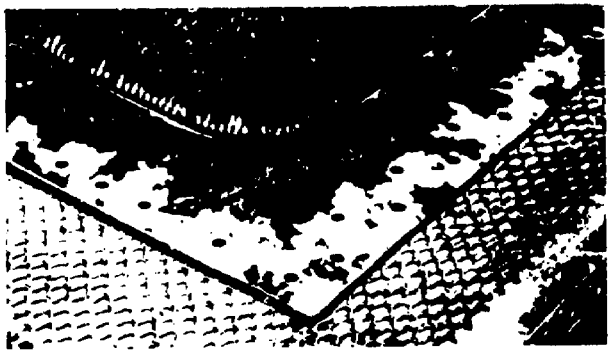

CREVICE CORROSION

ALD QUOTE

"THE INTEGRITY OF ALL BONDED HONEY-COMB STRUCTURE HAS BECOME AN AIR FORCE-WIDE PROBLEM. THE CURRENT TECHNOLOGY . . . IS NOT SATISFYING AIR FORCE REQUIREMENTS BY PROVIDING A REALISTIC AND RELIABLE END PRODUCT."

SA-ALC/MMIR LETTER
TO ASD/SD5E, 25 JANUARY 1977

HISTORICAL FLOW CHART

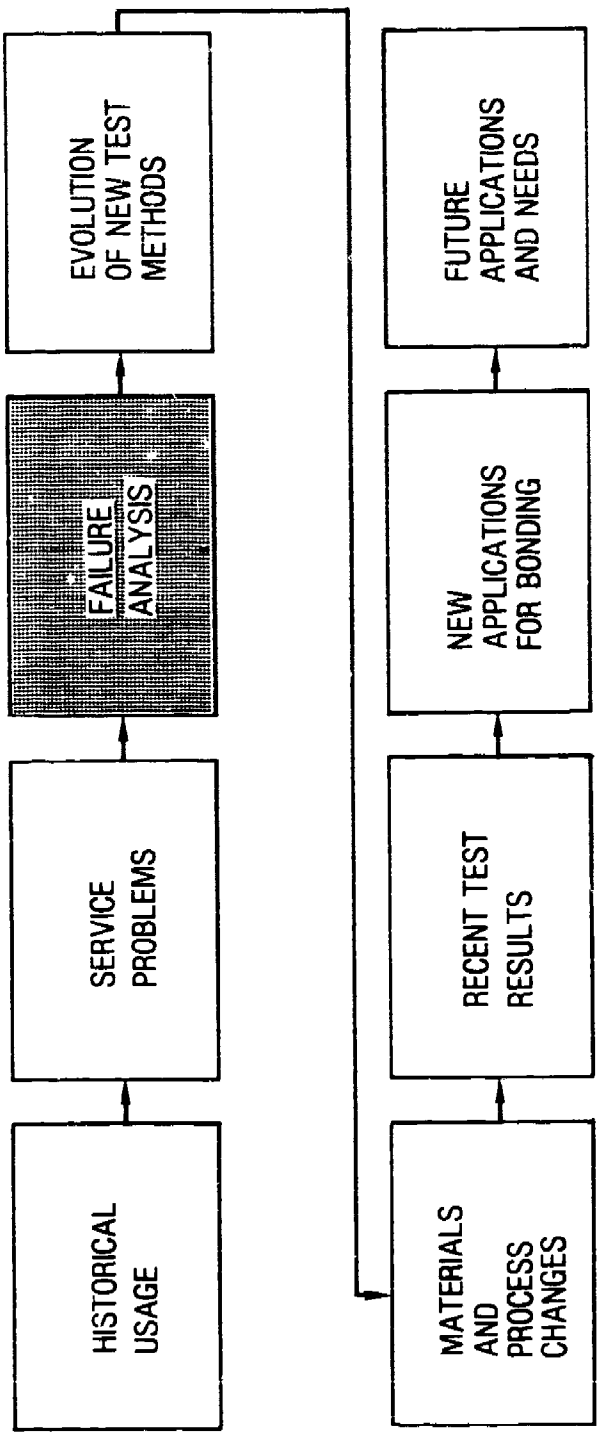

GALVANIC AND CREVICE CORROSION

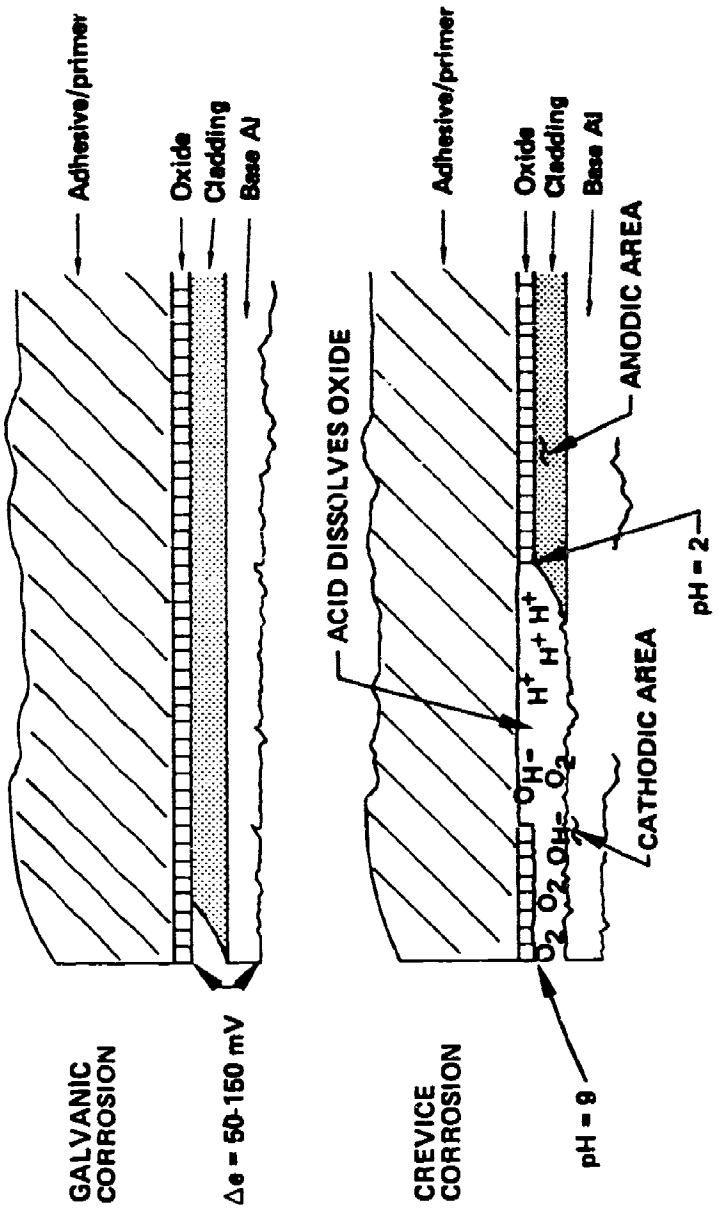

CHARACTERISTICS OF DELAMINATION FAILURES IN SERVICE

MECHANISM

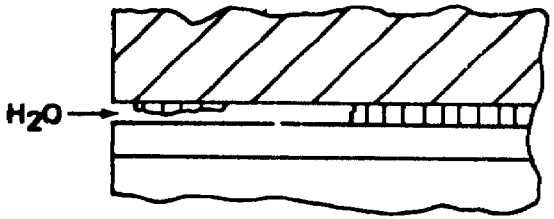

EXAMPLE

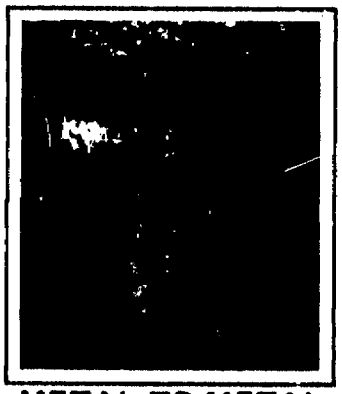

METAL TO METAL

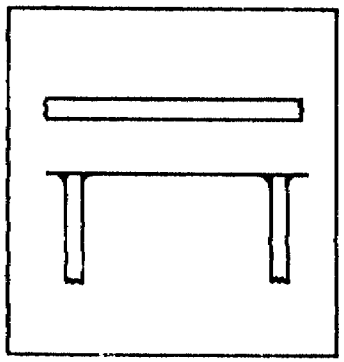

HONEYCOMB

CHARACTERISTICS

- INTERFACIAL FAILURE MODE
- PROGRESSIVE GROWTH
- LOW STRESS
- INITIATE AT FREE SURFACE

CREVICE CORROSION

MECHANISM

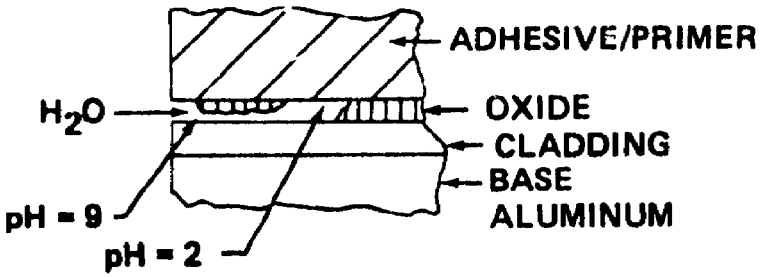

EXAMPLE

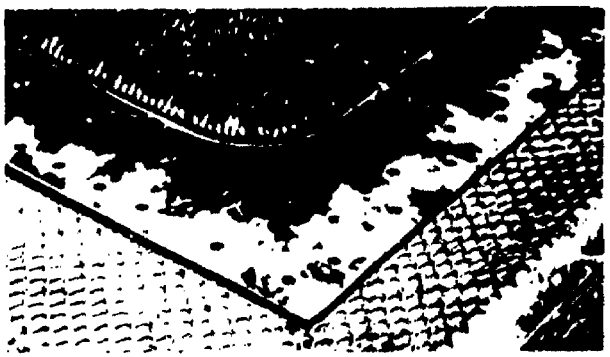

CHARACTERISTICS

- OXYGEN DEPLETION IN CRACK
- LOW pH AT CRACK TIP
- DISSOLUTION OF CLADDING AND OXIDE

WATER INGESTION

WATER INGESTION

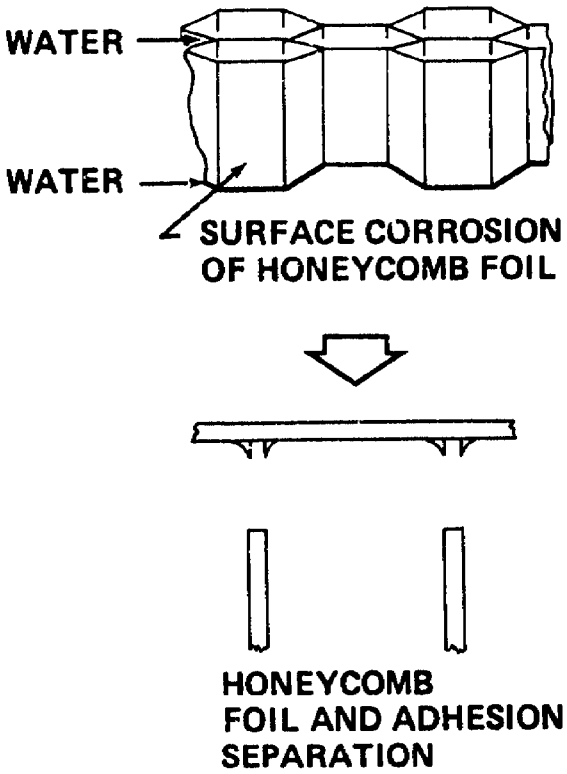

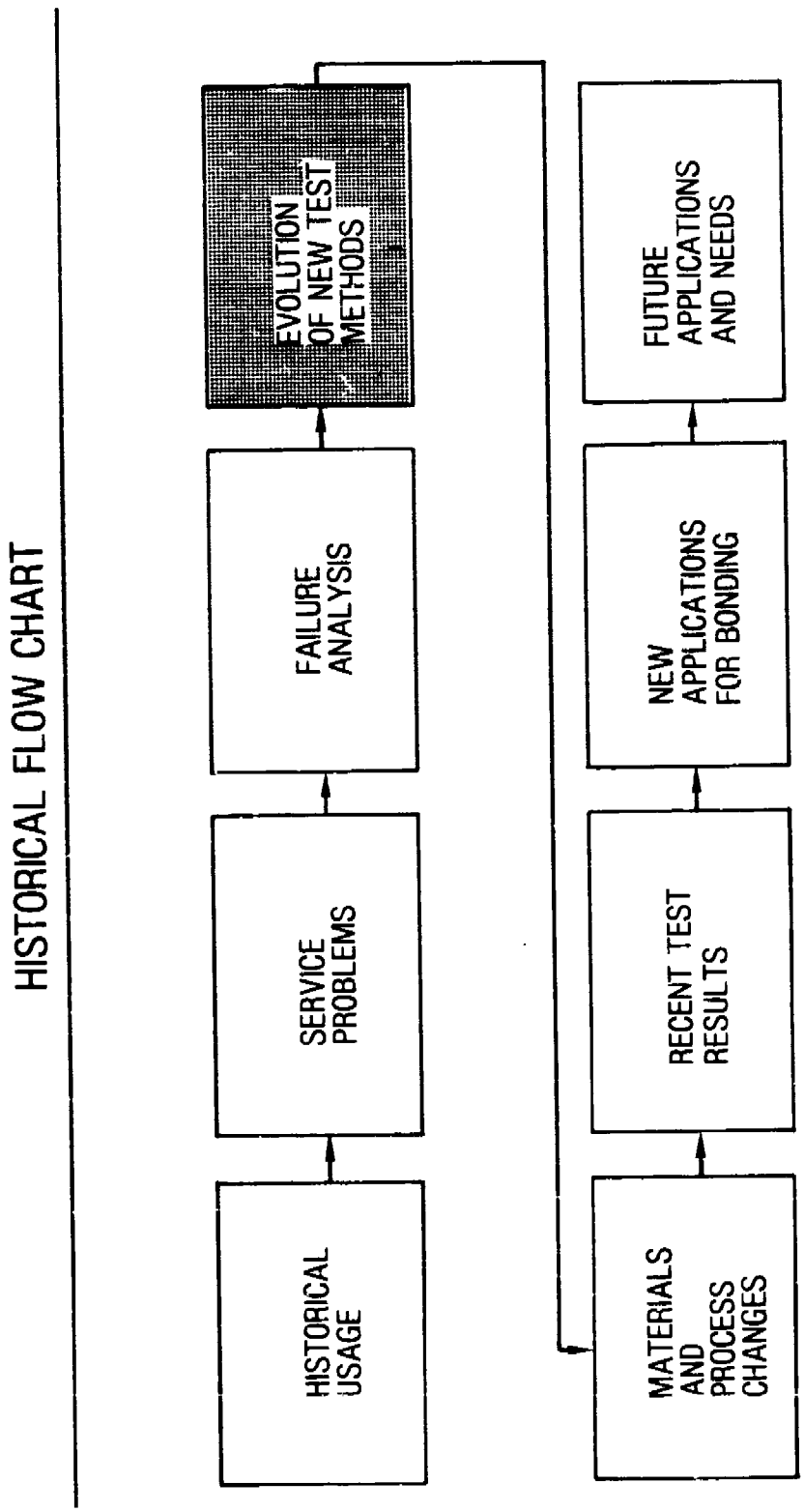
HISTORICAL FLOW CHART
HISTORICAL USAGE
SERVICE PROBLEMS
FAILURE ANALYSIS
EVOLUTION OF NEW TEST METHODS
MATERIALS AND PROCESS CHANGES
RECENT TEST RESULTS
NEW APPLICATIONS FOR BONDING
FUTURE APPLICATIONS AND NEEDS

BONDED 737 COMPONENT (CIRCA 1969) DELAMINATED IN SERVICE TESTS ON UNDELAMINATED SKIN-DOUBLER BOND AREA

- 9,000+ flight-hours—11,000+ landings
- 2024-T3 clad bonded with FM 123-2 adhesive and BR123 primer

1. PROOFLOADED TO 2,000 lb/in^2
2. SHEAR TEST TO 5,100 lb/in^2 WITH NO FAILURE

PORTA SHEAR SPECIMEN

WEDGE TEST SPECIMEN EXPOSED TO 120°F/100% R.H.

DOUBLER

SKIN

PRETEST FRACTURE | TEST | POSTTEST FRACTURE

FRACTURE

CRACK DIRECTION →

PORTA SHEAR SPECIMEN, 5,100 lb/in^2 WITH NO FAILURE

PEEL SPECIMEN ROOM TEMPERATURE TEST, 72 lb/in

SKIN

DOUBLER

PEEL DIRECTION →

| ADDED WATER—DELAMINATION OCCURRED

EVALUATION OF SERVICE PARTS

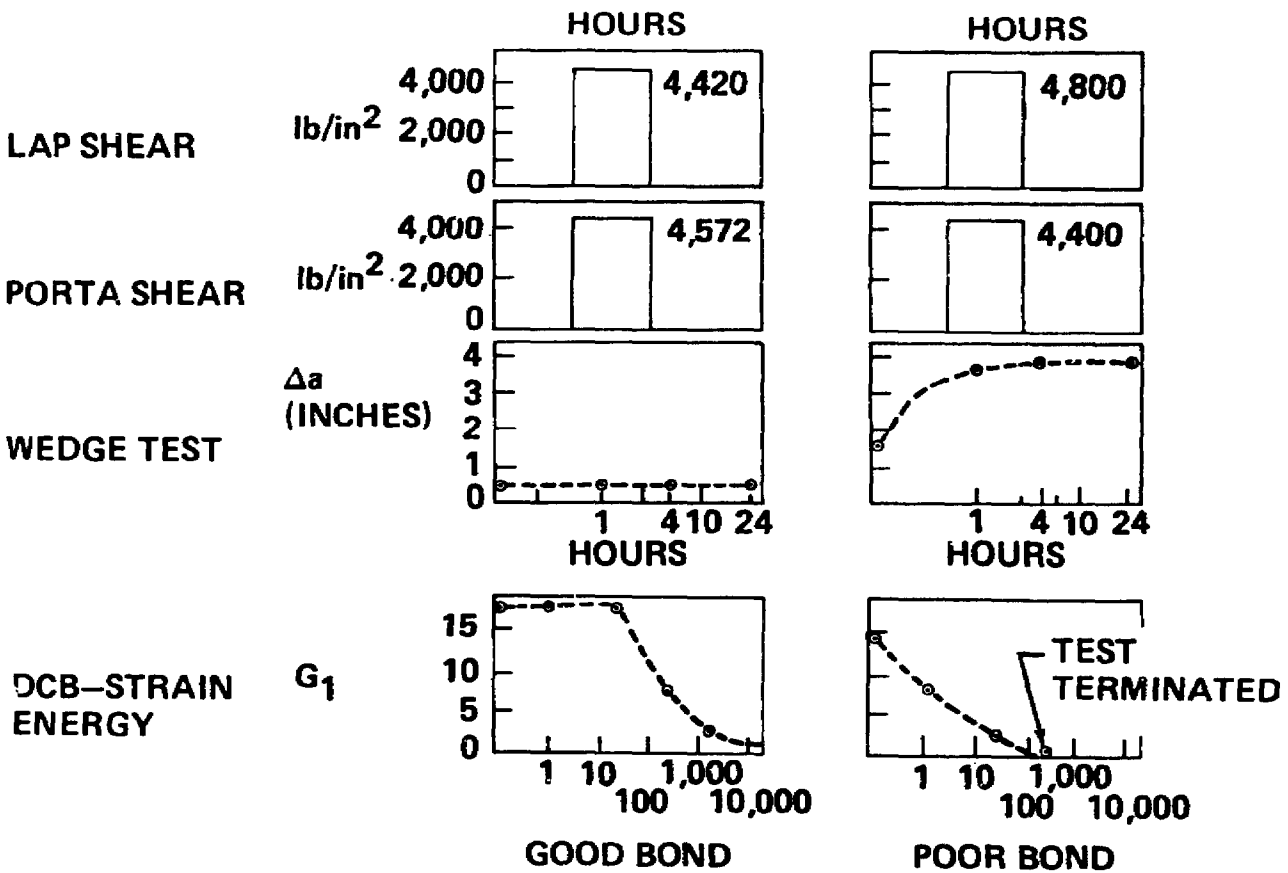

TYPICAL LOADING ARRANGEMENT

CYCLIC LOAD

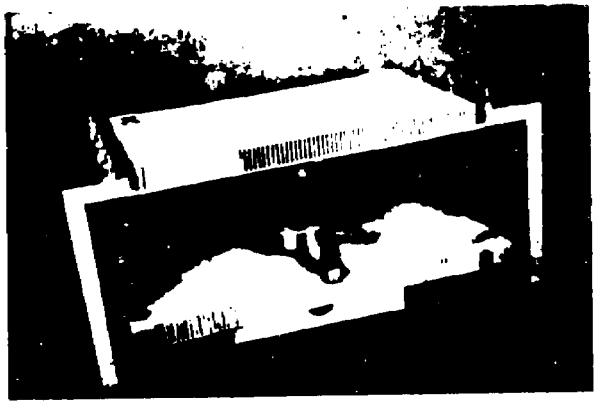

CYCLIC LOAD ARRANGEMENT

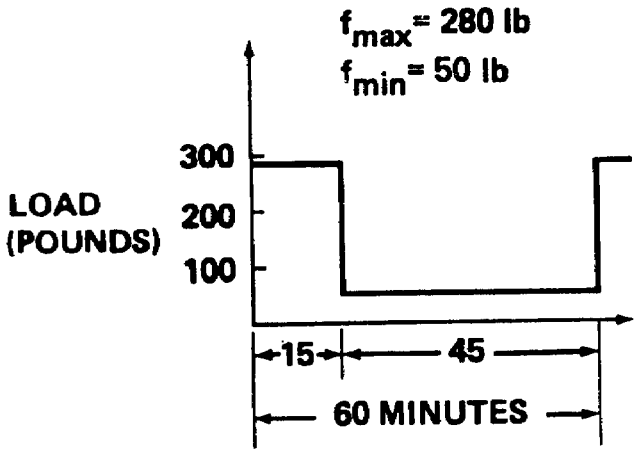

CYCLIC LOAD CYCLE

GROUND—AIR—GROUND ENVIRONMENT

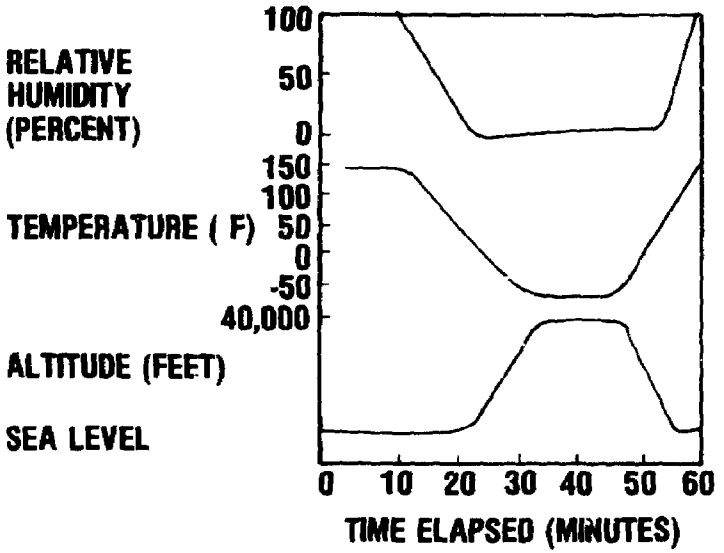

TYPICAL RESULTS

BONDING TECHNOLOGY	NO STRESS	STATIC STRESS	CYCLIC STRESS
OLD	100 CELLS, WATER, 4,000 CYCLES	50 CELLS, WATER, 760 CYCLES	FAILED, 260 CYCLES
NEW	NO WATER, 8,000 CYCLES	NO WATER 8,000 CYCLES	NO FAILURE, 3,000 CYCLES

EVOLUTION OF TEST METHODS

STATIC	➧	FATIGUE
AMBIENT	➧	RANGE OF TEST TEMPERATURES
DRY	➧	MOISTURE CONDITIONED
SINGLE LOAD	➧	SYNERGISTIC
SMALL	➧	LARGE

HISTORICAL FLOW CHART

ELEMENTS OF BONDING

SEM 5000X

METAL TO METAL

HONEYCOMB SANDWICH

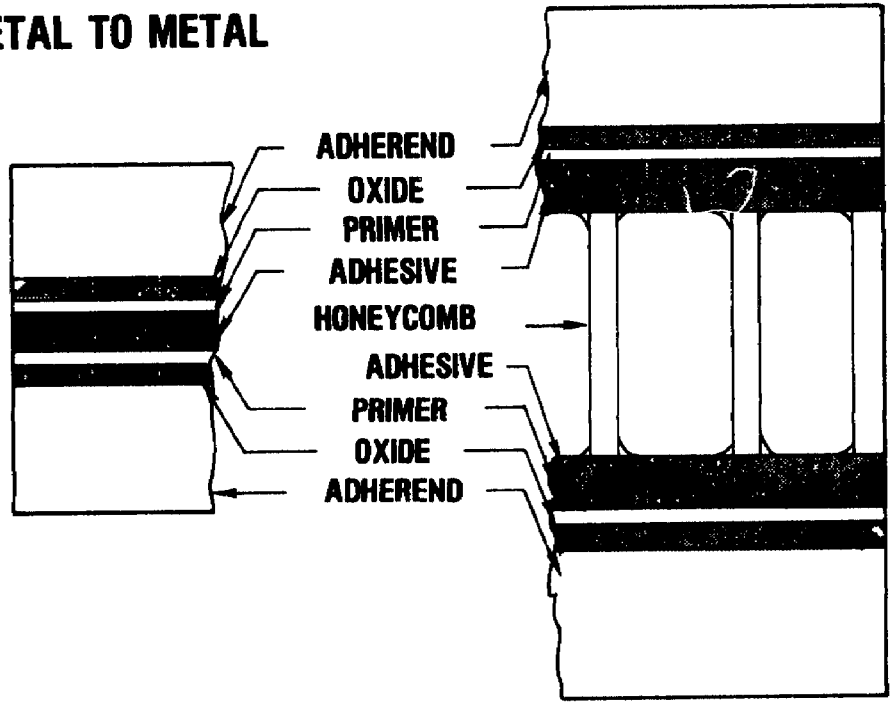

FRACTURE MECHANICS SPECIMEN— THIN ADHEREND

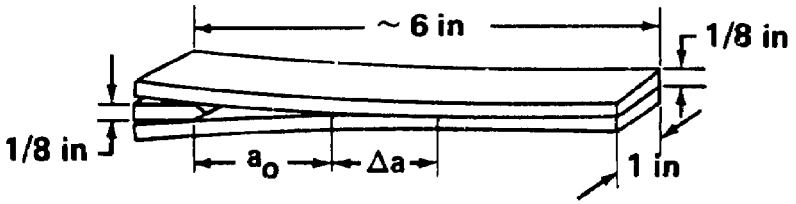

a_o = DISTANCE FROM LOAD POINT TO INITIAL CRACK TIP

Δa = GROWTH IN CRACK DURING ENVIRONMENTAL EXPOSURE

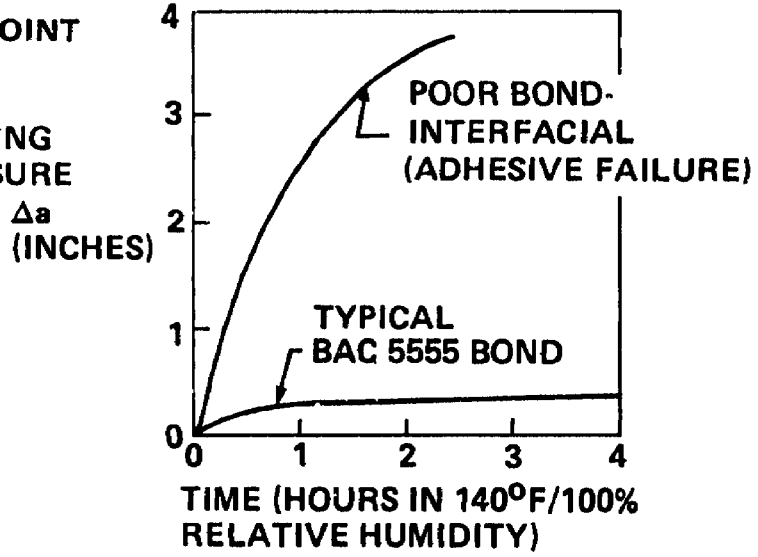

Comparison of FPL Etch and Phosphoric Acid Anodize Processes

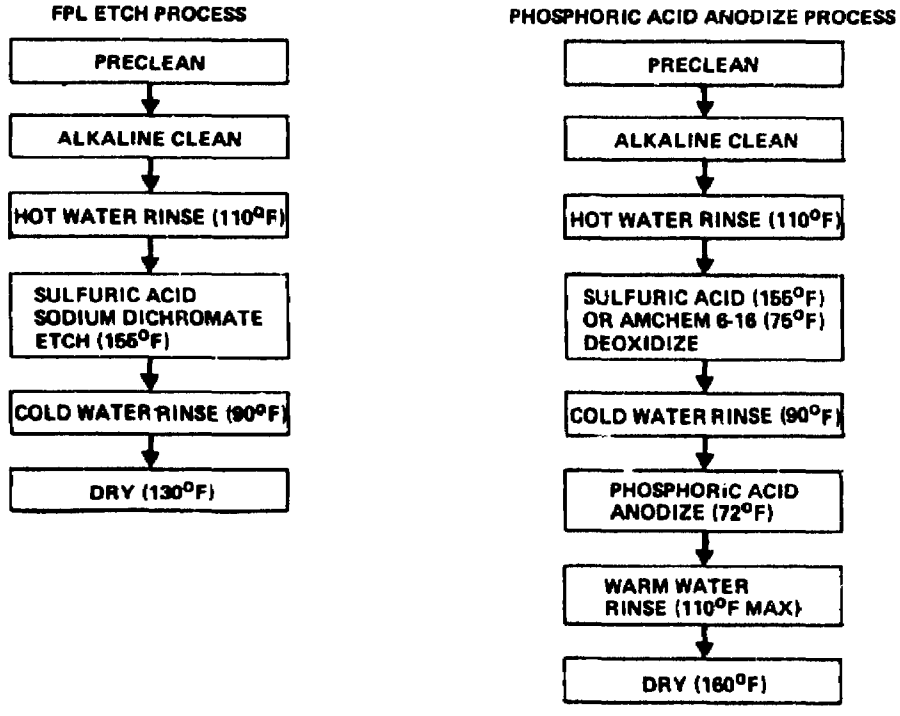

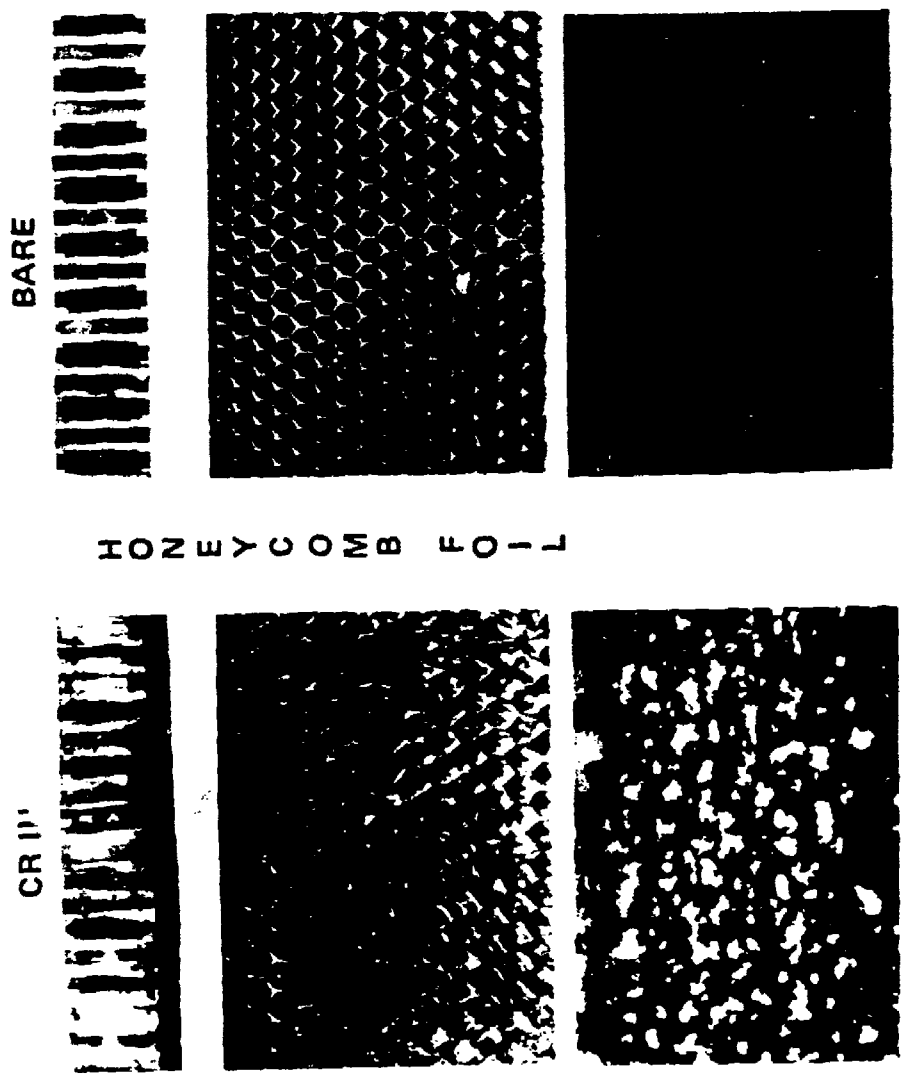
BARE
HONEYCOMB FOIL
CR II'

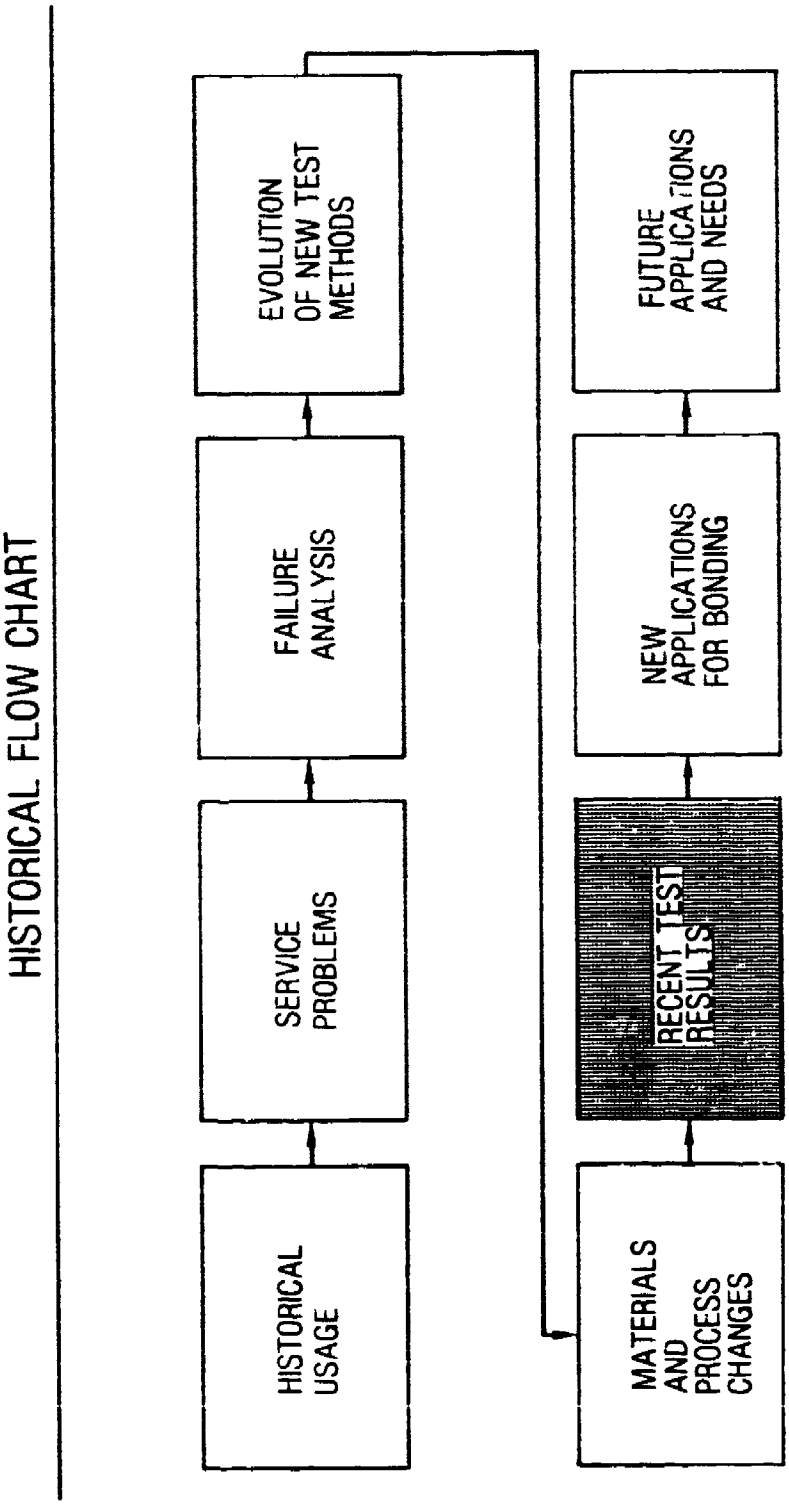
HISTORICAL FLOW CHART
HISTORICAL USAGE
SERVICE PROBLEMS
FAILURE ANALYSIS
EVOLUTION OF NEW TEST METHODS
MATERIALS AND PROCESS CHANGES
RECENT TEST RESULTS
NEW APPLICATIONS FOR BONDING
FUTURE APPLICATIONS AND NEEDS

COMPARISON OF PRIMERS ON PHOSPHORIC ACID

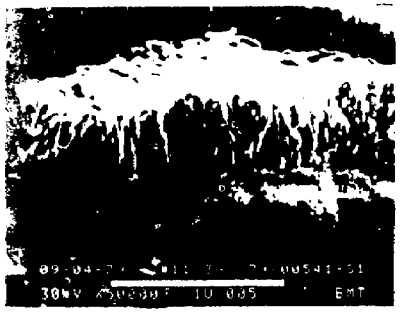

50,000X

PARTIAL PENETRATION
(THIN RUBBER CONTAINING
PRIMER ON 2024-T3 CLAD)

50,000X

COMPLETE PENETRATION
(THIN RUBBER CONTAINING
PRIMER ON 2024-T3 CLAD)

50,000X

EXCESSIVELY THICK PRIMER
(THICK RUBBER CONTAINING
PRIMER ON 2024-T3 BARE)

TEM Photo

TEM Photo

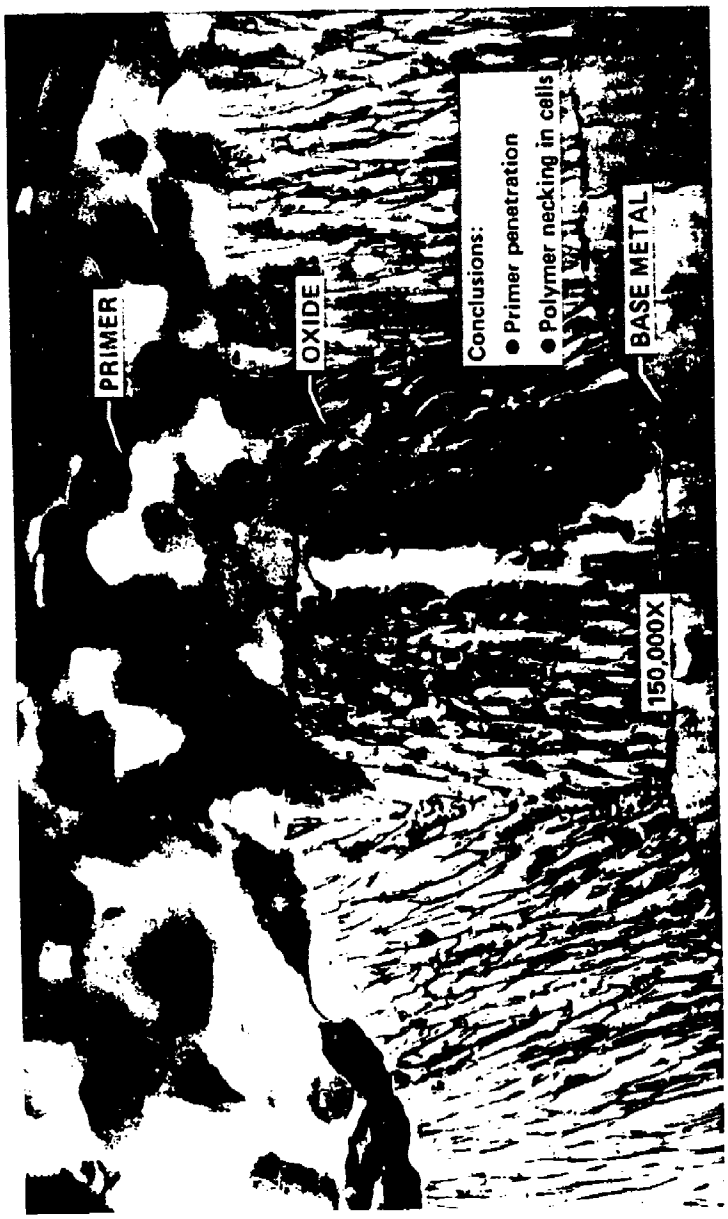
PRIMER
OXIDE
BASE METAL
150,000X
Conclusions:
● Primer penetration
● Polymer necking in cells

TEM Photo

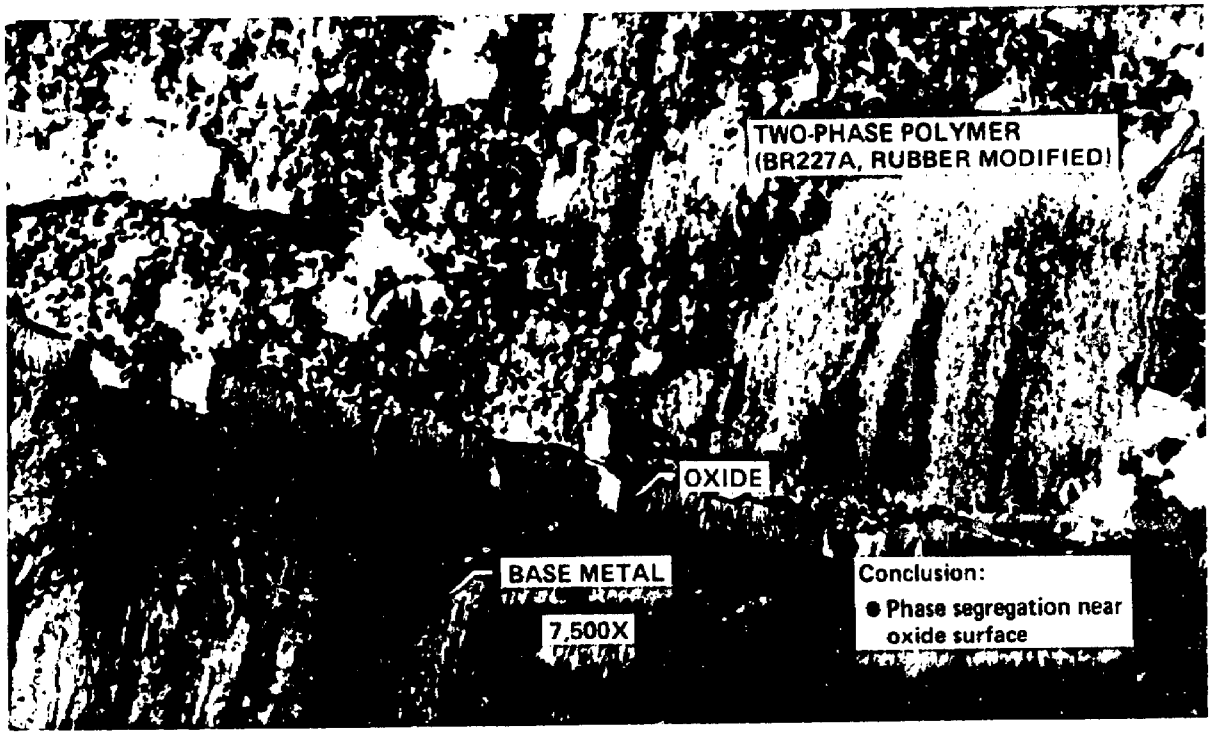
TWO-PHASE POLYMER
(BR227A, RUBBER MODIFIED)
OXIDE
BASE METAL
7,500X
Conclusion:
● Phase segregation near oxide surface

HISTORICAL FLOW CHART

BONDED STRUCTURE—YC-14 PROTOTYPE

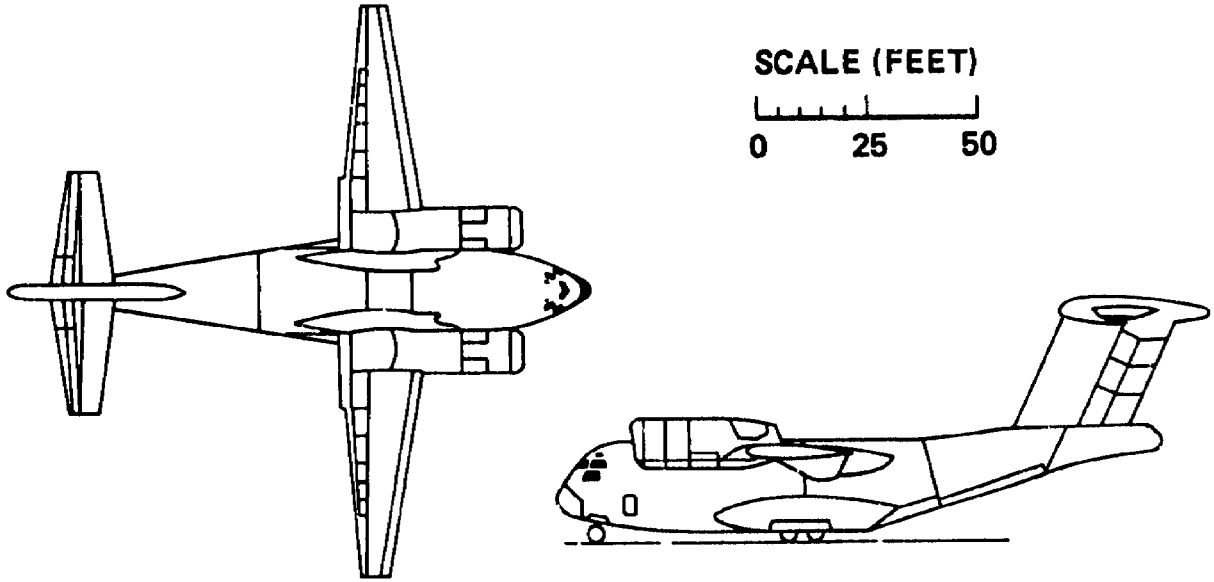

AREA OF BONDED STRUCTURE (ft^2) (65% OF TOTAL APL WETTED AREA)		
ALUMINUM HONEYCOMB	METAL TO METAL	FIBERGLASS HONEYCOMB
2,450	1,000	5,000

YC-14 EMPENNAGE DESIGN

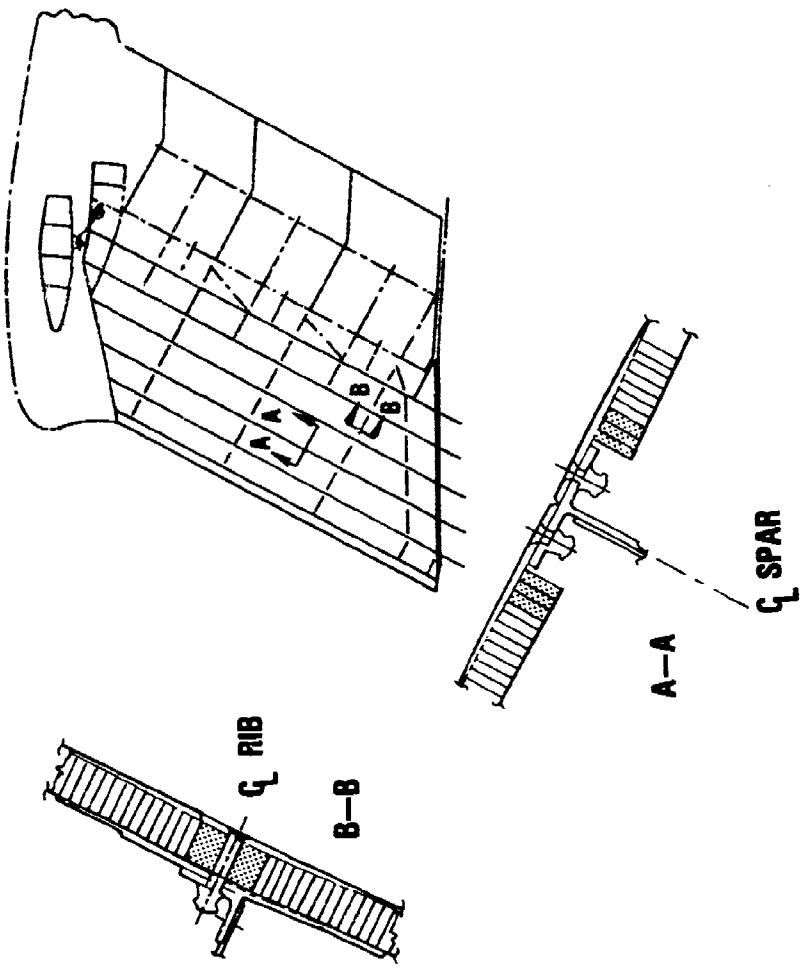

METAL BONDING

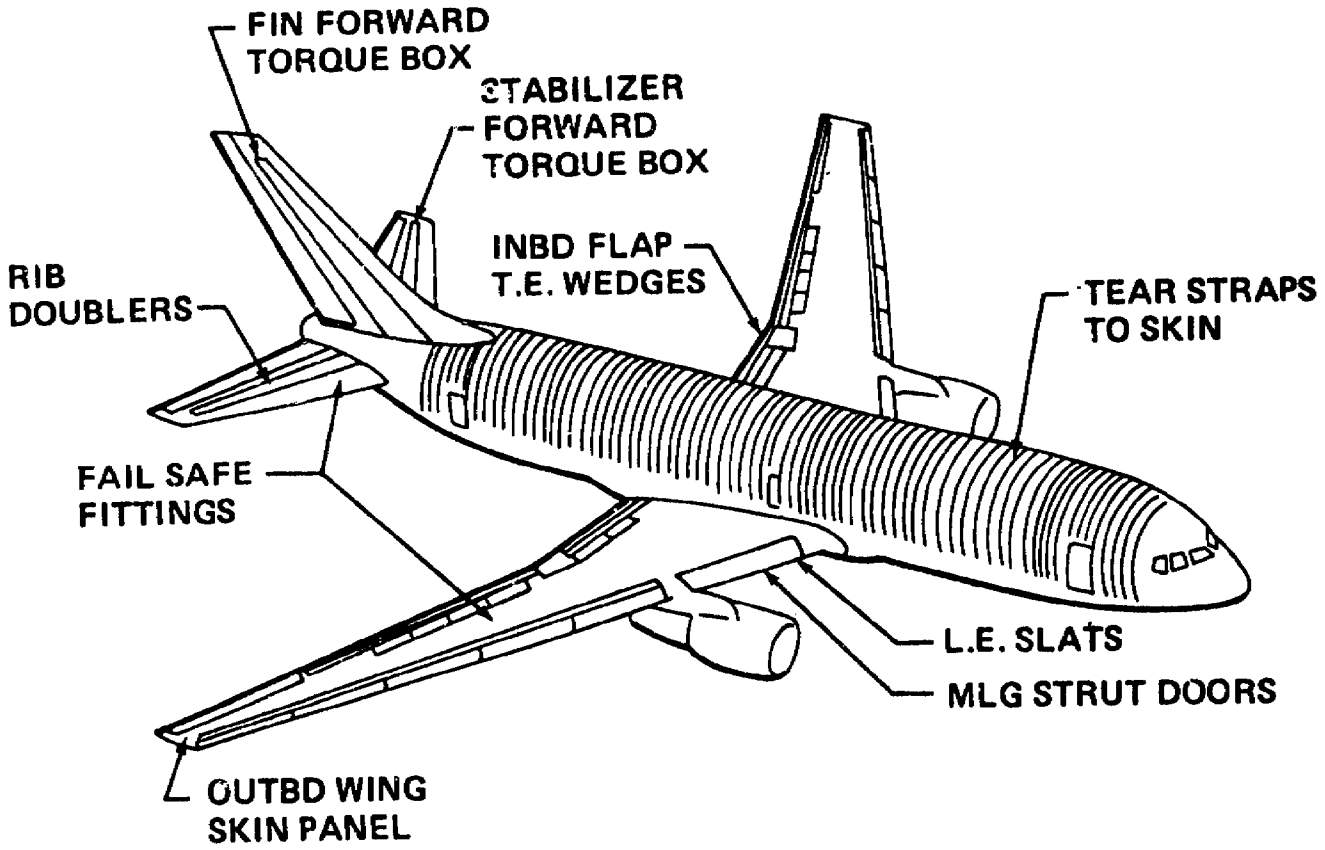

HISTORICAL FLOW CHART
HISTORICAL USAGE
SERVICE PROBLEMS
FAILURE ANALYSIS
EVOLUTION OF NEW TEST METHODS
MATERIALS AND PROCESS CHANGES
RECENT TEST RESULTS
NEW APPLICATIONS FOR BONDING
FUTURE APPLICATIONS AND NEEDS

FUTURE BONDING NEEDS

SECONDARY ➡ PRIMARY ➡ HIGH TEMPERATURE

REQUIRED TEST METHODS—

1. MEANINGFUL, DUPLICATE LOADS AND TEMPERATURE
2. SIMULATE SERVICE FAILURES
3. COMBINE EFFECTS OF MOISTURE, TEMPERATURE, SPECTRUM FATIGUE.

Biography

Name: Gilbert (Gib) L. Arthur

Present Affiliation: NAVAIR Engineering Support Office
Naval Air Rework Facility
MCAS Cherry Point, NC 28533

Title:
Chemical Branch Head

Field of Interest/Responsibilities: Chemical processes and materials involved with cleaning, metal surface treatment, electroplating, organic coatings, surface preparation for adhesive bonding and corrosion treatment and control.

Previous Affiliations/Titles:

Empire Menhaden Co., Empire, LA/
Chief Chemist

Academic Background:

B. S. in Chemistry, High Point College, High Point, NC/1949

Society Activities/Offices:

ACS, NACE, SAMPE

Publications/Papers:

Biography

Name:

F. L. (Fred) Banta

Present Affiliation:

Aerojet Strategic Propulsion Co.
Sacramento, Ca.

Title:

Senior Engineering Specialist

Field of Interest/Responsibilities:

Engineering Materials & Processes
Corrosion Prevention & Control MX Stage II
Adhesive Bonding MX Common EPM

Previous Affiliations/Titles:

Chemical Systems Division of United Technologies
Sunnyvale, Ca.
Manager, Materials & Processes-Eng. Branch

Academic Background:

B.S. Engineering, University of Wisconsin
M.S. Engineering, Stanford University

Society Activities/Offices:

ASTM - Member Main Committee E 24
AMS Div. of SAE

Publications/Papers:

"Structural Adhesives for Missile External Protection Material"
To be presented at 1981 JANNAF Propulsion Meeting - New Orleans

"Metallurgical Defects in Aerospace Materials"
Presented at Ninth Annual Technical Meeting of International Metallographic Society - Seattle, Washington

"Casting - A Means for Low Cost-High Strength Rocket Motor Fabrication"
Presented at ASM - Detroit, Michigan

"Low Cost Fabrication - Integral Rocket Ramjet Components"
Presented at SAMPE - Kiamisha Lake, New York

ASM Handbook, Vol 4 "Forming" Contributing author on Metal Spinning Section.

Biography

Name:

Hargrow Barber

Present Affiliation:

Naval Air Rework Facility, Code 120
Alameda Naval Air Station, Alameda, CA 94501

Title:

Training Instructor
Corrosion Engineer

Field of Interest/Responsibilities:

Training, Corrosion Control

Previous Affiliations/Titles:

None

Academic Background:

Degree in Chemistry, BS and MS
Two years Metallurgy

Society Activities/Offices:

National Association of Corrosion Engineers
Member T-9B and T-9D Technical Committee
License number 142, California Corrosion Engineer

Publications/Papers:

None

Biography

Name: LOUIS CAMPANAPO

Present Affiliation: Aeronutronic Division
Ford Aerospace & Communications Corporation

Title:
MATERIALS ENGINEER

Field of Interest/Responsibilities: Materials and Processes/ material and process call-outs for division programs, corrosion control, specifications, manufacturing support, proposals, etc.

Previous Affiliations/Titles:

Rockwell International--Space Division-- /
Member of Technical Staff

Academic Background:

PhD--Organic Chemistry--State University of Iowa

Society Activities/Offices:

SAMPE
Alpha Chi Sigma

Publications/Papers:

Company Internal

Biography

Name: Larry W. Campbell, PE

Present Affiliation: McDonnell Douglas
Astronautics Company-St. Louis

Title: Senior Engineer

Field of Interest/Responsibilities: Corrosion Control on the Harpoon Weapon System (Anti-ship Missile)

Previous Affiliations/Titles:

Martin Marietta Aerospace - Denver Division - Michoud Operations
Senior Engineer

Academic Background: B.S. - Ch. E. from University of Missouri at Rolla (1971)
NACE Courses 1 & 5
1980 MIT Corrosion Short Course
NACE Corrosion Specialist-In-Training

Society Activities/Offices:

Member NACE/T-9B Chairman
Member AIChE
Member ASTM/G-1 Committee
Member NSPE/Registered Professional Engineer in Louisianna

Publications/Papers: None

Biography

Name: Thomas A. Corboy

Present Affiliation:

Advanced Coatings and Chemicals

Title:

President

Field of Interest/Responsibilities:

Coating - Corrosion - Research as it relates

Previous Affiliations/Titles:

Dexter Corp. - General Manager

W.P. Fuller & Co. - Vice President

Academic Background:

AA City College S.F.
BS San Jose State College
MBA Goldedn Gate College S.F

Society Activities/Offices:

SAE / NACE / NPC / NPTC / SAMPLE / FCS /

Publications/Papers:

17 Patents Issued or pending

Biography

Name: Eugene R. Fannin

Present Affiliation: McDonnell Aircraft Company,
A Division of McDonnell Douglas Corp.

Title: Program Manager, Engineering Technology

Field of Interest/Responsibilities:

Corrosion control, electroplating and inorganic coatings, vacuum deposition, materials development application. Presently program manager responsible for the Ivadizer equipment development and marketing.

Previous Affiliations/Titles:

24 years with McDonnell Aircraft in Material and Process Development. Previous title - Manager - Nonmetallics Branch, Material and Process Development.

Academic Background: B.S. Chemical Engineering, University of Missouri, Rolla.

Society Activities/Offices:

SAMPE ASM AES
AIAA - Materials Technical Committee
SAE - Nonmetallics Committee
NMAB - Ion Implantation Committee

Publications/Papers:

Ion Vapor Deposited Aluminum Coatings for Improved Corrosion Protection, AGARD Meeting, September 1978.

Aluminum Coated Fasteners by Ion Vapor Deposition, Finishing Conference (SMB), October 1977.

Ion Vapor Deposited Aluminum, Alternative for Cadmium, Workshop on Alternatives for Cadmium, October 1977

Biography

Name: Catharine M. Flowers

Present Affiliation: Martin Marietta Aerospace
1979-present P.O. Box 179, Denver, CO 80201

Title: MX Corrosion Control Engineer
(Staff Engineer)

Field of Interest/Responsibilities:

Interest: Corrosion control, finishes, materials selection, failure analysis
Responsibilities: Corrosion control program for Martin Marietta part of MX contract.

Previous Affiliations/Titles:

1974-1979 - Northrop Corporation/Sr. Engr, Mtls & Processes
1972-1974 - NETCO, Inc., contracted to Aerospace Corp./Engr, Mtls. Lab.
1970-1972 - Chemistry Department, Univ. of So. Calif/Research
1969-1970 - Hughes Aircraft Co/Analyst
1968-1969 - Chemistry Department, Univ. of Ca. at L.A./Teacher

Academic Background:

B.S. Chemistry, Univ. of So. Calif., 1968
Graduate courses at UCLA and USC - 1969 - 1976

Society Activities/Offices:

Member of ASM, AES.

Publications/Papers:

Photochemistry of Complex Ions. XII. Photochemistry of Cobalt (III) Acidoammines: R.A. Pribush, C.K. Poon, C.M. Bruce (now Flowers), and A.W. Adamson, University of Southern California, JACS, 96, 3027 (1974).

Biography

Name: Albert J. Glueckert

Present Affiliation: GARD, INC./ GATX CORP.

Title: Research Engineer

Field of Interest/Responsibilities: Corrosion and Coatings, Air Pollution

Previous Affiliations/Titles:

Academic Background: B.S. Chemical Engineering

Society Activities/Offices: A.I.Ch.E.
N.A.C.E.
Soc. for Coating Technology

Publications/Papers:

Biography

Name: Jack D. Guttenplan

Present Affiliation: Autonetics Strategic Systems Division
Rockwell International
D/274-044, Mail Code: 031-GA25; 3370 Miraloma Avenue, Anaheim, CA 92803
Title: Member of the Technical Staff (MTS)

Field of Interest/Responsibilities: Corrosion, Electrochemistry, Material Science/Corrosion Prevention and Control Representative for Guidance and Control System of Missile X, Autonetics Representative on Corporate Technical Panel on Corrosion.

Previous Affiliations/Titles:

Magna Corporation (TRW), Anaheim, CA - Manager, Development
Chrysler Corporation, Highland Park, MI - Group Leader, Electrochemistry Research
C.F. Prutton and Associates, Cleveland, OH - Associate Engineer

Academic Background:

1945 Case Institute of Technology, Cleveland, Ohio - B.S. Chemical Engineering

1948 Case Institute of Technology, Cleveland, Ohio - M.S. Chemical Engineering

Society Activities/Offices:

ASM/Chairman, Orange Coast Chapter 1978-79
ASM/Chairman, Technical Program Committee, WESTEC 1980-1981
NACE/T9E/Corrosion Specialist
FAIC
SIGMA Xi, TAU Beta Pi, Professional Engineer in Corrosion Engineering, California

Publications/Papers:

35 Publications/Papers in the Areas of Corrosion, Electrochemistry and Materials Science.

Recent Papers:

E. G. Shafrin, J. S. Murday, J. D. Guttenplan, and L. N. Hashimoto, "Chromate Film Used For Chemical Corrosion Control On Gold Plated PCB Connectors", Applications of Surface Science 4, 456-465, 1980.

J. D. Guttenplan and L. N. Hashimoto, "Corrosion Control For Electrical Contacts In Submarine Based Electronic Equipment", Materials Performance, Vol. 18, No. 12, 49-55, Dec. 1979.

J. D. Guttenplan and L. N. Hashimoto, "Cleaning Process For The MARDAN Computer", 5TH Contamination Control Seminar, Los Angeles, CA., October 1979.

J. D. Guttenplan, "Corrosion Prevention and Control", Orange County Chapter SPHE, Buena Park, CA., March 1979.

J. D. Guttenplan, "SPD - A NDT Method for Detecting Surface Contamination", Plating and Surface Finishing, Vol. 65, No. 6, 51-58, June 1978.

Biography

Name: Alvin H. Ingram Jr.

Present Affiliation:
Naval Air Rework Facility
NAVAIR Engineering Support Office
Code: NESO 34200
Norfolk, VA. 23511

Title:
Chemist

Field of Interest/Responsibilities:

Electroplating, Surface Chemistry Corrosion, Inorganic Coatings, Analytical Chemistry.

Previous Affiliations/Titles:

Academic Background:

B. S. Chemistry, 1963, [illegible] Dominion University, Norfolk, VA.

Society Activities/Offices:
American Society for Metals
American Electroplaters Society

Publications/Papers:

U. S. Patent, 3, 994, 751, Paint Adhesion Improvement

Biography

Name: John R. Martin

Present Affiliation: The Foxboro Company
Foxboro, Mass.

Title: Manager, Materials Research

Field of Interest/Responsibilities: Applied research related to materials used in industrial instruments and control systems. These units are expected to operate within tight performance specs and with a high degree of reliability in a broad range of environments.

Previous Affiliations/Titles:

General Dynamics/Electric Boat Division

Academic Background:

BS, Tufts University, Chem. Eng.
MS, University of Connecticut, Chem. Eng.
PhD, University of Connecticut, Polymer Science

Society Activities/Offices:

Soc. Plastics Eng., Engineering Prop. & Struct. Div.; Chm. Tech. Prog. Comm.;
AIChE
ACS
NACE
Int'l Electronics Pkg. Soc.

Publications/Papers:

15 Technical publications in open literature - primarily related to test and evaluation of polymeric materials for long term performance

3 Reports for NAVSHIPS; investigated elastomer characteristics relevant to sonar systems

Biography

Name: J. B. Nathan, Jr.

Present Affiliation: Honeywell Inc.
Defense Systems Division
600 Second Street N.E.
Hopkins, MN 55343

Title: Principal Materials & Process Engineer

Field of Interest/Responsibilities:

Mr. Nathan is a Principal Materials and Process Engineer in Honeywell's Defense Systems Division. In this capacity he advises design engineering in the selection of materials, metal finishing treatments, heat treatments, metal joining techniques, encapsulation, fabrication methods, and sealing techniques for new electronic weaponry designs. For the past twelve years he has had the added responsibility of designing the long term - world wide storage corrosion protection systems of all DSD's electronic weaponry projects.

He served as project engineer for a multi-year corrosion study of various metal, paint coating, and sealant materials in ground burial environments. He was responsible for transferring the ground burial study results into the designs of Honeywell's buried sensor and traffic monitor product lines.

He was responsible for corrosion protection of Honeywell's sensor systems in the National Data Buoy System, a weather monitor attached to free floating marine buoys.

He was responsible for printed circuit assembly materials, and plastic molding compounds, encapsulating and potting compound selections for Honeywell's electronic fuze and scatterable mines programs.

For the past three-years he has been responsible for selecting the corrosion protection systems used on all U.S. Navy Torpedo systems designed and/or manufactured by Honeywell.

Previous Affiliations/Titles:

Prior to joining Honeywell in 1968, Mr. Nathan was a Materials Engineer at Beech Aircraft Corporation, Boulder, Colorado and Cessna Aircraft Company, Wichita, Kansas. In those capacities he was responsible for all material and process controls at a military aircraft production facility, and for material and process selection and controls for Apollo and LEM cryogenic fuel tanks.

Academic Background:

B.S., Chemical Engineering, Kansas State University

B.S., Physical Sciences, Kansas State University

Registered Professional Engineer, State of Kansas

Society Activities/Offices:

Member - American Society for Testing and Materials

Member - National Association of Corrosion Engineers

Active Member of Corrosion of Aerospace Equipment Committee (T-9)

Moderator of the Corrosion Protection Panel Discussion at the 1980 NACE North Central Regional Conference.

Publications/Papers:

"A Program to Evaluate Materials for Underground Exposure in Extreme Environments," 15th National SAMPE Symposium, April, 1969.

"Evaluation of Materials for Underground Exposure in Extreme Environments," 4th SAMPE National Technical Conference, October, 1972.

"Fabrication and Laser Sealing of a Powder Metal Mercury Switch," 5th National SAMPE Technical Conference, October, 1973.

"Improve Small Item Concealment with Indigious Adhesive Camouflage", USA MERDC Passive Countersurveillance Symposium, April, 1973.

1970 Seals and Sealing Burden Study - Final Report (distributed within Honeywell D.S.D. Engineering).

"Pressure Sensitive Adhesive Film Characterization by Accelerated Aging," Adhesives Age, Vol. 17, No. 9, Spetember, 1974.

"Electroless Nickel Plating on Powder Metal Substrates", Plating and Surface Finishing, Vol. 65, No. 6, June, 1978.

"A Method for Moisture Proofing Ground Buried Cable Connectors and Splices," National Association of Corrosion Engineers, March, 1978, Paper No. 200.

"Conflicting Requirements in Military Specifications", National Association of Corrosion Engineers, March, 1979, Paper No. 150.

"A Method of Moisture Proofing Buried Cable Connectors and Splices", Materials Performance, Vol. 18, No. 6, August, 1979.

Biography

Name:

James E. Preston

Present Affiliation:

Naval Coastal Systems Center, Panama City, Fla.

Title:

Mechanical Engineer

Field of Interest/Responsibilities:

Mechanical Design
Materials Selection
Failure Analysis
Corrosion Control

Previous Affiliations/Tities:

Adjunct Instructor, University of Florida, Gainesville, Fla.

Adjunct Instructor, Gulf Coast Community College, Panama City, Fla.

Consulting Engineer, Reg. P.E. (Fla.)

Academic Background:

Bachelor of Mechnical Engineering, University of Florida, 1963

Master of Materials Engineering, University of Florida, 1968

Various Short Courses in Materials and Corrosion Engineering

Society Activities/Offices:

American Society for Metals

National Association of Corrosion Engineers

American Society of Mechanical Engineers, Past Chmn. Panama City Section

Publications/Papers:

BIOGRAPHY

Name: Harold J. Singletary

Present Affiliation: Lockheed-Georgia Company

Title: Staff Engineer

Field of Interest/Responsibilities: Corrosion & Its Prevention in Aircraft Systems/Provide design guidance and support in the prevention of corrosion in Lockheed-built products; participate in Air Force CPAB activities for the C-130, C-141 and C-5; develop corrosion oriented information for service manuals and technical orders; initiate corrective action on corrosion related problems; establish corrosion testing procedures; conduct classes in corrosion for Lockheed and customer personnel; contribute to the Engineering Design Handbook.

Previous Affiliations/Titles: Cee Bee Chemical Co., salesman & technical representative; The Martin Company, senior engineer; Hayes International Corp., materials and processes engineer.

Academic Background: University of Alabama, 1949

Society Activities/Offices: SAMPE, first vice-chairman of Atlanta Chapter; NACE, past chairman, Atlanta Section; Registered Professional Engineer.

Publications/Papers: "Aircraft Lavatories, A Corrosive Royal Flush", 9th National SAMPE Technical Conference, October 1977; "Growing Procedural Problems of Washing Mammoth Aircraft", Journal of Aircraft, Sept. 1974; "Maintenance of Aircraft Integral Fuel Tanks", Airlifters, July 1967, October 1967, and January 1968.

BIOGRAPHY

NAME: Ronald J. Olson

Present Affiliation:

3M
Industrial Specialties

Title:

Technical Service Representative

Field of Interest/Responsibilities:

General Industry/Automotive/Aerospace as concerns surface protection and pressure sensitive bonding. Primary responsibilities include identifying new product opportunities, services and assuring product conformance to meet government, industry and 3M requirements.

Previous Affiliations/Titles:

Product Engineering and Development - 3M Industrial Specialties Div.

Academic Background:

University of Minnesota - Technical Course Study

Biography

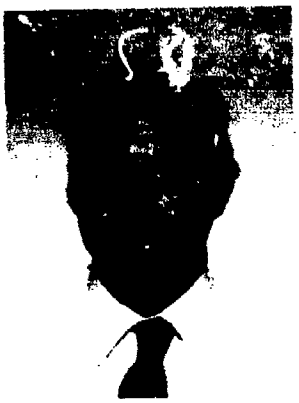

Name: NARVEL L. ROGERS

Present Affiliation: Bell Helicopter Textron

Title: Chemical and Process Laboratory
Assistant Group Engineer

Field of Interest/Responsibilities:
Metal Finishing and Corrosion Control

Previous Affiliations/Titles:

Academic Background:

Attended Tarleton State College and
The University of Texas

Society Activities/Offices:

NACE, T9B, T9D Committees
SAMPE, Chairman, Dallas-Ft. Worth Chapter
National Director - Dallas-Ft. Worth Chapter
AUSA

Publications/Papers:

(See Attached Sheet for listing)

PAPERS AND PUBLICATIONS:

1. "Surface Preparation of Metals for Adhesive Bonding", presented at Symposium on Structural Adhesive Bonding, September 1965, at Stevens Institute of Technology, Hoboken, N. J.; published in Journal of Applied Polymer Science.

2. "A Comparative Test for Corrosion Resistant Adhesive Primers", presented at SAMPE National Technical Conference, Aerospace Adhesives and Elastomers, October 1970, Dallas, Texas; published by SAMPE - National SAMPE Technical Conference Series, Vol. 2.

3. "Some Effects of Curing Conditions on Adhesion to Metal Surfaces", presented by SAE Automotive Engineering Congress and Exposition, Adhesive Symposium, January 1971, Detroit, Michigan; published by SAE.

4. "Corrosion of Adhesive Bonded Clad Aluminum", presented at SAE National Business Aircraft Meeting, March 1972, Wichita, Kansas; published by SAE.

5. "Developing a Reliable Surface Preparation for Adhesive Bonding", presented at Symposium on Processing for Adhesives Bonded Structures, August 1972, at Stevens Institute of Technology, Hoboken, N. J.; published in Journal of Applied Polymer Science.

6. "A Comparative Test for Bondline Corrosion - Clad Vs Bare Aluminum", presented at SAMPE National Technical Conference, Kiamesha Lake, N. Y., October 1973; published by SAMPE, National SAMPE Technical Conference Series, Vol. 5.

7. "Lead Interference in Bisulfate Etch Solution for Stainless Steel", presented at SAMPE National Symposium, April 1976, Los Angeles, California; published by SAMPE, 21st National SAMPE Symposium, Vol. 21.

8. "Bonding to Sealed Chromic Acid Anodize", presented at Symposium on Durability of Adhesive Bonded Structures, Picatinny Arsenal, Dover, N. J., October 1976; published by Journal of Applied Polymer Science.

9. "Characterization of Stainless Steel Surfaces Prepared for Adhesive Bonding", presented at Joint SAMPE/ASM Symposium, Los Angeles, California, February 1980; published by ASM.

BIOGRAPHY

NAME: Neil E. Ryan

Present Affiliation:

Aeronautical Research Laboratories

Title:

Principal Research Scientist

Field of Interest/Responsibilities:

Durability Performance of Aircraft
Materials - Corrosion and Environment Assisted cracking processes.

Previous Affiliations/Titles:

Academic Background:

Fellow Royal Melbourne Inst. Tech
D. Phil Oxford University
C. Eng., Member Inst. Metallurgists (London)
[FRMIT, D. Phil (Oxon), CE, NM.]

Society Activities/Offices:

Australasian Institute of Metals*
Chairman - Australian Fracture Group
*National Tech. Comm.
Phys. Met. Comm. (Victorian Branch)

Publications/Papers:

Some 36 Papers - High Temp. Alloy Development Fracture Mechanics and Corrosion Fatigue

BIOGRAPHY

NAME: Don Treadway

Present Affiliation:

General Dynamics/Convair

Title:

Senior Engineering Chemist

Field of Interest/Responsibilities:

Interests involve corrosion prevention procedures for military and aerospace hardware including corrosion testing using accelerated laboratory and natural environments. Responsibilities include preparation and implementation of the corrosion control plans and finish specification for Tomahawk Cruise Missile systems.

Previous Affiliations/Titles:

Academic Background:

B.S., Chemical Engineering, University of California at Berkeley

Society Activities/Offices:

National Association of Corrosion Engineers
American Society for Metals
Society for the Advancement of Materials and Process Engineers

Publications/Papers:

Corrosion Control at Graphite/Epoxy - Aluminum and Titanium Interfaces, Technical Report AFML-TR-74-150, Air Force Materials Laboratory, July 1974.

BIOGRAPHY

NAME: Frank T. Werner, Capt

Present Affiliation:

USAF, HQ SAC/LGME
Aircraft Engineering Division

Title:

Aircraft Systems Engineer

Field of Interest/Responsibilities:

Primarily involved with improving aircraft systems which have less than desirable reliability.

Previous Affilitation/Titles:

Fisher Body, General Motors - Production Engineer
USAF - Pilot On -135 Series Aircraft 7 Yrs

Academic Background:

BME from General Motors Institute, Flint Michigan
MBA from Creighton, University Omaha

Society Activities/Offices:

Publications/Papers:

BIOGRAPHY

NAME: Robert A. Williams

Present Affiliation:

McDonnell Aircraft Co.
St. Louis, Missouri

Title:

Technical Specialist, Engineering Technology

Field of Interest/Responsibilities:

Corrosion Prevention and Control. Member F-15 Corrosion Prevention and Control Panel 1970-71. Harpoon Missile Corrosion Prevention and Control 1971-72. F-4 Aircraft Corrosion Control 1972-74. Co-Chairman F-18 Corrosion Prevention and Control Panel 1975-78. Environmental Resistance Coordinator AV-8 Programs 1979-80.

Previous Affiliation/Titles:

Senior Engineer (M&P), North American Aviation (Later North American Rockwell), Columbus, Ohio 1961-68. Member Corporate Corrosion Panel 1967-68. Senior Engineer (M&P), Curtiss Wright-Corp., Caldwell, NJ 1959-61.

Academic Background:

Higher National Certificate, Royal Institute of Chemistry, London, England.

Society Activities/Offices:

NACE Accredited Corrosion Specialist. Member NACE T-9 Committee.

Publications/Paper:

"Corrosion is a Dirty Word", Three Part Article-Product Support Digest Magazine.

BIOGRAPHY

NAME: Phillip M. Winter

Present Affiliation:

3M Company - Building Service and
Cleaning Products Division Laboratory

Title:

R & D Supervisor

Field of Interest/Responsibilities:

Metal Surface Studies
New Technology Development

Previous Affiliations/Titles:

Rocketdyne - Materials Engineer

Academic Background:

BS Metallurgy - University of Minnesota

Society Activities/Offices:

ASM
NACE

Publications/Papers:

*U.S.Government Printing Office: 1982 — 559-008/5082